

Army

AD

69121669

USAAVLABS TECHNICAL REPORT 66-77

COMPARISON OF THEORETICAL AND EXPERIMENTAL MODEL ROTOR BLADE VIBRATORY SHEAR FORCES

By

Lawrence J. Bain

October 1967

**U. S. ARMY AVIATION MATERIEL LABORATORIES
FORT EUSTIS, VIRGINIA**

**CONTRACT DA 44-177,AMC-136(T)
UNITED AIRCRAFT CORPORATION
SIKORSKY AIRCRAFT DIVISION
STRATFORD, CONNECTICUT**

This document has been
approved for public release
and sale; its distribution is
unlimited.



Disclaimers

The findings in this report are not to be construed as an official Department of the Army position unless so designated by other authorized documents.

When Government drawings, specifications, or other data are used for any purpose other than in connection with a definitely related Government procurement operation, the United States Government thereby incurs no responsibility nor any obligation whatsoever; and the fact that the Government may have formulated, furnished, or in any way supplied the said drawings, specifications, or other data is not to be regarded by implication or otherwise as in any manner licensing the holder or any other person or corporation, or conveying any rights or permission, to manufacture, use, or sell any patented invention that may in any way be related thereto.

Disposition Instructions

Destroy this report when no longer needed. Do not return it to originator.

PAGE 1		PAGE 2	
NO		SECTION 1	
UNCLASSIFIED		<input type="checkbox"/>	
CLASSIFICATION			
DISTRIBUTION/AVAILABILITY CODES			
DIST.	AVAIL.	SPECIAL	



DEPARTMENT OF THE ARMY
U. S. ARMY AVIATION MATERIEL LABORATORIES
FORT EUSTIS, VIRGINIA 23604

This report has been reviewed by the U. S. Army
Aviation Materiel Laboratories and is considered
to be technically sound. It is published for the
dissemination and application of the information
contained herein.

Task 1D121401A14203

Contract DA 44-177-AMC-136(T)

USAAVLABS Technical Report 66-77

October 1967

COMPARISON OF THEORETICAL AND
EXPERIMENTAL MODEL ROTOR
BLADE VIBRATORY SHEAR FORCES

SER-50419

by

Lawrence J. Bain

Prepared by

United Aircraft Corporation
Sikorsky Aircraft Division
Stratford, Connecticut

for

U. S. ARMY AVIATION MATERIEL LABORATORIES
FORT EUSTIS, VIRGINIA

This document has been approved
for public release and sale; its
distribution is unlimited.

SUMMARY

An investigation was undertaken to obtain quantitative measurements of the vibratory forcing functions from the blades of rotary wing aircraft in the flight speed range encompassing both pure and compound helicopter operation. These measurements were made using dynamically scaled model rotor blades mounted on a specially instrumented rotor head. Testing was accomplished in the United Aircraft Corporation's 18 foot subsonic wind tunnel within a range of equivalent forward speeds from 75 to 300 knots and within a range of full scale rotor lifts from zero to 40,000 pounds. In addition to rotor performance, the final data include ten harmonics of the orthogonal blade root shear forces, rotor blade bending moments, and rotor control loads.

It was concluded from the experimental work that:

- 1) High harmonics of vibratory shear forces can be measured at the blade root over a wide range of speeds and lifts.
- 2) Only the first harmonic of flatwise and edgewise shear force is significantly effected by the flapping trim condition of the rotor.
- 3) Elimination of lag damping may increase or decrease the edgewise shear force, depending on its proximity of the operating condition to a blade natural frequency.
- 4) Increasing forward speed causes an increase in both flatwise and edgewise shear forces, the latter becoming predominant at the highest forward speeds.
- 5) Increasing rotor lift at constant forward speed causes a gradual increase in the magnitude of the flatwise shear force harmonics.
- 6) The radial shear force first harmonic longitudinal component takes on values which can be significant, but the fundamental nature of this force is not well defined.

The experimental results were correlated at seven test points with a fully coupled aeroelastic analysis. The evaluation of this work led to the following conclusions:

- 1) The inclusion of wake-induced velocity effects in the theoretical method shifts the calculated flatwise shear forces in a direction which improves the correlation but has no significant effect on the calculated edgewise shear forces.
- 2) The overall degree of correlation is strongly influenced by the accuracy to which the blade natural frequencies are known, the continuity of the calculated induced velocity distribution, and the predictability of the edgewise rotor blade behavior.

FOREWORD

This program was sponsored by the U. S. Army Aviation Materiel Laboratories (formerly U. S. Army Transportation Research Command) Fort Eustis, Virginia, and was monitored by Mr. Joseph McGarvey.

The experimental and theoretical research program was carried out from May 1964 through November 1965. Assisting in this program was Mr. P. J. Arcidiacono of the United Aircraft Corporation Research Laboratories, who directed the development of the rotor head and the impedance analysis.

CONTENTS

SUMMARY.....	<u>Page</u> iii
FOREWORD.....	v
LIST OF ILLUSTRATIONS.....	viii
LIST OF SYMBOLS.....	xv
INTRODUCTION.....	1
DESIGN DATA AND DESCRIPTION OF EQUIPMENT.....	2
EXPERIMENTAL PROCEDURE.....	7
EXPERIMENTAL RESULTS.....	9
EVALUATION OF EXPERIMENTAL RESULTS.....	11
CORRELATION OF THEORY AND EXPERIMENT.....	18
CONCLUSIONS.....	21
RECOMMENDATIONS.....	23
BIBLIOGRAPHY.....	24
DISTRIBUTION.....	123
APPENDIXES	
I. Experimental Flatwise and Edgewise Shear Force Figures.....	125
II. Experimental Radial Shear Force Figures.....	236
III. Experimental Vibratory Moment Amplitude Figures....	261
IV. Experimental Vibratory Control Load Amplitude Figures.....	284

ILLUSTRATIONS

<u>Figure</u>	<u>Page</u>
1 Vibratory Shear Force Rotor Head	44
2 Vibratory Shear Force Rotor Head Details	46
3 Dynamically Scaled Blade-Exploded View	48
4 Dynamic Blade Physical Properties	49
5 Model Rotor Blade Calculated Natural Frequencies	50
6 United Aircraft's Subsonic Wind Tunnel	51
7 Sikorsky Helicopter Rotor Test Rig	52
8 Wind Tunnel Test Conditions	54
9 Effect of Trim Condition on Shear Forces, $\mu = 0.2$	55
10 Effect of Lag Damping on Shear Forces, $\mu = 0.2$, $\alpha_s = -4$ Deg.	59
11 Effect of Lag Damping on Shear Forces, $\mu = 0.5$, $\alpha_s = -4$ Deg.	61
12 Effect of Lag Damping on Edgewise Blade Bending Moment	63
13 Effect of Advance Ratio on Nondimensional Shear Force, $C_L/\sigma = 0.035$, $\alpha_s = -4$ Deg.	66
14 Effect of Advance Ratio on Rotor Blade Vibratory Moments	70
15 Experimental Flatwise Vibratory Shear Force, $\alpha_s = -4$ Deg.	71
16 Experimental Edgewise Vibratory Shear Force, $\alpha_s = -4$ Deg.	73

<u>Figure</u>		<u>Page</u>
17	Experimental Radial Vibratory Shear Force, $\alpha_s = -4$ Deg.	75
18	Experimental Blade Moments, $\mu = 0.2$, $C_L/\sigma = 0.071$, $\alpha_s = -4$ Deg.	77
19	Experimental Blade Moments, $\mu = 0.3$, $C_L/\sigma = 0.019$, $\alpha_s = -4$ Deg.	80
20	Experimental Blade Moments, $\mu = 0.3$, $C_L/\sigma = 0.041$, $\alpha_s = -4$ Deg.	83
21	Experimental Blade Moments, $\mu = 0.3$, $C_L/\sigma = 0.062$, $\alpha_s = -4$ Deg.	86
22	Experimental Blade Moments, $\mu = 0.4$, $C_L/\sigma = 0.046$, $\alpha_s = -4$ Deg.	89
23	Experimental Blade Moments, $\mu = 0.5$, $C_L/\sigma = 0.048$, $\alpha_s = -4$ Deg.	92
24	Experimental Blade Moments, $\mu = 0.7$, $C_L/\sigma = 0.032$, $\alpha_s = -4$ Deg.	95
25	Effect of Rotor Lift on Flatwise Vibratory Shear Force, $\mu = 0.3$, $\alpha_s = -4$ Deg.	99
26	Effect of Rotor Lift on Edgewise Vibratory Shear Force, $\mu = 0.3$, $\alpha_s = -4$ Deg.	101
27	Effect of Rotor Lift on Radial Vibratory Shear Force, $\mu = 0.3$, $\alpha_s = -4$ Deg.	103
28	Effect of Rotor Lift on Nondimensional Shear Forces, $\mu = 0.3$, $\alpha_s = -4$ Deg.	105

<u>Figure</u>		<u>Page</u>
29	Comparison of Theoretical and Experimental Vibratory Shear Force Harmonic Amplitudes, $\mu = 0.2$, $C_L/\sigma = 0.071$, $\alpha_s = -4$ Deg. . .	109
30	Comparison of Theoretical and Experimental Vibratory Shear Force Harmonic Amplitudes, $\mu = 0.3$, $C_L/\sigma = 0.019$, $\alpha_s = -4$ Deg. . .	110
31	Comparison of Theoretical and Experimental Vibratory Shear Force Harmonic Amplitudes, $\mu = 0.3$, $C_L/\sigma = 0.041$, $\alpha_s = -4$ Deg. . .	111
32	Comparison of Theoretical and Experimental Vibratory Shear Force Harmonic Amplitudes, $\mu = 0.3$, $C_L/\sigma = 0.062$, $\alpha_s = -4$ Deg. . .	112
33	Comparison of Theoretical and Experimental Vibratory Shear Force Harmonic Amplitudes, $\mu = 0.4$, $C_L/\sigma = 0.046$, $\alpha_s = -4$ Deg. . .	113
34	Comparison of Theoretical and Experimental Vibratory Shear Force Harmonic Amplitudes, $\mu = 0.5$, $C_L/\sigma = 0.048$, $\alpha_s = -4$ Deg. . .	114
35	Comparison of Theoretical and Experimental Vibratory Shear Force Harmonic Amplitudes, $\mu = 0.7$, $C_L/\sigma = 0.032$, $\alpha_s = -4$ Deg. . .	115
36	Comparison of Theoretical and Experimental Flatwise Rotor Blade Bending Moments, $\alpha_s = -4$ Deg. . .	116
37	Comparison of Theoretical and Experimental Flatwise Rotor Blade Bending Moments, $\alpha_s = -4$ Deg. . .	118
38	Comparison of Theoretical and Experimental Edgewise Rotor Blade Bending Moments, $\mu = 0.5$, $C_L/\sigma = 0.048$, $\alpha_s = -4$ Deg.	119

<u>Figure</u>		<u>Page</u>
39	Azimuthal Variation of Vibratory Shear Force, $\alpha_s = -4$ Deg.	120

APPENDIX I

40	Experimental Shear Force, $\mu = 0.2$, $\alpha_s = 0$ Deg. .	125
41	Experimental Shear Force, $\mu = 0.2$, $\alpha_s = -4$ Deg. .	131
42	Experimental Shear Force, $\mu = 0.2$, $\alpha_s = -8$ Deg. .	137
43	Experimental Shear Force, $\mu = 0.2$, $\alpha_s = 0$ Deg., Out-of-Trim, -4 Degree Longitudinal Flapping . .	143
44	Experimental Shear Force, $\mu = 0.2$, $\alpha_s = -4$ Deg., Zero Lag Damping	147
45	Experimental Shear Force, $\mu = 0.3$, $\alpha_s = 0$ Deg. .	152
46	Experimental Shear Force, $\mu = 0.3$, $\alpha_s = -4$ Deg. .	158
47	Experimental Shear Force, $\mu = 0.3$, $\alpha_s = -8$ Deg. .	163
48	Experimental Shear Force, $\mu = 0.4$, $\alpha_s = 4$ Deg. .	168
49	Experimental Shear Force, $\mu = 0.4$, $\alpha_s = 0$ Deg. .	173
50	Experimental Shear Force, $\mu = 0.4$, $\alpha_s = -4$ Deg. .	178
51	Experimental Shear Force, $\mu = 0.4$, $\alpha_s = -8$ Deg. .	183
52	Experimental Shear Force, $\mu = 0.5$, $\alpha_s = 0$ Deg. .	187
53	Experimental Shear Force, $\mu = 0.5$, $\alpha_s = -4$ Deg. .	193

<u>Figure</u>		<u>Page</u>
54	Experimental Shear Force, $\mu = 0.5$, $\alpha_s = -8$ Deg. .	199
55	Experimental Shear Force, $\mu = 0.5$, $\alpha_s = -4$ Deg. Zero Lag Damping	205
56	Experimental Shear Force, $\mu = 0.7$, $\alpha_s = 4$ Deg. .	211
57	Experimental Shear Force, $\mu = 0.7$, $\alpha_s = 0$ Deg. .	217
58	Experimental Shear Force, $\mu = 0.7$, $\alpha_s = -4$ Deg. .	222
59	Experimental Shear Force, $\mu = 1.0$, $\alpha_s = 0$ Deg. .	228

APPENDIX II

60	Experimental Radial Shear Force, $\mu = 0.2$. . .	236
61	Experimental Radial Shear Force, $\mu = 0.3$. . .	237
62	Experimental Radial Shear Force, $\mu = 0.4$. . .	238
63	Experimental Radial Shear Force, $\mu = 0.5$. . .	239
64	Experimental Radial Shear Force, $\mu = 0.7$. . .	240
65	Experimental Radial Shear Force, $\mu = 0.2$, $\alpha_s = 0$ Deg.	241
66	Experimental Radial Shear Force, $\mu = 0.2$, $\alpha_s = -4$ Deg.	242
67	Experimental Radial Shear Force, $\mu = 0.2$, $\alpha_s = -8$ Deg.	243
68	Experimental Radial Shear Force, $\mu = 0.2$, $\alpha_s = 0$ Deg. Out-of-Trim, -4 Degree Longitudinal Flapping . . .	244
69	Experimental Radial Shear Force, $\mu = 0.2$, $\alpha_s = -4$ Deg. Zero Lag Damping	245

<u>Figure</u>		<u>Page</u>
70	Experimental Radial Shear Force, $\mu = 0.3$, $\alpha_s = 0$ Deg.	246
71	Experimental Radial Shear Force, $\mu = 0.3$, $\alpha_s = -4$ Deg.	247
72	Experimental Radial Shear Force, $\mu = 0.3$, $\alpha_s = -8$ Deg.	248
73	Experimental Radial Shear Force, $\mu = 0.4$, $\alpha_s = 4$ Deg.	249
74	Experimental Radial Shear Force, $\mu = 0.4$, $\alpha_s = 0$ Deg.	250
75	Experimental Radial Shear Force, $\mu = 0.4$, $\alpha_s = -4$ Deg.	251
76	Experimental Radial Shear Force, $\mu = 0.4$, $\alpha_s = -8$ Deg.	252
77	Experimental Radial Shear Force, $\mu = 0.5$, $\alpha_s = 0$ Deg.	253
78	Experimental Radial Shear Force, $\mu = 0.5$, $\alpha_s = -4$ Deg.	254
79	Experimental Radial Shear Force, $\mu = 0.5$, $\alpha_s = -8$ Deg.	255
80	Experimental Radial Shear Force, $\mu = 0.5$, $\alpha_s = -4$ Deg. Zero Lag Damping	256
81	Experimental Radial Shear Force, $\mu = 0.7$, $\alpha_s = 4$ Deg.	257
82	Experimental Radial Shear Force, $\mu = 0.7$, $\alpha_s = 0$ Deg.	258
83	Experimental Radial Shear Force, $\mu = 0.7$, $\alpha_s = -4$ Deg.	259
84	Experimental Radial Shear Force, $\mu = 1.0$, $\alpha_s = 0$ Deg.	260

<u>Figure</u>	<u>APPENDIX III</u>	<u>Page</u>
85	Experimental Vibratory Moment Amplitude, $\mu = 0.2$	261
86	Experimental Vibratory Moment Amplitude, $\mu = 0.3$	265
87	Experimental Vibratory Moment Amplitude, $\mu = 0.4$	269
88	Experimental Vibratory Moment Amplitude, $\mu = 0.5$	273
89	Experimental Vibratory Moment Amplitude, $\mu = 0.7$	277
90	Experimental Vibratory Moment Amplitude, $\mu = 1.0$	281

APPENDIX IV

91	Experimental Vibratory Control Load Amplitude, $\mu = 0.2$	284
92	Experimental Vibratory Control Load Amplitude, $\mu = 0.3$	285
93	Experimental Vibratory Control Load Amplitude, $\mu = 0.4$	286
94	Experimental Vibratory Control Load Amplitude, $\mu = 0.5$	287
95	Experimental Vibratory Control Load Amplitude, $\mu = 0.7$	288
96	Experimental Vibratory Control Load Amplitude, $\mu = 1.0$	289

SYMBOLS

<u>Dimensional</u>		<u>Unit</u>
A_{ls}	lateral cyclic pitch	degrees
B_{ls}	longitudinal cyclic pitch	degrees
c	blade chord	feet
D	rotor drag	pounds
L	rotor lift	pounds
Q	rotor torque	foot-pounds
r	radial distance to local blade station	feet
R	rotor radius	feet
V	forward speed	feet per second
V_k	forward speed	knots
α_s	shaft angle of attack	degrees
α	rotor angle of attack, $\alpha_s - B_{ls}$	degrees
θ	collective pitch	degrees
ρ	mass density of air	slugs per cubic foot
ψ	azimuth angle, measured from downwind position in direction of rotation	degrees
Ω	rotor angular velocity	radians per second

SYMBOLS

(continued)

Nondimensional

b number of blades

C_D/σ rotor drag coefficient-solidity ratio, $D/\pi R^2 \rho (\Omega R)^2 \sigma$
 $= D/R^3 \rho \Omega^2 bc$

C_L/σ rotor lift coefficient-solidity ratio, $L/\pi R^2 \rho (\Omega R)^2 \sigma$
 $= L/R^3 \rho \Omega^2 bc$

C_Q/σ rotor torque coefficient-solidity ratio, $Q/\pi R^2 \rho (\Omega R)^2 R \sigma$

$M_{(x, \psi)}$ Mach number at radius station x and azimuth position ψ .

x radius station, r/R

μ advance ratio, $V/\Omega R$

σ rotor solidity, $bc/\pi R$

Note: All Fourier series coefficients for shear forces and
 rotor blade flapping and lagging motions are based
 on the assumption of a positive series; i.e.,

$$f(t) = A_0 + A_1 \cos \Omega t + A_2 \cos 2\Omega t + \dots + A_N \cos N \Omega t + \dots \\
+ B_1 \sin \Omega t + B_2 \sin 2\Omega t + \dots + B_N \sin N \Omega t + \dots$$

where A_N = Nth harmonic cosine coefficient

B_N = Nth harmonic sine coefficient

N = harmonic order

INTRODUCTION

As continual improvements have been made in the performance characteristics of rotary wing aircraft, attention to the problems of vibratory loading and associated structural fatigue has increased. The achievement of low fuselage vibration levels and subsequent improvement in aircraft component life and crew efficiency requires, however, a detailed knowledge of the origin of the forces which excite the fuselage. Prior to the start of this investigation, the cause-effect relationship between vibratory loading and fuselage response was not well defined. Previous studies, such as Reference 1, have presented rotor blade vibratory airloads and stresses, and successful attempts have been made to measure vibratory loads by instrumenting the rotor shaft, as in Reference 2. None of these studies, however, have reached the source of fuselage forced response; that is, the vibratory forces fed into the fuselage from the rotor blades at the blade root.

It was not considered feasible to design and fabricate a rotor head which could be instrumented to measure these vibratory forces until two conflicting objectives were resolved. First, maximum sensitivity had to be achieved so that higher harmonics of the loads could be accurately measured; second, the stress in the structural components of such a rotor head had to be minimized to reduce the probability of failure. The development of the semiconductor strain gage effectively closed the gap between these two objectives, thus making possible a detailed investigation of rotor blade vibratory root shear forces.

The purpose of the present investigation was to obtain quantitative measurements of the vibratory forcing functions from blades of rotary wing aircraft within the flight speed range encompassing both pure and compound helicopter operations. In addition, the degree of correlation between experimental results and theoretical calculations, including the effects of wake-induced velocities, was to be determined. The experimental data were to be obtained from wind tunnel tests of dynamically scaled model rotor blades mounted on a specially designed rotor head instrumented to measure flatwise, edgewise, and radial vibratory root shear forces.

The objective of this report is to present the experimentally obtained data and to place these data into a meaningful context by discussing, with specific examples, the effects of forward speed, rotor loading, lag damping, and flapping trim condition. The experimental results are correlated with a theory developed at Sikorsky Aircraft, described in Reference 3.

DESIGN DATA AND DESCRIPTION OF EQUIPMENT

ROTOR HEAD

The model rotor head was designed to utilize semiconductor strain gages having a gage factor of approximately 100. The structural components of the head, namely, the upper and lower plates, are 7075-T6 aluminum alloy. A fail-safe mechanism with a safety factor of 20 was provided to prevent major damage in the event of failure in the instrumented section. Figure 1 (a) shows the basic rotor head with the installed semiconductor strain gages, and Figure 1 (b) shows the assembly of the head. The pitch control horns are adaptable to pitch-flap coupling ratios of zero and unity, but the present investigation was conducted entirely in the $\delta_3=0$ configuration. Figure 2 is a schematic diagram showing the force and moment conventions and the location of the strain gages.

CALIBRATION

The model rotor head instrumentation was statically calibrated to determine primary slopes, interaction constants, and temperature compensation factors. In the course of this work it was found that to obtain a satisfactory calibration matrix, it was necessary to include measurements of the tangential moment on the instrumented section caused by the lag damper reaction and the edgewise shear force. The resolution of the shear force measurements based on the static calibrations and the noise level of the data acquisition system was determined to be:

Flatwise ± 0.17 pound

Edgewise ± 0.12 pound

Radial ± 0.05 pound

The repeatability of the shear forces determined during the wind tunnel testing and the magnitude of the calibration matrix elements resulted in a final shear force accuracy of ± 0.2 pound in all three directions. The flatwise and edgewise shear force strain gage circuits were each composed of two active and two dummy gages wired to measure the total shear force and to cancel bending in the instrumented section caused by the shear force. The radial shear force circuit was composed of four active gages in the Poisson arrangement. This circuit also measured the total shear force and cancelled bending. The tangential moment circuit was composed

of two active and two dummy gages to measure the bending moment on the upper instrumented section. All of the dummy gages were mounted on the unstressed center section of the upper plate.

ROTOR BLADES

The model rotor blades were untwisted, 9-foot diameter, 2.69-inch chord with an NACA 0012 airfoil section, and were dynamically scaled in flatwise, edgewise, and torsional stiffness properties from the Sikorsky S-56 (CH-37) main rotor blades.* With the specially instrumented, four-bladed rotor head, the rotor solidity is 0.0634. Figure 3 shows the components of a model blade and a fully assembled blade. The model spar was built up of laminations of fiber glass and paper. Trailing edge pockets were composed of balsa wood ribs covered with magnesium and were bonded to the spar. Figure 4 shows the blade spanwise mass and stiffness distributions, and Figure 5 shows the flatwise, edgewise, and torsional natural frequencies of the blade as functions of rotor speed.

The development of the fiber glass model blades evolved from dynamically scaled model rotor blades made of aluminum, used in studies such as Reference 4. These metal blades were designed to operate at full scale tip speeds, but the investigation of rotor behavior at high forward speeds necessitated the development of blades which would retain their dynamic similarity while operating at reduced tip speeds. The reduced speeds resulted from the desire to simulate forward speeds higher than the wind tunnel limit of 175 knots. Reference 5 describes the development of this type of blade using reduced-stiffness spars of fiber glass-paper laminate construction. The various scaling ratios, listed in Table III, are taken from reference 5. The stiffness of the composite spars is scaled in the flatwise, edgewise, and torsional directions from full scale values. The resulting stiffnesses are reduced from those of the aluminum model blades by a factor of 5.5, so that the reduced experimental velocities are $1/\sqrt{5.5}$ times the full scale velocities. For example, at an actual tunnel speed of 100 knots, the fiber glass rotor blades are dynamically similar to the full scale blades operating at $100\sqrt{5.5}$ or 235 knots, and this speed is referred to as the equivalent forward speed.

* The full scale S-56 main rotor blades are twisted -8 degrees

WIND TUNNEL

Testing was conducted in the United Aircraft Corporation's large subsonic wind tunnel. This is an atmospheric-density, closed-return tunnel powered by a 9000-horsepower motor and having a maximum speed of approximately 175 knots. The test section is octagonal in cross section, 18 feet across the opposite flats. Remotely controlled air exchangers are employed to maintain constant stagnation temperature during operation. Figure 6 is an artist's drawing depicting the general arrangement of the tunnel.

HELICOPTER ROTOR TEST RIG

The helicopter rotor test rig (HRTR) is equipped with a six-component strain gaged balance and is powered by a variable frequency electric motor rated at 375 horsepower at 6000 rpm. Figure 7 (a) shows an overall view of the HRTR mounted in the wind tunnel, and Figure 7 (b) shows the details of the hub and swash plate area. The coincident flapping and lagging hinges are located at the 5.6 percent radius station. Lagging motion is restrained by rotary viscous dampers having a nominal damping factor of 1.9 foot-pound-second for a lag motion amplitude of 1 degree. This value represents 55 percent critical damping. The model dampers have an adjustable damping feature which permits the selection of any desired damping factor within a moderate range determined by the working fluid in the damper. The dampers were set to the above value by calibrating them in a special calibration fixture which operates the damper at a specified frequency and amplitude and records the resulting torque output. The damper was adjusted in small increments until the proper combination of frequency, amplitude and torque was reached. There was a small phase difference between the application of the force to the damper and the minimum force output indicating the presence of spring force in the damper. This was taken into account in the calibration so the value stated above represents the pure damping output. Rotary transformers are used to sense flapping and lagging motion. A conventional swash plate is driven by three precision electric actuators. Collective and cyclic pitch are remotely set from a servo system in the wind tunnel control room, and the yaw table of the wind tunnel provides variation in shaft angle of attack.

The HRTR drive motor is supported by frictionless hydrostatic oil bearings. The motor case is restrained from rotation by a strain gage torque beam to measure rotor torque. Axial displacement of the motor-shaft system is limited by a strain gage thrust beam. The rotor head is supported by a four-component strain gage balance which was not used in

this test program, as this balance is sized for larger forces than were anticipated for this test. Electric signals are transmitted from the rotating system to the stationary system through a 100-channel slip ring assembly.

Dynamic data from the rotor test rig are recorded on a 20-channel EPSCO data acquisition system. Each channel is scanned 36 times per revolution for six revolutions. The information is received from the HRTR in analog form, digitized, and recorded on magnetic tape. These data are transmitted to an IBM 7094 data processing unit and reduced. The primary data reduction program reduces the performance data to dimensional and coefficient form in the wind and shaft axes systems. Tare forces and moments on the rotor hub, obtained with the blades removed, are subtracted from the measured data, so that the reduced performance data correspond to that from the rotor blades alone. Blade motions and bending moment data are reduced to average and peak-to-peak values. The secondary data reduction program performs a harmonic analysis on all 20 channels of information. The measured shear force and tangential moment data are further reduced to correct for calibration interactions and blades-off tares, and finally these data are corrected for the effects of hub flexibility, as discussed in the section on experimental procedures.

THEORETICAL METHOD

The theoretical method of Reference 3 was used to correlate the experimental data obtained in this program. This method is a fully coupled flatwise, edgewise, torsional aeroelastic analysis based on an extension of Myklestad's method for rotating beams. A variable inflow analysis, developed by the Cornell Aeronautical Laboratory, Inc. (CAL) and described in Reference 6, was combined with the blade aeroelastic analysis. The analytical procedure included an initial determination of flatwise and torsional rotor blade motion with a uniform inflow iteration to obtain required values of rotor lift and propulsive force. This information was used in the CAL analysis to obtain a distribution of induced velocity at ten radial blade stations and twenty-four azimuth locations. With this distribution, using the first flatwise shear force harmonic as a boundary condition, a second iteration was made on the rotor lift and propulsive force, which gave final values of blade motions and loadings.

SIGN CONVENTIONS

The sign convention used is that a positive sign indicates:

<u>Measurement</u>	<u>Direction</u>
Flatwise Shear Force	Upward
Edgewise Shear Force	In direction of rotor rotation
Radial Shear Force	Radially outward from rotor ϕ
Flatwise Bending Moment	Upper surface in compression
Edgewise Bending Moment	Trailing edge in compression
Torsion Moment	Leading edge upward
θ	Leading edge upward
α_s	Rotor Shaft tilted downstream
A_{1s}	Pitch reduction at $\psi = 0$ degrees
B_{1s}	Pitch reduction at $\psi = 90$ degrees

EXPERIMENTAL PROCEDURE

HELICOPTER ROTOR TEST RIG IMPEDANCE

Since it is desirable to have vibratory shear force results which are independent of the particular rotor test rig employed, the measured shear forces must be corrected for the effects of the displacements of the hub, which induce extraneous forces in the instrumented section of the rotor head. These displacements are caused by the shear forces themselves; therefore, the correction factors must be determined from the test data in conjunction with predetermined properties of the rotor test rig.

The analytical background of this procedure is based on the fact that the deflections of the rotor hub can be predicted with a knowledge of the applied forces. Such deflections are determined by dividing the measured shear forces by an experimentally determined rotor hub impedance. The product of this quotient and the rotor blade impedance, determined analytically, yields the force induced on the blade by the hub motion. This force is then subtracted from the measured results to produce the final shear force, reflecting only the effects of the rotor blade loading and no effects of the supporting structure motion. The correction can be written in the form of a matrix equation, as follows:

$$\{\text{corrected shear force}\} = \{\text{measured shear force}\} - \left[\begin{array}{c} \text{theoretical} \\ \text{blade impedance} \end{array} \right] \times \left[\begin{array}{c} \text{experimental} \\ \text{HRTR impedance} \end{array} \right]^{-1} \times \left\{ \begin{array}{c} \text{measured} \\ \text{shear force} \end{array} \right\}$$

To determine the rotor test rig impedance, a special rotor head was fabricated which matched the weight of the one to be used in the wind tunnel testing. This head was mounted on the HRTR in the wind tunnel, and to it was attached an electromagnetic shaker with appropriate instrumentation to measure forces and displacements. By taking measurements over a range of excitation frequencies in the axial and in-plane directions, the variation of HRTR impedance and principal axes was determined within the range of frequencies to which the rig would be subjected during actual testing. For a rotor with "n" blades, the nth harmonic of the flatwise root shear forces combine to produce an n/rev vertical excitation of the fuselage. The (n + 1) and (n - 1) harmonics of the flatwise root shears combine to form n/rev hub moments resulting in vibratory pitching and rolling moments of the airframe. The (n + 1) and (n - 1) harmonics of the edgewise root shear forces combine to form n/rev longitudinal and lateral in-plane forces at the rotor head. Since the

test rotor was a four-bladed configuration, only the third, fourth, fifth, seventh, eighth, and ninth shear force harmonics affected hub motions. Because in an "n" bladed rotor system only integer multiples of the $n\Omega$ frequency will be seen in the fixed system, the hub motion corrections were confined to the four-per-revolution and eight-per-revolution frequencies. The final test conditions were selected, whenever possible, so that the rotor speeds would correspond to frequencies away from those of low HRTR impedance, in order to minimize the correction factors on the measured data. The corrections of the shear forces based on this analysis were approximately 0.1 pound throughout the test, and the maximum correction was approximately 0.7 pound. It was determined prior to testing that the motion of the HRTR would not alter the rotor blade impedance characteristics by a significant amount, so that these characteristics were reduced to functions of rotor speed only. An example of the HRTR impedance matrix for a rotor speed of 636 rpm is given below.

	upstream direction		advancing blade direction	
	real	imaginary	real	imaginary
4 per rev.	- 1570 lb/in.	- 765 lb/in.	- 7050 lb/in.	- 2420 lb/in.
8 per rev.	- 3750 lb/in.	- 4920 lb/in.	- 4920 lb/in.	- 4750 lb/in.

The impedances in the rotor shaft direction were large enough to be considered infinite in comparison to the impedances shown in the above matrix.

WIND TUNNEL TESTING

The wind tunnel testing procedure was to set a desired rotor tip speed, shaft angle of attack, and tunnel speed and then to record data at each of a series of increasing collective pitch settings. The minimum value of collective pitch was that required for zero thrust; and at each collective pitch, longitudinal and lateral cyclic pitch were adjusted to eliminate first harmonic flapping in respect to the rotor shaft. This cyclic pitch condition was defined as trimmed. For some test conditions, the cyclic pitch values were set to yield longitudinal first harmonic flapping of -4 degrees (forward), while holding the lateral flapping at zero to determine the influence of out-of-trim flapping on the vibratory shear forces. The maximum collective pitch was determined by the limiting vibratory stress amplitude on the rotor head or blades. The tested rotor operating conditions are shown in Figure 8 and Table I. In the remainder of the report these conditions are referred to by the nominal advance ratio values, 0.2, 0.3, 0.4, 0.5, 0.7, and 1.0.

EXPERIMENTAL RESULTS

Table I is a listing of each test point in this program. Shaft and rotor angle of attack, non-dimensionalized thrust and torque, nominal collective pitch, and flapping and lagging motion are listed for each advance ratio. The flapping and lagging motion harmonic amplitudes are printed to three decimal places since the reproduction of the table was done directly from the test data through the data processing unit, but these amplitudes are only accurate to one decimal place or 0.1 degree.

The complete test results are presented in the appendices, and the most significant of these are presented again and discussed in the following section.

The first through tenth harmonic orthogonal components of flatwise and edgewise vibratory shear force obtained in the wind tunnel tests are presented in Appendix I. The flatwise force coefficients are shown as functions of rotor lift coefficient-solidity ratio, and the edgewise force coefficients as functions of rotor torque coefficient-solidity ratio. These data are grouped by advance ratio, each group covering a range of shaft angle of attack.

The first through fourth harmonic orthogonal components of radial shear force are presented in Appendix II. The first harmonic cosine coefficient is shown as a function of rotor angle of attack for constant collective pitch at each advance ratio. The variation of this coefficient with changes in trim and lag damping is indicated by flagged and double flagged symbols, respectively. None of the other harmonic coefficients of radial shear force reached magnitudes approaching those of the first cosine harmonic, instead, they were approximately one pound or 0.3 percent of the steady radial load. The radial shear force harmonics above the fourth did not exceed the one pound level at any test point and are not presented. The remaining radial shear force coefficients are given as functions of rotor lift coefficient-solidity ratio.

Flatwise rotor blade bending moments were measured at four radial stations on the blade at 21, 33, 47, and 64 percent radius. Throughout the range of test conditions, the flatwise moment at the inboard station, 21 percent radius, was consistently the largest measured moment. This fact is substantiated in the following section of the report. The radial locations of the largest measured edgewise and torsional moments are also verified in that section. Part (a) of the figures in Appendix III gives the one-half peak-to-peak values of the flatwise moment at 0.21R as it varies with rotor angle of attack for constant collective pitch and

advance ratio. A flatwise moment of 21 inch-pounds at this radial station on the blade corresponds to a stress of 10,000 psi on an equivalent rotor blade made of aluminum; i.e., it has the same unit strain. Edgewise bending moments were measured at 21, 33, and 47 percent radial stations on the blade. The location of the maximum measured value varied between the inboard and outboard stations within the range of test conditions. Part (b) of the figures in Appendix III presents the one-half peak-to-peak edgewise moment at the 21 percent station as a function of rotor angle of attack for constant collective pitch and advance ratio. An edgewise moment of 56 inch-pounds at this station on the blade corresponds to 10,000 psi edgewise stress on an equivalent aluminum blade. Part (c) of the same set of figures is a plot of the moments measured in the edgewise direction at the 47 percent radial station, with 29 inch-pounds giving the equivalent of 10,000 psi stress. The rotor blade torsional moment was measured at the 17.5, 38, and 90 percent radial stations. The inboard moment was largest at all test points, and its one-half peak-to-peak value is presented in part (d) of the figures of Appendix III in a manner identical to that of the other blade moments. A 35 inch-pound torsional moment at the 17.5 percent radial station corresponds to 10,000 psi on the equivalent aluminum blade. The change in each of the three blade bending moments resulting from out-of-trim operation is indicated by the flagged symbols on the plots for the advance ratio of 0.2. The change resulting from elimination of lag damping is indicated by double-flagged symbols on the plots for advance ratios 0.2 and 0.5.

Rotor control loads were measured on the push rod for the instrumented blade. The one-half peak-to-peak values of this load are presented in Appendix IV in a form identical to that of the blade bending moments.

EVALUATION OF EXPERIMENTAL RESULTS

OUT-OF-TRIM OPERATION

The effect of out-of-trim operation of the flatwise and edgewise vibratory shear forces can be seen by comparing parts (a) and (b) of Figure 9, which are taken directly from Appendix I. The only force harmonic which is significantly altered by adjusting the first harmonic flapping with respect to the shaft to -4 degrees in the longitudinal direction is the first harmonic, which produces a pitching moment in the fixed system of coordinates. In particular, the amplitude of the first harmonic shear in both the flatwise and edgewise directions takes on a value on the order of double that of trimmed operation. This behavior is what would be expected since a one per revolution forcing function is being introduced in the system. Figure 9 also shows that the phase of the first harmonic shear force becomes less sensitive to changes in rotor lift when the rotor is taken out-of-trim. The effect on the cosine component of the first radial shear force harmonic is not well defined, but the points in Figure 60 of Appendix II indicate that this component is generally increased by operation out-of-trim. The data in Figure 85 of Appendix III reveal that the principal effect of out-of-trim operation on blade bending moments is an increase in the one-half peak-to-peak flatwise moment approximately equivalent to that resulting from a 2-degree increase in collective pitch or roughly a 7500-pound increase in full-scale rotor lift. However, the edgewise and torsional moments are not significantly altered. It should be noted that because of the flapping and lagging motion of the blades, the blade bending, and the variation of the blade pitch over the rotor disk; the axis system in which the blade bending moments are measured is being continually displaced in both translational and rotational directions with respect to the axis system in which the root shear forces are measured. As a result, there is a large interaction between events occurring in any one direction of the blade axis system and the three directions of the shear force axis system. This effect is seen above where operation out-of-trim caused a change in the edgewise shear force with no significant change in the edgewise blade bending moment.

EFFECT OF LAG DAMPING

The effect of lag damping on the vibratory shear forces and blade moments must be evaluated in light of the proximity of the rotor operating condition to an edgewise blade natural frequency. For this reason two rotor speeds are considered. At the advance ratio of 0.2, the first edgewise bending frequency is very nearly three per revolution, whereas

at the higher advance ratio , 0.5, at which the rotor tip speed is reduced, the first edgewise bending frequency is farther removed from a resonance point, as shown in Figure 5. Comparing parts (a) and (b) of Figure 10, which is taken directly from Appendix I, it is seen that removal of the lag damping at the condition near the edgewise natural frequency results in an increase in the edgewise shear force harmonics shown, particularly the third; which displays an increase in maximum amplitude of about 25 percent. Removal of lag damping at the other condition results in a decrease in the edgewise shears, as seen by comparing parts (a) and (b) of Figure 11. The third harmonic amplitude decreases 20 percent at $C_Q/\sigma = 0.005$ for this case. The remaining shear force harmonics for these four test conditions, given in Appendix I, show that the edgewise force harmonics above the fourth behave essentially the same as those shown in Figures 10 and 11 and that the flatwise shear force increases with the removal of lag damping at both rotor speeds. The latter effect results from the increase in flatwise blade bending moments discussed below. The effect of lag damping on the radial shear force is not clearly indicated by the data taken from $\mu = 0.2$, but Figure 63 of Appendix II for $\mu = 0.5$ shows a definite pattern in which the first cosine harmonic is initially reduced but later reverses as the collective pitch is increased and eventually increases at the higher collective pitches.

The data in Appendix III show that removal of lag damping results in a slight increase in flatwise and torsional blade bending moments at both rotor speeds. This moment increase is largest at the high collective pitch settings and is essentially zero at the low settings. This effect is a result of the fact that, experimentally, more longitudinal cyclic pitch was required to maintain the rotor in a trimmed condition when the lag damping was removed than with full lag damping. It is not clear why this additional cyclic pitch is necessary, but the effect is consistent throughout the test. The edgewise bending moments at the inboard radial station are increased at both rotor speeds by an amount equivalent to a one degree increase in collective pitch or an increase in full scale lift of approximately 4000 pounds. At the outboard station the increment in edgewise moment due to the removal of lag damping is much larger at the higher rotor speed than it is at the lower speed. The increase at the lower speed at this station is of the same order of magnitude as the increases on the inboard station. This is seen in Figure 12, which is a plot of data extracted from Appendix IV. This effect of rotor speed on the edgewise response to changes in lag damping, is related to the effects of the rotor operating condition's being near an edgewise natural frequency, already discussed in connection with the edgewise shear force. It would be expected that the removal or reduction of lag damping at rotor speeds

remote from an edgewise natural frequency would cause a reduction rather than an increase in the edgewise bending moments because the restraining load on the blade root is reduced. For the rotor speed in question, however, Figure 5 shows that the test point is not sufficiently removed from the critical speed to preclude the presence of resonant excitation effects. The trend of reduction in edgewise bending moment and shear force with changes in rotor speed away from the critical value is clear, nevertheless, and for an advance ratio of 0.7, Figure 12 shows edgewise moments which are considerably lower than those measured with full lag damping.

EFFECT OF FORWARD SPEED

Figure 13 shows the effect of forward speed on the flatwise and edgewise shear forces. The amplitudes of the second through tenth harmonic coefficients, derived from the data presented in Appendix I, are presented as functions of advance ratio for a constant rotor lift coefficient - solidity ratio of 0.035 and a shaft angle of attack of -4 degrees with the rotor trimmed to zero flapping with respect to the shaft. The shear force amplitudes are nondimensionalized by the lift per blade to provide an indication of the magnitude of the vibratory loads relative to the steady loading on the rotor. The flatwise vibratory loading shows a general increase with forward speed in all harmonics. In some harmonics, particularly the third and fourth, the increase is very rapid as the advance ratio exceeds 0.5. The same pattern is evident in the edgewise vibratory loading, with the third and fourth harmonics again reaching very large values at $\mu = 0.7$. This flatwise and edgewise shear force response stems directly from the change in the behavior of the rotor blade in the edgewise direction as the forward speed is increased. This change is discussed below. The effect of forward speed on the first cosine harmonic of the radial shear force can be assessed from Figures 60 through 64 in Appendix II. In general, increasing forward speed causes this shear component to change from a nose down pitching moment component to a nose up component. The magnitude of this shear force was not anticipated and the cause of the measured behavior could not be determined without an extensive analytical effort, beyond the scope of the present study.

Figure 14 presents the one-half peak-to-peak blade bending moments as functions of advance ratio. The test points, listed in Table II, included those for $\alpha_s = -4$ degrees for $\mu = 0.2, 0.4, 0.5$, and 0.7 , and for $\mu = 0.3$ with $C_L/\sigma = 0.062$. The lift coefficient-solidity ratios are not constant for these five points but decrease with forward speed, as would be the case in compound helicopter operation, from

$C_L/\sigma = 0.071$ at $\mu = 0.2$ to $C_L/\sigma = 0.032$ at $\mu = 0.7$. The results shown represent a more realistic situation as compared, for instance, to the case with a constant C_L/σ equal to 0.032. The blade moments in all three directions increase with advance ratio. The edgewise and torsional moments are strongly influenced by the forward speed above the 0.5 advance ratio. It is notable that the maximum flatwise bending moment occurs at the inboard radial station throughout the forward speed range as does the maximum torsional moment, while the edgewise moment shifts from the inboard end of the blade to the outboard end as the forward speed is increased. The time histories of these moments can be seen in Figures 18, 21, 22, 23, and 24; and it is evident that the shift of the maximum edgewise bending moment station is a result of the change in the participation of edgewise bending modes. At the low advance ratios the first elastic mode predominates, but as the speed is increased additional modes become significant so the station of maximum bending moment is changed accordingly. It should also be noted that with the flatwise stiffness distribution given in Figure 4, the maximum bending stress tends to occur at the 64 percent radial station, which is in accord with flight measurements.

The time histories of the flatwise, edgewise, and radial shear forces at the same five test points are shown in Figures 15, 16, and 17; from them the change in harmonic content with forward speed can be observed. As the advance ratio is increased from 0.2 to 0.4, the first harmonic predominates in all three directions with some high harmonics of small amplitude appearing in no definite pattern. Above 0.4, all of the forces are predominately fourth harmonic. This effect would cause a change in the fuselage forcing functions from a steady moment at the low speeds to a four per revolution excitation at the high speeds. The cause of this variation of shear force harmonic content can be determined from the points in question shown in Figures 18 through 24, which present the azimuthal plots of blade bending moments at all seven points listed in Table II. The striking feature in these plots is the character of the edgewise bending moment at the high advance ratios. Essentially, it is composed of the fourth harmonic with an amplitude on the outboard station reaching 20 inch-pounds. Since the flatwise bending moment does not exhibit the same character, it can be concluded that at the 0.7 advance ratio the shear forces are primarily influenced by the edgewise blade bending through the mechanism of the displacement of the blade axis system from the shear force axes system.

Looking now at the change in harmonic content of the blade bending moments with forward speed in Figures 18, 21, 22, 23, and 24, the edgewise moment is seen to be essentially third harmonic at the lower

advance ratios as would be expected because of the nearness of the rotor speed to the edgewise natural frequency point. At the higher advance ratios, however, the rotor speed is reduced and moves away from the critical speed, but does not closely approach the four per revolution natural frequency. Therefore, the edgewise behavior at these high advance ratios cannot be categorically attributed to resonant excitation. The list of lag motion harmonics in Table I for the $\mu = 0.7$ data point shows a fourth harmonic amplitude larger than any others but the first, and a comparison in Table I with the lower speed points reveals that the first harmonic lag motion dominates all other harmonics in amplitude. Although the magnitudes being compared are on the borderline of the measuring system accuracy, an aerodynamic source of the high speed edgewise behavior is implied; but this has not been positively determined. It was observed during testing that removal of the lag damping at the high forward speeds resulted in a reduction of the fourth harmonic magnitude and in an increase in the third harmonic magnitude of the edgewise blade response. It should also be noted that the test data at $\mu = 1.0$ show the same effect: a large fourth harmonic with lag damping and a shift toward the third harmonic with reduced lag damping, even though the rotor speed is 15 percent lower at this condition than it is in the $\mu = 0.7$ condition. Investigation of this phenomenon is impeded by the shortage of experimental dynamic data at high forward speeds and by the complexity of the actual lag damper behavior. While the moment output is nominally pure damping linearly related to the velocity, as discussed in the section entitled "Helicopter Rotor Test Rig"; there is some spring content which varies in a complex manner with frequency and amplitude. The exact determination of these characteristics is beyond the scope of the present study. In this program, the structural limitations of the special rotor head precluded extensive data taking at the high advance ratios because of the very large vibratory forces involved. Designing for such large forces would have reduced measuring accuracy at lower values of advance ratio, μ .

The torsional moment in Figures 18 through 21 is essentially first harmonic in character at the low forward speeds, reflecting the cyclic pitch input. At the higher speeds, appearing first at an advance ratio of 0.4, the torsional moment has an increasing content of high harmonics, particularly at the inboard stations. At the two highest advance ratios, 0.5 and 0.7, presented in Figures 23 and 24, the eighth harmonic response can be traced to the proximity of a natural frequency at 580 rpm. The harmonic content of the flatwise bending moments is difficult to visualize because of the effects of high seventh, eighth, ninth, and tenth airload harmonics at all forward speeds. It is apparent, however, from Figures 18 through 24, that the third and fourth harmonics

show a large increase with increasing forward speed relative to the increases that take place in the high harmonics. None of this is attributable to resonant excitation of flatwise modes, but coupling with edgewise blade response undoubtedly contributes to this part of the flatwise response, particularly since both the collective and cyclic pitch settings are high under these conditions; i.e., $\theta = 12$ degrees, $B_{1s} = 13.7$ degrees at $\mu = 0.7$.

EFFECT OF ROTOR LIFT

Figures 25, 26, and 27 present the time histories of the flatwise, edgewise, and radial shear forces at a constant advance ratio of 0.3 for a range of rotor lift under trimmed conditions. A phase change in the first harmonic is readily apparent in all three components. In addition, the initial reduction and subsequent increase in this harmonic can be seen by comparing the middle load conditions with the high and low conditions. This comparison also reveals that the magnitude of the higher harmonics changes very little over the range of lift. It should be noted that the lowest equivalent forward speed in this program was approximately 75 knots, and due to the variation of wake-induced velocity effects with forward speed, the results discussed herein cannot generally be extrapolated to lower speeds.

The correlation between rotor thrust level and vibratory loading is shown in Figure 28. The amplitudes of the flatwise and edgewise shear force harmonics, obtained from Figure 50 of Appendix I, are presented as functions of rotor lift coefficient - solidity ratio at an advance ratio of 0.3 and a shaft angle of attack of -4 degrees. The amplitudes are nondimensionalized by the lift per blade, and data for C_L/σ below 0.04 are not plotted in order to avoid the distortion that takes place as the lift goes to zero. The low flatwise harmonics show an increase as the rotor lift increases. Except for the seventh and tenth, the harmonics above the fourth remain low throughout the range of lift. The rotor speed at this advance ratio, $\mu = 0.3$, yields an operating condition close to the seven per revolution natural frequency of the third flatwise blade bending mode and the ten per revolution natural frequency of the fourth flatwise mode, explaining the departure of the seventh and tenth harmonics from the pattern of the others. Looking at the harmonics of flapping motion for $\mu = 0.3$ and $\alpha_s = -4$ degrees, it is seen that the amplitudes of second, third, and fourth harmonic flapping increase with rotor lift. It is this effect which produces the increase in the flatwise shear force second, third, and fourth harmonics seen in Figure 28. The correlation between the rotor thrust level and the nondimensional edgewise shear force harmonic amplitudes is similar to that of the flatwise case for the

low harmonics although it is not as marked. The edgewise amplitudes above the fourth harmonic remain low throughout the lift range and do not exhibit even the small increase at the highest lift that was seen in the flatwise harmonic amplitudes.

The vibratory shear forces data presented in Figures 9, 10, 11, 13, 15, 17, and 25 through 28 are taken from only a very small number of the test conditions included in Appendix I. Sufficient information is given in Table I and Appendix I to enable the reader to replot the data of any of the 116 test conditions in any of the forms used herein and to evaluate specific operating conditions in more detail.

CORRELATION OF THEORY AND EXPERIMENT

The experimental data for the seven test points listed in Table II were correlated with the theoretical method of Reference 3.

Figures 29 through 35 present the measured and calculated shear force harmonic amplitudes. In Figures 29, 32, 33, and 35, the results of uniform inflow computations are also shown. In comparing the measured flatwise shear force harmonic amplitudes with the calculated variable inflow values, the second and fifth harmonics show the most consistent difference among the seven subject points. In all cases, except at $\mu = 0.7$, it was found that the fourth and/or fifth harmonic of induced velocity on the inboard segment of the blade, as computed in the variable inflow analysis, was higher than any other harmonics above the second. The effect of this on blade response can also be seen in the calculated flatwise blade bending moments at $\mu = 0.3, 0.4, 0.5$, shown in Figure 36. In the case of a large second harmonic difference, it was found that the calculated rotor wake produced a flatwise loading on the outboard portion of the blade which was essentially composed of a two per revolution load. This resulted in a blade flapping motion in which the primary component was second harmonic. For example, examination of the flapping coefficients given in Table I for the $\mu = 0.5$ point reveals a second harmonic magnitude of 0.8 degrees as opposed to the calculated value of 1.3 degrees.

Looking in particular at the $\mu = 0.2$ case, the flatwise bending moment presented in Figure 37 shows a sharp peak at the 165-degree azimuth in the calculated values that are present, but is greatly attenuated in the measured values. The cause of this peak was traced to the representation of the rotor wake, in which a tip vortex from one blade is passing under the inboard end of the following blade. Since the circulation is assumed to be concentrated at the vortex core, a rapid increase in induced velocity is felt by the blade, and the high peak in bending moment results. In the physical case with a finite vortex core, the increase in induced velocity is more gradual and the blade response is less drastic, as seen from the measured results in Figure 37. It was analytically determined that a peak such as that given by the calculations would cause an increase in the magnitudes of all harmonics, and it is seen that a downward shift of the calculated shear force harmonics in Figure 29 would yield a much better correlation in every harmonic. As the forward speed and rotor lift are increased and the wake is washed away from the rotor, this peaking effect is diminished as the subject vortex passes under the aft part of the rotor.

The remaining significant differences in the measured and calculated flatwise shear forces are in the seventh harmonic at $\mu = 0.2$ and the fourth harmonic at $\mu = 0.7$, as shown in Figures 29 and 35, respectively. The latter difference stems from the fact that the large fourth harmonic edgewise blade bending discussed earlier in conjunction with the measured shear force data is not predicted in the computations, even though the flatwise blade bending moment correlation is not unreasonable, as seen in Figure 37. The magnitude of the computed seventh harmonic at the low speed is a result of a resonant excitation of the third flatwise bending mode of the blade caused by a seventh harmonic-induced velocity component over the inboard blade segments having a value nearly equal to the steady induced velocity.

The flatwise shear force harmonics calculated with the assumption of uniform inflow show a steady decrease in magnitude as the harmonic order is increased. The measured results, however, do not follow this pattern, and it is evident that without the higher harmonic excitation provided by a variation in induced velocities, there is no possibility of accurately predicting the harmonic content of the vibratory shear forces. At the high advance ratio, $\mu = 0.7$, the difference between the uniform and variable inflow results is very small, but the analysis of wake-induced velocities used in this program was not developed for use at high speed. Therefore, the similarity of the two results does not necessarily imply that the effects of wake-induced velocities can be neglected at high speeds. Figure 39a, which shows the measured and calculated flatwise shear forces as functions of azimuth position, verifies that an accurate knowledge of harmonics is the key to vibratory shear force analysis.

Comparison of the measured values of edgewise shear force harmonic coefficients with the calculated variable inflow values, Figures 29 and 32 through 35, reveals a steady decrease in the degree of correlation as forward speed is increased. This is primarily evident in the low harmonics, where the measured values display a magnitude increase not matched by the theoretical values. The agreement of the higher harmonics is better, but only to the extent that both calculated and measured values remain small. It was shown earlier that all the harmonics of edgewise shear force tend to increase with forward speed, but no such trend is evident in the calculations. This absence, then, is the major deficiency in the edgewise shear force analysis. Since the nature of the blade edgewise behavior at the high advance ratios is not well understood because of the undefined effects of such things as the lag dampers and the blade counterweights, and even though calculated results compare favorably at an advance ratio as high as 0.5, as seen in Figure 38, very little can be said about the correlation of edgewise shear forces.

The results presented do, however, highlight the need for additional theoretical and experimental analyses of rotor behavior at high forward speeds.

The uniform inflow results and the comparative time histories of the edgewise shear forces, Figure 39b, add nothing to the understanding of the problem at hand. There is no significant difference between the uniform and variable inflow results, and both results differ from the measured values to a large extent. The induced velocity analysis does not account for variations of in-plane velocities, but whether or not the inclusion of these would effect the degree of correlation of the edgewise shear forces could not be determined within the scope of this investigation.

With respect to the overall correlation effort, it is felt that although there is considerable room for improvement, the results are encouraging in view of the fact that it has been impossible to even attempt such a correlation in the past for lack of detailed experimental data. The deficiencies in the flatwise shear force calculations clearly point to the areas in which improvements should be made. Namely, the especially restrictive comparison by harmonics demands that the wake-induced velocities be free of sudden large variations and that the rotor blade natural frequencies be well defined through the high modes. In addition, the strong influence of the aeroelastic behavior of the rotor blade in the edgewise direction necessitates a fundamental understanding of this behavior before a better degree of correlation can be achieved at high speeds.

CONCLUSIONS

The results of the experimental investigation of the vibratory shear forces generated by an individual helicopter rotor blade of a four bladed rotor system led to the following principal conclusions:

1) The harmonic content of vibratory shear forces can be accurately determined over a wide range of forward speeds and rotor lifts through the use of high sensitivity semiconductor strain gages.

2) The trim condition of the rotor exerts a strong influence on the amplitude and phase of the first harmonic flatwise and edgewise shear forces, but has no appreciable effect on other harmonics. The change in amplitude of the first harmonic forces is proportional to the amount of out-of-trim flapping. The trim condition exhibited no well defined effect on radial shear forces.

3) Removal of linear viscous lag damping results in a slight increase in the flatwise shear force and either an increase or a decrease in the edgewise shear force, depending on the nearness of the rotor speed to a rotor blade edgewise natural frequency.

4) Increasing forward speed over a range of from 75 to 300 knots results in a gradual increase in the flatwise shear force. The edgewise shear force remains essentially constant from 75 to 175 knots and then increases rapidly from 175 to 300 knots, becoming the predominate force at the highest speeds. At forward speeds above 200 knots, the edgewise bending of the blade dominates the shear forces in all three directions to result in a significant change in the harmonic content of the shear forces over the total speed range.

5) Increasing the rotor lift at constant forward speed produces a gradual increase in the flatwise vibratory shear force. A similar effect takes place in the edgewise shear force, but it is confined to the low harmonics.

6) The longitudinal first harmonic component of the radial shear force can take on values having a magnitude equal to those of the other shear forces under high rotor lift conditions at low forward speeds and under low rotor lift conditions at high forward speeds. The fundamental nature and significance of the radial shear force could not be determined within the scope of this investigation.

The comparison of experimental results and theoretical results obtained with a fully coupled aeroelastic analysis led to the following

principal conclusions:

- 1) The inclusion of the effects of wake-induced velocities alters the theoretical results in a direction which improves the correlation of the flatwise shear forces.
- 2) The natural frequencies of the rotor blade must be well defined through the high harmonic range, because the use of wake-induced velocities in the theoretical analysis necessarily introduces high harmonic forcing functions which excite a response in the blade that can be directly reflected in the vibratory shear force harmonics.
- 3) The theoretical distribution of induced velocities must be free of singular points having velocities greater by an order of magnitude than the surrounding points, because the singular points tend to introduce errors in all the harmonics of a force under consideration.
- 4) The deterioration of the degree of correlation of edgewise shear forces with increasing forward speed indicates the need for an improved theoretical and experimental definition of edgewise rotor blade aeroelastic behavior.
- 5) The inclusion of wake-induced velocities has no significant effect on the degree of correlation of edgewise shear forces.

RECOMMENDATIONS

A more complete understanding of the origin of fuselage excitation requires additional research in the following areas:

1) The existing model rotor should be tested through the low speed range in a wind tunnel having a larger cross section than that of the tunnel used in this investigation. Such a test will provide not only an indication of the magnitude of the effects of the tunnel-rotor diameter ratio (2:1 in this program) on the vibratory shear forces, but will also provide supplementary data at forward speeds below those evaluated herein.

2) A new rotor head having strengthened instrumented sections and fitted with the existing fiber glass blades should be tested to provide more data at forward speeds in the vicinity of 300 knots. Theoretical analyses should be made in conjunction with this experimental work so that specific questions can be answered, such as those arising in connection with the dominance of the edgewise rotor blade bending over the vibratory shear forces.

BIBLIOGRAPHY

1. Scheiman, J., A Tabulation of Helicopter Rotor Blade Differential Pressures, Stresses, and Motions as Measured in Flight, NASA TM X-952, March 1964.
2. Gabel, R., In-Flight Measurement of Steady and Oscillatory Rotor Shaft Loads, CAL/TRECOM Symposium, Buffalo, New York, June 1963.
3. Carlson, R., and Hilzinger, K., Analysis and Correlation of Helicopter Rotor Blade Response in a Variable Inflow Environment, USAAVLABS Technical Report 65-51, September 1965. (Sikorsky Engineering Report 50405).
4. Rabbott, J. P., Jr., Comparison of Theoretical and Experimental Model Helicopter Rotor Performance in Forward Flight, TCREC Technical Report 61-103, July 1961. (Sikorsky Engineering Report 50129).
5. Fradenburgh, E. A., and Kiely, E. F., Development of Dynamic Model Rotor Blades for High Speed Helicopter Research, Symposium on Aeroelastic and Dynamic Modeling Technology, Wright-Patterson Air Force Base, Ohio, September 1963.
6. Piziali, R. A., and DuWaldt, F. A., A Method for Computing Rotary Wing Airload Distributions in Forward Flight, TCREC Technical Report 62-44, July 1962. (Cornell Aeronautical Laboratories Report BB-1495-S-1).

TABLE I FLAPPING AND LAGGING MOTIONS AS FOURIER COEFFICIENTS, DEG.

LOVANCE RATIO = 0.181		
<p>ALPHA S = 0 CL/BIC = -0.000 THETA = -1 C/SIC = 0.0001 ALPHA C = -0.1</p> <p>FLAPPING</p> <p>A0 -0.142 A1 0.071 A2 0.016 A3 -0.033 A4 -0.074 A5 -0.184 A6 -0.004 A7 0.004 A8 0.042 A9 -0.024 A10 0.003 A11 -0.003 A12 0.043 A13 0.031 A14 0.003 A15 0.004 A16 -0.011 A17 -0.009 A18 -0.004 A19 -0.004 A20 0.004 A21 -0.009 A22 0.007 A23 -0.001 A24 0.002 A25 0.003 A26 -0.007 A27 0.001 A28 0.005 A29 0.003 A30 -0.003 A31 0.004 A32 0.004 A33 -0.004 A34 0.004 A35 0.005 A36 0.004 A37 -0.004 A38 0.004 A39 0.005 A40 0.004 A41 -0.004 A42 0.004 A43 0.005 A44 0.004 A45 -0.004 A46 0.004 A47 0.005 A48 0.004 A49 -0.004 A50 0.004 A51 0.005 A52 0.004 A53 -0.004 A54 0.004 A55 0.005 A56 0.004 A57 -0.004 A58 0.004 A59 0.005 A60 0.004 A61 -0.004 A62 0.004 A63 0.005 A64 0.004 A65 -0.004 A66 0.004 A67 0.005 A68 0.004 A69 -0.004 A70 0.004 A71 0.005 A72 0.004 A73 -0.004 A74 0.004 A75 0.005 A76 0.004 A77 -0.004 A78 0.004 A79 0.005 A80 0.004 A81 -0.004 A82 0.004 A83 0.005 A84 0.004 A85 -0.004 A86 0.004 A87 0.005 A88 0.004 A89 -0.004 A90 0.004 A91 0.005 A92 0.004 A93 -0.004 A94 0.004 A95 0.005 A96 0.004 A97 -0.004 A98 0.004 A99 0.005 A100 0.004</p>	<p>ALPHA S = 0 CL/BIC = 0.038 THETA = 2 C/SIC = 0.0002 ALPHA C = -1.0</p> <p>FLAPPING</p> <p>A0 1.933 A1 -0.124 A2 0.129 A3 0.003 A4 -0.028 A5 -0.047 A6 -0.007 A7 0.007 A8 0.004 A9 0.004 A10 0.038 A11 0.034 A12 0.032 A13 0.004 A14 0.004 A15 0.011 A16 0.019 A17 0.002 A18 0.002 A19 0.002 A20 0.012 A21 -0.008 A22 0.001 A23 0.001 A24 0.001 A25 0.012 A26 -0.008 A27 0.001 A28 0.001 A29 0.001 A30 0.012 A31 -0.008 A32 0.001 A33 0.001 A34 0.001 A35 0.012 A36 -0.008 A37 0.001 A38 0.001 A39 0.001 A40 0.012 A41 -0.008 A42 0.001 A43 0.001 A44 0.001 A45 0.012 A46 -0.008 A47 0.001 A48 0.001 A49 0.001 A50 0.012 A51 -0.008 A52 0.001 A53 0.001 A54 0.001 A55 0.012 A56 -0.008 A57 0.001 A58 0.001 A59 0.001 A60 0.012 A61 -0.008 A62 0.001 A63 0.001 A64 0.001 A65 0.012 A66 -0.008 A67 0.001 A68 0.001 A69 0.001 A70 0.012 A71 -0.008 A72 0.001 A73 0.001 A74 0.001 A75 0.012 A76 -0.008 A77 0.001 A78 0.001 A79 0.001 A80 0.012 A81 -0.008 A82 0.001 A83 0.001 A84 0.001 A85 0.012 A86 -0.008 A87 0.001 A88 0.001 A89 0.001 A90 0.012 A91 -0.008 A92 0.001 A93 0.001 A94 0.001 A95 0.012 A96 -0.008 A97 0.001 A98 0.001 A99 0.001 A100 0.012</p>	<p>ALPHA S = 0 CL/SIC = 0.004 THETA = 4 C/SIC = 0.0009 ALPHA C = -2.0</p> <p>FLAPPING</p> <p>A0 3.436 A1 -0.002 A2 0.008 A3 0.004 A4 -0.021 A5 -0.034 A6 -0.004 A7 0.004 A8 0.004 A9 0.004 A10 0.011 A11 0.017 A12 0.013 A13 0.008 A14 0.008 A15 0.003 A16 0.003 A17 0.003 A18 0.003 A19 0.003 A20 0.003 A21 0.003 A22 0.003 A23 0.003 A24 0.003 A25 0.003 A26 0.003 A27 0.003 A28 0.003 A29 0.003 A30 0.003 A31 0.003 A32 0.003 A33 0.003 A34 0.003 A35 0.003 A36 0.003 A37 0.003 A38 0.003 A39 0.003 A40 0.003 A41 0.003 A42 0.003 A43 0.003 A44 0.003 A45 0.003 A46 0.003 A47 0.003 A48 0.003 A49 0.003 A50 0.003 A51 0.003 A52 0.003 A53 0.003 A54 0.003 A55 0.003 A56 0.003 A57 0.003 A58 0.003 A59 0.003 A60 0.003 A61 0.003 A62 0.003 A63 0.003 A64 0.003 A65 0.003 A66 0.003 A67 0.003 A68 0.003 A69 0.003 A70 0.003 A71 0.003 A72 0.003 A73 0.003 A74 0.003 A75 0.003 A76 0.003 A77 0.003 A78 0.003 A79 0.003 A80 0.003 A81 0.003 A82 0.003 A83 0.003 A84 0.003 A85 0.003 A86 0.003 A87 0.003 A88 0.003 A89 0.003 A90 0.003 A91 0.003 A92 0.003 A93 0.003 A94 0.003 A95 0.003 A96 0.003 A97 0.003 A98 0.003 A99 0.003 A100 0.003</p>
<p>ALPHA S = 0 CL/BIC = 0.085 THETA = 6 C/SIC = 0.0025 ALPHA C = -3.1</p> <p>FLAPPING</p> <p>A0 4.178 A1 0.035 A2 -0.148 A3 0.008 A4 -0.008 A5 -0.124 A6 -0.103 A7 0.016 A8 0.010 A9 0.010 A10 0.011 A11 0.014 A12 0.008 A13 0.016 A14 0.016 A15 0.038 A16 -0.027 A17 0.008 A18 0.003 A19 0.003 A20 0.037 A21 -0.016 A22 0.004 A23 0.001 A24 0.001 A25 0.038 A27 -0.028 A28 0.002 A29 0.004 A30 0.004 A31 0.021 A32 -0.009 A33 0.004 A34 0.004 A35 0.003 A36 0.007 A37 -0.008 A38 0.001 A39 0.001 A40 0.001 A41 0.007 A42 -0.026 A43 0.001 A44 0.001 A45 0.001 A46 0.007 A47 -0.026 A48 0.001 A49 0.001 A50 0.001 A51 0.007 A52 -0.026 A53 0.001 A54 0.001 A55 0.001 A56 0.007 A57 -0.026 A58 0.001 A59 0.001 A60 0.001 A61 0.007 A62 -0.026 A63 0.001 A64 0.001 A65 0.001 A66 0.007 A67 -0.026 A68 0.001 A69 0.001 A70 0.001 A71 0.007 A72 -0.026 A73 0.001 A74 0.001 A75 0.001 A76 0.007 A77 -0.026 A78 0.001 A79 0.001 A80 0.001 A81 0.007 A82 -0.026 A83 0.001 A84 0.001 A85 0.001 A86 0.007 A87 -0.026 A88 0.001 A89 0.001 A90 0.001 A91 0.007 A92 -0.026 A93 0.001 A94 0.001 A95 0.001 A96 0.007 A97 -0.026 A98 0.001 A99 0.001 A100 0.001</p>	<p>ALPHA S = -4 CL/BIC = 0.002 THETA = 1 C/SIC = 0.0001 ALPHA C = -0.3</p> <p>FLAPPING</p> <p>A0 -0.000 A1 0.000 A2 0.000 A3 0.000 A4 0.000 A5 0.000 A6 0.000 A7 0.000 A8 0.000 A9 0.000 A10 0.000 A11 0.000 A12 0.000 A13 0.000 A14 0.000 A15 0.000 A16 0.000 A17 0.000 A18 0.000 A19 0.000 A20 0.000 A21 0.000 A22 0.000 A23 0.000 A24 0.000 A25 0.000 A26 0.000 A27 0.000 A28 0.000 A29 0.000 A30 0.000 A31 0.000 A32 0.000 A33 0.000 A34 0.000 A35 0.000 A36 0.000 A37 0.000 A38 0.000 A39 0.000 A40 0.000 A41 0.000 A42 0.000 A43 0.000 A44 0.000 A45 0.000 A46 0.000 A47 0.000 A48 0.000 A49 0.000 A50 0.000 A51 0.000 A52 0.000 A53 0.000 A54 0.000 A55 0.000 A56 0.000 A57 0.000 A58 0.000 A59 0.000 A60 0.000 A61 0.000 A62 0.000 A63 0.000 A64 0.000 A65 0.000 A66 0.000 A67 0.000 A68 0.000 A69 0.000 A70 0.000 A71 0.000 A72 0.000 A73 0.000 A74 0.000 A75 0.000 A76 0.000 A77 0.000 A78 0.000 A79 0.000 A80 0.000 A81 0.000 A82 0.000 A83 0.000 A84 0.000 A85 0.000 A86 0.000 A87 0.000 A88 0.000 A89 0.000 A90 0.000 A91 0.000 A92 0.000 A93 0.000 A94 0.000 A95 0.000 A96 0.000 A97 0.000 A98 0.000 A99 0.000 A100 0.000</p>	<p>ALPHA S = -4 CL/SIC = 0.001 THETA = 2 C/SIC = 0.0003 ALPHA C = -0.8</p> <p>FLAPPING</p> <p>A0 -0.000 A1 0.000 A2 0.000 A3 0.000 A4 0.000 A5 0.000 A6 0.000 A7 0.000 A8 0.000 A9 0.000 A10 0.000 A11 0.000 A12 0.000 A13 0.000 A14 0.000 A15 0.000 A16 0.000 A17 0.000 A18 0.000 A19 0.000 A20 0.000 A21 0.000 A22 0.000 A23 0.000 A24 0.000 A25 0.000 A26 0.000 A27 0.000 A28 0.000 A29 0.000 A30 0.000 A31 0.000 A32 0.000 A33 0.000 A34 0.000 A35 0.000 A36 0.000 A37 0.000 A38 0.000 A39 0.000 A40 0.000 A41 0.000 A42 0.000 A43 0.000 A44 0.000 A45 0.000 A46 0.000 A47 0.000 A48 0.000 A49 0.000 A50 0.000 A51 0.000 A52 0.000 A53 0.000 A54 0.000 A55 0.000 A56 0.000 A57 0.000 A58 0.000 A59 0.000 A60 0.000 A61 0.000 A62 0.000 A63 0.000 A64 0.000 A65 0.000 A66 0.000 A67 0.000 A68 0.000 A69 0.000 A70 0.000 A71 0.000 A72 0.000 A73 0.000 A74 0.000 A75 0.000 A76 0.000 A77 0.000 A78 0.000 A79 0.000 A80 0.000 A81 0.000 A82 0.000 A83 0.000 A84 0.000 A85 0.000 A86 0.000 A87 0.000 A88 0.000 A89 0.000 A90 0.000 A91 0.000 A92 0.000 A93 0.000 A94 0.000 A95 0.000 A96 0.000 A97 0.000 A98 0.000 A99 0.000 A100 0.000</p>
<p>ALPHA S = -4 CL/BIC = 0.004 THETA = 4 C/SIC = 0.0010 ALPHA C = -3.9</p> <p>FLAPPING</p> <p>A0 -0.000 A1 0.000 A2 0.000 A3 0.000 A4 0.000 A5 0.000 A6 0.000 A7 0.000 A8 0.000 A9 0.000 A10 0.000 A11 0.000 A12 0.000 A13 0.000 A14 0.000 A15 0.000 A16 0.000 A17 0.000 A18 0.000 A19 0.000 A20 0.000 A21 0.000 A22 0.000 A23 0.000 A24 0.000 A25 0.000 A26 0.000 A27 0.000 A28 0.000 A29 0.000 A30 0.000 A31 0.000 A32 0.000 A33 0.000 A34 0.000 A35 0.000 A36 0.000 A37 0.000 A38 0.000 A39 0.000 A40 0.000 A41 0.000 A42 0.000 A43 0.000 A44 0.000 A45 0.000 A46 0.000 A47 0.000 A48 0.000 A49 0.000 A50 0.000 A51 0.000 A52 0.000 A53 0.000 A54 0.000 A55 0.000 A56 0.000 A57 0.000 A58 0.000 A59 0.000 A60 0.000 A61 0.000 A62 0.000 A63 0.000 A64 0.000 A65 0.000 A66 0.000 A67 0.000 A68 0.000 A69 0.000 A70 0.000 A71 0.000 A72 0.000 A73 0.000 A74 0.000 A75 0.000 A76 0.000 A77 0.000 A78 0.000 A79 0.000 A80 0.000 A81 0.000 A82 0.000 A83 0.000 A84 0.000 A85 0.000 A86 0.000 A87 0.000 A88 0.000 A89 0.000 A90 0.000 A91 0.000 A92 0.000 A93 0.000 A94 0.000 A95 0.000 A96 0.000 A97 0.000 A98 0.000 A99 0.000 A100 0.000</p>	<p>ALPHA S = -4 CL/BIC = 0.071 THETA = 6 C/SIC = 0.0024 ALPHA C = -6.9</p> <p>FLAPPING</p> <p>A0 -0.000 A1 0.000 A2 0.000 A3 0.000 A4 0.000 A5 0.000 A6 0.000 A7 0.000 A8 0.000 A9 0.000 A10 0.000 A11 0.000 A12 0.000 A13 0.000 A14 0.000 A15 0.000 A16 0.000 A17 0.000 A18 0.000 A19 0.000 A20 0.000 A21 0.000 A22 0.000 A23 0.000 A24 0.000 A25 0.000 A26 0.000 A27 0.000 A28 0.000 A29 0.000 A30 0.000 A31 0.000 A32 0.000 A33 0.000 A34 0.000 A35 0.000 A36 0.000 A37 0.000 A38 0.000 A39 0.000 A40 0.000 A41 0.000 A42 0.000 A43 0.000 A44 0.000 A45 0.000 A46 0.000 A47 0.000 A48 0.000 A49 0.000 A50 0.000 A51 0.000 A52 0.000 A53 0.000 A54 0.000 A55 0.000 A56 0.000 A57 0.000 A58 0.000 A59 0.000 A60 0.000 A61 0.000 A62 0.000 A63 0.000 A64 0.000 A65 0.000 A66 0.000 A67 0.000 A68 0.000 A69 0.000 A70 0.000 A71 0.000 A72 0.000 A73 0.000 A74 0.000 A75 0.000 A76 0.000 A77 0.000 A78 0.000 A79 0.000 A80 0.000 A81 0.000 A82 0.000 A83 0.000 A84 0.000 A85 0.000 A86 0.000 A87 0.000 A88 0.000 A89 0.000 A90 0.000 A91 0.000 A92 0.000 A93 0.000 A94 0.000 A95 0.000 A96 0.000 A97 0.000 A98 0.000 A99 0.000 A100 0.000</p>	<p>ALPHA S = -4 CL/SIC = 0.007 THETA = 8 C/SIC = 0.0007 ALPHA C = -8.2</p> <p>FLAPPING</p> <p>A0 -0.000 A1 0.000 A2 0.000 A3 0.000 A4 0.000 A5 0.000 A6 0.000 A7 0.000 A8 0.000 A9 0.000 A10 0.000 A11 0.000 A12 0.000 A13 0.000 A14 0.000 A15 0.000 A16 0.000 A17 0.000 A18 0.000 A19 0.000 A20 0.000 A21 0.000 A22 0.000 A23 0.000 A24 0.000 A25 0.000 A26 0.000 A27 0.000 A28 0.000 A29 0.000 A30 0.000 A31 0.000 A32 0.000 A33 0.000 A34 0.000 A35 0.000 A36 0.000 A37 0.000 A38 0.000 A39 0.000 A40 0.000 A41 0.000 A42 0.000 A43 0.000 A44 0.000 A45 0.000 A46 0.000 A47 0.000 A48 0.000 A49 0.000 A50 0.000 A51 0.000 A52 0.000 A53 0.000 A54 0.000 A55 0.000 A56 0.000 A57 0.000 A58 0.000 A59 0.000 A60 0.000 A61 0.000 A62 0.000 A63 0.000 A64 0.000 A65 0.000 A66 0.000 A67 0.000 A68 0.000 A69 0.000 A70 0.000 A71 0.000 A72 0.000 A73 0.000 A74 0.000 A75 0.000 A76 0.000 A77 0.000 A78 0.000 A79 0.000 A80 0.000 A81 0.000 A82 0.000 A83 0.000 A84 0.000 A85 0.000 A86 0.000 A87 0.000 A88 0.000 A89 0.000 A90 0.000 A91 0.000 A92 0.000 A93 0.000 A94 0.000 A95 0.000 A96 0.000 A97 0.000 A98 0.000 A99 0.000 A100 0.000</p>

NOTE: COEFFICIENTS ARE ALL LISTED AS -0. WHEN NO BLADE MOTION DATA WAS OBTAINED DUE TO INSTRUMENTATION DIFFICULTIES.

TABLE I CONTINUED.

ADVANCE RATIO = 0.181		
<p>ALPHA 5 = -4 CL/316 = 0.007 THETA = 10 CO/316 = 0.0081 ALPHA C = -9.1</p> <p>PLAPPING</p> <p>A0 -0. A1 -0. A2 -0. A3 -0. A4 -0. A5 -0. A6 -0. A7 -0. A8 -0. A9 -0. A10 -0.</p> <p>LAGGING</p> <p>A0 -0. A1 -0. A2 -0. A3 -0. A4 -0. A5 -0. A6 -0. A7 -0. A8 -0. A9 -0. A10 -0.</p>	<p>ALPHA 5 = -8 CL/316 = 0.004 THETA = 2 CO/316 = 0.0001 ALPHA C = -8.7</p> <p>PLAPPING</p> <p>A0 -0. A1 -0. A2 -0. A3 -0. A4 -0. A5 -0. A6 -0. A7 -0. A8 -0. A9 -0. A10 -0.</p> <p>LAGGING</p> <p>A0 -0. A1 -0. A2 -0. A3 -0. A4 -0. A5 -0. A6 -0. A7 -0. A8 -0. A9 -0. A10 -0.</p>	<p>ALPHA 5 = -8 CL/316 = 0.032 THETA = 4 CO/316 = 0.0010 ALPHA C = -9.4</p> <p>PLAPPING</p> <p>A0 -0. A1 -0. A2 -0. A3 -0. A4 -0. A5 -0. A6 -0. A7 -0. A8 -0. A9 -0. A10 -0.</p> <p>LAGGING</p> <p>A0 -0. A1 -0. A2 -0. A3 -0. A4 -0. A5 -0. A6 -0. A7 -0. A8 -0. A9 -0. A10 -0.</p>
<p>ALPHA 5 = -8 CL/316 = 0.017 THETA = 4 CO/316 = 0.0024 ALPHA C = -18.9</p> <p>PLAPPING</p> <p>A0 -0. A1 -0. A2 -0. A3 -0. A4 -0. A5 -0. A6 -0. A7 -0. A8 -0. A9 -0. A10 -0.</p> <p>LAGGING</p> <p>A0 -0. A1 -0. A2 -0. A3 -0. A4 -0. A5 -0. A6 -0. A7 -0. A8 -0. A9 -0. A10 -0.</p>	<p>ALPHA 5 = -8 CL/316 = 0.078 THETA = 8 CO/316 = 0.0044 ALPHA C = -11.4</p> <p>PLAPPING</p> <p>A0 -0. A1 -0. A2 -0. A3 -0. A4 -0. A5 -0. A6 -0. A7 -0. A8 -0. A9 -0. A10 -0.</p> <p>LAGGING</p> <p>A0 -0. A1 -0. A2 -0. A3 -0. A4 -0. A5 -0. A6 -0. A7 -0. A8 -0. A9 -0. A10 -0.</p>	<p>ALPHA 5 = -8 CL/316 = 0.889 THETA = 10 CO/316 = 0.0074 ALPHA C = -13.5</p> <p>PLAPPING</p> <p>A0 -0. A1 -0. A2 -0. A3 -0. A4 -0. A5 -0. A6 -0. A7 -0. A8 -0. A9 -0. A10 -0.</p> <p>LAGGING</p> <p>A0 -0. A1 -0. A2 -0. A3 -0. A4 -0. A5 -0. A6 -0. A7 -0. A8 -0. A9 -0. A10 -0.</p>
<p>ALPHA 5 = -8 CL/316 = 0.092 THETA = 11 CO/316 = 0.0089 ALPHA C = -13.7</p> <p>PLAPPING</p> <p>A0 -0. A1 -0. A2 -0. A3 -0. A4 -0. A5 -0. A6 -0. A7 -0. A8 -0. A9 -0. A10 -0.</p> <p>LAGGING</p> <p>A0 -0. A1 -0. A2 -0. A3 -0. A4 -0. A5 -0. A6 -0. A7 -0. A8 -0. A9 -0. A10 -0.</p>	<p>OUT-OF-THIN</p> <p>ALPHA 5 = 0 CL/316 = 0.007 THETA = 0 CO/316 = 0.0000 ALPHA C = -4.9</p> <p>PLAPPING</p> <p>A0 -0.288 A1 0.329 A2 -0.228 A3 -0.038 A4 0.028 A5 -0.004 A6 0.001 A7 -0.001 A8 0.001 A9 0.003 A10 0.002</p> <p>LAGGING</p> <p>A0 0.043 A1 0.019 A2 0.009 A3 -0.004 A4 0.004 A5 0.001 A6 -0.001 A7 0.001 A8 -0.001 A9 -0.001 A10 0.001</p>	<p>OUT-OF-THIN</p> <p>ALPHA 5 = 0 CL/316 = 0.021 THETA = 2 CO/316 = 0.0005 ALPHA C = -3.6</p> <p>PLAPPING</p> <p>A0 1.242 A1 0.213 A2 -0.044 A3 -0.007 A4 0.044 A5 0.017 A6 -0.028 A7 0.013 A8 0.003 A9 0.009 A10 0.001</p> <p>LAGGING</p> <p>A0 0.099 A1 0.018 A2 0.008 A3 -0.001 A4 0.001 A5 0.002 A6 0.001 A7 -0.001 A8 0.001 A9 0.002 A10 0.002</p>

TABLE I CONTINUED.

ADVANCE RATIO = 0.181		OUT-OF-TRIM		ZERO LAG DAMPING	
OUT-OF-TRIM		OUT-OF-TRIM		OUT-OF-TRIM	
ALPHA S = 0 CL/SIC = 0.047 THETA = 4 CO/SIC = 0.0012 ALPHA C = -0.2		ALPHA S = 0 CL/SIC = 0.071 THETA = 9 CO/SIC = 0.0025 ALPHA C = -7.2		ALPHA S = -4 CL/SIC = -0.004 THETA = 0 CO/SIC = 0.0001 ALPHA C = -4.0	
FLAPPING	LAGGING	FLAPPING	LAGGING	FLAPPING	LAGGING
A0 2.422	A0 0.245	A0 4.084	A0 0.915	A0 0.048	A0 -0.103
A1 0.152	A1 0.104	A1 0.207	A1 0.199	A1 0.213	A1 0.078
A2 -0.122	A2 -0.093	A2 -0.245	A2 -0.048	A2 0.040	A2 -0.205
A3 0.180	A3 0.131	A3 0.081	A3 0.118	A3 0.040	A3 -0.039
A4 0.180	A4 0.131	A4 0.081	A4 0.118	A4 0.040	A4 -0.039
A5 0.180	A5 0.131	A5 0.081	A5 0.118	A5 0.040	A5 -0.039
A6 0.180	A6 0.131	A6 0.081	A6 0.118	A6 0.040	A6 -0.039
A7 0.180	A7 0.131	A7 0.081	A7 0.118	A7 0.040	A7 -0.039
A8 0.180	A8 0.131	A8 0.081	A8 0.118	A8 0.040	A8 -0.039
A9 0.180	A9 0.131	A9 0.081	A9 0.118	A9 0.040	A9 -0.039
A10 0.180	A10 0.131	A10 0.081	A10 0.118	A10 0.040	A10 -0.039
A11 0.180	A11 0.131	A11 0.081	A11 0.118	A11 0.040	A11 -0.039
A12 0.180	A12 0.131	A12 0.081	A12 0.118	A12 0.040	A12 -0.039
A13 0.180	A13 0.131	A13 0.081	A13 0.118	A13 0.040	A13 -0.039
A14 0.180	A14 0.131	A14 0.081	A14 0.118	A14 0.040	A14 -0.039
A15 0.180	A15 0.131	A15 0.081	A15 0.118	A15 0.040	A15 -0.039
A16 0.180	A16 0.131	A16 0.081	A16 0.118	A16 0.040	A16 -0.039
A17 0.180	A17 0.131	A17 0.081	A17 0.118	A17 0.040	A17 -0.039
A18 0.180	A18 0.131	A18 0.081	A18 0.118	A18 0.040	A18 -0.039
A19 0.180	A19 0.131	A19 0.081	A19 0.118	A19 0.040	A19 -0.039
A20 0.180	A20 0.131	A20 0.081	A20 0.118	A20 0.040	A20 -0.039
A21 0.180	A21 0.131	A21 0.081	A21 0.118	A21 0.040	A21 -0.039
A22 0.180	A22 0.131	A22 0.081	A22 0.118	A22 0.040	A22 -0.039
A23 0.180	A23 0.131	A23 0.081	A23 0.118	A23 0.040	A23 -0.039
A24 0.180	A24 0.131	A24 0.081	A24 0.118	A24 0.040	A24 -0.039
A25 0.180	A25 0.131	A25 0.081	A25 0.118	A25 0.040	A25 -0.039
A26 0.180	A26 0.131	A26 0.081	A26 0.118	A26 0.040	A26 -0.039
A27 0.180	A27 0.131	A27 0.081	A27 0.118	A27 0.040	A27 -0.039
A28 0.180	A28 0.131	A28 0.081	A28 0.118	A28 0.040	A28 -0.039
A29 0.180	A29 0.131	A29 0.081	A29 0.118	A29 0.040	A29 -0.039
A30 0.180	A30 0.131	A30 0.081	A30 0.118	A30 0.040	A30 -0.039
A31 0.180	A31 0.131	A31 0.081	A31 0.118	A31 0.040	A31 -0.039
A32 0.180	A32 0.131	A32 0.081	A32 0.118	A32 0.040	A32 -0.039
A33 0.180	A33 0.131	A33 0.081	A33 0.118	A33 0.040	A33 -0.039
A34 0.180	A34 0.131	A34 0.081	A34 0.118	A34 0.040	A34 -0.039
A35 0.180	A35 0.131	A35 0.081	A35 0.118	A35 0.040	A35 -0.039
A36 0.180	A36 0.131	A36 0.081	A36 0.118	A36 0.040	A36 -0.039
A37 0.180	A37 0.131	A37 0.081	A37 0.118	A37 0.040	A37 -0.039
A38 0.180	A38 0.131	A38 0.081	A38 0.118	A38 0.040	A38 -0.039
A39 0.180	A39 0.131	A39 0.081	A39 0.118	A39 0.040	A39 -0.039
A40 0.180	A40 0.131	A40 0.081	A40 0.118	A40 0.040	A40 -0.039
A41 0.180	A41 0.131	A41 0.081	A41 0.118	A41 0.040	A41 -0.039
A42 0.180	A42 0.131	A42 0.081	A42 0.118	A42 0.040	A42 -0.039
A43 0.180	A43 0.131	A43 0.081	A43 0.118	A43 0.040	A43 -0.039
A44 0.180	A44 0.131	A44 0.081	A44 0.118	A44 0.040	A44 -0.039
A45 0.180	A45 0.131	A45 0.081	A45 0.118	A45 0.040	A45 -0.039
A46 0.180	A46 0.131	A46 0.081	A46 0.118	A46 0.040	A46 -0.039
A47 0.180	A47 0.131	A47 0.081	A47 0.118	A47 0.040	A47 -0.039
A48 0.180	A48 0.131	A48 0.081	A48 0.118	A48 0.040	A48 -0.039
A49 0.180	A49 0.131	A49 0.081	A49 0.118	A49 0.040	A49 -0.039
A50 0.180	A50 0.131	A50 0.081	A50 0.118	A50 0.040	A50 -0.039
A51 0.180	A51 0.131	A51 0.081	A51 0.118	A51 0.040	A51 -0.039
A52 0.180	A52 0.131	A52 0.081	A52 0.118	A52 0.040	A52 -0.039
A53 0.180	A53 0.131	A53 0.081	A53 0.118	A53 0.040	A53 -0.039
A54 0.180	A54 0.131	A54 0.081	A54 0.118	A54 0.040	A54 -0.039
A55 0.180	A55 0.131	A55 0.081	A55 0.118	A55 0.040	A55 -0.039
A56 0.180	A56 0.131	A56 0.081	A56 0.118	A56 0.040	A56 -0.039
A57 0.180	A57 0.131	A57 0.081	A57 0.118	A57 0.040	A57 -0.039
A58 0.180	A58 0.131	A58 0.081	A58 0.118	A58 0.040	A58 -0.039
A59 0.180	A59 0.131	A59 0.081	A59 0.118	A59 0.040	A59 -0.039
A60 0.180	A60 0.131	A60 0.081	A60 0.118	A60 0.040	A60 -0.039
A61 0.180	A61 0.131	A61 0.081	A61 0.118	A61 0.040	A61 -0.039
A62 0.180	A62 0.131	A62 0.081	A62 0.118	A62 0.040	A62 -0.039
A63 0.180	A63 0.131	A63 0.081	A63 0.118	A63 0.040	A63 -0.039
A64 0.180	A64 0.131	A64 0.081	A64 0.118	A64 0.040	A64 -0.039
A65 0.180	A65 0.131	A65 0.081	A65 0.118	A65 0.040	A65 -0.039
A66 0.180	A66 0.131	A66 0.081	A66 0.118	A66 0.040	A66 -0.039
A67 0.180	A67 0.131	A67 0.081	A67 0.118	A67 0.040	A67 -0.039
A68 0.180	A68 0.131	A68 0.081	A68 0.118	A68 0.040	A68 -0.039
A69 0.180	A69 0.131	A69 0.081	A69 0.118	A69 0.040	A69 -0.039
A70 0.180	A70 0.131	A70 0.081	A70 0.118	A70 0.040	A70 -0.039
A71 0.180	A71 0.131	A71 0.081	A71 0.118	A71 0.040	A71 -0.039
A72 0.180	A72 0.131	A72 0.081	A72 0.118	A72 0.040	A72 -0.039
A73 0.180	A73 0.131	A73 0.081	A73 0.118	A73 0.040	A73 -0.039
A74 0.180	A74 0.131	A74 0.081	A74 0.118	A74 0.040	A74 -0.039
A75 0.180	A75 0.131	A75 0.081	A75 0.118	A75 0.040	A75 -0.039
A76 0.180	A76 0.131	A76 0.081	A76 0.118	A76 0.040	A76 -0.039
A77 0.180	A77 0.131	A77 0.081	A77 0.118	A77 0.040	A77 -0.039
A78 0.180	A78 0.131	A78 0.081	A78 0.118	A78 0.040	A78 -0.039
A79 0.180	A79 0.131	A79 0.081	A79 0.118	A79 0.040	A79 -0.039
A80 0.180	A80 0.131	A80 0.081	A80 0.118	A80 0.040	A80 -0.039
A81 0.180	A81 0.131	A81 0.081	A81 0.118	A81 0.040	A81 -0.039
A82 0.180	A82 0.131	A82 0.081	A82 0.118	A82 0.040	A82 -0.039
A83 0.180	A83 0.131	A83 0.081	A83 0.118	A83 0.040	A83 -0.039
A84 0.180	A84 0.131	A84 0.081	A84 0.118	A84 0.040	A84 -0.039
A85 0.180	A85 0.131	A85 0.081	A85 0.118	A85 0.040	A85 -0.039
A86 0.180	A86 0.131	A86 0.081	A86 0.118	A86 0.040	A86 -0.039
A87 0.180	A87 0.131	A87 0.081	A87 0.118	A87 0.040	A87 -0.039
A88 0.180	A88 0.131	A88 0.081	A88 0.118	A88 0.040	A88 -0.039
A89 0.180	A89 0.131	A89 0.081	A89 0.118	A89 0.040	A89 -0.039
A90 0.180	A90 0.131	A90 0.081	A90 0.118	A90 0.040	A90 -0.039
A91 0.180	A91 0.131	A91 0.081	A91 0.118	A91 0.040	A91 -0.039
A92 0.180	A92 0.131	A92 0.081	A92 0.118	A92 0.040	A92 -0.039
A93 0.180	A93 0.131	A93 0.081	A93 0.118	A93 0.040	A93 -0.039
A94 0.180	A94 0.131	A94 0.081	A94 0.118	A94 0.040	A94 -0.039
A95 0.180	A95 0.131	A95 0.081	A95 0.118	A95 0.040	A95 -0.039
A96 0.180	A96 0.131	A96 0.081	A96 0.118	A96 0.040	A96 -0.039
A97 0.180	A97 0.131	A97 0.081	A97 0.118	A97 0.040	A97 -0.039
A98 0.180	A98 0.131	A98 0.081	A98 0.118	A98 0.040	A98 -0.039
A99 0.180	A99 0.131	A99 0.081	A99 0.118	A99 0.040	A99 -0.039
A100 0.180	A100 0.131	A100 0.081	A100 0.118	A100 0.040	A100 -0.039
A101 0.180	A101 0.131	A101 0.081	A101 0.118	A101 0.040	A101 -0.039
A102 0.180	A102 0.131	A102 0.081	A102 0.118	A102 0.040	A102 -0.039
A103 0.180	A103 0.131	A103 0.081	A103 0.118	A103 0.040	A103 -0.039
A104 0.180	A104 0.131	A104 0.081	A104 0.118	A104 0.040	A104 -0.039
A105 0.180	A105 0.131	A105 0.081	A105 0.118	A105 0.040	A105 -0.039
A106 0.180	A106 0.131	A106 0.081	A106 0.118	A106 0.040	A106 -0.039
A107 0.180	A107 0.131	A107 0.081	A107 0.118	A107 0.040	A107 -0.039
A108 0.180	A108 0.131	A108 0.081	A108 0.118	A108 0.040	A108 -0.039
A109 0.180	A109 0.131	A109 0.081	A109 0.118	A109 0.040	A109 -0.039
A110 0.180	A110 0.131	A110 0.081	A110 0.118	A110 0.040	A110 -0.039
A111 0.180	A111 0.131	A111 0.081	A111 0.118	A111 0.040	A111 -0.039
A112 0.180	A112 0.131	A112 0.081	A112 0.118	A112 0.040	A112 -0.039
A113 0.180	A113 0.131	A113 0.081	A113 0.118	A113 0.040	A113 -0.039
A114 0.180	A114 0.131	A114 0.081	A114 0.118	A114 0.040	A114 -0.039
A115 0.180	A115 0.131	A115 0.081	A115 0.118	A115 0.040	A115 -0.039
A116 0.180	A116 0.131	A116 0.081	A116 0.118	A116 0.040	A116 -0.039
A117 0.180	A117 0.131	A117 0.081	A117 0.118	A117 0.040	A117 -0.039
A118 0.180	A118 0.131	A118 0.081	A118 0.118	A118 0.040	A118 -0.039
A119 0.180	A119 0.131	A119 0.081	A119 0.118	A119 0.040	A119 -0.039
A120 0.180	A120 0.131	A120 0.081	A120 0.118	A120 0.040	A120 -0.039
A121 0.180	A121 0.131	A121 0.081	A121 0.118	A121 0.040	A121 -0.039
A122 0.180	A122 0.131	A122 0.081	A122 0.118	A122 0.040	A122 -0.039
A123 0.180	A123 0.131	A123 0.081	A123 0.118	A123 0.040	A123 -0.039
A124 0.180	A124 0.131	A124 0.081	A124 0.118	A124 0.040	A124 -0.039
A125 0.180	A125 0.131	A125 0.081	A125 0.118	A125 0.040	A125 -0.039
A126 0.180	A126 0.131	A126 0.081	A126 0.118	A126 0.040	A126 -0.039
A127 0.180	A127 0.131	A127 0.081	A127 0.118	A127 0.040	A127 -0.039
A128 0.180	A128 0.131	A128 0.081	A128 0.118	A128 0.040	A128 -0.039
A129 0.180	A129 0.131	A129 0.081	A129 0.118	A129 0.040	A129 -0.039
A130 0.180	A130 0.131	A130 0.081	A130 0.118	A130 0.040	A130 -0.039
A131 0.180	A131 0.131	A131 0.081	A131 0.118	A131 0.040	A131 -0.039
A132 0.180	A132 0.131	A132 0.081	A132 0.118	A132 0.040	A132 -0.039
A133 0.180	A133 0.131	A133 0.081	A133 0.118	A133 0.040	A133 -0.039
A134 0.180	A134 0.131	A134 0.081	A134 0.118	A134 0.040	A134 -0.039
A135 0.180	A135 0.131	A135 0.081	A135 0.118	A135 0.040	A135 -0.039
A136 0.180	A136 0.131	A136 0.081	A136 0.118	A136 0.040	A136 -0.039
A137 0.180	A137 0.131	A137 0.081	A137 0.118	A137 0.040	A137 -0.039
A138 0.180	A138 0.131	A138 0.081	A138 0.118	A138 0.040	A138 -0.039
A139 0.180	A139 0.131	A139 0.081	A139 0.118	A139 0.040	A139 -0.039
A140 0.180	A140 0.131	A140 0.081	A140 0.118	A140 0.040	A14

TABLE I CONTINUED.

ADVANCE RATIO = 0.283		
<p>ALPHA 5 = 0 CL/SIC = -0.023 THETA = -2 CO/SIC = 0.0008 ALPHA C = 0.5</p> <p>FLAPPING</p> <p>AO 0.435 A1 -0.047 A2 0.049 A3 -0.043 A4 -0.235 A5 -0.324 A6 -0.009 A7 0.007 A8 0.092 A9 0.316 A10 -0.001 A11 0.003 A12 0.077 A13 0.025 A14 0.003 A15 -0.002 A16 0.816 A17 0.810 A18 -0.001 A19 0.001 A20 0.015 A21 0.017 A22 0.015 A23 0.015 A24 0.015 A25 0.015 A26 0.015 A27 0.015 A28 0.015 A29 0.015 A30 0.015 A31 0.015 A32 0.015 A33 0.015 A34 0.015 A35 0.015 A36 0.015 A37 0.015 A38 0.015 A39 0.015 A40 0.015 A41 0.015 A42 0.015 A43 0.015 A44 0.015 A45 0.015 A46 0.015 A47 0.015 A48 0.015 A49 0.015 A50 0.015 A51 0.015 A52 0.015 A53 0.015 A54 0.015 A55 0.015 A56 0.015 A57 0.015 A58 0.015 A59 0.015 A60 0.015 A61 0.015 A62 0.015 A63 0.015 A64 0.015 A65 0.015 A66 0.015 A67 0.015 A68 0.015 A69 0.015 A70 0.015 A71 0.015 A72 0.015 A73 0.015 A74 0.015 A75 0.015 A76 0.015 A77 0.015 A78 0.015 A79 0.015 A80 0.015 A81 0.015 A82 0.015 A83 0.015 A84 0.015 A85 0.015 A86 0.015 A87 0.015 A88 0.015 A89 0.015 A90 0.015 A91 0.015 A92 0.015 A93 0.015 A94 0.015 A95 0.015 A96 0.015 A97 0.015 A98 0.015 A99 0.015 A100 0.015</p>	<p>ALPHA 5 = 0 CL/SIC = -0.007 THETA = 0 CO/SIC = 0.0007 ALPHA C = -0.5</p> <p>FLAPPING</p> <p>AO 0.432 A1 -0.247 A2 0.188 A3 -0.079 A4 -0.870 A5 0.134 A6 -0.297 A7 -0.003 A8 0.003 A9 -0.004 A10 0.894 A11 -0.040 A12 0.004 A13 0.003 A14 -0.011 A15 0.003 A16 0.003 A17 0.003 A18 0.015 A19 0.015 A20 0.015 A21 0.015 A22 0.015 A23 0.015 A24 0.015 A25 0.015 A26 0.015 A27 0.015 A28 0.015 A29 0.015 A30 0.015 A31 0.015 A32 0.015 A33 0.015 A34 0.015 A35 0.015 A36 0.015 A37 0.015 A38 0.015 A39 0.015 A40 0.015 A41 0.015 A42 0.015 A43 0.015 A44 0.015 A45 0.015 A46 0.015 A47 0.015 A48 0.015 A49 0.015 A50 0.015 A51 0.015 A52 0.015 A53 0.015 A54 0.015 A55 0.015 A56 0.015 A57 0.015 A58 0.015 A59 0.015 A60 0.015 A61 0.015 A62 0.015 A63 0.015 A64 0.015 A65 0.015 A66 0.015 A67 0.015 A68 0.015 A69 0.015 A70 0.015 A71 0.015 A72 0.015 A73 0.015 A74 0.015 A75 0.015 A76 0.015 A77 0.015 A78 0.015 A79 0.015 A80 0.015 A81 0.015 A82 0.015 A83 0.015 A84 0.015 A85 0.015 A86 0.015 A87 0.015 A88 0.015 A89 0.015 A90 0.015 A91 0.015 A92 0.015 A93 0.015 A94 0.015 A95 0.015 A96 0.015 A97 0.015 A98 0.015 A99 0.015 A100 0.015</p>	<p>ALPHA 5 = 0 CL/SIC = 0.015 THETA = 2 CO/SIC = 0.0008 ALPHA C = -2.4</p> <p>FLAPPING</p> <p>AO 1.038 A1 -0.224 A2 0.141 A3 -0.034 A4 -0.038 A5 0.009 A6 -0.240 A7 -0.001 A8 0.001 A9 0.007 A10 0.058 A11 0.040 A12 0.001 A13 0.007 A14 -0.003 A15 -0.007 A16 -0.001 A17 -0.001 A18 -0.003 A19 -0.007 A20 -0.001 A21 -0.001 A22 -0.003 A23 -0.007 A24 -0.001 A25 -0.001 A26 -0.003 A27 -0.007 A28 -0.001 A29 -0.001 A30 -0.003 A31 -0.007 A32 -0.001 A33 -0.001 A34 -0.003 A35 -0.007 A36 -0.001 A37 -0.001 A38 -0.003 A39 -0.007 A40 -0.001 A41 -0.001 A42 -0.003 A43 -0.007 A44 -0.001 A45 -0.001 A46 -0.003 A47 -0.007 A48 -0.001 A49 -0.001 A50 -0.003 A51 -0.007 A52 -0.001 A53 -0.001 A54 -0.003 A55 -0.007 A56 -0.001 A57 -0.001 A58 -0.003 A59 -0.007 A60 -0.001 A61 -0.001 A62 -0.003 A63 -0.007 A64 -0.001 A65 -0.001 A66 -0.003 A67 -0.007 A68 -0.001 A69 -0.001 A70 -0.003 A71 -0.007 A72 -0.001 A73 -0.001 A74 -0.003 A75 -0.007 A76 -0.001 A77 -0.001 A78 -0.003 A79 -0.007 A80 -0.001 A81 -0.001 A82 -0.003 A83 -0.007 A84 -0.001 A85 -0.001 A86 -0.003 A87 -0.007 A88 -0.001 A89 -0.001 A90 -0.003 A91 -0.007 A92 -0.001 A93 -0.001 A94 -0.003 A95 -0.007 A96 -0.001 A97 -0.001 A98 -0.003 A99 -0.007 A100 -0.001</p>
<p>ALPHA 5 = 0 CL/SIC = 0.040 THETA = 4 CO/SIC = 0.0013 ALPHA C = -5.5</p> <p>FLAPPING</p> <p>AO 3.074 A1 0.134 A2 -0.043 A3 -0.014 A4 -0.540 A5 -0.177 A6 0.003 A7 0.014 A8 0.212 A9 -0.177 A10 0.011 A11 0.000 A12 0.045 A13 0.155 A14 0.011 A15 0.000 A16 0.050 A17 0.049 A18 -0.002 A19 0.000 A20 0.017 A21 -0.011 A22 0.002 A23 0.000 A24 0.022 A25 0.002 A26 0.001 A27 0.001 A28 0.032 A29 0.071 A30 -0.001 A31 0.001 A32 0.017 A33 0.000 A34 0.001 A35 0.001 A36 0.017 A37 0.000 A38 0.001 A39 0.001 A40 0.017 A41 0.000 A42 0.001 A43 0.001 A44 0.017 A45 0.000 A46 0.001 A47 0.001 A48 0.017 A49 0.000 A50 0.001 A51 0.001 A52 0.017 A53 0.000 A54 0.001 A55 0.001 A56 0.017 A57 0.000 A58 0.001 A59 0.001 A60 0.017 A61 0.000 A62 0.001 A63 0.001 A64 0.017 A65 0.000 A66 0.001 A67 0.001 A68 0.017 A69 0.000 A70 0.001 A71 0.001 A72 0.017 A73 0.000 A74 0.001 A75 0.001 A76 0.017 A77 0.000 A78 0.001 A79 0.001 A80 0.017 A81 0.000 A82 0.001 A83 0.001 A84 0.017 A85 0.000 A86 0.001 A87 0.001 A88 0.017 A89 0.000 A90 0.001 A91 0.001 A92 0.017 A93 0.000 A94 0.001 A95 0.001 A96 0.017 A97 0.000 A98 0.001 A99 0.001 A100 0.017</p>	<p>ALPHA 5 = 0 CL/SIC = 0.009 THETA = 4 CO/SIC = 0.0031 ALPHA C = -5.2</p> <p>FLAPPING</p> <p>AO 4.014 A1 -0.345 A2 0.090 A3 -0.131 A4 0.041 A5 0.414 A6 -0.576 A7 -0.003 A8 0.033 A9 0.093 A10 -0.133 A11 0.033 A12 0.033 A13 0.093 A14 -0.133 A15 0.033 A16 0.033 A17 0.093 A18 -0.133 A19 0.033 A20 0.033 A21 0.093 A22 -0.133 A23 0.033 A24 0.033 A25 0.093 A26 -0.133 A27 0.033 A28 0.033 A29 0.093 A30 -0.133 A31 0.033 A32 0.033 A33 0.093 A34 -0.133 A35 0.033 A36 0.033 A37 0.093 A38 -0.133 A39 0.033 A40 0.033 A41 0.093 A42 -0.133 A43 0.033 A44 0.033 A45 0.093 A46 -0.133 A47 0.033 A48 0.033 A49 0.093 A50 -0.133 A51 0.033 A52 0.033 A53 0.093 A54 -0.133 A55 0.033 A56 0.033 A57 0.093 A58 -0.133 A59 0.033 A60 0.033 A61 0.093 A62 -0.133 A63 0.033 A64 0.033 A65 0.093 A66 -0.133 A67 0.033 A68 0.033 A69 0.093 A70 -0.133 A71 0.033 A72 0.033 A73 0.093 A74 -0.133 A75 0.033 A76 0.033 A77 0.093 A78 -0.133 A79 0.033 A80 0.033 A81 0.093 A82 -0.133 A83 0.033 A84 0.033 A85 0.093 A86 -0.133 A87 0.033 A88 0.033 A89 0.093 A90 -0.133 A91 0.033 A92 0.033 A93 0.093 A94 -0.133 A95 0.033 A96 0.033 A97 0.093 A98 -0.133 A99 0.033 A100 0.033</p>	<p>ALPHA 5 = 0 CL/SIC = 0.045 THETA = 8 CO/SIC = 0.0056 ALPHA C = -4.8</p> <p>FLAPPING</p> <p>AO 4.497 A1 -0.316 A2 -0.108 A3 -0.283 A4 0.159 A5 -0.197 A6 -0.185 A7 -0.182 A8 0.035 A9 0.074 A10 0.218 A11 -0.182 A12 0.035 A13 0.074 A14 0.049 A15 0.090 A16 0.034 A17 0.004 A18 0.007 A19 0.079 A20 -0.034 A21 0.006 A22 0.007 A23 0.048 A24 0.031 A25 0.001 A26 0.001 A27 0.048 A28 0.031 A29 0.001 A30 0.001 A31 0.048 A32 0.031 A33 0.001 A34 0.001 A35 0.048 A36 0.031 A37 0.001 A38 0.001 A39 0.048 A40 0.031 A41 0.001 A42 0.001 A43 0.048 A44 0.031 A45 0.001 A46 0.001 A47 0.048 A48 0.031 A49 0.001 A50 0.001 A51 0.048 A52 0.031 A53 0.001 A54 0.001 A55 0.048 A56 0.031 A57 0.001 A58 0.001 A59 0.048 A60 0.031 A61 0.001 A62 0.001 A63 0.048 A64 0.031 A65 0.001 A66 0.001 A67 0.048 A68 0.031 A69 0.001 A70 0.001 A71 0.048 A72 0.031 A73 0.001 A74 0.001 A75 0.048 A76 0.031 A77 0.001 A78 0.001 A79 0.048 A80 0.031 A81 0.001 A82 0.001 A83 0.048 A84 0.031 A85 0.001 A86 0.001 A87 0.048 A88 0.031 A89 0.001 A90 0.001 A91 0.048 A92 0.031 A93 0.001 A94 0.001 A95 0.048 A96 0.031 A97 0.001 A98 0.001 A99 0.048 A100 0.031</p>
<p>ALPHA 5 = 0 CL/SIC = 0.074 THETA = 10 CO/SIC = 0.0083 ALPHA C = -8.0</p> <p>FLAPPING</p> <p>AO 3.074 A1 -0.034 A2 -0.033 A3 0.181 A4 -0.774 A5 -0.608 A6 -0.033 A7 0.070 A8 0.131 A9 -0.127 A10 0.041 A11 0.014 A12 0.151 A13 0.052 A14 0.013 A15 0.015 A16 -0.033 A17 -0.034 A18 0.000 A19 0.001 A20 0.083 A21 -0.084 A22 -0.004 A23 0.001 A24 0.034 A25 0.133 A26 0.003 A27 0.007 A28 0.081 A29 0.009 A30 0.003 A31 0.002 A32 0.010 A33 0.007 A34 0.003 A35 0.002 A36 0.033 A37 0.023 A38 0.003 A39 0.003 A40 0.023 A41 0.003 A42 0.003 A43 0.003 A44 0.023 A45 0.003 A46 0.003 A47 0.003 A48 0.023 A49 0.003 A50 0.003 A51 0.003 A52 0.023 A53 0.003 A54 0.003 A55 0.003 A56 0.023 A57 0.003 A58 0.003 A59 0.003 A60 0.023 A61 0.003 A62 0.003 A63 0.003 A64 0.023 A65 0.003 A66 0.003 A67 0.003 A68 0.023 A69 0.003 A70 0.003 A71 0.003 A72 0.023 A73 0.003 A74 0.003 A75 0.003 A76 0.023 A77 0.003 A78 0.003 A79 0.003 A80 0.023 A81 0.003 A82 0.003 A83 0.003 A84 0.023 A85 0.003 A86 0.003 A87 0.003 A88 0.023 A89 0.003 A90 0.003 A91 0.003 A92 0.023 A93 0.003 A94 0.003 A95 0.003 A96 0.023 A97 0.003 A98 0.003 A99 0.003 A100 0.023</p>	<p>ALPHA 5 = -5 CL/SIC = 0.002 THETA = 1 CO/SIC = 0.0001 ALPHA C = -4.6</p> <p>FLAPPING</p> <p>AO -0.508 A1 -0.132 A2 -0.019 A3 0.088 A4 -0.075 A5 0.132 A6 -0.280 A7 -0.001 A8 0.003 A9 0.075 A10 -0.033 A11 -0.001 A12 0.003 A13 0.082 A14 -0.001 A15 0.004 A16 -0.001 A17 0.000 A18 0.004 A19 0.002 A20 0.002 A21 0.011 A22 0.017 A23 0.001 A24 0.001 A25 0.011 A26 0.017 A27 0.001 A28 0.001 A29 0.011 A30 0.017 A31 0.001 A32 0.001 A33 0.011 A34 0.017 A35 0.001 A36 0.001 A37 0.011 A38 0.017 A39 0.001 A40 0.001 A41 0.011 A42 0.017 A43 0.001 A44 0.001 A45 0.011 A46 0.017 A47 0.001 A48 0.001 A49 0.011 A50 0.017 A51 0.001 A52 0.001 A53 0.011 A54 0.017 A55 0.001 A56 0.001 A57 0.011 A58 0.017 A59 0.001 A60 0.001 A61 0.011 A62 0.017 A63 0.001 A64 0.001 A65 0.011 A66 0.017 A67 0.001 A68 0.001 A69 0.011 A70 0.017 A71 0.001 A72 0.001 A73 0.011 A74 0.017 A75 0.001 A76 0.001 A77 0.011 A78 0.017 A79 0.001 A80 0.001 A81 0.011 A82 0.017 A83 0.001 A84 0.001 A85 0.011 A86 0.017 A87 0.001 A88 0.001 A89 0.011 A90 0.017 A91 0.001 A92 0.001 A93 0.011 A94 0.017 A95 0.001 A96 0.001 A97 0.011 A98 0.017 A99 0.001 A100 0.001</p>	<p>ALPHA 5 = -5 CL/SIC = 0.010 THETA = 2 CO/SIC = 0.0004 ALPHA C = -4.8</p> <p>FLAPPING</p> <p>AO 0.845 A1 -0.392 A2 -0.099 A3 0.043 A4 -0.047 A5 0.004 A6 -0.227 A7 -0.002 A8 0.001 A9 0.083 A10 -0.089 A11 0.002 A12 0.001 A13 0.079 A14 0.014 A15 0.004 A16 0.002 A17 -0.004 A18 -0.001 A19 0.005 A20 0.001 A21 0.014 A22 0.013 A23 0.001 A24 0.001 A25 0.014 A26 0.013 A27 0.001 A28 0.001 A29 0.014 A30 0.013 A31 0.001 A32 0.001 A33 0.014 A34 0.013 A35 0.001 A36 0.001 A37 0.014 A38 0.013 A39 0.001 A40 0.001 A41 0.014 A42 0.013 A43 0.001 A44 0.001 A45 0.014 A46 0.013 A47 0.001 A48 0.001 A49 0.014 A50 0.013 A51 0.001 A52 0.001 A53 0.014 A54 0.013 A55 0.001 A56 0.001 A57 0.014 A58 0.013 A59 0.001 A60 0.001 A61 0.014 A62 0.013 A63 0.001 A64 0.001 A65 0.014 A66 0.013 A67 0.001 A68 0.001 A69 0.014 A70 0.013 A71 0.001 A72 0.001 A73 0.014 A74 0.013 A75 0.001 A76 0.001 A77 0.014 A78 0.013 A79 0.001 A80 0.001 A81 0.014 A82 0.013 A83 0.001 A84 0.001 A85 0.014 A86 0.013 A87 0.001 A88 0.001 A89 0.014 A90 0.013 A91 0.001 A92 0.001 A93 0.014 A94 0.013 A95 0.001 A96 0.001 A97 0.014 A98 0.013 A99 0.001 A100 0.001</p>

TABLE I CONTINUED.

[illegible]

TABLE I CONTINUED.

ADVANCE RATIO = 0.283		ALPHA S = -8 CL/SIG = 0.039 THETA = 6 CQ/SIG = 0.0021 ALPHA C = -11.5		ALPHA S = -8 CL/SIG = 0.059 THETA = 8 CQ/SIG = 0.0038 ALPHA C = -13.2	
FLAPPING		LAGGING		FLAPPING	
A0 2.238	A0 1.272	A0 0.003	B1 -0.015	A0 3.365	A0 2.225
A1 -0.010	A1 0.399	A1 0.003	B2 0.002	A1 -0.381	B1 0.012
A2 -0.295	A2 -0.164	A2 -0.008	B3 0.002	A2 -0.473	B2 0.012
A3 0.127	A3 -0.199	A3 0.008	B4 0.002	A3 0.174	B3 0.010
A4 0.087	A4 0.022	A4 0.002	B5 0.001	A4 0.083	B4 0.007
A5 0.022	A5 -0.001	A5 0.003	B6 0.001	A5 0.032	B5 0.002
A6 0.017	A6 0.008	A6 -0.001	B7 0.002	A6 0.017	B6 0.002
A7 -0.019	A7 0.031	A7 -0.001	B8 0.001	A7 -0.022	B7 -0.001
A8 -0.001	A8 0.003	A8 -0.001	B9 0.001	A8 -0.001	B8 0.001
A9 0.006	A9 0.006	A9 -0.001	B10 0.001	A9 0.005	B9 0.002
A10 -0.002	A10 0.020	A10 0.001	B10 -0.001	A10 -0.015	B10 0.025
ALPHA S = -8 CL/SIG = 0.069 THETA = 10 CQ/SIG = 0.0061 ALPHA C = -14.8		ALPHA S = -8 CL/SIG = 0.078 THETA = 11 CQ/SIG = 0.0079 ALPHA C = -15.7		ALPHA S = -8 CL/SIG = 0.078 THETA = 11 CQ/SIG = 0.0079 ALPHA C = -15.7	
FLAPPING		LAGGING		FLAPPING	
A0 4.269	A0 3.523	A0 -0.215	B1 0.092	A0 4.634	A0 4.314
A1 0.309	A1 0.125	A1 -0.215	B2 0.028	A1 0.710	A1 -0.302
A2 -0.652	A2 -0.352	A2 -0.215	B3 0.025	A2 -0.762	A2 -0.302
A3 0.223	A3 -0.216	A3 0.051	B4 0.016	A3 0.280	A3 0.054
A4 0.060	A4 0.105	A4 -0.006	B5 0.008	A4 0.078	A4 -0.009
A5 0.025	A5 0.032	A5 -0.001	B6 0.005	A5 0.048	A5 0.003
A6 -0.005	A6 0.040	A6 0.023	B7 0.004	A6 -0.012	A6 -0.001
A7 -0.029	A7 0.037	A7 -0.001	B8 0.002	A7 -0.022	A7 0.005
A8 0.002	A8 0.007	A8 -0.001	B9 0.002	A8 0.001	A8 -0.001
A9 0.007	A9 0.014	A9 -0.001	B10 0.004	A9 0.007	A9 -0.003
A10 -0.021	A10 0.028	A10 0.001	B10 0.002	A10 -0.007	A10 0.006

TABLE I CONTINUED.

ADVANCE RATIO = 0.389			ALPHA 3 = 0 CL/SIG = -0.004 ALPHA C = 4.0 CC/SIG = 0.0003 ALPHA C = 4.0			ALPHA 3 = 0 CL/SIG = 0.017 ALPHA C = 3.0 CC/SIG = -0.0004 ALPHA C = 3.0			ALPHA 5 = 0 CL/SIG = 0.039 ALPHA C = 1.2 CC/SIG = -0.0006 ALPHA C = 1.2		
FLAPPING			LAGGING			LAGGING			FLAPPING		
A0	0.128	0.021	A0	2.333	0.074	A0	1.166	0.083	A0	2.131	0.089
A1	0.097	0.011	A1	0.048	0.074	A1	0.088	0.003	A1	0.044	0.132
A2	0.027	0.001	A2	0.001	0.074	A2	0.244	0.001	A2	0.030	0.044
A3	0.031	0.001	A3	0.001	0.074	A3	0.030	0.001	A3	0.031	0.135
A4	0.031	0.001	A4	0.001	0.074	A4	0.031	0.001	A4	0.031	0.135
A5	0.031	0.001	A5	0.001	0.074	A5	0.031	0.001	A5	0.031	0.135
A6	0.031	0.001	A6	0.001	0.074	A6	0.031	0.001	A6	0.031	0.135
A7	0.031	0.001	A7	0.001	0.074	A7	0.031	0.001	A7	0.031	0.135
A8	0.031	0.001	A8	0.001	0.074	A8	0.031	0.001	A8	0.031	0.135
A9	0.031	0.001	A9	0.001	0.074	A9	0.031	0.001	A9	0.031	0.135
A10	0.031	0.001	A10	0.001	0.074	A10	0.031	0.001	A10	0.031	0.135
ALPHA 5 = 0 CL/SIG = 0.031 ALPHA C = 2 CC/SIG = -0.0002 ALPHA C = -0.5			ALPHA 5 = 0 CL/SIG = 0.031 ALPHA C = 2 CC/SIG = 0.0002 ALPHA C = -1.7			ALPHA 5 = 0 CL/SIG = 0.031 ALPHA C = 2 CC/SIG = 0.0002 ALPHA C = -1.7			ALPHA 5 = 0 CL/SIG = 0.031 ALPHA C = 2 CC/SIG = 0.0002 ALPHA C = -1.7		
FLAPPING			LAGGING			LAGGING			FLAPPING		
A0	0.176	0.120	A0	2.200	0.093	A0	3.363	0.150	A0	0.390	0.160
A1	0.281	0.025	A1	0.025	0.093	A1	0.023	0.150	A1	0.043	0.160
A2	0.291	0.025	A2	0.025	0.093	A2	0.023	0.150	A2	0.043	0.160
A3	0.018	0.025	A3	0.025	0.093	A3	0.051	0.150	A3	0.078	0.160
A4	0.018	0.025	A4	0.025	0.093	A4	0.051	0.150	A4	0.078	0.160
A5	0.018	0.025	A5	0.025	0.093	A5	0.051	0.150	A5	0.078	0.160
A6	0.018	0.025	A6	0.025	0.093	A6	0.051	0.150	A6	0.078	0.160
A7	0.018	0.025	A7	0.025	0.093	A7	0.051	0.150	A7	0.078	0.160
A8	0.018	0.025	A8	0.025	0.093	A8	0.051	0.150	A8	0.078	0.160
A9	0.018	0.025	A9	0.025	0.093	A9	0.051	0.150	A9	0.078	0.160
A10	0.021	0.021	A10	0.021	0.093	A10	0.024	0.150	A10	0.024	0.160
ALPHA 5 = 0 CL/SIG = 0.010 ALPHA C = 0 CC/SIG = 0.0001 ALPHA C = -1.9			ALPHA 5 = 0 CL/SIG = 0.010 ALPHA C = 0 CC/SIG = 0.0001 ALPHA C = -1.9			ALPHA 5 = 0 CL/SIG = 0.010 ALPHA C = 0 CC/SIG = 0.0001 ALPHA C = -1.9			ALPHA 5 = 0 CL/SIG = 0.010 ALPHA C = 0 CC/SIG = 0.0001 ALPHA C = -1.9		
FLAPPING			LAGGING			LAGGING			FLAPPING		
A0	0.024	0.004	A0	2.310	0.075	A0	1.663	0.183	A0	2.034	0.173
A1	0.130	0.004	A1	0.071	0.075	A1	0.160	0.183	A1	0.045	0.173
A2	0.115	0.004	A2	0.005	0.075	A2	0.084	0.183	A2	0.045	0.173
A3	0.082	0.004	A3	0.004	0.075	A3	0.084	0.183	A3	0.045	0.173
A4	0.098	0.004	A4	0.002	0.075	A4	0.120	0.183	A4	0.104	0.173
A5	0.013	0.004	A5	0.002	0.075	A5	0.004	0.183	A5	0.004	0.173
A6	0.001	0.004	A6	0.001	0.075	A6	0.004	0.183	A6	0.004	0.173
A7	0.001	0.004	A7	0.001	0.075	A7	0.001	0.183	A7	0.001	0.173
A8	0.001	0.004	A8	0.001	0.075	A8	0.001	0.183	A8	0.001	0.173
A9	0.001	0.004	A9	0.001	0.075	A9	0.001	0.183	A9	0.001	0.173
A10	0.025	0.004	A10	0.003	0.075	A10	0.038	0.183	A10	0.004	0.173

TABLE I CONTINUED.

ADVANCE RATIO = 0.500		
ALPHA 5 = 0 CL/SIG = 0.045 THETA = 4 COSIG = 0.0026 ALPHA C = -7.1		
FLAPPING	LAGGING	
AQ 3-921	AQ 3-755	
A1 -0.017	A1 -0.115	01 0.031
A2 -0.057	A2 -0.315	A2 -0.025
A3 -0.132	A3 -0.452	A3 -0.035
A4 -0.144	A4 -0.504	A4 -0.016
A5 -0.024	A5 -0.056	A5 -0.004
A6 -0.021	A6 -0.070	A6 -0.001
A7 -0.023	A7 -0.022	A7 -0.005
A8 -0.022	A8 -0.001	A8 -0.001
A9 -0.033	A9 -0.042	A9 -0.001
A10 -0.032	A10 -0.021	A10 -0.001
ALPHA 5 = -4 CL/SIG = -0.004 THETA = 4 COSIG = 0.0022 ALPHA C = -9.2		
FLAPPING	LAGGING	
AQ 2-754	AQ 3-575	
A1 -0.278	A1 -0.147	01 0.001
A2 -0.442	A2 -0.389	A2 -0.009
A3 -0.111	A3 -0.385	A3 -0.008
A4 -0.124	A4 -0.040	A4 -0.004
A5 -0.024	A5 -0.026	A5 -0.001
A6 -0.006	A6 -0.006	A6 -0.002
A7 -0.031	A7 -0.004	A7 -0.002
A8 -0.031	A8 -0.012	A8 -0.001
A9 -0.008	A9 -0.020	A9 -0.001
A10 -0.018	A10 -0.015	A10 -0.001
ALPHA 5 = 0 CL/SIG = 0.040 THETA = 8 COSIG = 0.0041 ALPHA C = -11.5		
FLAPPING	LAGGING	
AQ 5-540	AQ 4-542	
A1 -0.071	A1 -0.019	01 0.057
A2 -0.075	A2 -0.041	A2 -0.020
A3 -0.248	A3 -0.502	A3 -0.019
A4 -0.104	A4 -0.107	A4 -0.002
A5 -0.052	A5 -0.040	A5 -0.001
A6 -0.006	A6 -0.005	A6 -0.001
A7 -0.007	A7 -0.007	A7 -0.002
A8 -0.007	A8 -0.040	A8 -0.004
A9 -0.022	A9 -0.037	A9 -0.001
A10 -0.017	A10 -0.010	A10 -0.001
ALPHA 5 = -8 CL/SIG = -0.007 THETA = 8 COSIG = 0.0063 ALPHA C = -10.6		
FLAPPING	LAGGING	
AQ -0.019	AQ -0.128	01 2-755
A1 -0.024	A1 -0.340	A1 -0.003
A2 -0.114	A2 -0.154	A2 -0.002
A3 -0.100	A3 -0.015	A3 -0.003
A4 -0.073	A4 -0.015	A4 -0.003
A5 -0.018	A5 -0.021	A5 -0.001
A6 -0.004	A6 -0.005	A6 -0.001
A7 -0.014	A7 -0.021	A7 -0.001
A8 -0.001	A8 -0.004	A8 -0.001
A9 -0.005	A9 -0.004	A9 -0.001
A10 -0.016	A10 -0.016	A10 -0.001
ALPHA 5 = -4 CL/SIG = -0.025 THETA = 2 COSIG = 0.0010 ALPHA C = -7.9		
FLAPPING	LAGGING	
AQ 1-607	AQ 2-913	
A1 -0.109	01 0.075	A1 -0.028
A2 -0.173	A2 -0.350	A2 -0.003
A3 -0.115	A3 -0.220	A3 -0.008
A4 -0.120	A4 -0.014	A4 -0.003
A5 -0.021	A5 -0.024	A5 -0.003
A6 -0.009	A6 -0.004	A6 -0.001
A7 -0.018	A7 -0.019	A7 -0.001
A8 -0.001	A8 -0.014	A8 -0.002
A9 -0.004	A9 -0.012	A9 -0.001
A10 -0.029	A10 -0.008	A10 -0.001

TABLE I CONTINUED.

ADVANCE RATIO = 0.389			
ALPHA S = -8 CL/SIG = 0.018 7ME7A = 6 CO/SIG = 0.0015 ALPHA C = -12.6		ALPHA S = -8 CL/SIG = 0.027 7ME7A = 7 CO/SIG = 0.0022 ALPHA C = -13.5	
FLAPPING A0 0.183 A1 0.127 A2 -0.294 A3 0.111 A4 0.093 A5 0.044 A6 0.001 A7 0.025 A8 0.004 A9 0.005 A10 -0.008		FLAPPING A0 1.454 A1 0.056 A2 -0.393 A3 0.125 A4 0.100 A5 0.047 A6 0.007 A7 0.020 A8 0.006 A9 -0.001 A10 -0.011	
LAGGING A0 3.267 A1 0.025 A2 0.001 A3 0.007 A4 0.008 A5 0.002 A6 -0.001 A7 0.001 A8 -0. A9 0.001 A10 0.001		LAGGING A0 3.675 A1 -0.012 A2 -0.006 A3 0.008 A4 0.009 A5 0.002 A6 0.002 A7 -0. A8 -0.002 A9 0.001 A10 -0.	
A1 -0.088 A2 -0.311 A3 -0.253 A4 -0.006 A5 0.006 A6 0.006 A7 0.008 A8 0.007 A9 0.009 A10 0.008		A1 -0.077 A2 -0.31A A3 -0.309 A4 -0.007 A5 0.004 A6 0.010 A7 -0.009 A8 0.007 A9 0.006 A10 0.008	
B1 -0.027 B2 0.005 B3 -0.010 B4 0.004 B5 -0. B6 -0.001 B7 0.001 B8 -0.001 B9 0.001 B10 -0.		B1 -0.010 B2 -0.003 B3 -0.008 B4 0.003 B5 0.001 B6 0.001 B7 -0. B8 -0.001 B9 0.001 B10 -0.	
ALPHA S = -8 CL/SIG = 0.038 7ME7A = 8 CO/SIG = 0.0032 ALPHA C = -14.6		ALPHA S = -8 CL/SIG = 0.046 7ME7A = 9 CO/SIG = 0.0042 ALPHA C = -15.1	
FLAPPING A0 2.073 A1 -0.037 A2 -0.535 A3 0.170 A4 0.095 A5 0.061 A6 0.003 A7 0.029 A8 0.008 A9 -0. A10 0.001		FLAPPING A0 2.304 A1 -0.009 A2 -0.437 A3 0.203 A4 0.104 A5 0.077 A6 0.007 A7 0.030 A8 0.005 A9 -0.003 A10 0.007	
LAGGING A0 4.209 A1 -0.067 A2 -0. A3 0.021 A4 0.009 A5 0.001 A6 -0. A7 -0. A8 -0. A9 -0.001 A10 0.001		LAGGING A0 4.707 A1 -0.114 A2 -0.002 A3 0.035 A4 0.027 A5 0.001 A6 -0. A7 0.001 A8 0.013 A9 -0.001 A10 0.003	
A1 -0.145 A2 -0.323 A3 -0.378 A4 0.013 A5 0.006 A6 0.014 A7 -0.002 A8 0.013 A9 0.010 A10 0.001		A1 -0.223 A2 -0.363 A3 -0.440 A4 0.027 A5 -0.005 A6 0.024 A7 -0.012 A8 0.013 A9 0.008 A10 0.003	
B1 0.011 B2 0.008 B3 -0.010 B4 0.009 B5 0.001 B6 -0. B7 -0.001 B8 -0.001 B9 0.002 B10 -0.001		B1 0.038 B2 0.005 B3 -0.015 B4 0.012 B5 0.003 B6 0.001 B7 -0.002 B8 -0.002 B9 -0. B10 0.001	

TABLE I CONTINUED.

ADVANCE MATIC = 0.488			
ALPHA 5 = 0 CL/SIG = 0.003 THETA = -2 CO/SIG = 0.0001 ALPHA C = 0.0	ALPHA 5 = 0 CL/SIG = 0.015 THETA = 0 CO/SIG = 0.0000 ALPHA C = -1.0	ALPHA 5 = 0 CL/SIG = 0.033 THETA = 2 CO/SIG = 0.0001 ALPHA C = -3.5	
FLAPPING A0 0.163 A1 -0.348 A2 -0.385 A3 0.084 A4 0.014 A5 -0.014 A6 -0.041 A7 -0.021 A8 -0.014 A9 -0.005 A10 -0.005	FLAPPING A0 0.783 A1 -0.048 A2 -0.144 A3 0.053 A4 0.010 A5 -0.003 A6 -0.003 A7 0.003 A8 -0.013 A9 -0.002 A10 -0.003	FLAPPING A0 1.726 A1 -0.406 A2 -0.115 A3 0.012 A4 0.000 A5 0.024 A6 -0.007 A7 -0.020 A8 -0.014 A9 -0.003 A10 -0.016	LAGGING A0 2.337 A1 0.007 A2 -0.020 A3 0.007 A4 0.000 A5 0.000 A6 0.000 A7 0.000 A8 0.000 A9 0.000 A10 0.000
ALPHA 5 = 0 CL/SIG = 0.003 THETA = 4 CO/SIG = 0.0000 ALPHA C = -5.0	ALPHA 5 = 0 CL/SIG = 0.022 THETA = 0 CO/SIG = 0.0002 ALPHA C = -7.5	ALPHA 5 = 0 CL/SIG = 0.070 THETA = 8 CO/SIG = 0.0042 ALPHA C = -9.0	
FLAPPING A0 2.373 A1 -0.382 A2 -0.400 A3 0.084 A4 0.014 A5 -0.014 A6 -0.041 A7 -0.021 A8 -0.014 A9 -0.005 A10 -0.005	FLAPPING A0 5.078 A1 -0.078 A2 -0.144 A3 0.053 A4 0.010 A5 -0.003 A6 -0.003 A7 0.003 A8 -0.013 A9 -0.002 A10 -0.003	FLAPPING A0 3.873 A1 -0.340 A2 -0.140 A3 0.078 A4 0.024 A5 0.050 A6 -0.041 A7 -0.041 A8 0.024 A9 -0.001 A10 -0.024	LAGGING A0 4.283 A1 0.036 A2 -0.055 A3 0.001 A4 0.001 A5 0.001 A6 0.001 A7 0.001 A8 0.001 A9 0.001 A10 0.001
ALPHA 5 = 0 CL/SIG = 0.000 THETA = 10 CO/SIG = 0.0046 ALPHA C = -11.7	ALPHA 5 = 0 CL/SIG = 0.005 THETA = 11 CO/SIG = 0.0077 ALPHA C = -12.8	ALPHA 5 = 0 CL/SIG = 0.008 THETA = 0 CO/SIG = 0.0001 ALPHA C = -4.0	
FLAPPING A0 4.264 A1 0.014 A2 -0.044 A3 0.027 A4 0.014 A5 -0.014 A6 -0.041 A7 -0.021 A8 -0.014 A9 -0.005 A10 -0.005	FLAPPING A0 4.553 A1 -0.460 A2 -1.144 A3 0.363 A4 0.075 A5 0.072 A6 0.072 A7 0.072 A8 0.072 A9 0.072 A10 0.072	FLAPPING A0 -0.016 A1 -0.460 A2 -0.310 A3 0.035 A4 0.035 A5 0.035 A6 0.035 A7 0.035 A8 0.035 A9 0.035 A10 0.035	LAGGING A0 2.543 A1 0.135 A2 -0.002 A3 0.004 A4 0.004 A5 0.004 A6 0.004 A7 0.004 A8 0.004 A9 0.004 A10 0.004

TABLE I CONTINUED.

GOVANCE RATIO = 0.400		
<p>ALPHA S = -4 CL/SIG = 0.003 TMEYA = 2 CO/SIG = 0.0004 ALPHA C = -3.9</p>		
FLAPPING	LAGGING	
A0 0.114	A0 2.373	
A1 -0.114	A1 -0.131	
A2 -0.081	A2 -0.097	
A3 0.070	A3 -0.097	
A4 0.014	A4 -0.013	
A5 0.014	A5 -0.013	
A6 -0.014	A6 -0.021	
A7 -0.014	A7 -0.021	
A8 -0.002	A8 -0.004	
A9 0.002	A9 0.004	
A10 0.013	A10 0.021	
FLAPPING	LAGGING	
A0 0.114	A0 2.373	
A1 -0.114	A1 -0.131	
A2 -0.081	A2 -0.097	
A3 0.070	A3 -0.097	
A4 0.014	A4 -0.013	
A5 0.014	A5 -0.013	
A6 -0.014	A6 -0.021	
A7 -0.014	A7 -0.021	
A8 -0.002	A8 -0.004	
A9 0.002	A9 0.004	
A10 0.013	A10 0.021	
<p>ALPHA S = -4 CL/SIG = 0.008 TMEYA = 8 CO/SIG = 0.0034 ALPHA C = -11.9</p>		
FLAPPING	LAGGING	
A0 2.318	A0 1.500	
A1 -0.248	A1 -0.011	
A2 -0.925	A2 -0.027	
A3 0.109	A3 -0.027	
A4 0.109	A4 -0.027	
A5 0.109	A5 -0.027	
A6 0.039	A6 -0.036	
A7 -0.032	A7 -0.071	
A8 0.014	A8 -0.009	
A9 0.006	A9 0.019	
A10 -0.016	A10 0.008	
<p>ALPHA S = -4 CL/SIG = 0.073 TMEYA = 13 CO/SIG = 0.0099 ALPHA C = -16.8</p>		
FLAPPING	LAGGING	
A0 3.112	A0 1.009	
A1 -0.114	A1 -0.002	
A2 -1.242	A2 -0.971	
A3 0.423	A3 -0.932	
A4 0.263	A4 -0.168	
A5 0.131	A5 -0.023	
A6 -0.004	A6 -0.104	
A7 -0.010	A7 -0.249	
A8 0.033	A8 -0.038	
A9 -0.017	A9 0.017	
A10 0.004	A10 -0.031	
<p>ALPHA S = -4 CL/SIG = 0.030 TMEYA = 6 CO/SIG = 0.0019 ALPHA C = -9.9</p>		
FLAPPING	LAGGING	
A0 1.738	A0 0.039	
A1 -0.137	A1 -0.007	
A2 -0.137	A2 -0.007	
A3 0.033	A3 -0.072	
A4 0.122	A4 -0.076	
A5 0.041	A5 -0.043	
A6 0.007	A6 -0.007	
A7 -0.011	A7 -0.019	
A8 0.013	A8 -0.008	
A9 0.004	A9 0.013	
A10 -0.019	A10 0.018	
<p>ALPHA S = -4 CL/SIG = 0.070 TMEYA = 12 CO/SIG = 0.0080 ALPHA C = -15.6</p>		
FLAPPING	LAGGING	
A0 3.212	A0 0.017	
A1 -0.137	A1 -0.017	
A2 -1.119	A2 -0.031	
A3 0.113	A3 -0.021	
A4 0.272	A4 -0.084	
A5 0.148	A5 -0.043	
A6 0.023	A6 -0.043	
A7 0.024	A7 -0.198	
A8 0.042	A8 0.033	
A9 -0.011	A9 0.026	
A10 -0.009	A10 -0.033	
<p>ALPHA S = -8 CL/SIG = 0.010 TMEYA = 6 CO/SIG = 0.0011 ALPHA C = -12.2</p>		
FLAPPING	LAGGING	
A0 0.311	A0 0.028	
A1 -0.232	A1 -0.000	
A2 -0.232	A2 -0.240	
A3 0.073	A3 -0.014	
A4 0.073	A4 -0.027	
A5 0.038	A5 -0.027	
A6 0.003	A6 -0.024	
A7 0.049	A7 0.000	
A8 0.011	A8 0.008	
A9 0.010	A9 0.007	
A10 0.011	A10 0.018	

TABLE I CONTINUED.

ADVANCE RATIO = 0.400			ALPHA S = -8 CL/SIG = 0.021 THETA = 0 CO/SIG = 0.0023 ALPHA C = -14.8			ALPHA S = -8 CL/SIG = 0.039 THETA = 10 CO/SIG = 0.0043 ALPHA C = -16.1			ALPHA S = -8 CL/SIG = 0.050 THETA = 12 CO/SIG = 0.0067 ALPHA C = -18.2		
FLAPPING			LAGGING			FLAPPING			LAGGING		
A0	1.036	0.074	A0	-1.184	0.010	A0	2.034	0.036	A0	2.408	0.198
A1	0.131	0.076	A1	0.010	0.010	A1	-0.473	0.038	A1	-0.270	0.197
A2	0.443	0.328	A2	0.002	0.001	A2	-0.721	0.038	A2	-0.968	0.389
A3	0.101	0.035	A3	0.022	0.035	A3	-0.152	0.038	A3	-0.152	0.038
A4	0.123	0.040	A4	0.022	0.035	A4	0.163	0.037	A4	0.172	0.037
A5	0.012	0.030	A5	-0.004	0.033	A5	-0.112	0.037	A5	-0.112	0.037
A6	0.013	0.002	A6	-0.004	0.033	A6	0.004	0.037	A6	0.004	0.037
A7	0.013	0.002	A7	-0.004	0.033	A7	0.004	0.037	A7	0.004	0.037
A8	0.013	0.002	A8	-0.004	0.033	A8	0.004	0.037	A8	0.004	0.037
A9	0.013	0.002	A9	-0.004	0.033	A9	0.004	0.037	A9	0.004	0.037
A10	0.002	0.011	A10	0.002	0.033	A10	0.002	0.033	A10	0.002	0.033
ZERO LAG DAMPING			ZERO LAG DAMPING			ZERO LAG DAMPING			ZERO LAG DAMPING		
ALPHA S = -8 CL/SIG = 0.022 THETA = 0 CO/SIG = 0.0017 ALPHA C = -10.8			ALPHA S = -8 CL/SIG = 0.042 THETA = 10 CO/SIG = 0.0056 ALPHA C = -19.8			ALPHA S = -8 CL/SIG = 0.007 THETA = 2 CO/SIG = 0.0002 ALPHA C = -8.4			ALPHA S = -8 CL/SIG = 0.010 THETA = 4 CO/SIG = 0.0009 ALPHA C = -8.4		
FLAPPING			LAGGING			FLAPPING			LAGGING		
A0	1.483	0.024	A0	2.428	0.012	A0	0.132	0.034	A0	1.013	0.359
A1	0.134	0.024	A1	0.011	0.012	A1	-0.440	0.034	A1	-0.950	0.197
A2	0.502	0.379	A2	0.014	0.012	A2	0.003	0.034	A2	-0.249	0.389
A3	0.045	0.035	A3	0.012	0.035	A3	0.093	0.034	A3	0.045	0.035
A4	0.123	0.040	A4	0.012	0.035	A4	0.025	0.034	A4	0.025	0.035
A5	0.012	0.030	A5	-0.004	0.033	A5	-0.112	0.034	A5	-0.112	0.037
A6	0.013	0.002	A6	-0.004	0.033	A6	0.004	0.034	A6	0.004	0.037
A7	0.013	0.002	A7	-0.004	0.033	A7	0.004	0.034	A7	0.004	0.037
A8	0.013	0.002	A8	-0.004	0.033	A8	0.004	0.034	A8	0.004	0.037
A9	0.013	0.002	A9	-0.004	0.033	A9	0.004	0.034	A9	0.004	0.037
A10	0.002	0.011	A10	0.002	0.033	A10	0.002	0.033	A10	0.002	0.033
ZERO LAG DAMPING			ZERO LAG DAMPING			ZERO LAG DAMPING			ZERO LAG DAMPING		
ALPHA S = -8 CL/SIG = 0.022 THETA = 0 CO/SIG = 0.0017 ALPHA C = -10.8			ALPHA S = -8 CL/SIG = 0.042 THETA = 10 CO/SIG = 0.0056 ALPHA C = -19.8			ALPHA S = -8 CL/SIG = 0.007 THETA = 2 CO/SIG = 0.0002 ALPHA C = -8.4			ALPHA S = -8 CL/SIG = 0.010 THETA = 4 CO/SIG = 0.0009 ALPHA C = -8.4		
FLAPPING			LAGGING			FLAPPING			LAGGING		
A0	1.483	0.024	A0	2.428	0.012	A0	0.132	0.034	A0	1.013	0.359
A1	0.134	0.024	A1	0.011	0.012	A1	-0.440	0.034	A1	-0.950	0.197
A2	0.502	0.379	A2	0.014	0.012	A2	0.003	0.034	A2	-0.249	0.389
A3	0.045	0.035	A3	0.012	0.035	A3	0.093	0.034	A3	0.045	0.035
A4	0.123	0.040	A4	0.012	0.035	A4	0.025	0.034	A4	0.025	0.035
A5	0.012	0.030	A5	-0.004	0.033	A5	-0.112	0.034	A5	-0.112	0.037
A6	0.013	0.002	A6	-0.004	0.033	A6	0.004	0.034	A6	0.004	0.037
A7	0.013	0.002	A7	-0.004	0.033	A7	0.004	0.034	A7	0.004	0.037
A8	0.013	0.002	A8	-0.004	0.033	A8	0.004	0.034	A8	0.004	0.037
A9	0.013	0.002	A9	-0.004	0.033	A9	0.004	0.034	A9	0.004	0.037
A10	0.002	0.011	A10	0.002	0.033	A10	0.002	0.033	A10	0.002	0.033

TABLE I CONTINUED.

ADVANCE RATIO = 0.005		
<p>ALPHA 3 = A CL/316 = 0.008 THETA = -7 CO/316 = -0.0002 ALPHA C = 7.1</p> <p>FLAPPING</p> <p>AO 0.037 01 0.087 A1 -0. 01 -0. A2 0.026 02 -1.468 A2 -0. 02 -0. A3 0.022 03 0.103 A3 -0. 03 -0. A4 0.006 04 0.086 A4 -0. 04 -0. A5 0.112 05 0.026 A5 -0. 05 -0. A6 0.004 06 0.016 A6 -0. 06 -0. A7 0.214 07 0.031 A7 -0. 07 -0. A8 0.042 08 0.031 A8 -0. 08 -0. A9 0.042 09 0.019 A9 -0. 09 -0. A10 0.008 10 0.009 A10 -0. 10 -0.</p>	<p>ALPHA 3 = A CL/316 = 0.015 THETA = -9 CO/316 = -0.0004 ALPHA C = 9.0</p> <p>FLAPPING</p> <p>AO 0.208 01 -0.125 A1 -0. 01 -0. A2 0.226 02 -1.410 A2 -0. 02 -0. A3 0.047 03 0.068 A3 -0. 03 -0. A4 0.113 04 0.011 A4 -0. 04 -0. A5 0.113 05 0.011 A5 -0. 05 -0. A6 0.113 06 0.011 A6 -0. 06 -0. A7 0.214 07 0.031 A7 -0. 07 -0. A8 0.042 08 0.031 A8 -0. 08 -0. A9 0.042 09 0.019 A9 -0. 09 -0. A10 0.008 10 0.009 A10 -0. 10 -0.</p>	<p>ALPHA 9 = A CL/316 = 0.021 THETA = -4 CO/316 = -0.0004 ALPHA C = 3.7</p> <p>FLAPPING</p> <p>AO 0.443 01 -0.092 A1 -0. 01 -0. A2 0.208 02 -1.351 A2 -0. 02 -0. A3 0.098 03 0.010 A3 -0. 03 -0. A4 0.079 04 0.031 A4 -0. 04 -0. A5 0.031 05 0.009 A5 -0. 05 -0. A6 0.031 06 0.009 A6 -0. 06 -0. A7 0.031 07 0.009 A7 -0. 07 -0. A8 0.031 08 0.011 A8 -0. 08 -0. A9 0.031 09 0.009 A9 -0. 09 -0. A10 0.010 10 0.001 A10 -0. 10 -0.</p>
<p>ALPHA 5 = A CL/316 = 0.031 THETA = -2 CO/316 = -0.0007 ALPHA C = 1.4</p> <p>FLAPPING</p> <p>AO 1.093 01 0.003 A1 -0. 01 -0. A2 0.104 02 -1.222 A2 -0. 02 -0. A3 0.094 03 0.390 A3 -0. 03 -0. A4 0.024 04 0.098 A4 -0. 04 -0. A5 0.021 05 0.021 A5 -0. 05 -0. A6 0.021 06 0.001 A6 -0. 06 -0. A7 0.013 07 0.048 A7 -0. 07 -0. A8 0.012 08 0.019 A8 -0. 08 -0. A9 0.012 09 0.008 A9 -0. 09 -0. A10 0.013 10 0.008 A10 -0. 10 -0.</p>	<p>ALPHA 3 = A CL/316 = 0.059 THETA = -0 CO/316 = -0.0009 ALPHA C = -0.8</p> <p>FLAPPING</p> <p>AO 1.404 01 0.109 A1 -0. 01 -0. A2 0.421 02 -1.198 A2 -0. 02 -0. A3 0.180 03 0.809 A3 -0. 03 -0. A4 0.098 04 0.210 A4 -0. 04 -0. A5 0.074 05 0.025 A5 -0. 05 -0. A6 0.026 06 0.028 A6 -0. 06 -0. A7 0.094 07 0.078 A7 -0. 07 -0. A8 0.003 08 0.028 A8 -0. 08 -0. A9 0.004 09 0.017 A9 -0. 09 -0. A10 0.002 10 0.011 A10 -0. 10 -0.</p>	<p>ALPHA 3 = A CL/316 = 0.030 THETA = 2 CO/316 = -0.0001 ALPHA C = -3.1</p> <p>FLAPPING</p> <p>AO 2.044 01 0.062 A1 -0. 01 -0. A2 0.449 02 -1.022 A2 -0. 02 -0. A3 0.249 03 0.489 A3 -0. 03 -0. A4 0.040 04 0.221 A4 -0. 04 -0. A5 0.044 05 0.032 A5 -0. 05 -0. A6 0.029 06 0.042 A6 -0. 06 -0. A7 0.030 07 0.062 A7 -0. 07 -0. A8 0.041 08 0.012 A8 -0. 08 -0. A9 0.041 09 0.012 A9 -0. 09 -0. A10 0.002 10 0.009 A10 -0. 10 -0.</p>
<p>ALPHA 5 = A CL/316 = 0.022 THETA = 4 CO/316 = 0.0009 ALPHA C = -9.3</p> <p>FLAPPING</p> <p>AO 2.252 01 0.046 A1 -0. 01 -0. A2 0.924 02 0.987 A2 -0. 02 -0. A3 0.251 03 0.084 A3 -0. 03 -0. A4 0.022 04 0.568 A4 -0. 04 -0. A5 0.044 05 0.022 A5 -0. 05 -0. A6 0.001 06 0.058 A6 -0. 06 -0. A7 0.031 07 0.052 A7 -0. 07 -0. A8 0.019 08 0.010 A8 -0. 08 -0. A9 0.004 09 0.007 A9 -0. 09 -0. A10 0.013 10 0.009 A10 -0. 10 -0.</p>	<p>ALPHA 5 = A CL/316 = 0.042 THETA = -7.6 CO/316 = 0.0020 ALPHA C = -7.6</p> <p>FLAPPING</p> <p>AO 2.764 01 -0.041 A1 -0. 01 -0. A2 1.259 02 -1.092 A2 -0. 02 -0. A3 0.251 03 1.000 A3 -0. 03 -0. A4 0.193 04 0.598 A4 -0. 04 -0. A5 0.021 05 0.017 A5 -0. 05 -0. A6 0.012 06 0.031 A6 -0. 06 -0. A7 0.037 07 0.026 A7 -0. 07 -0. A8 0.012 08 0.056 A8 -0. 08 -0. A9 0.003 09 0.020 A9 -0. 09 -0. A10 0.006 10 0.024 A10 -0. 10 -0.</p>	<p>ALPHA 3 = 0 CL/316 = 0.004 THETA = -2 CO/316 = 0.0009 ALPHA C = -0.4</p> <p>FLAPPING</p> <p>AO 0.107 01 0.044 A1 -0. 01 -0. A2 0.292 02 -1.071 A2 -0. 02 -0. A3 0.054 03 0.098 A3 -0. 03 -0. A4 0.122 04 0.015 A4 -0. 04 -0. A5 0.169 05 0.002 A5 -0. 05 -0. A6 0. 06 0.023 A6 -0. 06 -0. A7 0.041 07 0.008 A7 -0. 07 -0. A8 0.003 08 0.027 A8 -0. 08 -0. A9 0.014 09 0.312 A9 -0. 09 -0. A10 0.007 10 0.002 A10 -0. 10 -0.</p>

TABLE I CONTINUED.

ADVANCE RATIO = 0.003			ADVANCE RATIO = 0.003			ADVANCE RATIO = 0.003		
ALPHA 3 = 0 CL/SIG = 0.010 THETA = 0 CO/SIG = 0.0005 ALPHA C = -2.5			ALPHA 3 = 0 CL/SIG = 0.010 THETA = 2 CO/SIG = 0.0005 ALPHA C = -4.7			ALPHA 3 = 0 CL/SIG = 0.020 THETA = 4 CO/SIG = 0.0008 ALPHA C = -7.0		
FLAPPING	LAGGING		FLAPPING	LAGGING		FLAPPING	LAGGING	
A0 0.000	A0 -0.0		A0 0.000	A0 -0.0		A0 0.000	A0 -0.0	
A1 0.000	A1 -0.0		A1 0.000	A1 -0.0		A1 0.000	A1 -0.0	
A2 0.000	A2 -0.0		A2 0.000	A2 -0.0		A2 0.000	A2 -0.0	
A3 0.000	A3 -0.0		A3 0.000	A3 -0.0		A3 0.000	A3 -0.0	
A4 0.000	A4 -0.0		A4 0.000	A4 -0.0		A4 0.000	A4 -0.0	
A5 0.000	A5 -0.0		A5 0.000	A5 -0.0		A5 0.000	A5 -0.0	
A6 0.000	A6 -0.0		A6 0.000	A6 -0.0		A6 0.000	A6 -0.0	
A7 0.000	A7 -0.0		A7 0.000	A7 -0.0		A7 0.000	A7 -0.0	
A8 0.000	A8 -0.0		A8 0.000	A8 -0.0		A8 0.000	A8 -0.0	
A9 0.000	A9 -0.0		A9 0.000	A9 -0.0		A9 0.000	A9 -0.0	
A10 0.000	A10 -0.0		A10 0.000	A10 -0.0		A10 0.000	A10 -0.0	
ALPHA 1 = 0 CL/SIG = 0.004 THETA = 0 CO/SIG = 0.0011 ALPHA C = -9.4			ALPHA 3 = 0 CL/SIG = 0.040 THETA = 8 CO/SIG = 0.0028 ALPHA C = -11.5			ALPHA 3 = 0 CL/SIG = 0.055 THETA = 9 CO/SIG = 0.0035 ALPHA C = -13.7		
FLAPPING	LAGGING		FLAPPING	LAGGING		FLAPPING	LAGGING	
A0 0.000	A0 -0.0		A0 0.000	A0 -0.0		A0 0.000	A0 -0.0	
A1 0.000	A1 -0.0		A1 0.000	A1 -0.0		A1 0.000	A1 -0.0	
A2 0.000	A2 -0.0		A2 0.000	A2 -0.0		A2 0.000	A2 -0.0	
A3 0.000	A3 -0.0		A3 0.000	A3 -0.0		A3 0.000	A3 -0.0	
A4 0.000	A4 -0.0		A4 0.000	A4 -0.0		A4 0.000	A4 -0.0	
A5 0.000	A5 -0.0		A5 0.000	A5 -0.0		A5 0.000	A5 -0.0	
A6 0.000	A6 -0.0		A6 0.000	A6 -0.0		A6 0.000	A6 -0.0	
A7 0.000	A7 -0.0		A7 0.000	A7 -0.0		A7 0.000	A7 -0.0	
A8 0.000	A8 -0.0		A8 0.000	A8 -0.0		A8 0.000	A8 -0.0	
A9 0.000	A9 -0.0		A9 0.000	A9 -0.0		A9 0.000	A9 -0.0	
A10 0.000	A10 -0.0		A10 0.000	A10 -0.0		A10 0.000	A10 -0.0	

TABLE I CONTINUED.

ADVANCE RATIO = 0.83			ALPHA 5 = -4 CL/SIG = -0.007 THETA = 2 CG/SIG = 0.0003 ALPHA C = -6.4			ALPHA 5 = -4 CL/SIG = 0.001 THETA = 4 CG/SIG = 0.0006 ALPHA C = -8.4			ALPHA 5 = -4 CL/SIG = 0.004 THETA = 6 CG/SIG = 0.0009 ALPHA C = -11.0		
FLAPPING			LAGGING			FLAPPING			LAGGING		
A0	-0.047	0.1	0.040	A1	-0.138	0.1	0.124	A0	0.518	0.1	0.001
A1	-0.291	0.2	-0.550	A2	-0.130	0.2	0.002	A1	0.518	0.2	0.073
A2	0.114	0.3	-0.047	A3	0.009	0.3	0.014	A2	0.518	0.3	0.027
A3	0.113	0.4	-0.047	A4	0.025	0.4	-0.018	A3	0.518	0.4	0.008
A4	-0.046	0.5	-0.003	A5	0.025	0.5	0.018	A4	0.518	0.5	0.004
A5	0.132	0.6	-0.018	A6	0.004	0.6	-0.004	A5	0.518	0.6	0.004
A6	-0.002	0.7	0.018	A7	0.004	0.7	0.004	A6	0.518	0.7	0.001
A7	0.011	0.8	-0.043	A8	0.002	0.8	-0.001	A7	0.518	0.8	0.002
A8	0.024	0.9	0.014	A9	0.002	0.9	0.002	A8	0.518	0.9	0.001
A9	0.005	1.0	0.011	A10	0.004	1.0	0.004	A9	0.518	1.0	0.001
A10	0.007	0.10	-0.001	A10	-0.002	0.10	-0.001	A10	0.518	0.10	0.001
FLAPPING			LAGGING			FLAPPING			LAGGING		
A0	1.164	0.1	0.024	A1	0.718	0.1	-0.085	A0	1.021	0.1	0.218
A1	-1.131	0.2	-0.284	A2	0.034	0.2	0.020	A1	1.021	0.2	0.174
A2	-0.474	0.3	-0.704	A3	0.023	0.3	-0.059	A2	1.021	0.3	0.048
A3	0.057	0.4	-0.228	A4	0.109	0.4	-0.004	A3	1.021	0.4	0.059
A4	-0.024	0.5	-0.050	A5	-0.005	0.5	0.003	A4	1.021	0.5	0.150
A5	-0.004	0.6	-0.007	A6	-0.009	0.6	0.003	A5	1.021	0.6	0.010
A6	0.005	0.7	0.044	A7	0.001	0.7	0.003	A6	1.021	0.7	0.015
A7	0.005	0.8	-0.027	A8	0.007	0.8	-0.003	A7	1.021	0.8	0.001
A8	0.004	0.9	-0.009	A9	-0.002	0.9	0.004	A8	1.021	0.9	0.003
A9	0.004	1.0	-0.003	A10	-0.002	1.0	0.003	A9	1.021	1.0	0.001
A10	-0.010	0.10	-0.003	A10	-0.002	0.10	-0.003	A10	1.021	0.10	0.001
FLAPPING			LAGGING			FLAPPING			LAGGING		
A0	1.021	0.1	0.024	A1	0.718	0.1	-0.085	A0	1.021	0.1	0.218
A1	-1.131	0.2	-0.284	A2	0.034	0.2	0.020	A1	1.021	0.2	0.174
A2	-0.474	0.3	-0.704	A3	0.023	0.3	-0.059	A2	1.021	0.3	0.048
A3	0.057	0.4	-0.228	A4	0.109	0.4	-0.004	A3	1.021	0.4	0.059
A4	-0.024	0.5	-0.050	A5	-0.005	0.5	0.003	A4	1.021	0.5	0.150
A5	-0.004	0.6	-0.007	A6	-0.009	0.6	0.003	A5	1.021	0.6	0.010
A6	0.005	0.7	0.044	A7	0.001	0.7	0.003	A6	1.021	0.7	0.015
A7	0.005	0.8	-0.027	A8	0.007	0.8	-0.003	A7	1.021	0.8	0.001
A8	0.004	0.9	-0.009	A9	-0.002	0.9	0.004	A8	1.021	0.9	0.003
A9	0.004	1.0	-0.003	A10	-0.002	1.0	0.003	A9	1.021	1.0	0.001
A10	-0.010	0.10	-0.003	A10	-0.002	0.10	-0.003	A10	1.021	0.10	0.001

TABLE I CONCLUDED.

ADVANCE RATIO = 0.995		
<p>ALPHA S = 0 CL/SIG = -0.009 THETA = 4 CG/SIG = -0.0007 ALPHA C = -8.1</p> <p>FLAPPING</p> <p>A0 -0.345 A1 0.002 A2 -0.398 A3 0.213 A4 0.031 A5 0.048 A6 0.035 A7 0.031 A8 -0.043 A9 -0.018 A10 -0.017</p> <p>B1 0.140 B2 -0.271 B3 -0.383 B4 -0.290 B5 -0.125 B6 0.108 B7 0.019 B8 0.160 B9 0.049 B10 0.031</p> <p>LAGGING</p> <p>A0 2.480 A1 0.181 A2 0.067 A3 0.033 A4 0.042 A5 0.021 A6 -0.009 A7 0.004 A8 -0.003 A9 0.006 A10 0.003</p>	<p>ALPHA S = 0 CL/SIG = -0.006 THETA = 6 CG/SIG = -0.0014 ALPHA C = -10.5</p> <p>FLAPPING</p> <p>A0 -0.266 A1 0.041 A2 -0.601 A3 0.067 A4 0.024 A5 0.448 A6 0.096 A7 0.100 A8 0.006 A9 0.030 A10 -0.001</p> <p>B1 -0.025 B2 -0.015 B3 -0.611 B4 -0.449 B5 0.040 B6 0.171 B7 0.043 B8 0.227 B9 0.079 B10 0.062</p> <p>LAGGING</p> <p>A0 2.061 A1 0.125 A2 0.398 A3 0.053 A4 -0.009 A5 0.031 A6 0.001 A7 0.007 A8 0.009 A9 0.005 A10 0.004</p>	<p>ALPHA S = 0 CL/SIG = -0.004 THETA = 2 CG/SIG = -0.0007 ALPHA C = -5.8</p> <p>FLAPPING</p> <p>A0 -0.092 A1 -0.169 A2 -0.296 A3 0.133 A4 -0.037 A5 0.347 A6 0.082 A7 0.025 A8 0.047 A9 0.005 A10 -0.002</p> <p>B1 -0.138 B2 -0.603 B3 -0.284 B4 -0.110 B5 -0.344 B6 0.079 B7 -0.019 B8 0.088 B9 0.035 B10 0.016</p> <p>LAGGING</p> <p>A0 2.944 A1 0.204 A2 0.030 A3 0.008 A4 0.005 A5 0.010 A6 -0.004 A7 -0.001 A8 -0.001 A9 0.003 A10 0.002</p>
<p>ALPHA S = 0 CL/SIG = -0.007 THETA = 8 CG/SIG = -0.0018 ALPHA C = -12.8</p> <p>FLAPPING</p> <p>A0 -0.015 A1 0.082 A2 -1.001 A3 -0.121 A4 -0.061 A5 0.061 A6 0.182 A7 0.204 A8 0.021 A9 0.056 A10 0.021</p> <p>B1 -0.118 B2 0.058 B3 -0.857 B4 -0.620 B5 0.276 B6 0.161 B7 0.014 B8 0.245 B9 0.072 B10 0.069</p> <p>LAGGING</p> <p>A0 1.868 A1 0.055 A2 0.095 A3 0.060 A4 0.029 A5 0.035 A6 0.033 A7 0.018 A8 -0.005 A9 0.007 A10 0.001</p>	<p>ALPHA S = 0 CL/SIG = 0.004 THETA = 0 CG/SIG = 0.0007 ALPHA C = -3.4</p> <p>FLAPPING</p> <p>A0 0.245 A1 -0.036 A2 -0.084 A3 0.081 A4 -0.132 A5 0.333 A6 0.135 A7 0.045 A8 0.042 A9 0.016 A10 0.005</p> <p>B1 -0.147 B2 -1.140 B3 -0.409 B4 0.063 B5 -0.457 B6 0.021 B7 -0.008 B8 0.103 B9 0.033 B10 0.004</p> <p>LAGGING</p> <p>A0 3.183 A1 0.233 A2 0.008 A3 -0.002 A4 -0.026 A5 0.004 A6 -0.007 A7 -0.001 A8 -0.001 A9 0.002 A10 -0.001</p>	<p>ALPHA S = 0 CL/SIG = 0.004 THETA = 0 CG/SIG = 0.0007 ALPHA C = -3.4</p> <p>FLAPPING</p> <p>A0 0.245 A1 -0.036 A2 -0.084 A3 0.081 A4 -0.132 A5 0.333 A6 0.135 A7 0.045 A8 0.042 A9 0.016 A10 0.005</p> <p>B1 -0.147 B2 -1.140 B3 -0.409 B4 0.063 B5 -0.457 B6 0.021 B7 -0.008 B8 0.103 B9 0.033 B10 0.004</p> <p>LAGGING</p> <p>A0 3.183 A1 0.233 A2 0.008 A3 -0.002 A4 -0.026 A5 0.004 A6 -0.007 A7 -0.001 A8 -0.001 A9 0.002 A10 -0.001</p>

TABLE II SHEAR FORCE HARMONIC COEFFICIENTS, LB.

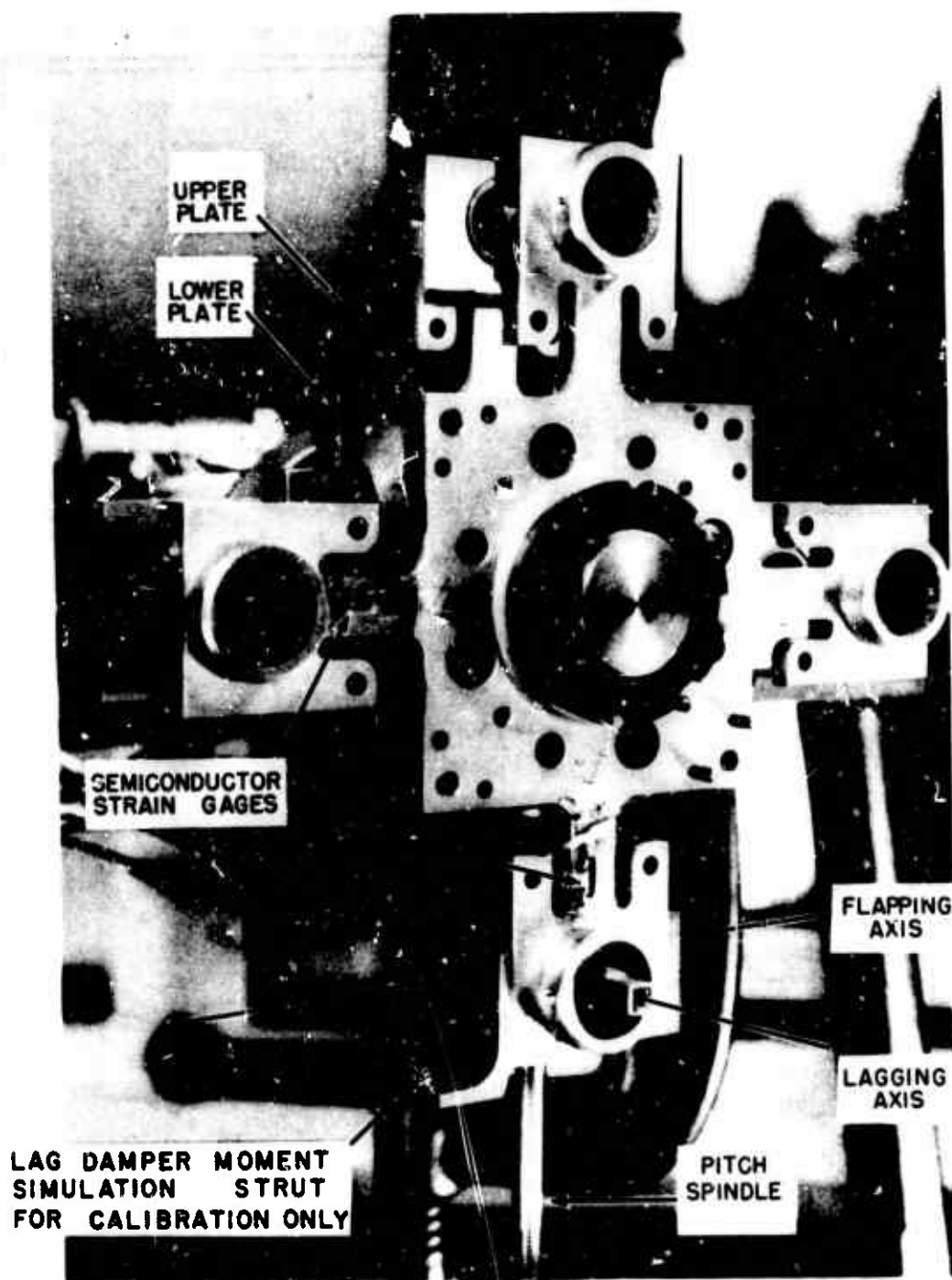
ADVANCE RATIO = 0.191						
ALPHA S = -4		ALPHA C = -6.9		THETA = 6		
CL/SIG = 0.071		CD/SIG = -0.0041		CQ/SIG = 0.0024		
FLATWISE		EDGEWISE		RADIAL		
N	COSINE	SINE	COSINE	SINE	COSINE	SINE
1	0.5	0.9	1.8	1.1	-7.9	0.9
2	-0.6	0.0	-0.3	0.0	0.4	1.1
3	1.6	0.0	-0.5	-0.5	0.6	1.2
4	-0.2	0.3	0.2	-0.2	-0.5	0.4
5	0.3	0.1	0.0	-0.1	0.3	0.0
6	0.1	0.0	-0.1	0.2	-0.2	0.2
7	0.2	0.1	-0.5	0.0	0.0	-0.1
8	0.0	-0.1	-0.2	0.0	0.0	0.0
9	-0.1	0.0	-0.2	0.1	-0.1	-0.0
10	0.2	0.1	-0.1	0.2	-0.2	0.2
ADVANCE RATIO = 0.283						
ALPHA S = -4		ALPHA C = -4.8		THETA = 2		
CL/SIG = 0.019		CD/SIG = 0.0007		CQ/SIG = 0.0004		
1	-0.4	-3.3	2.3	1.1	-2.3	1.6
2	0.3	-0.3	-0.2	0.3	0.1	-0.7
3	0.4	-0.1	-0.4	-0.3	-0.0	0.4
4	0.2	0.0	0.2	-0.2	-0.2	0.0
5	0.0	-0.0	-0.1	-0.0	-0.0	0.1
6	0.0	0.1	-0.0	-0.1	0.0	0.0
7	-0.3	-0.0	-0.0	-0.0	-0.0	0.0
8	0.0	0.0	-0.0	-0.0	0.0	0.0
9	-0.1	0.1	-0.0	-0.0	-0.1	0.0
10	-0.3	-0.1	0.2	0.1	-0.1	-0.1
ALPHA S = -4		ALPHA C = -6.5		THETA = 4		
CL/SIG = 0.041		CD/SIG = -0.0008		CQ/SIG = 0.0011		
1	-1.0	-2.3	0.5	-0.1	-1.2	0.1
2	-0.3	-0.3	-0.3	0.5	-0.0	-0.7
3	0.7	-0.2	0.0	0.2	-0.2	0.2
4	0.2	0.4	-0.2	0.1	-0.2	-0.1
5	0.1	-0.0	0.1	0.1	0.1	0.1
6	-0.0	0.1	0.0	-0.1	-0.0	0.0
7	-0.3	-0.1	-0.1	-0.0	-0.1	-0.0
8	0.0	-0.1	0.0	0.1	-0.1	-0.1
9	0.1	-0.2	-0.1	0.3	-0.2	-0.2
10	-0.3	-0.2	0.1	-0.0	-0.0	-0.1
ALPHA S = -4		ALPHA C = -7.9		THETA = 6		
CL/SIG = 0.062		CD/SIG = -0.0029		CQ/SIG = 0.0022		
1	-2.4	-1.0	-2.2	-0.3	-0.5	-0.2
2	-0.7	-0.6	0.0	0.9	-0.2	-0.9
3	1.4	-0.7	0.5	0.8	-0.5	-0.1
4	0.0	0.4	-0.2	-0.1	0.1	-0.2
5	0.3	-0.2	0.3	0.3	0.2	-0.1
6	0.0	0.1	0.0	0.0	-0.0	-0.1
7	-0.6	-0.2	0.2	-0.0	-0.0	-0.1
8	-0.1	-0.4	0.1	0.2	-0.2	-0.2
9	0.2	0.1	-0.3	-0.0	0.1	0.1
10	0.4	-0.3	0.1	0.0	-0.0	-0.0

TABLE II CONCLUDED

ADVANCE RATIO = 0.389						
ALPHA S = -4		ALPHA C = -9.5		THETA = 6		
CL/SIC = 0.046		CD/SIC = -0.0018		CQ/SIC = 0.0022		
FLATWISE		EDGEWISE		RADIAL		
N	COSINE	SINE	COSINE	SINE	COSINE	SINE
1	-2.1	-1.5	-0.5	-0.2	-0.6	-0.2
2	-1.2	-1.8	-0.6	-1.2	0.0	1.0
3	1.0	-1.4	-0.9	0.5	0.8	0.5
4	0.7	0.3	-0.2	-0.4	-0.3	0.3
5	0.2	0.0	0.0	-0.3	0.4	0.2
6	-0.2	0.2	-0.2	0.1	-0.1	-0.1
7	0.2	0.3	0.1	0.1	-0.3	-0.1
8	-0.4	0.1	-0.1	-0.2	0.2	-0.1
9	-0.2	0.3	-0.2	-0.2	0.0	0.3
10	0.0	0.1	-0.1	-0.1	0.0	-0.0
ADVANCE RATIO = 0.488						
ALPHA S = -4		ALPHA C = -11.9		THETA = 8		
CL/SIC = 0.048		CD/SIC = -0.0024		CQ/SIC = 0.0034		
1	-0.5	-0.2	0.0	0.4	0.2	-0.3
2	-1.3	-2.4	-0.9	-1.5	0.5	1.4
3	0.0	-2.6	-1.3	1.2	0.6	0.3
4	0.6	-1.0	-0.7	-1.0	-0.3	0.5
5	0.4	-0.2	-0.1	0.0	0.4	-0.1
6	-0.2	0.2	0.0	0.3	-0.1	-0.0
7	0.3	-1.1	-0.3	-0.2	0.1	1.0
8	0.1	0.4	0.3	0.3	-0.4	-0.2
9	-0.2	0.3	0.0	0.3	0.1	-0.7
10	-0.3	-0.1	0.0	0.0	0.2	-0.2
ADVANCE RATIO = 0.683						
ALPHA S = -4		ALPHA C = -17.7		THETA = 12		
CL/SIC = 0.032		CD/SIC = 0.0033		CQ/SIC = 0.0042		
1	2.0	0.0	2.0	0.0	-1.0	-0.7
2	-2.9	-2.4	-2.9	2.4	2.3	1.1
3	-2.0	-2.7	-2.0	2.7	2.2	-1.0
4	-4.3	-4.3	-4.3	-4.3	4.6	2.9
5	0.3	0.0	0.0	0.3	0.3	-1.3
6	1.0	-0.1	1.0	-0.1	-0.7	0.1
7	0.0	0.4	0.0	0.4	0.1	0.3
8	0.4	-0.9	0.4	-0.8	-0.6	0.4
9	0.3	0.2	0.3	0.3	-0.1	-0.1
0	0.8	0.3	0.8	0.3	-0.4	-0.0

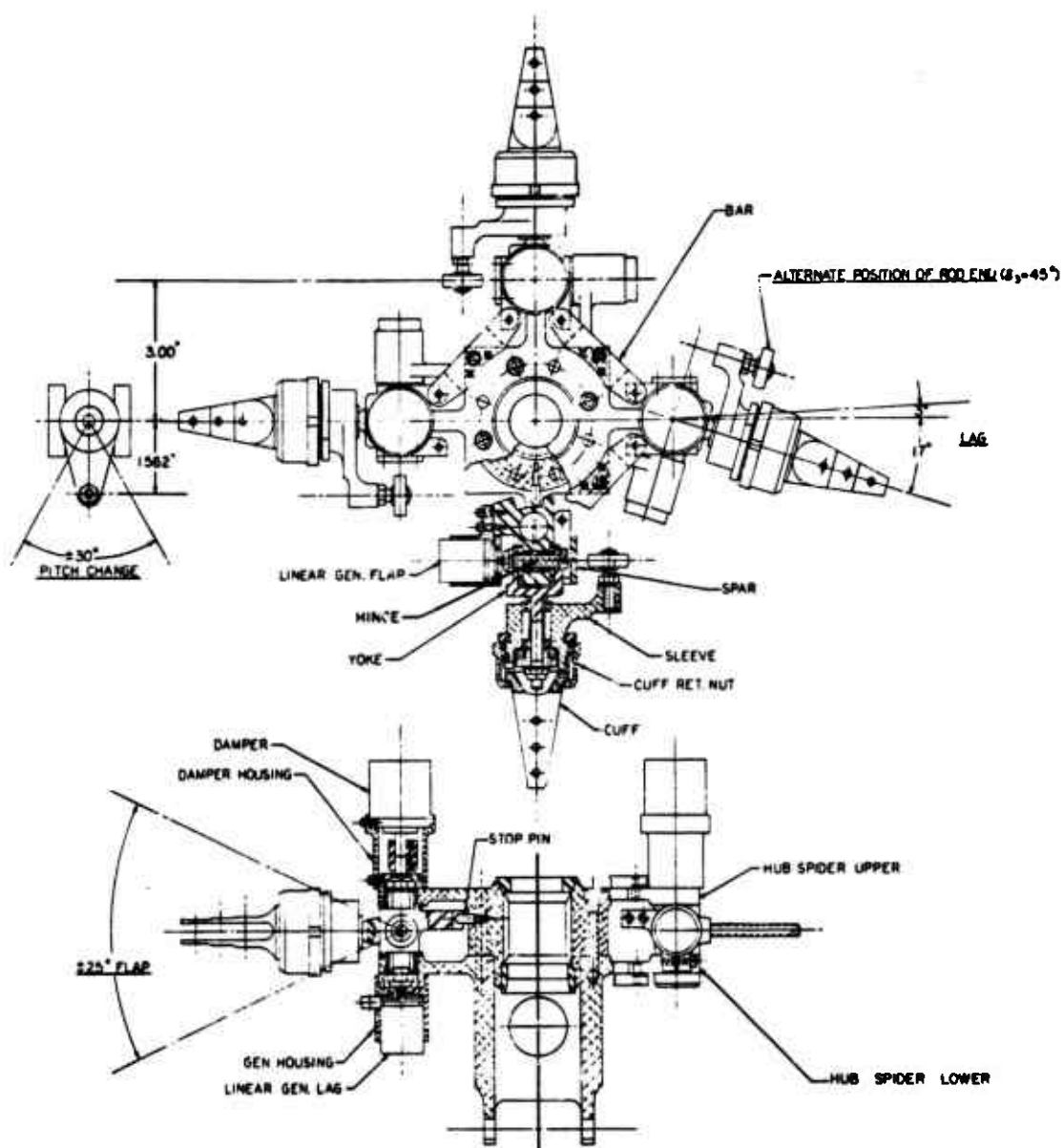
TABLE III - SCALING RATIOS

Model linear dimension = $1/S$ x full scale linear dimension	
Subscript m - model Subscript fs - full scale	
Parameter	Full Scale Blade
Radius & other linear dimensions R_m/R_{fs}	$1/S$
Areas- A_m/A_{fs}	$1/S^2$
Mass per unit length m_m/m_{fs}	$1/S^2$
Total mass M_{bm}/M_{bfs}	$1/S^3$
Stiffness EI_{xxm}/EI_{xxfs} , etc.	$1/S^5$
Angular velocity Ω_m/Ω_{fs}	\sqrt{S}
Linear velocities $(\Omega R)_m/(\Omega R)_{fs}$	$1/\sqrt{S}$
Mach number M_m/M_{fs}	$1/\sqrt{S}$
Froude number $(\Omega^2 R/g)_m/(\Omega^2 R/g)_{fs}$	1
Reynolds number RN_m/RN_{fs}	$1/S^{3/2}$
Output forces F_m/F_{fs}	$1/S^3$
Output moments $Mom._m/Mom._{fs}$	$1/S^4$
Output elastic strains ϵ_m/ϵ_{fs}	1
Natural frequencies ω_m/ω_{fs}	\sqrt{S}



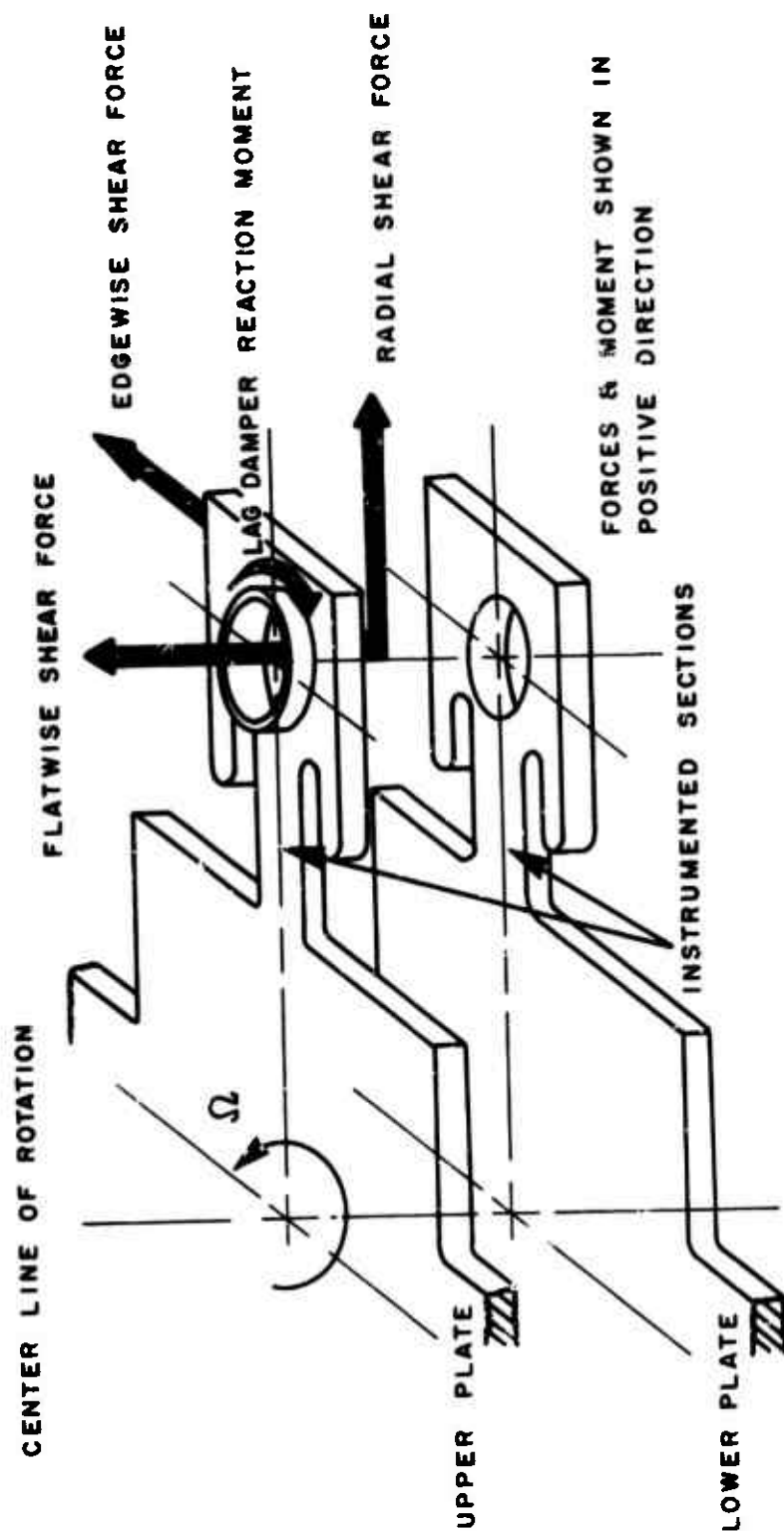
(a) BASIC INSTALLATION

Figure 1. Vibratory Shear Force Rotor Head.



(b) ASSEMBLY DRAWING

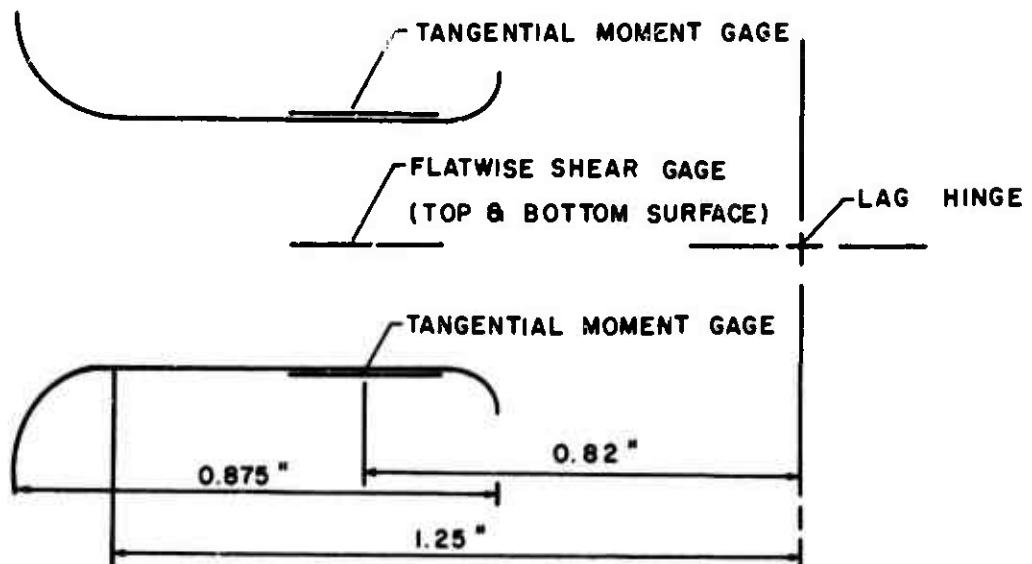
Figure 1. Concluded.



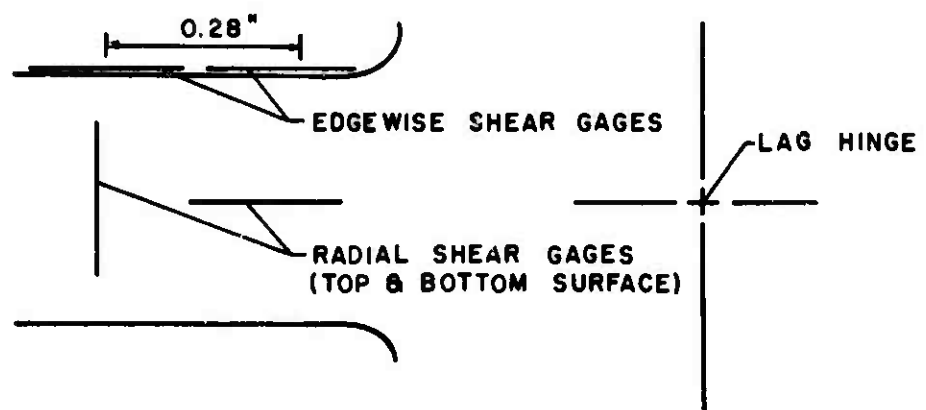
(a) DEFINITION OF SHEAR FORCES AND LAG DAMPER REACTION MOMENT

Figure 2. Vibratory Shear Force Rotor Head Details.

UPPER INSTRUMENTED SECTION - TOP VIEW



LOWER INSTRUMENTED SECTION - TOP VIEW



(b) SEMICONDUCTOR STRAIN GAGE LOCATIONS

Figure 2. Concluded.

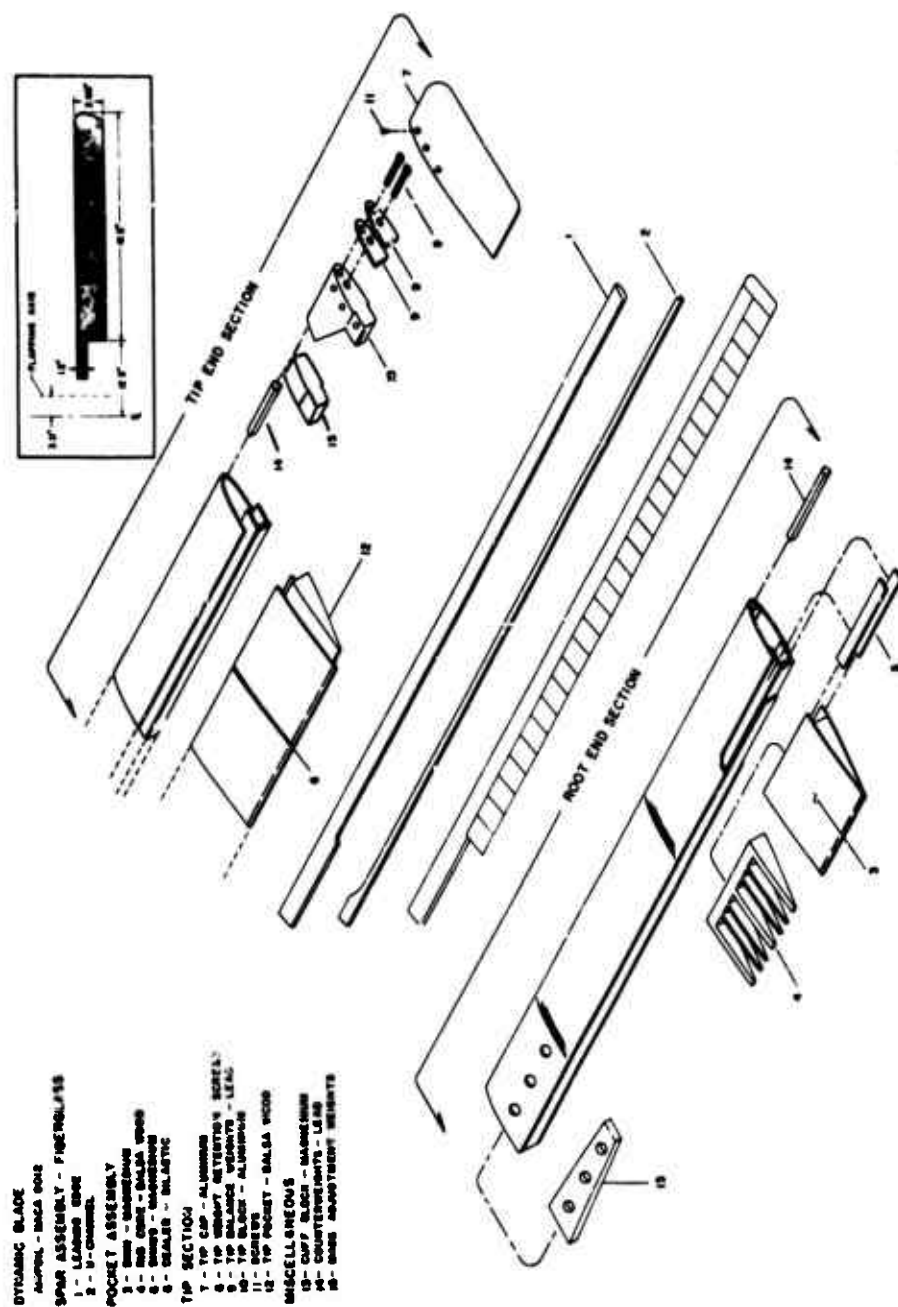


Figure 3. Dynamically Scaled Blade-Exploded View.

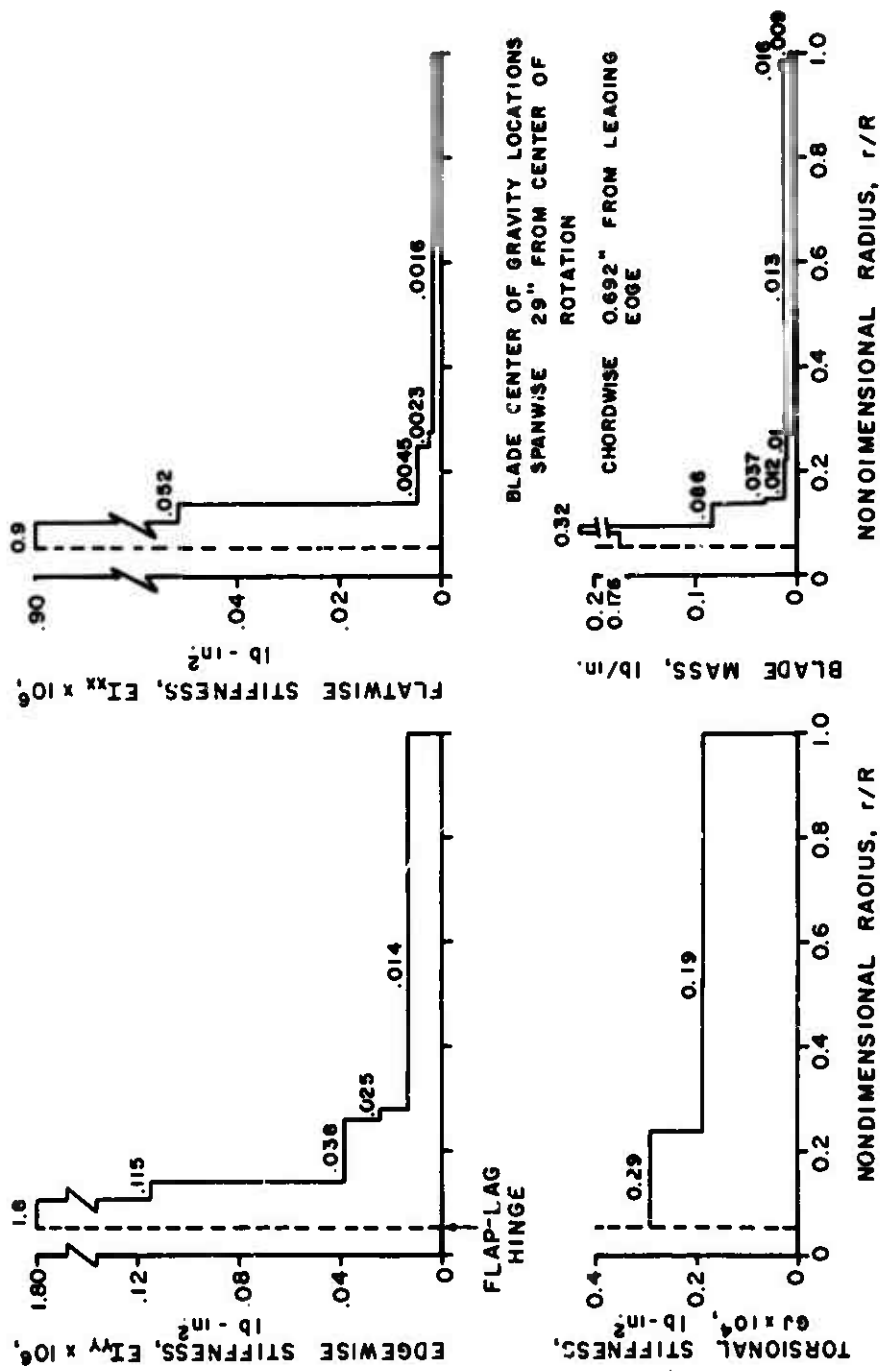


Figure 4. Dynamic Blade Physical Properties.

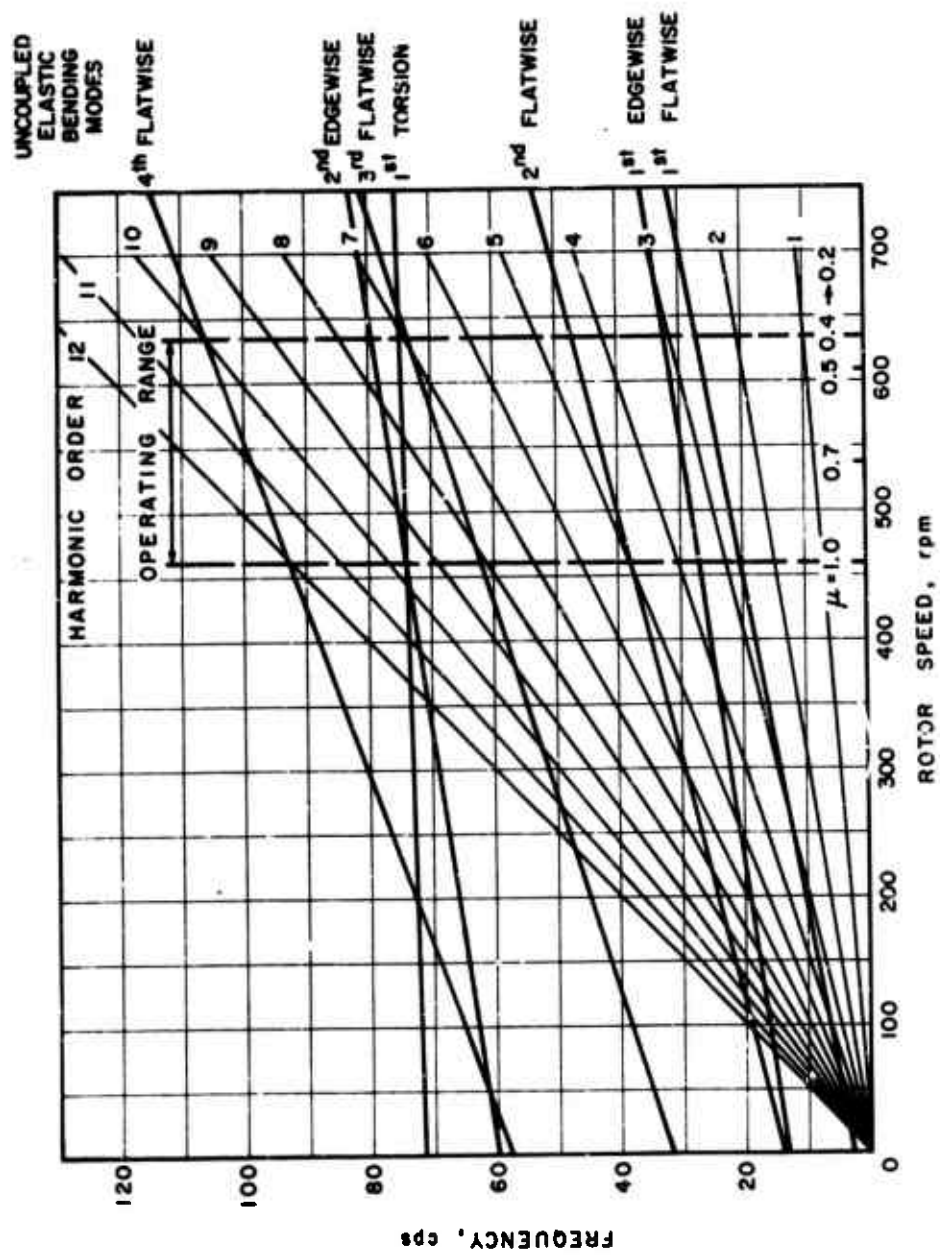


Figure 5. Model Rotor Blade Calculated Natural Frequencies.

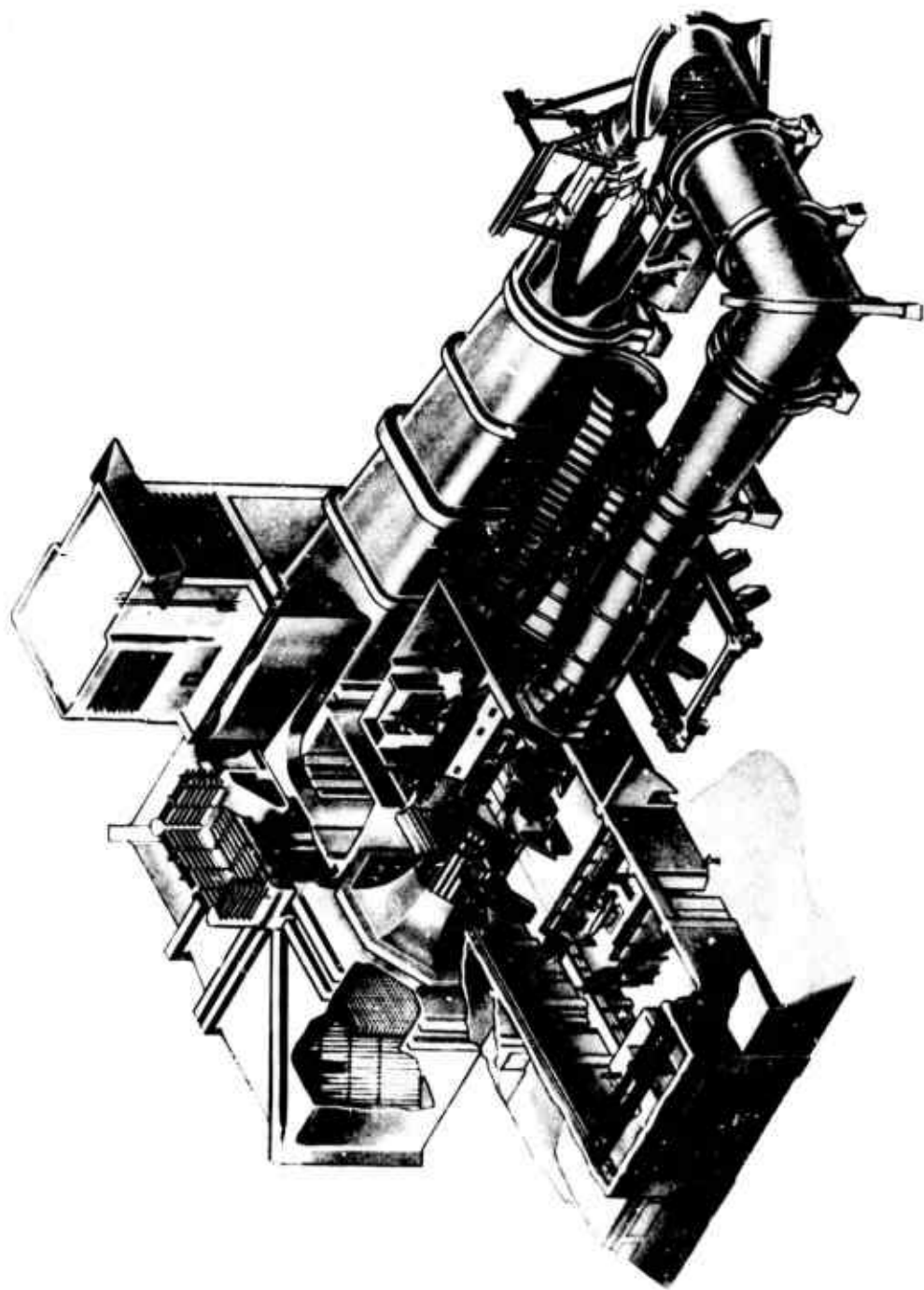
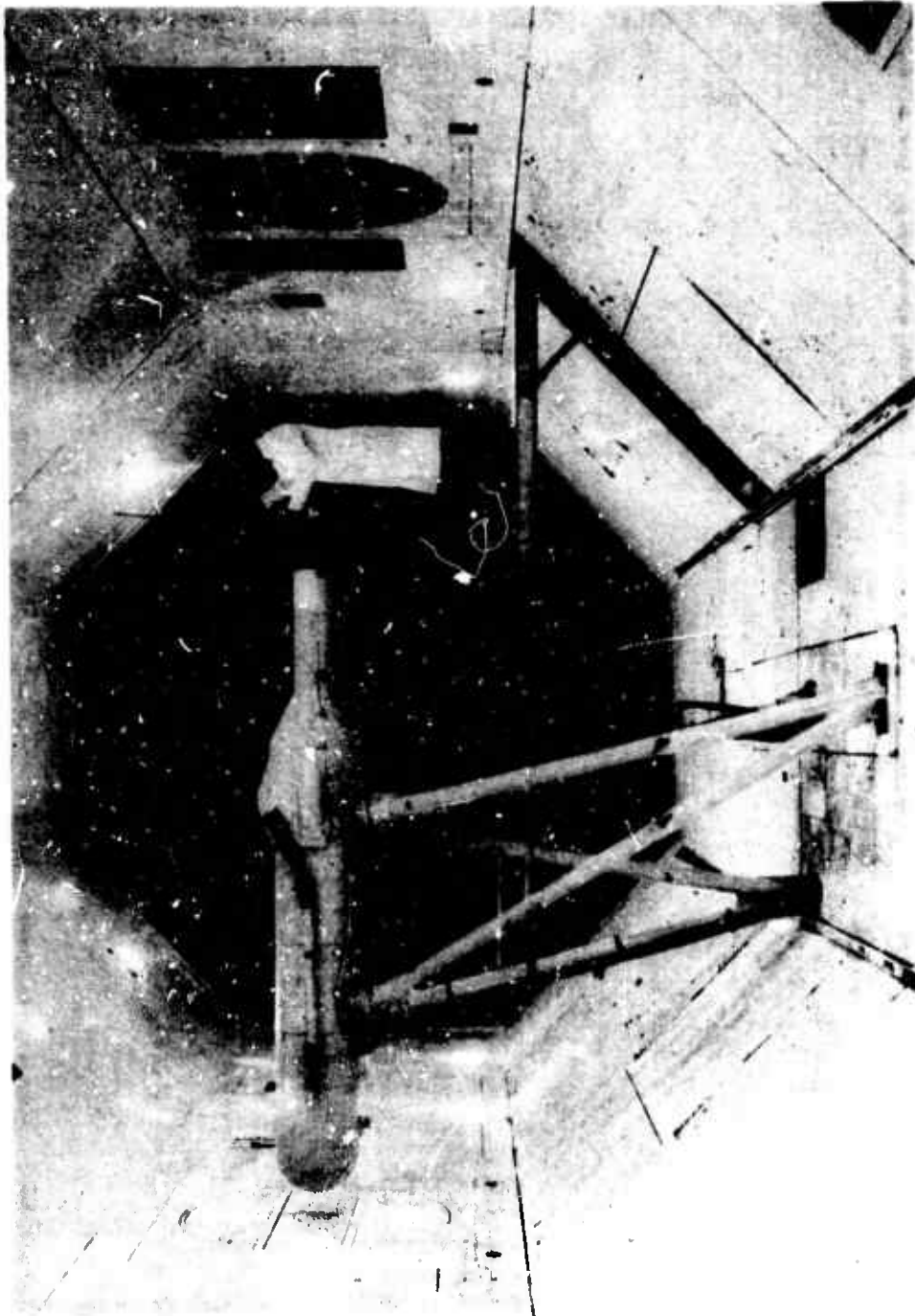
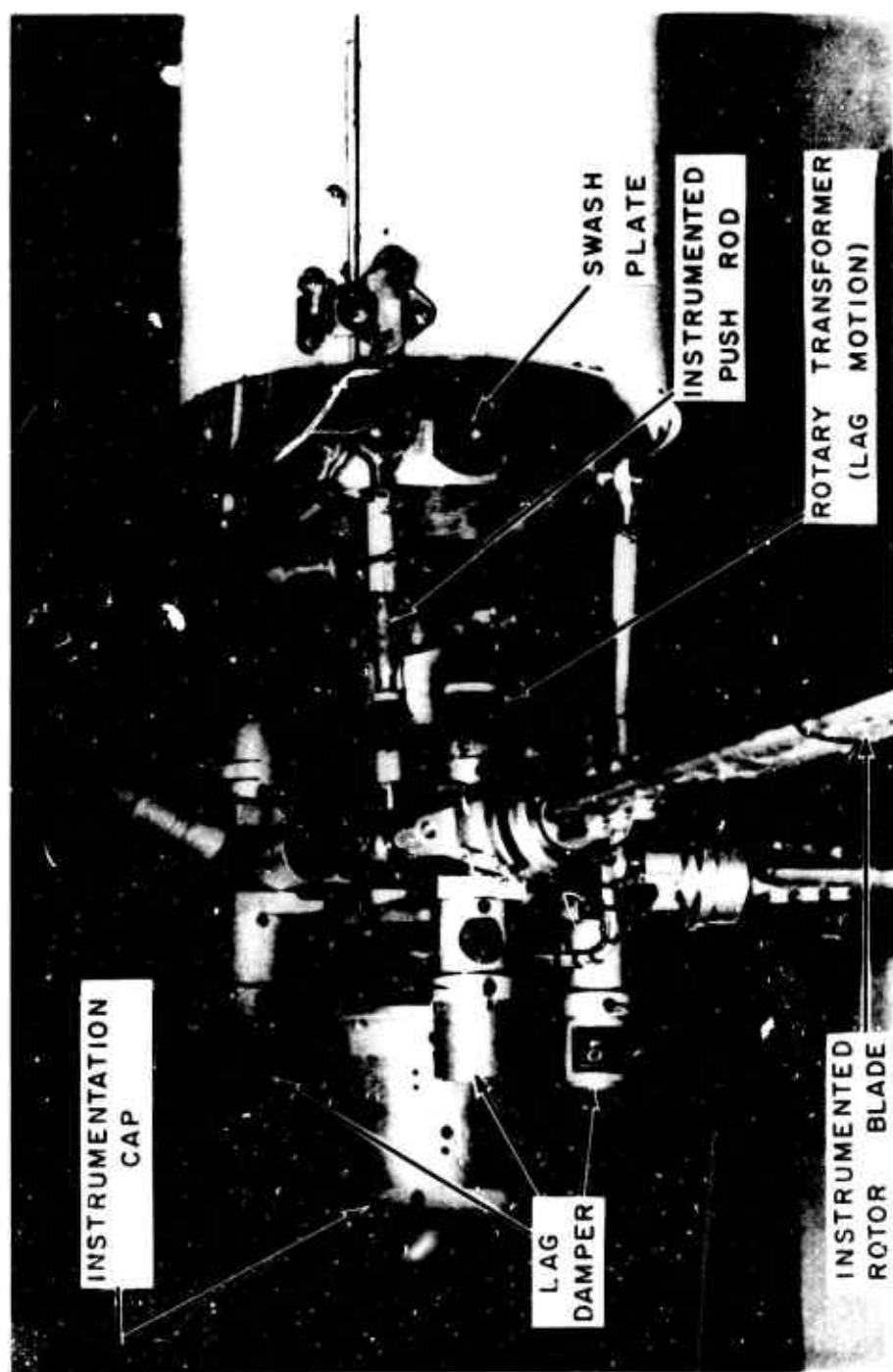


Figure 6. United Aircraft's Subsonic Wind Tunnel.



(a) GENERAL VIEW OF MODEL INSTALLATION IN WIND TUNNEL

Figure 7. Sikorsky Helicopter Rotor Test Rig.



(b) DETAILS OF HUB AND SWASH PLATE AREA

Figure 7. Concluded.

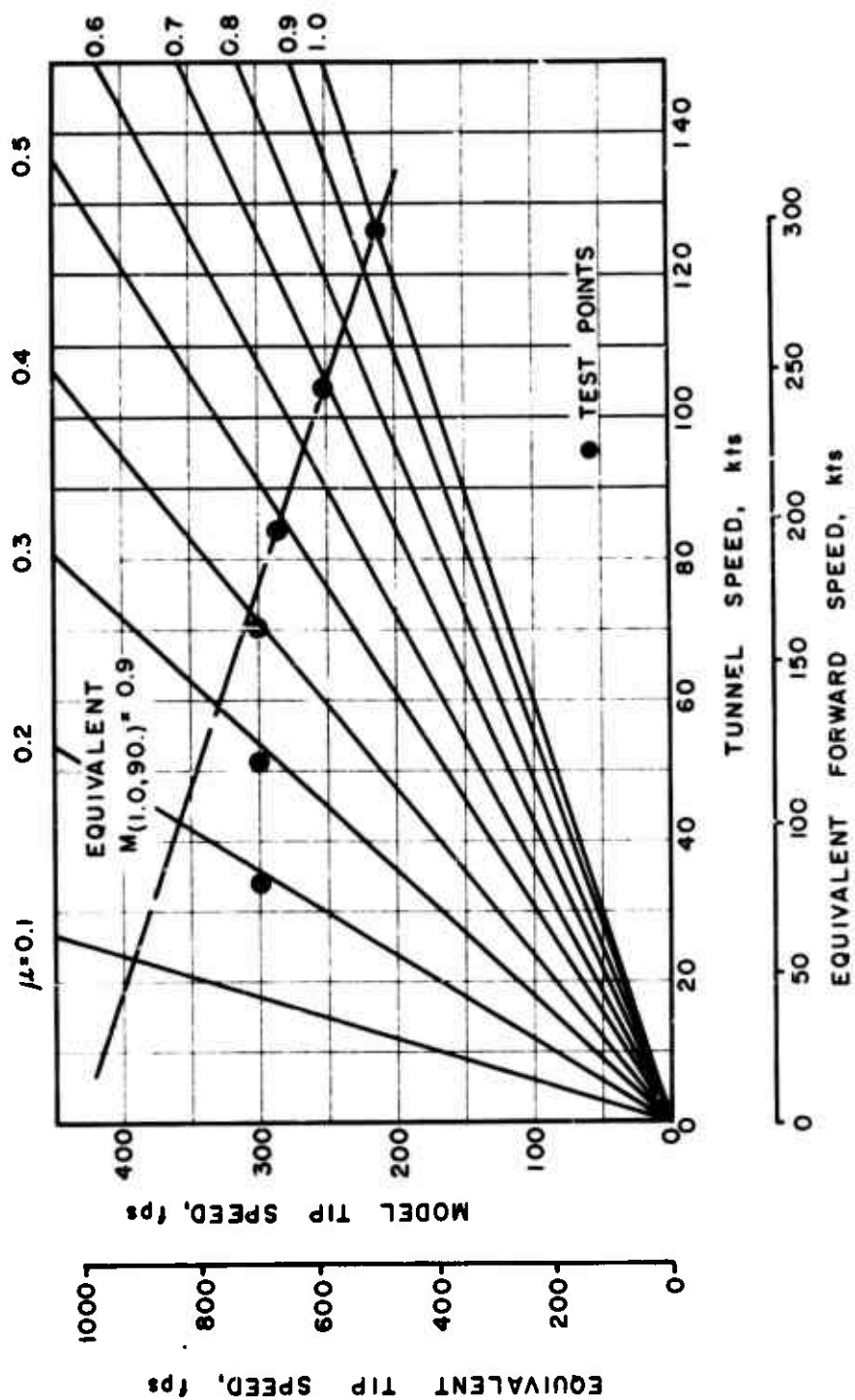
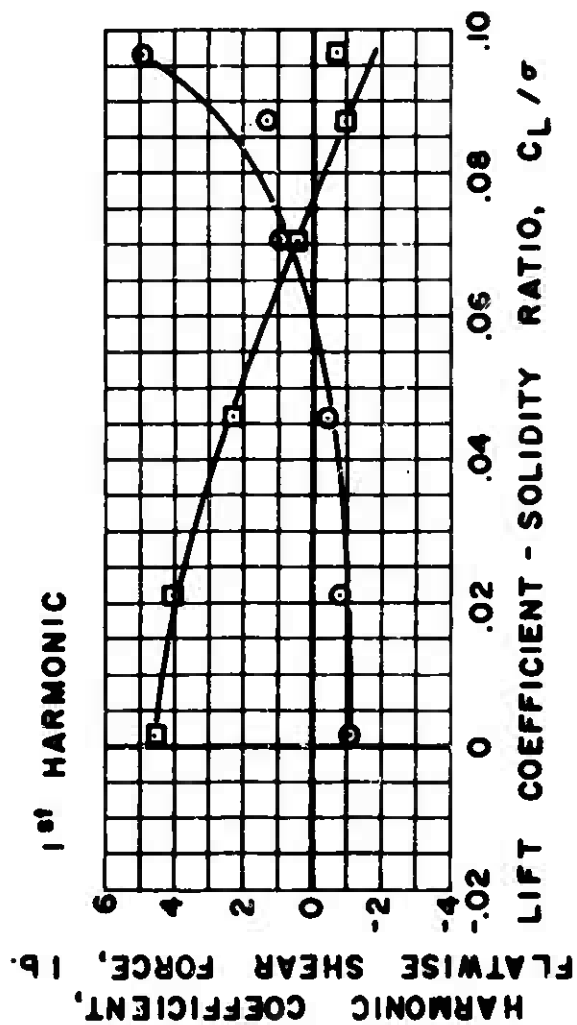


Figure 8. Wind Tunnel Test Conditions.

○ SINE COEFFICIENTS
 □ COSINE COEFFICIENTS



$\alpha_s = -4 \text{ deg. } \mu = 0.2$

(a) TRIMMED

Figure 9. Effect of Trim Condition on Shear Forces.

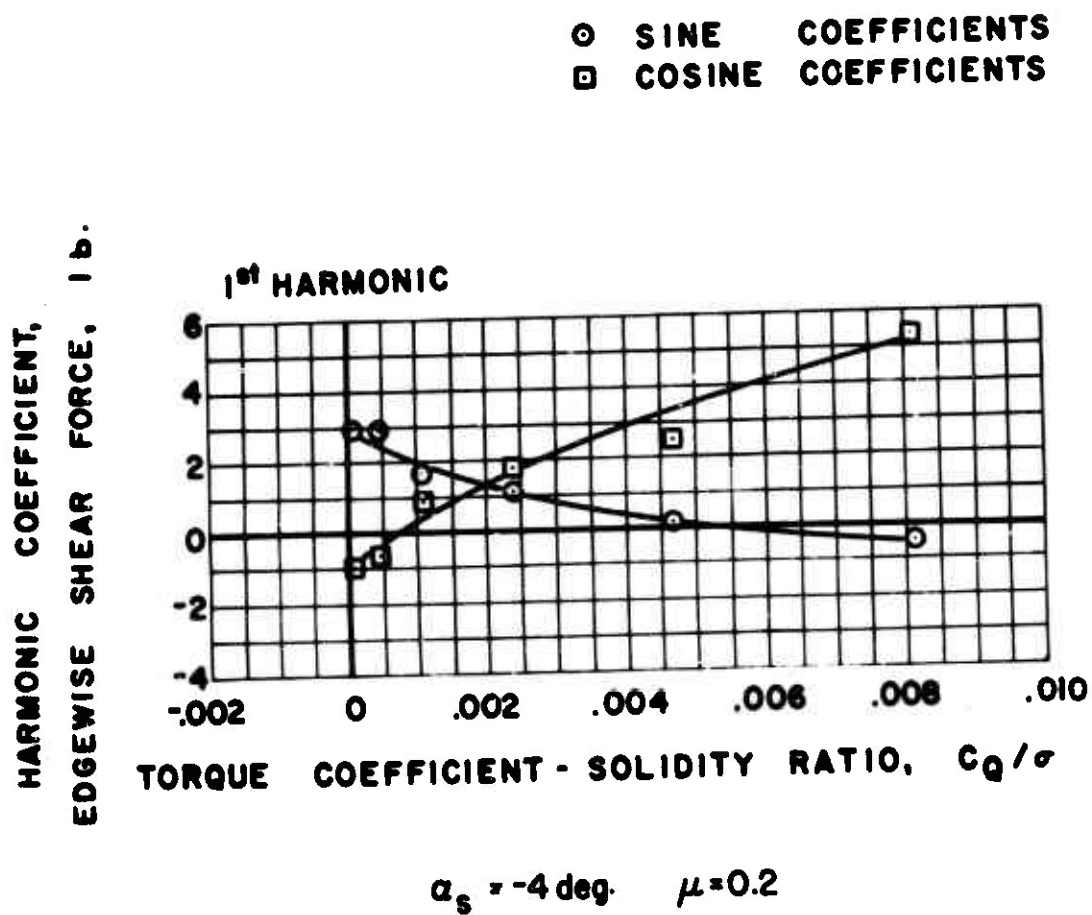
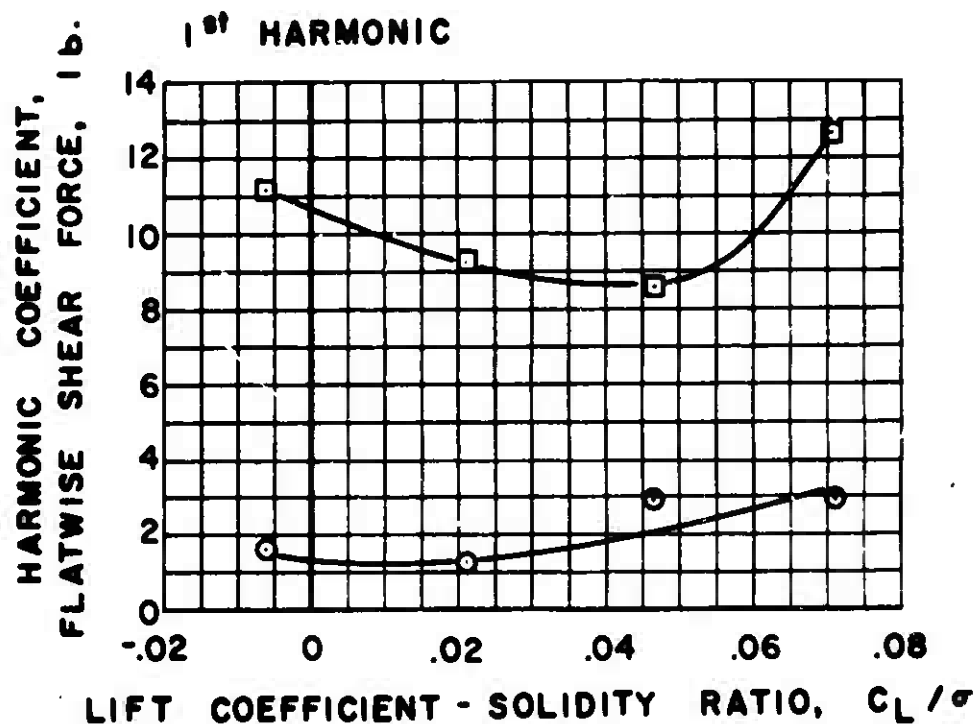


Figure 9(a) Continued.

○ SINE COEFFICIENTS
 □ COSINE COEFFICIENTS

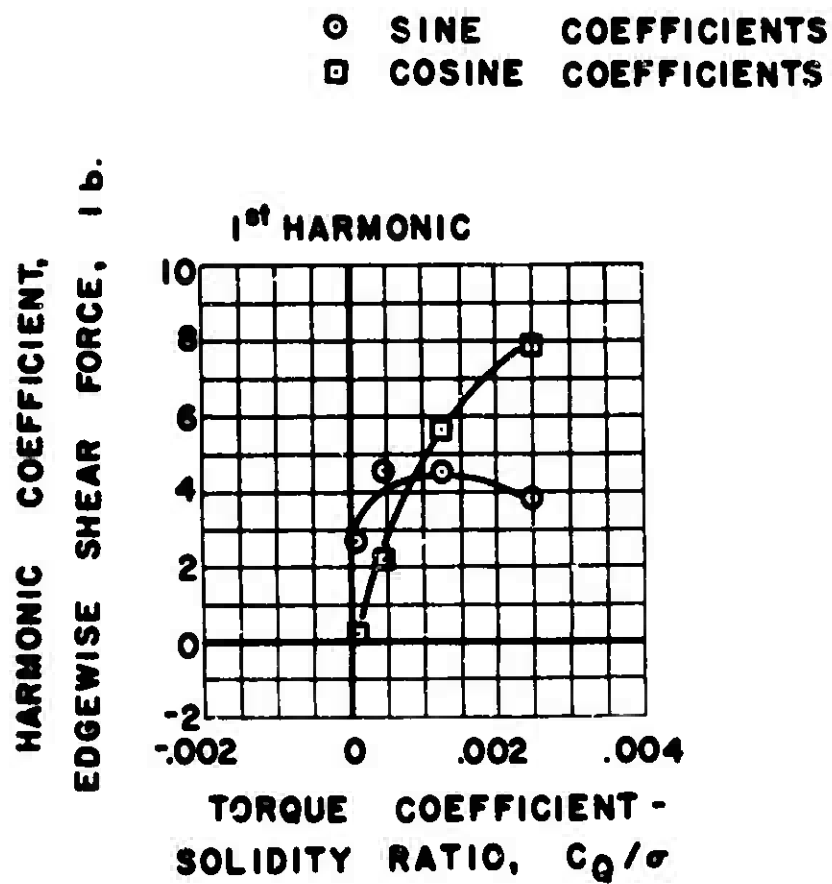


$\alpha_s = 0 \text{ deg. } \mu = 0.2$

-4 deg. FIRST HARMONIC LONGITUDINAL FLAPPING

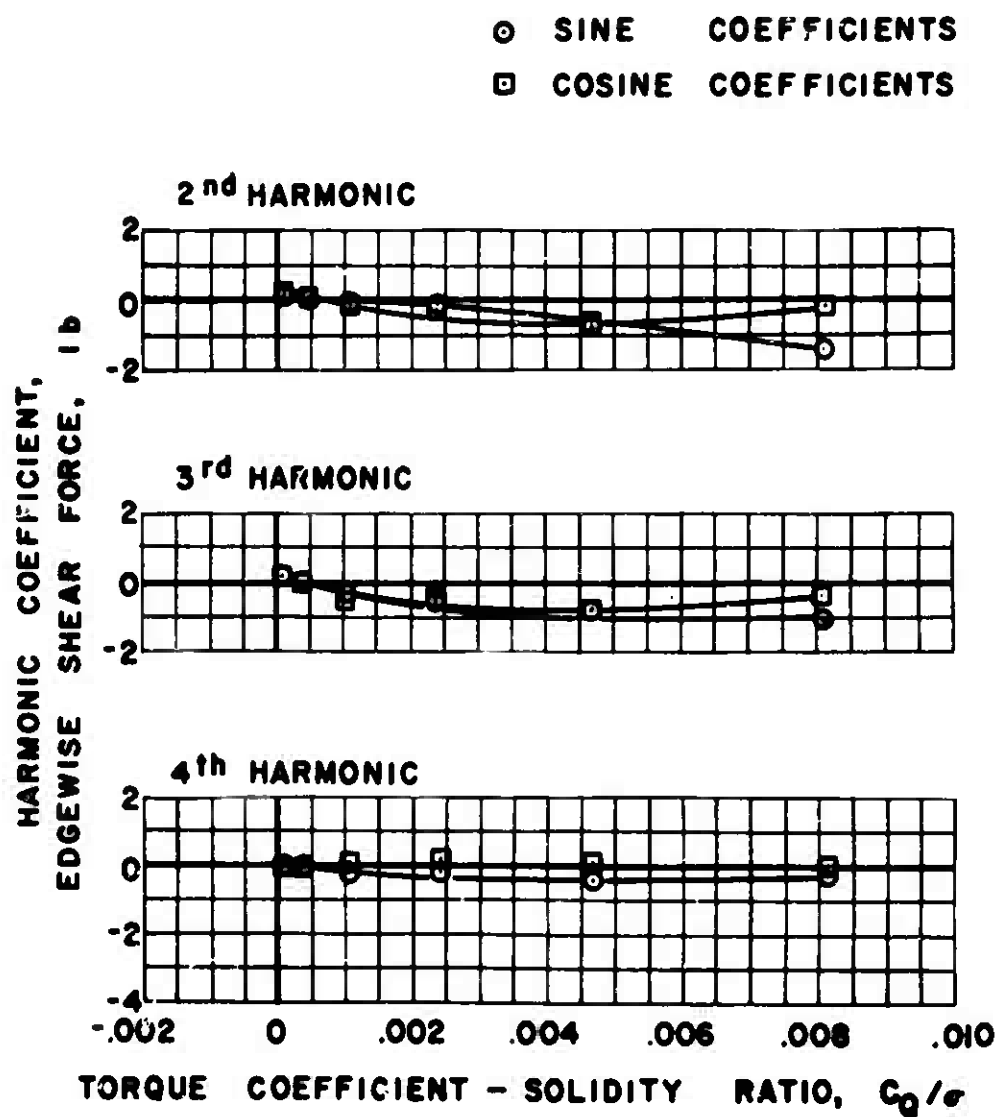
(b) OUT-OF-TRIM

Figure 9. Continued.



$$\alpha_s = 0 \text{ deg.} \quad \mu = 0.2$$

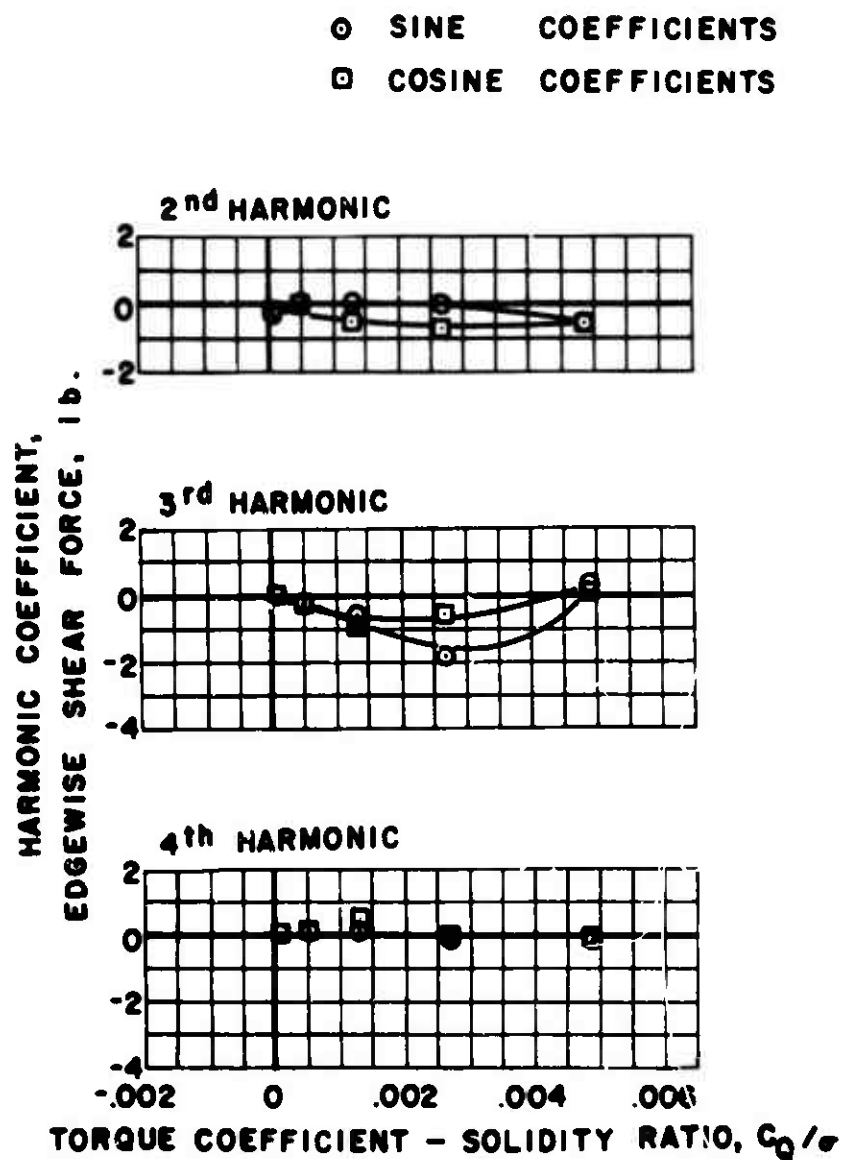
Figure 9(b) Concluded.



$$\alpha_s = -4 \text{ deg. } \mu = 0.2$$

(a) FULL LAG DAMPING

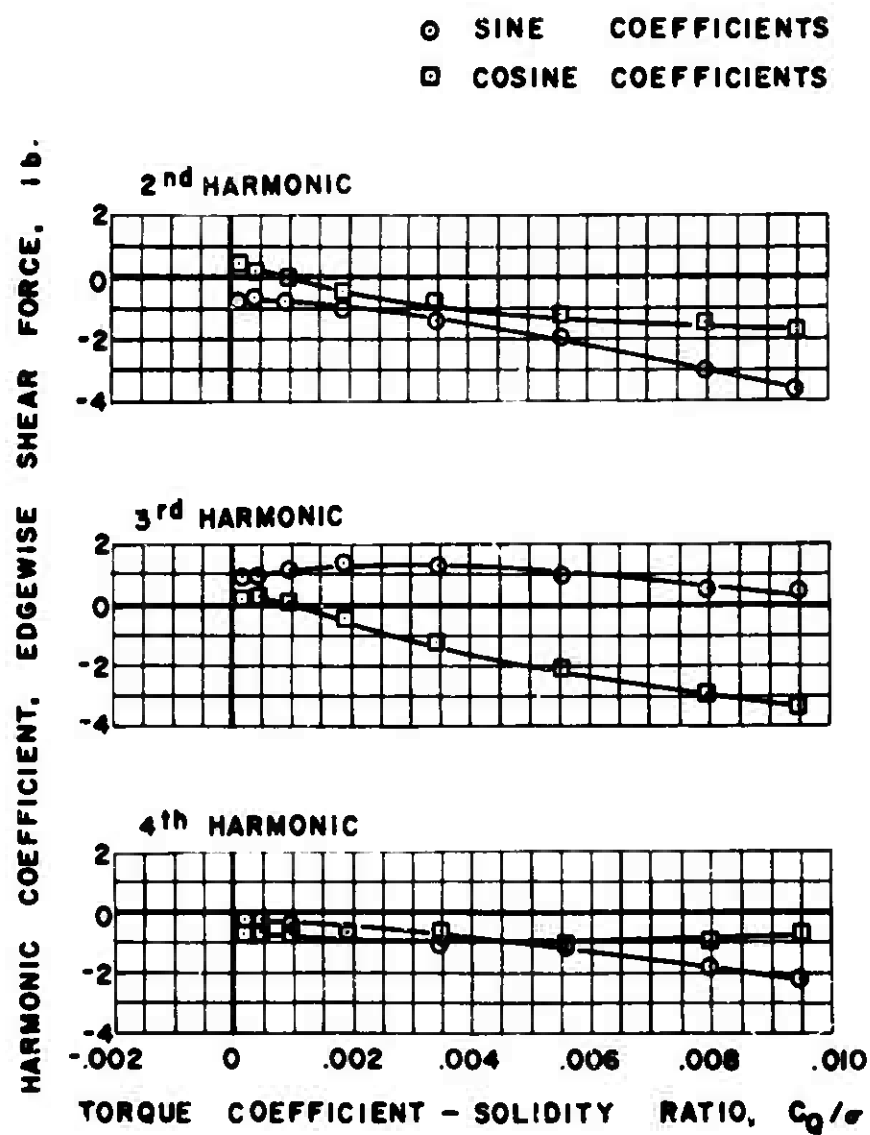
Figure 10. Effect of Lag Damping on Shear Forces.



$\alpha_s = -4 \text{ deg.} \quad \mu = 0.2$

(b) ZERO LAG DAMPING

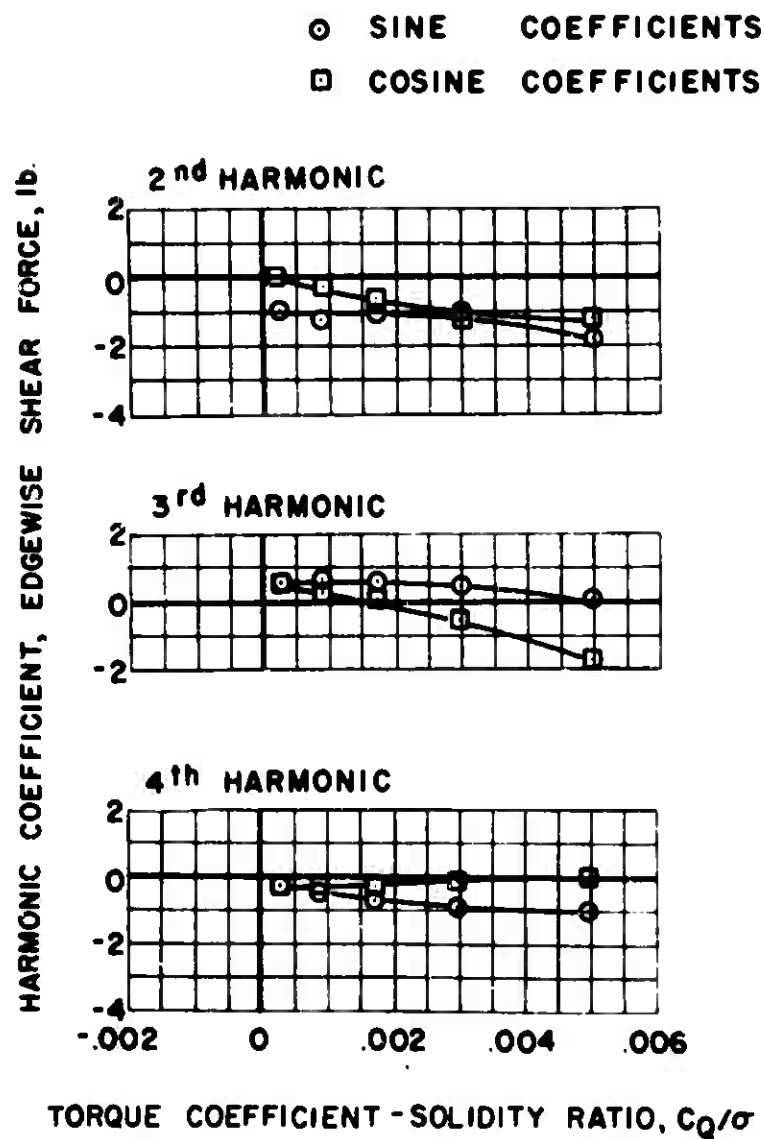
Figure 10. Concluded.



$\alpha_s = -4\text{deg.}$ $\mu = 0.5$

(a) FULL LAG DAMPING

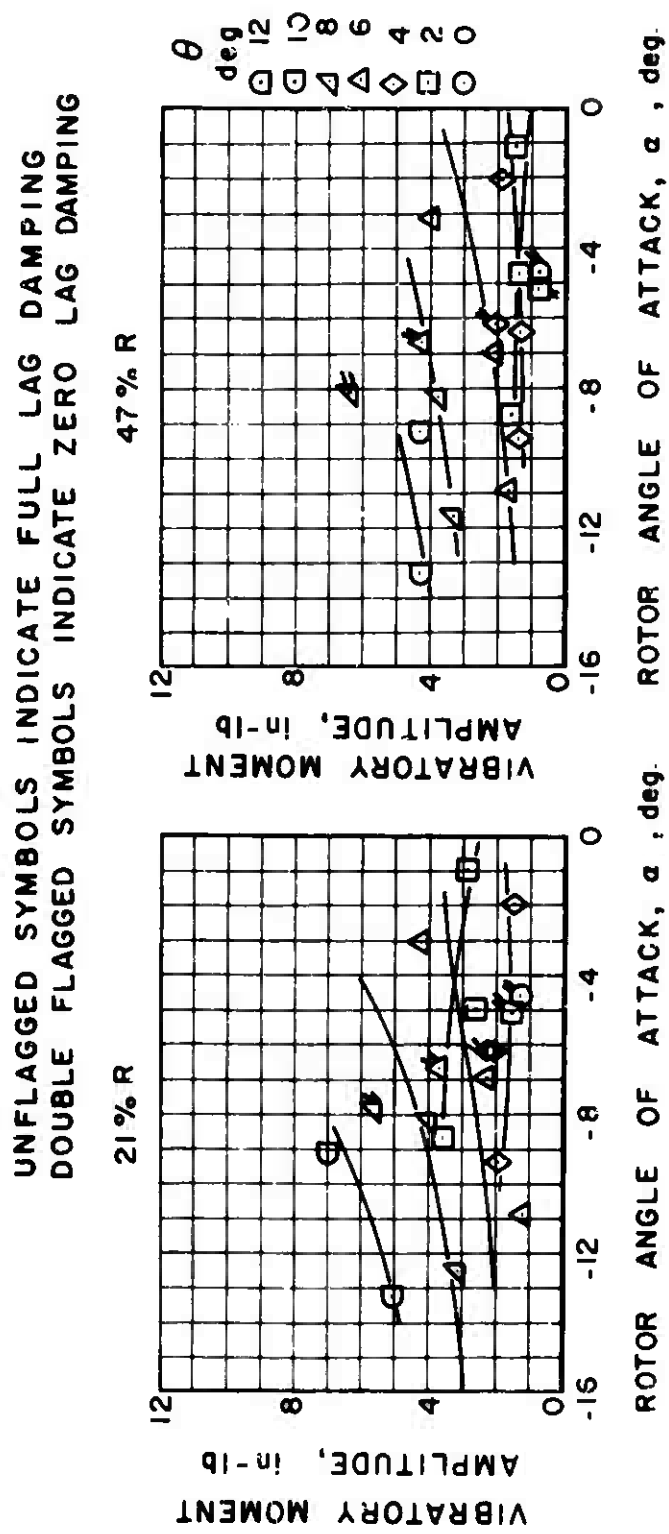
Figure 11. Effect of Lag Damping on Shear Forces.



$$\alpha_s = -4 \text{ deg. } \mu = 0.5$$

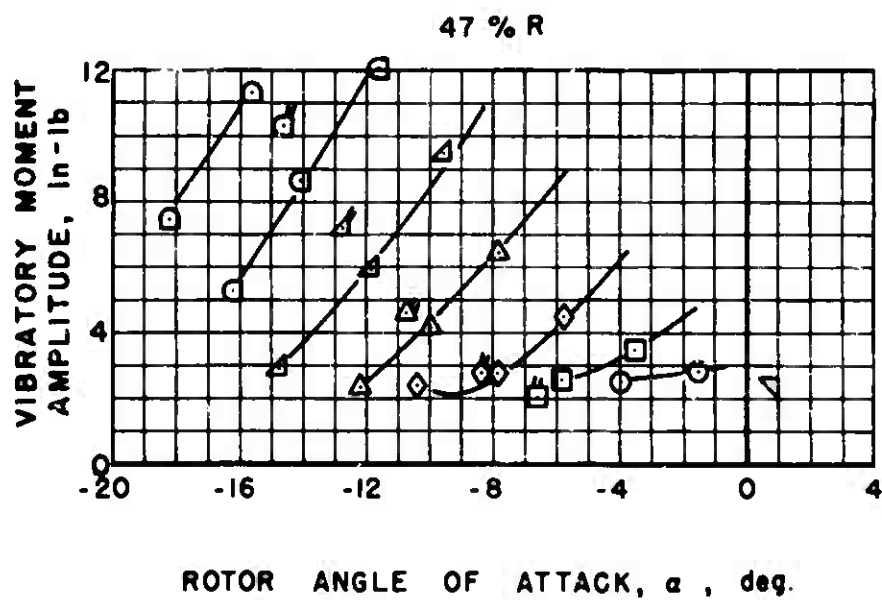
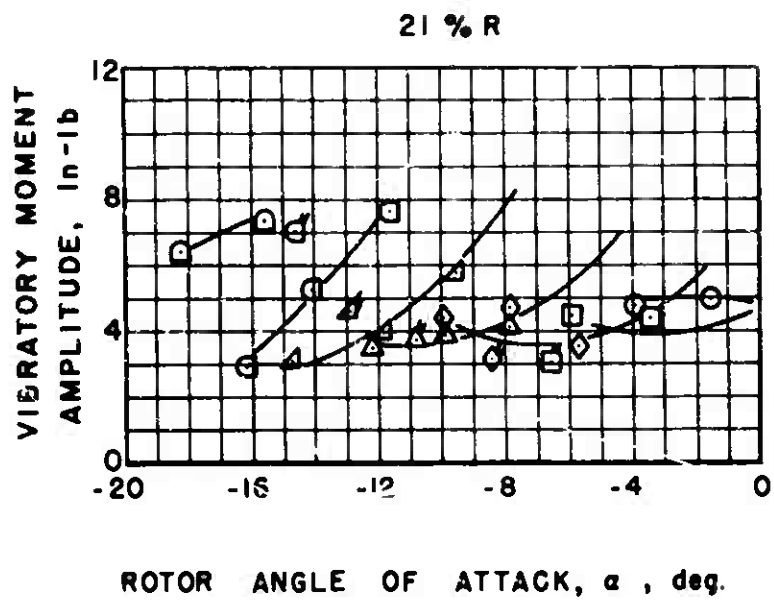
(b) ZERO LAG DAMPING

Figure 11. Concluded.



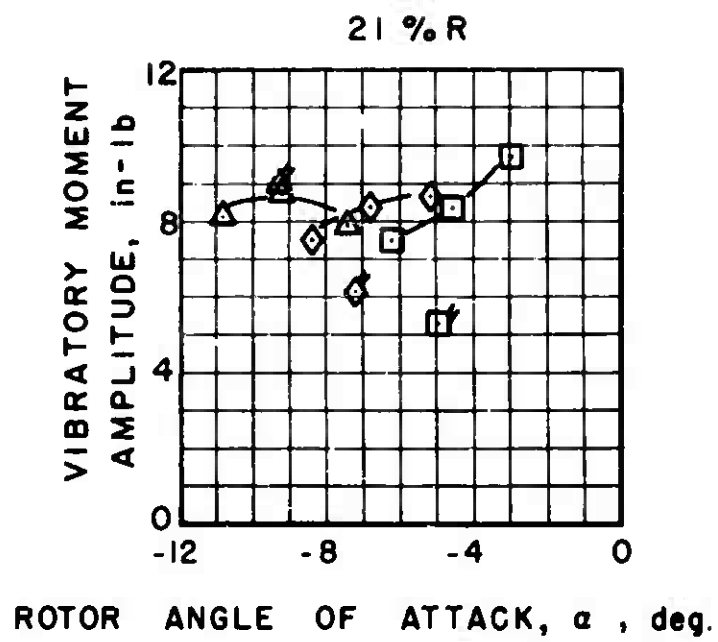
(a) $\mu = 0.2$

Figure 12. Effect of Lag Damping on Edgewise Blade Bending Moment.



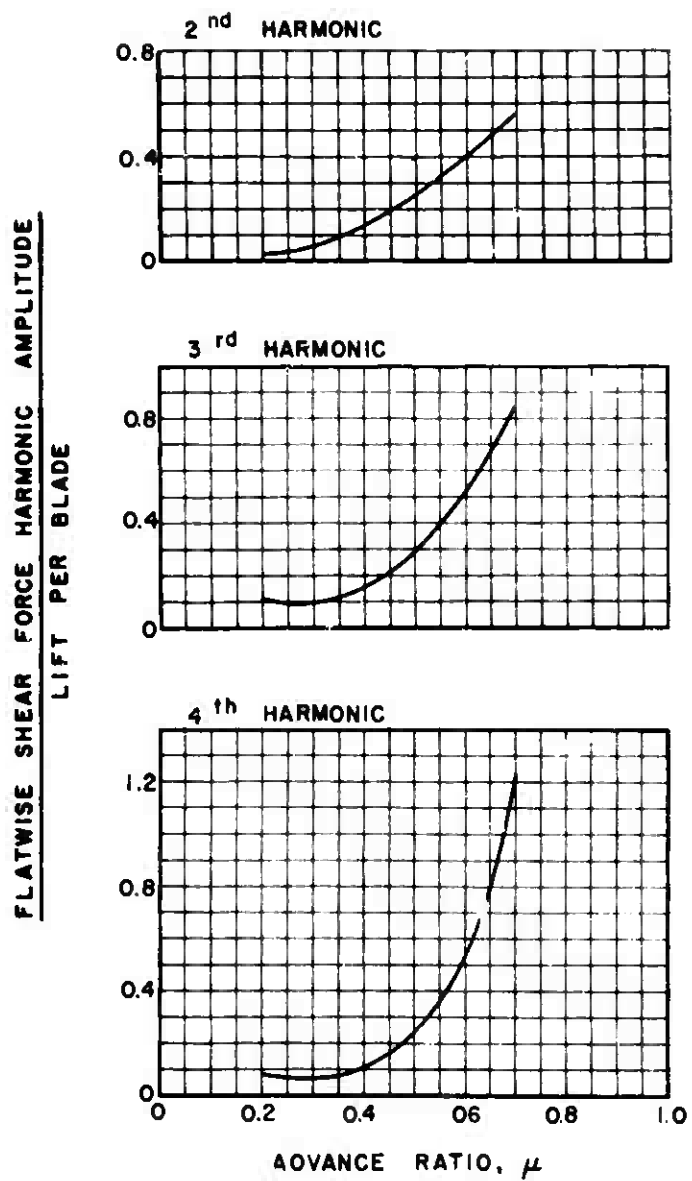
(b) $\mu = 0.5$

Figure 12. Continued.



(c) $\mu = 0.7$

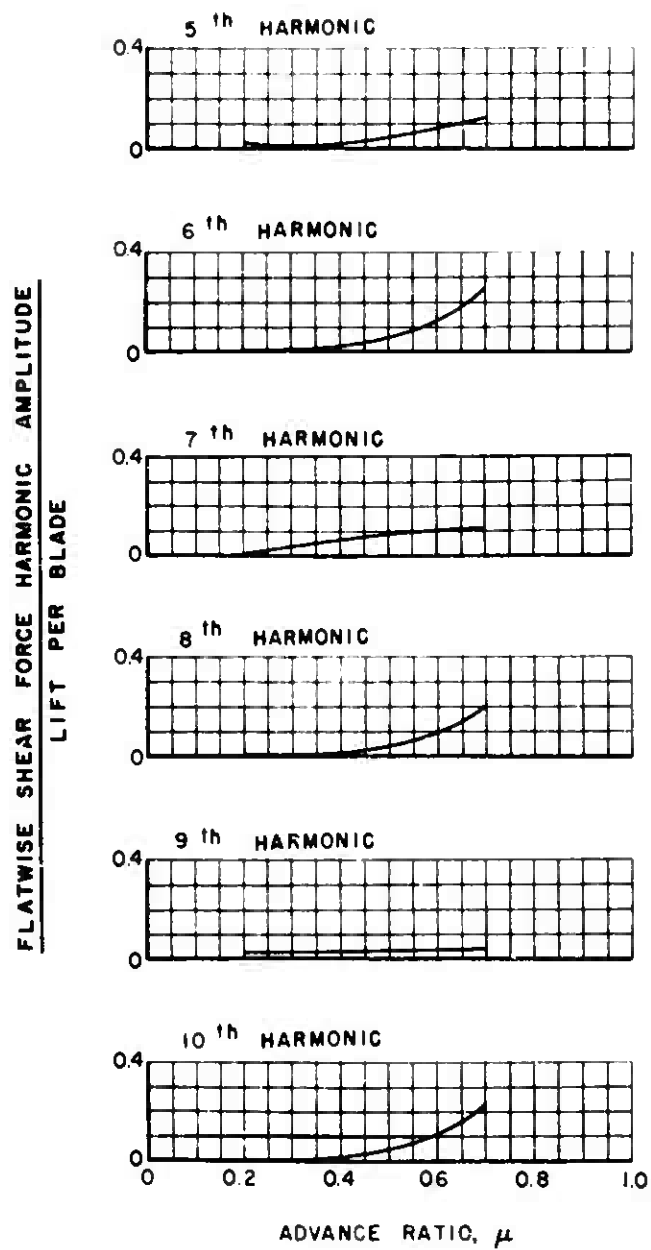
Figure 12. Concluded.



$C_L/\sigma = 0.035$, $\alpha_s = -4 \text{ deg.}$

(a) FLATWISE SHEAR

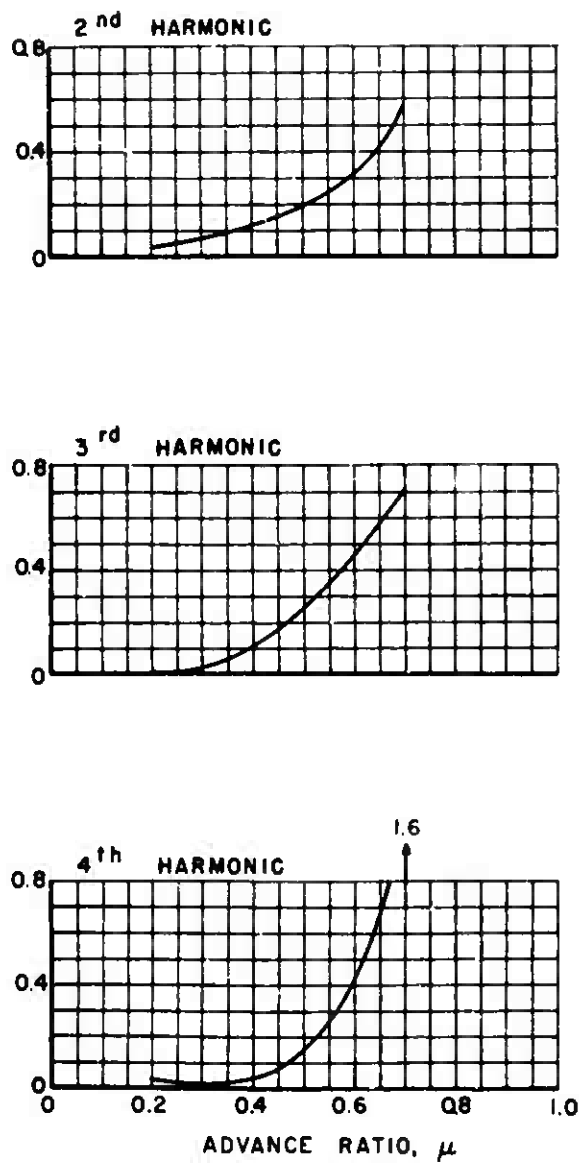
Figure 13. Effect of Advance Ratio on Nondimensional Shear Forces.



$$C_L/\sigma = 0.035, \quad \alpha_s = -4 \text{ deg.}$$

Figure 13(a). Continued.

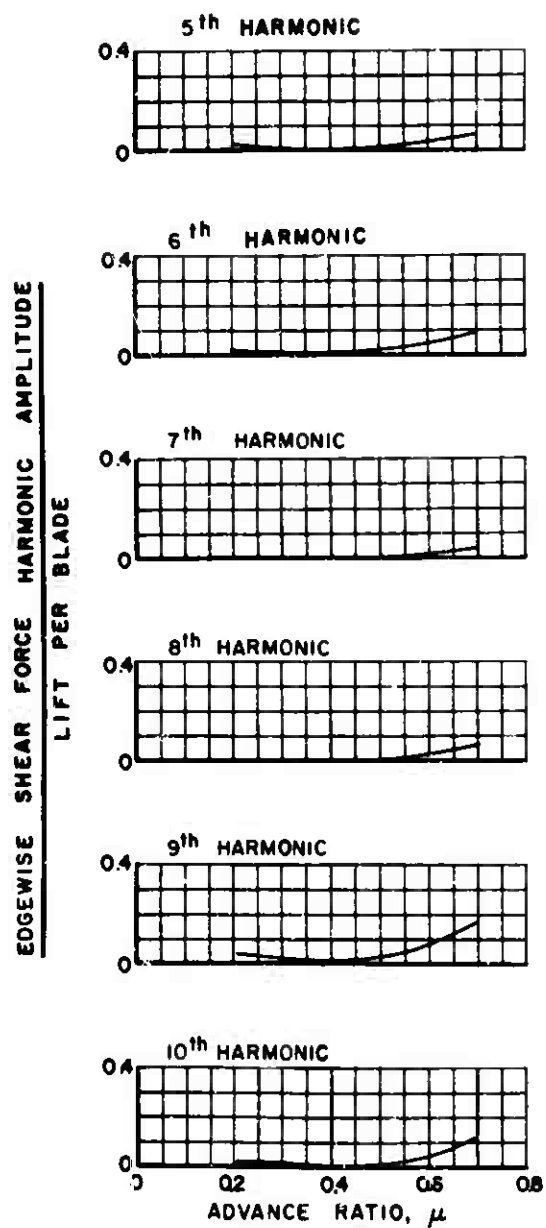
EDGEWISE SHEAR FORCE HARMONIC AMPLITUDE
LIFT PER BLADE



$$C_L/\sigma = 0.035, \quad \alpha_s = -4 \text{ deg.}$$

(b) EDGEWISE SHEAR

Figure 13. Continued.



$$C_L/\sigma = 0.035, \quad \alpha_s = -4 \text{ deg.}$$

Figure 13(b). Concluded.

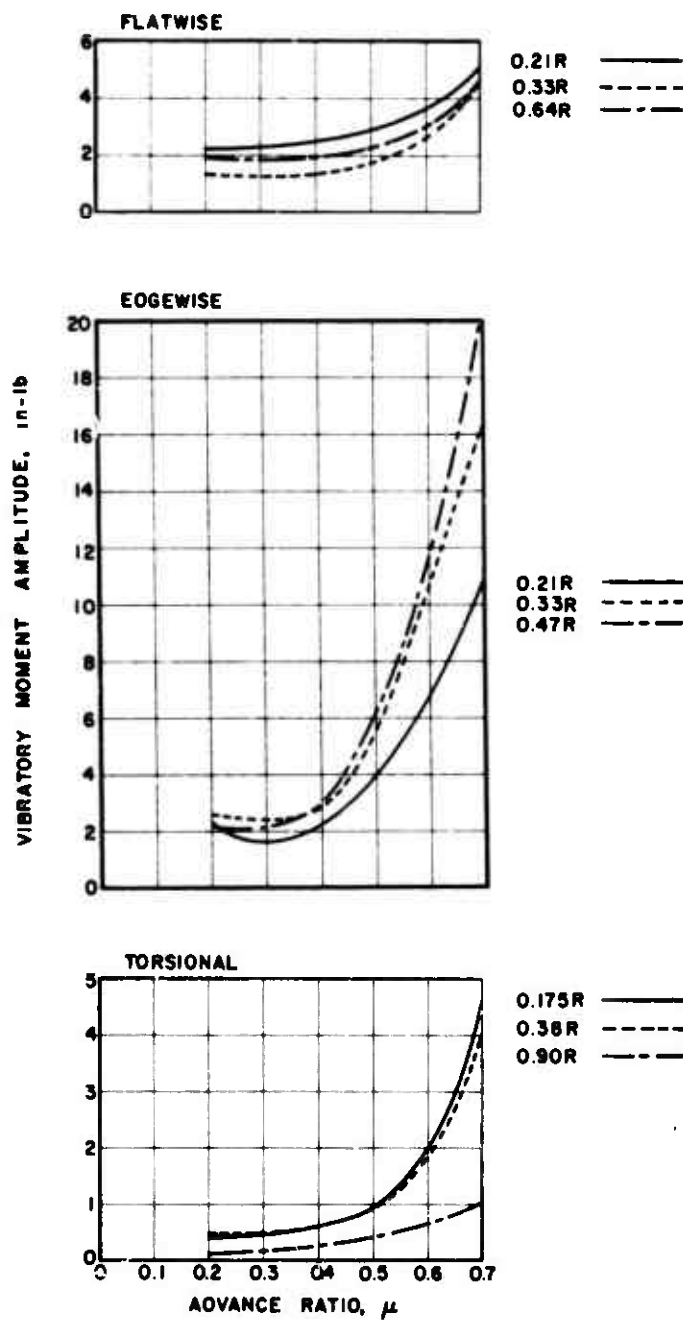


Figure 14. Effect of Advance Ratio on Rotor Blade Vibratory Moments.

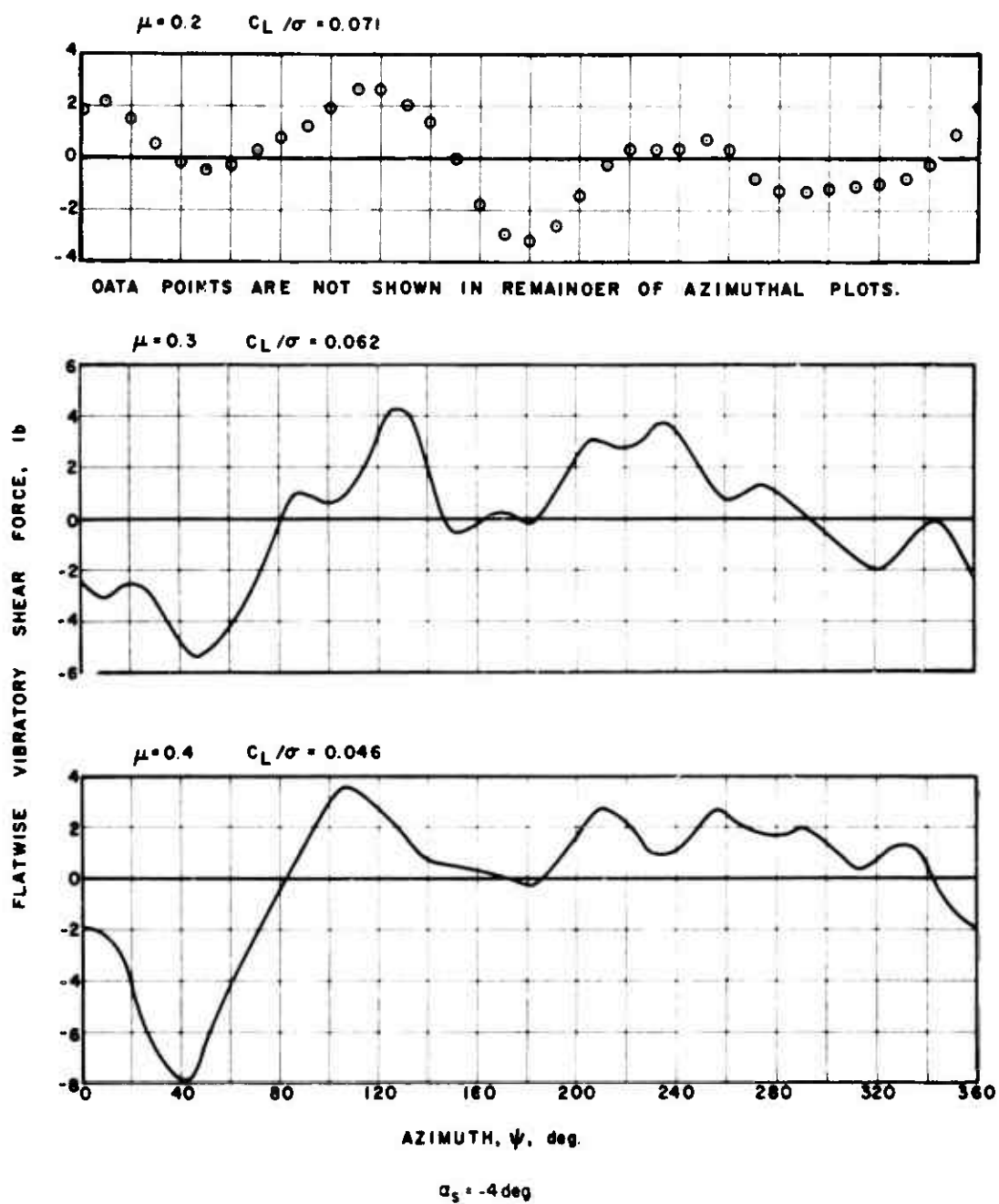


Figure 15. Experimental Flatwise Vibratory Shear Force.

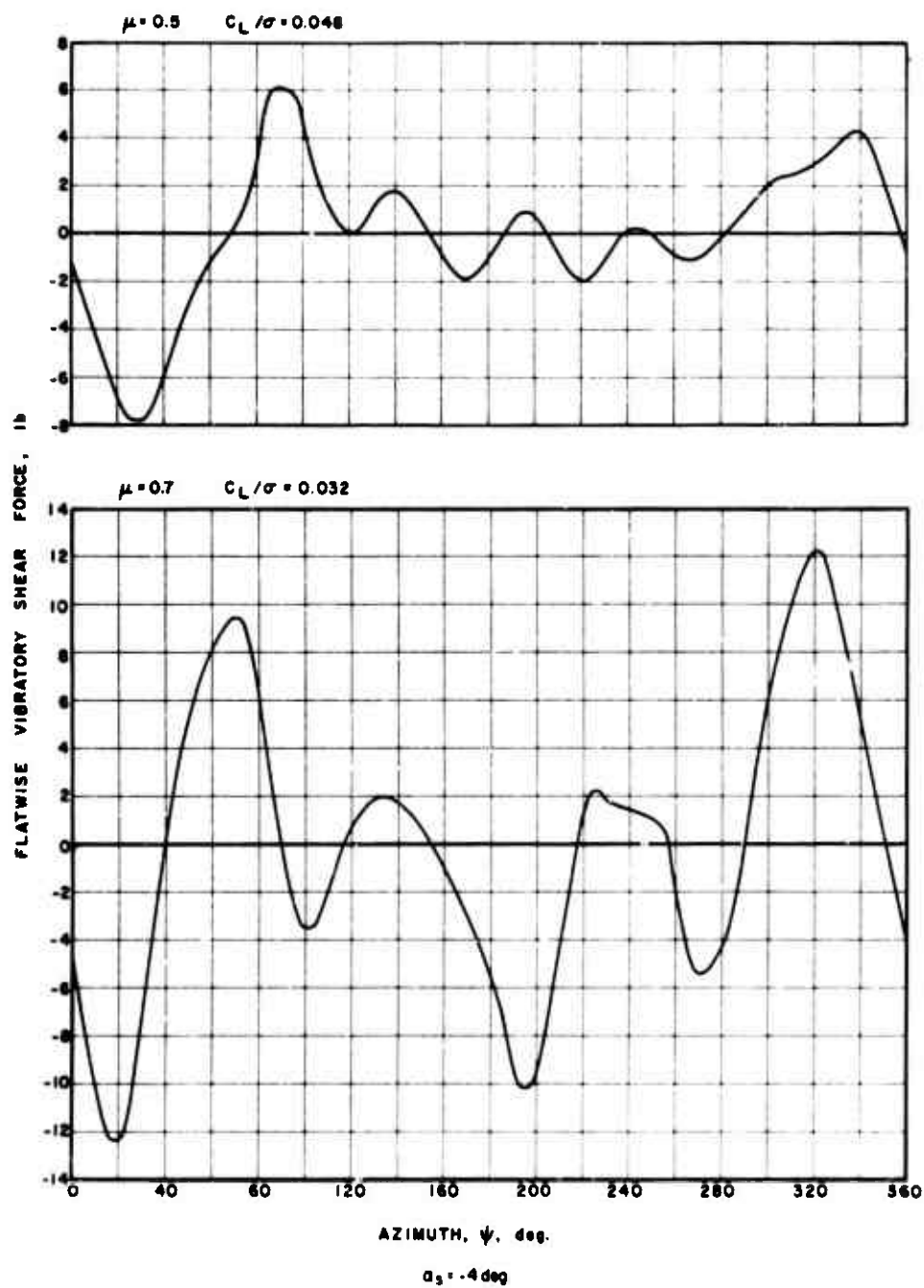


Figure 15. Concluded.

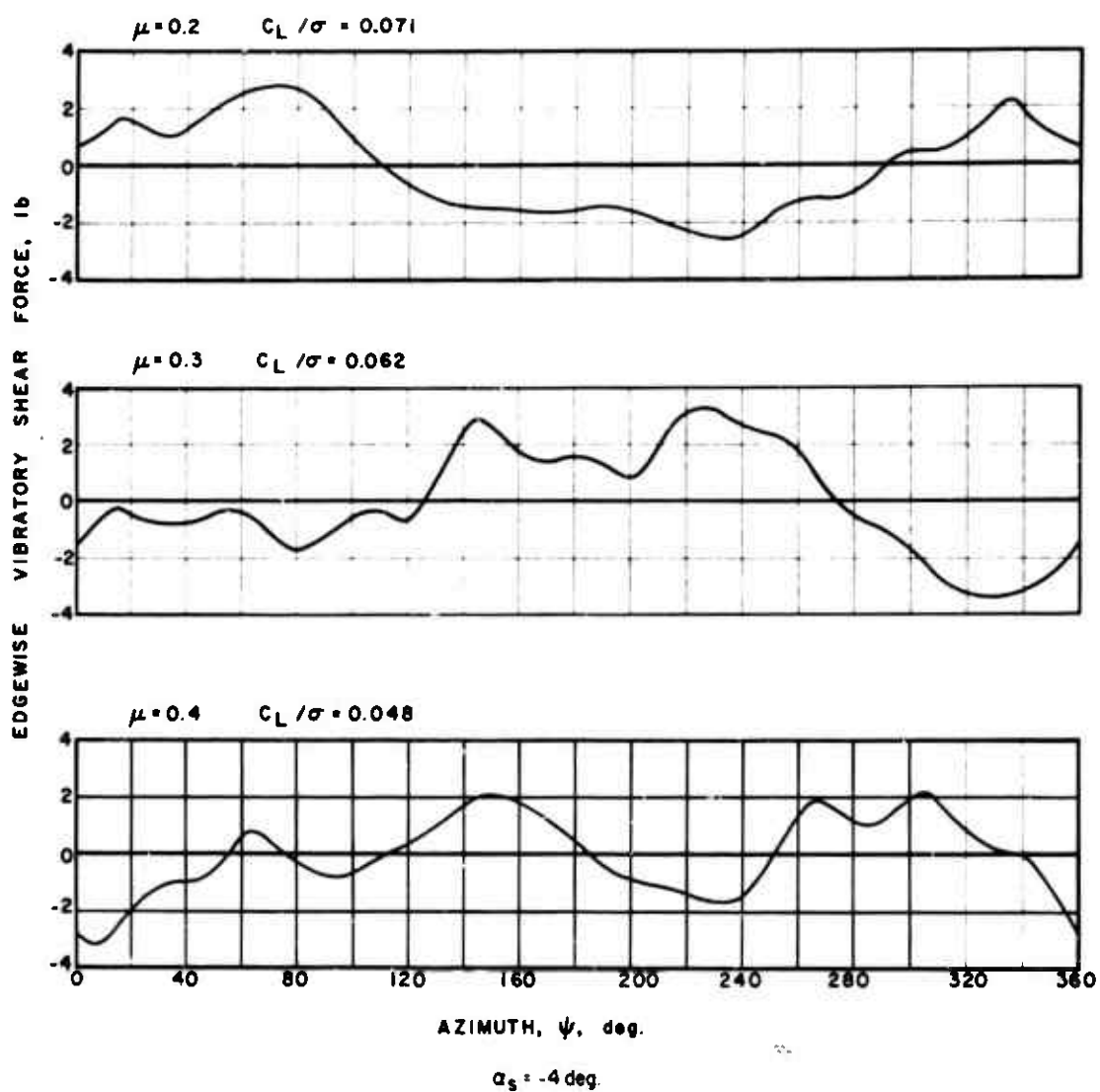


Figure 16. Experimental Edgewise Vibratory Shear Force.

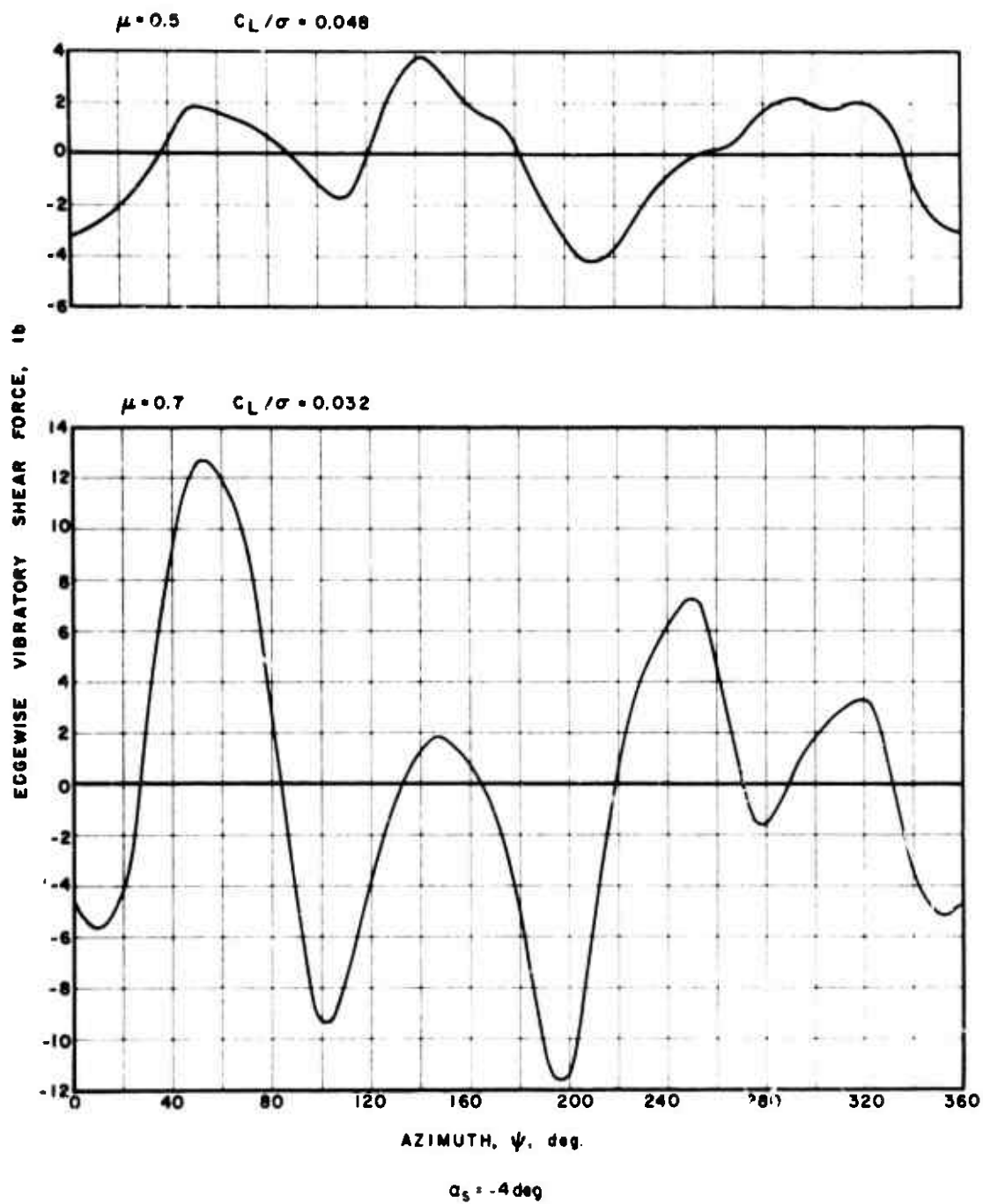


Figure 16. Concluded.

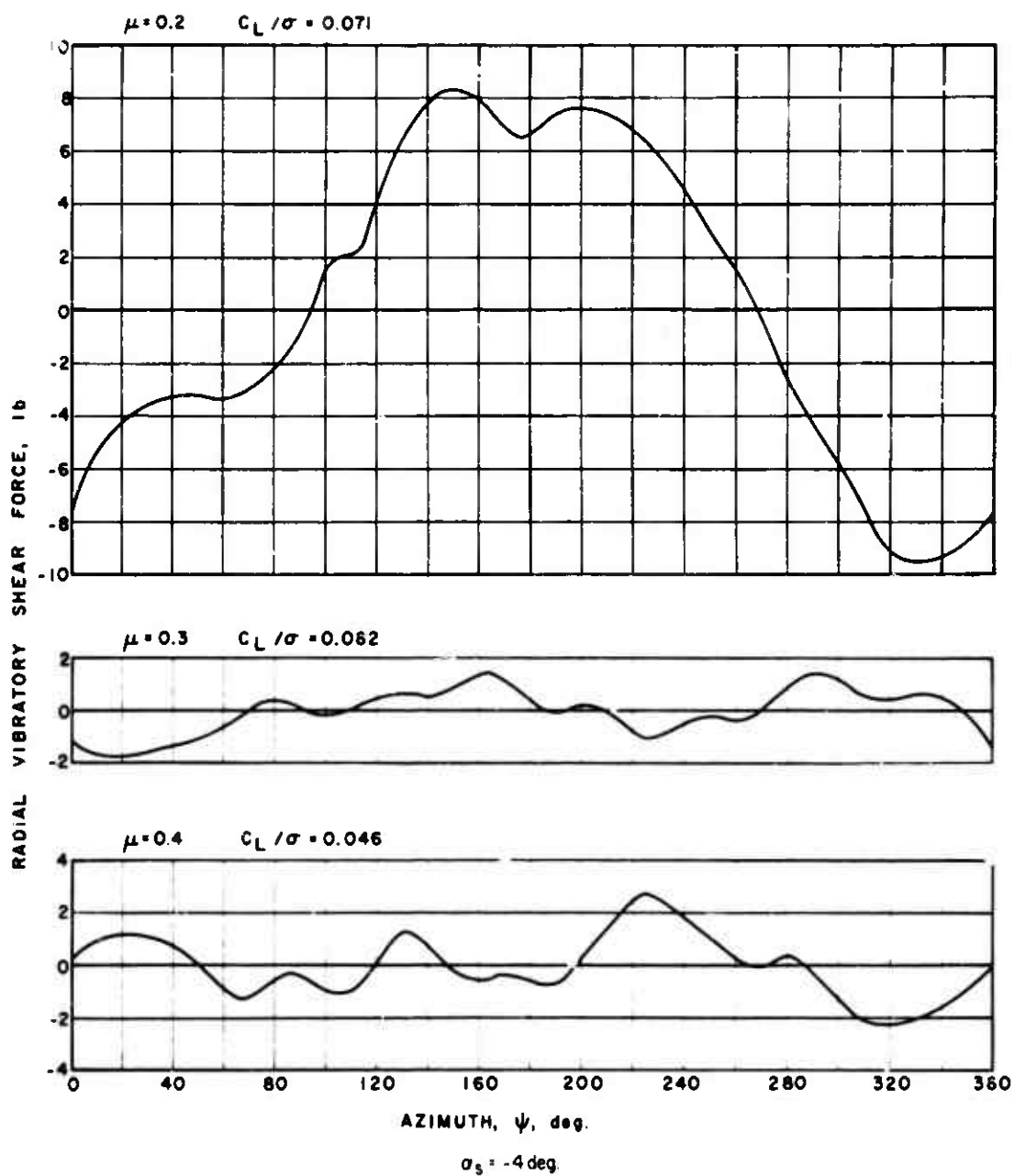


Figure 17. Experimental Radial Vibratory Shear Force.

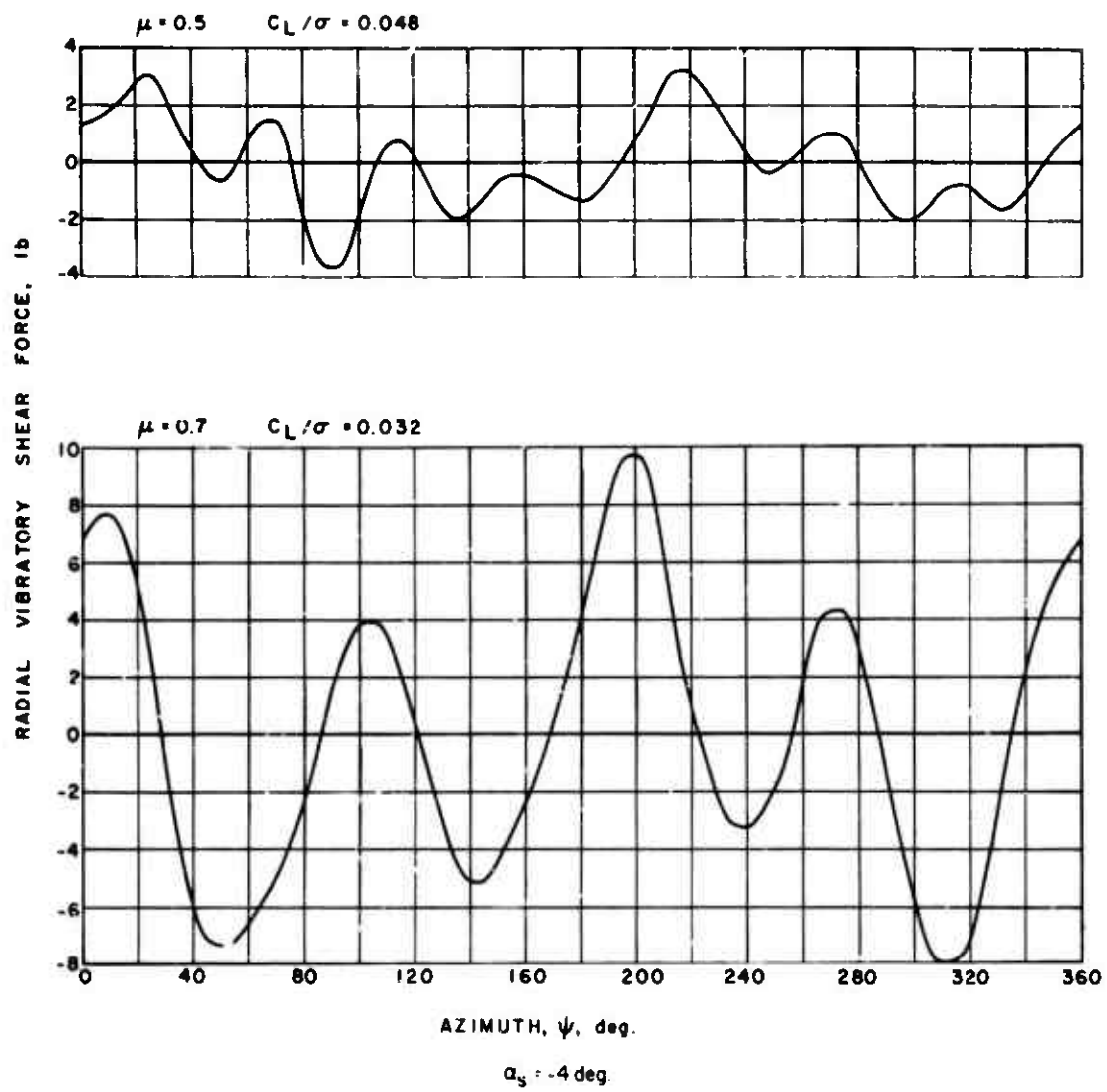
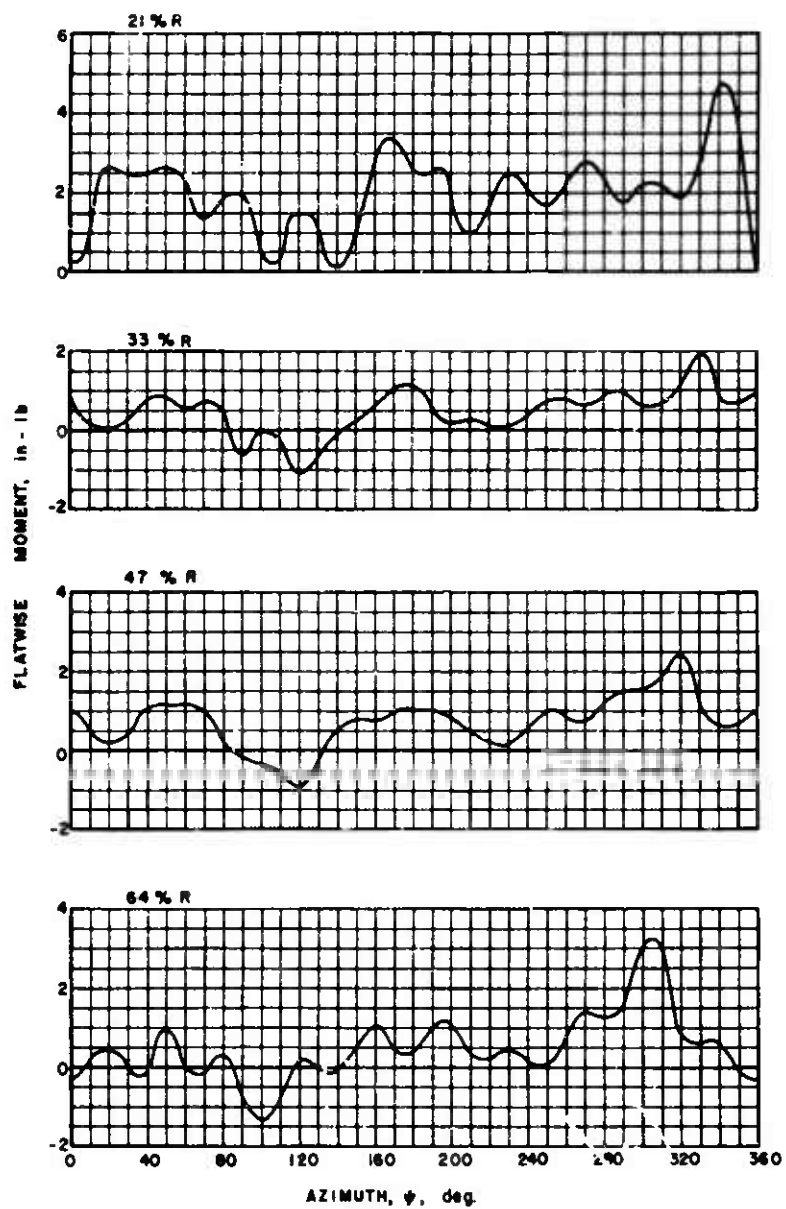


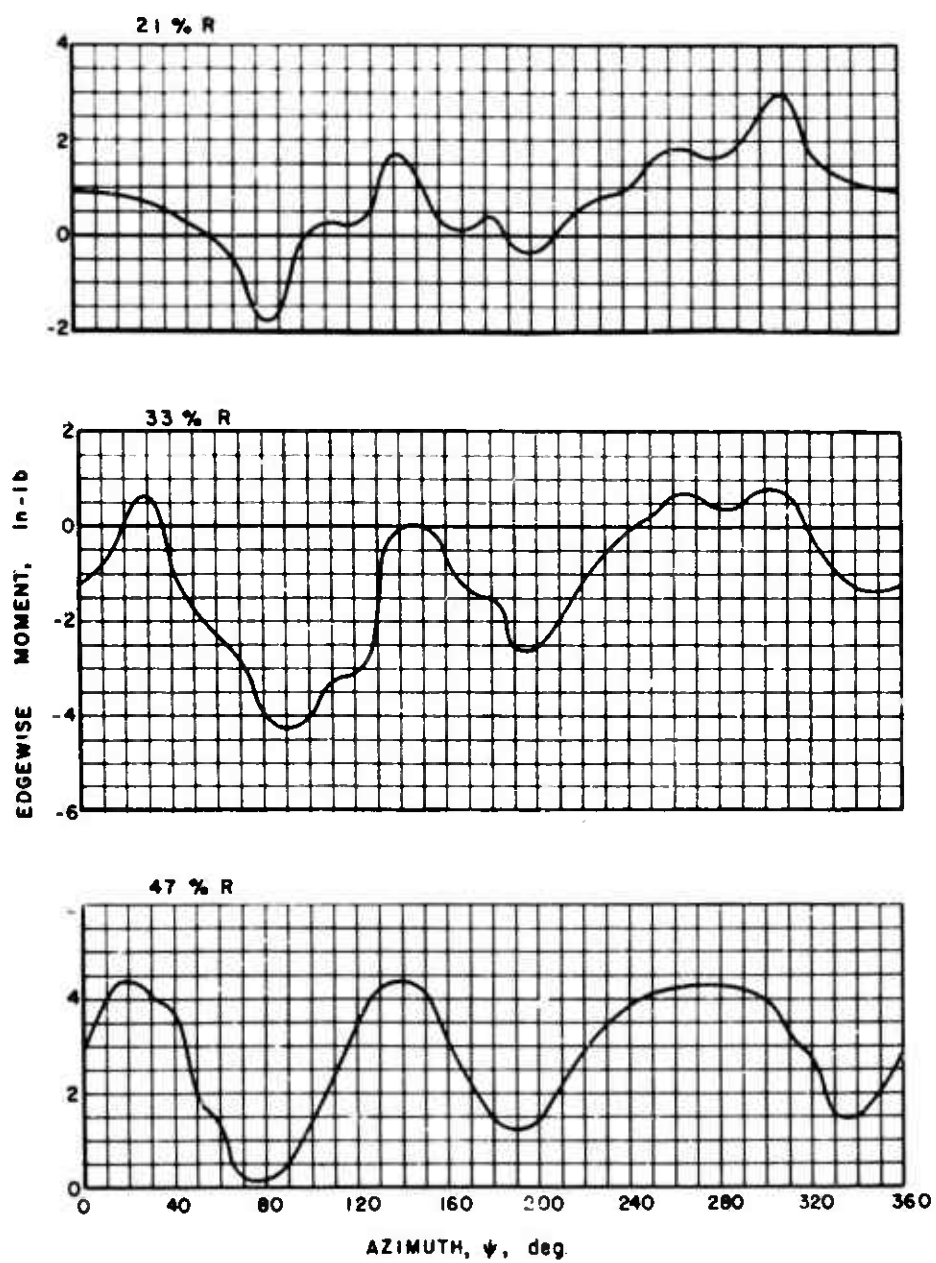
Figure 17. Concluded.



$$\mu = 0.2 \quad C_L / \sigma = 0.071 \quad \alpha_g = -4 \text{ deg}$$

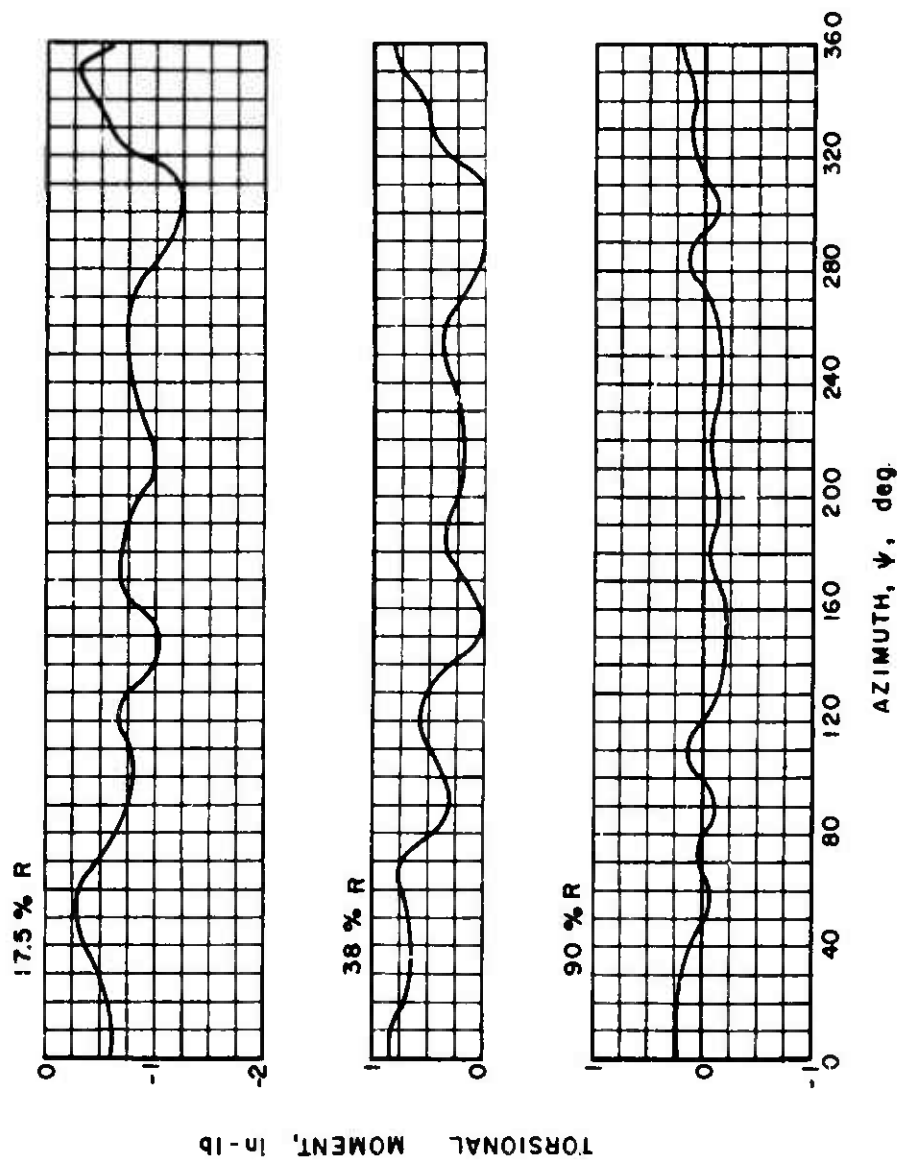
(a) FLATWISE MOMENTS

Figure 18. Experimental Blade Moments.



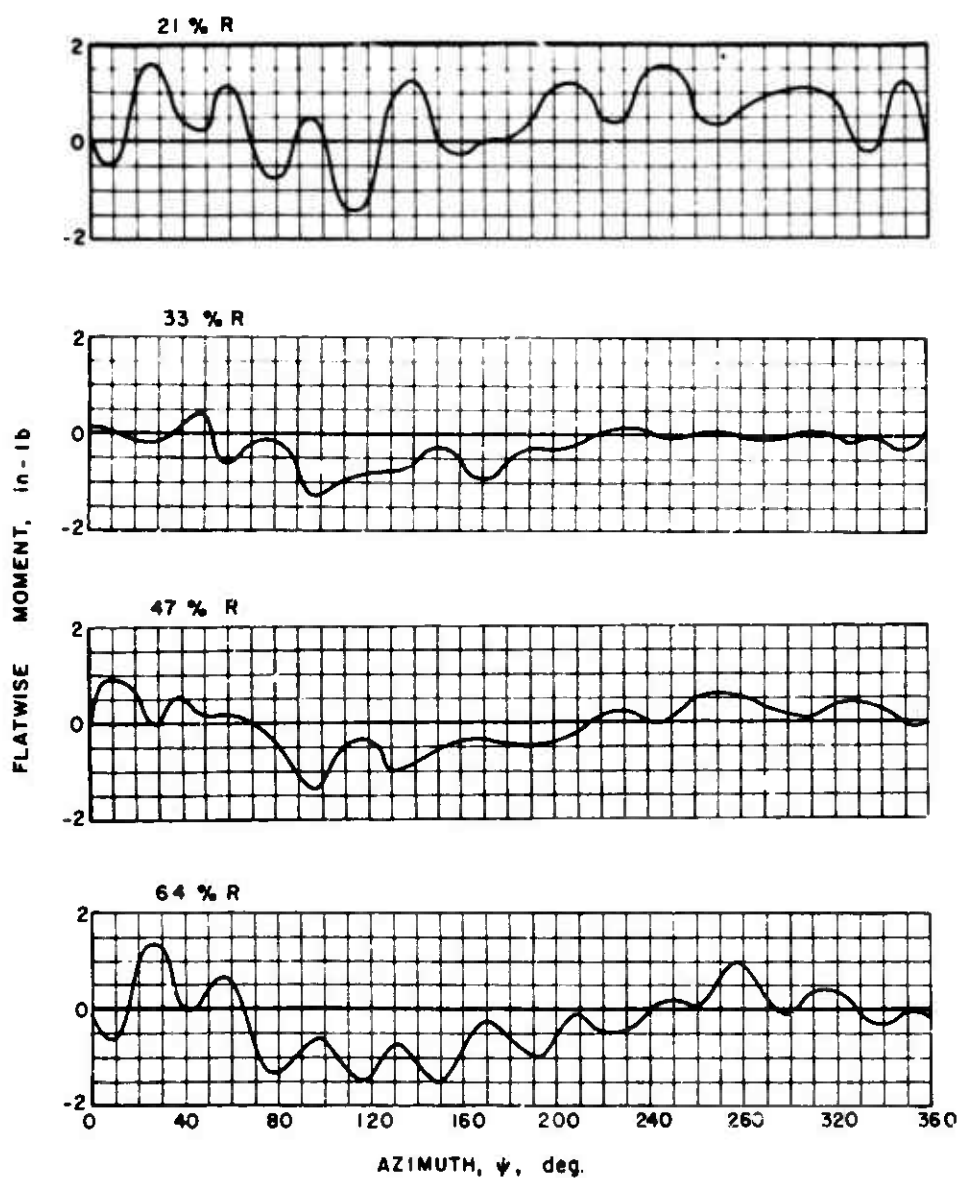
(b) EDGEWISE MOMENTS

Figure 18. Continued.



(c) TORSIONAL MOMENTS

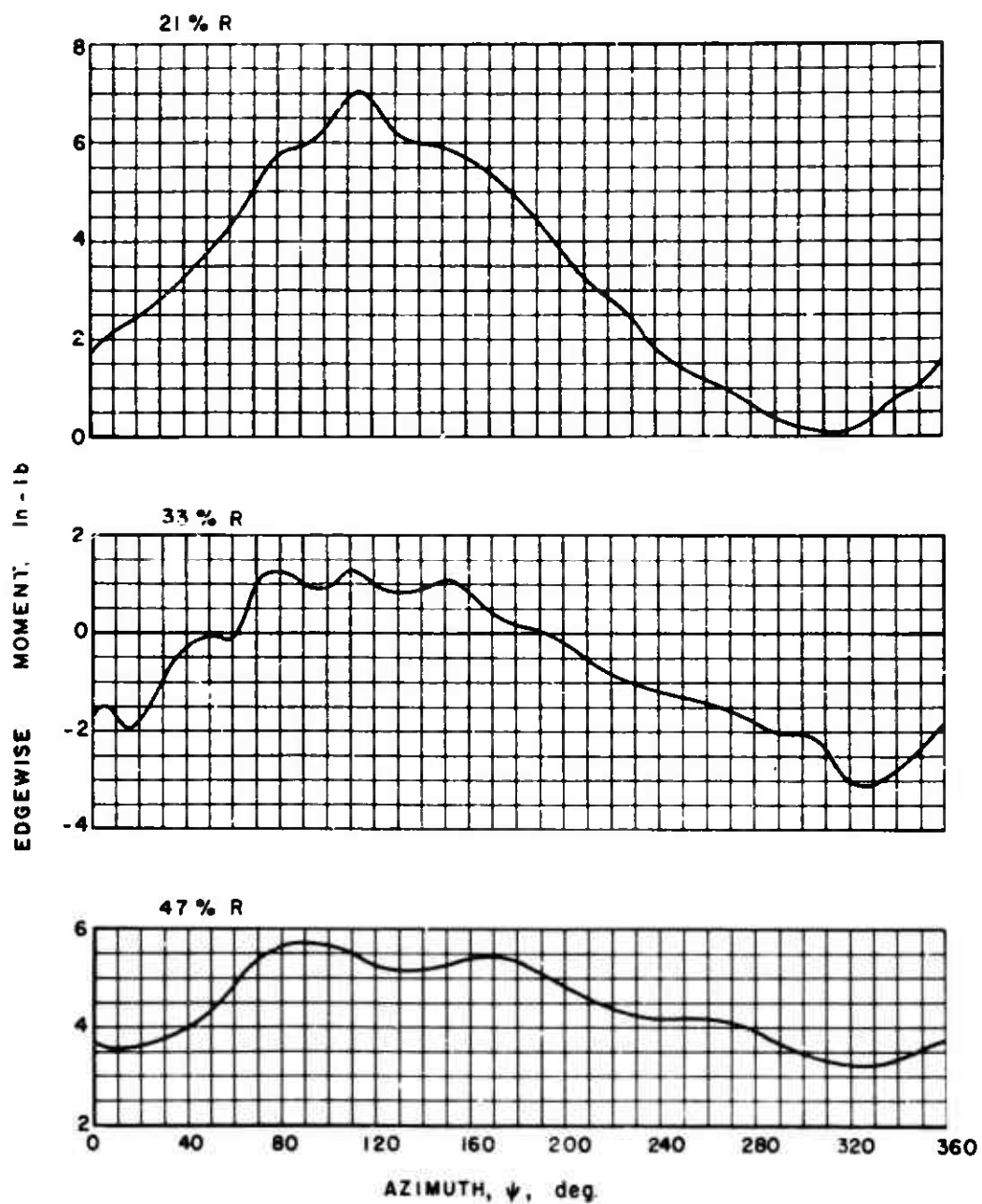
Figure 18. Concluded.



$$\mu = 0.3 \quad C_L / \sigma = 0.019 \quad \alpha_s = -4 \text{ deg.}$$

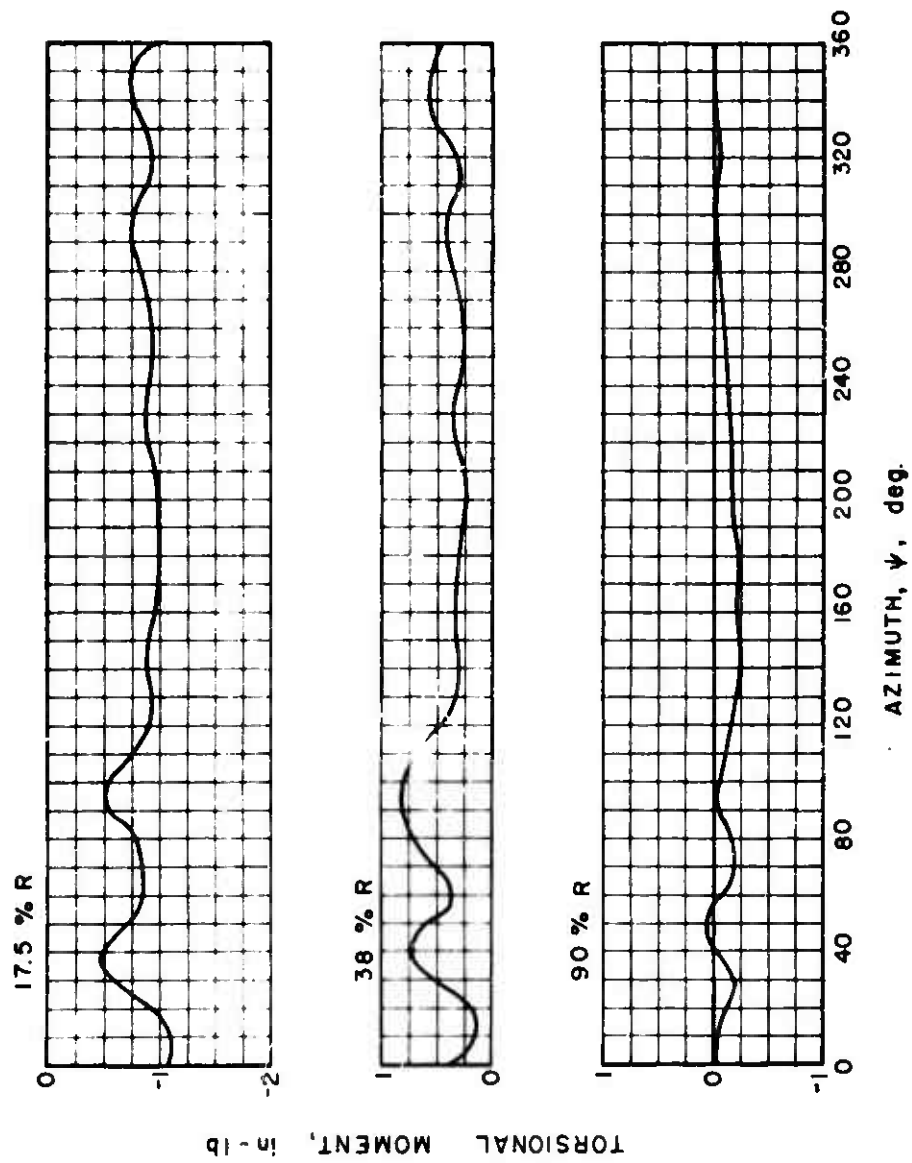
(a) FLATWISE MOMENTS

Figure 19. Experimental Blade Moments.



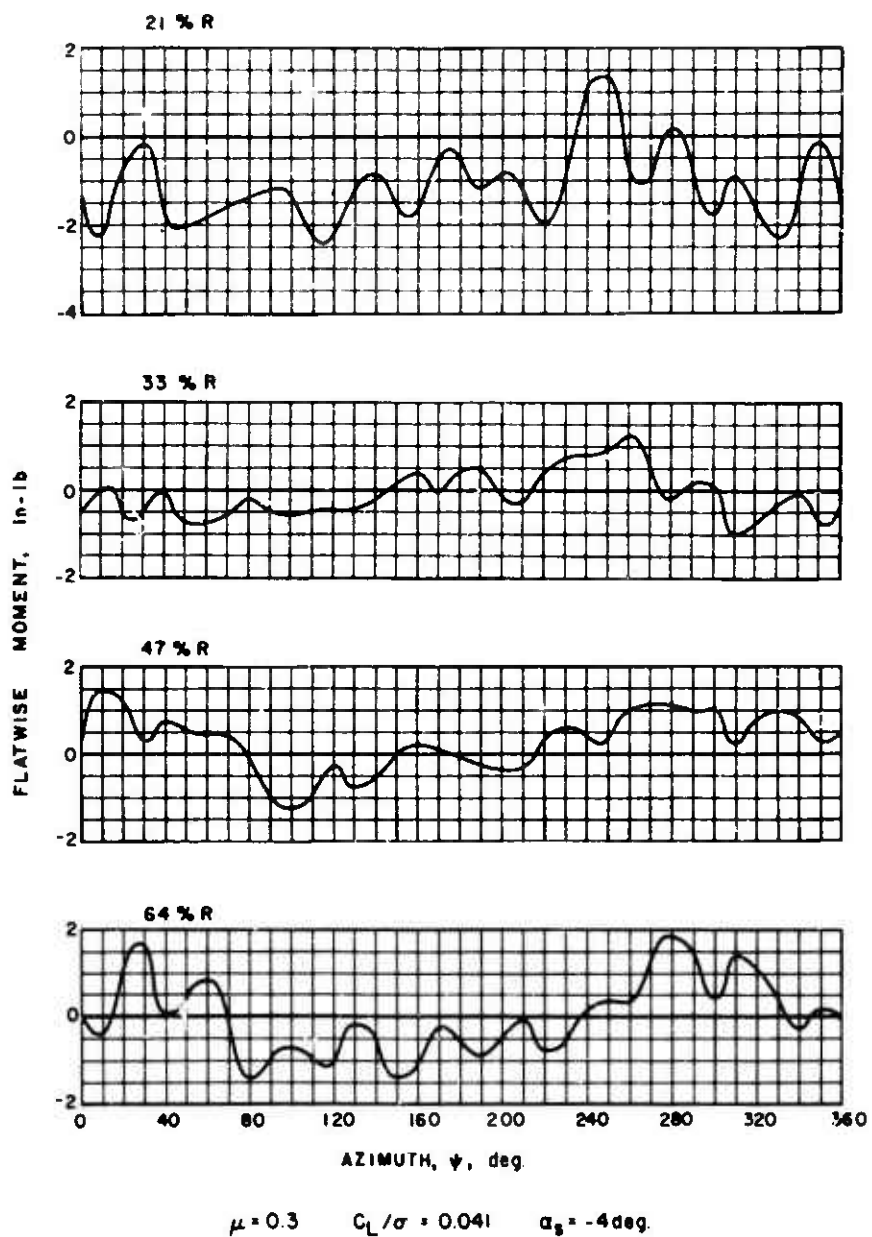
(b) EDGEWISE MOMENTS

Figure 19. Continued.



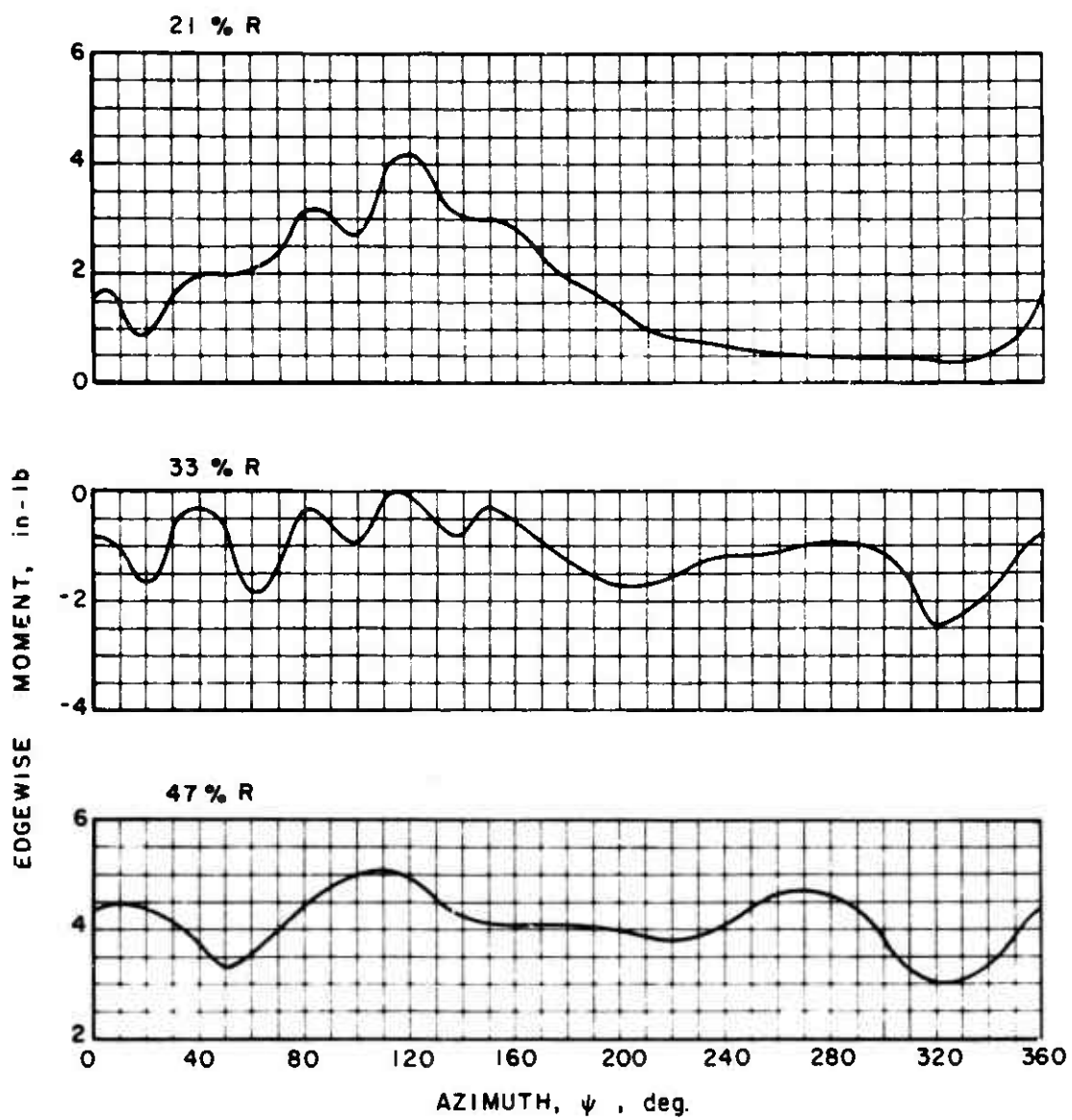
(c) TORSIONAL MOMENTS

Figure 19. Concluded.



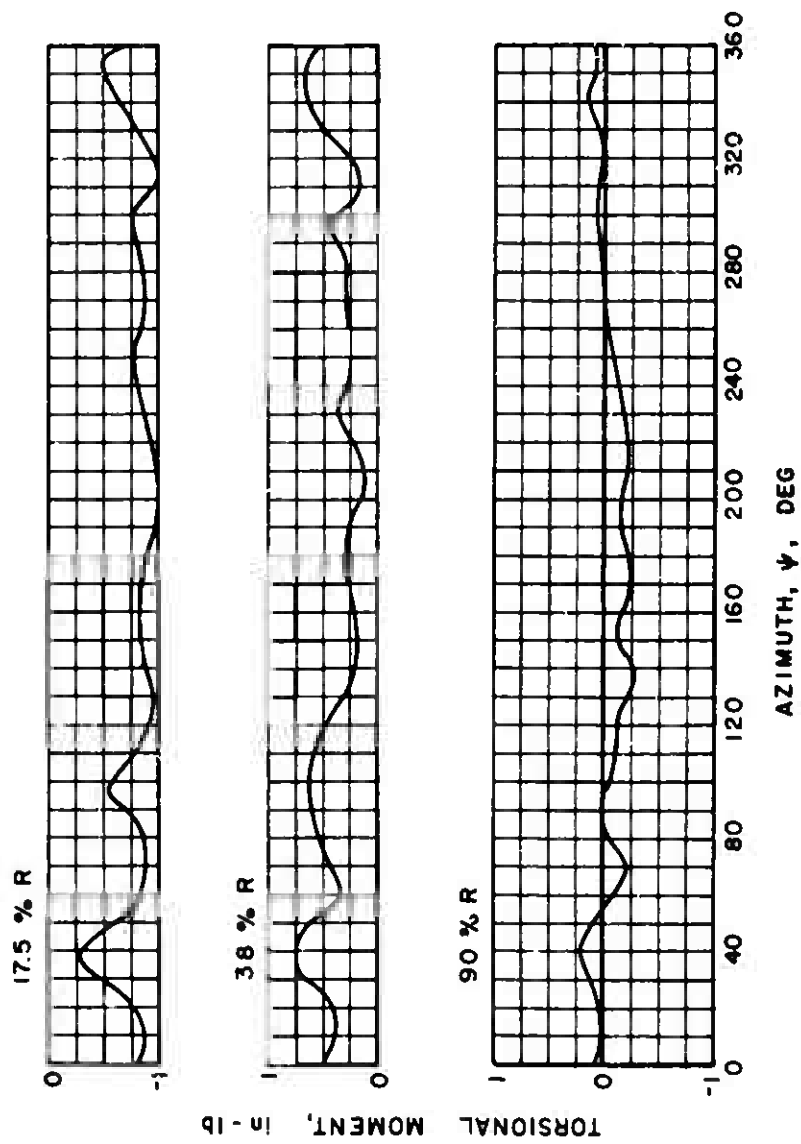
(a) FLATWISE MOMENTS

Figure 20. Experimental Blade Moments.



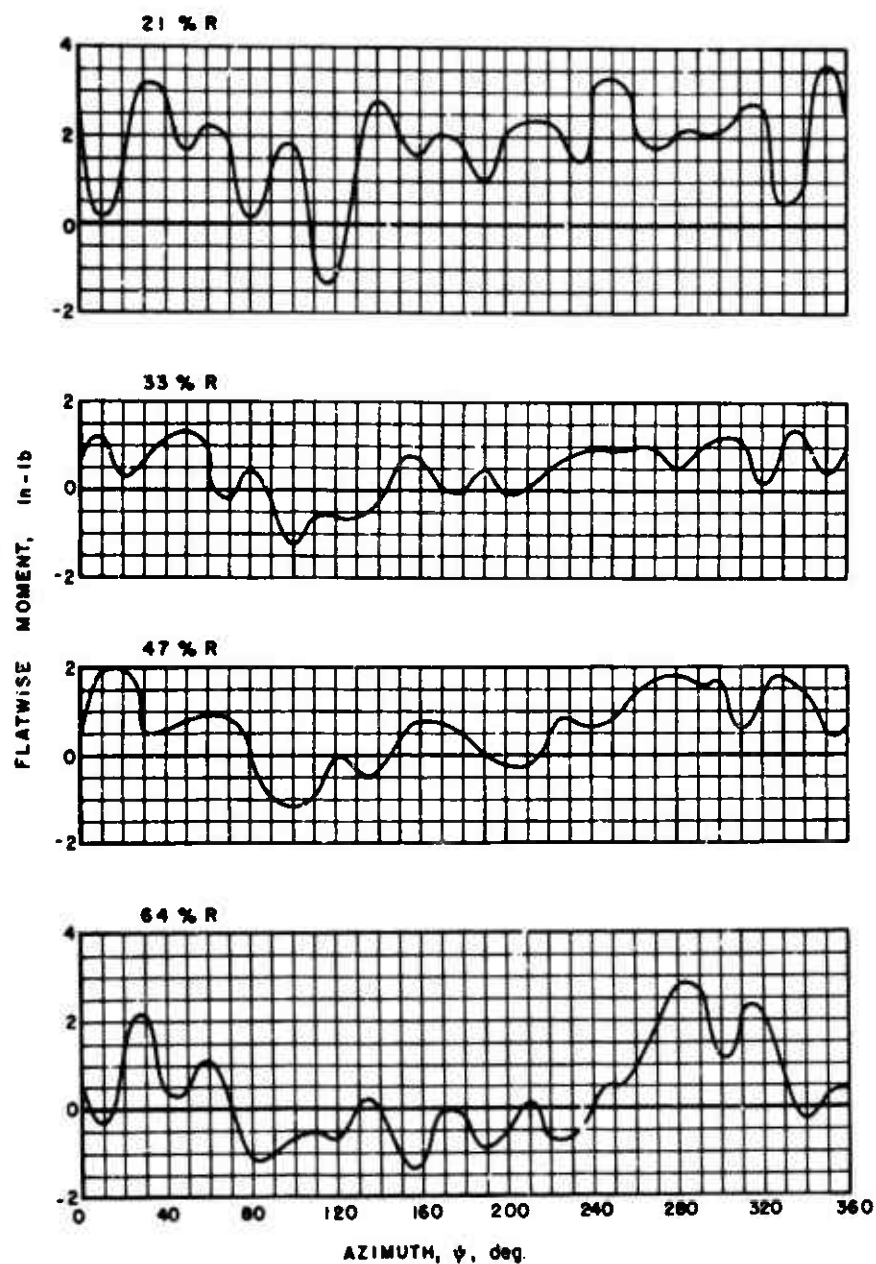
(b) EDGEWISE MOMENTS

Figure 20. Continued.



(c) TORSIONAL MOMENTS

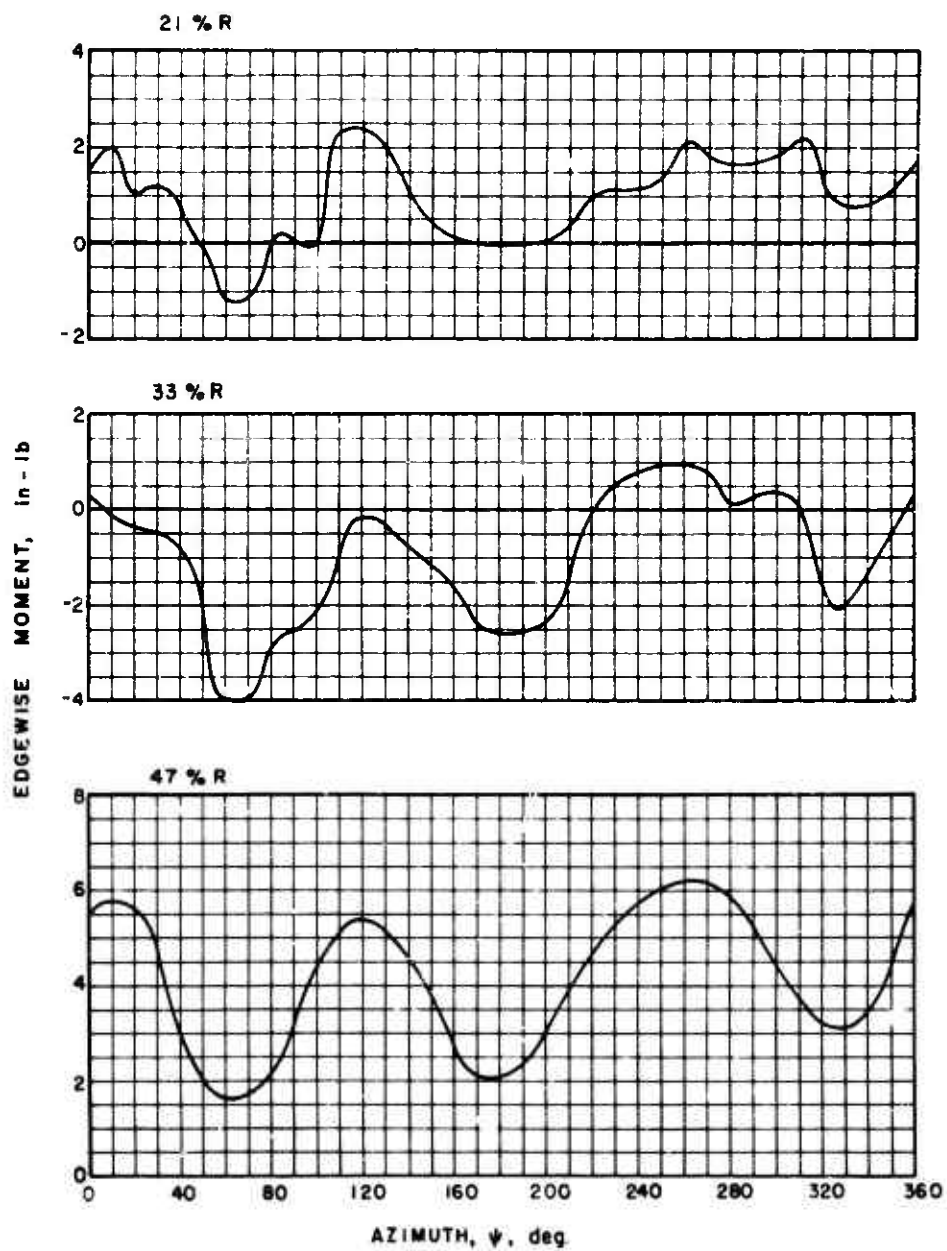
Figure 20. Concluded.



$\mu = 0.3$ $C_L / \sigma = 0.062$ $\alpha_s = -4 \text{ deg.}$

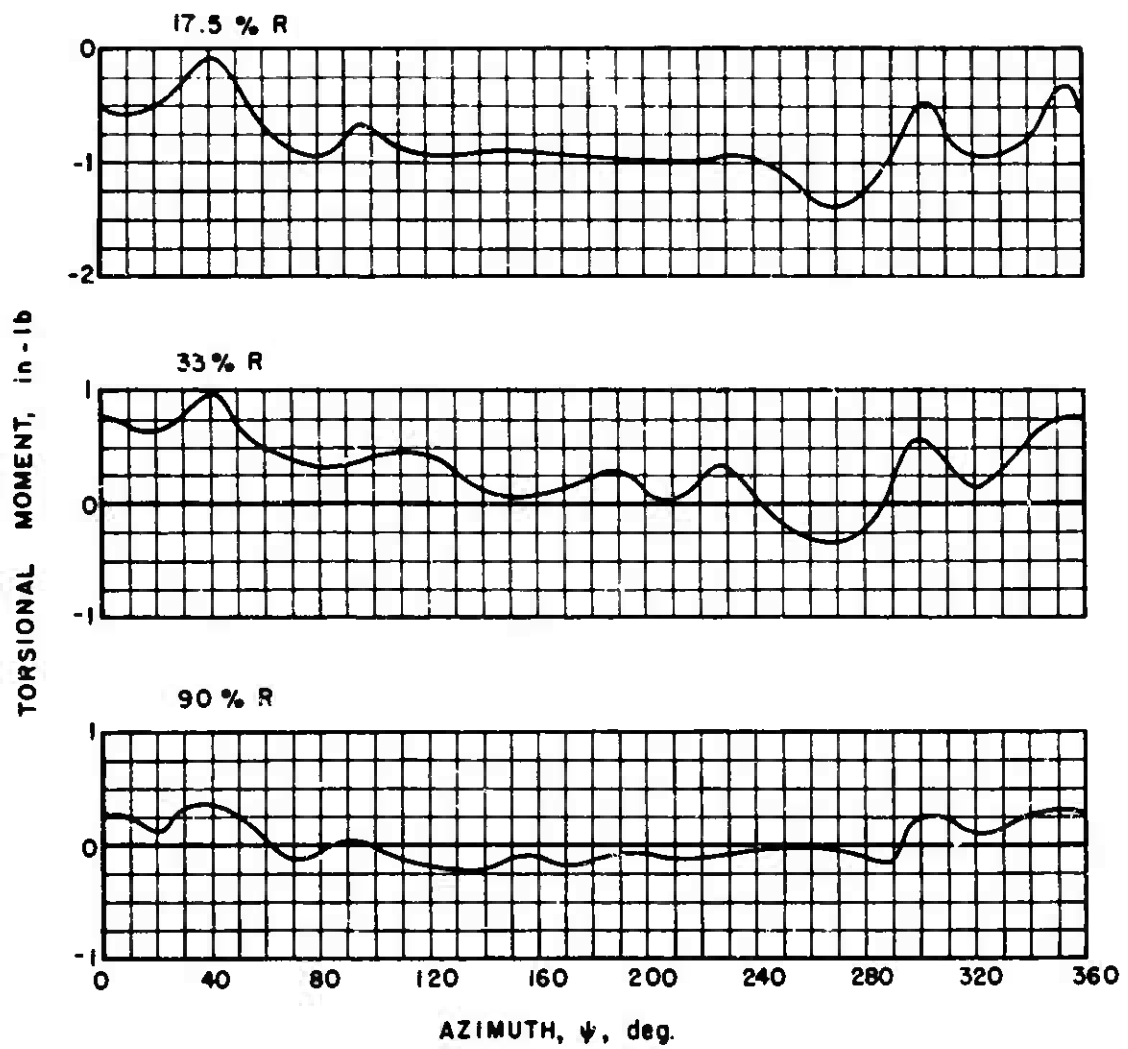
(a) FLATWISE MOMENTS

Figure 21. Experimental Blade Moments.



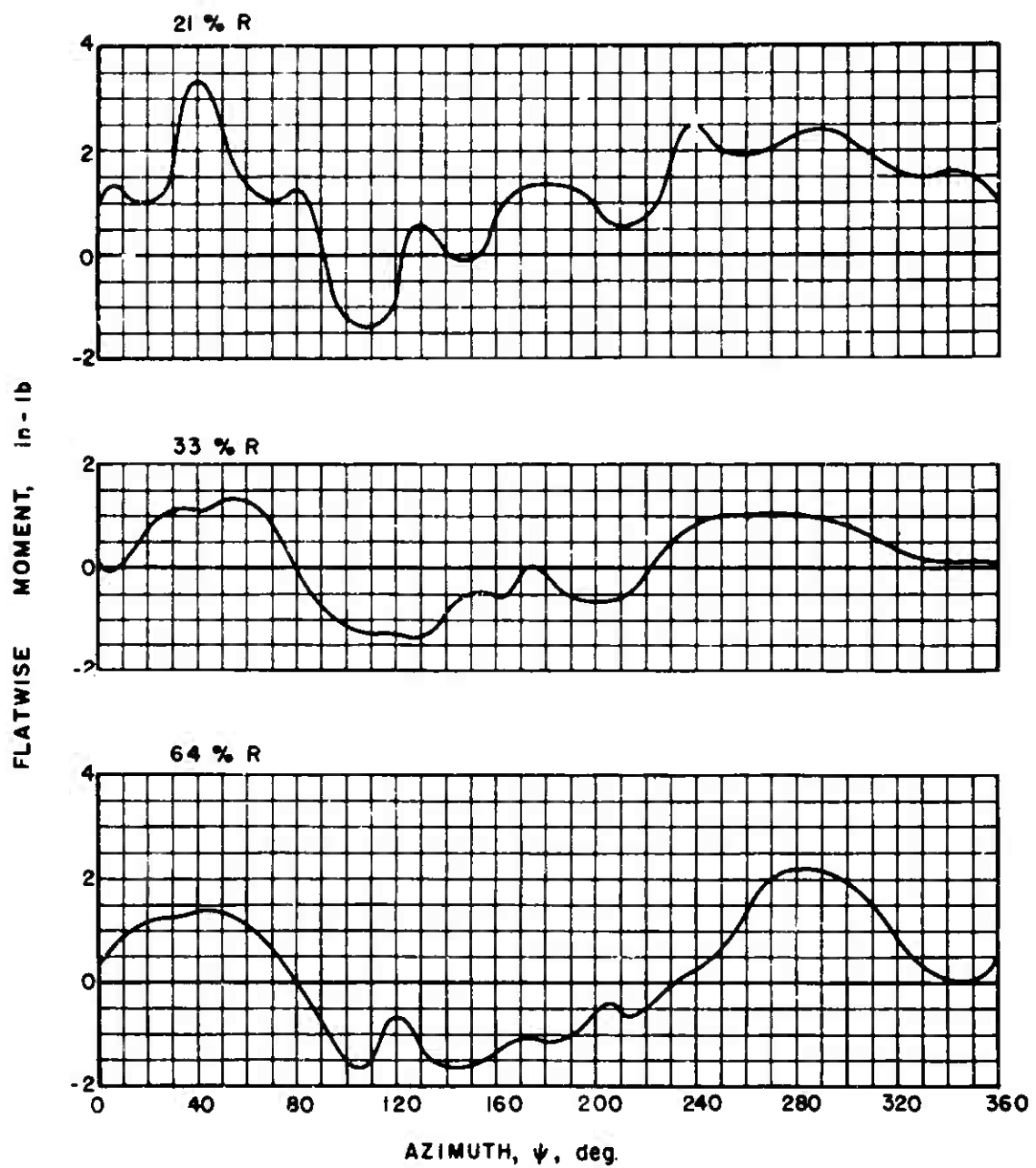
(b) EDGEWISE MOMENTS

Figure 21. Continued.



(c) TORSIONAL MOMENTS

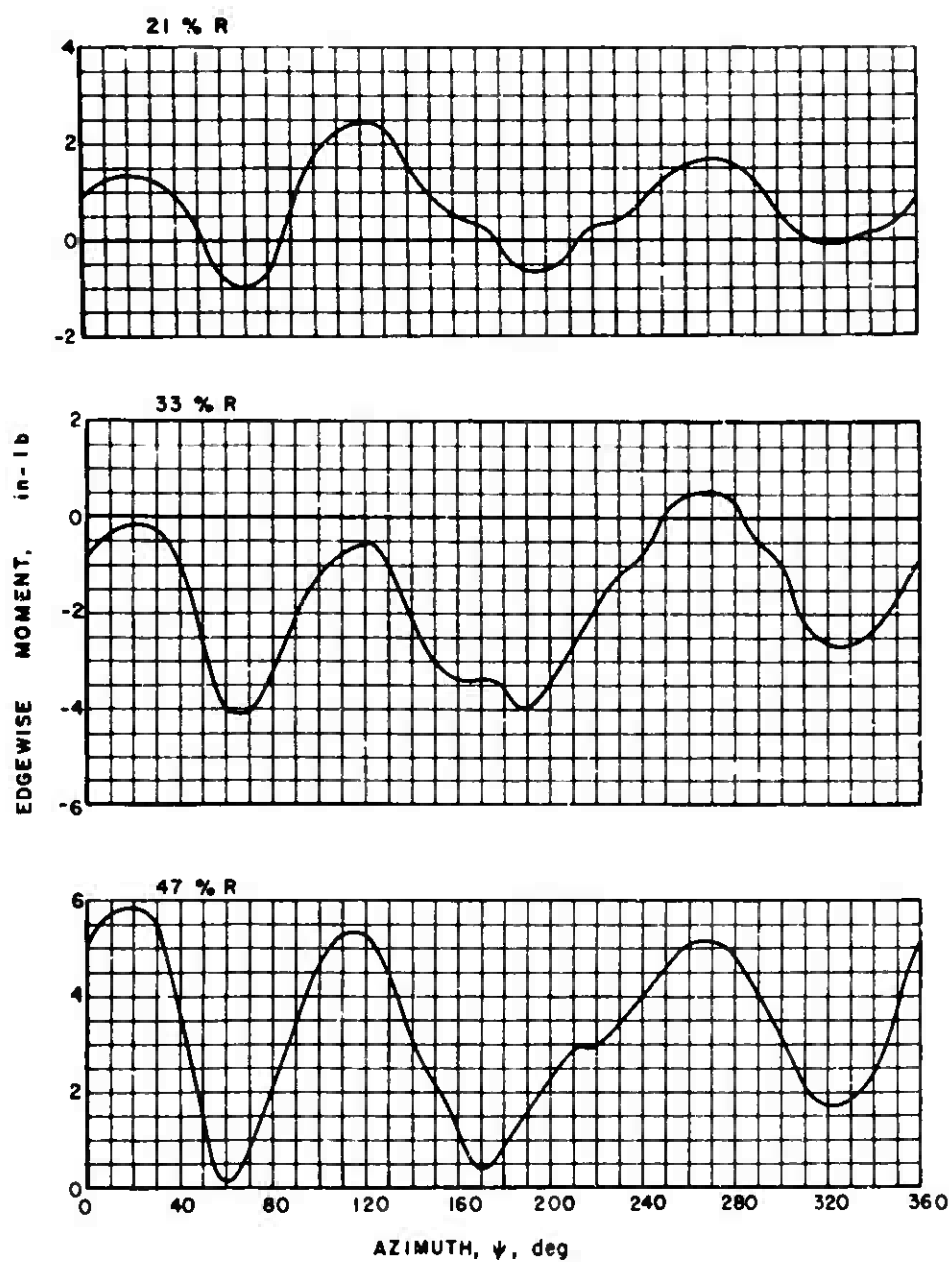
Figure 21. Concluded.



$$\mu = 0.4 \quad C_L / \sigma = 0.046 \quad \alpha_s = -4 \text{ deg.}$$

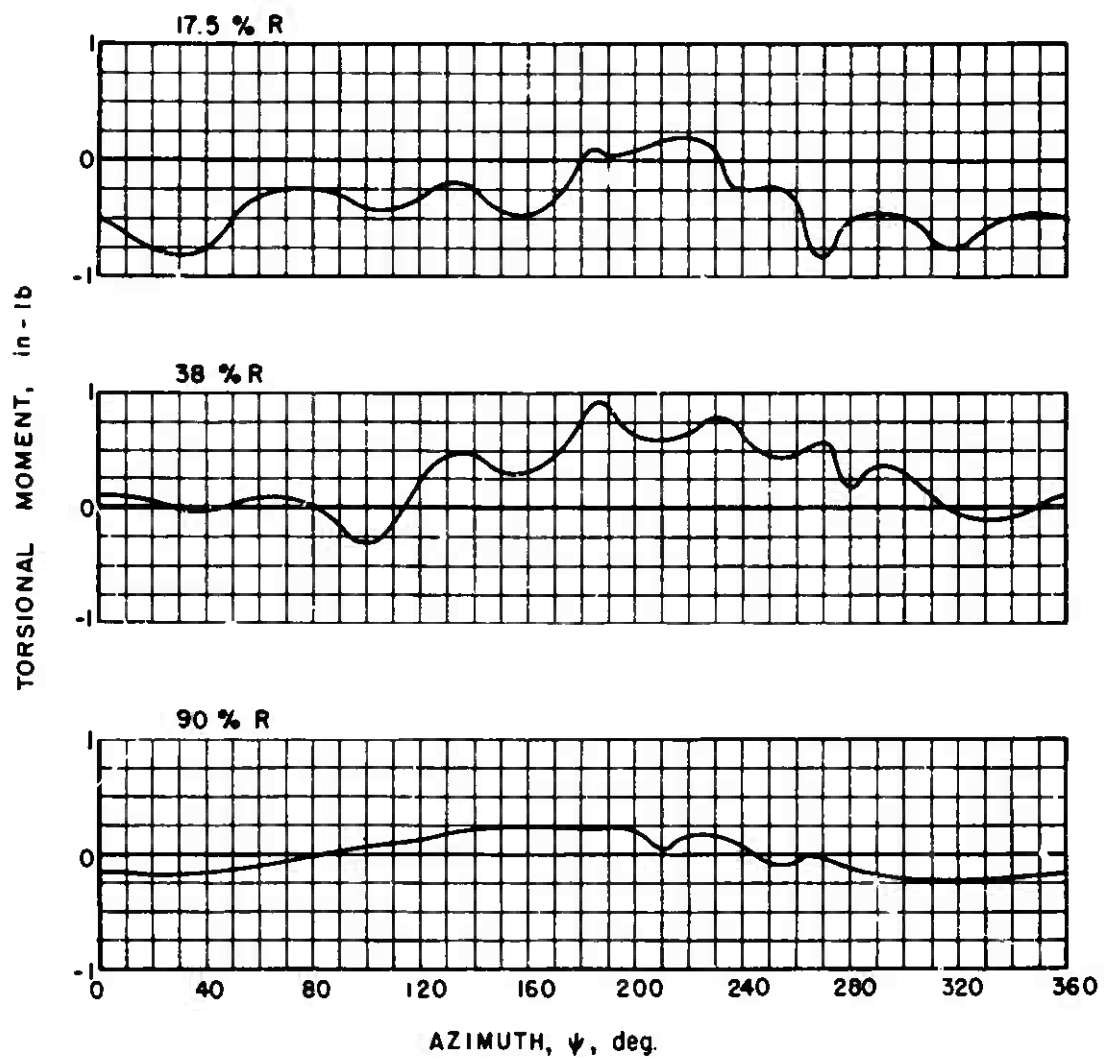
(a) FLATWISE MOMENTS

Figure 22. Experimental Blade Moments.



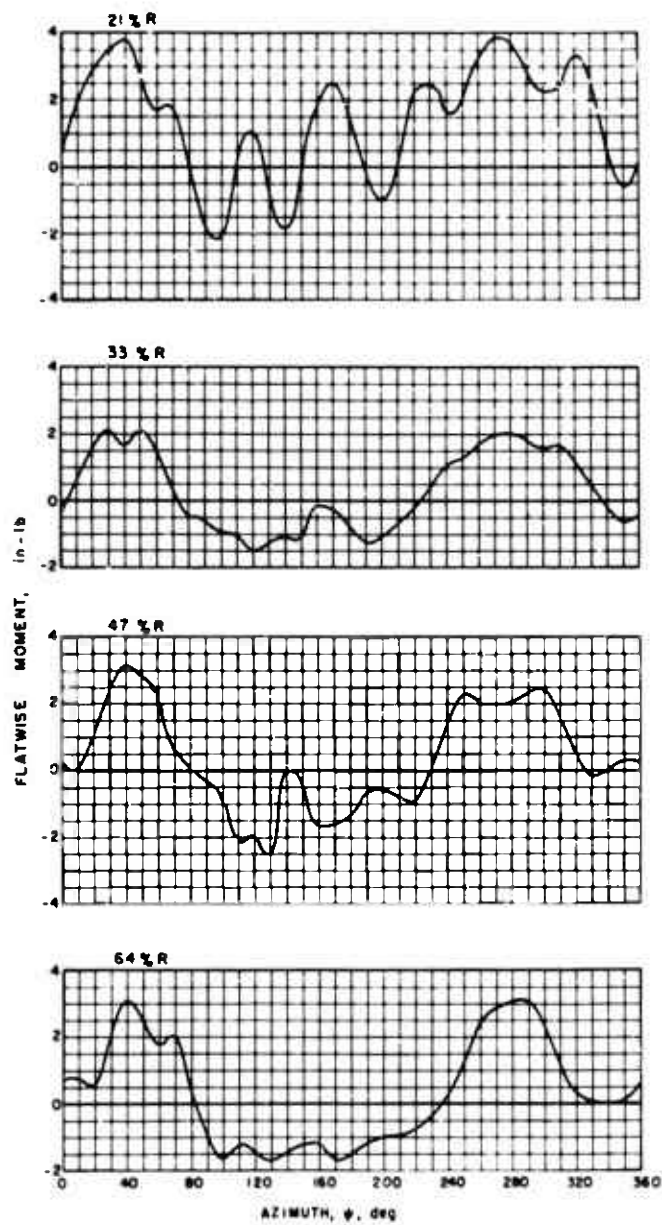
(b) EDGEWISE MOMENTS

Figure 22. Continued.



(c) TORSIONAL MOMENTS

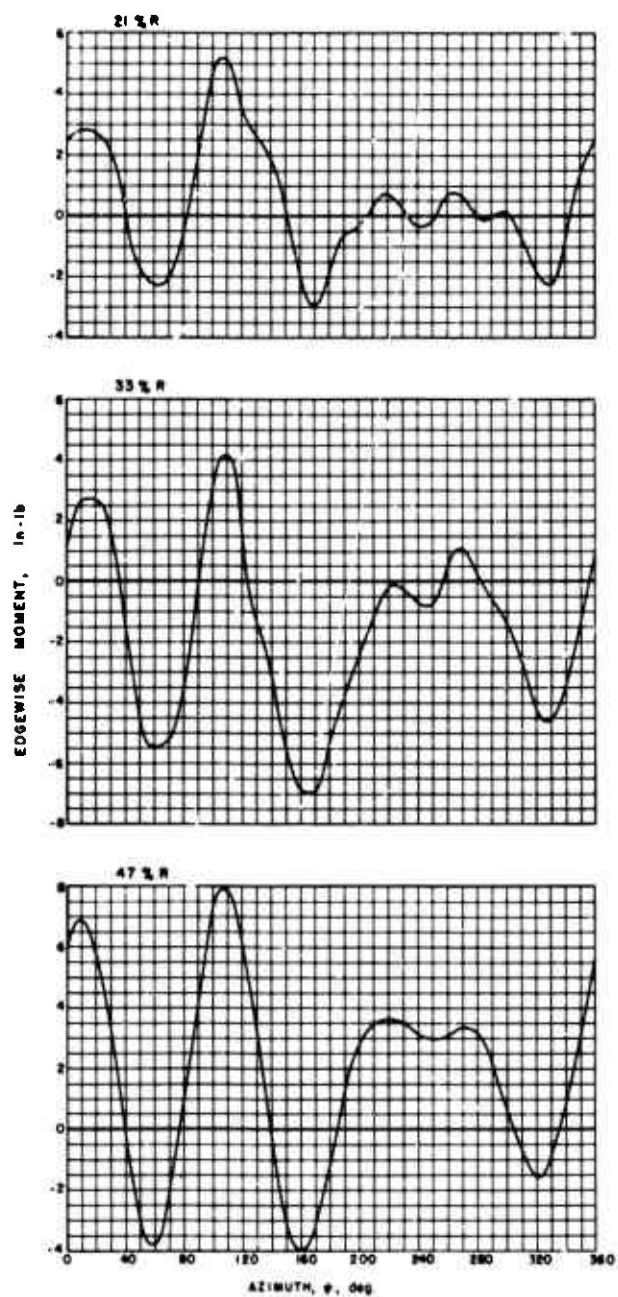
Figure 22. Concluded.



$\mu = 0.5$ $C_L / \sigma = 0.048$ $\alpha_s = -4 \text{ deg}$

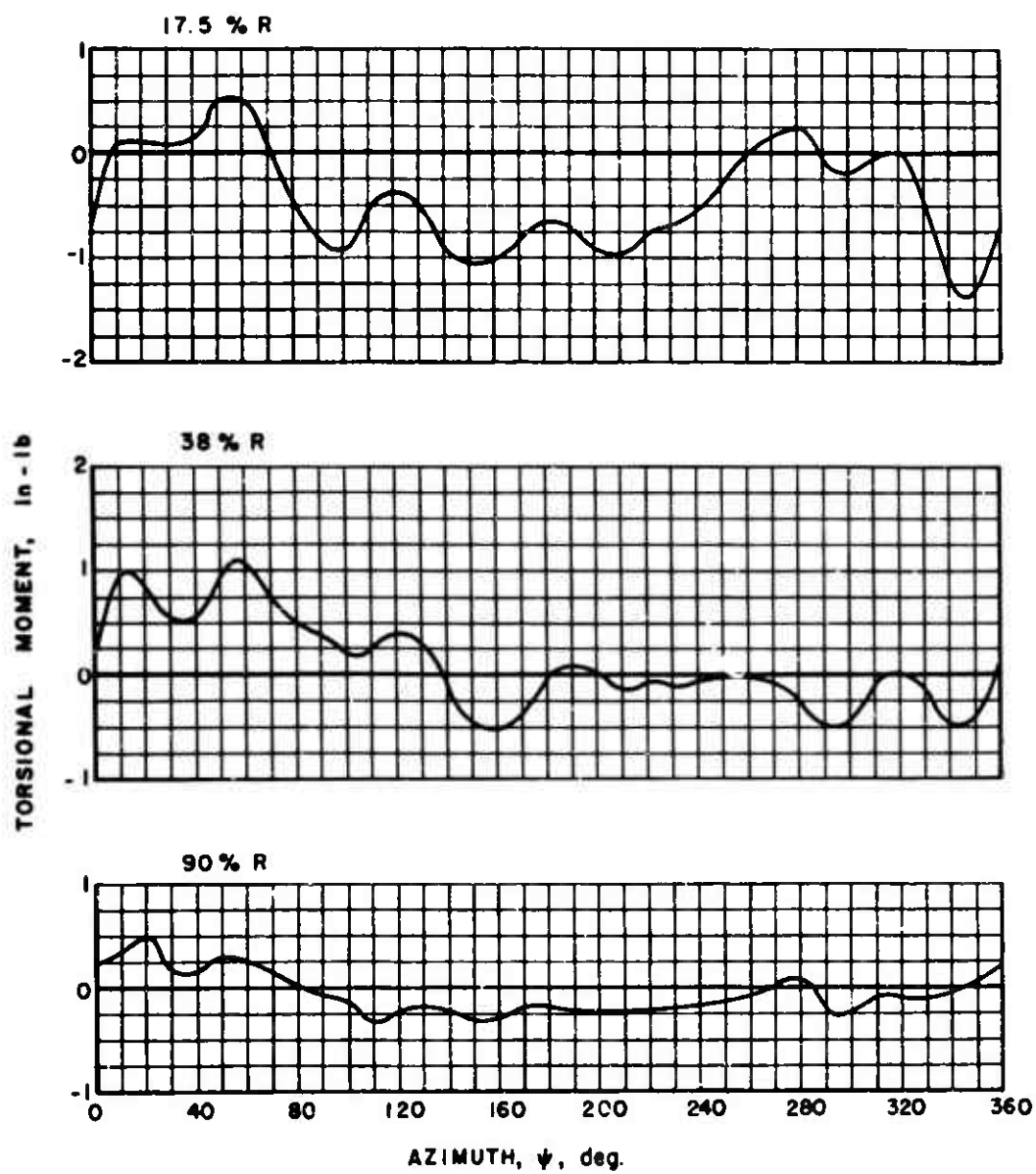
(a) FLATWISE MOMENTS

Figure 23. Experimental Blade Moments.



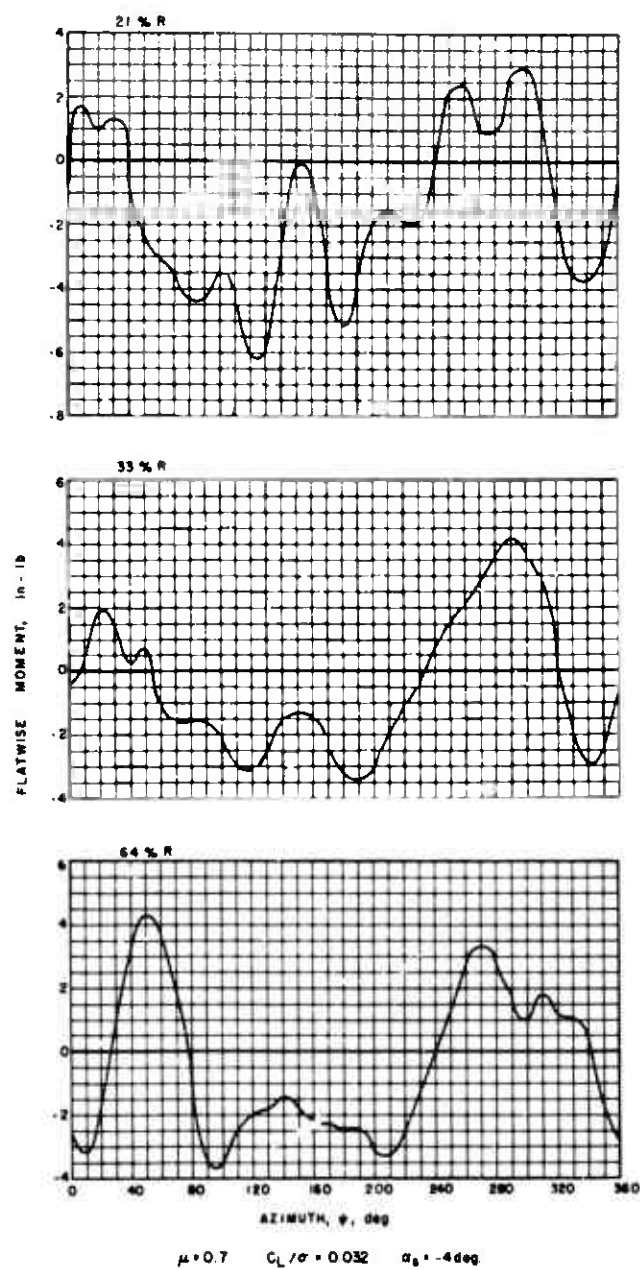
(b) EDGEWISE MOMENTS

Figure 23. Continued.



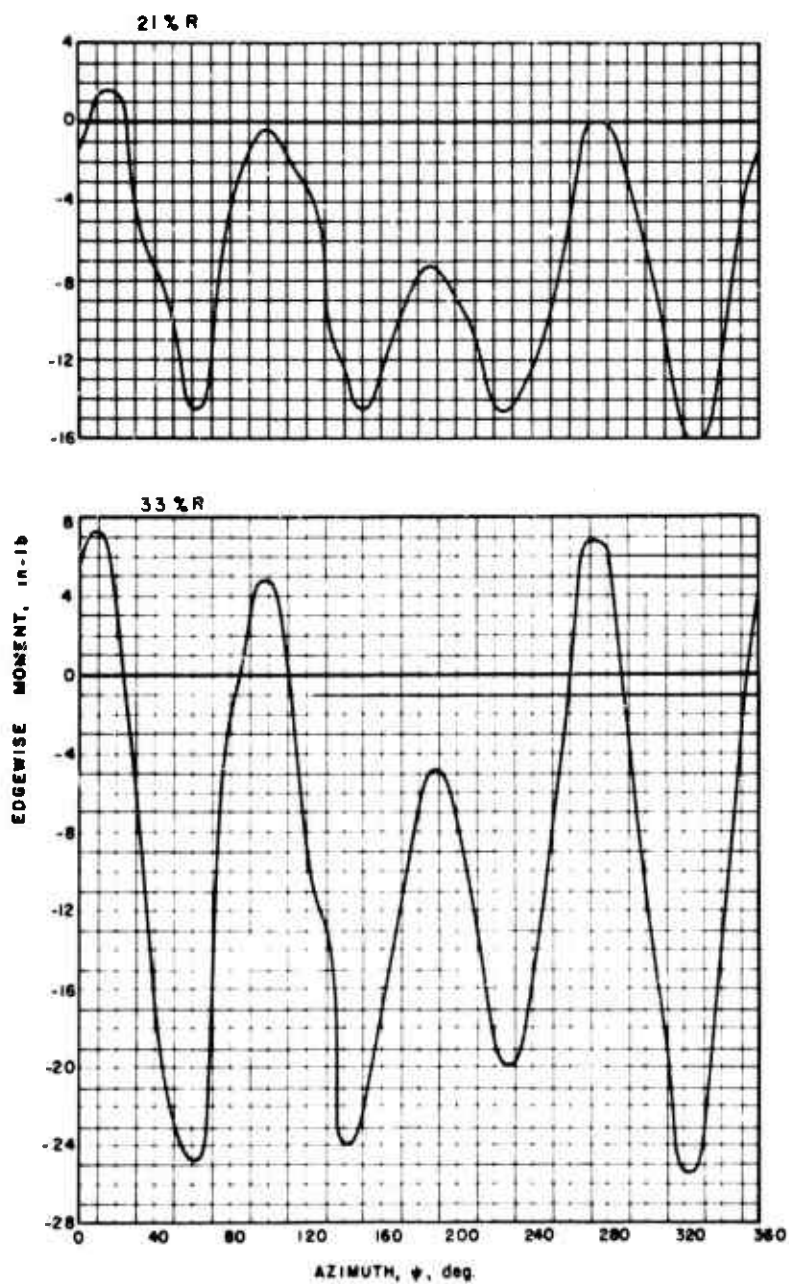
(c) TORSIONAL MOMENTS

Figure 23. Concluded.



(a) FLATWISE MOMENTS

Figure 24. Experimental Blade Moments.



(b) EDGEWISE MOMENTS

Figure 24. Continued.

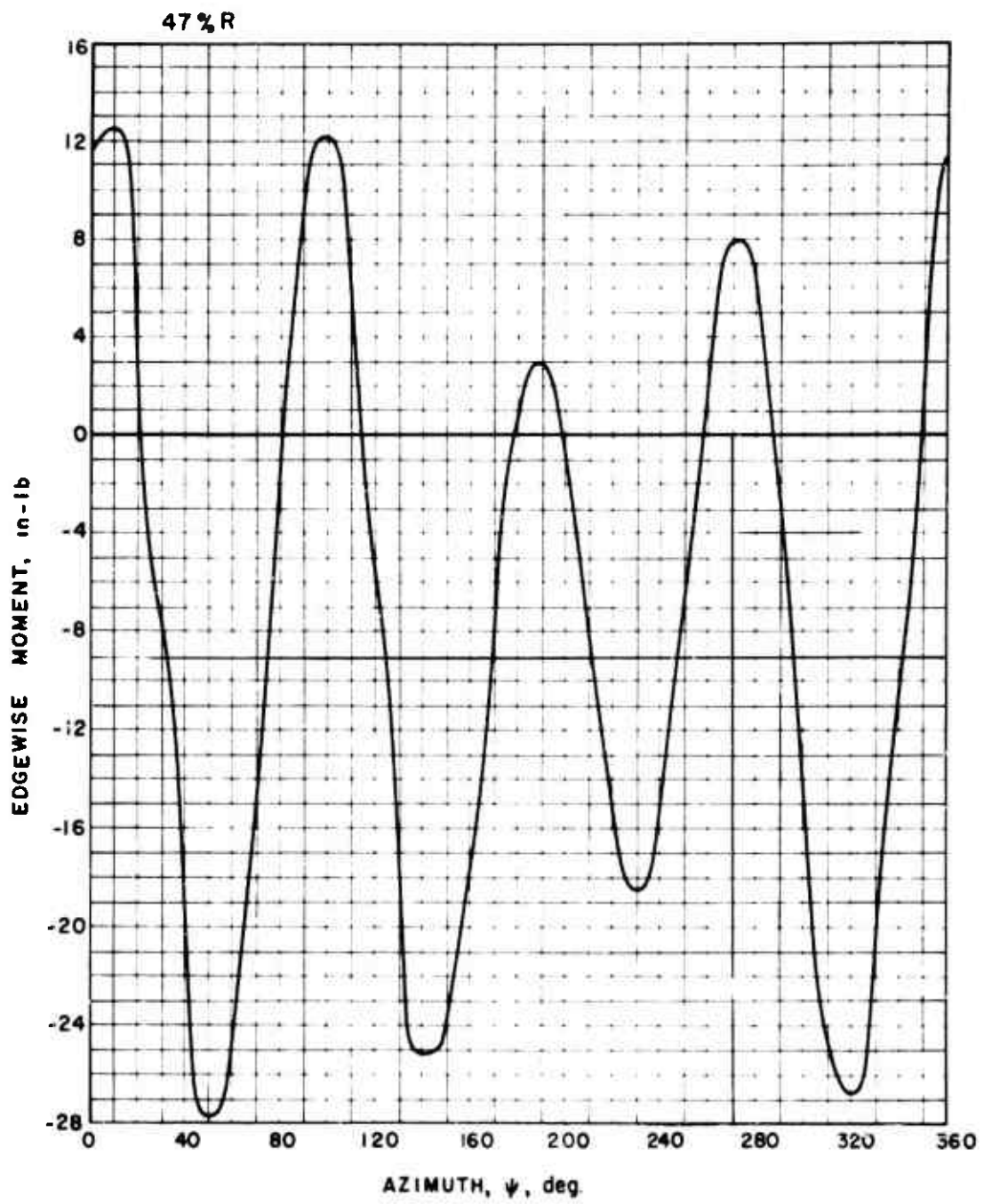
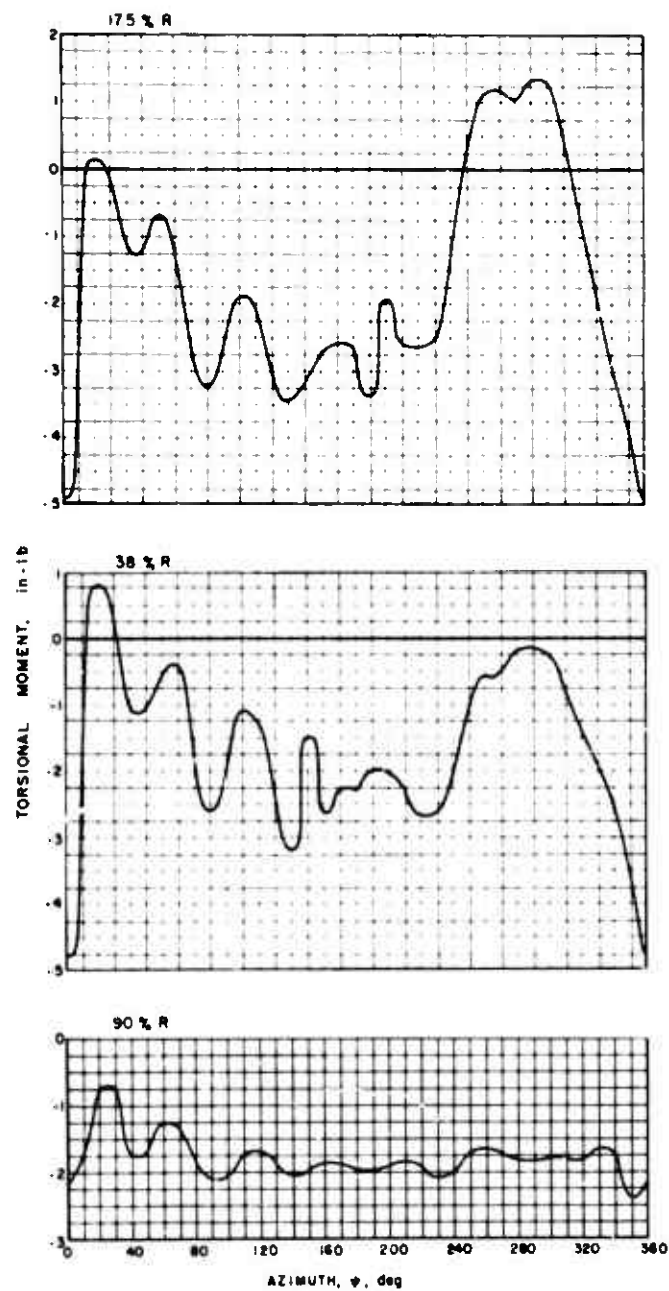


Figure 24(b). Continued.



(c) TORSIONAL MOMENTS

Figure 24. Concluded.

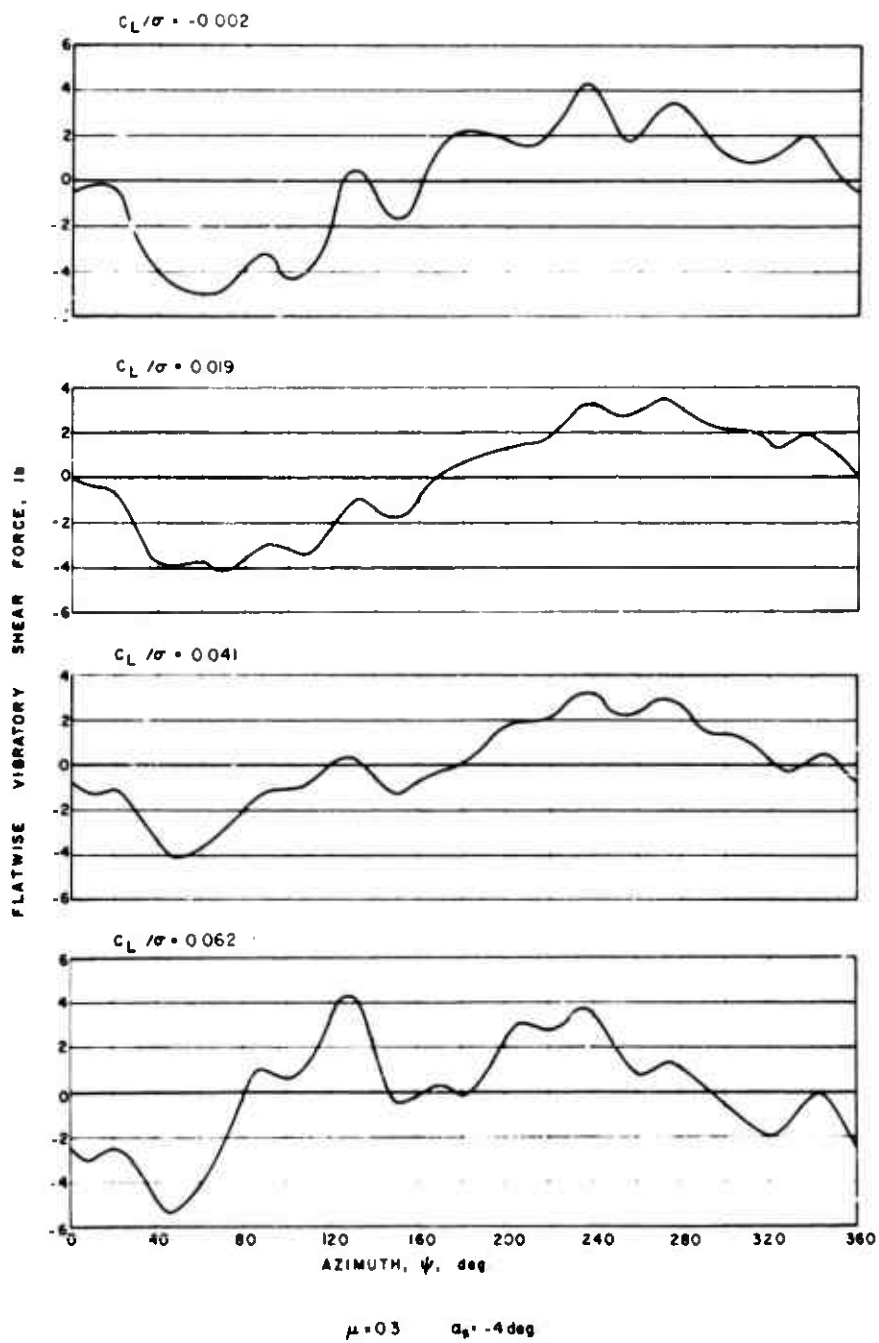
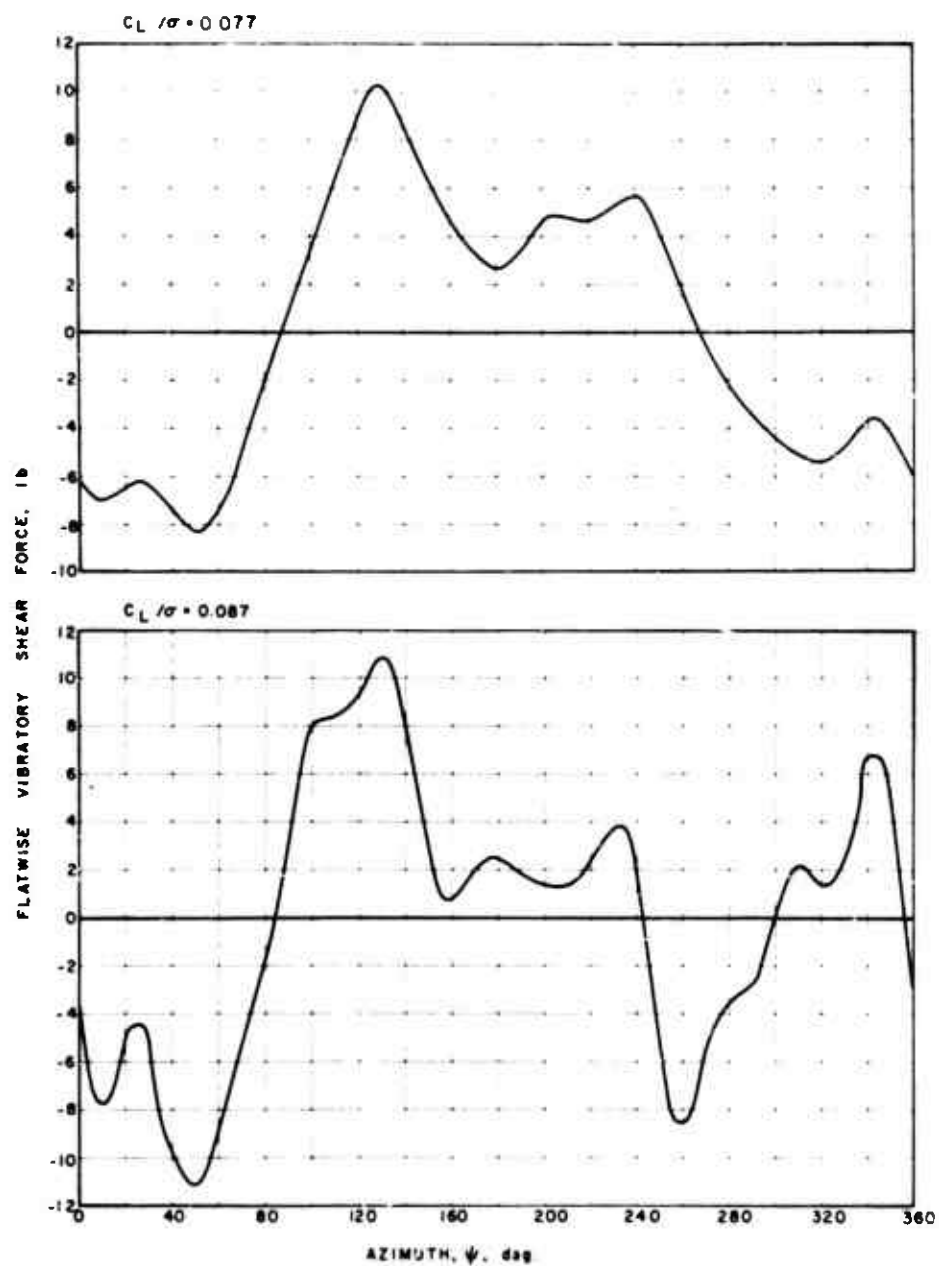


Figure 25. Effect of Rotor Lift on Flatwise Vibratory Shear Force.



$\mu = 0.3$ $\alpha_g = -4 \text{ deg}$

Figure 25. Concluded.

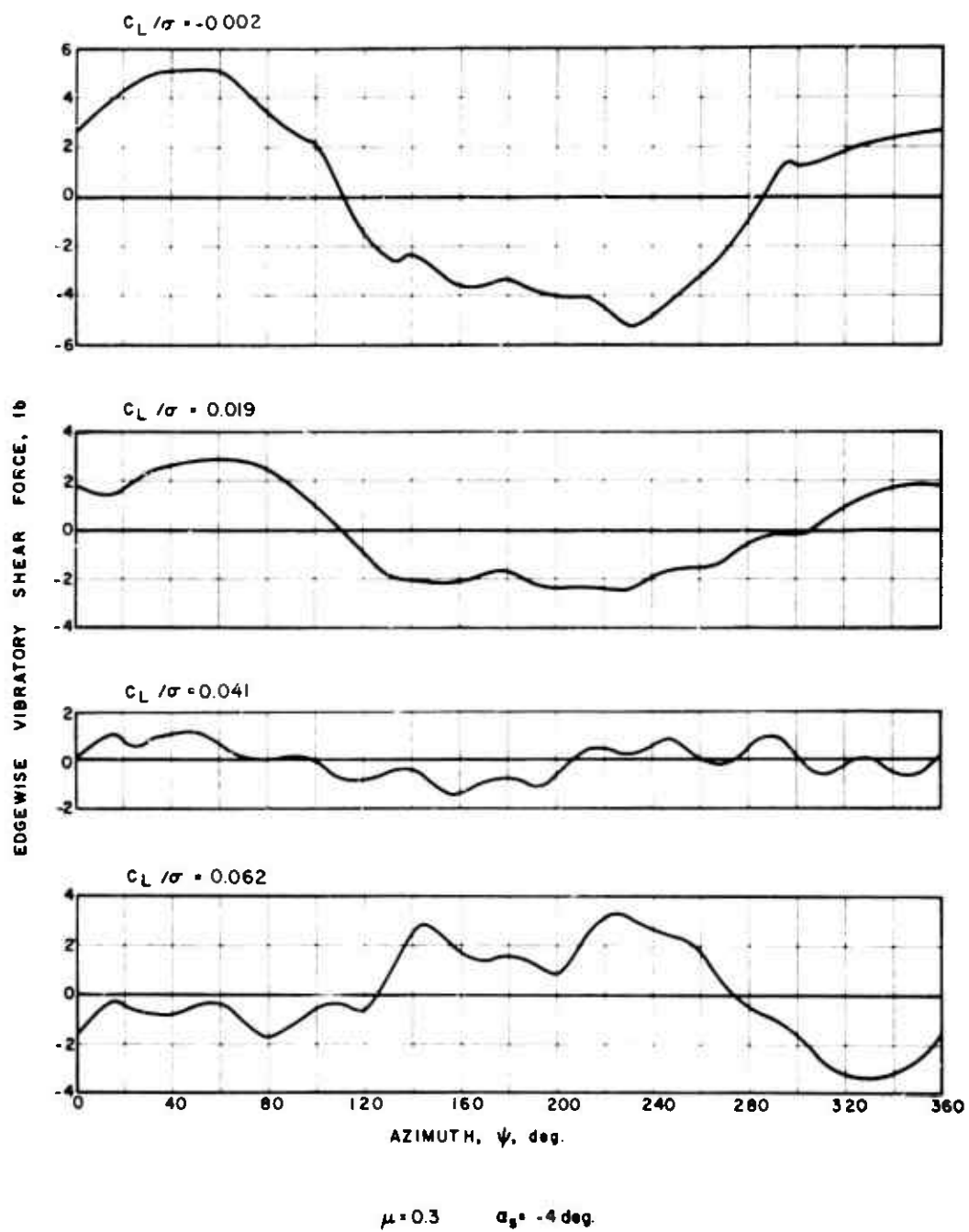


Figure 26. Effect of Rotor Lift on Edgewise Vibratory Shear Force.

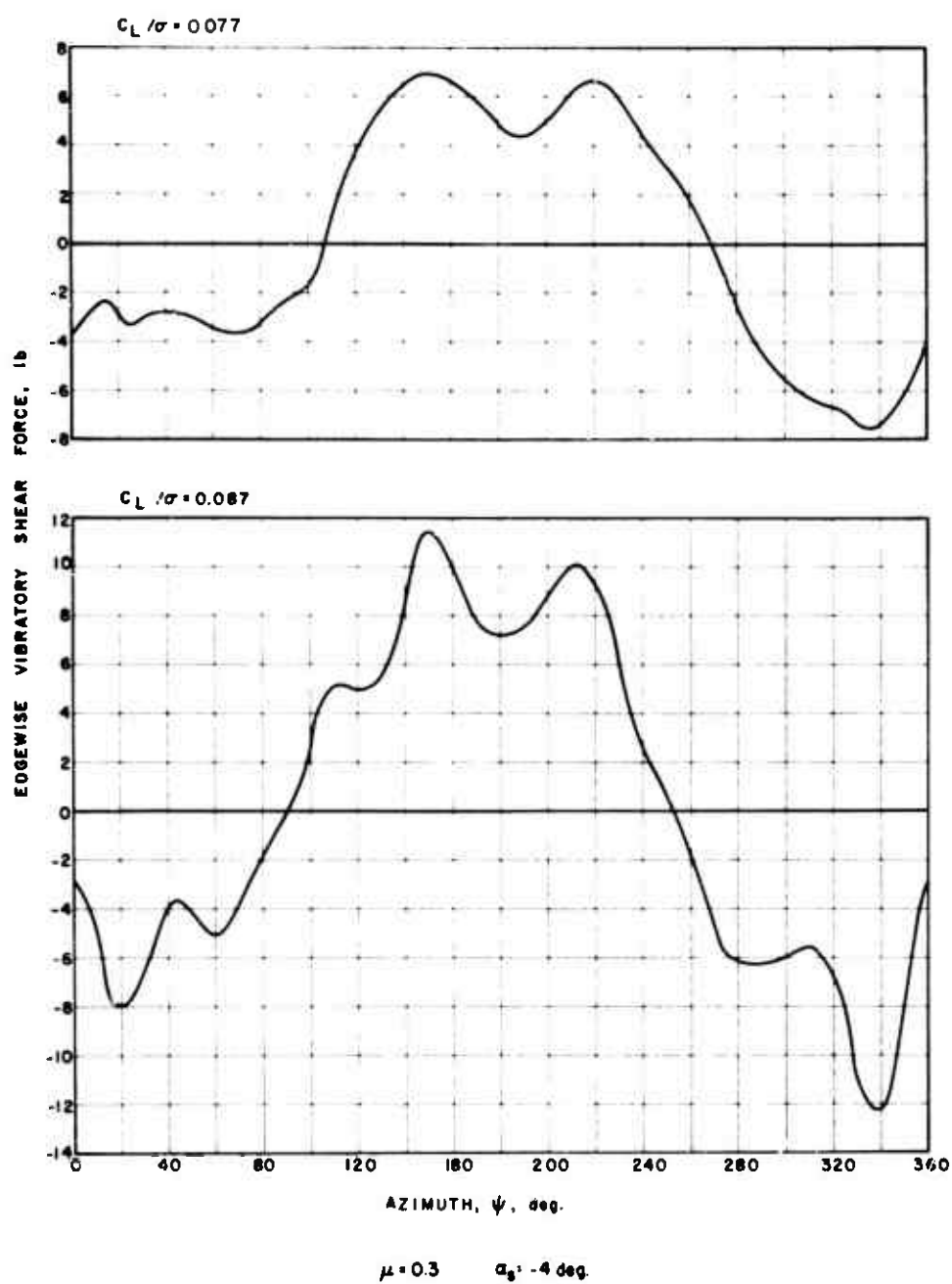


Figure 26. Concluded.

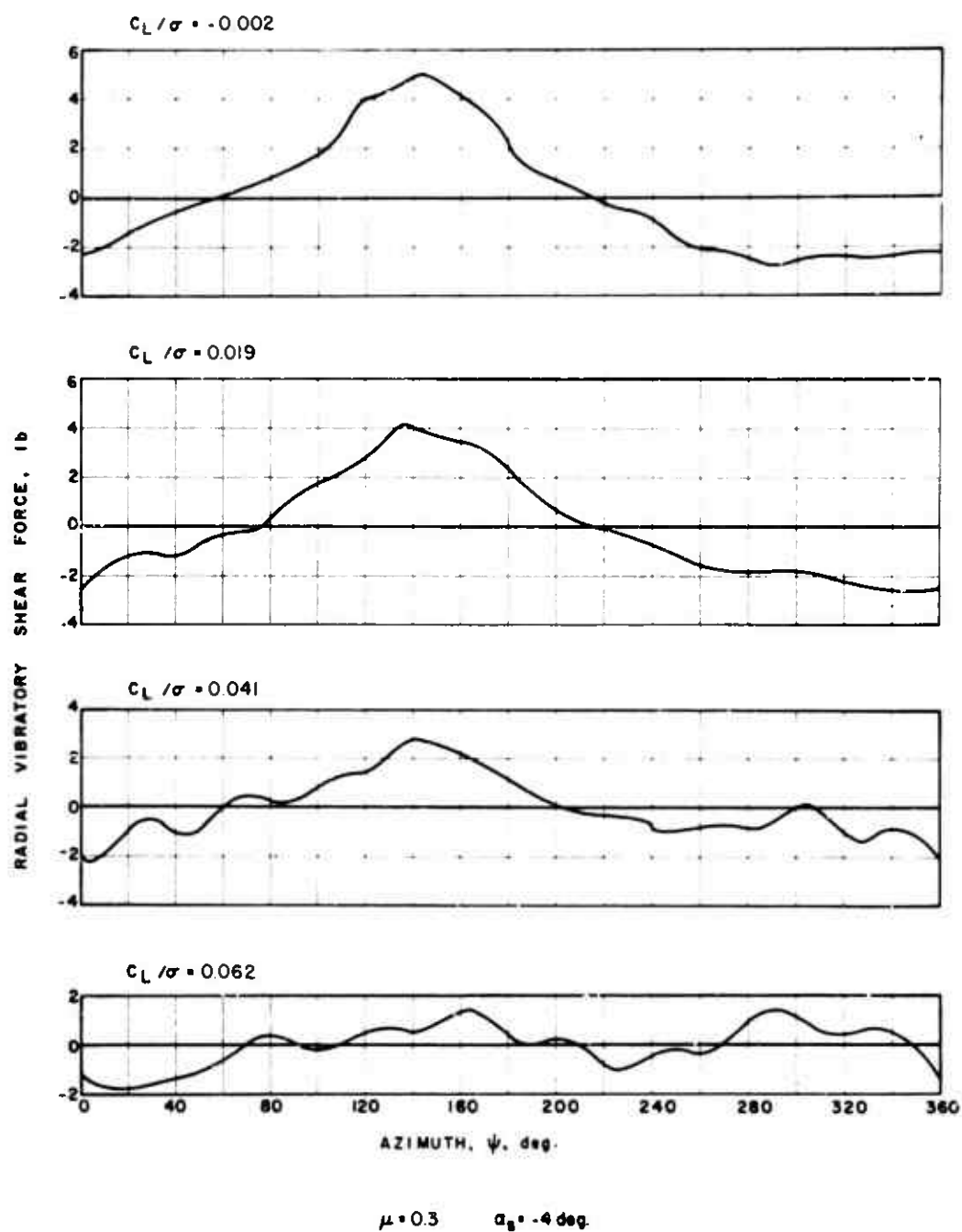


Figure 27. Effect of Rotor Lift on Radial Vibratory Shear Force.

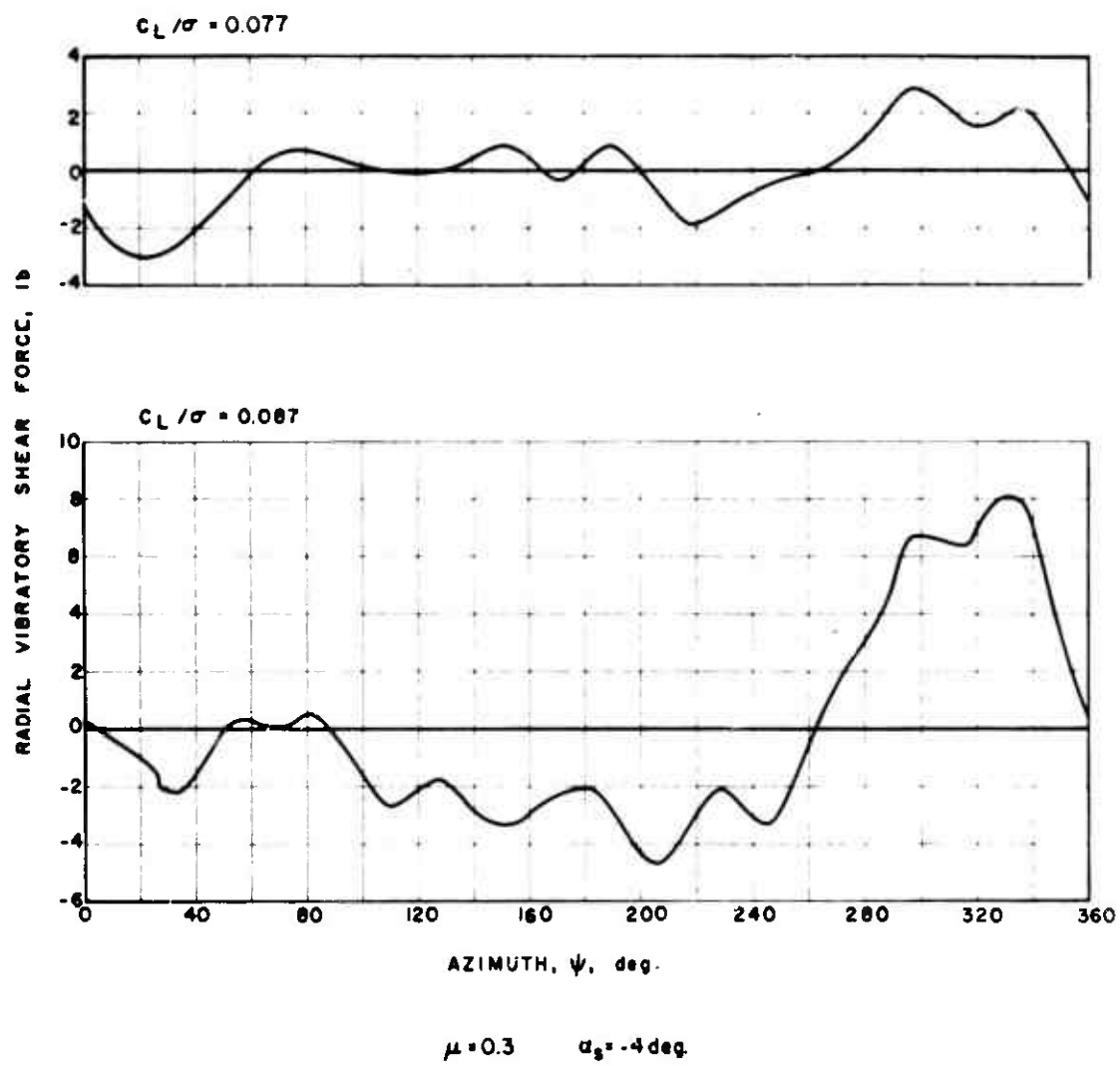
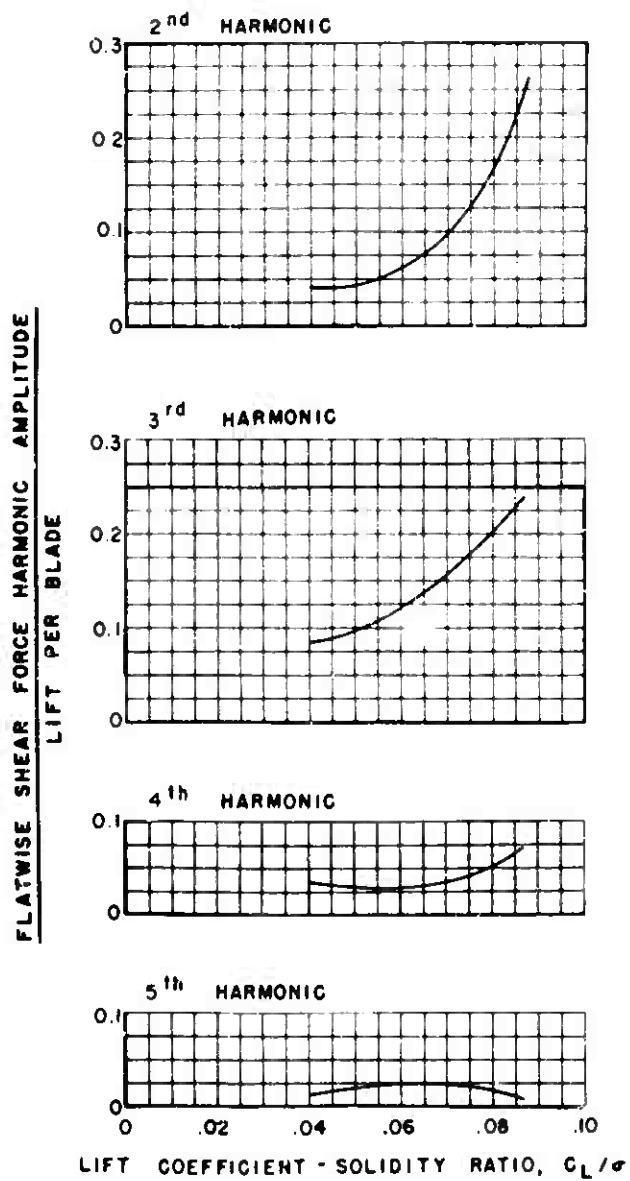


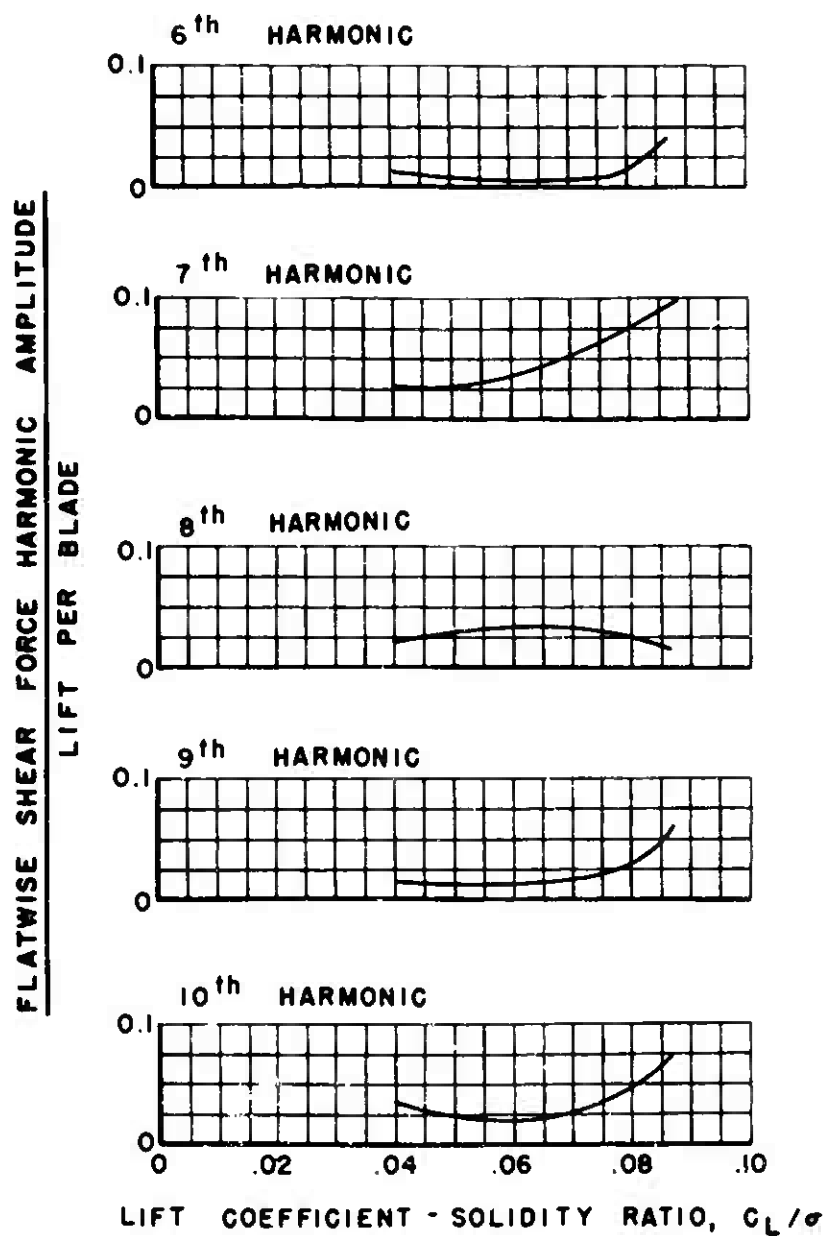
Figure 27. Concluded.



$$\mu = 0.3, \alpha_s = -4 \text{ deg}$$

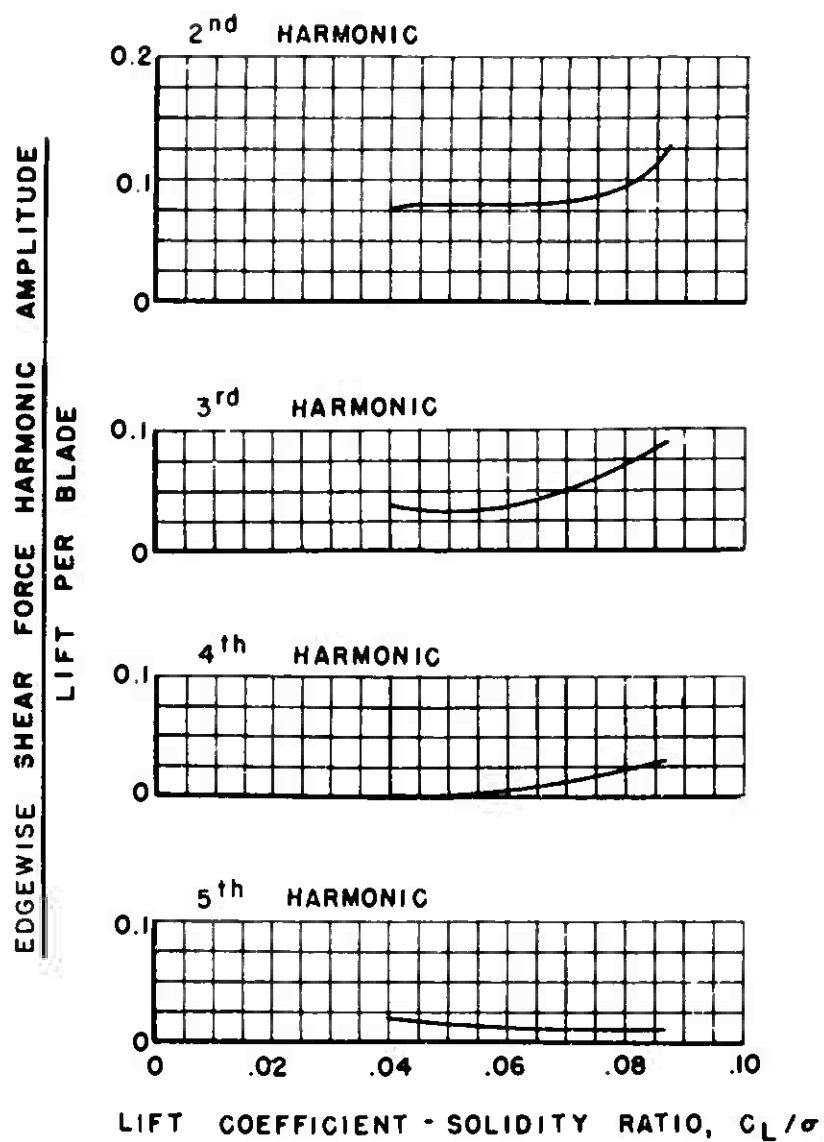
(a) FLATWISE

Figure 28. Effect of Rotor Lift on Nondimensional Shear Forces.



$$\mu = 0.3, \alpha_s = -4 \text{ deg.}$$

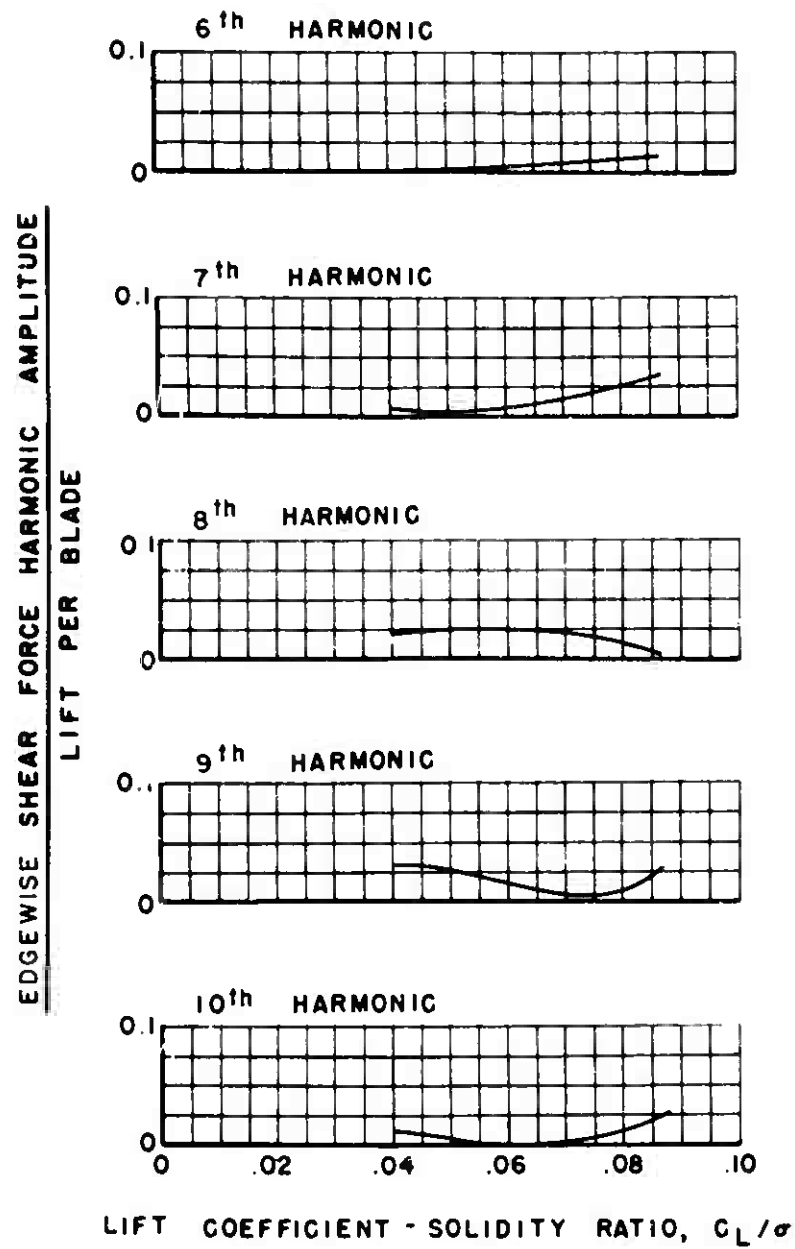
Figure 28(a). Continued.



$$\mu = 0.3 \quad \alpha_s = -4 \text{ deg.}$$

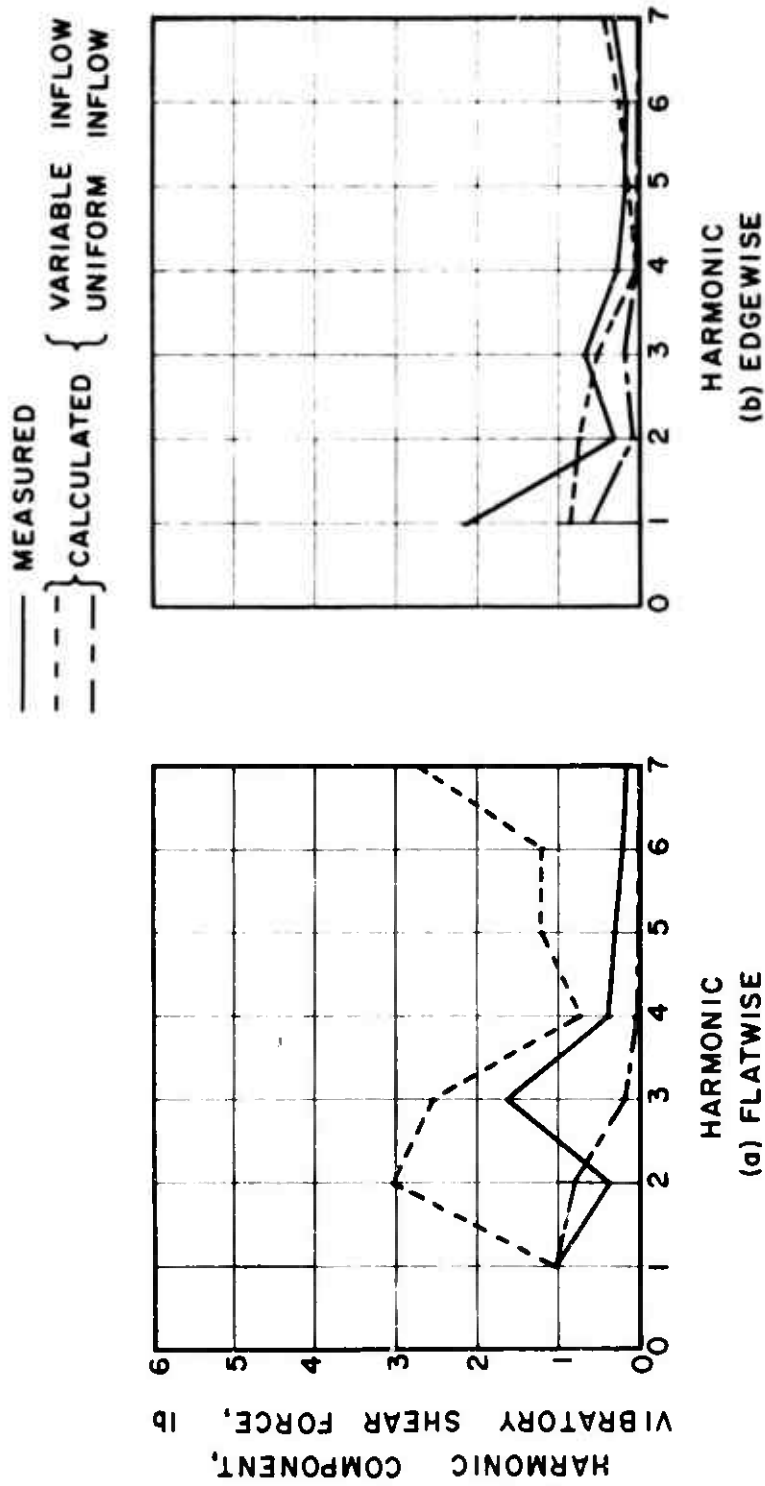
(b) EDGEWISE

Figure 28. Continued.



$$\mu = 0.3 \quad \alpha_s = -4 \text{ deg}$$

Figure 28(b). Concluded.



$$\mu = 0.2$$

$$c_L/\sigma = 0.071$$

$$\alpha_s = -4 \text{ deg.}$$

Figure 29. Comparison of Theoretical and Experimental Vibratory Shear Force Harmonic Amplitudes.

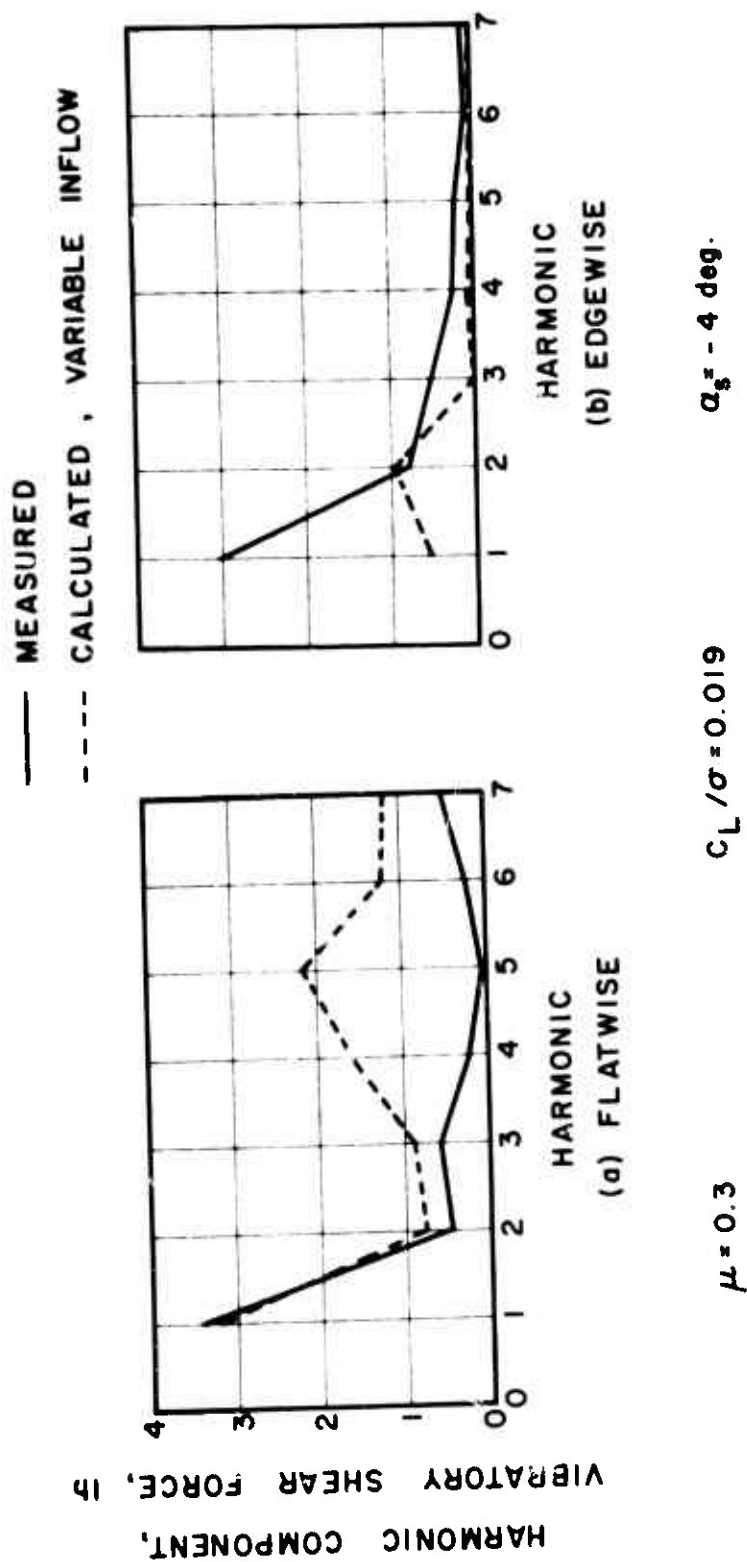


Figure 30. Comparison of Theoretical and Experimental Vibratory Shear Force Harmonic Amplitudes.

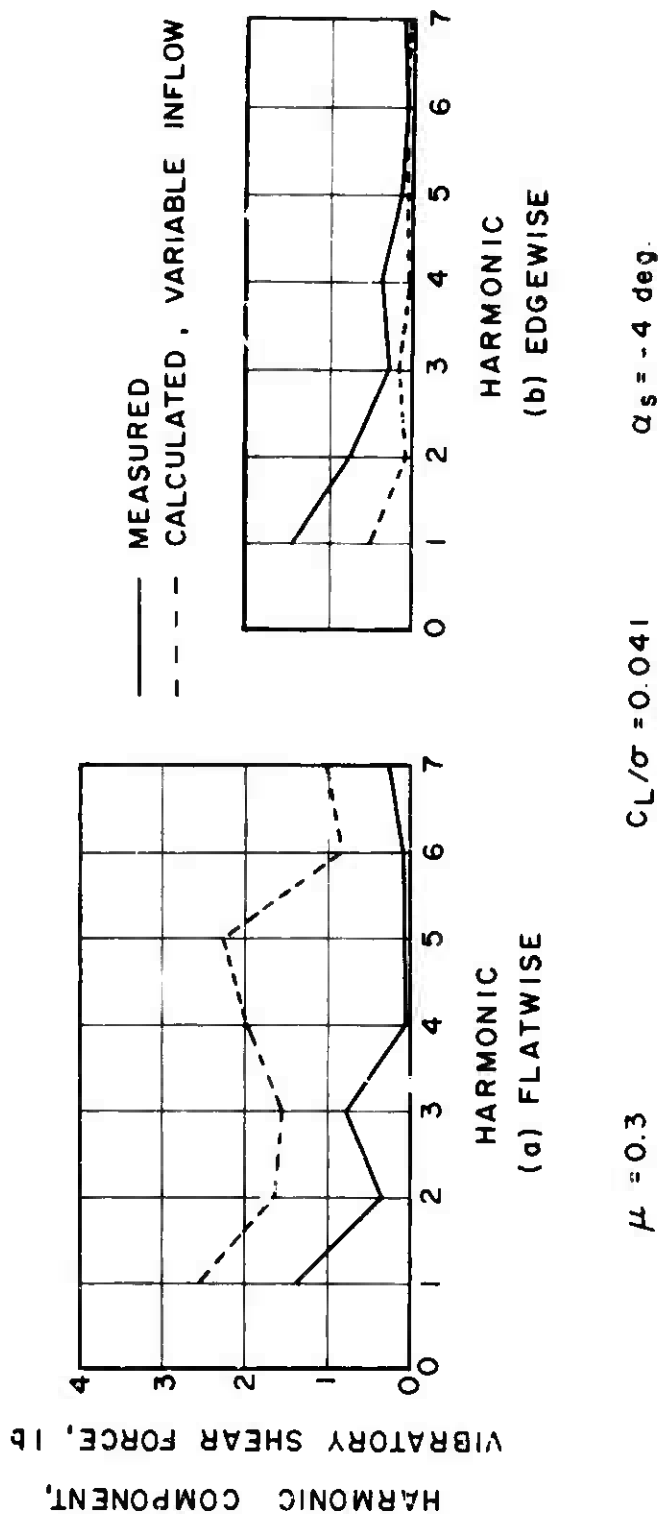
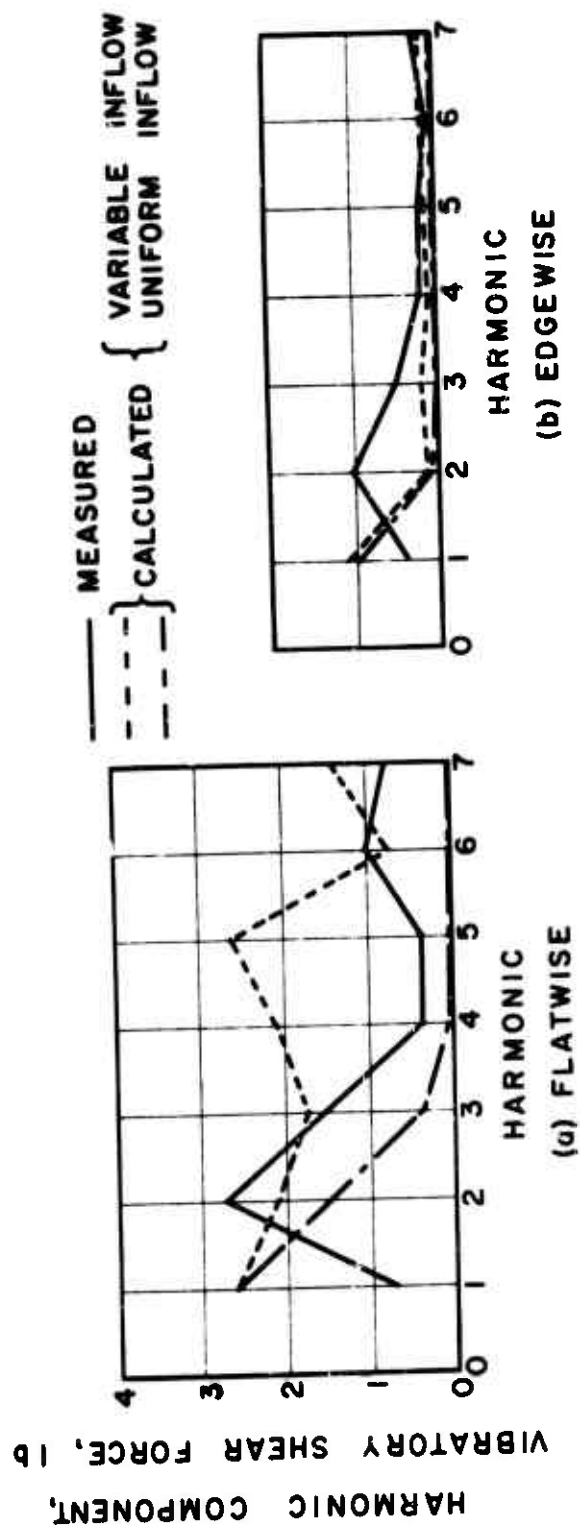


Figure 31. Comparison of Theoretical and Experimental Vibratory Shear Force Harmonic Amplitudes.



$$\mu = 0.3 \qquad c_L / \sigma = 0.062 \qquad \alpha_s = -4 \text{ deg.}$$

Figure 32. Comparison of Theoretical and Experimental Vibratory Shear Force Harmonic Amplitudes.

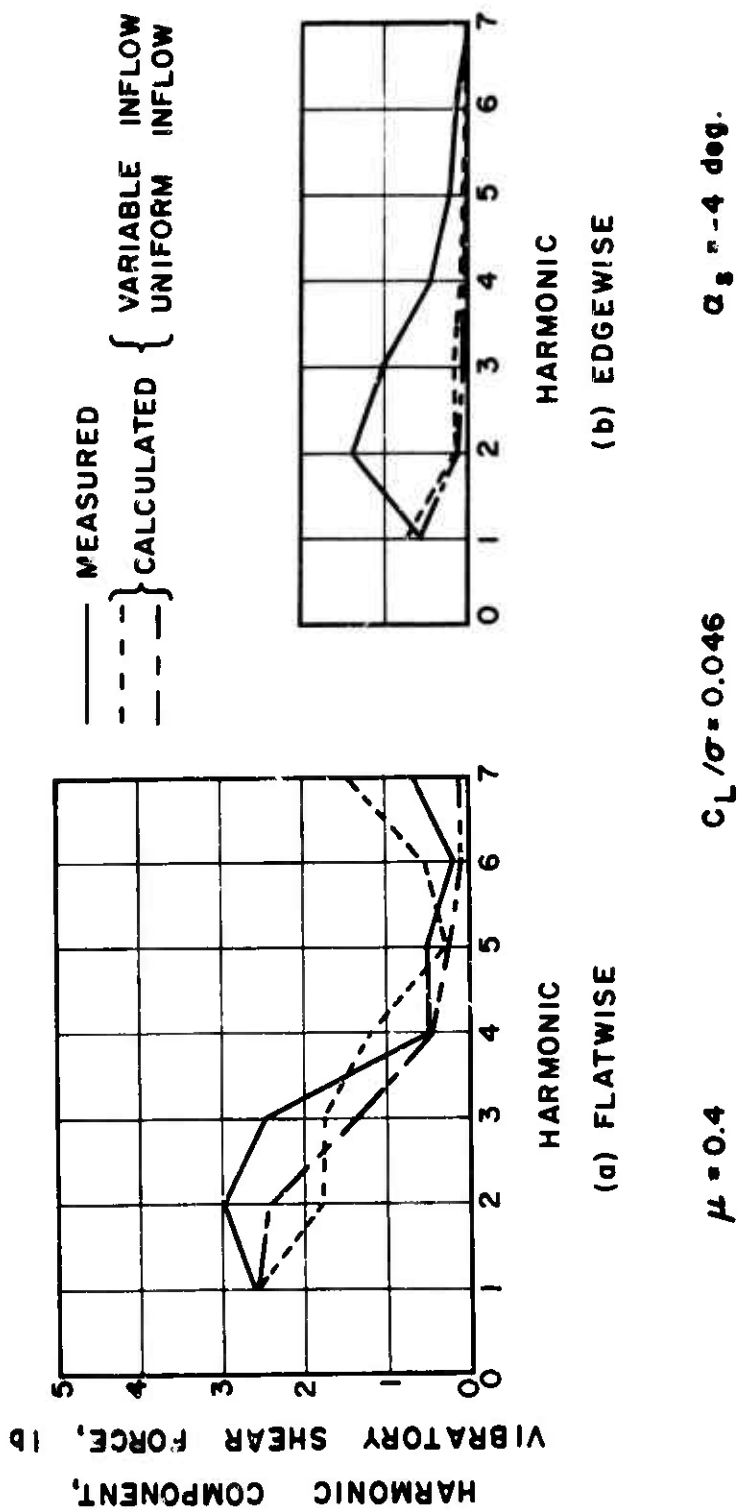
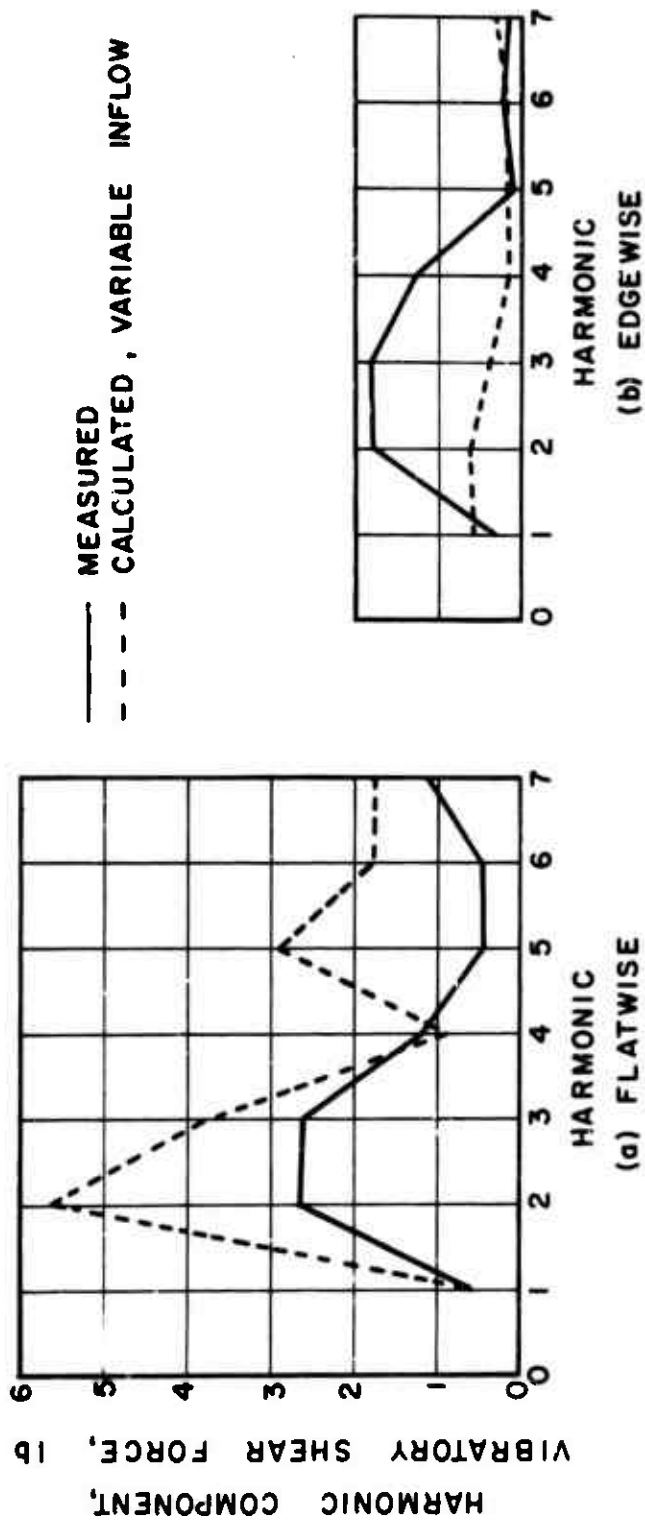


Figure 33. Comparison of Theoretical and Experimental Vibratory Shear Force Harmonic Amplitudes.



$\mu = 0.5$

$CL/\sigma = 0.048$

$\alpha_s = -4 \text{ deg.}$

Figure 34. Comparison of Theoretical and Experimental Vibratory Shear Force Harmonic Amplitudes.

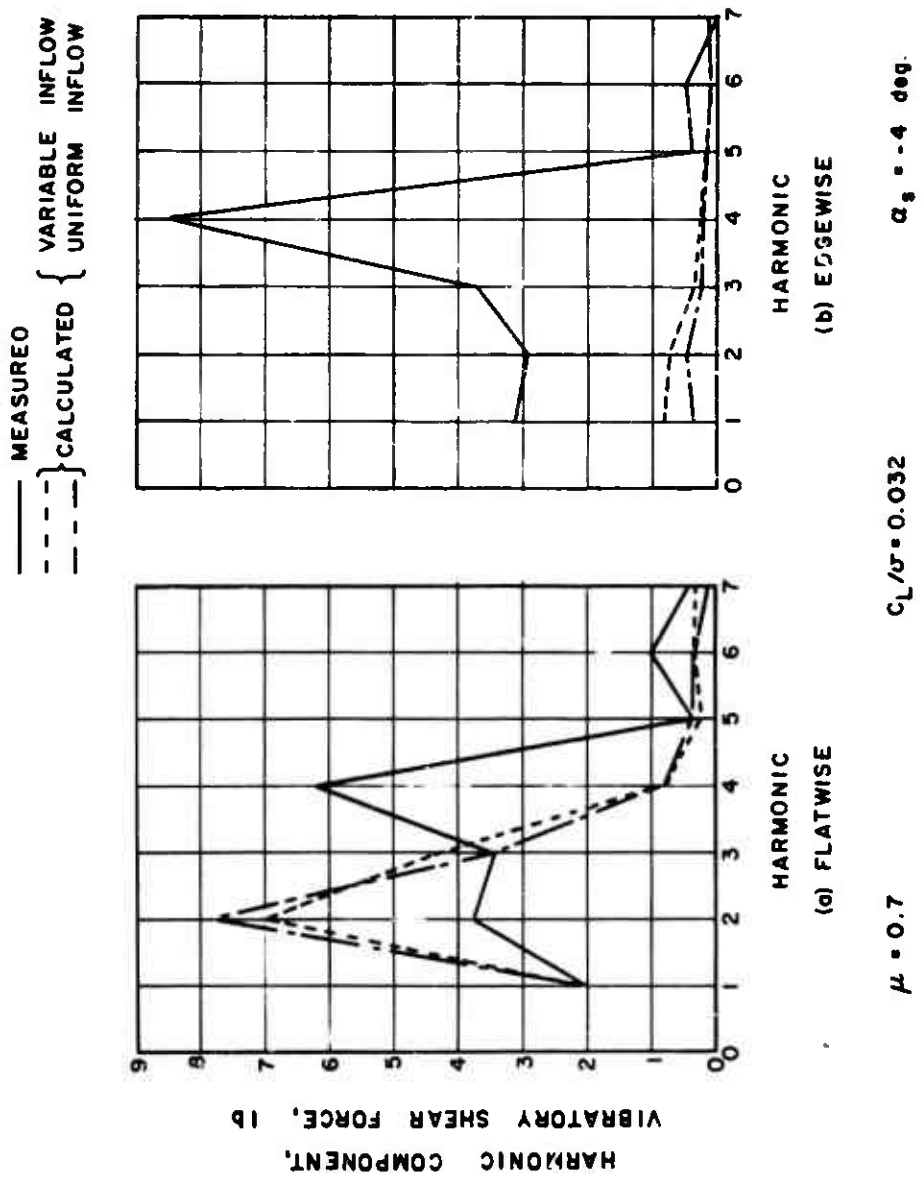


Figure 35. Comparison of Theoretical and Experimental Vibratory Shear Force Harmonic Amplitudes.

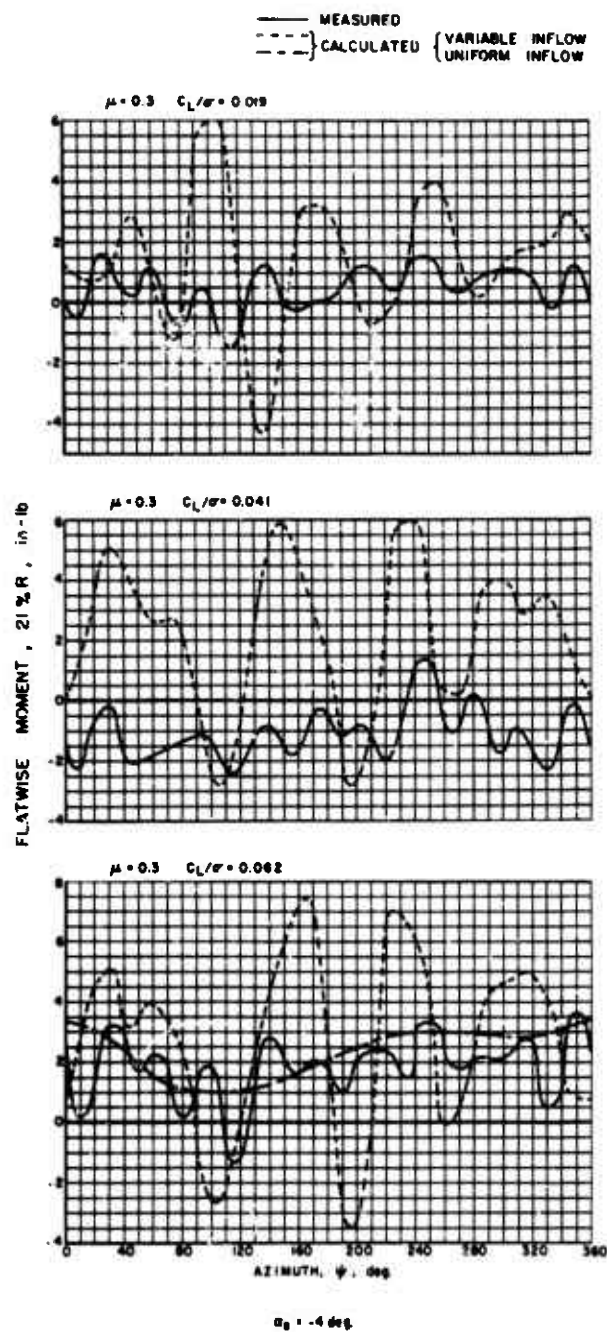


Figure 36. Comparison of Theoretical and Experimental Flatwise Rotor Blade Bending Moments.

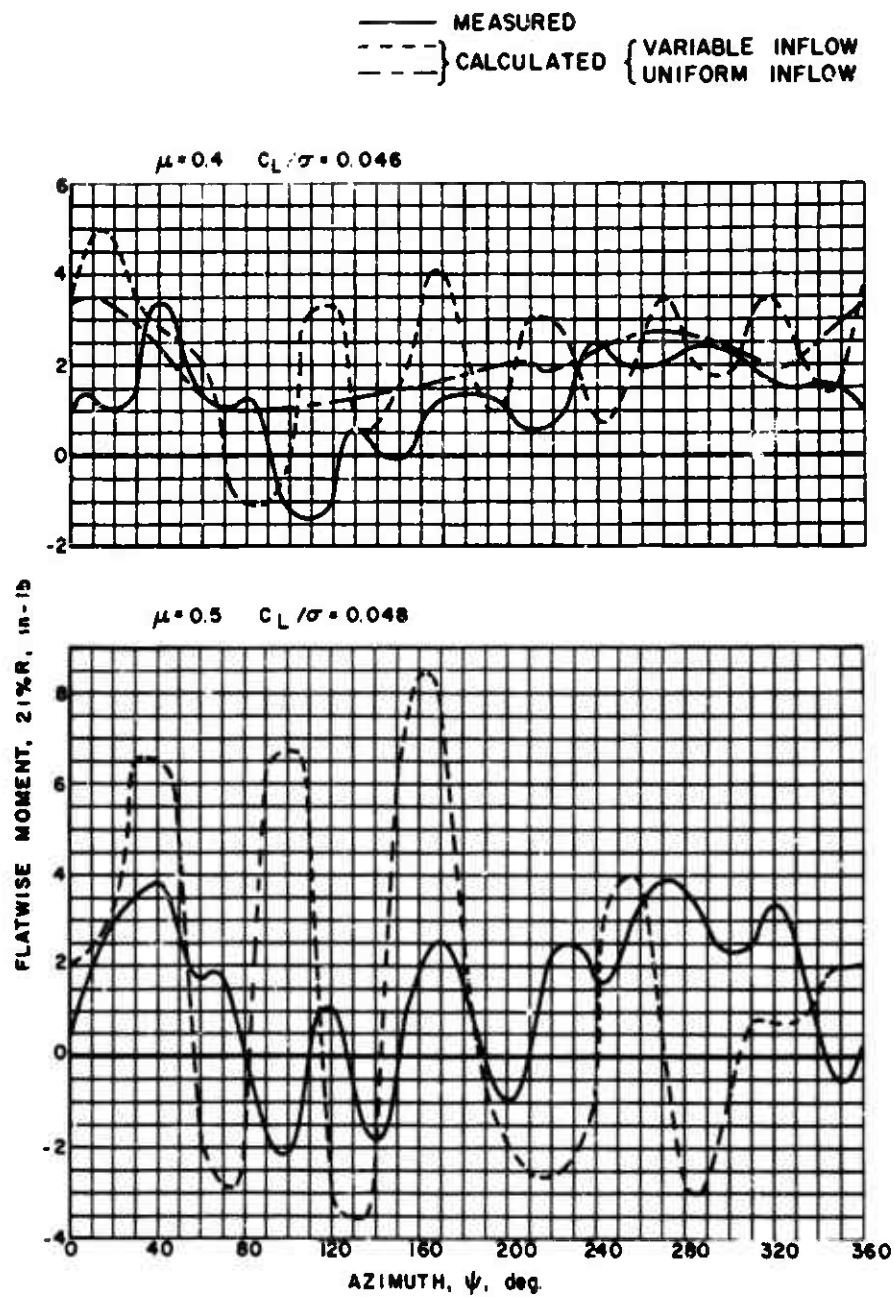


Figure 36. Concluded.

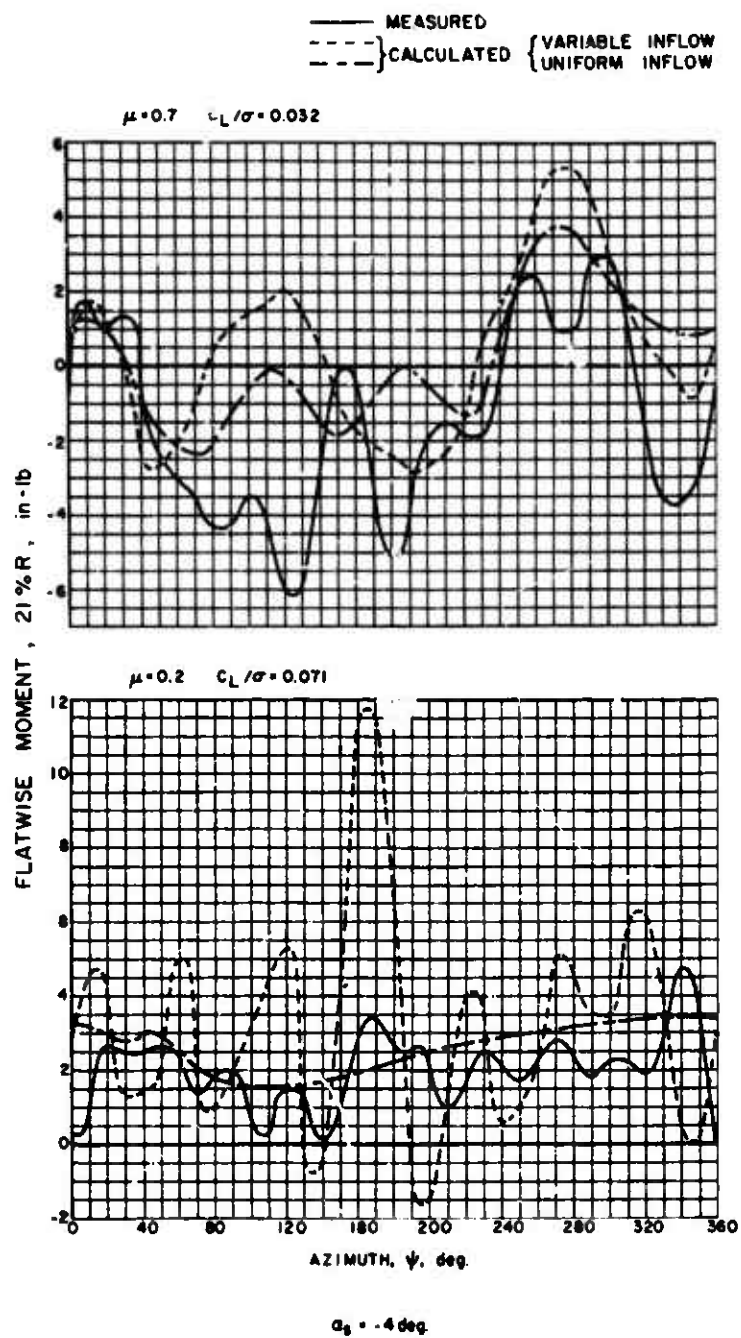
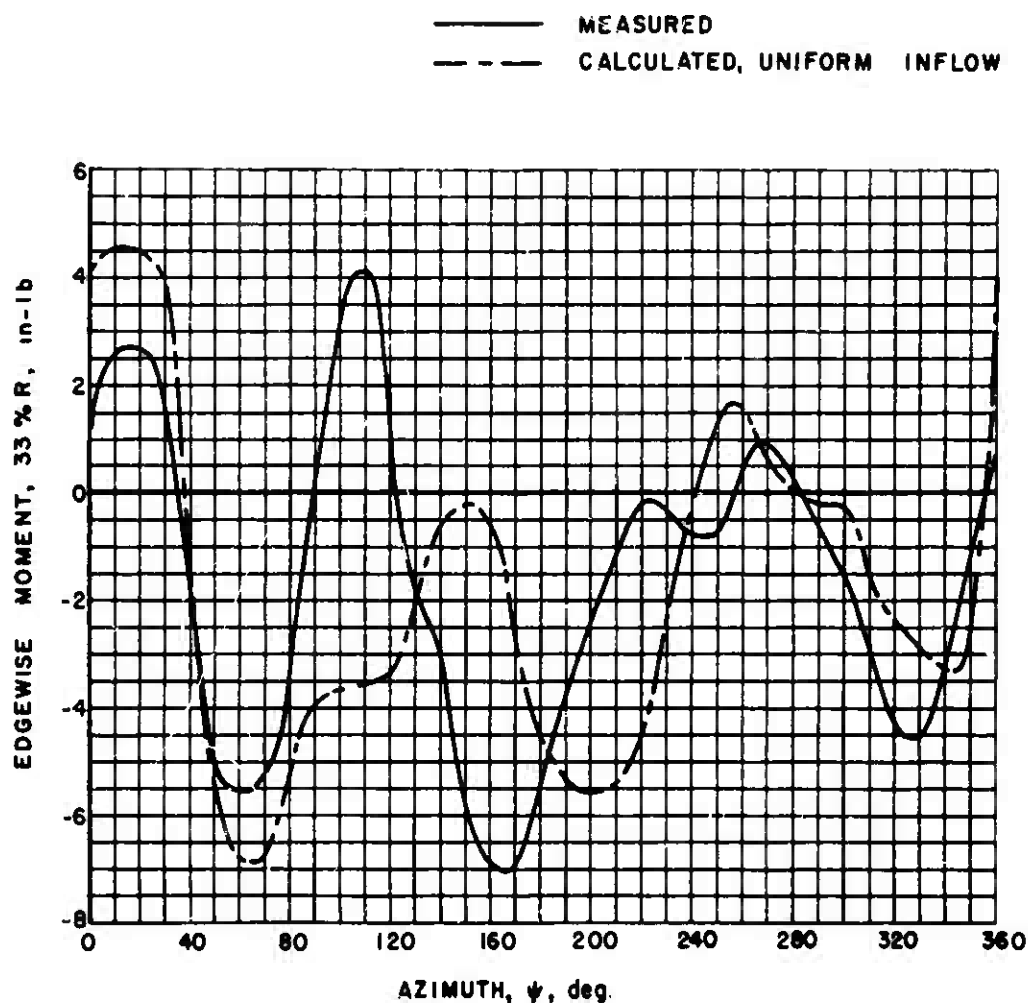


Figure 37. Comparison of Theoretical and Experimental Flatwise Rotor Blade Bending Moments.



$$\mu = 0.5$$

$$C_L / \sigma = 0.048$$

$$\alpha_s = -4 \text{ deg.}$$

Figure 38. Comparison of Theoretical and Experimental Edgewise Rotor Blade Bending Moments.

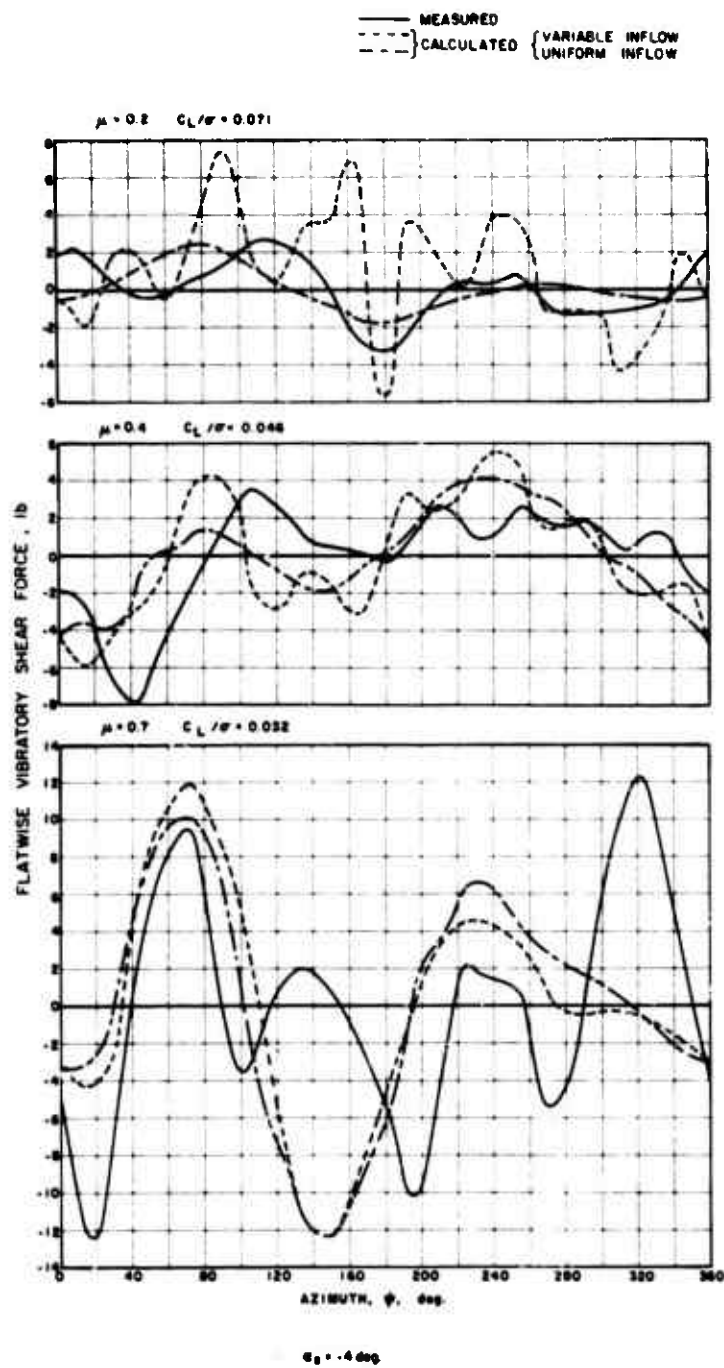


Figure 39. Azimuthal Variation of Vibratory Shear Force.

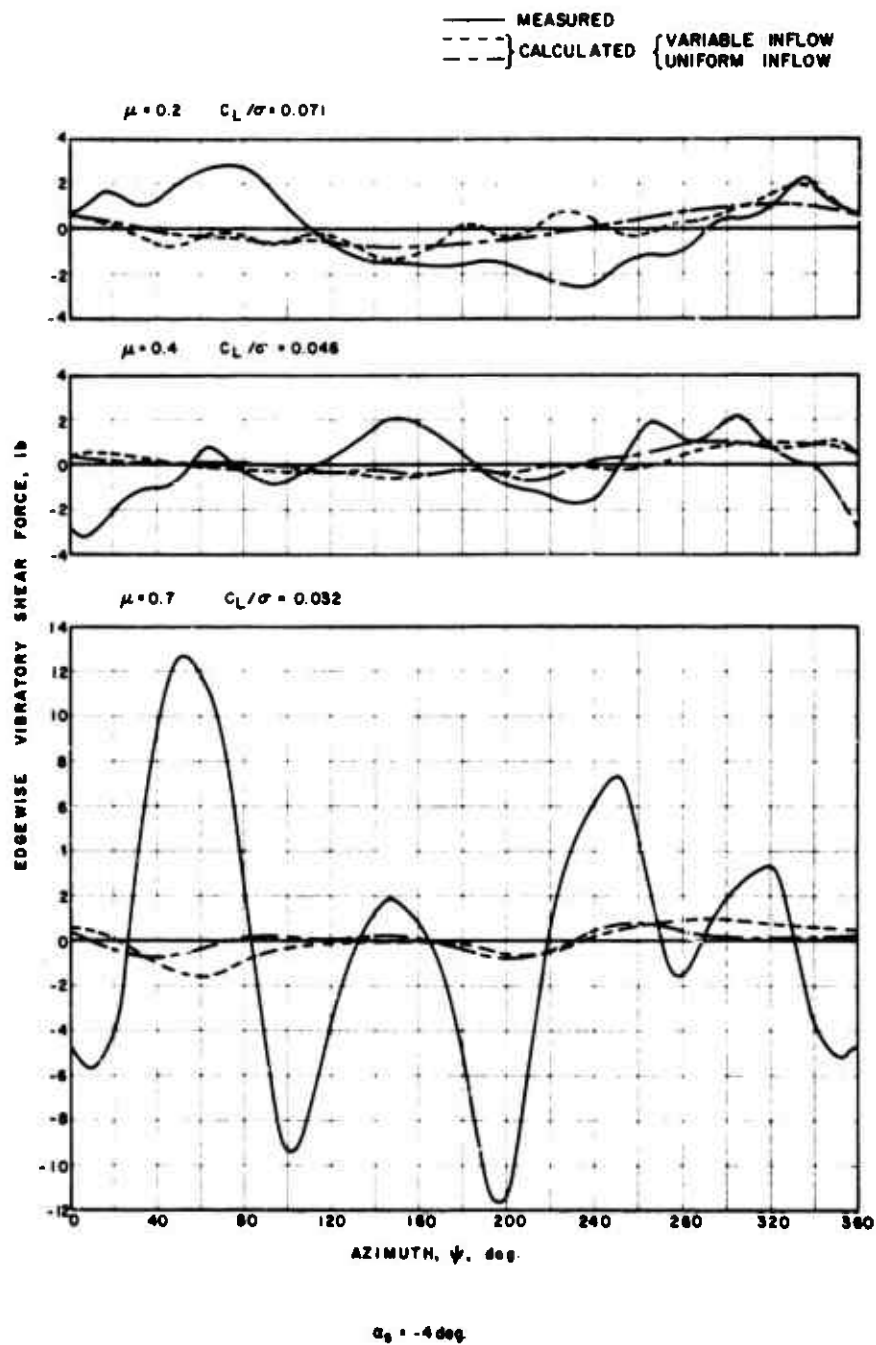


Figure 39. Concluded.

DISTRIBUTION

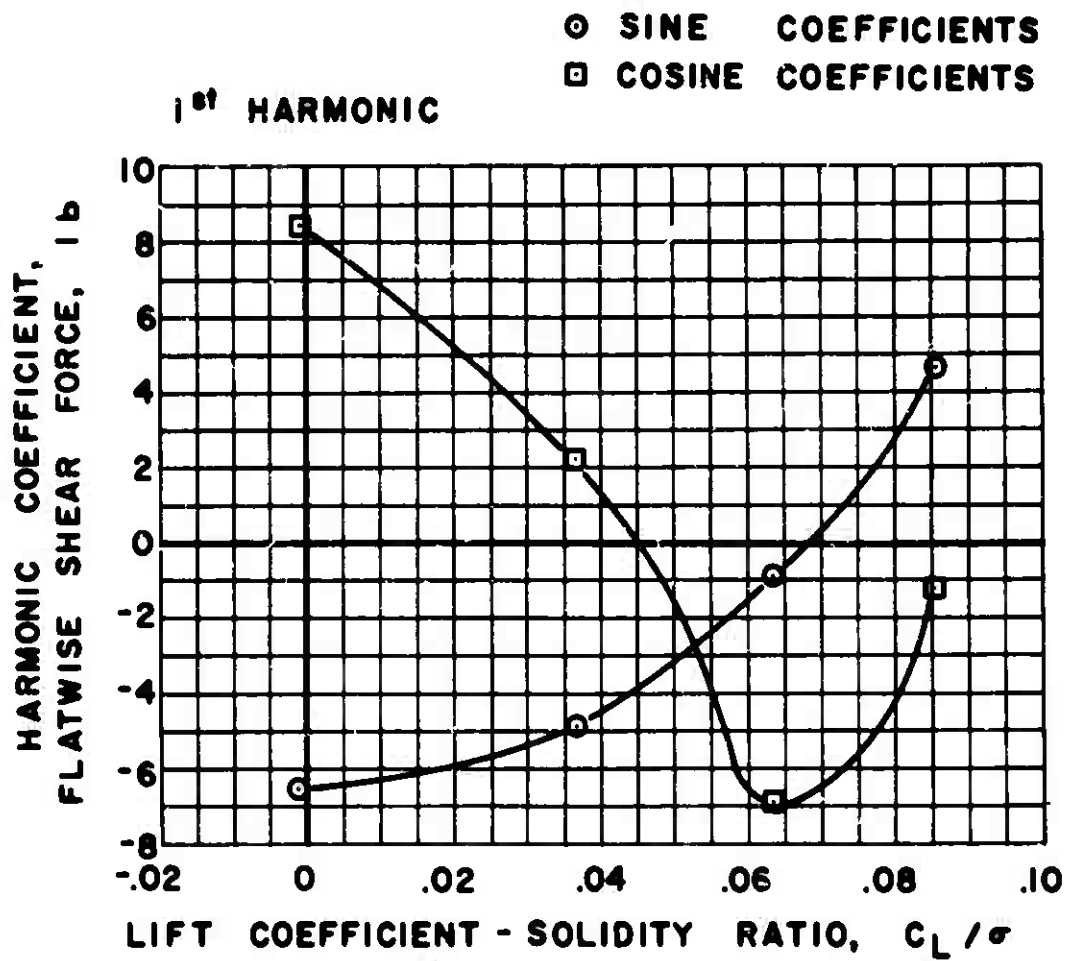
US Army Materiel Command	3
US Army Aviation Materiel Command	5
United States Army, Pacific	1
Chief of R&D, DA	1
Director of Defense Research and Engineering	1
US Army R&D Group (Europe)	2
US Army Aviation Materiel Laboratories	28
Army Aeronautical Research Laboratory, Ames Research Center	1
US Army Research Office-Durham	1
Plastics Technical Evaluation Center	1
US Army Engineer Waterways Experiment Station	1
US Army Test and Evaluation Command	1
US Army Electronics Command	2
US Army Combat Developments Command Experimentation Command	1
US Army Aviation School	1
US Army Aviation Test Activity	2
Air Force Flight Test Center, Edwards AFB	2
Air Proving Ground Center, Eglin AFB	1
US Army Field Office, AFSC, Andrews AFB	1
Systems Engineering Group, Wright-Patterson AFB	1
Naval Air Systems Command, DN	7

PRECEDING PAGE BLANK

Office of Naval Research	1
Commandant of the Marine Corps	1
Marine Corps Liaison Officer, US Army Transportation School	1
Lewis Research Center, NASA	1
Manned Spacecraft Center, NASA	1
NASA Scientific and Technical Information Facility	2
NAFEC Library (FAA)	2
US Army Board for Aviation Accident Research	1
Bureau of Safety, Civil Aeronautics Board	2
US Naval Aviation Safety Center	1
Federal Aviation Agency, Washington, DC	2
US Army Medical R&D Command	1
US Government Printing Office	1
Defense Documentation Center	20

APPENDIX I

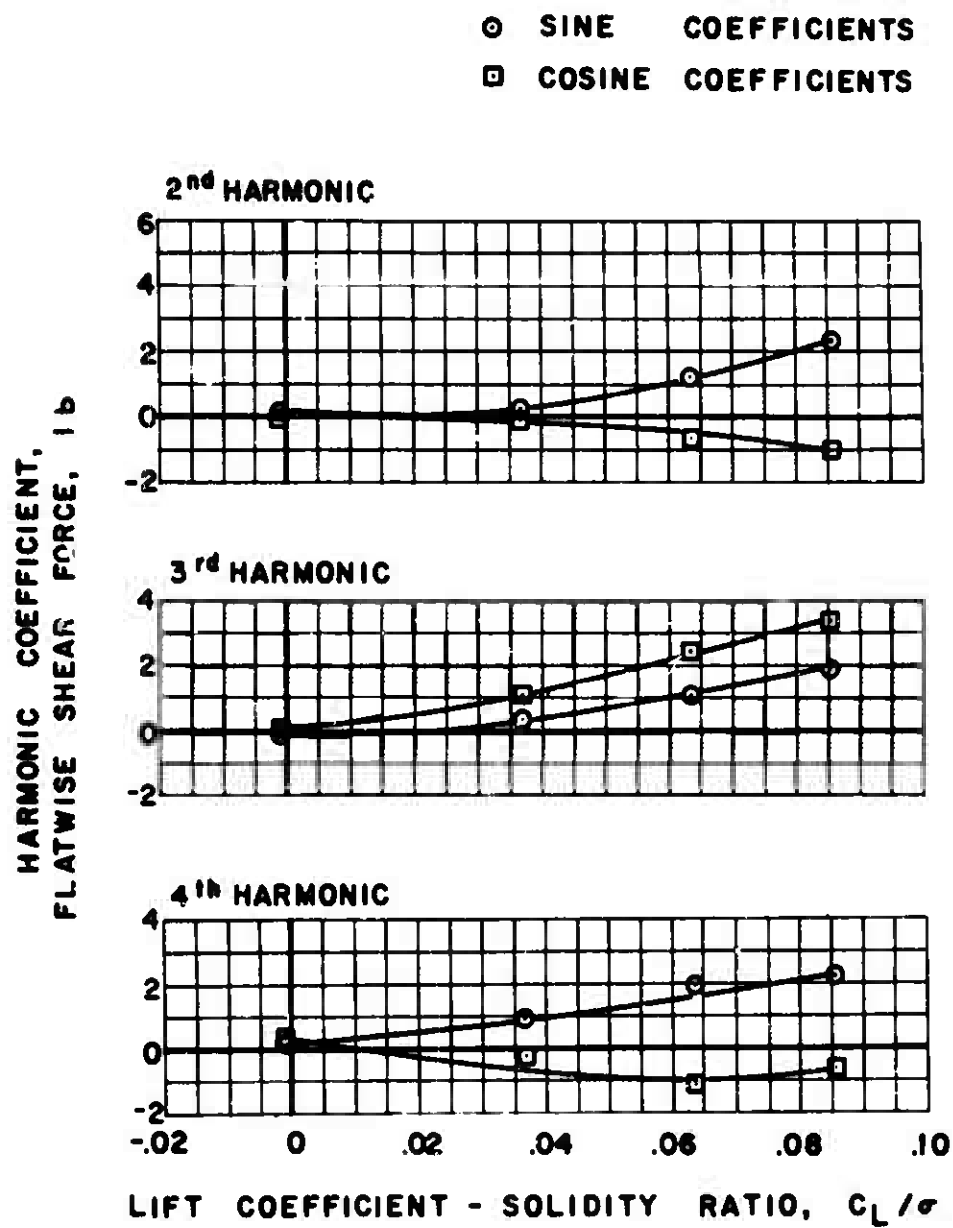
EXPERIMENTAL FLATWISE AND EDGEWISE SHEAR FORCE FIGURES



$$\mu = 0.2 \quad \alpha_s = 0 \text{ deg.}$$

(a) FLATWISE

Figure 40. Experimental Shear Force.



$\mu = 0.2 \quad \alpha_s = 0 \text{ deg.}$

Figure 40(a). Continued.

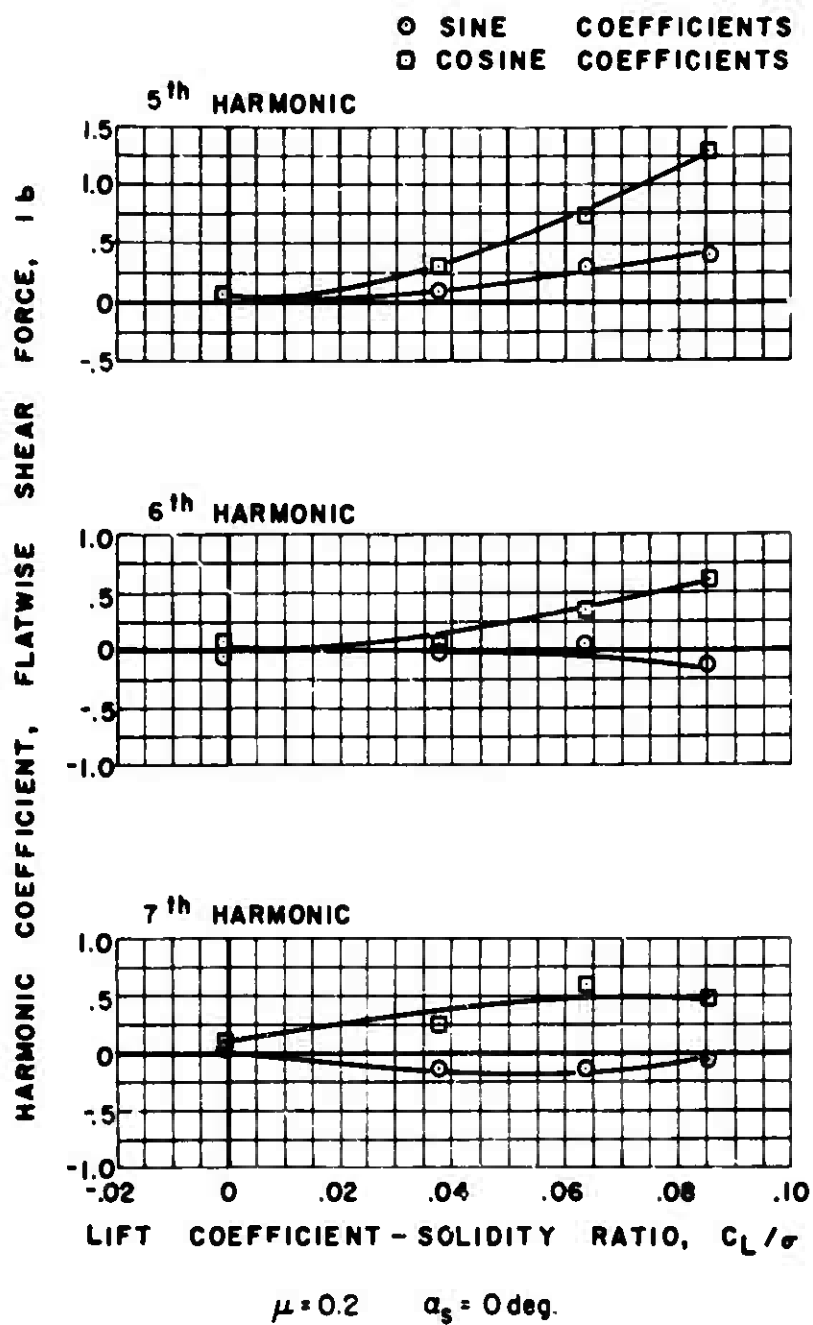


Figure 40(a). Continued.

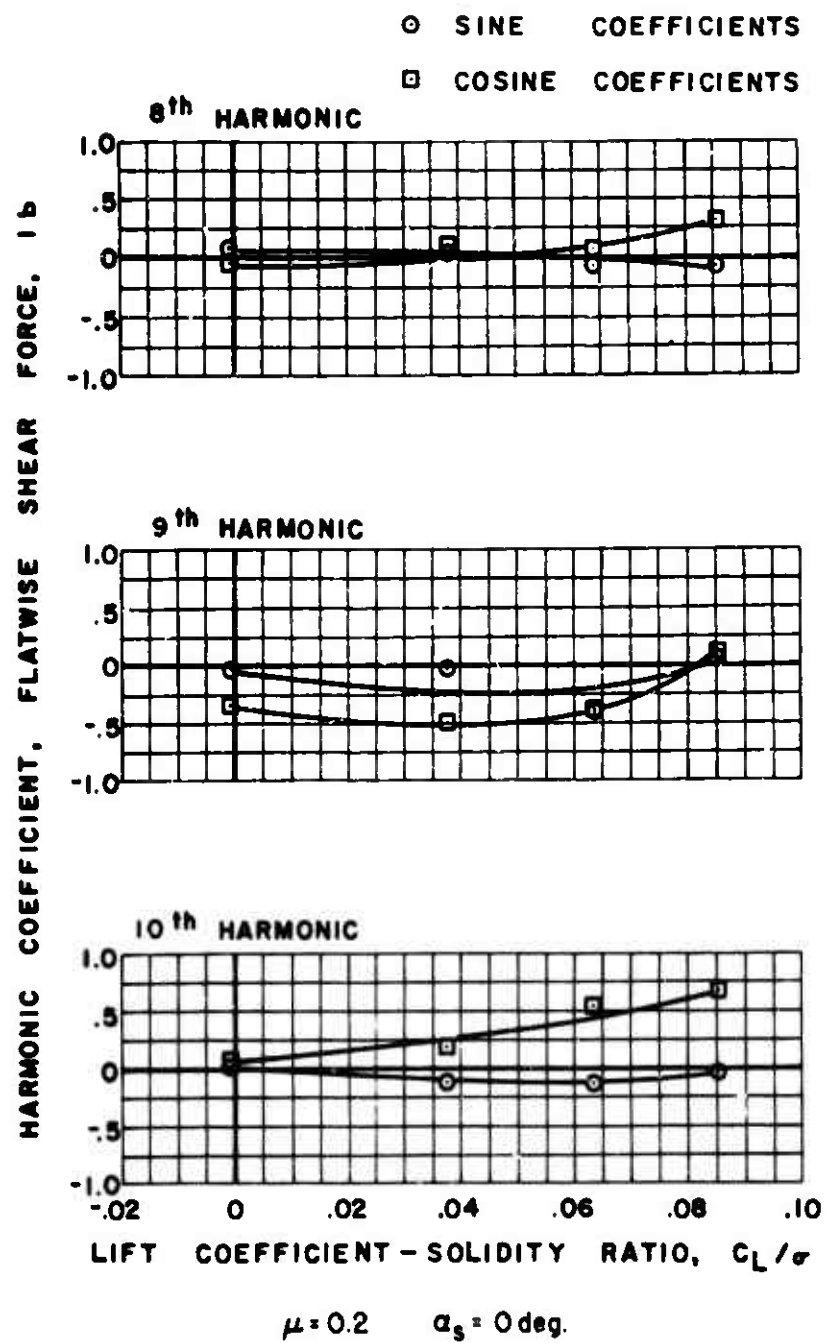
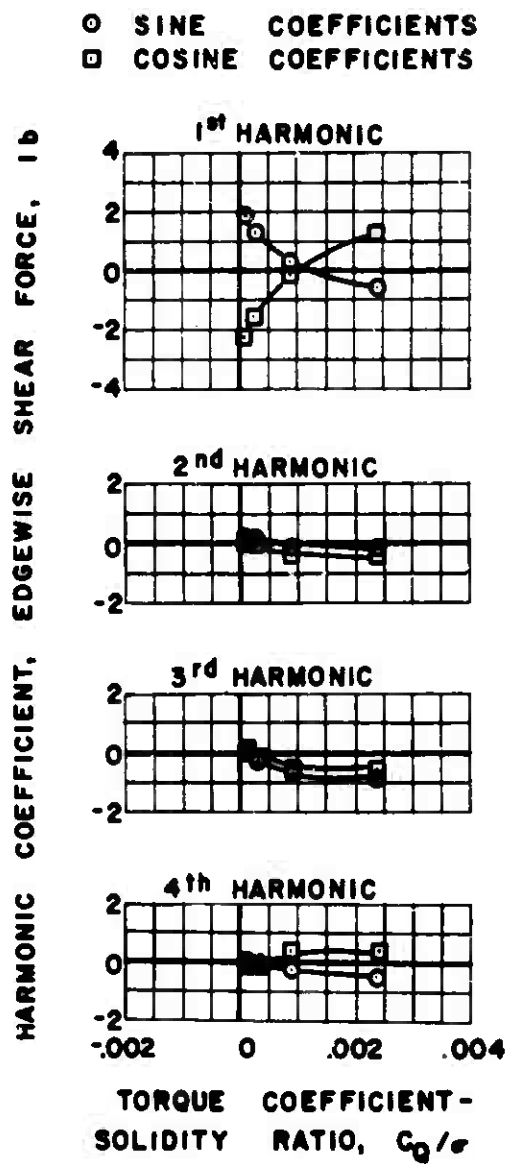


Figure 40(a). Continued.



$\mu = 0.2$ $\alpha_s = 0 \text{ deg.}$

(b) EDGEWISE

Figure 40. Continued.

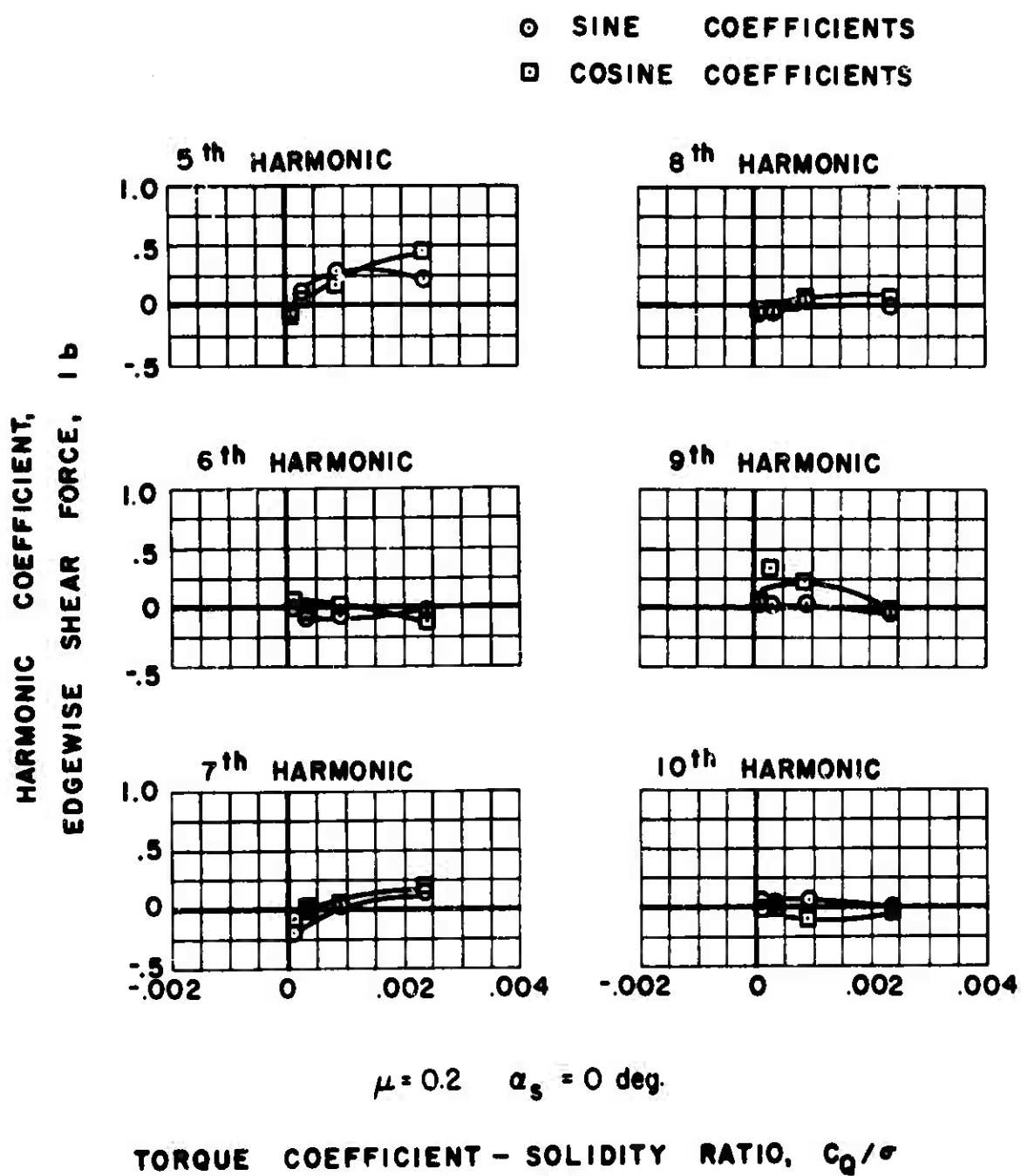


Figure 40(b). Concluded.

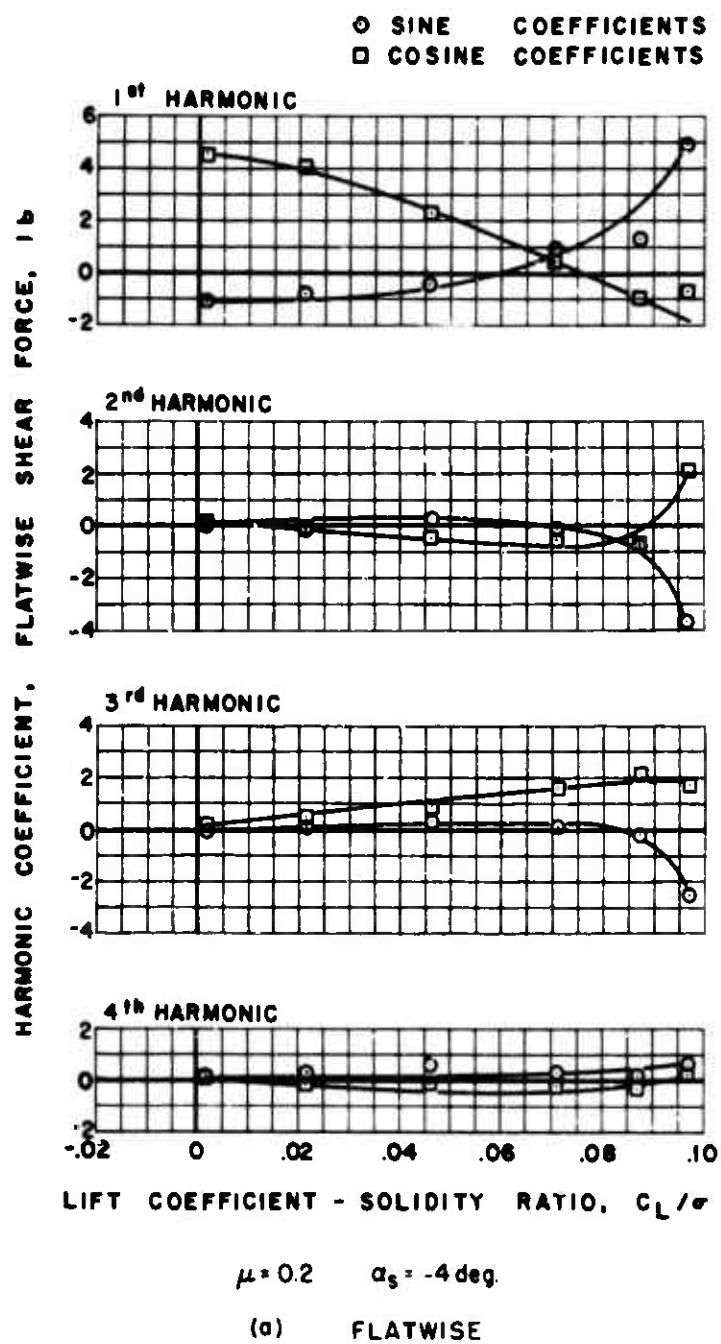


Figure 41. Experimental Shear Force.

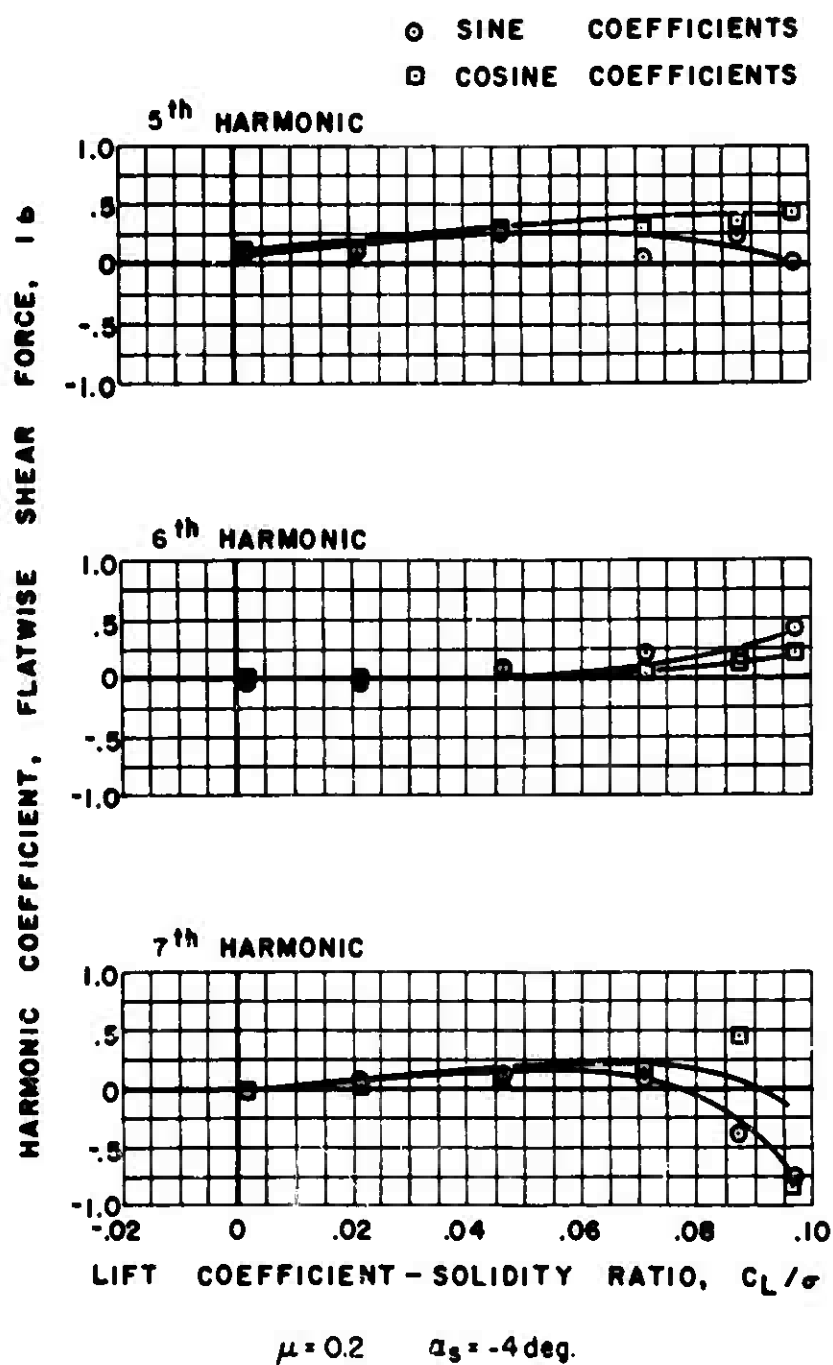


Figure 41(a). Continued.

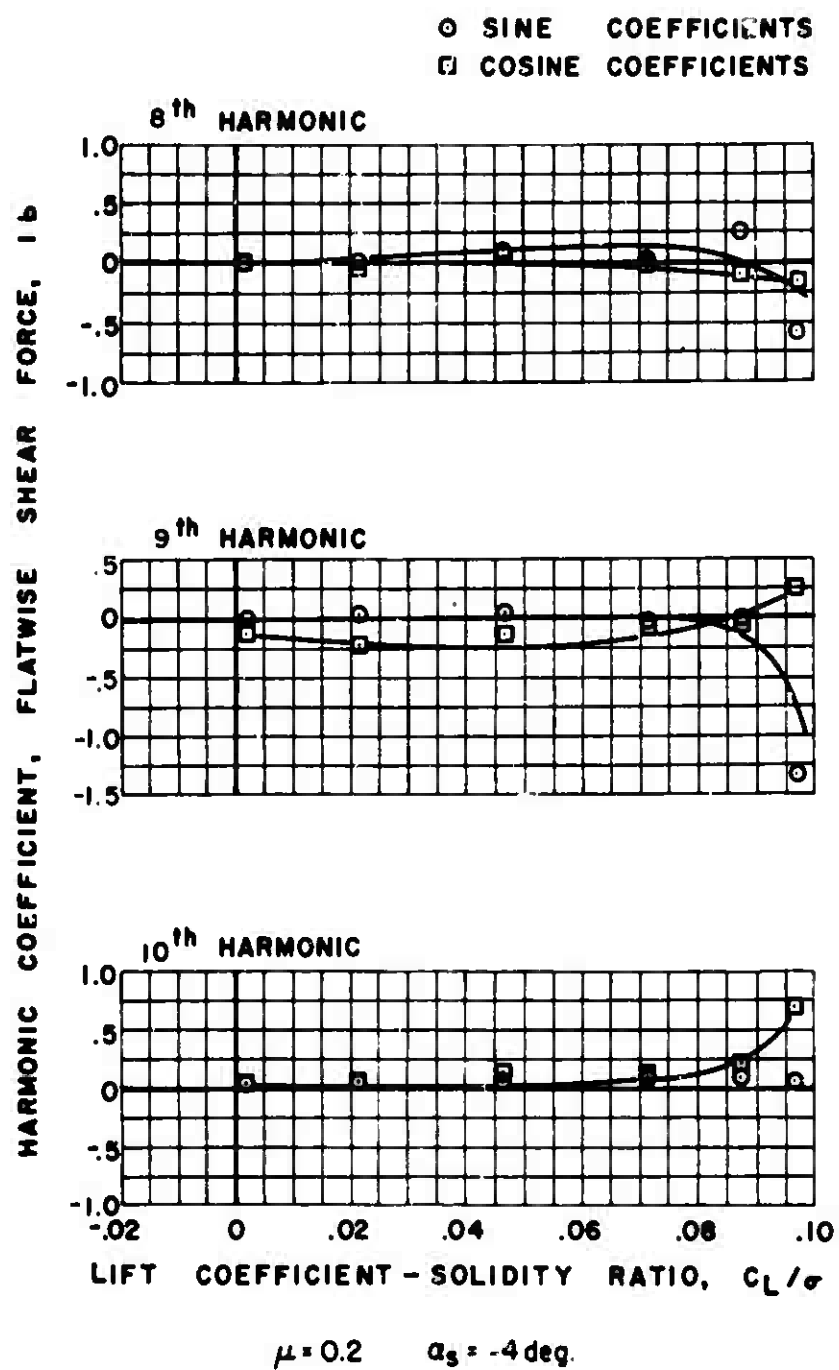
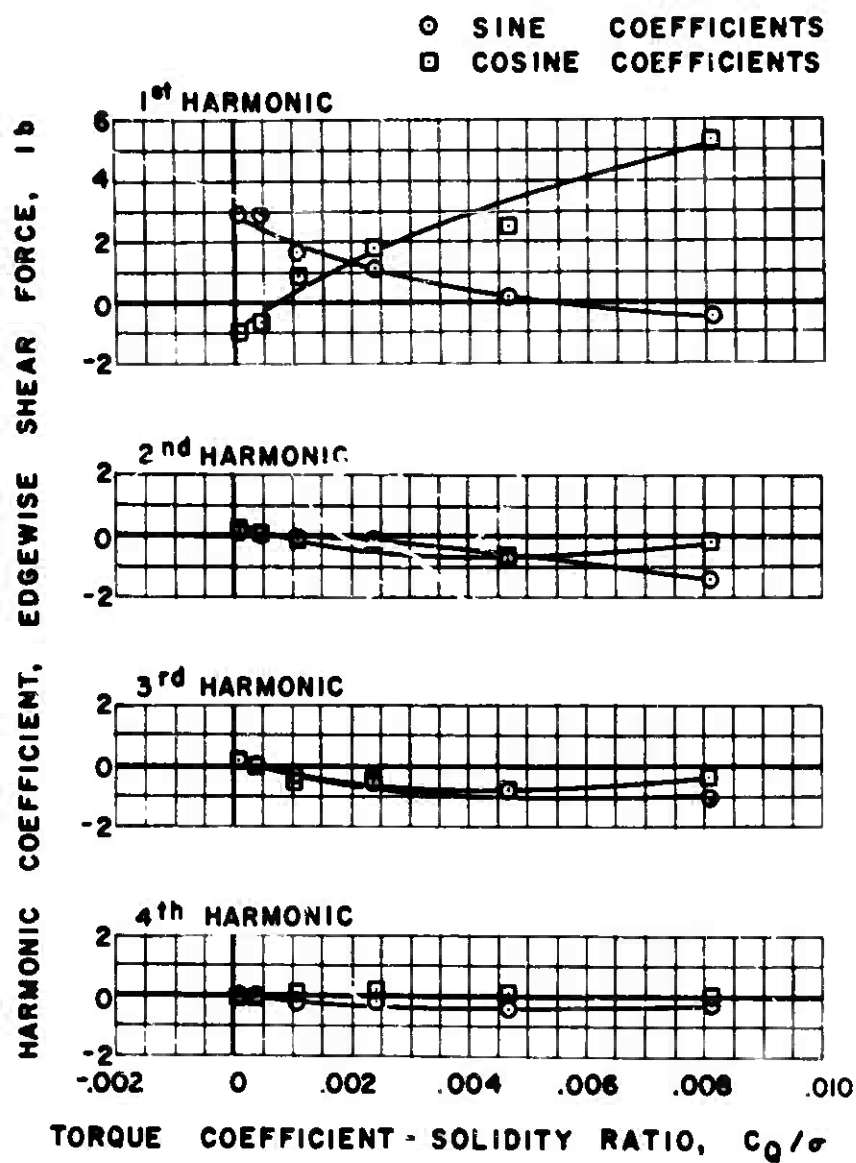


Figure 41(a). Continued.



$$\mu = 0.2 \quad \alpha_s = -4 \text{ deg.}$$

(b) EDGEWISE

Figure 41. Continued.

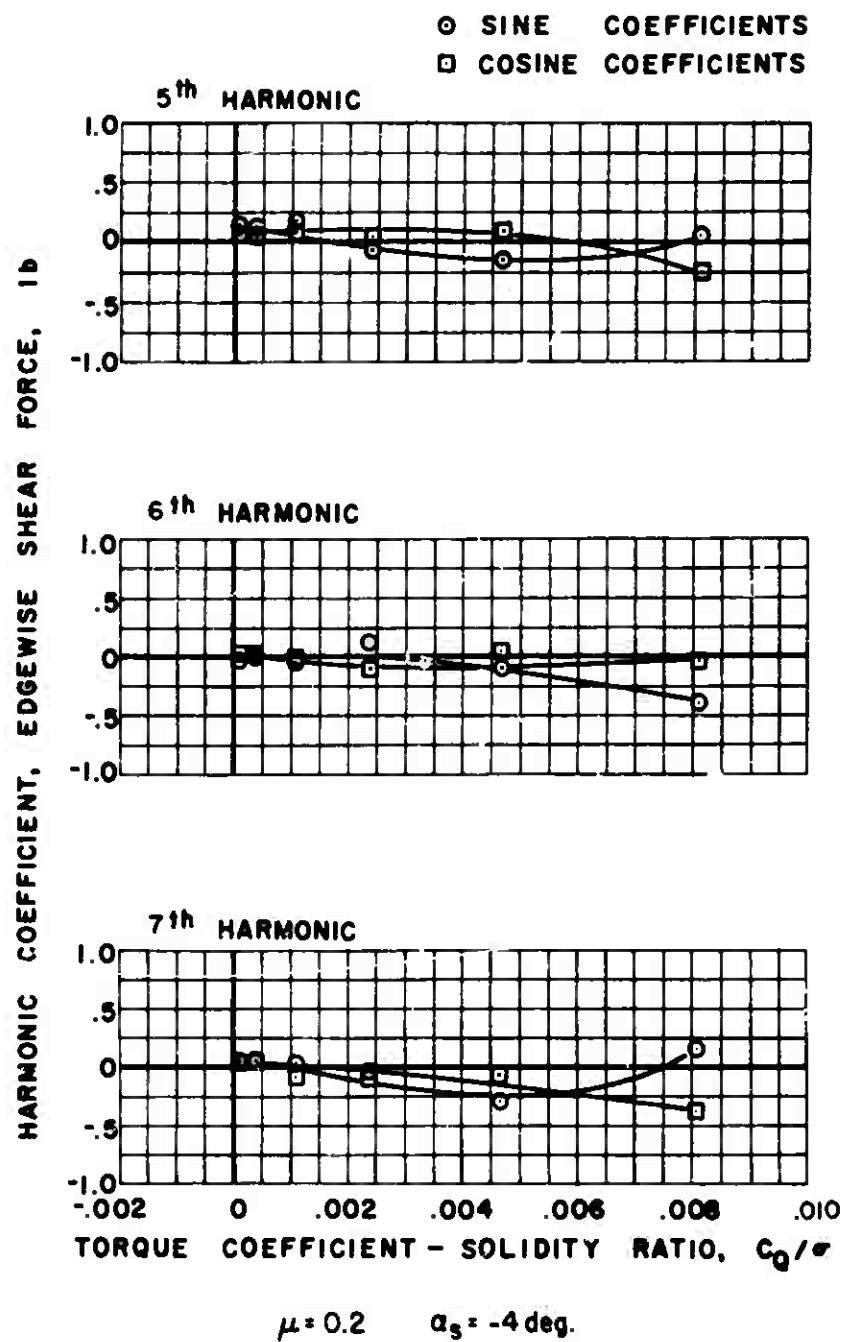


Figure 41(b). Continued.

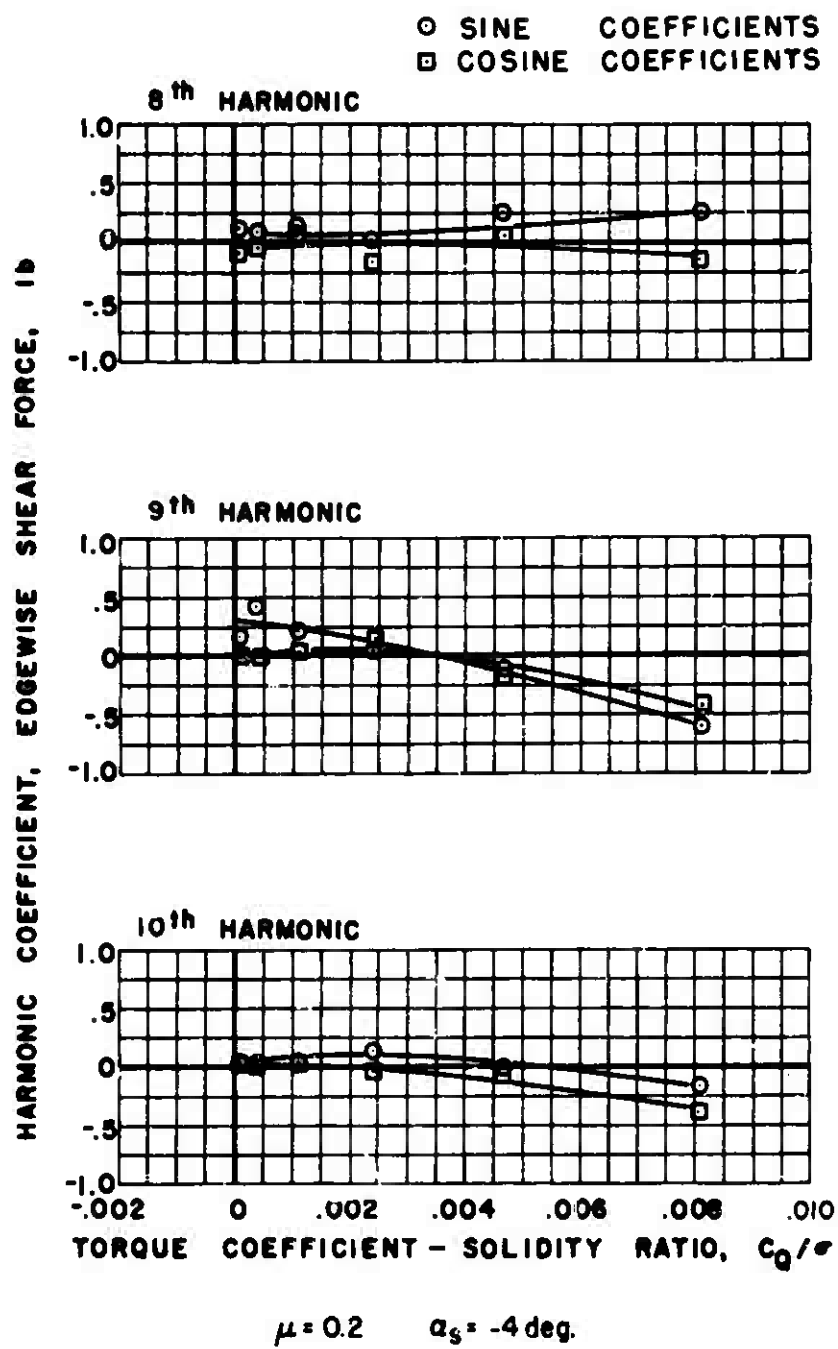
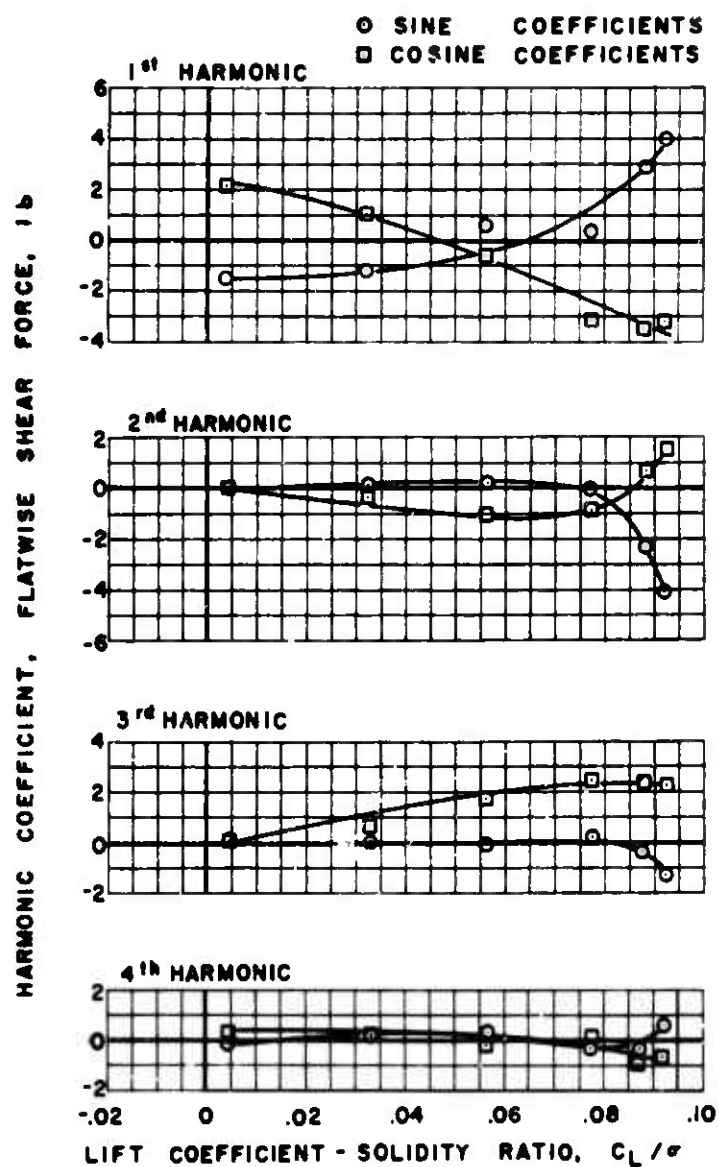


Figure 41(b). Concluded.



$\mu = 0.2 \quad \alpha_s = -8 \text{ deg.}$

(a) FLATWISE

Figure 42. Experimental Shear Force.

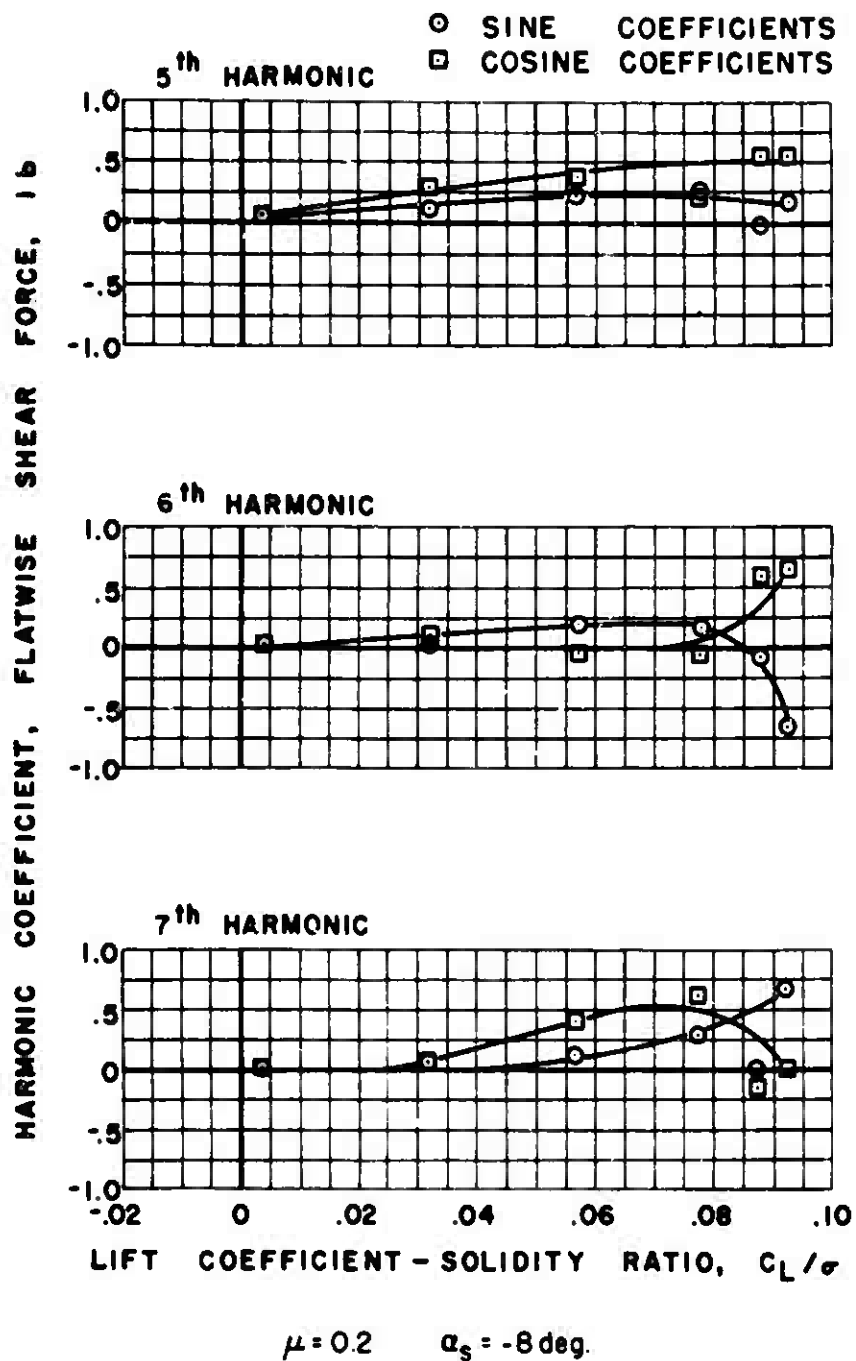
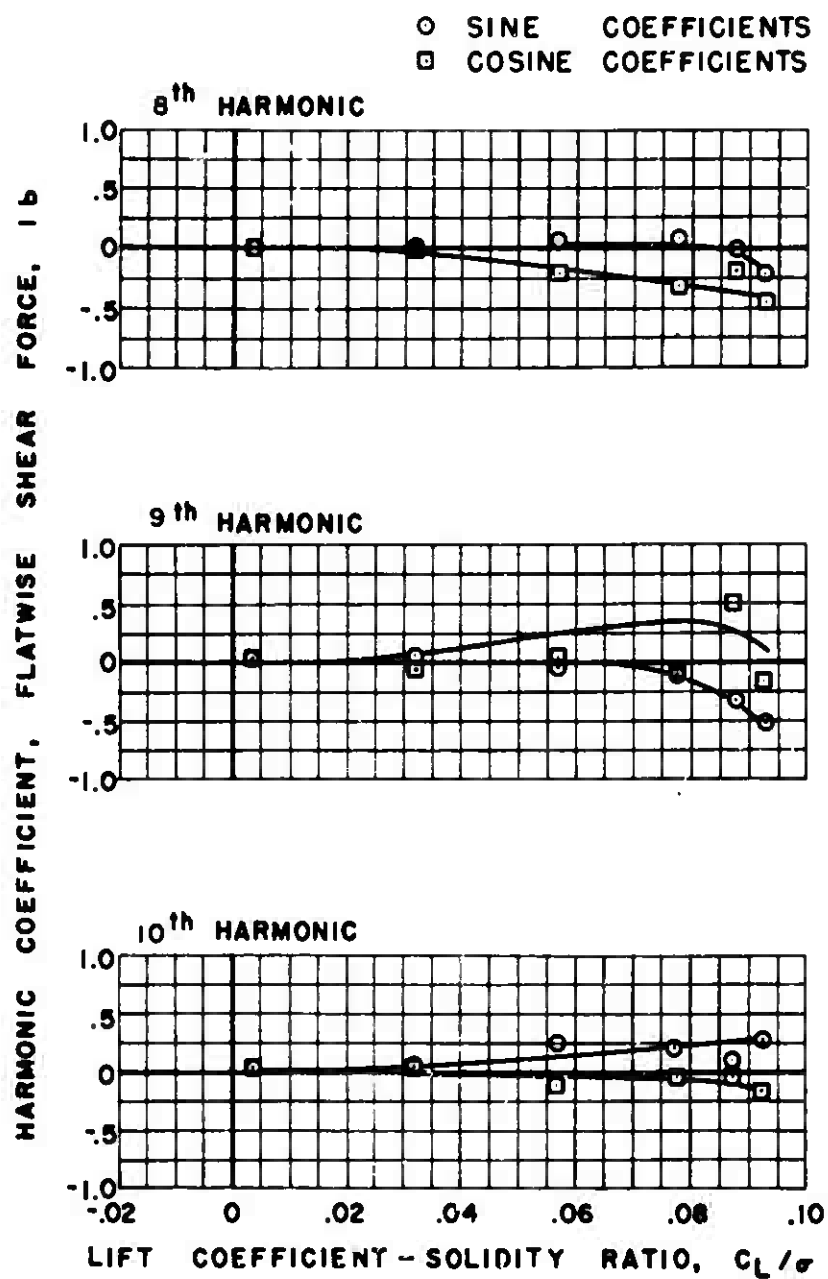
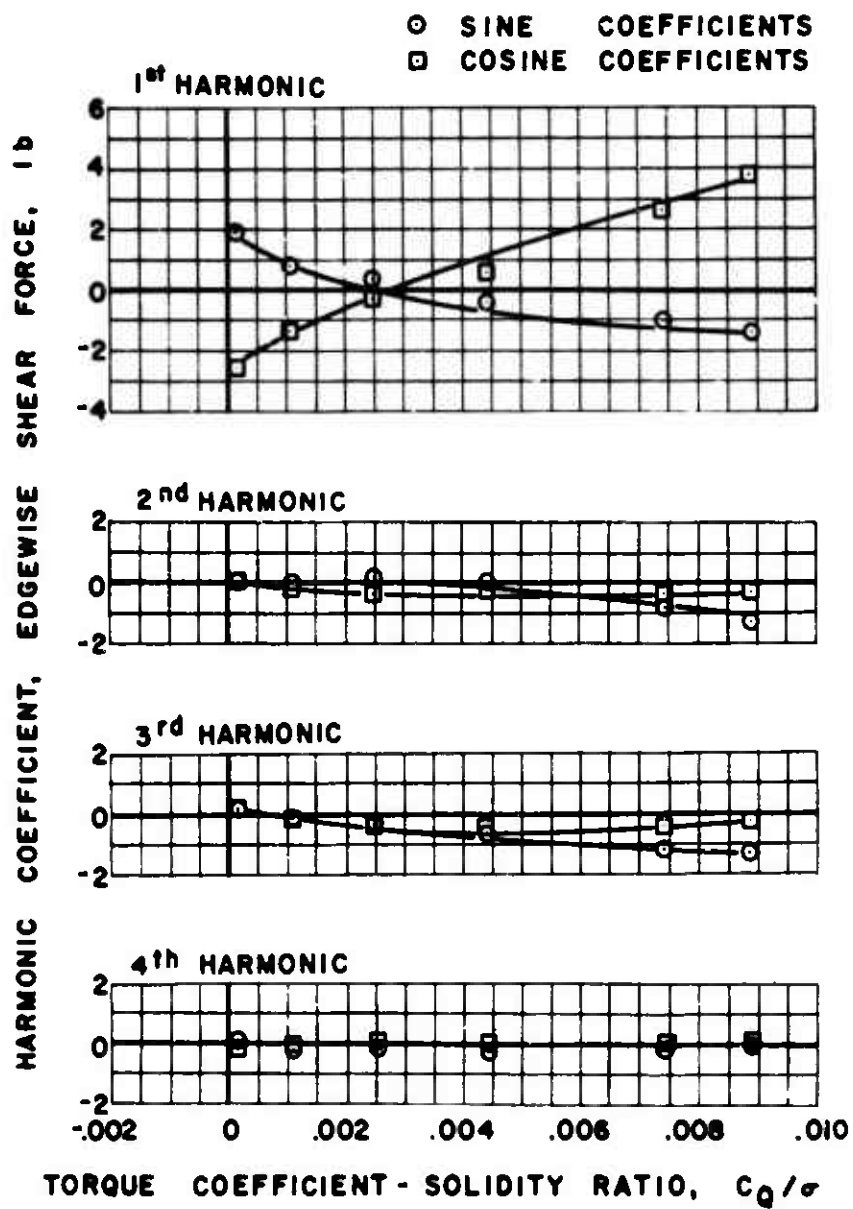


Figure 42(a). Continued.



$\mu = 0.2 \quad \alpha_s = -8 \text{ deg.}$

Figure 42(a). Continued.



$\mu = 0.2$ $\alpha_s = -8 \text{ deg.}$

(b) EDGEWISE

Figure 42. Continued.

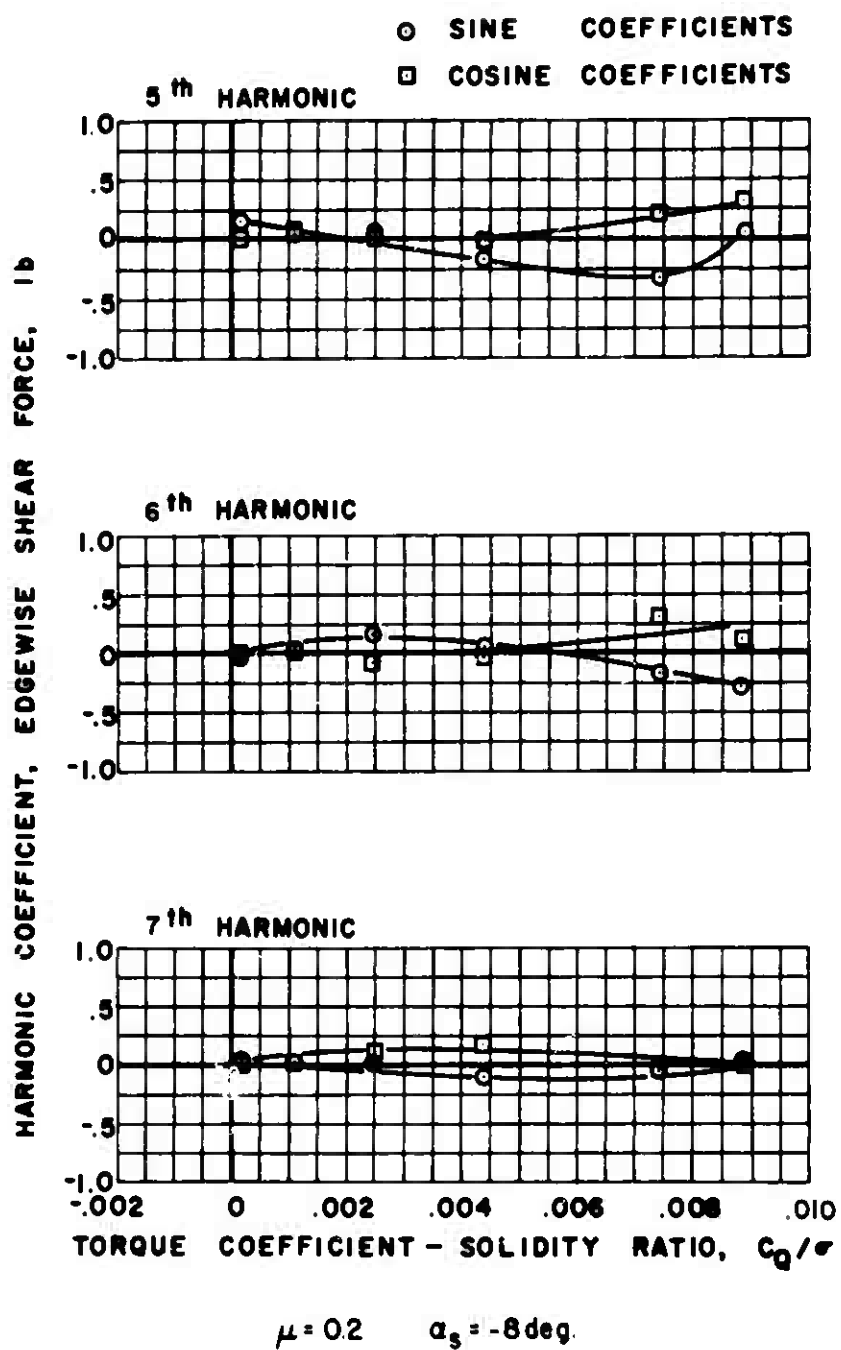


Figure 42(b). Continued.

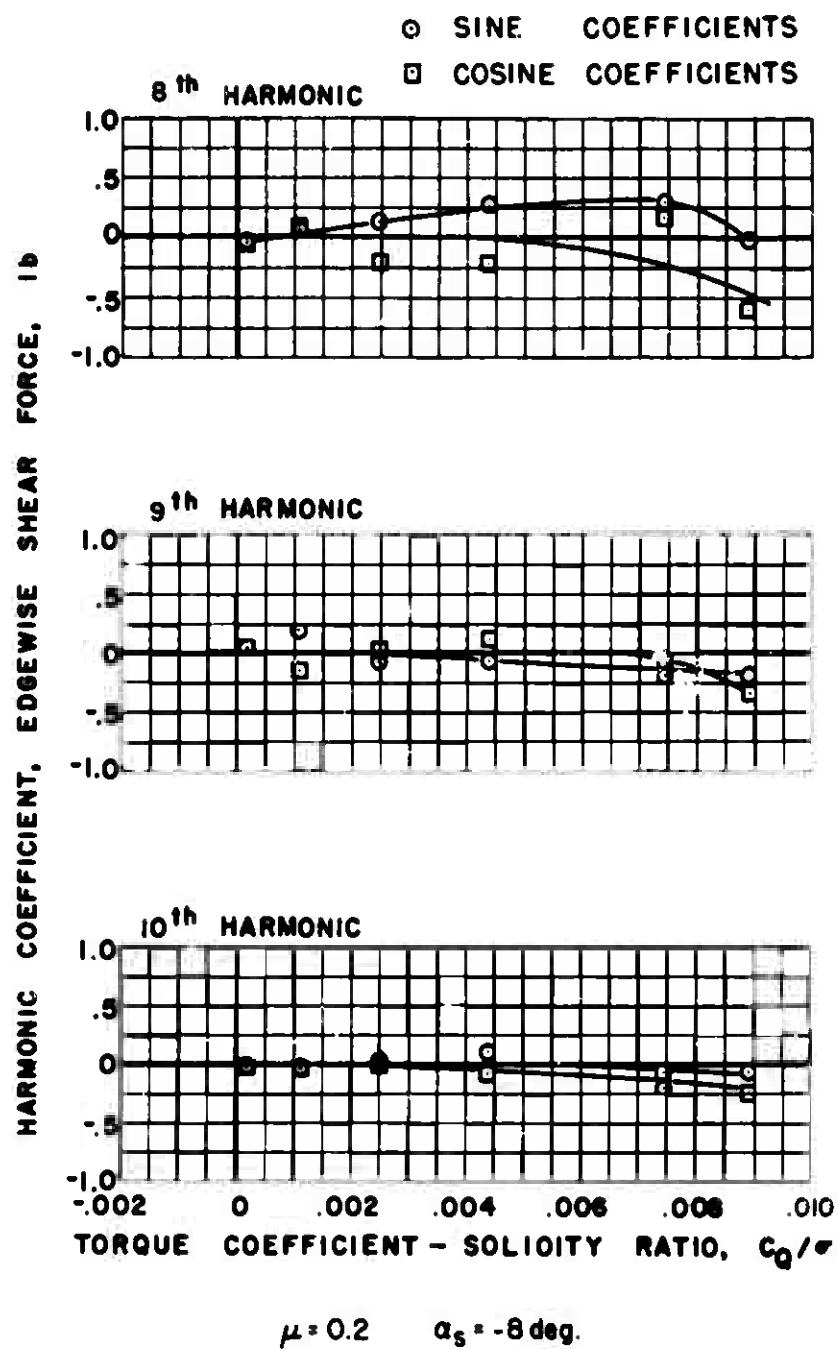
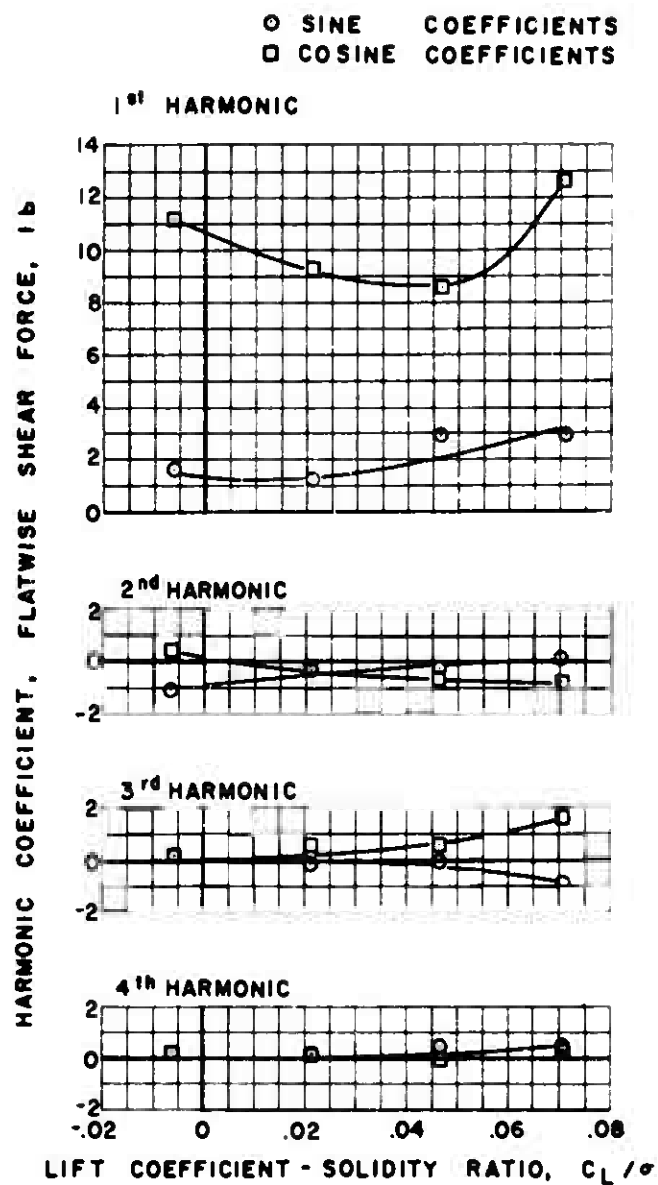


Figure 42(b). Concluded.



$\mu = 0.2 \quad \alpha_s = 0 \text{ deg.}$

(a) FLATWISE

Figure 43. Experimental Shear Force, Out of Trim, -4 Degree Longitudinal Flapping.

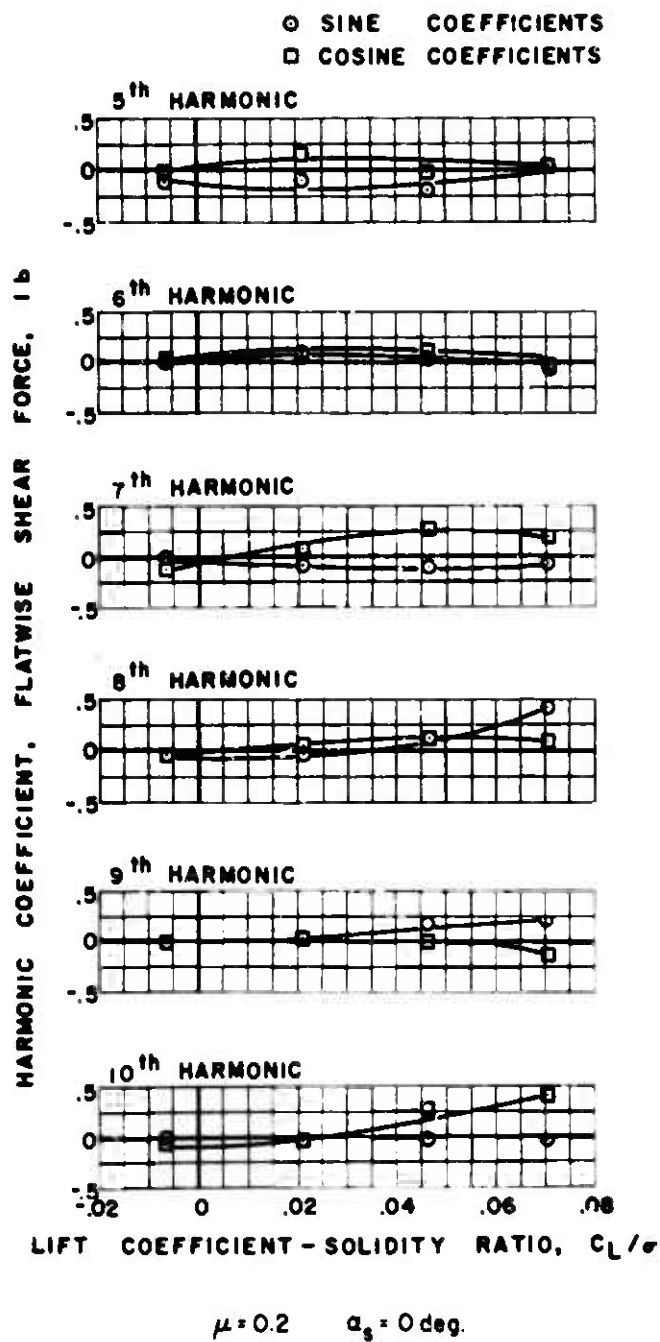
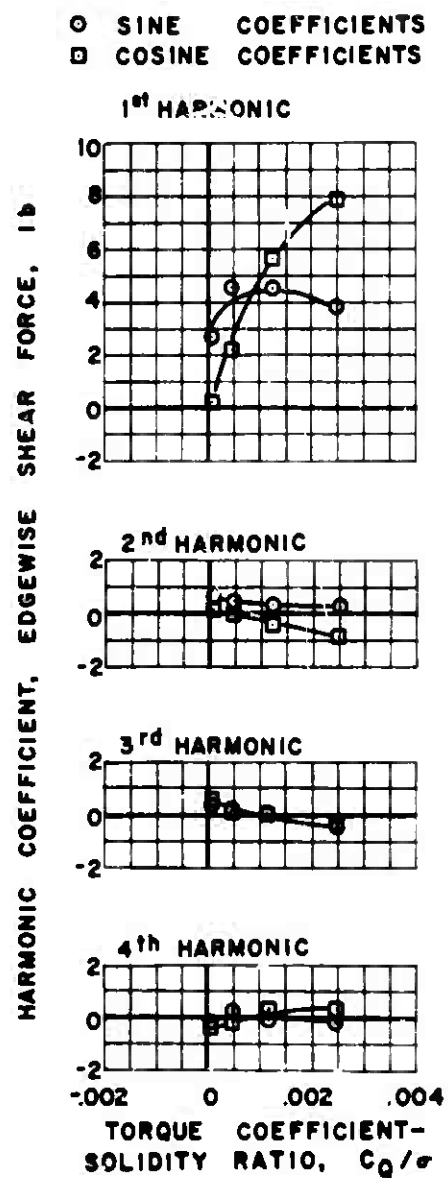


Figure 43(a). Continued



$\mu = 0.2$ $\alpha_s = 0^\circ$

(b) EDGEWISE

Figure 43. Continued.

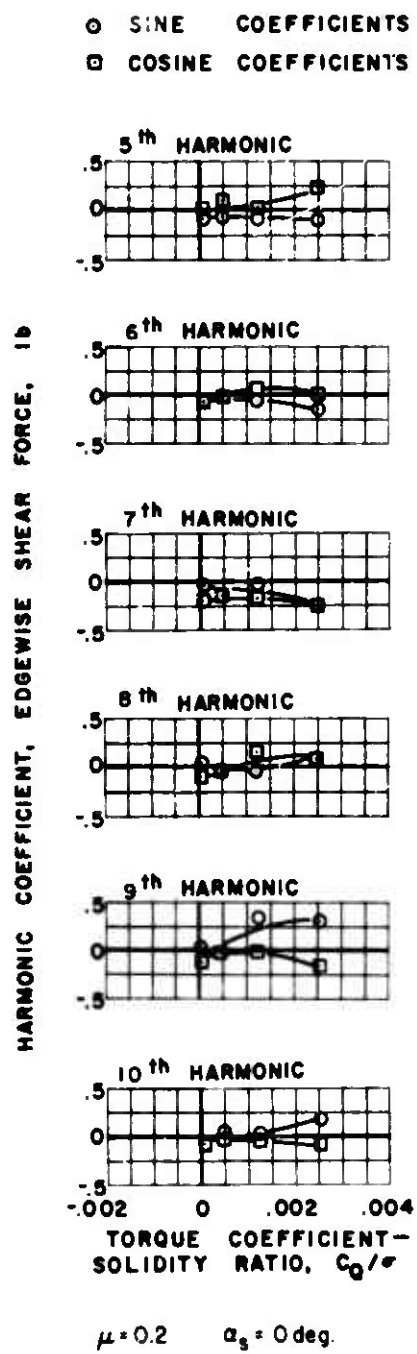
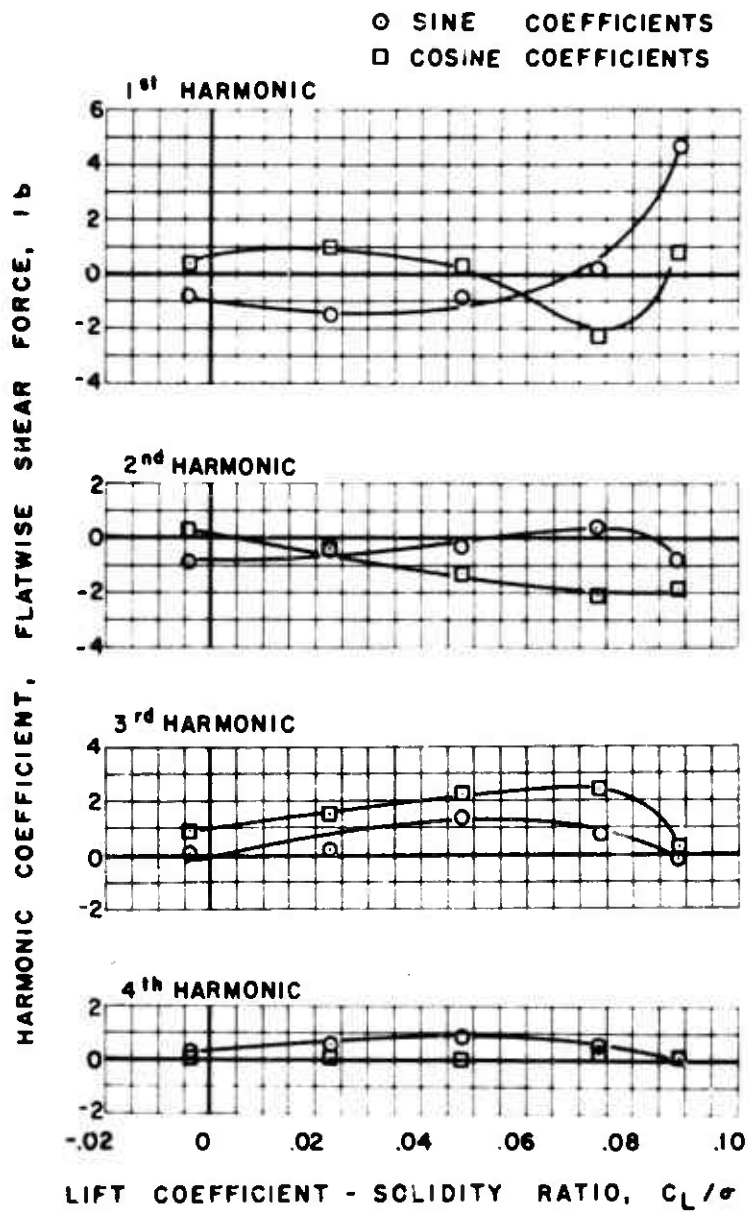


Figure 43(b). Concluded.



$\mu = 0.2$ $\alpha_s = -4^\circ$

(a) FLATWISE

Figure 44. Experimental Shear Force, Zero Lag Damping.

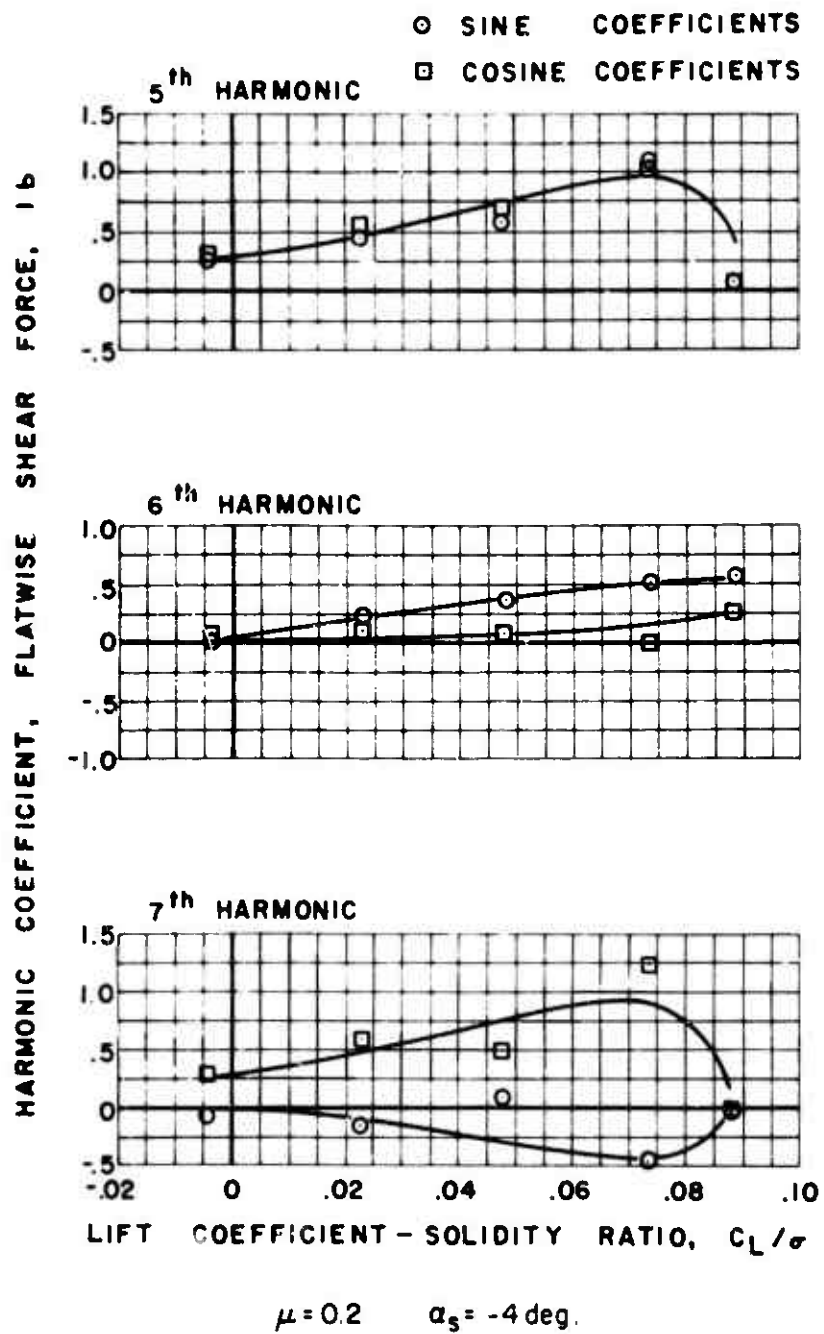


Figure 44(a). Continued.

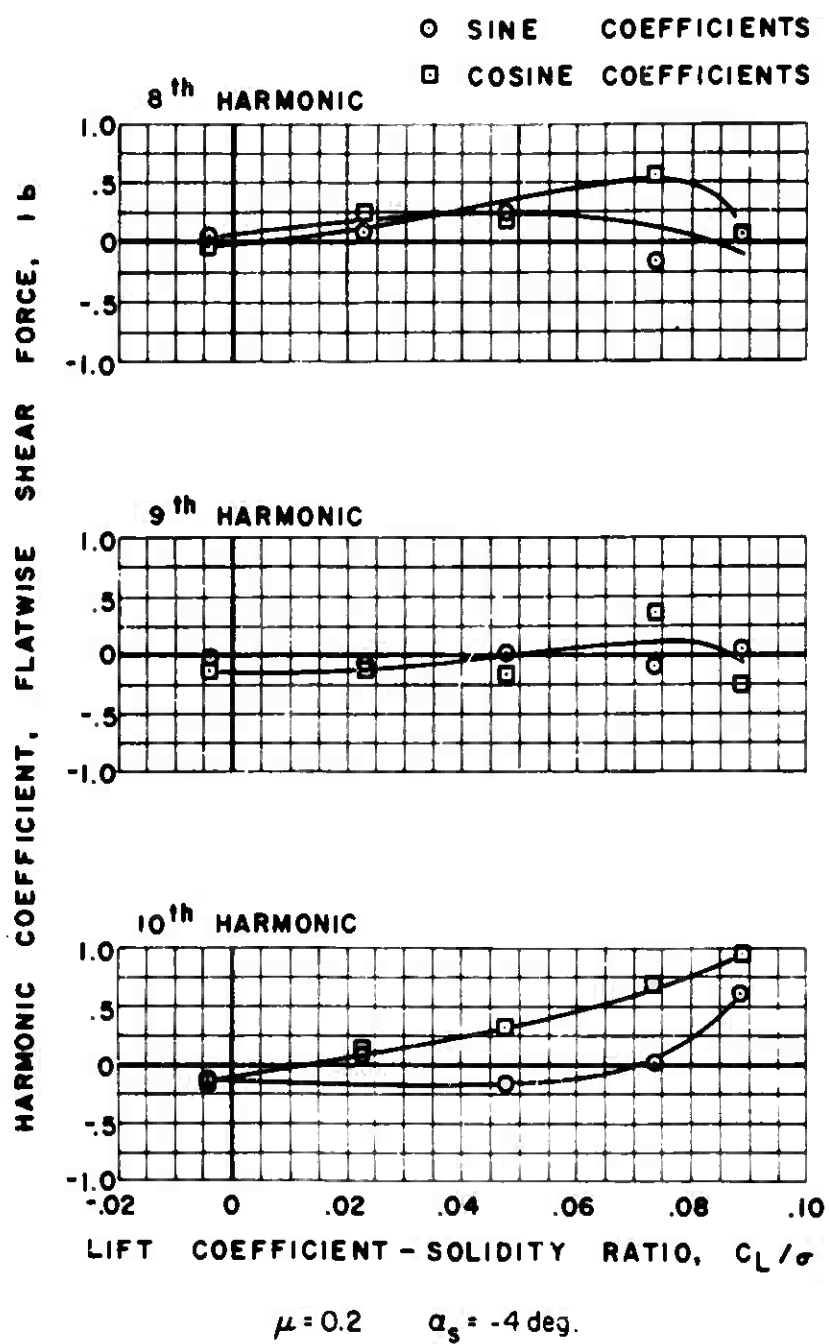
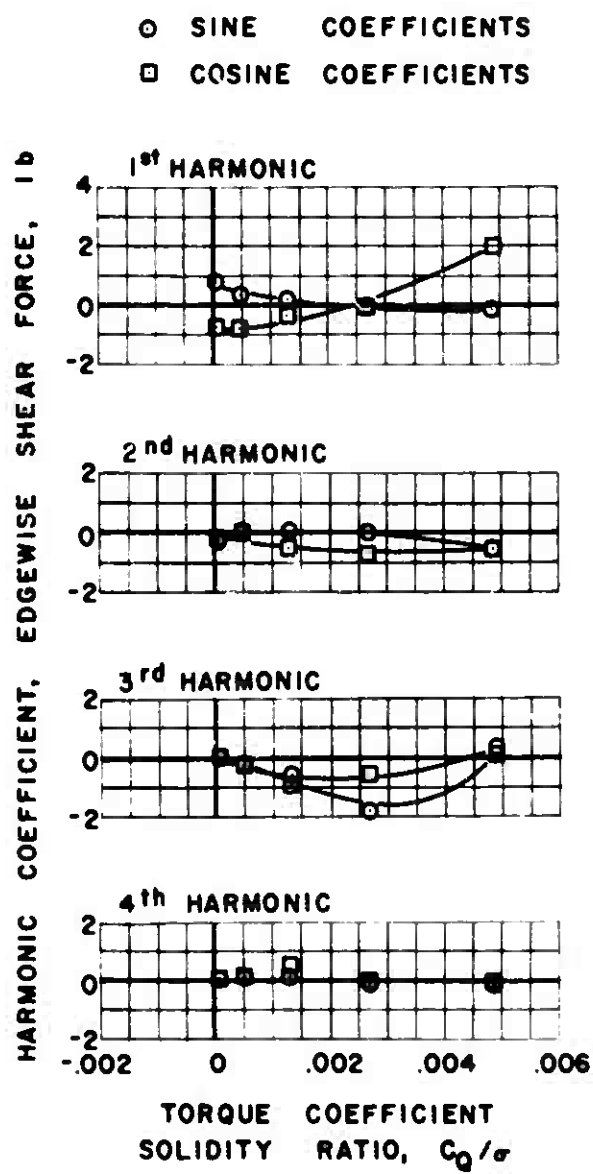


Figure 44(a). Continued.



$\mu = 0.2$ $\alpha_s = -4$ deg.

(b) EDGEWISE

Figure 44. Continued.

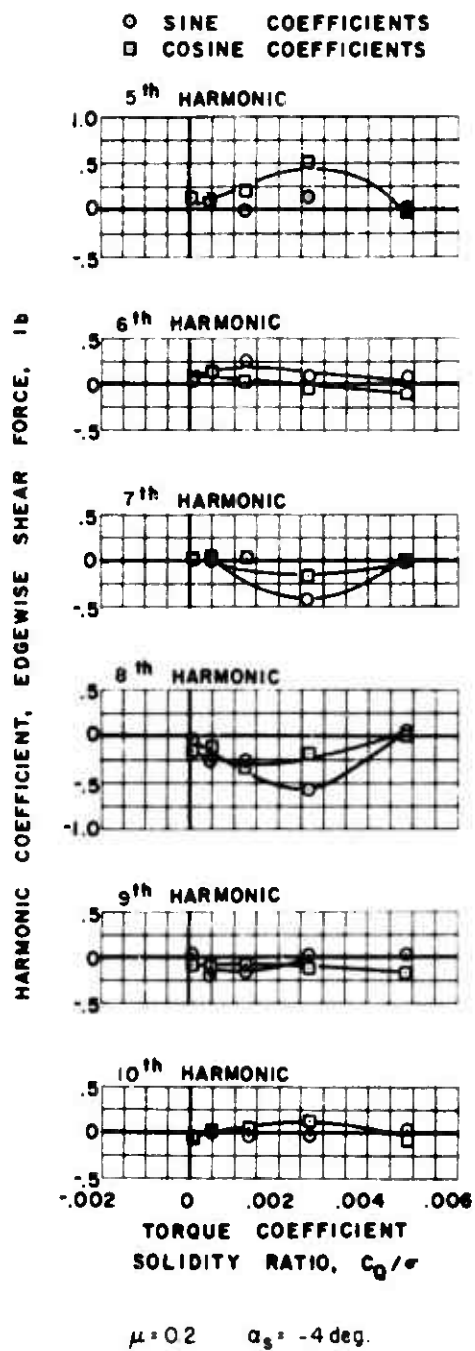


Figure 44(b). Concluded.

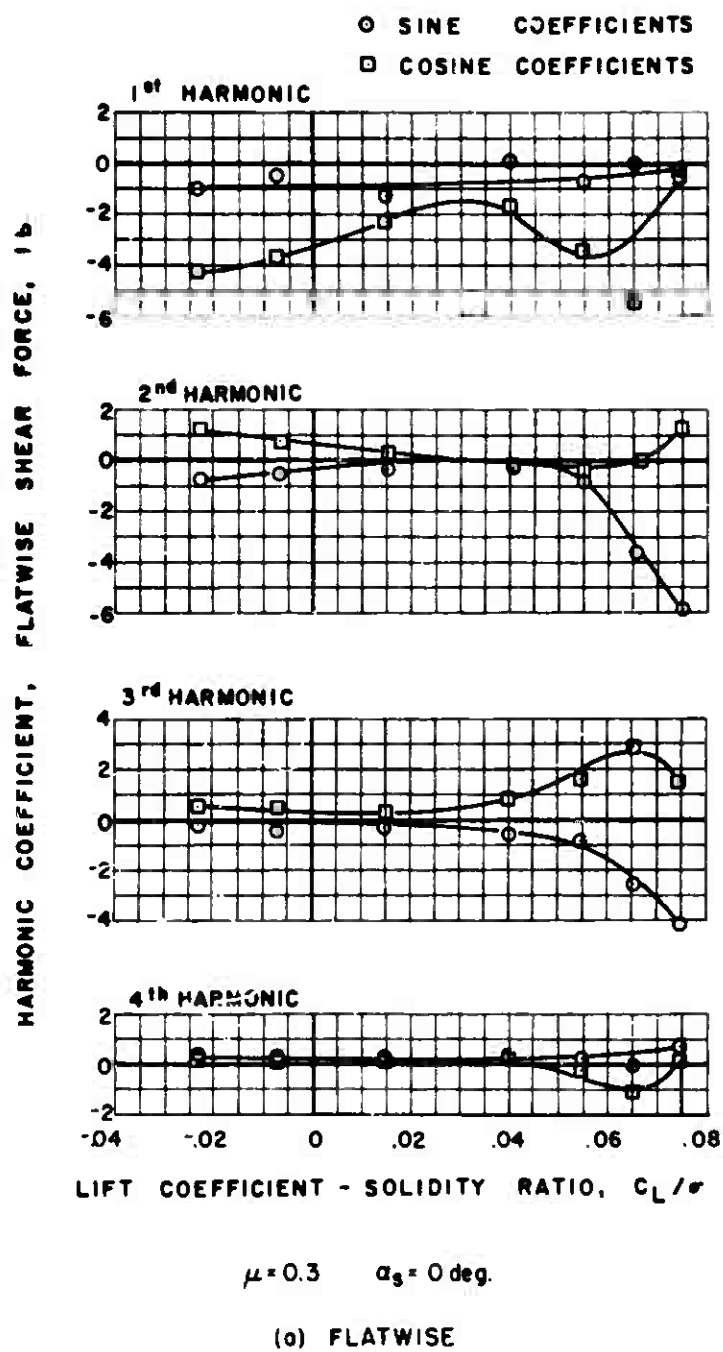


Figure 45. Experimental Shear Force.

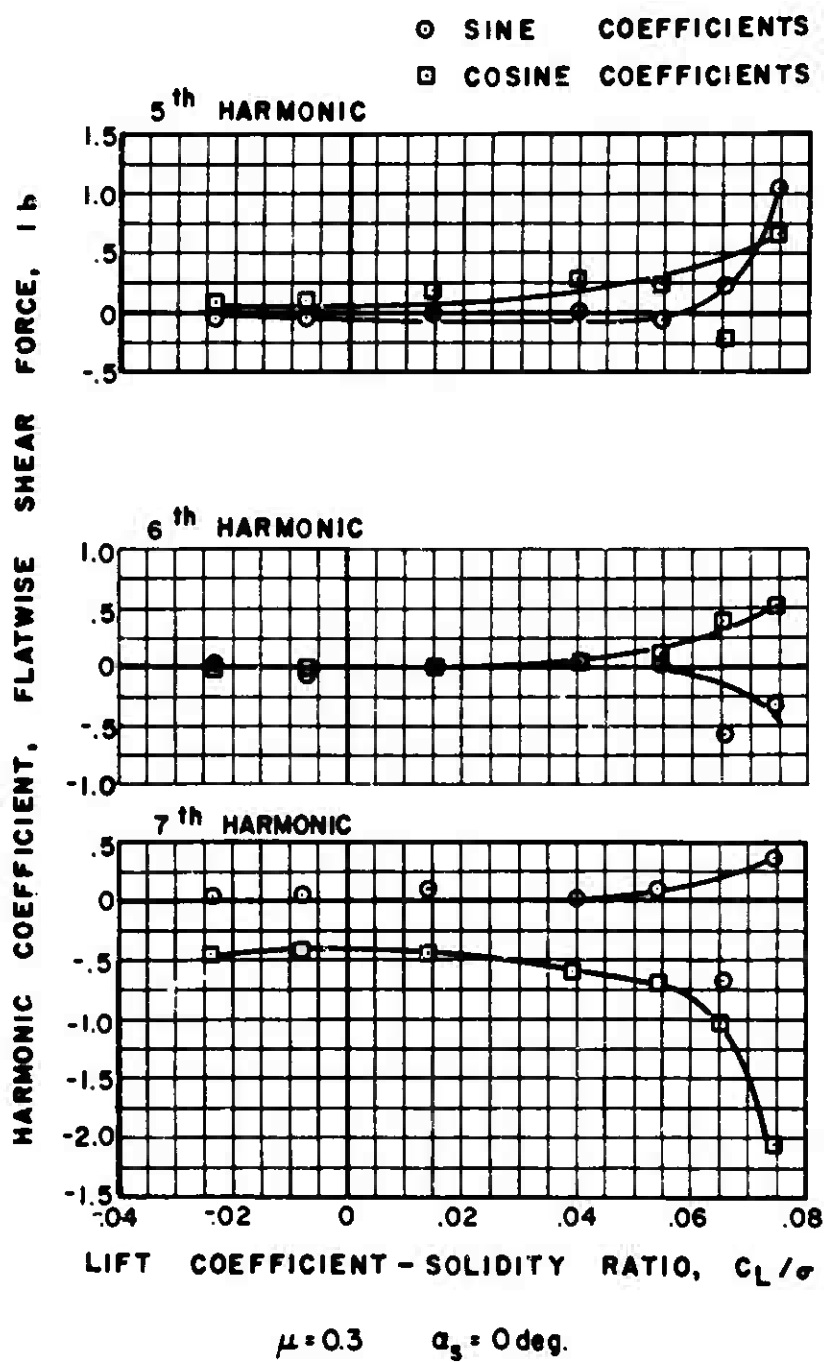


Figure 45(a). Continued.

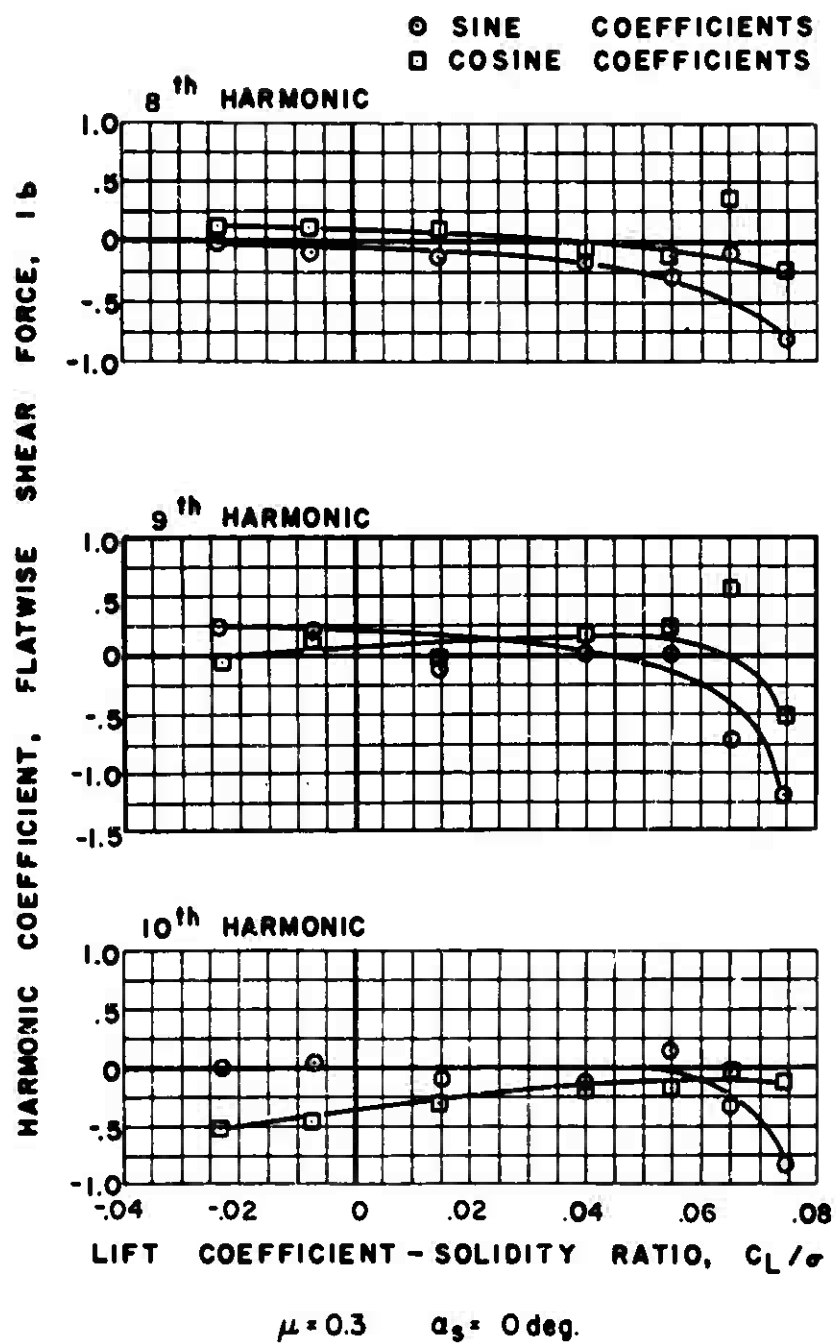
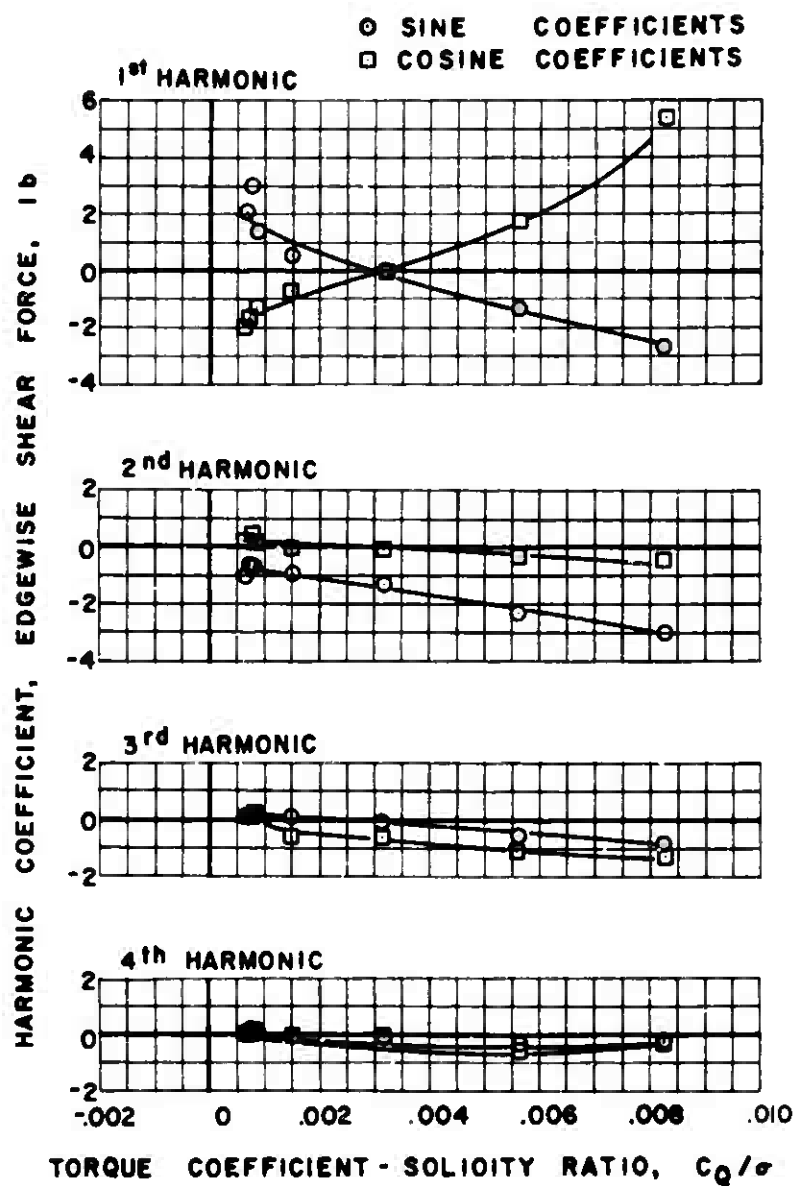


Figure 45(a). Continued.



$\mu = 0.3 \quad \alpha_s = 0 \text{ deg.}$

(b) EDGEWISE

Figure 45. Continued.

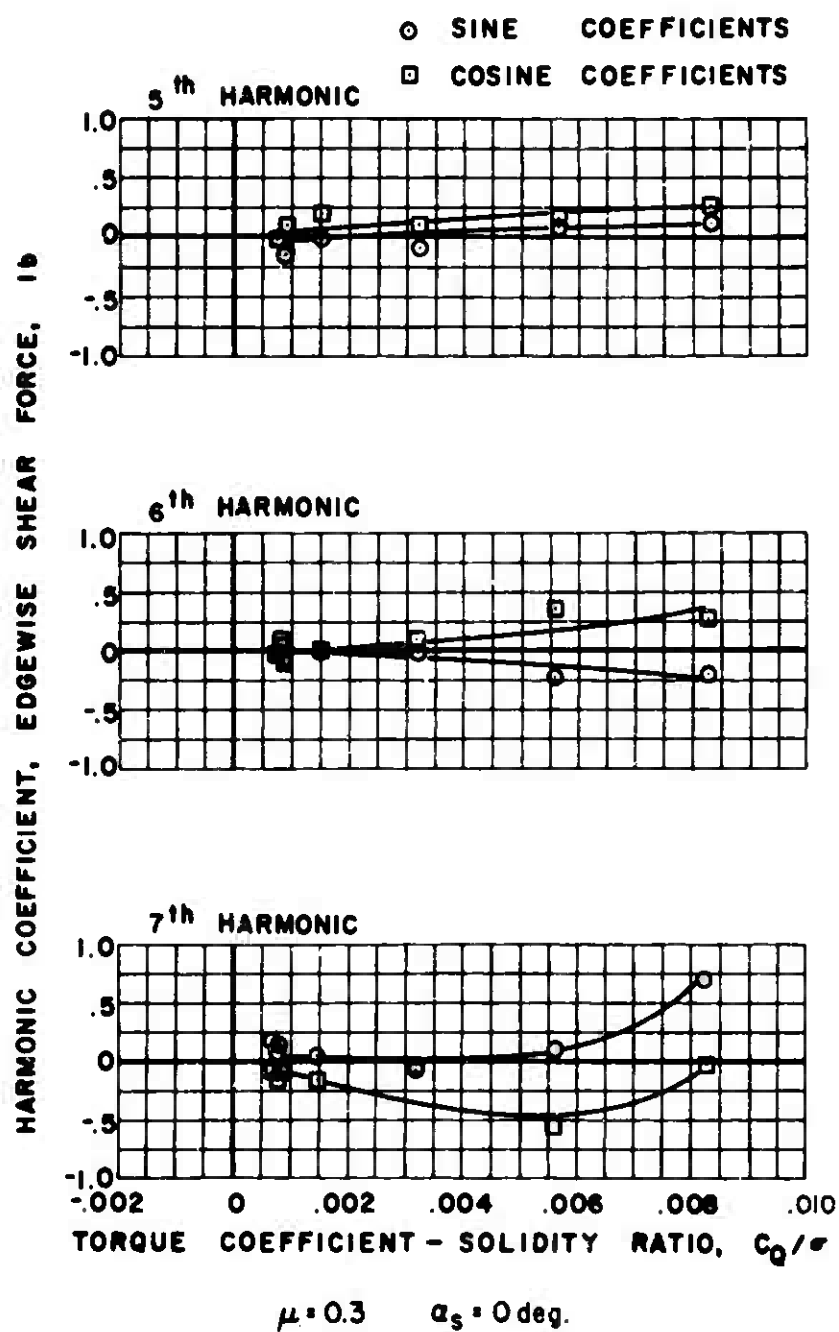


Figure 45(b). Continued.

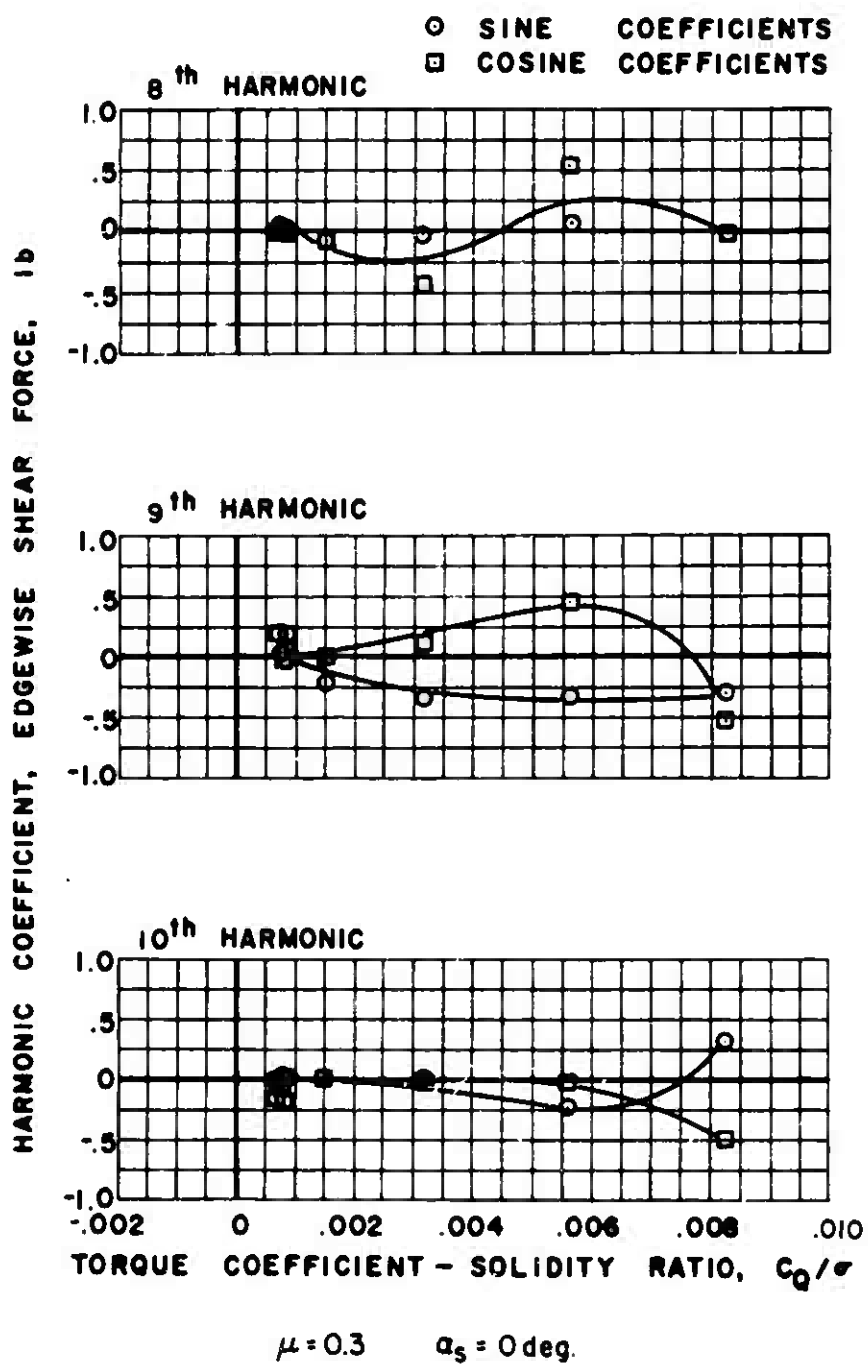
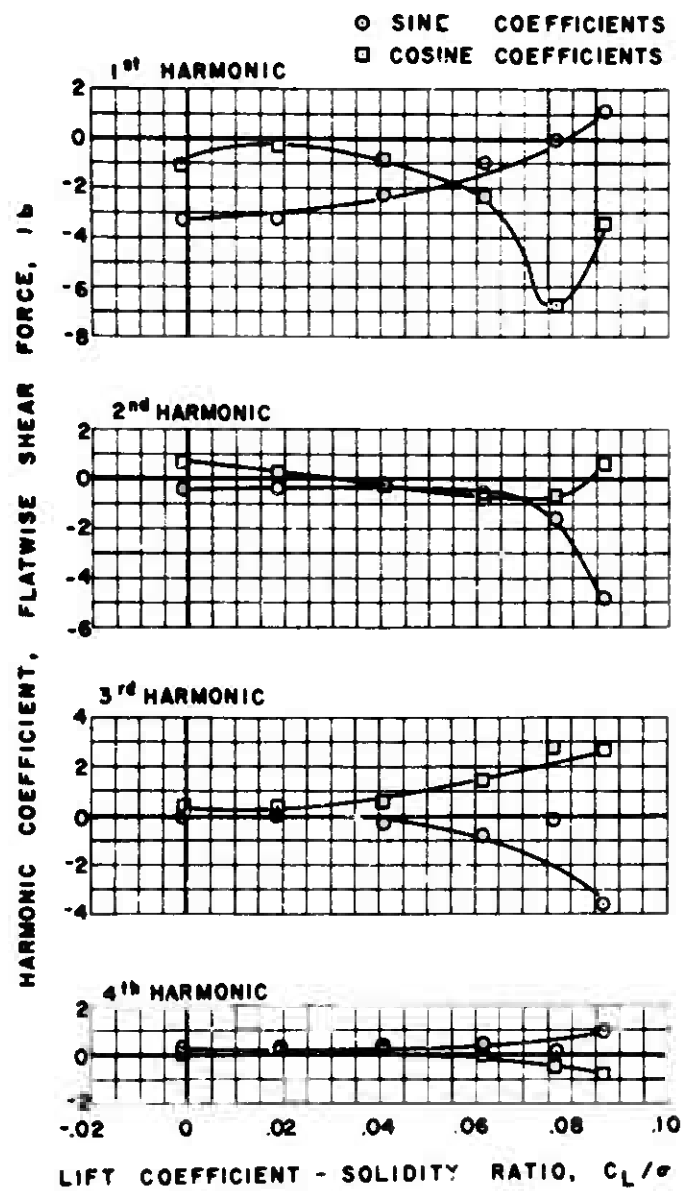


Figure 45(b). Concluded.



$\mu = 0.3$ $\alpha_s = -4 \text{ deg.}$

(a) FLATWISE

Figure 46. Experimental Shear Force.

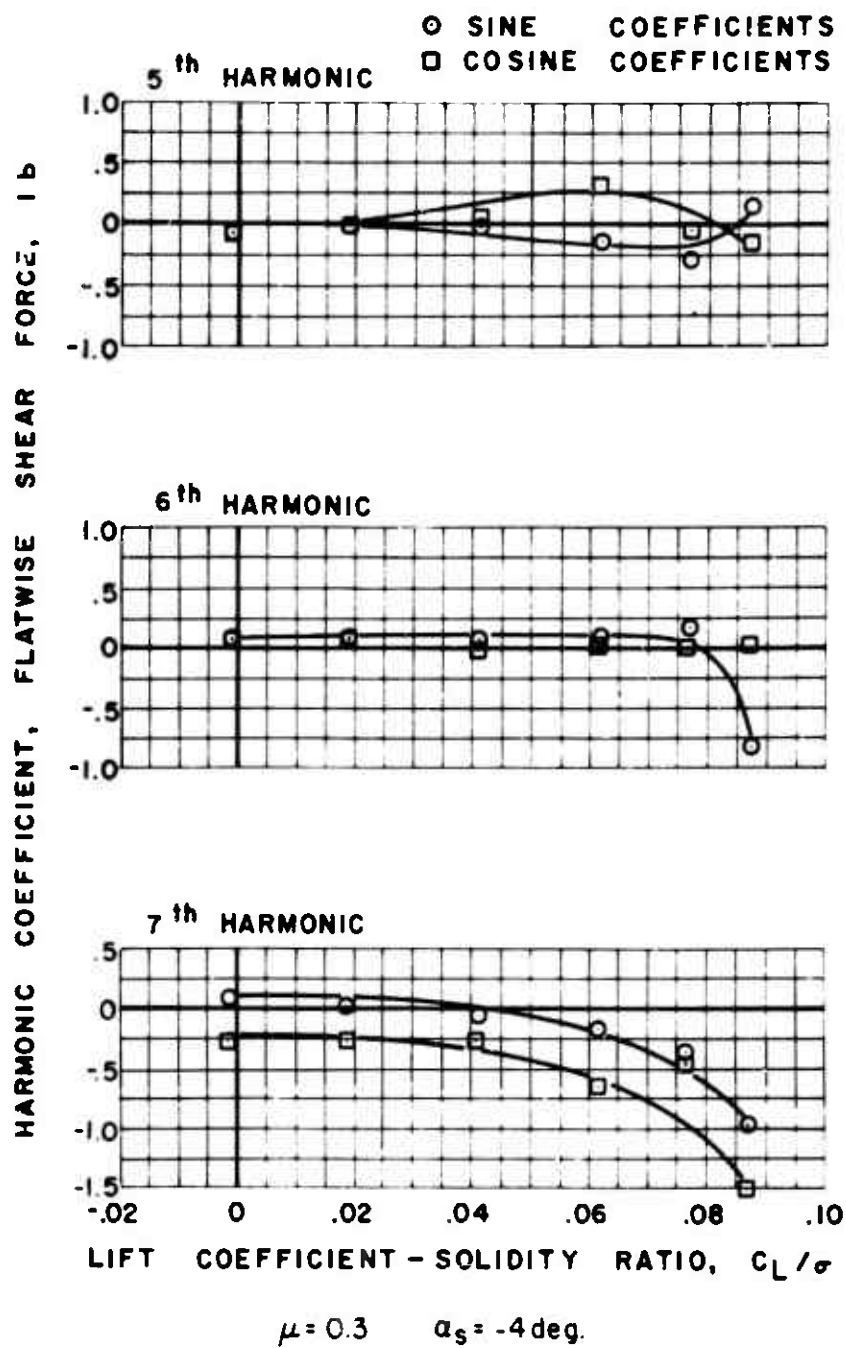


Figure 46(a). Continued.

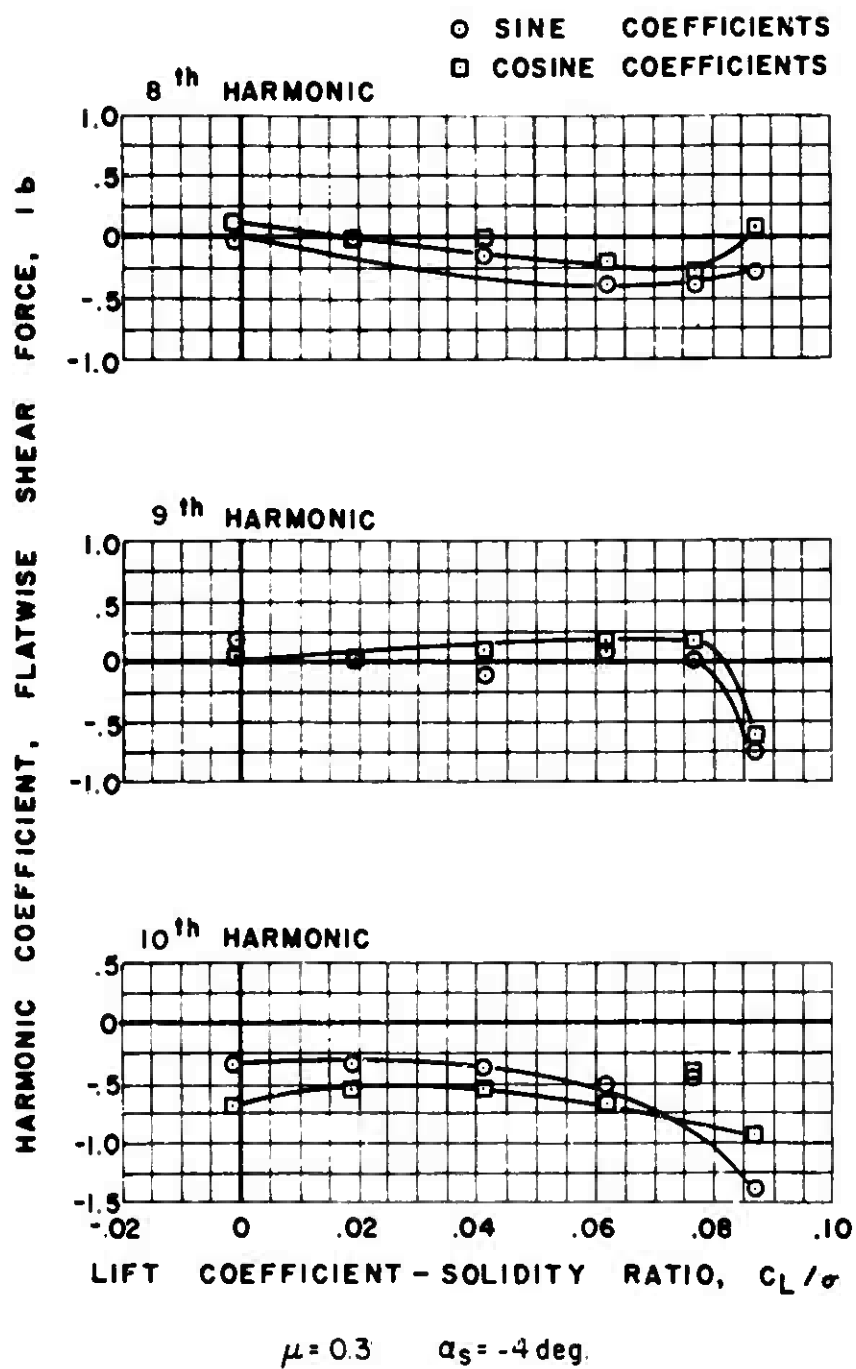
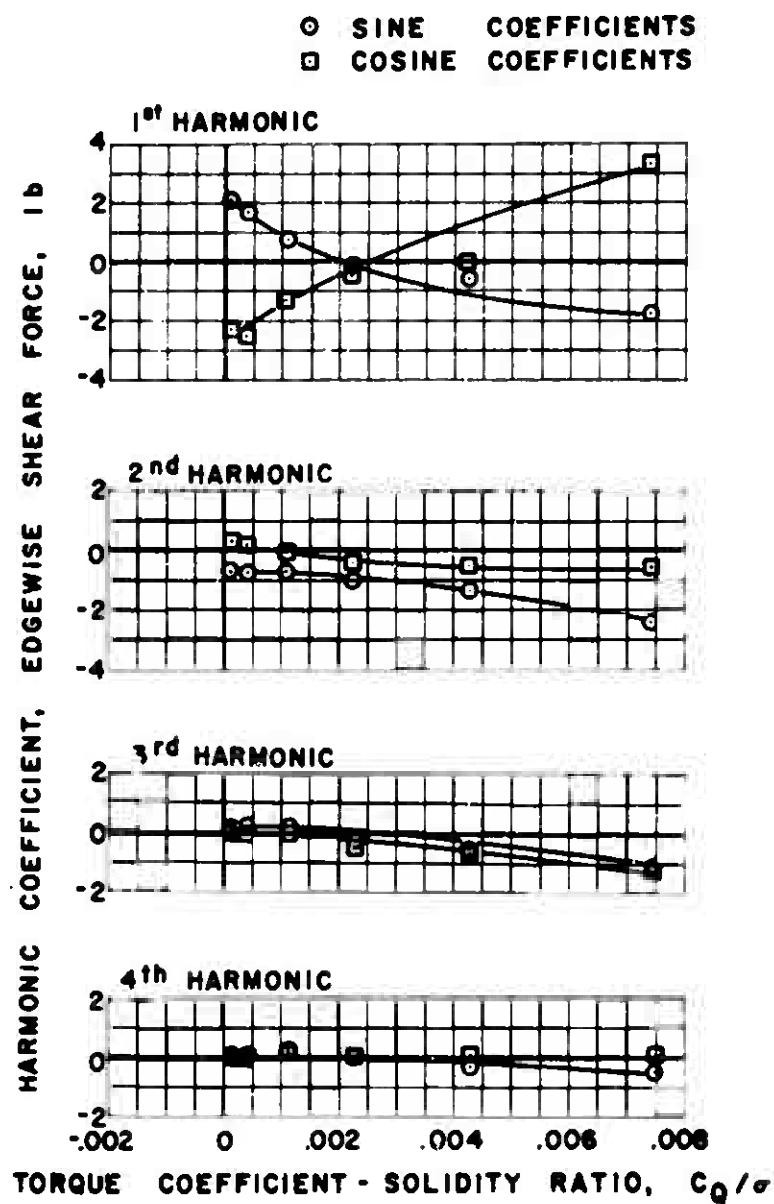


Figure 46(a). Continued.



$\mu = 0.3$ $\alpha_s = -4\text{deg.}$

(b) EDGEWISE

Figure 46. Continued.

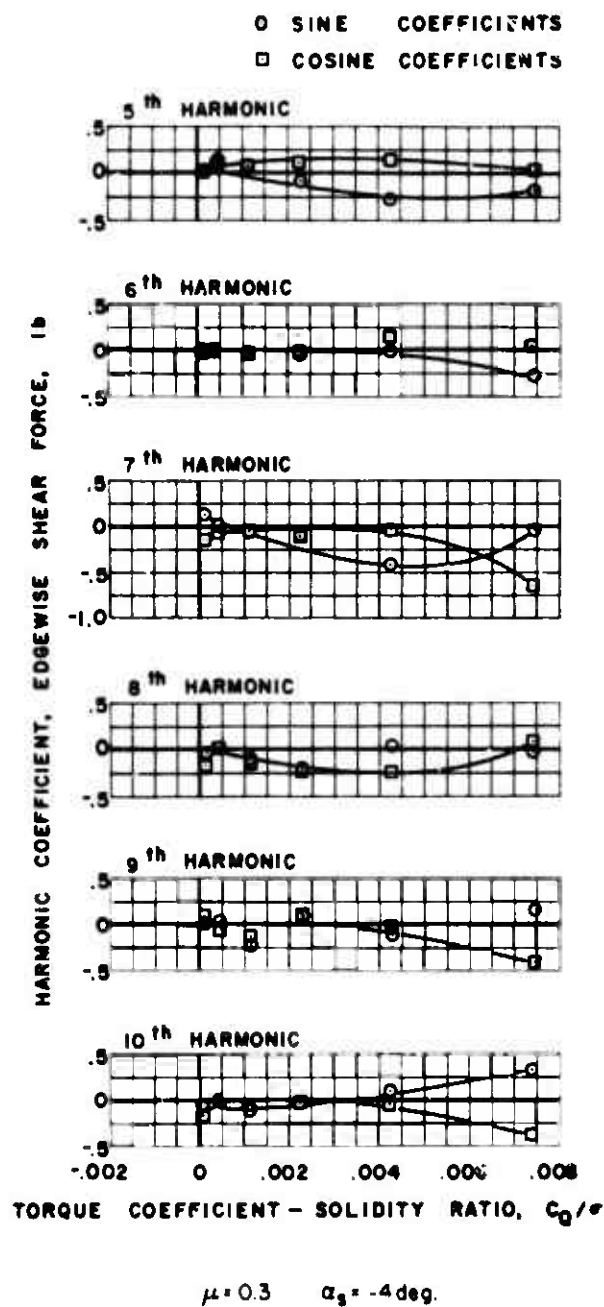
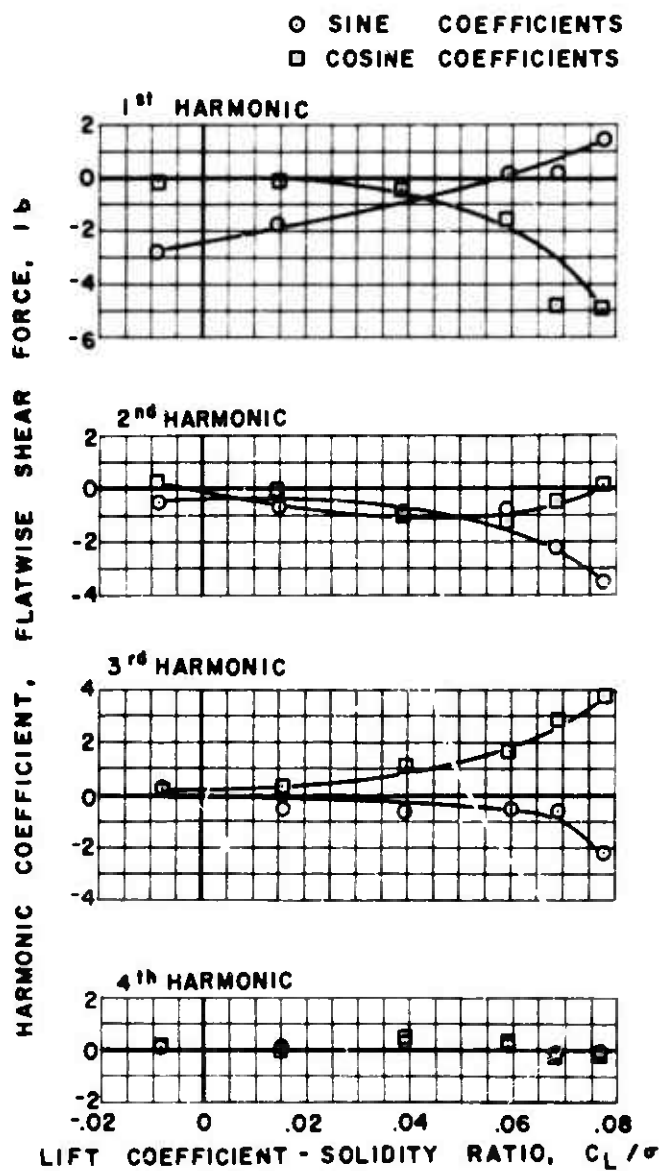


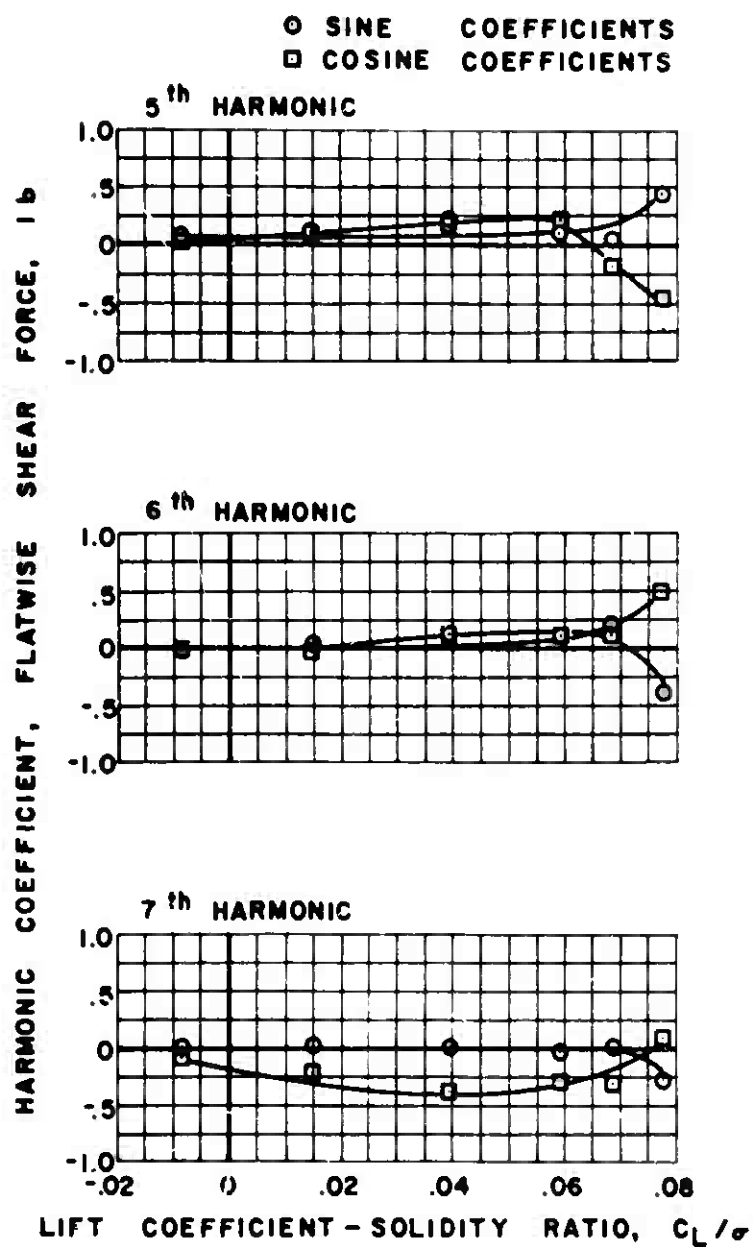
Figure 46(b). Concluded.



$\mu = 0.3 \quad \alpha_s = -8 \text{ deg.}$

(a) FLATWISE

Figure 47. Experimental Shear Force.



$\mu = 0.3 \quad \alpha_s = -8 \text{ deg.}$

Figure 47(a). Continued.

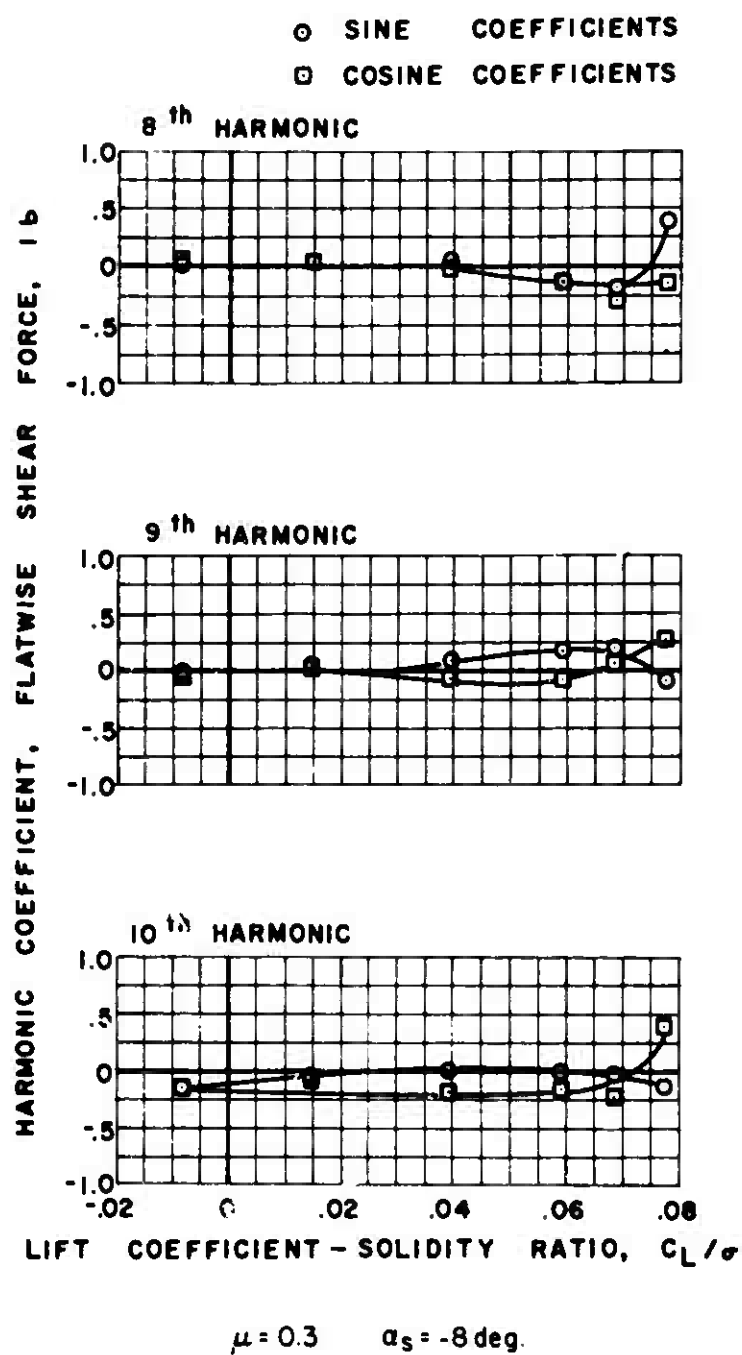
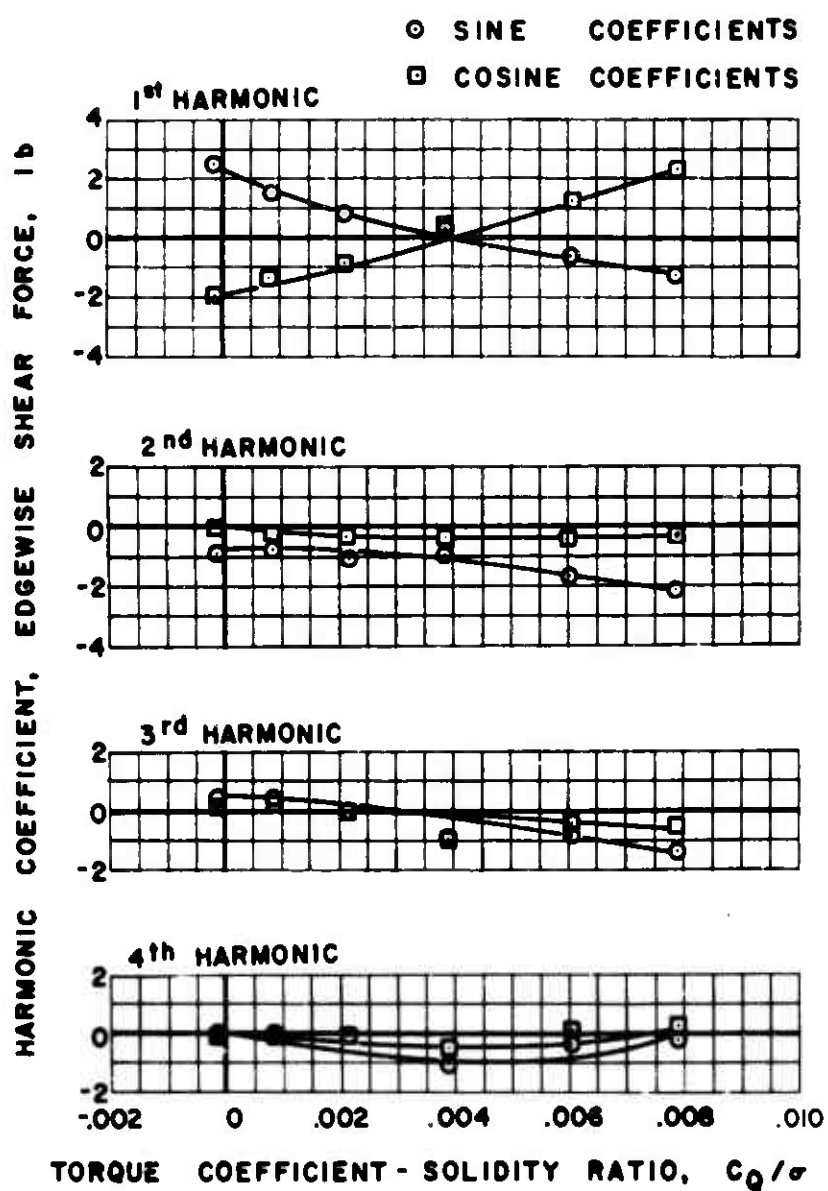


Figure 47(a). Continued.



$\mu = 0.3 \quad \alpha_s = -8 \text{ deg.}$

(b) EDGEWISE

Figure 47. Continued.

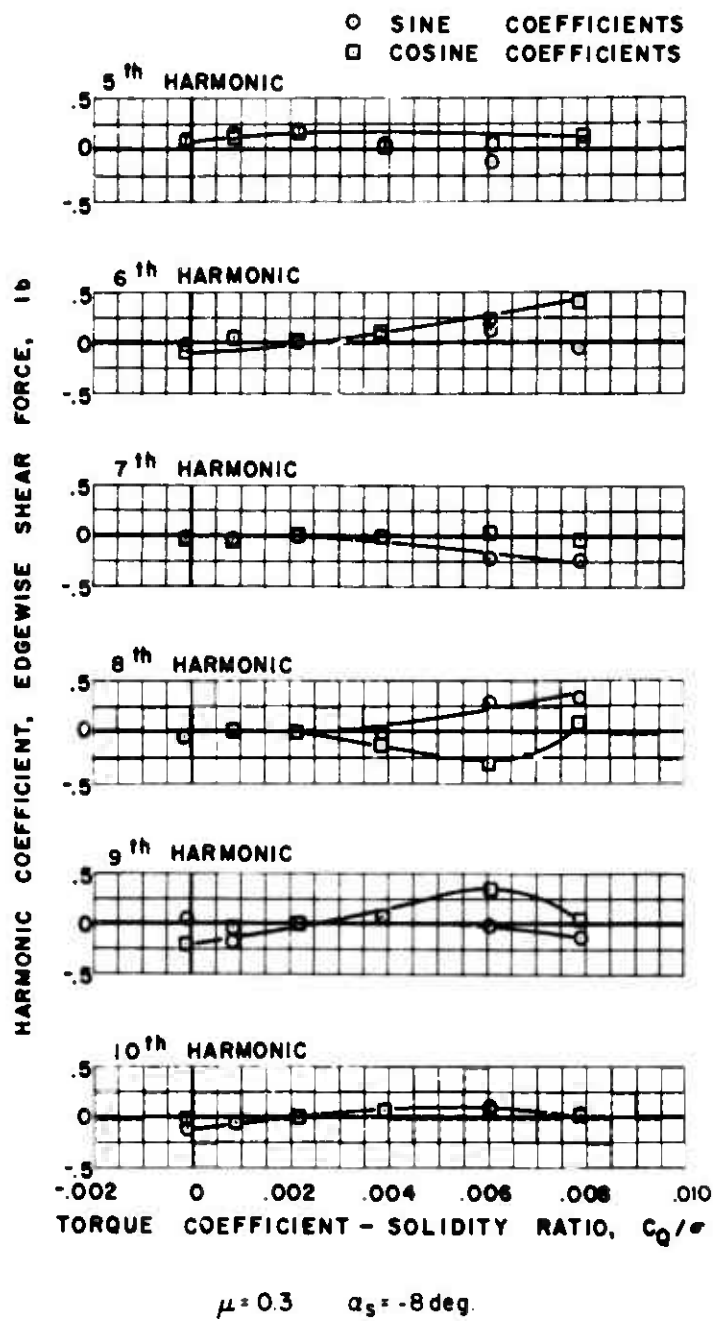
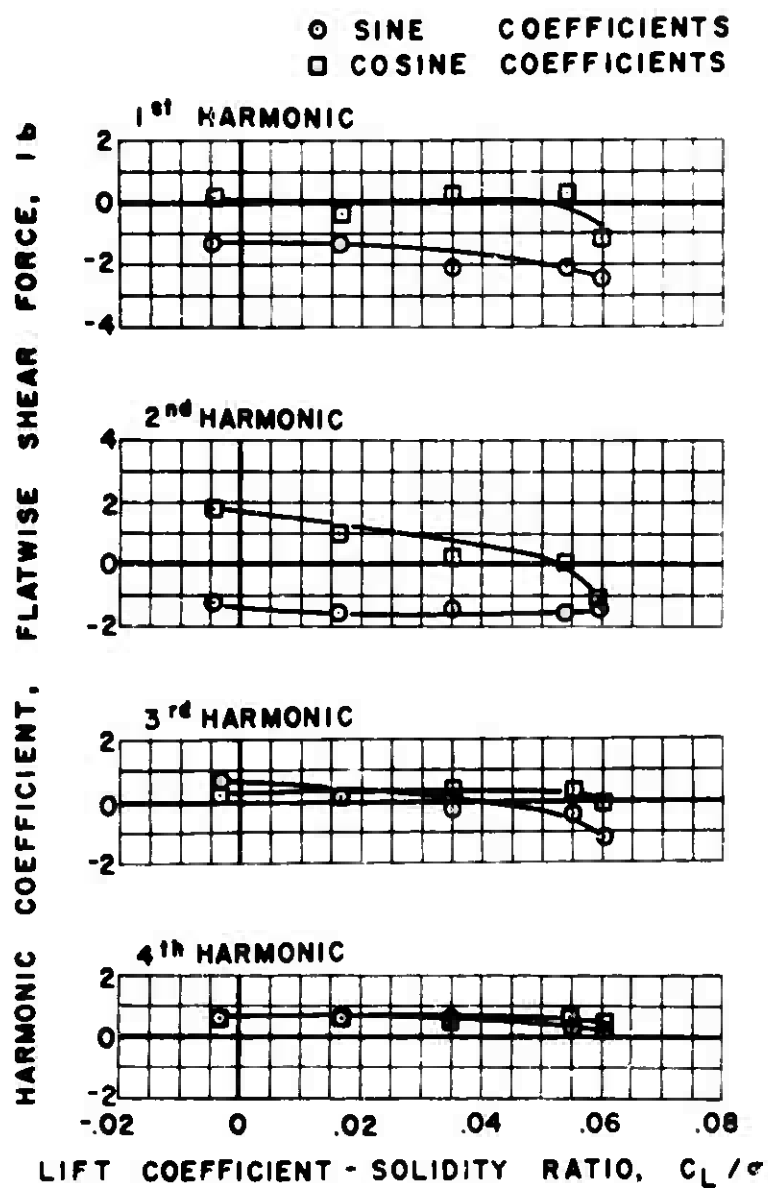


Figure 47(b). Concluded.



$$\mu = 0.4 \quad \alpha_s = 4 \text{ deg.}$$

(a) FLATWISE

Figure 48. Experimental Shear Force.

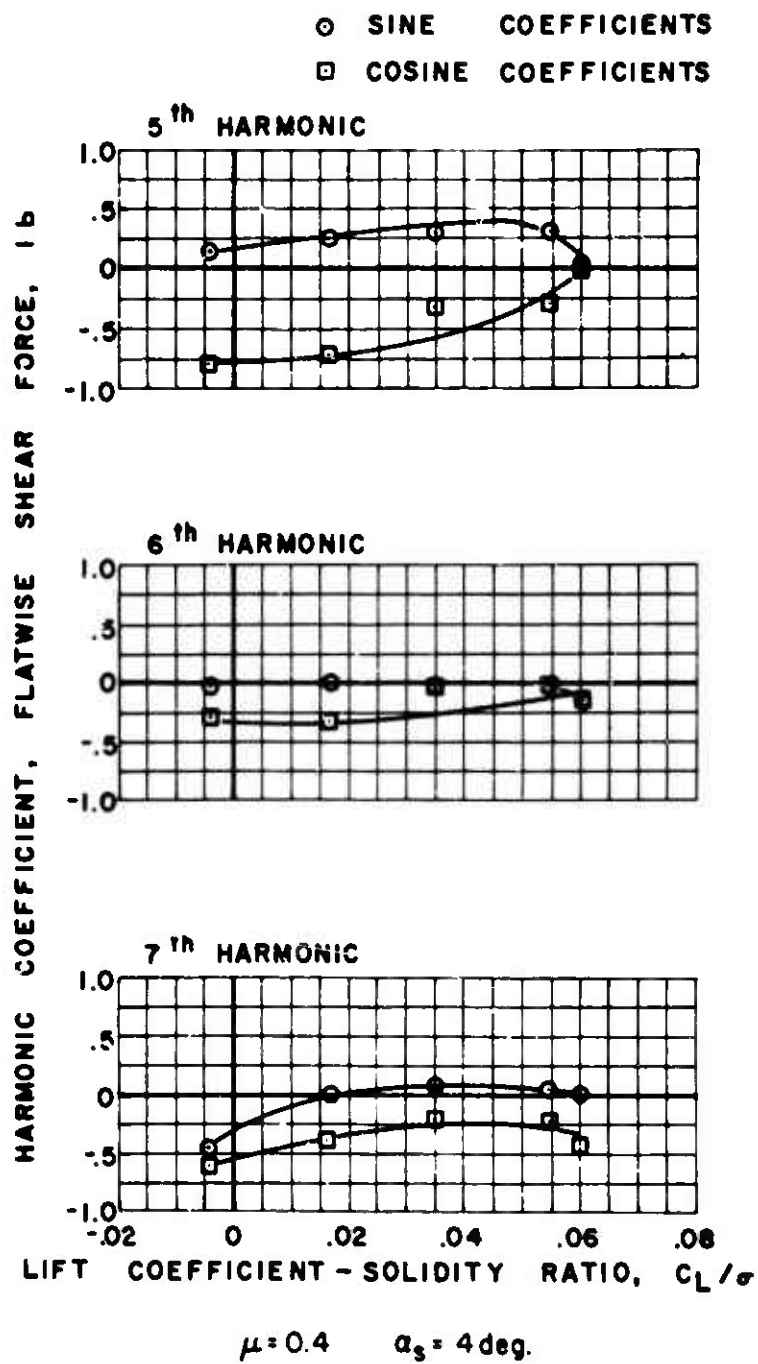


Figure 48(a). Continued.

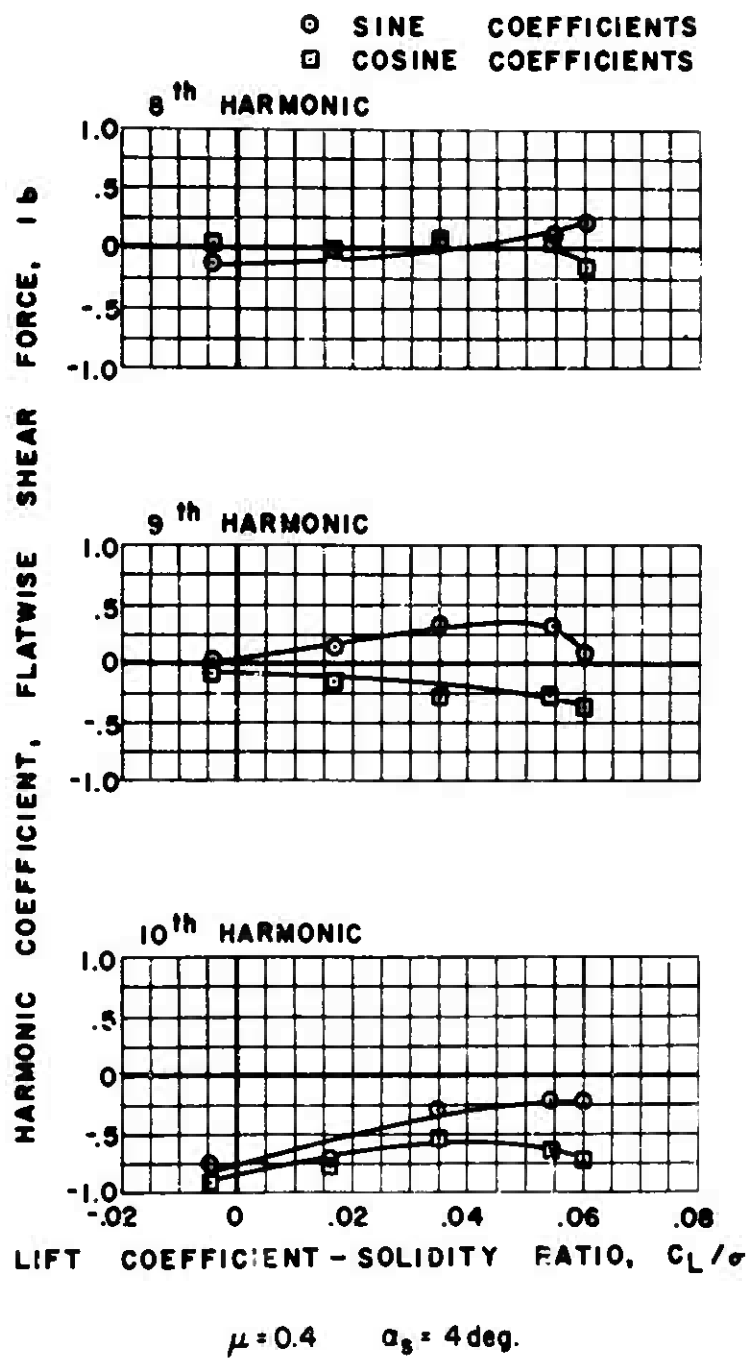
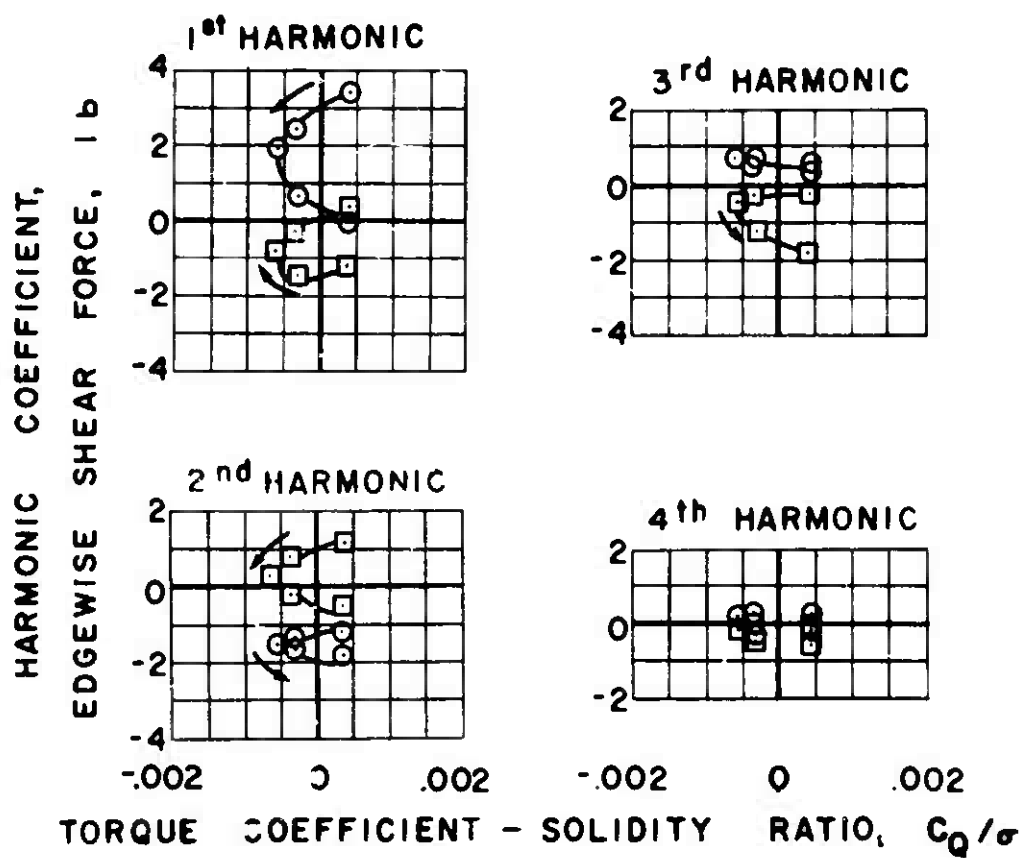


Figure 48(a). Continued.

ARROWS INDICATE DIRECTION OF
INCREASING COLLECTIVE PITCH

○ SINE COEFFICIENTS
□ COSINE COEFFICIENTS



$\mu = 0.4$ $\alpha_s = 4$ deg.

(b) EDGEWISE

Figure 48. Continued.

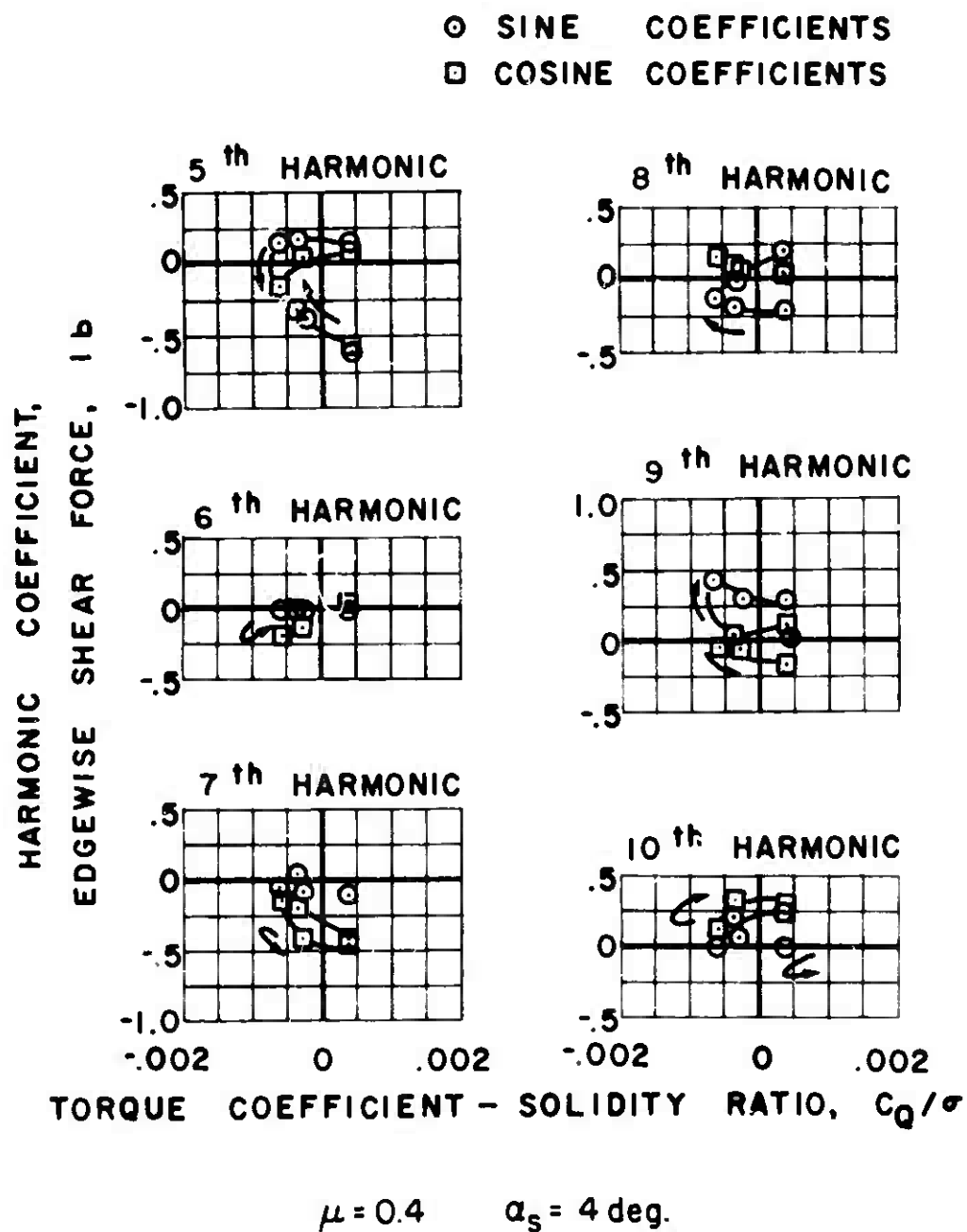
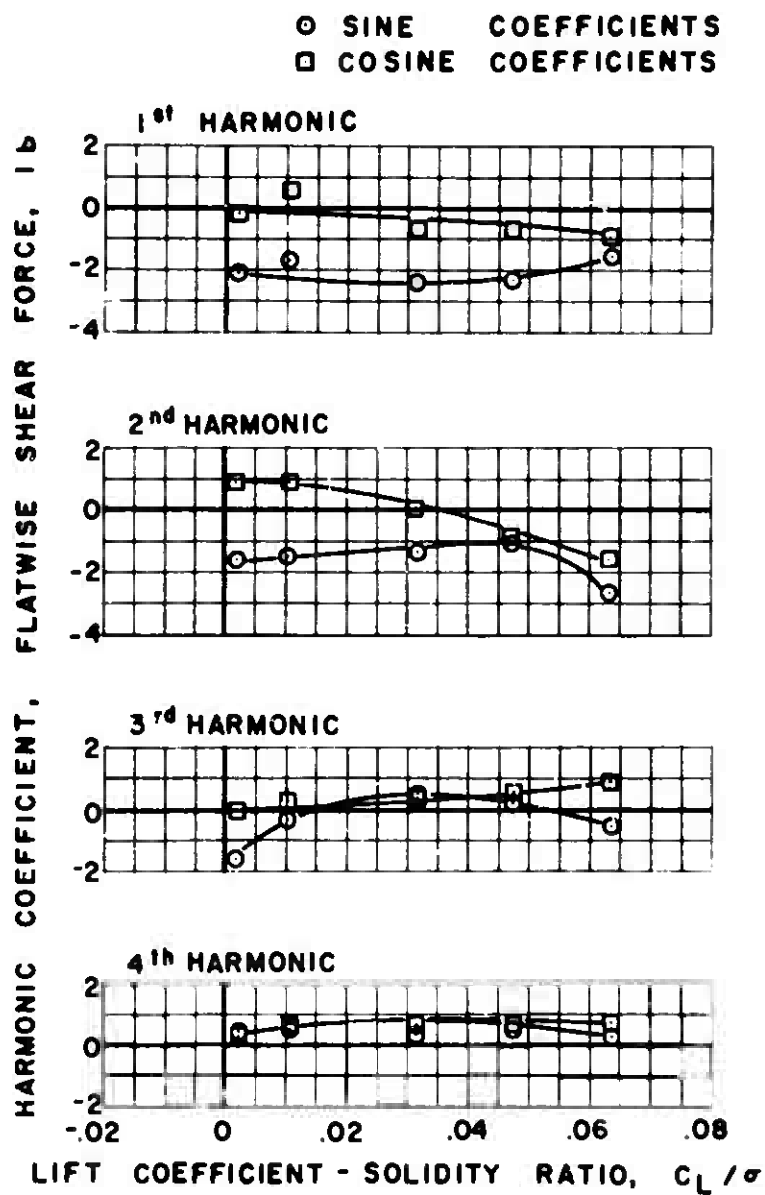


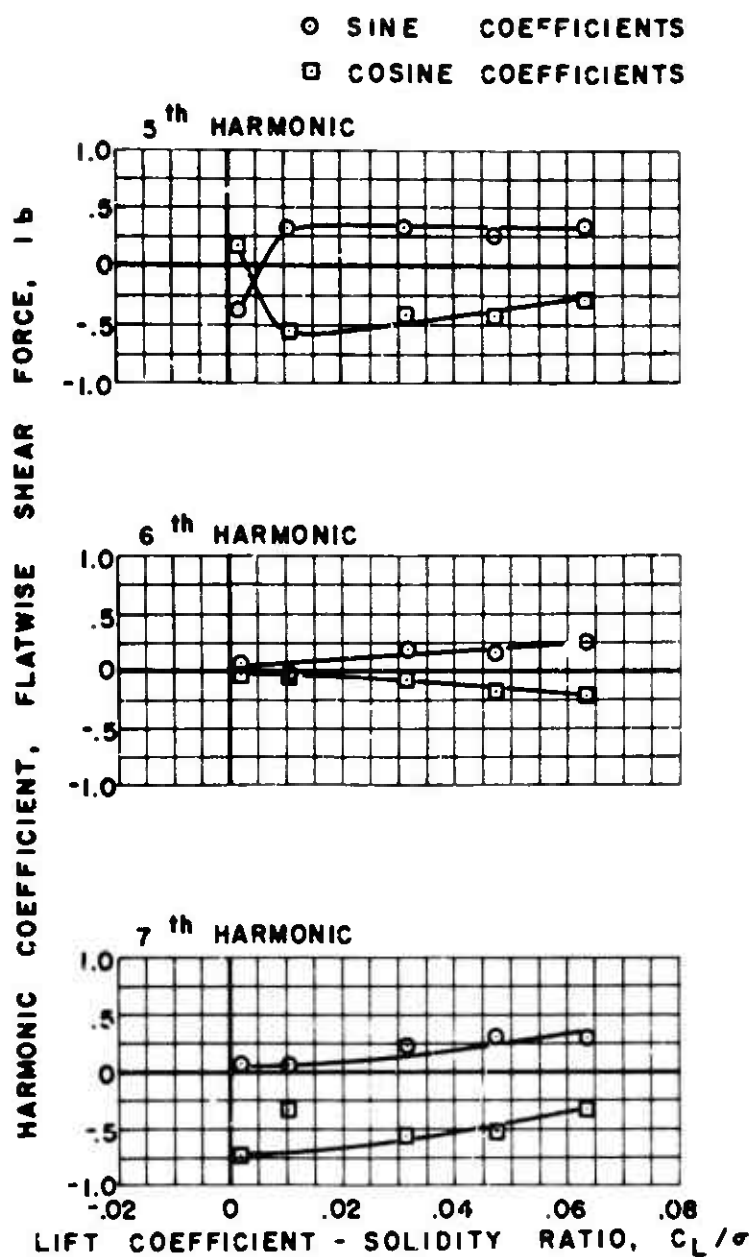
Figure 48(b). Concluded.



$$\mu = 0.4 \quad \alpha_s = 0 \text{ deg.}$$

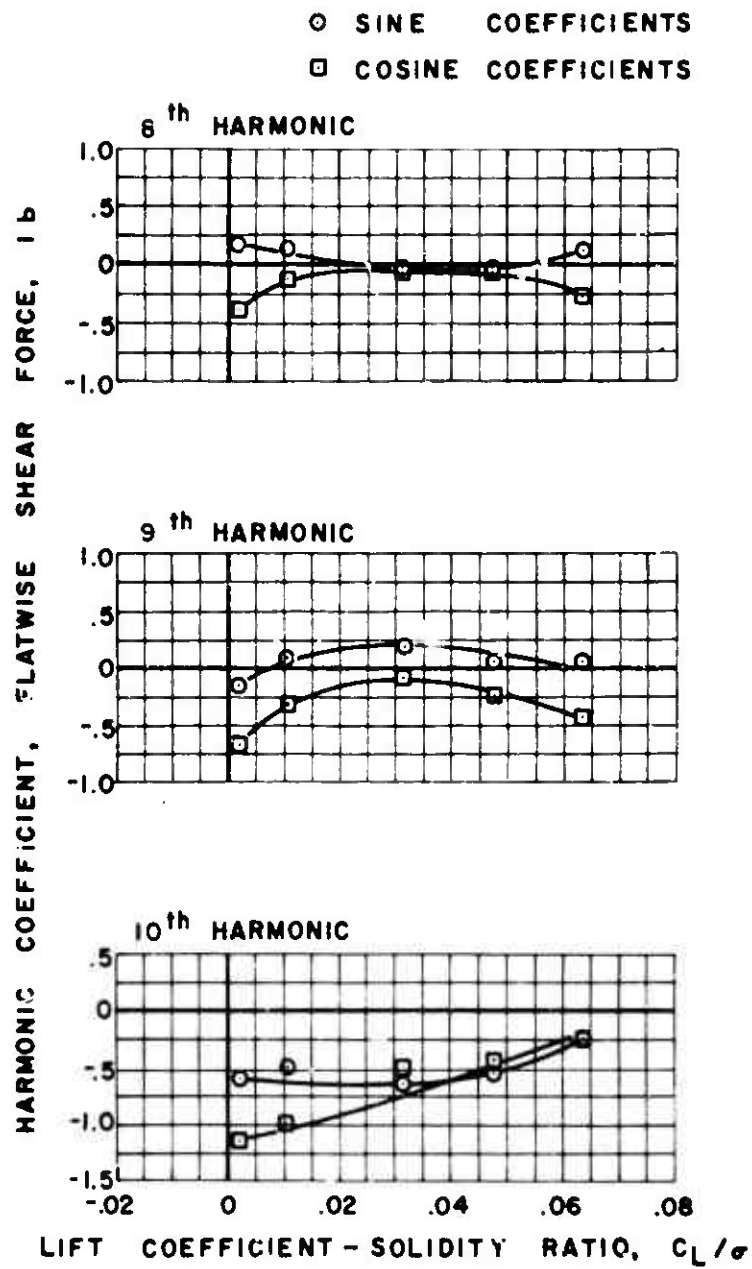
(a) FLATWISE

Figure 49. Experimental Shear Force.



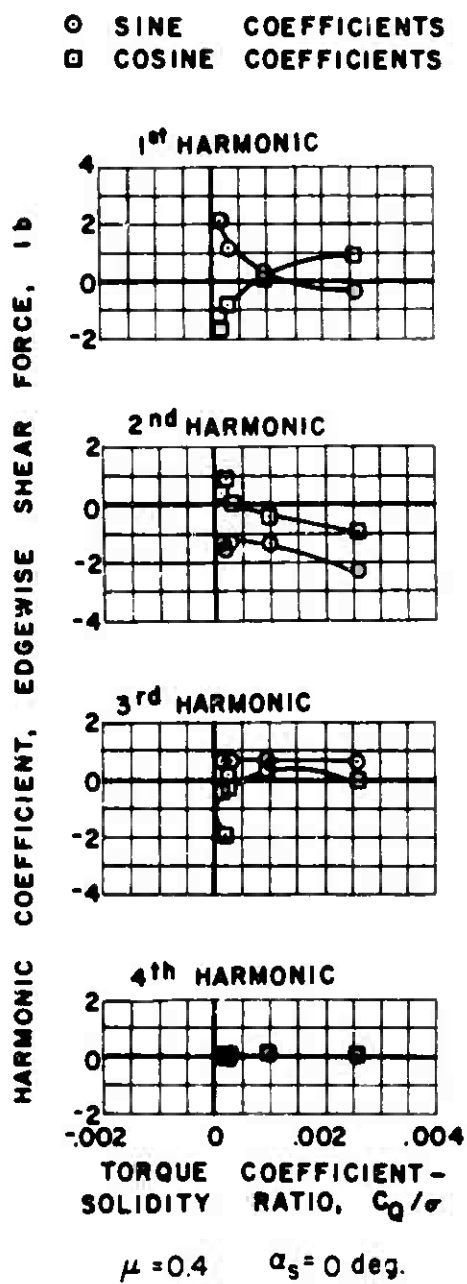
$\mu = 0.4 \quad \alpha_s = 0 \text{ deg.}$

Figure 49(a). Continued.



$\mu = 0.4$ $\alpha_s = 0 \text{ deg.}$

Figure 49(a). Continued.



(b) EDGEWISE

Figure 49. Continued.

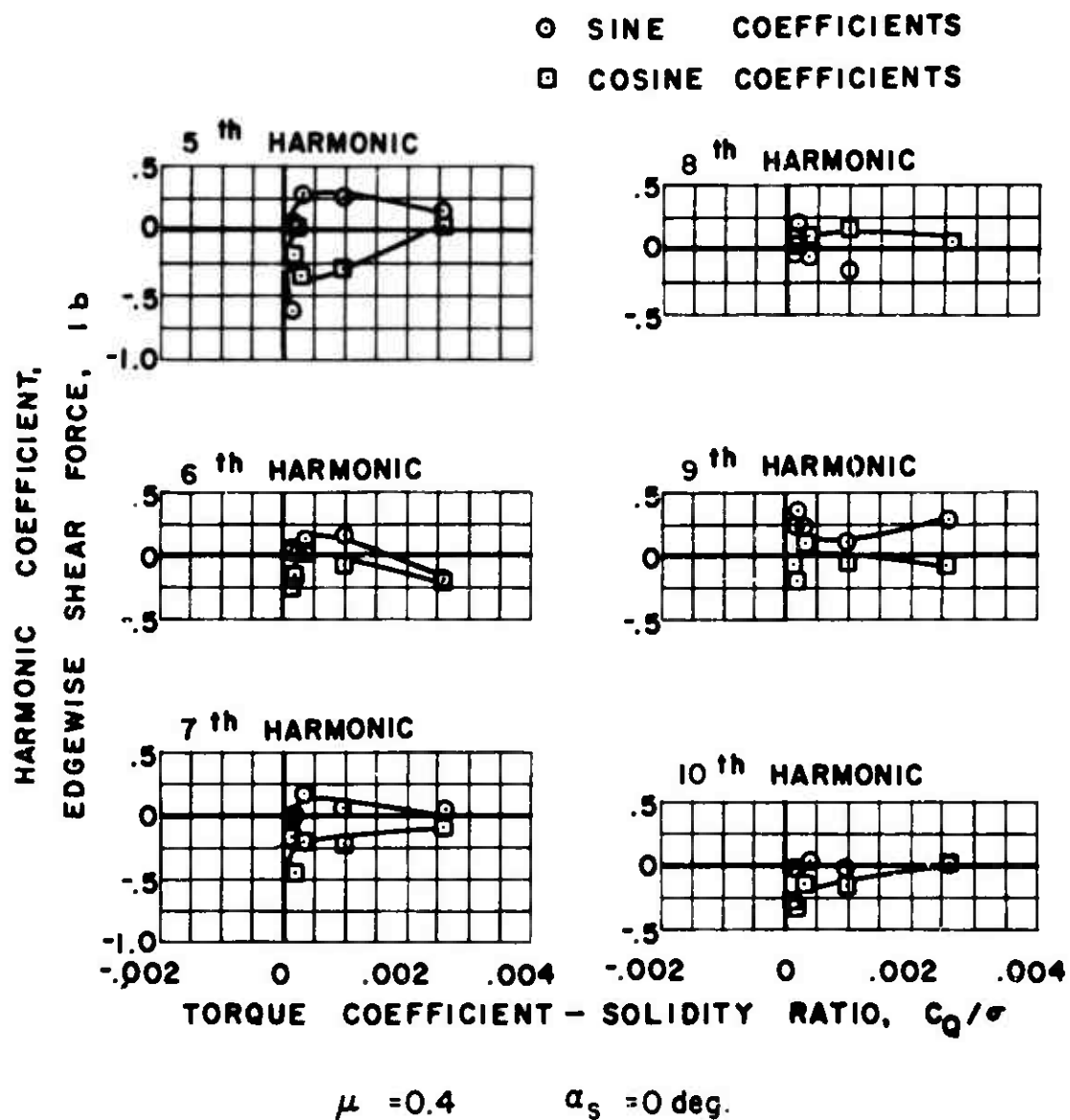
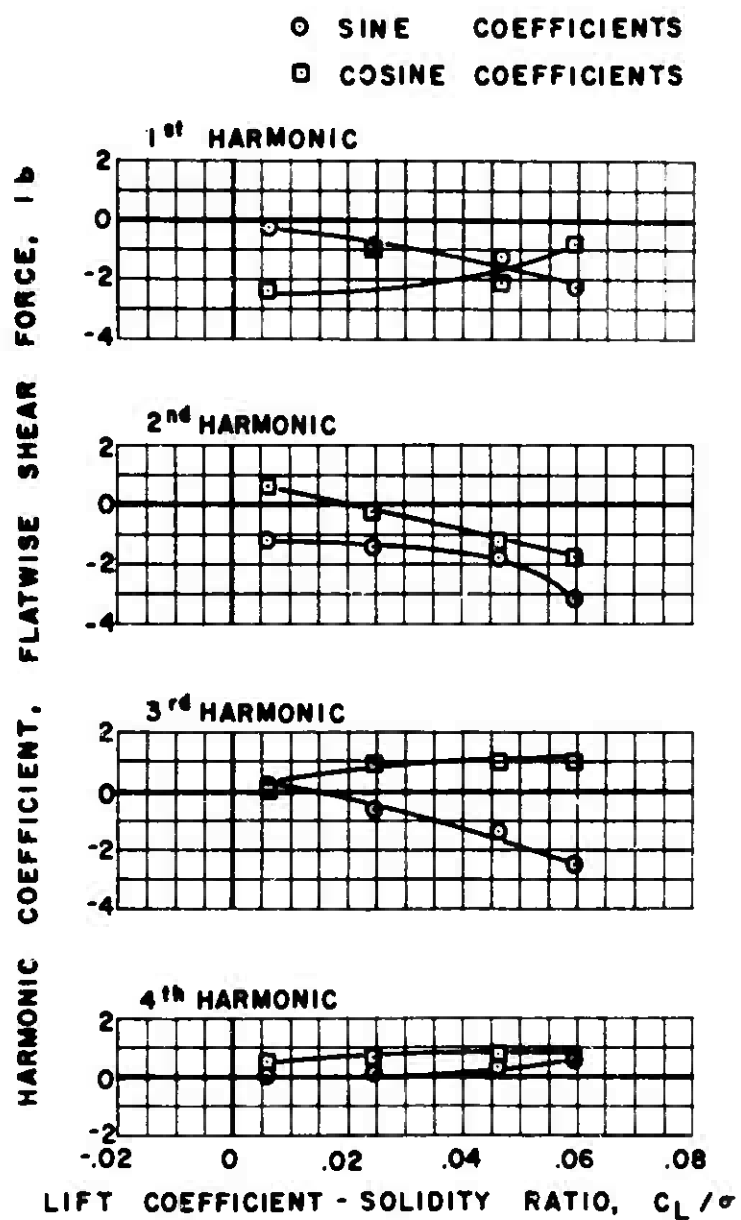


Figure 49(b). Concluded.



$$\mu = 0.4 \quad \alpha_s = -4 \text{ deg.}$$

(a) FLATWISE

Figure 50. Experimental Shear Force.

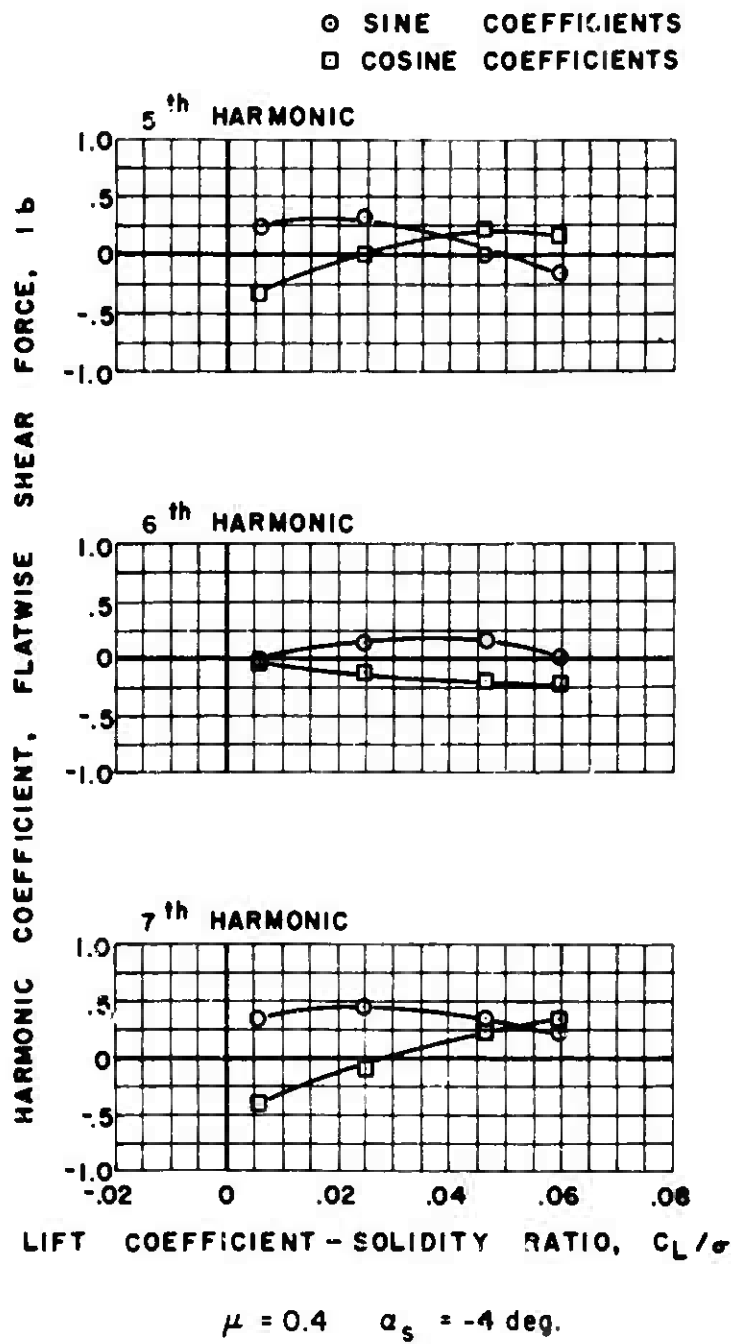


Figure 50(a). Continued.

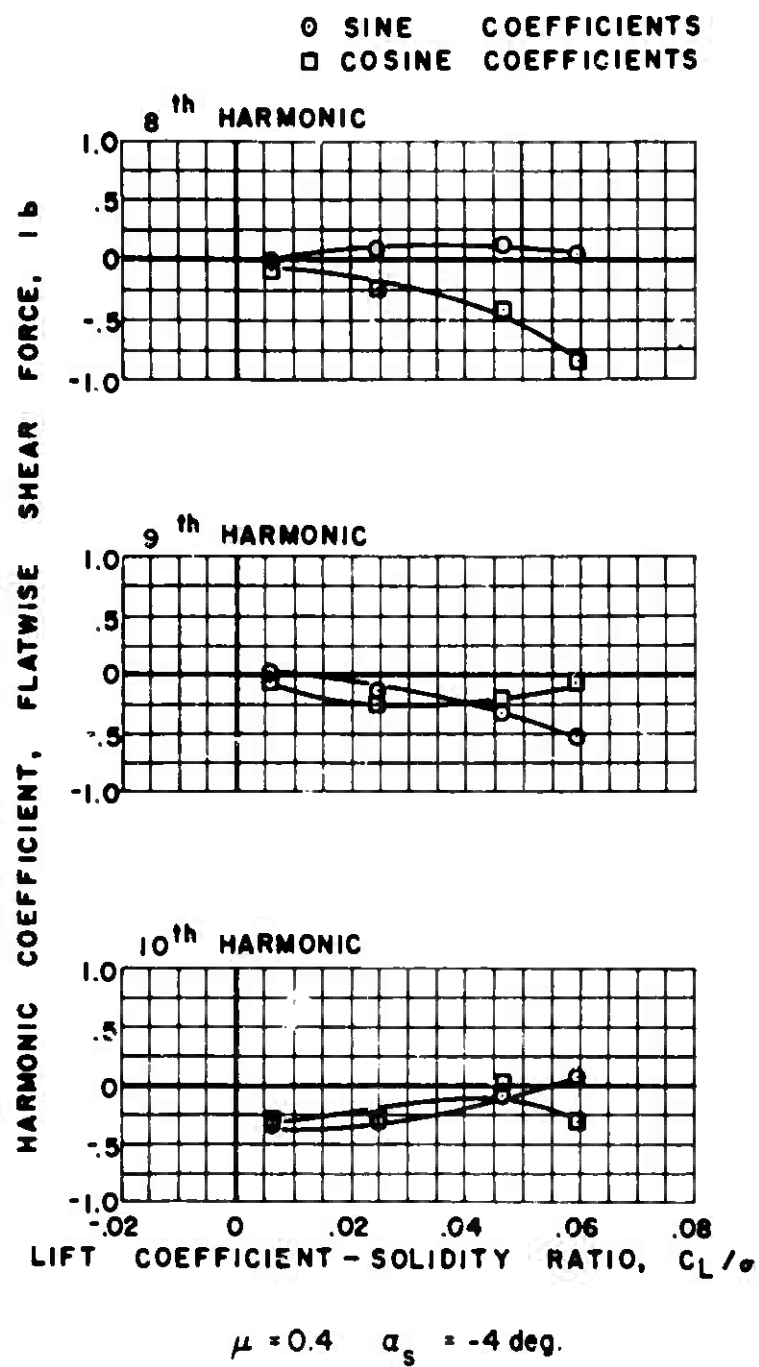
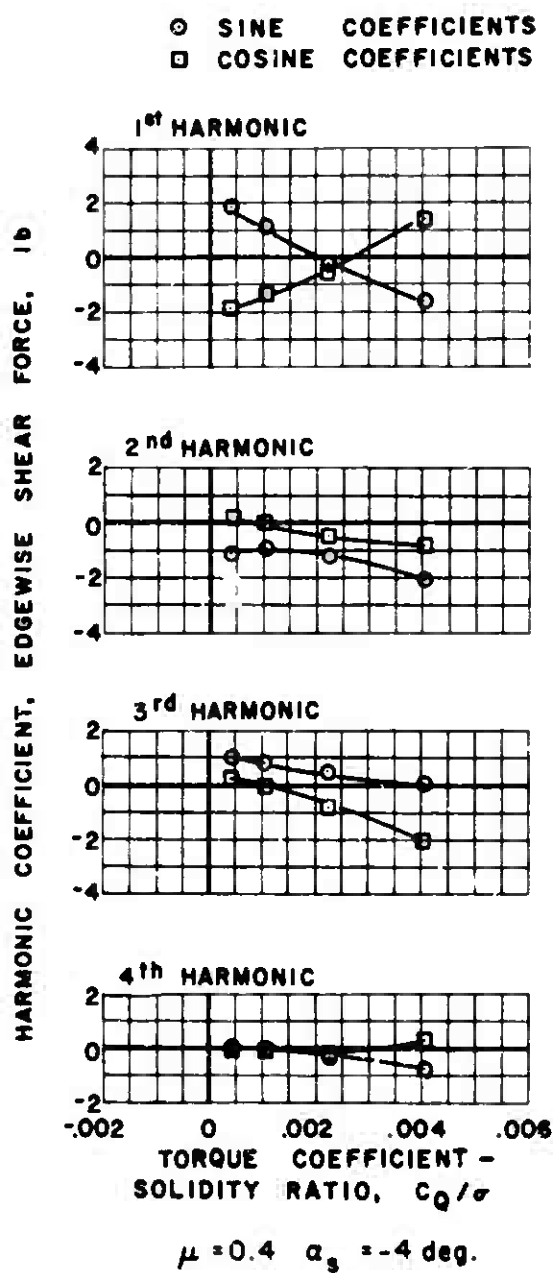


Figure 50(a). Continued.



(b) EDGEWISE

Figure 50. Continued.

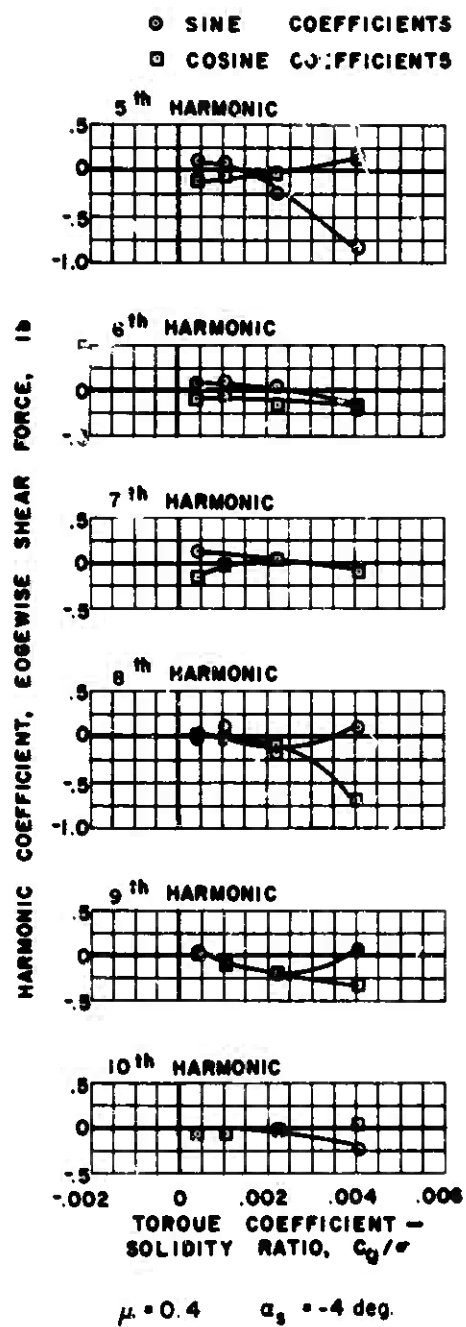


Figure 50(b). Concluded.

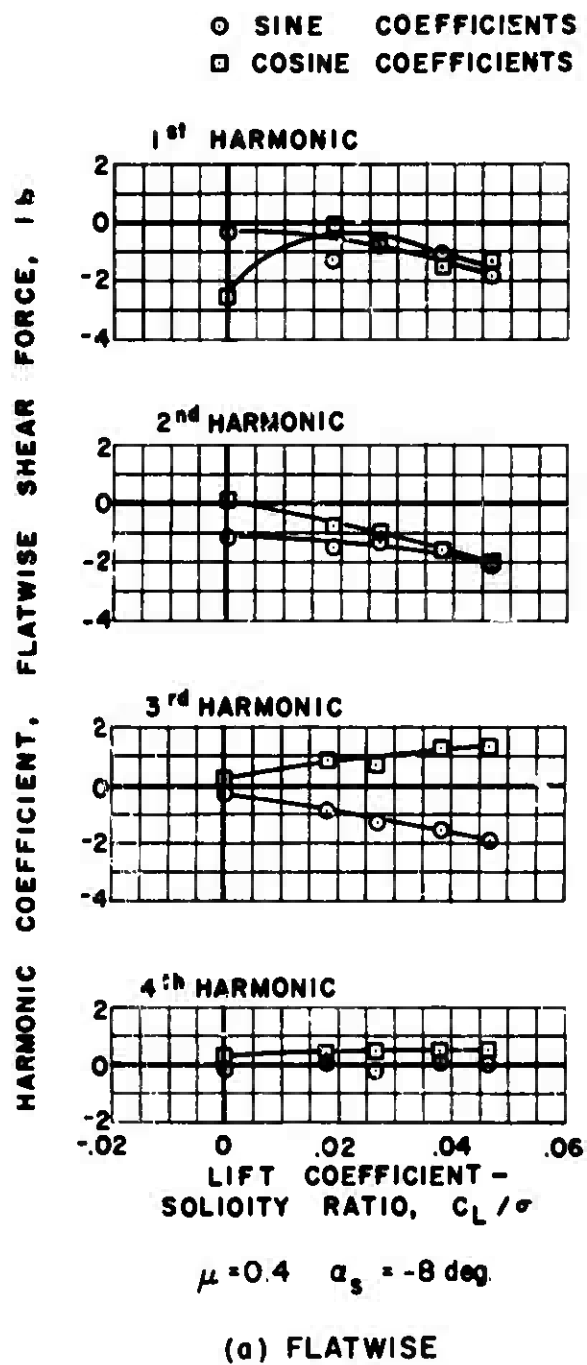


Figure 51. Experimental Shear Force.

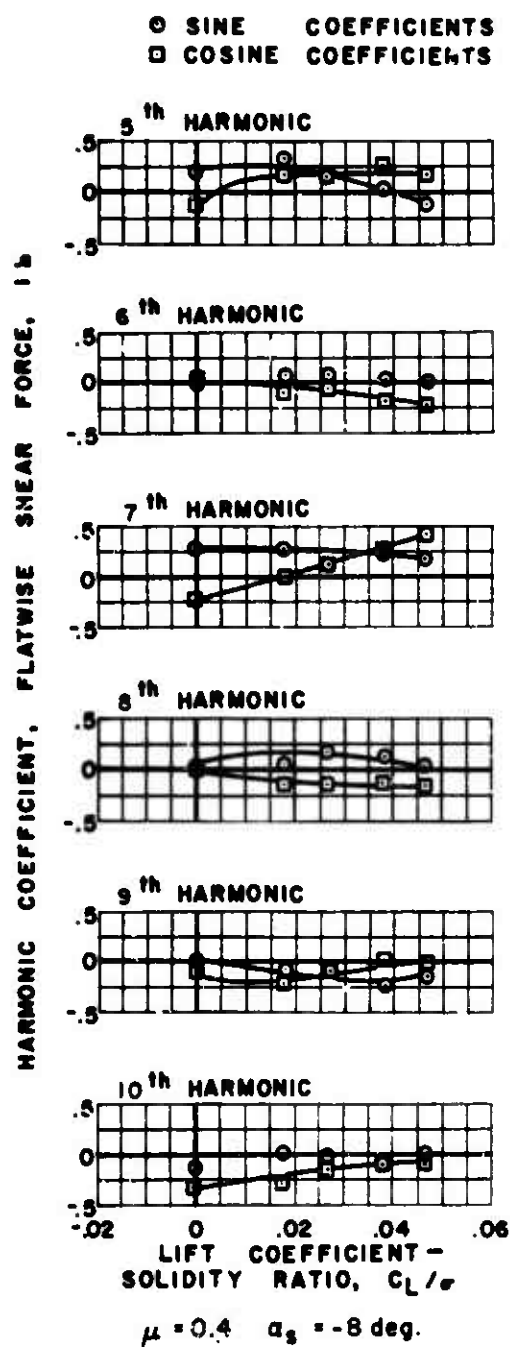
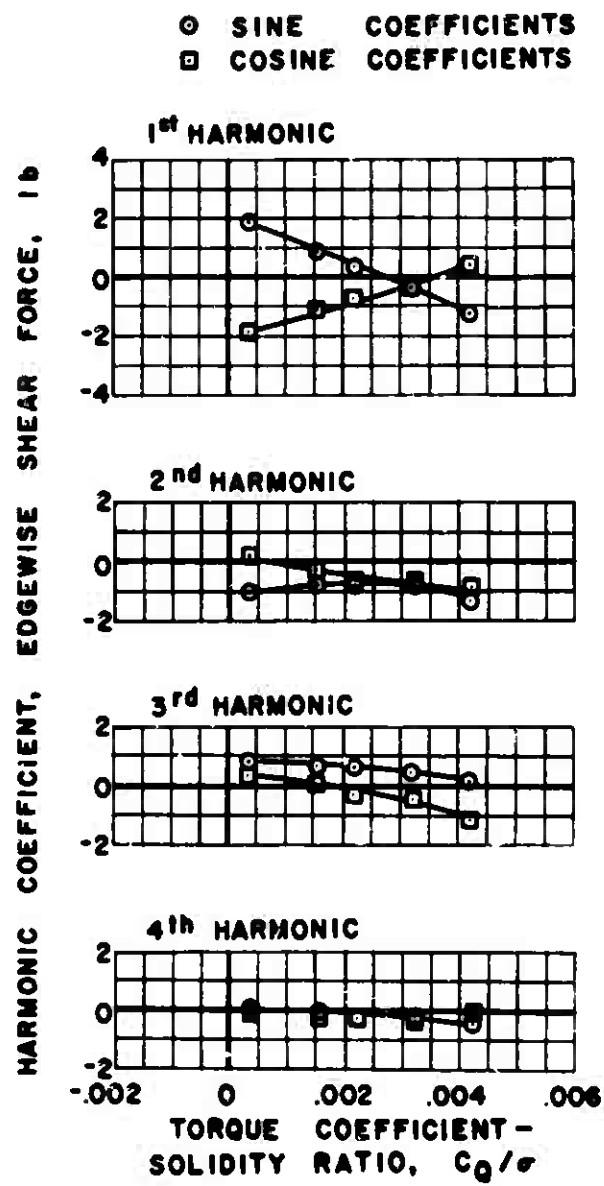


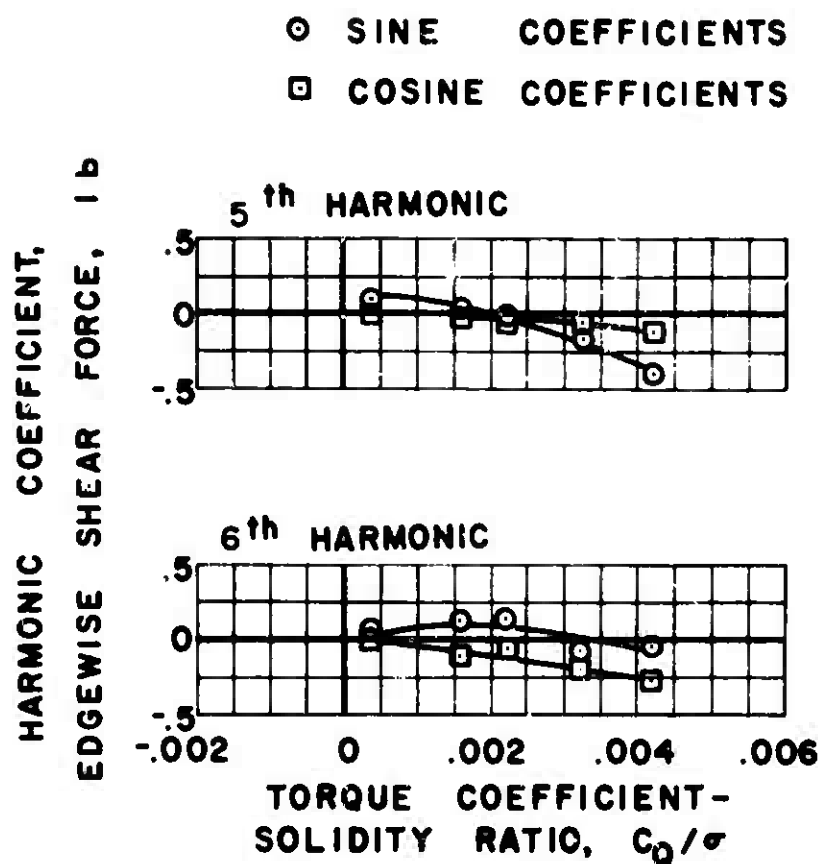
Figure 51(a). Continued.



$\mu = 0.4 \quad \alpha_s = -8 \text{ deg.}$

(b) EDGEWISE

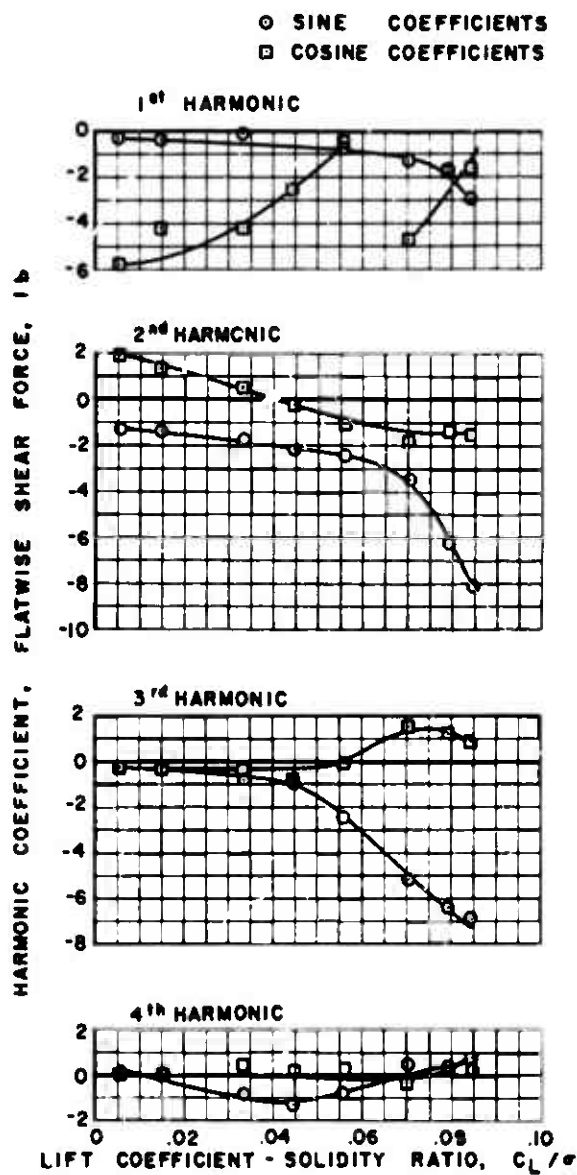
Figure 51. Continued.



IN THIS TEST CONDITION THE MAGNITUDE OF THE EDGEWISE HARMONICS ABOVE THE SIXTH DID NOT EXCEED THE REPEATABILITY OF THE SYSTEM AND ARE NOT PRESENTED.

$$\mu = 0.4 \quad \alpha_s = -8 \text{ deg.}$$

Figure 51(b). Concluded.



$\mu = 0.5 \quad \alpha_s = 0 \text{ deg.}$

(a) FLATWISE

Figure 52. Experimental Shear Force.

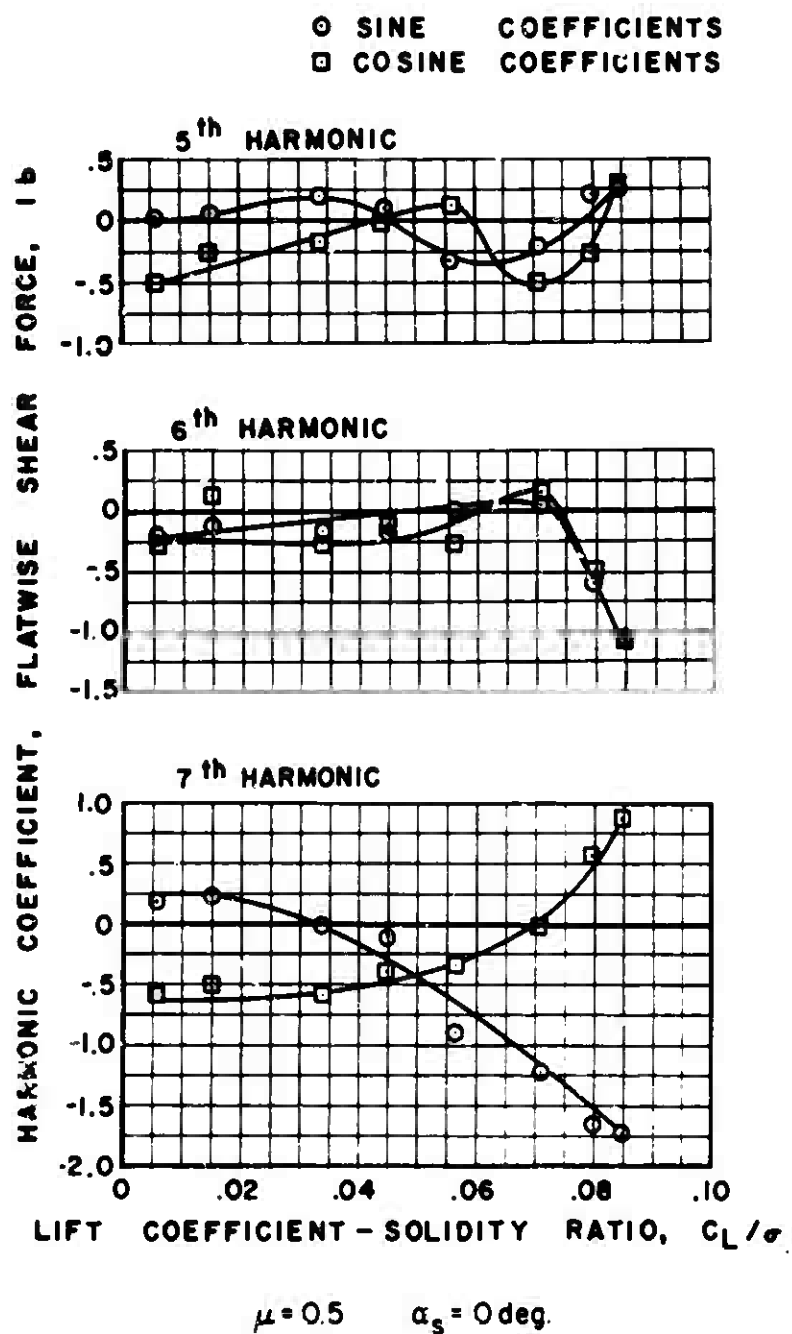
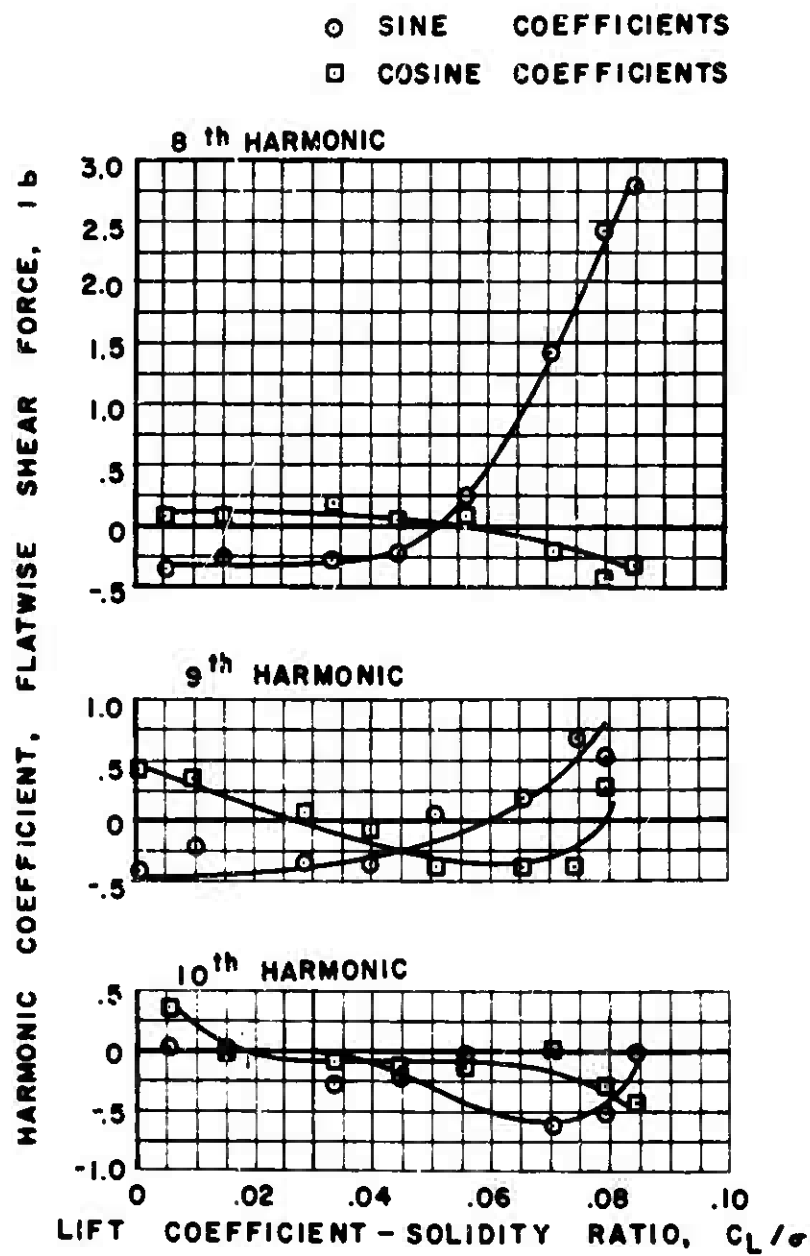


Figure 52(a). Continued.



$$\mu = 0.5 \quad \alpha_s = 0 \text{ deg.}$$

Figure 52(a). Continued.

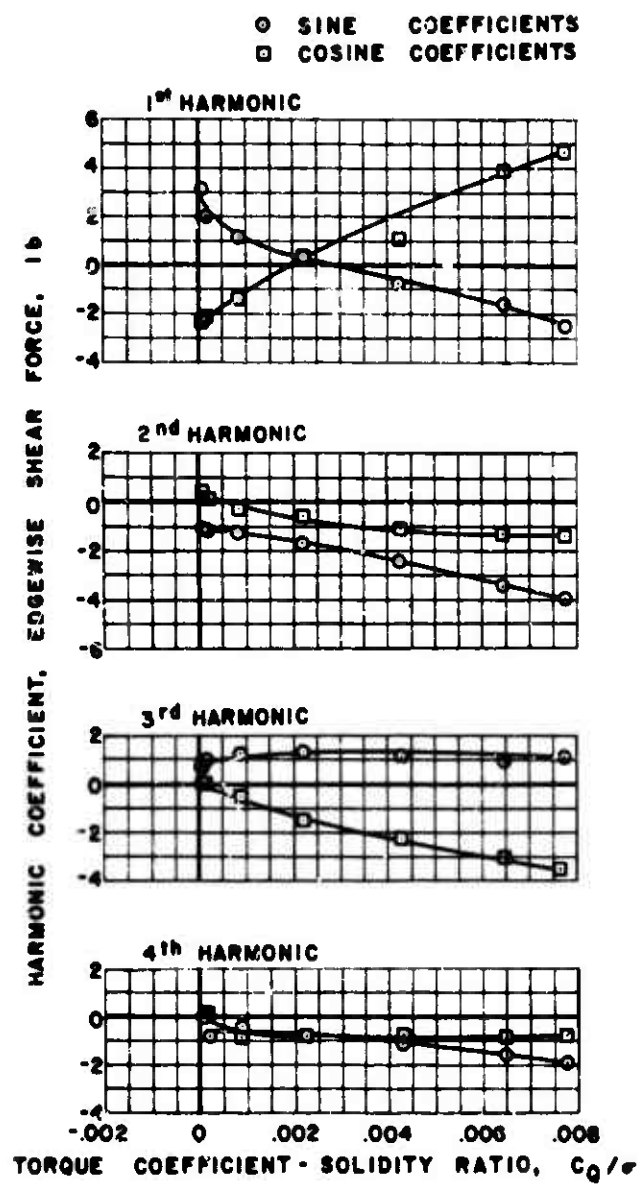


Figure 52. Continued.

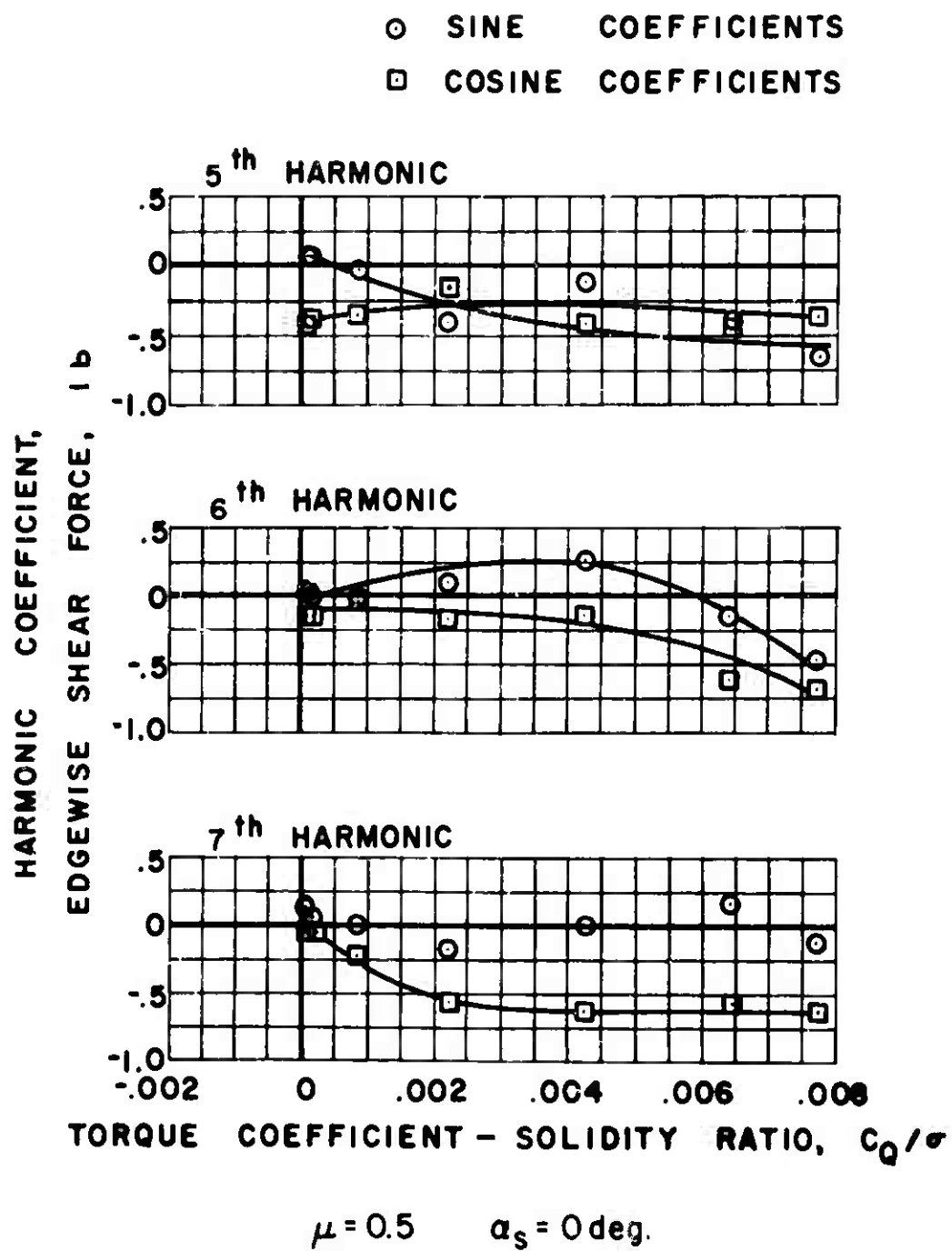


Figure 52(b). Continued.

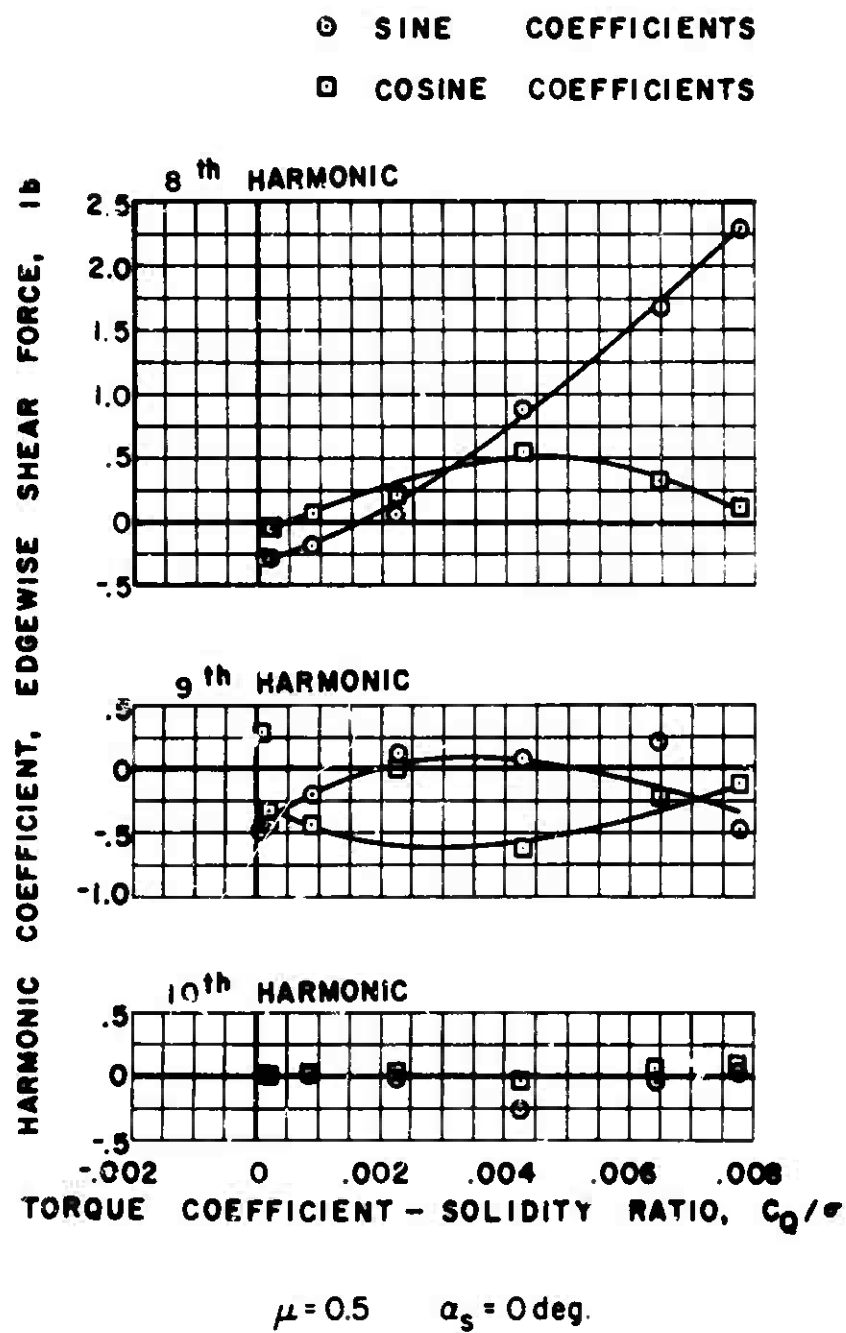
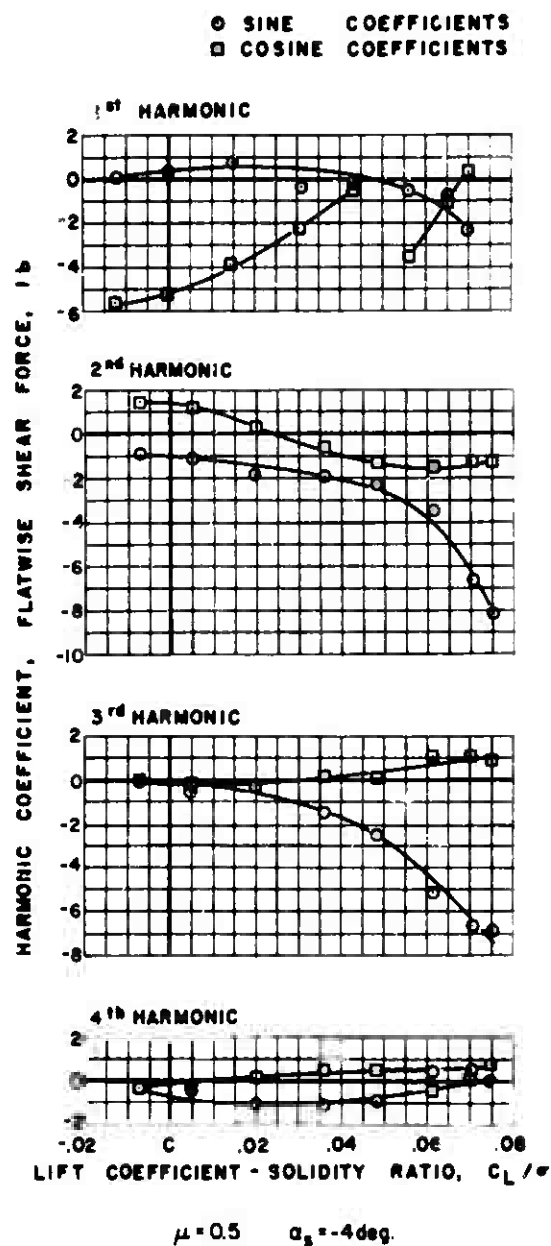


Figure 52(b). Concluded.



(a) FLATWISE

Figure 53. Experimental Shear Force.

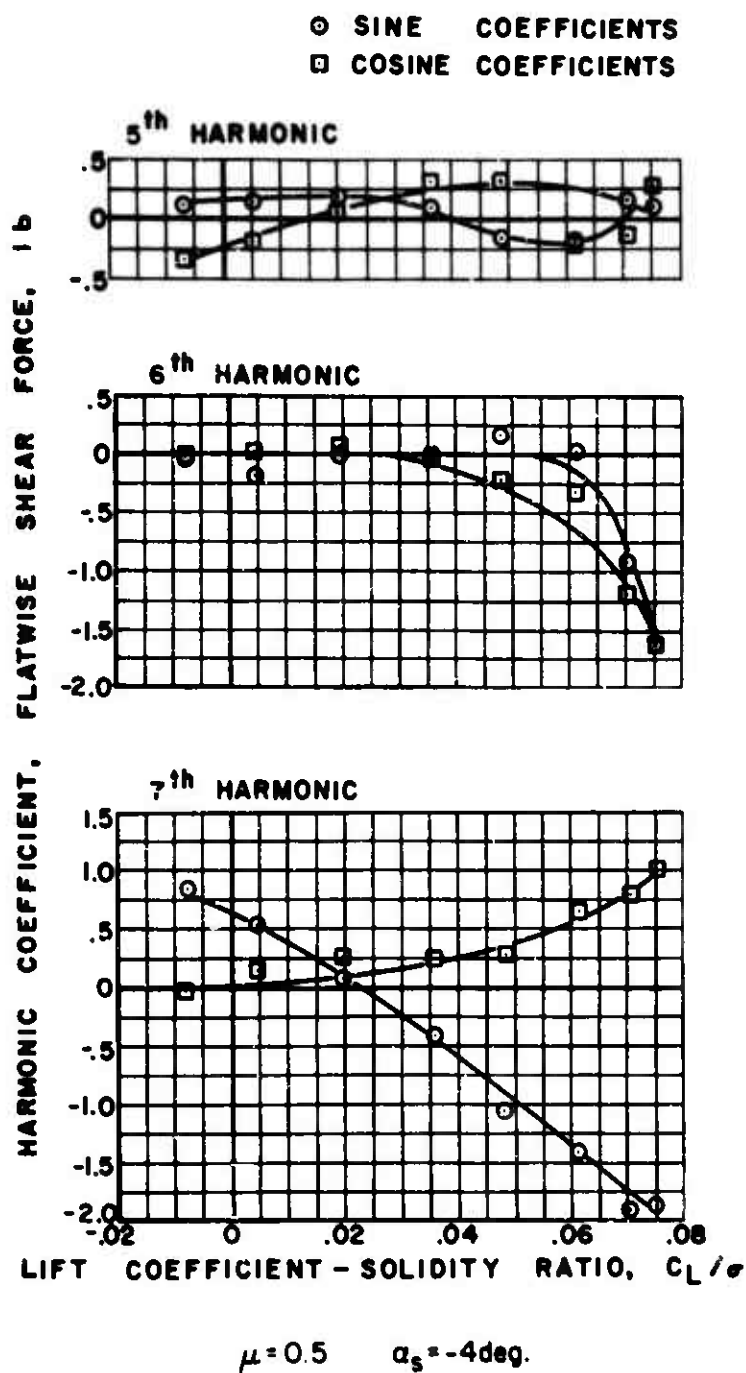


Figure 53(a). Continued.

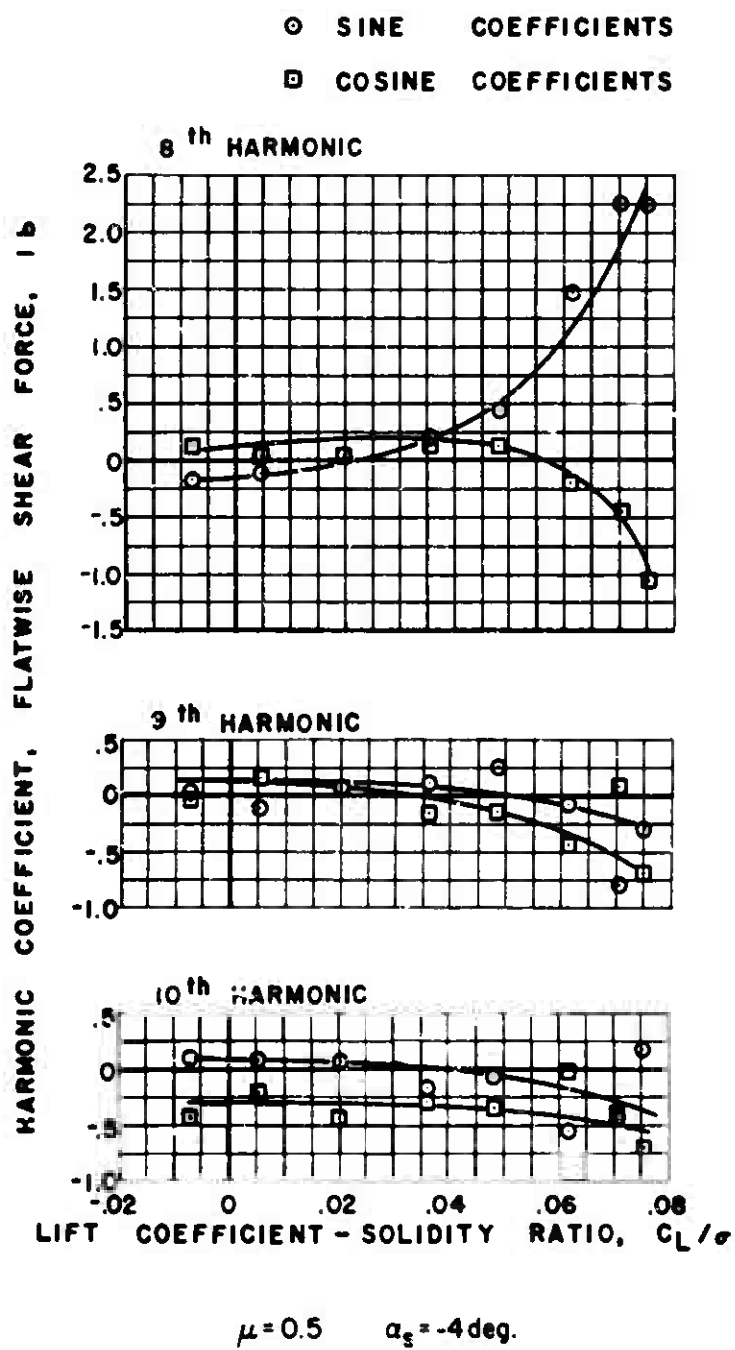
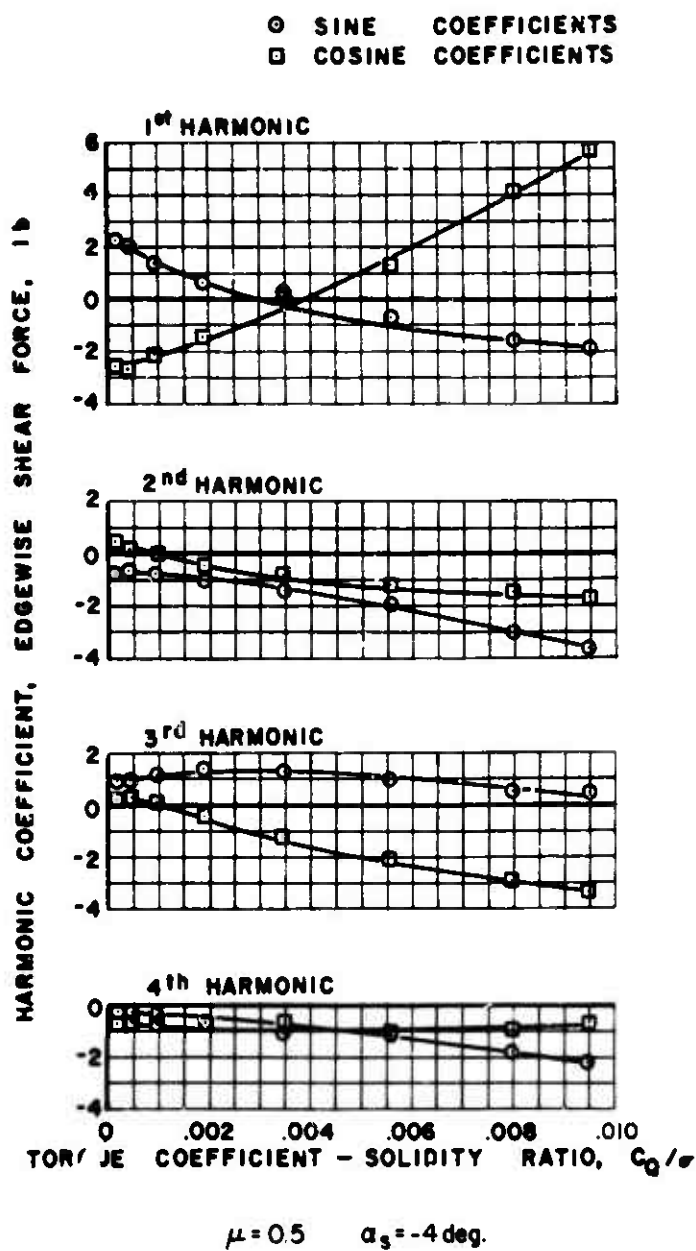
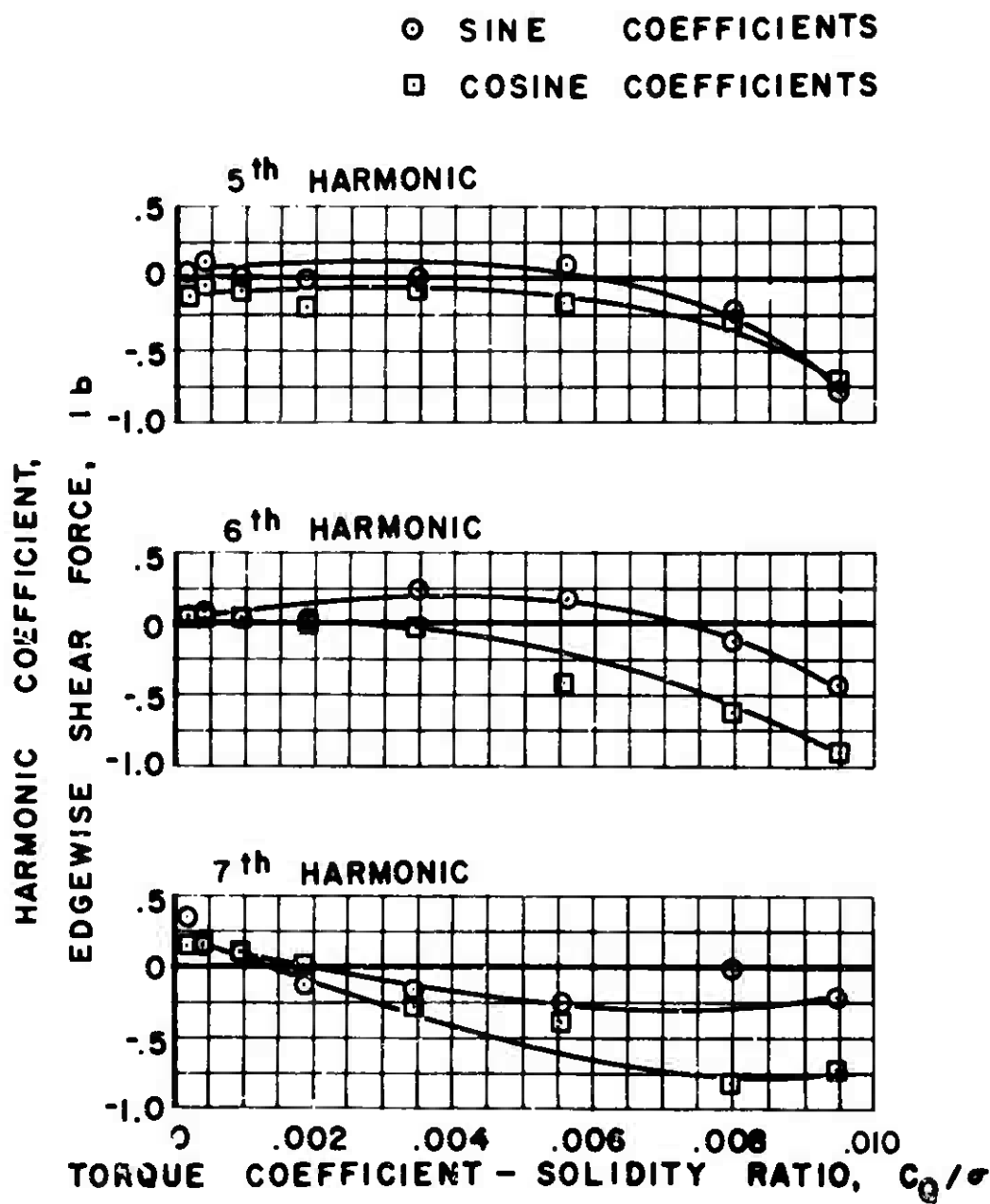


Figure 53(a). Continued.



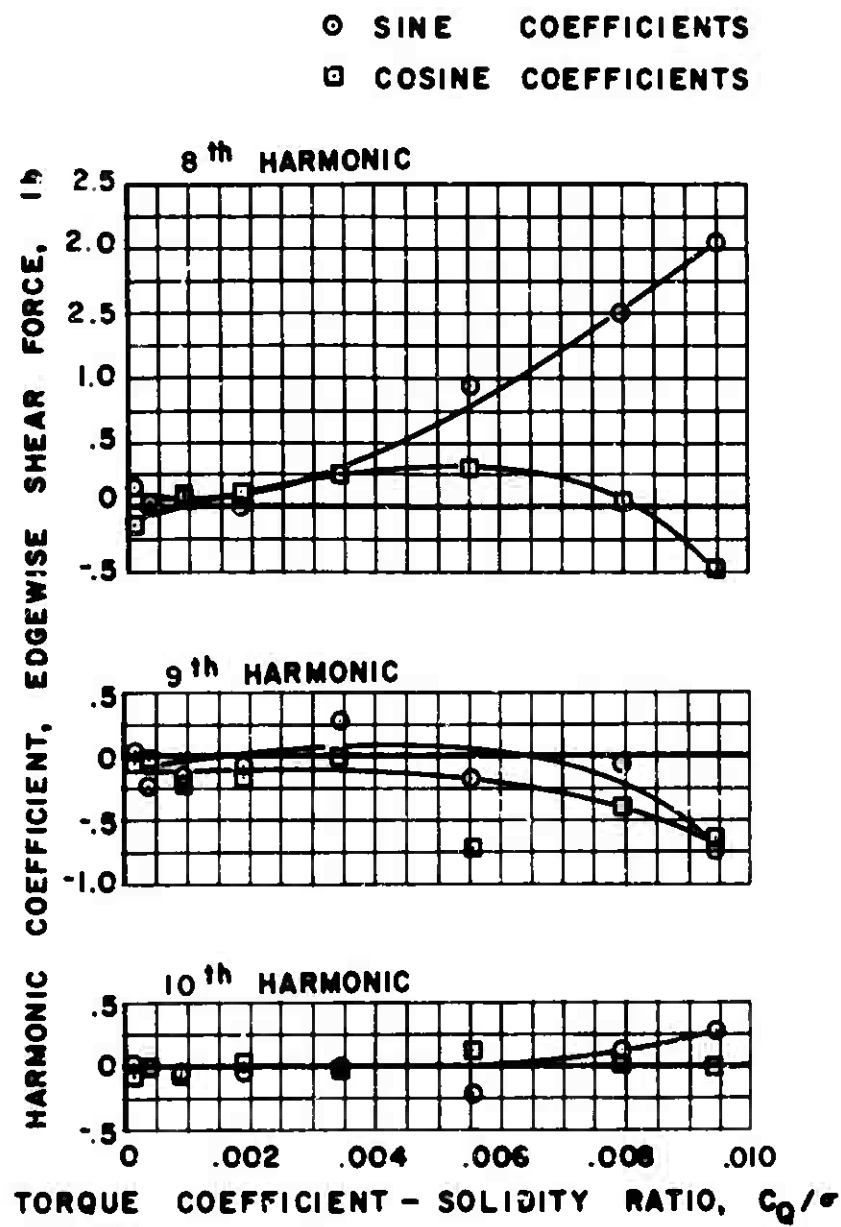
(b) EDGEWISE

Figure 53. Continued.



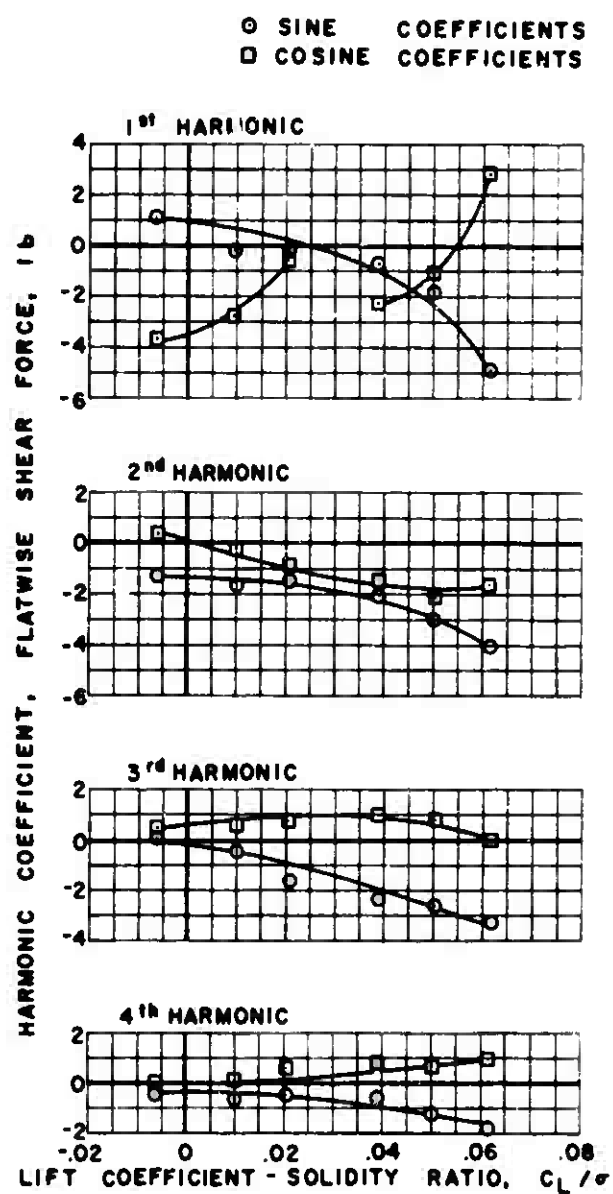
$$\mu = 0.5 \quad \alpha_s = -4 \text{ deg.}$$

Figure 53(b). Continued.



$$\mu = 0.5 \quad \alpha_s = -4 \text{ deg.}$$

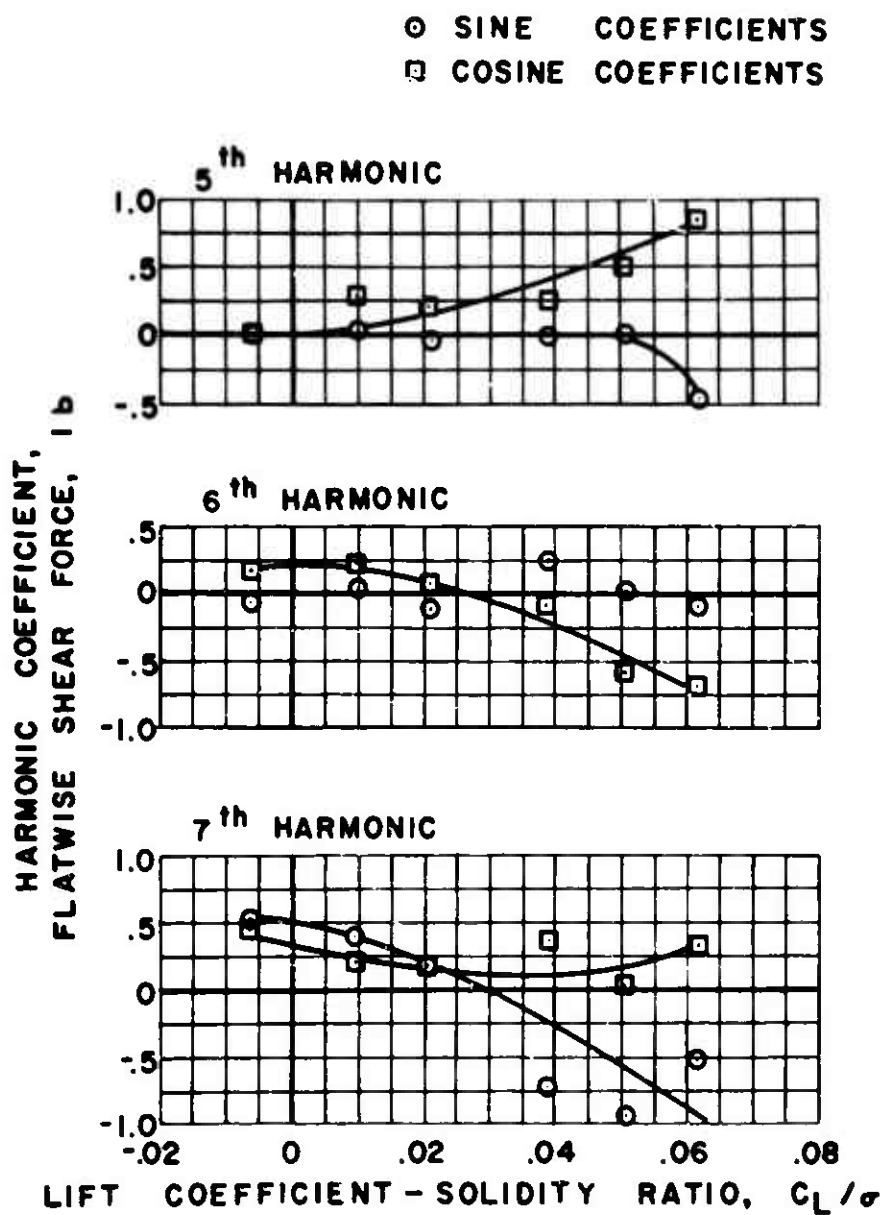
Figure 53(b). Concluded.



$\mu = 0.5$ $\alpha_s = -8 \text{ deg.}$

(a) FLATWISE

Figure 54. Experimental Shear Force.



$$\mu = 0.5 \quad \alpha_s = -8 \text{ deg.}$$

Figure 54(a). Continued.

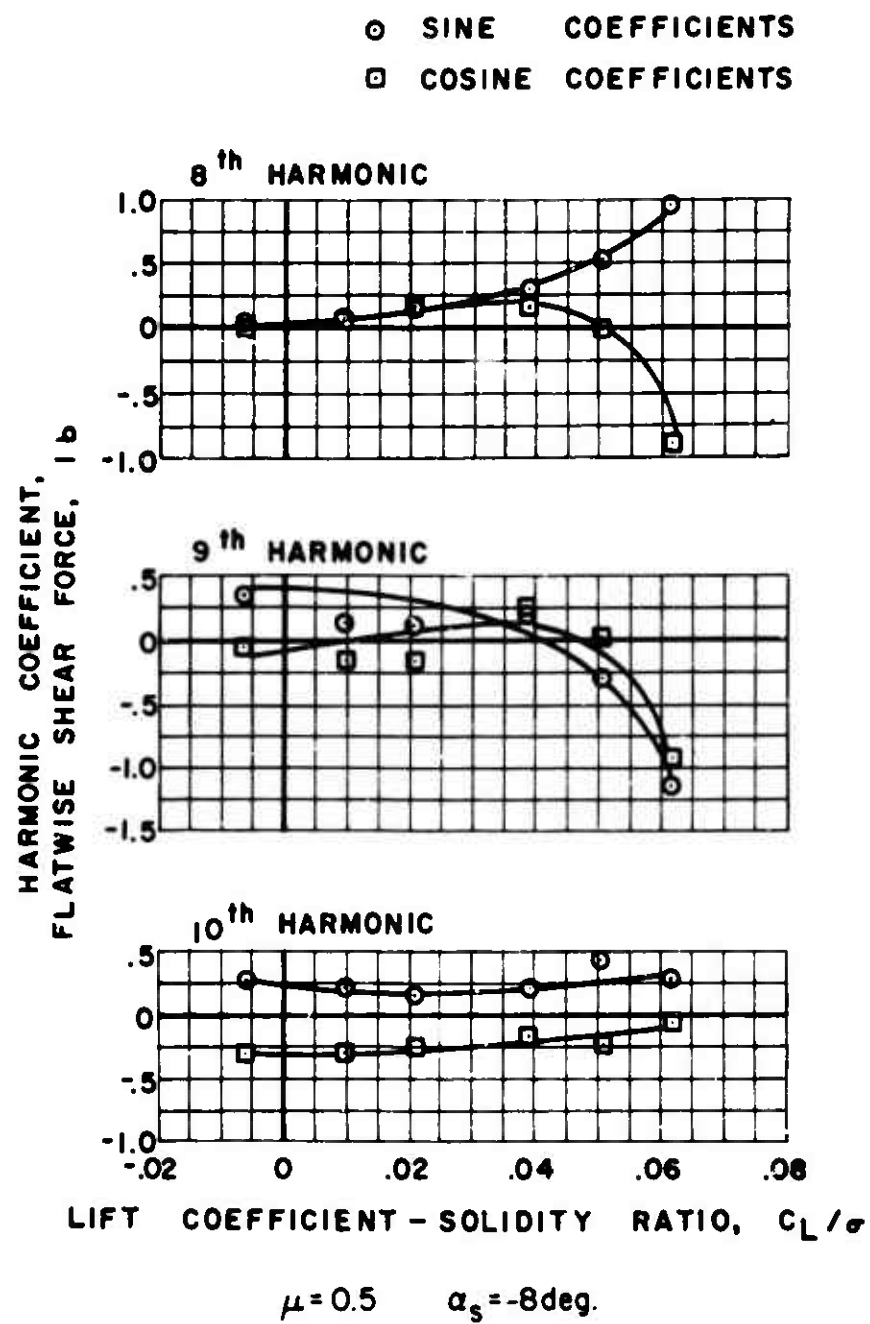
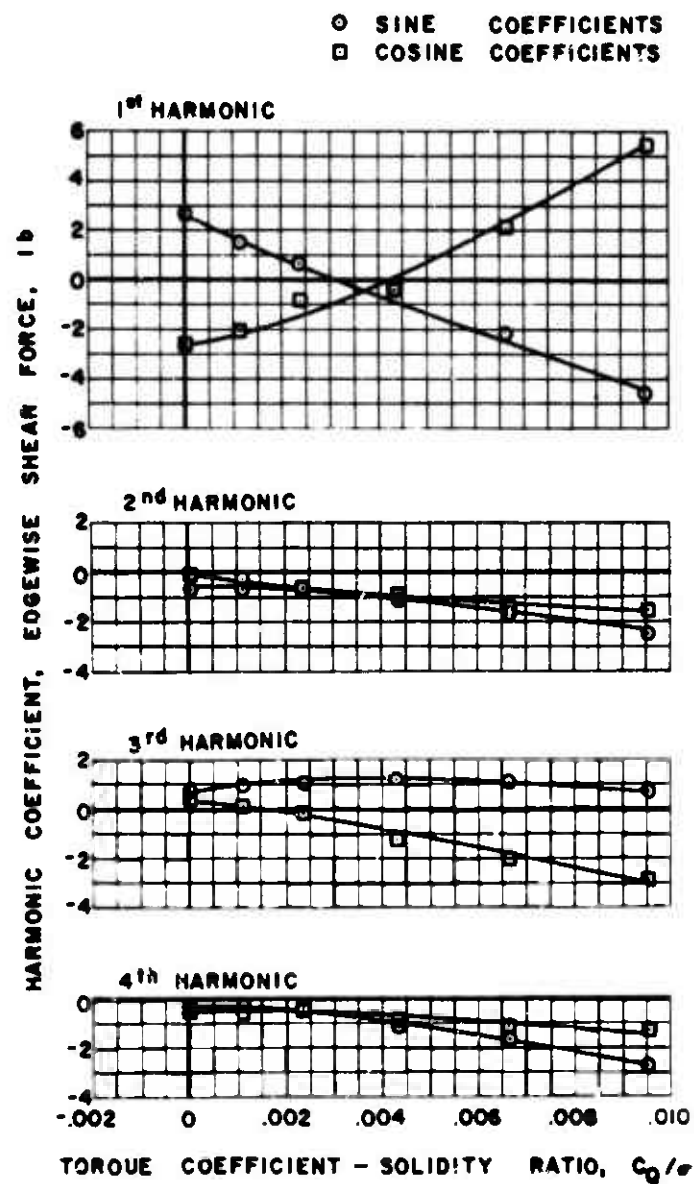


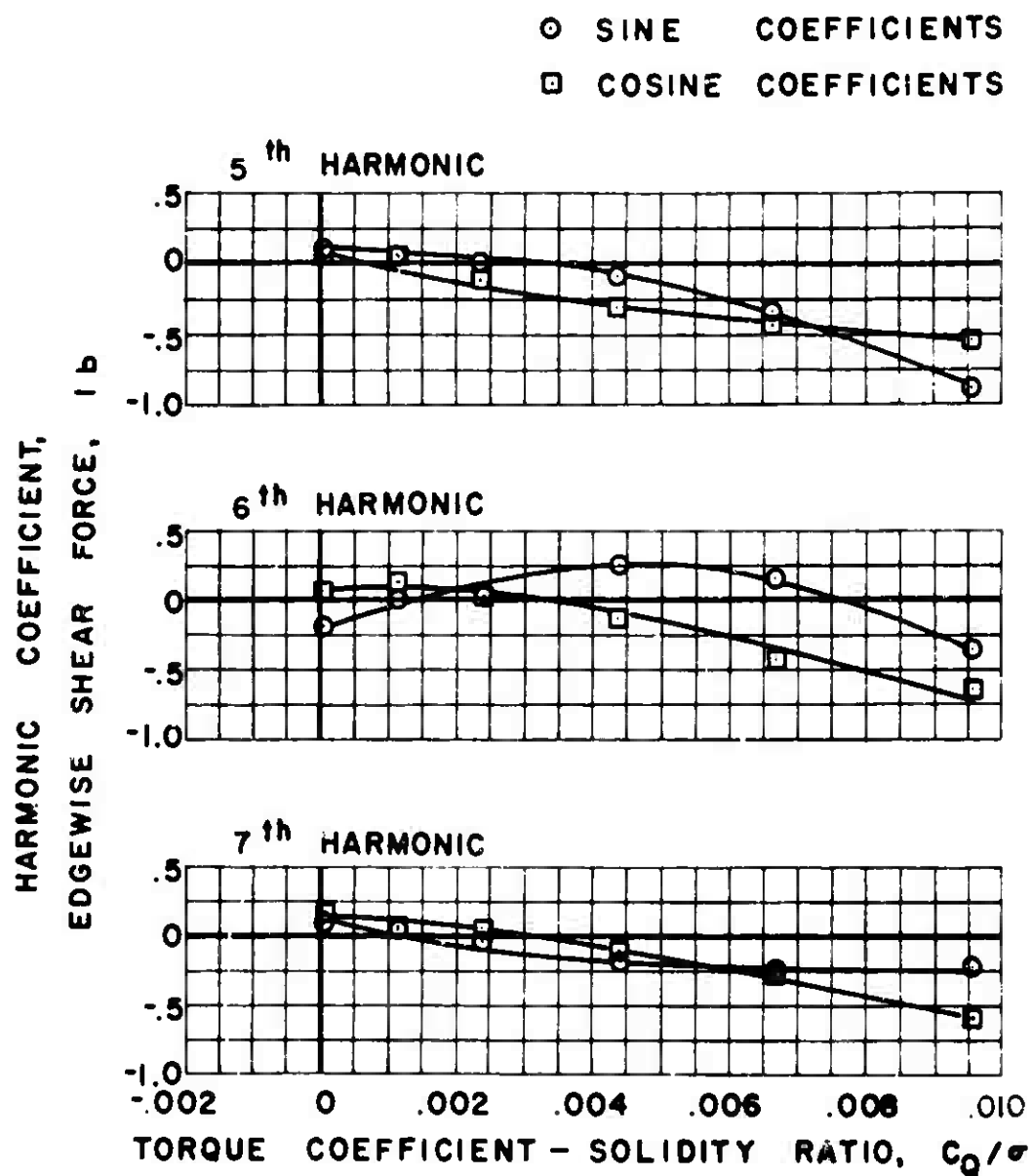
Figure 54(a). Continued.



$\mu = 0.5$ $\alpha_s = -8\text{deg.}$

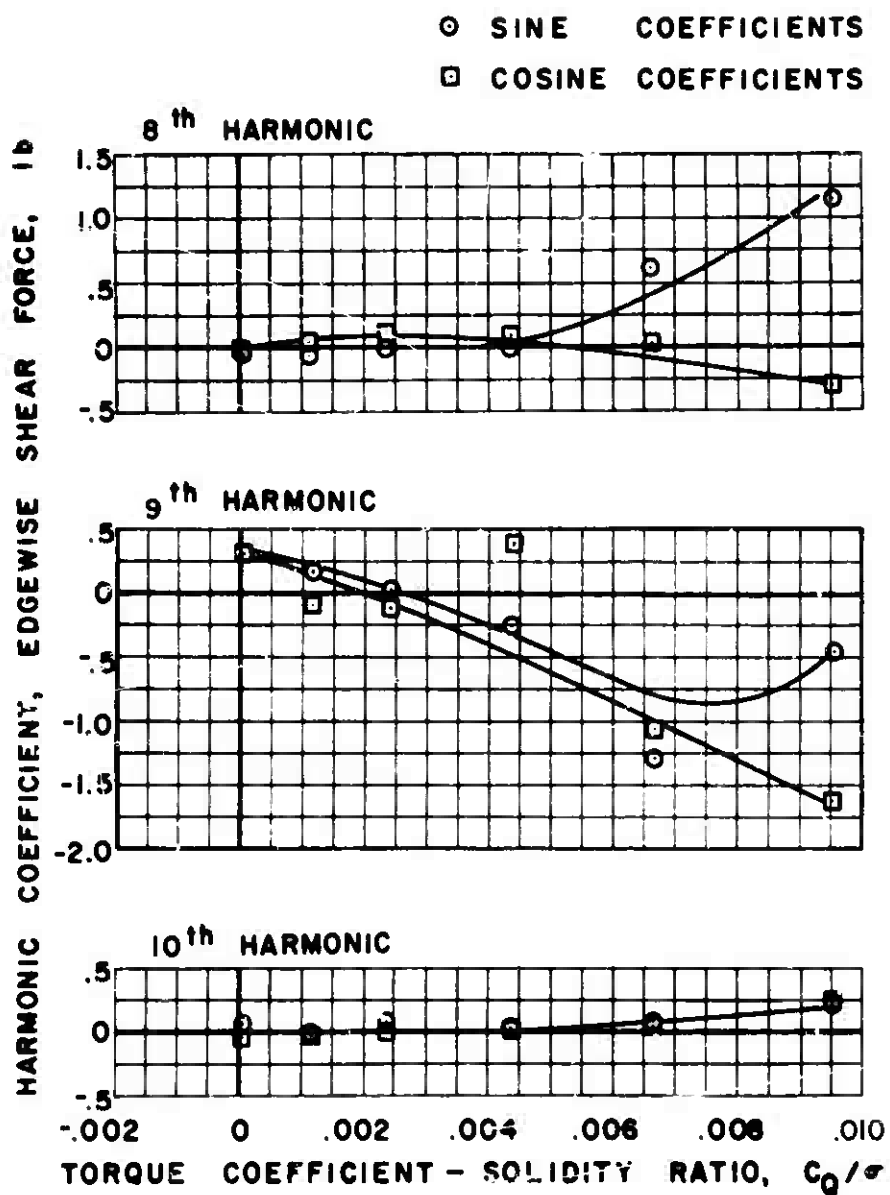
(b) EDGEWISE

Figure 54. Continued.



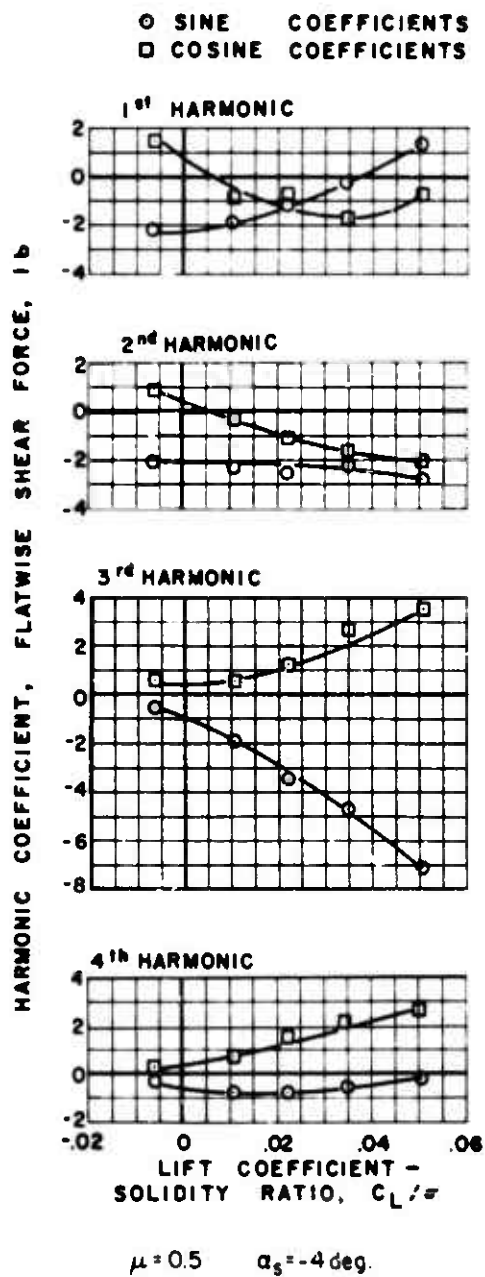
$\mu = 0.5 \quad \alpha_s = -8 \text{ deg.}$

Figure 54(b). Continued.



$$\mu = 0.5 \quad \alpha_s = -8 \text{ deg.}$$

Figure 54(b). Concluded.



(a) FLATWISE

Figure 55. Experimental Shear Force, Zero Lag Damping.

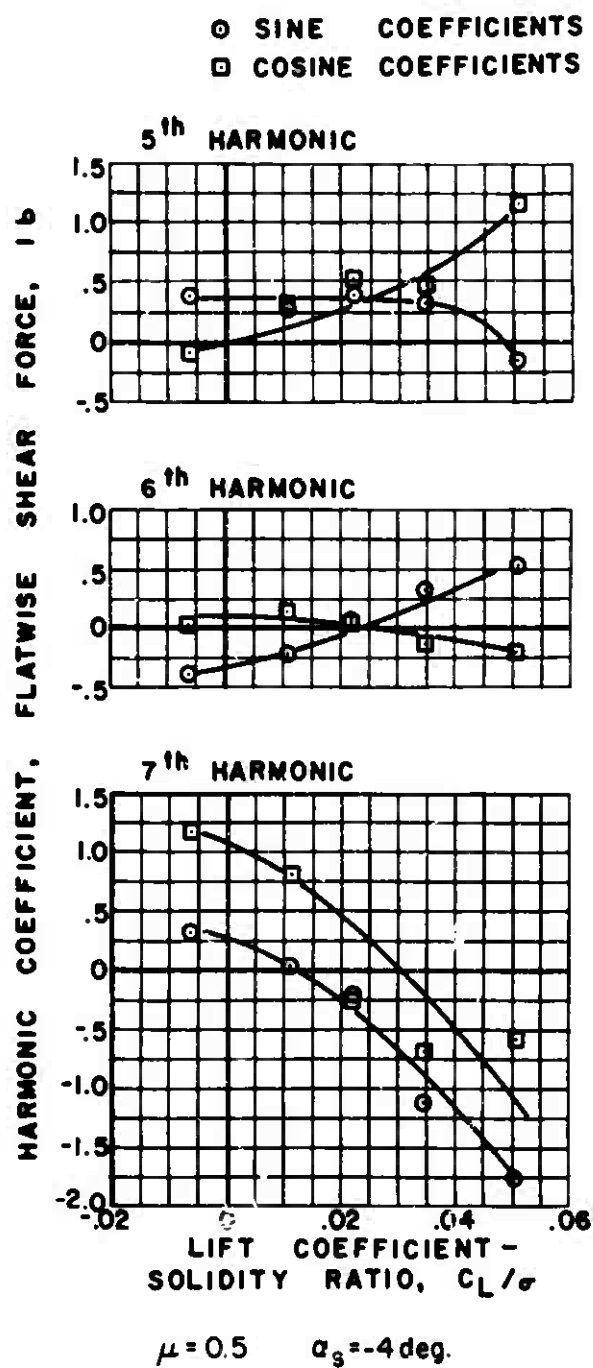
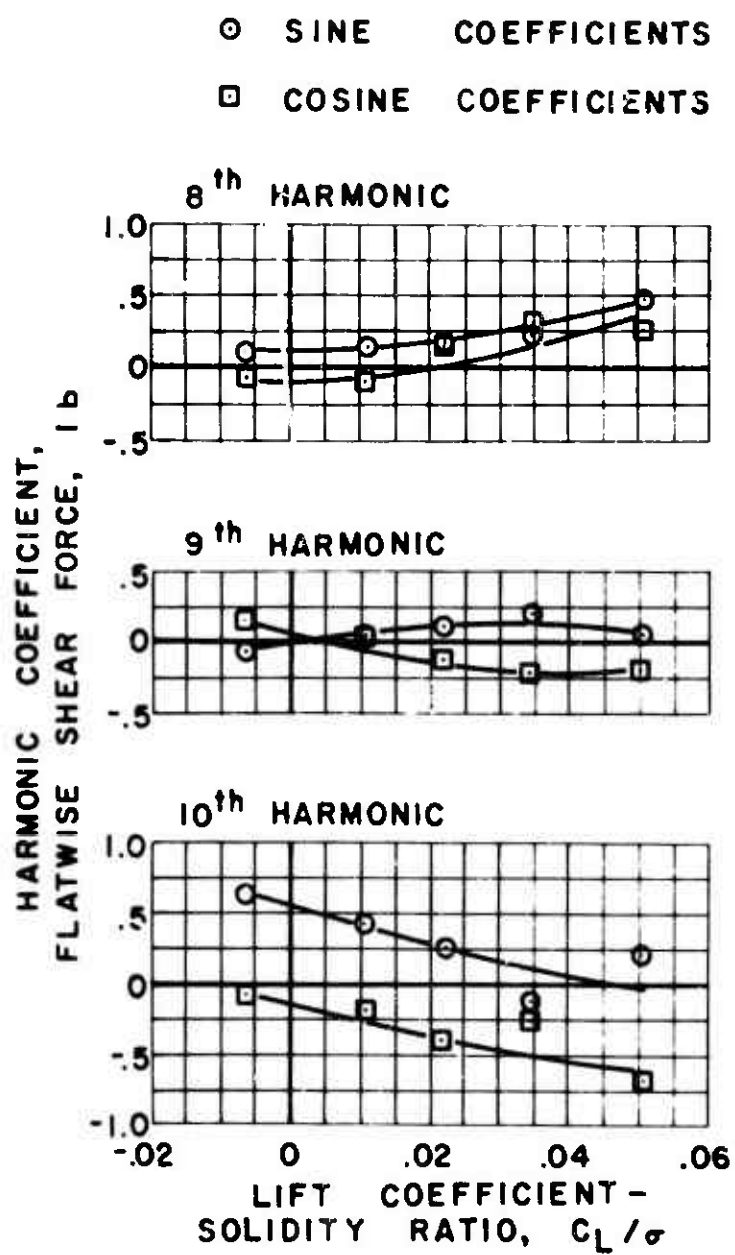
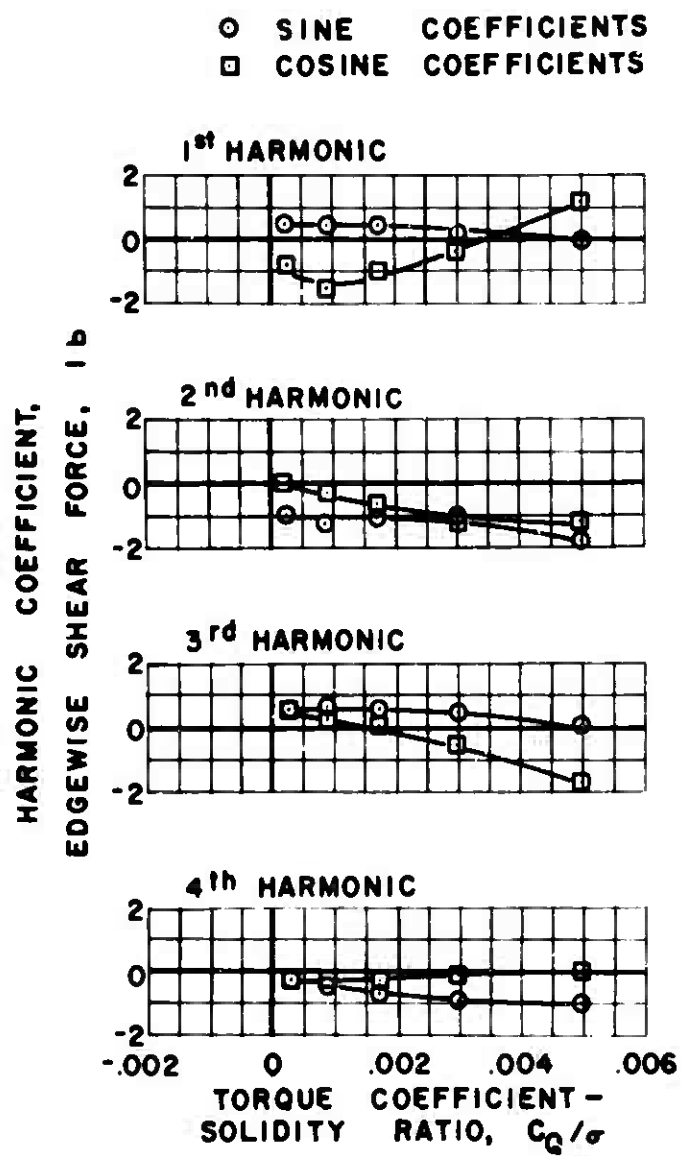


Figure 55(a). Continued.



$\mu = 0.5$ $\alpha_s = -4 \text{ deg.}$

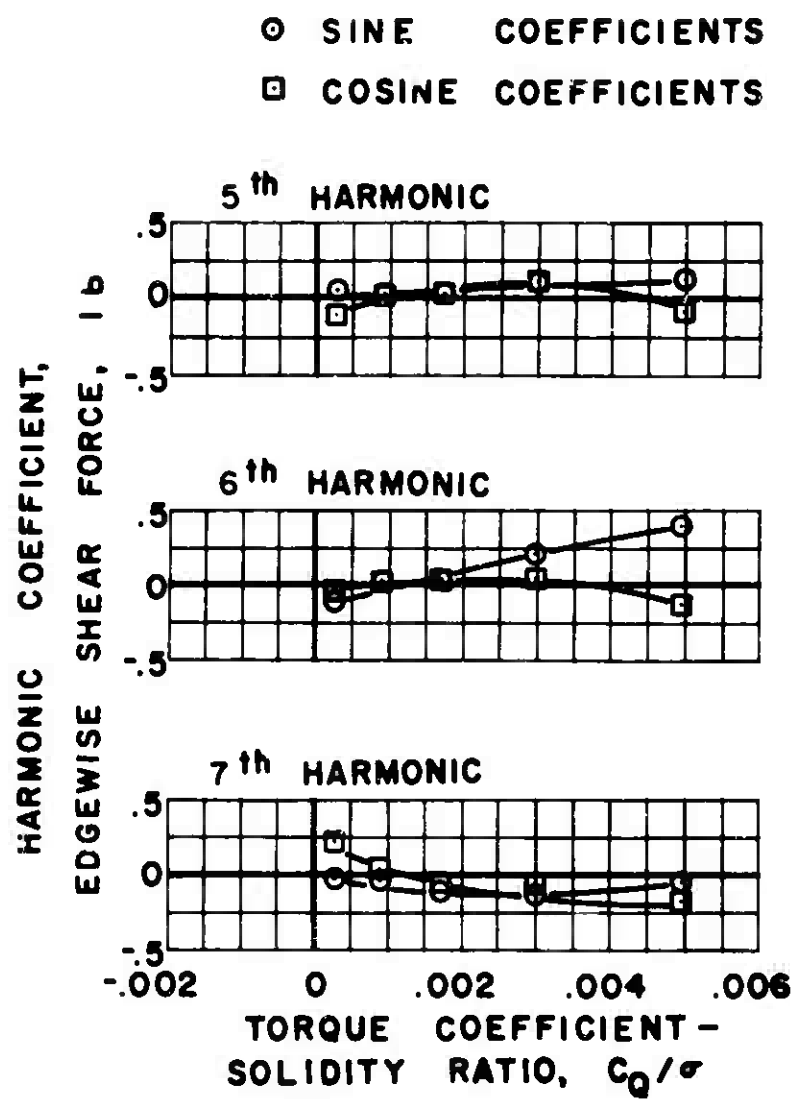
Figure 55(a). Continued.



$\mu = 0.5$ $\alpha_s = -4\text{deg.}$

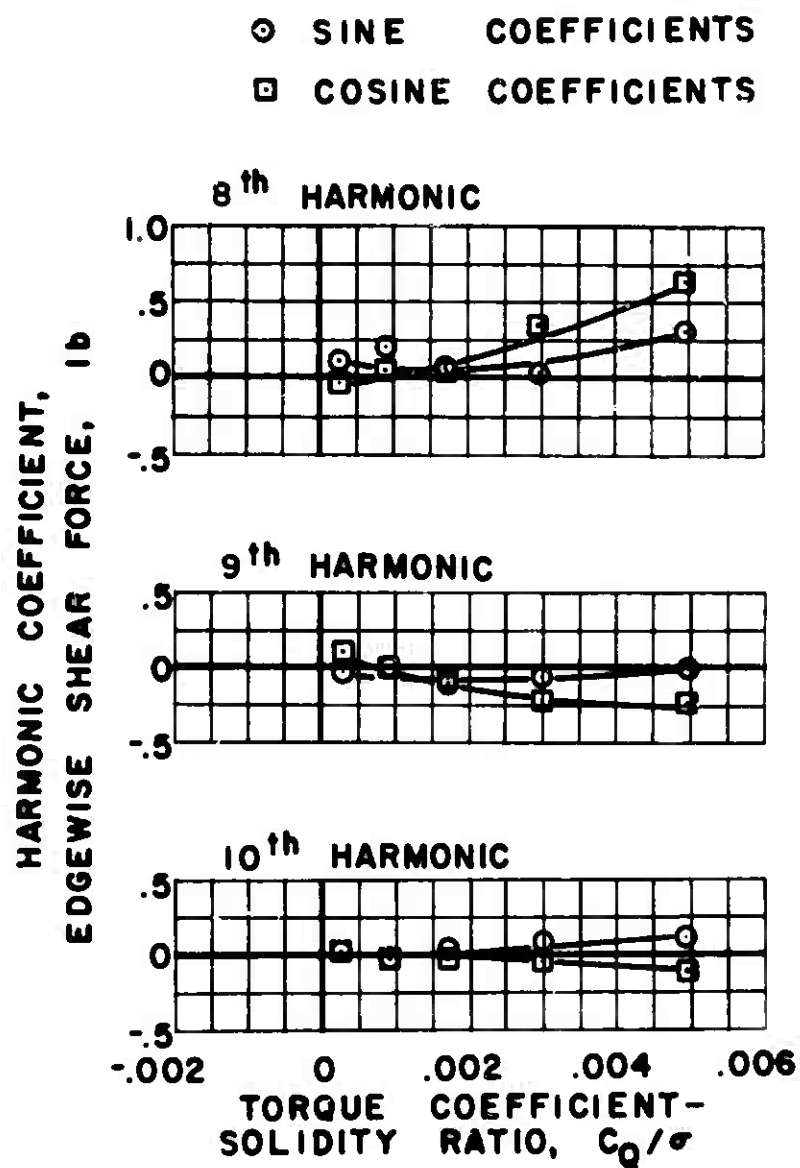
(b) EDGEWISE

Figure 55. Continued.



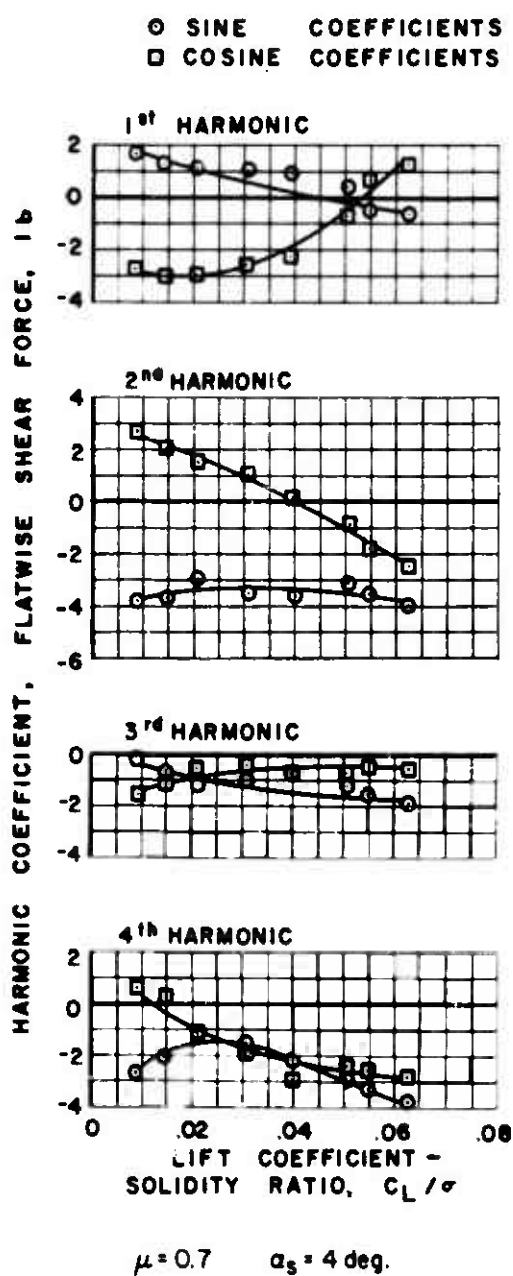
$$\mu = 0.5 \quad \alpha_s = -4\text{deg.}$$

Figure 55(b). Continued.



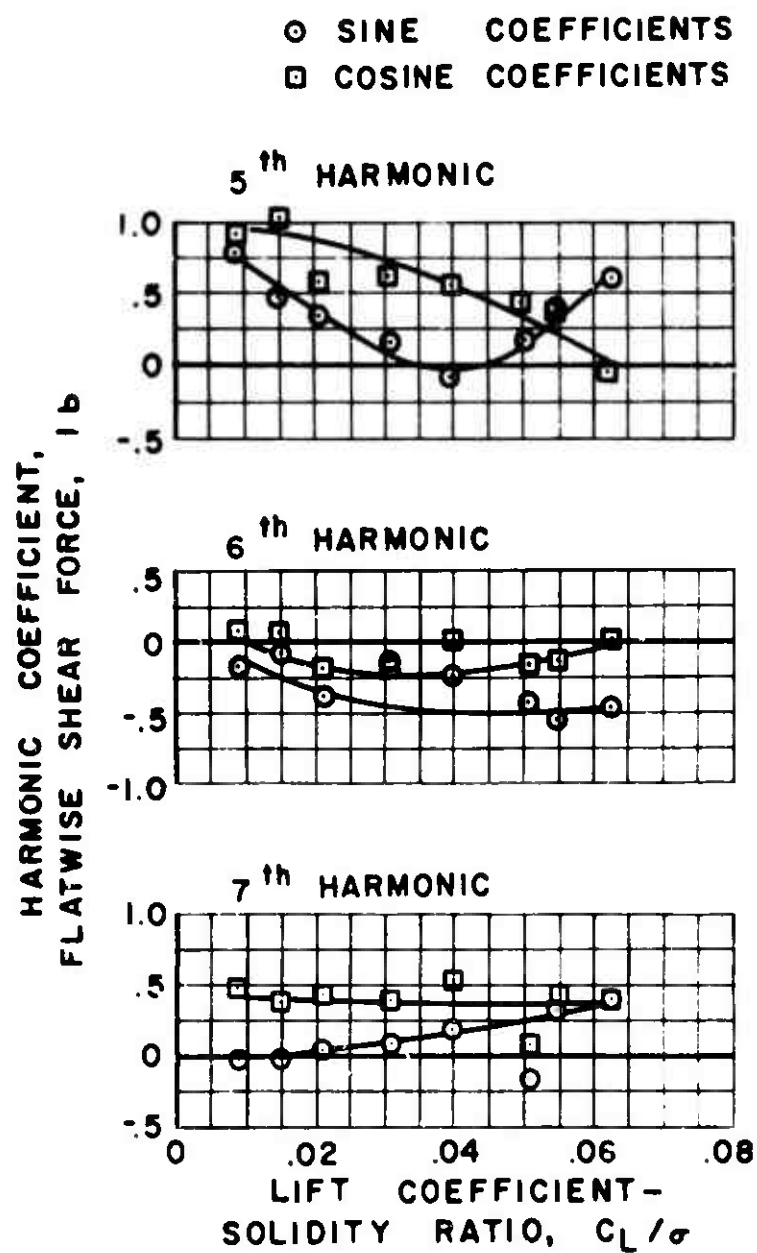
$\mu = 0.5$ $\alpha_s = -4$ deg.

Figure 55(b). Concluded.



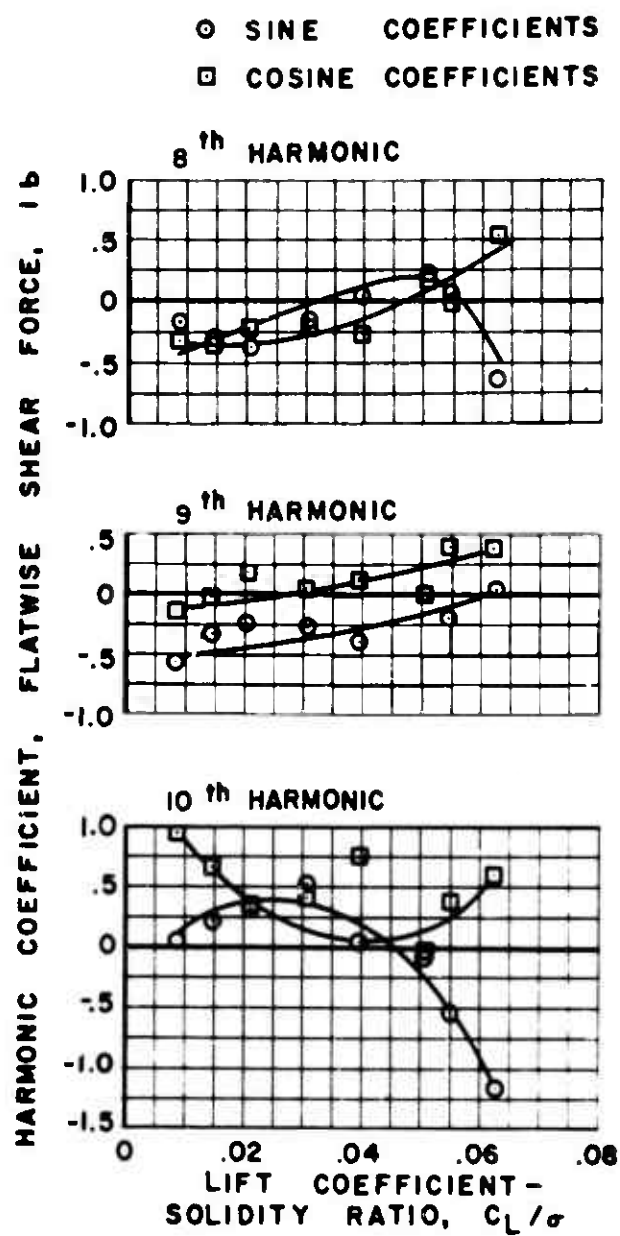
(a) FLATWISE

Figure 56. Experimental Shear Force.



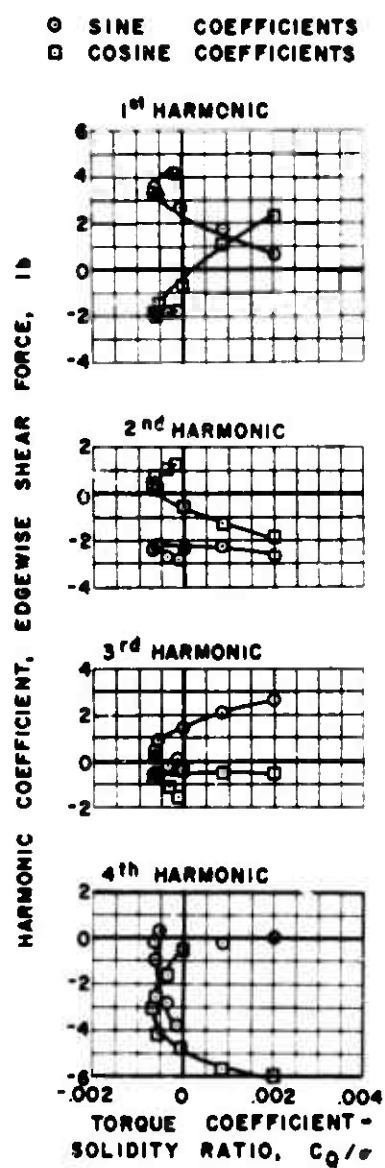
$\mu = 0.7$ $\alpha_s = 4$ deg.

Figure 56(a). Continued.



$\mu = 0.7$ $\alpha_s = 4$ deg.

Figure 56(a). Continued.

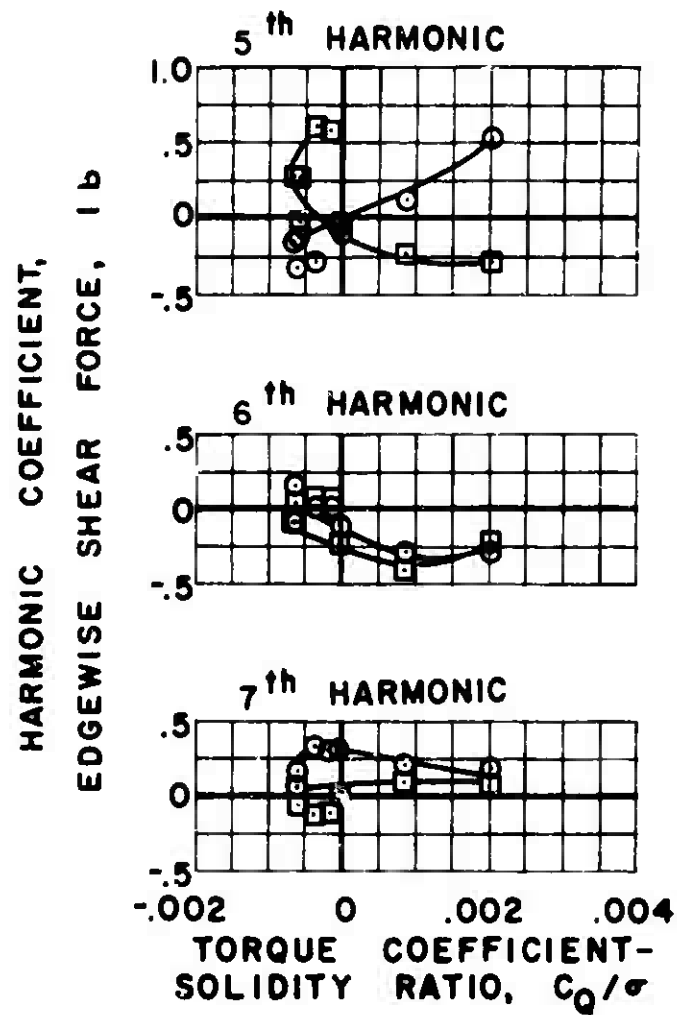


$\mu = 0.7$ $\alpha_s = 4 \text{ deg.}$

(b) EDGEWISE

Figure 56. Continued.

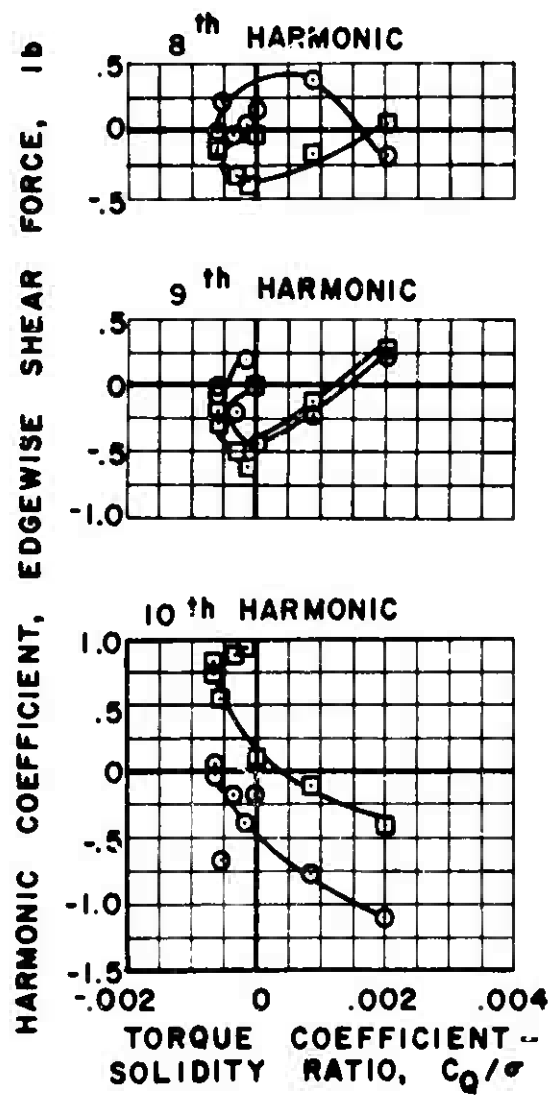
○ SINE COEFFICIENTS
 □ COSINE COEFFICIENTS



$\mu = 0.7$ $\alpha_s = 4 \text{ deg.}$

Figure 56(b). Continued.

○ SINE COEFFICIENTS
 □ COSINE COEFFICIENTS



$\mu = 0.7$ $\alpha_s = 4 \text{ deg.}$

Figure 56(b). Concluded.

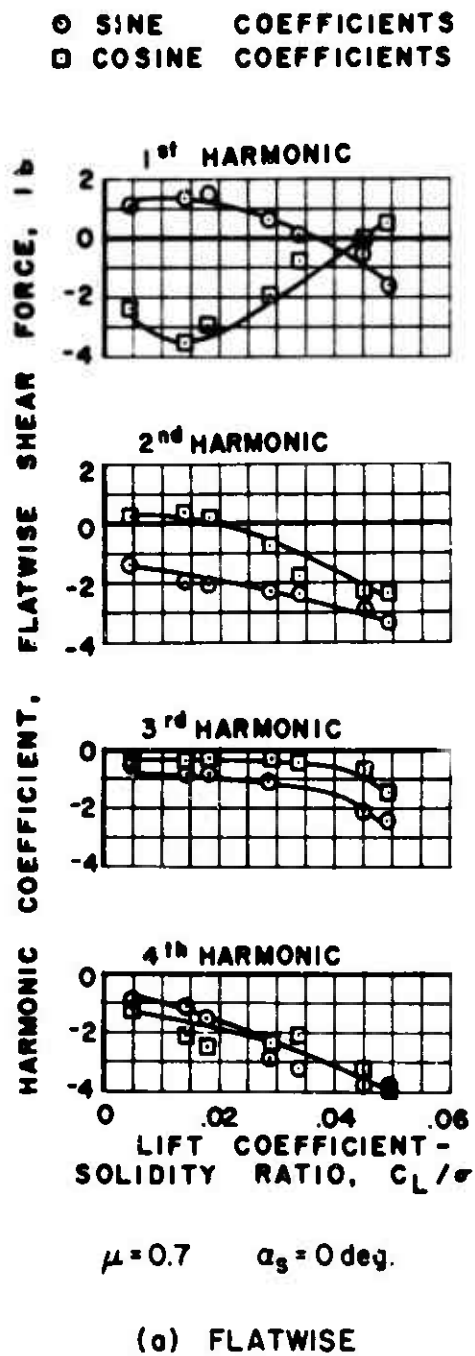
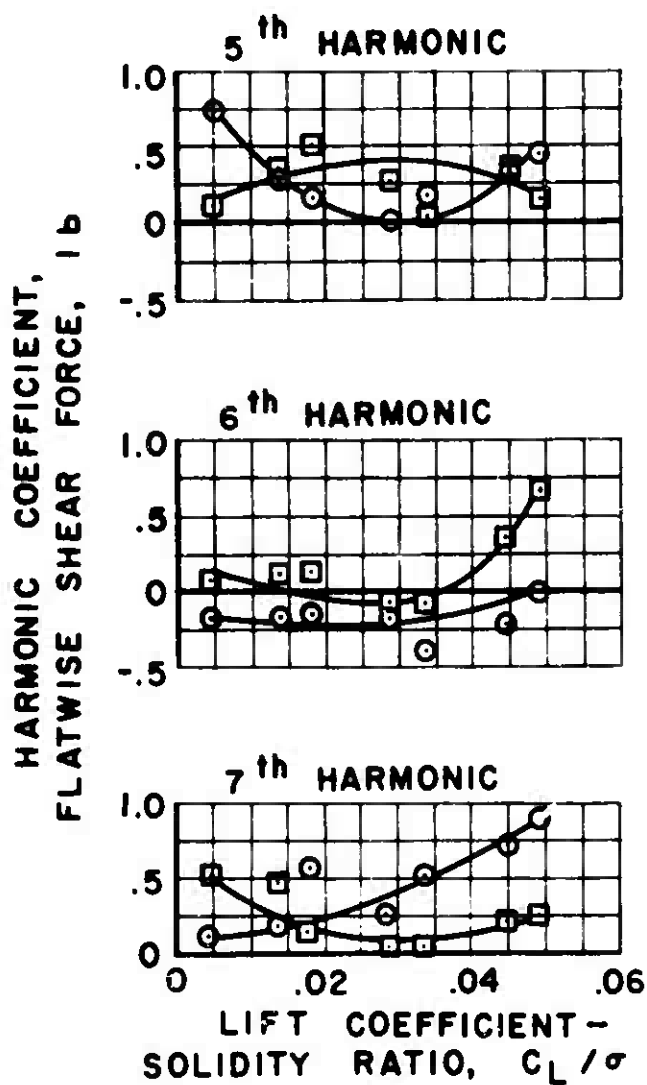


Figure 57. Experimental Shear Force.

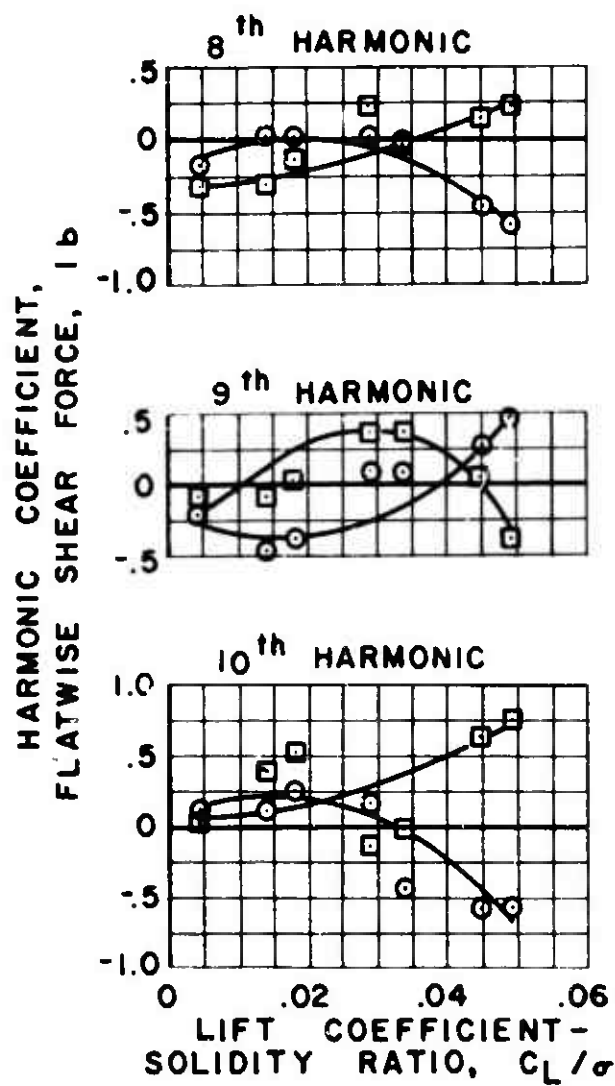
○ SINE COEFFICIENTS
 □ COSINE COEFFICIENTS



$\mu = 0.7$ $\alpha_s = 0 \text{ deg.}$

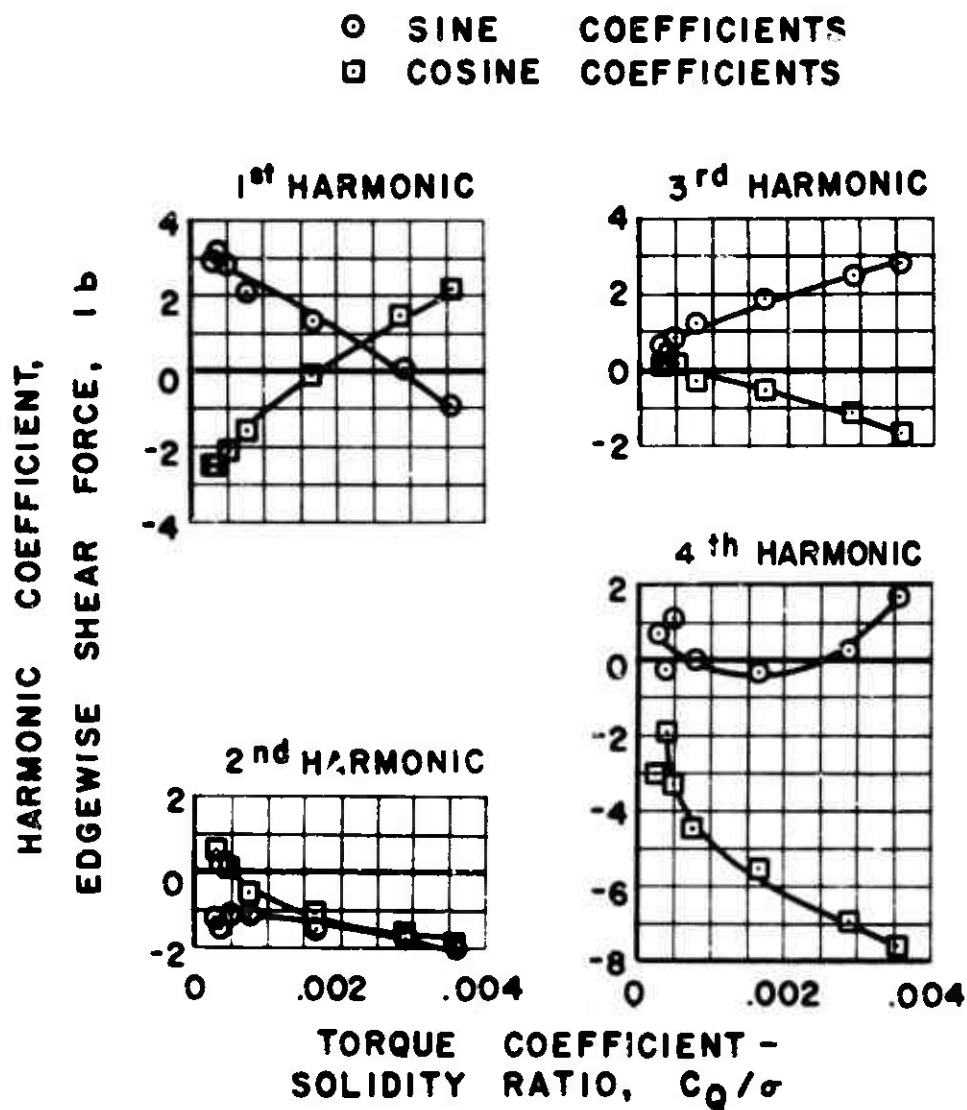
Figure 57(a). Continued.

○ SINE COEFFICIENTS
 □ COSINE COEFFICIENTS



$\mu = 0.7$ $\alpha_s = 0 \text{ deg.}$

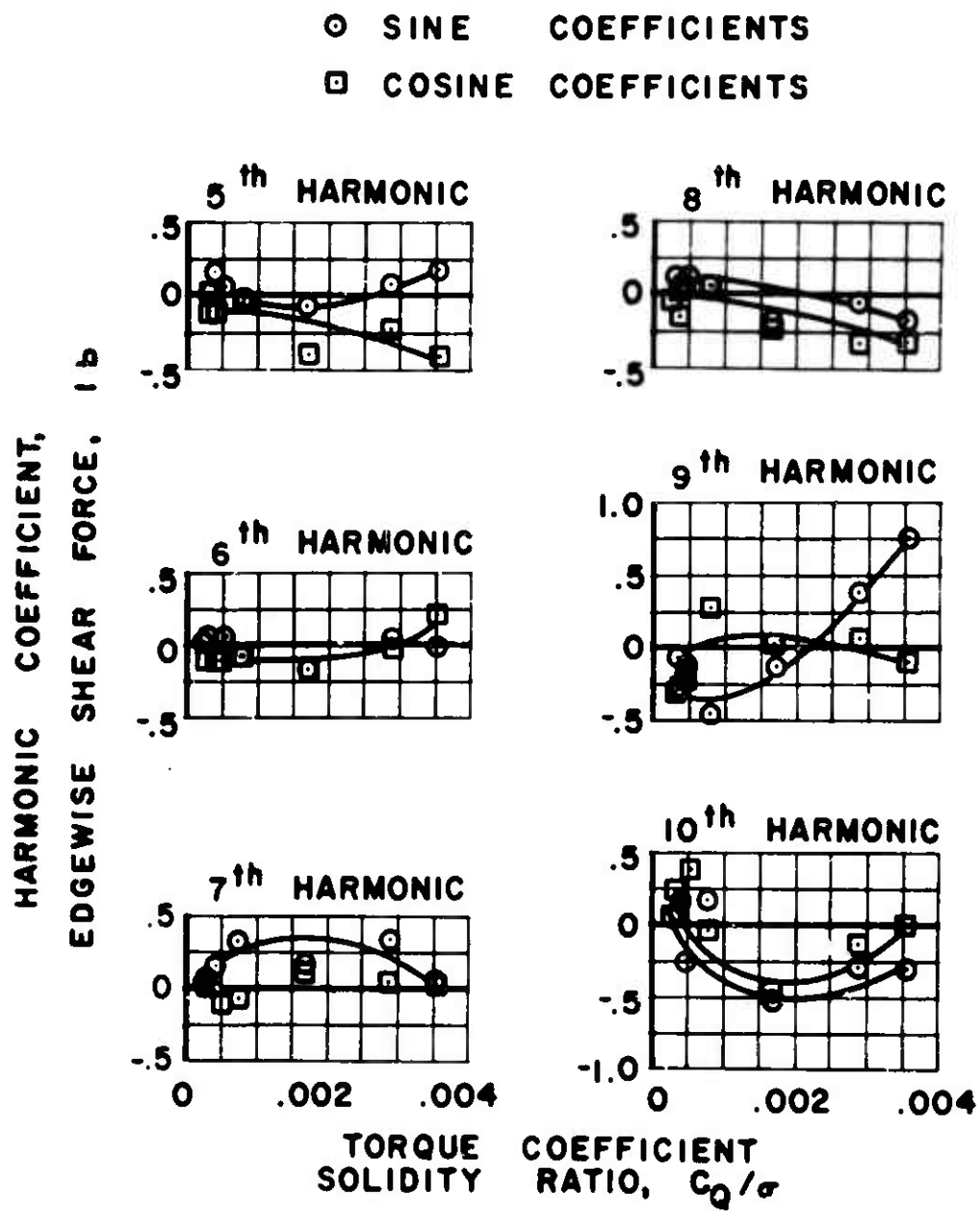
Figure 57(a). Continued.



$\mu = 0.7$ $\alpha_s = 0 \text{ deg.}$

(b) EDGEWISE

Figure 57. Continued.



$\mu = 0.7 \quad \alpha_s = 0 \text{ deg.}$

Figure 57(b). Concluded.

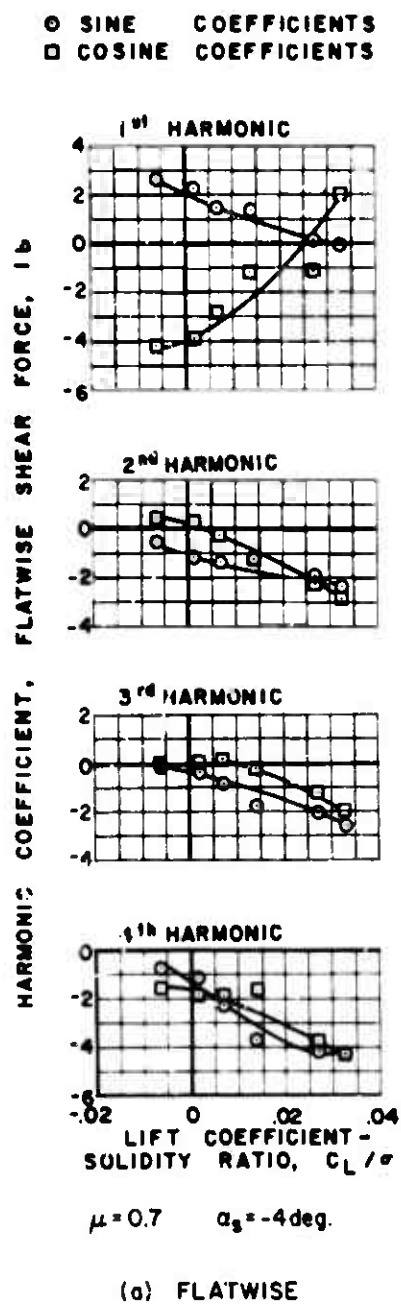
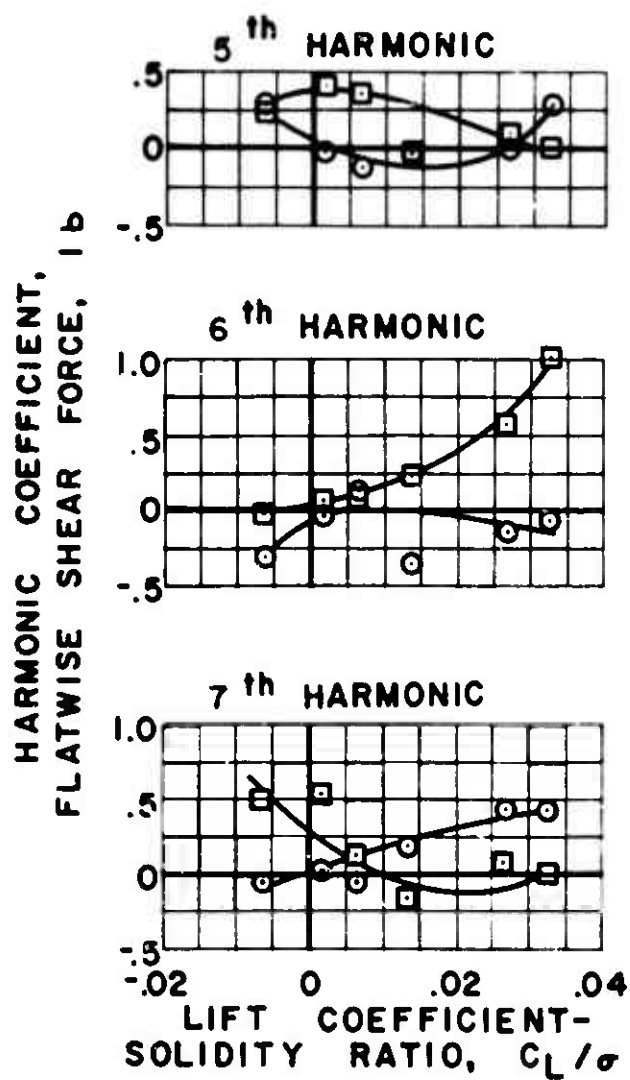


Figure 58. Experimental Shear Force.

○ SINE COEFFICIENTS
 □ COSINE COEFFICIENTS

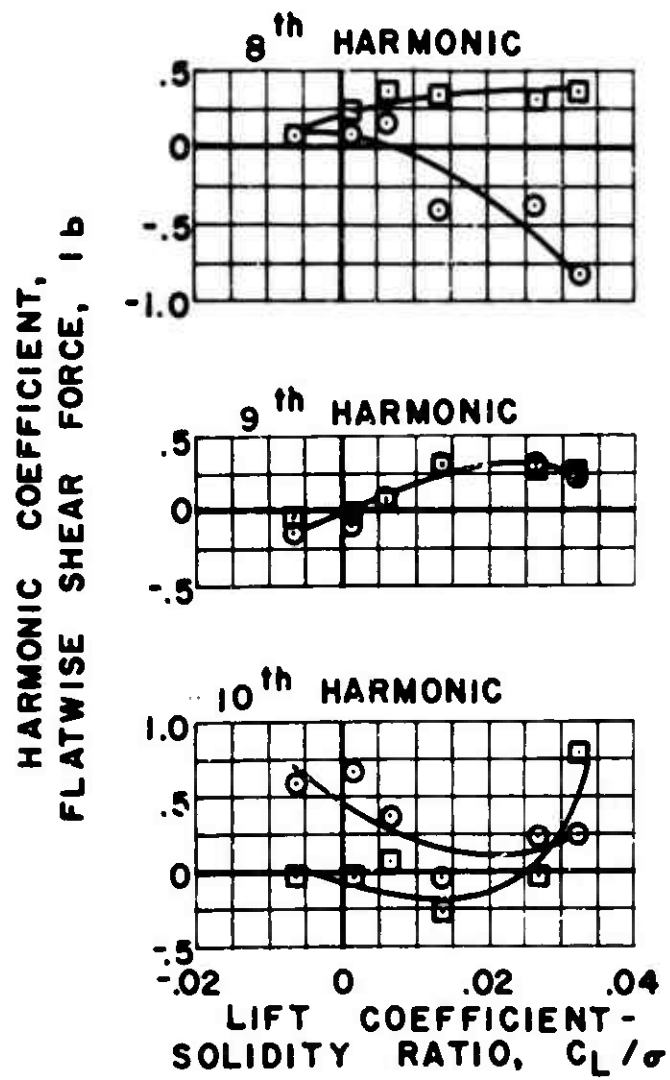


$\mu = 0.7$ $\alpha_s = -4\text{deg.}$

Figure 58(a). Continued.

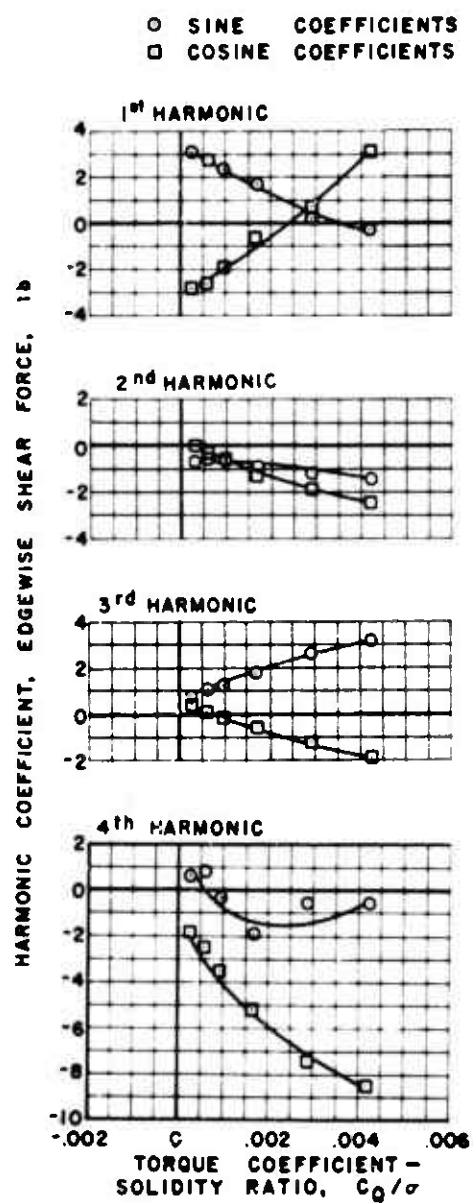
○ SINE COEFFICIENTS

□ COSINE COEFFICIENTS



$\mu = 0.7$ $\alpha_s = -4 \text{ deg.}$

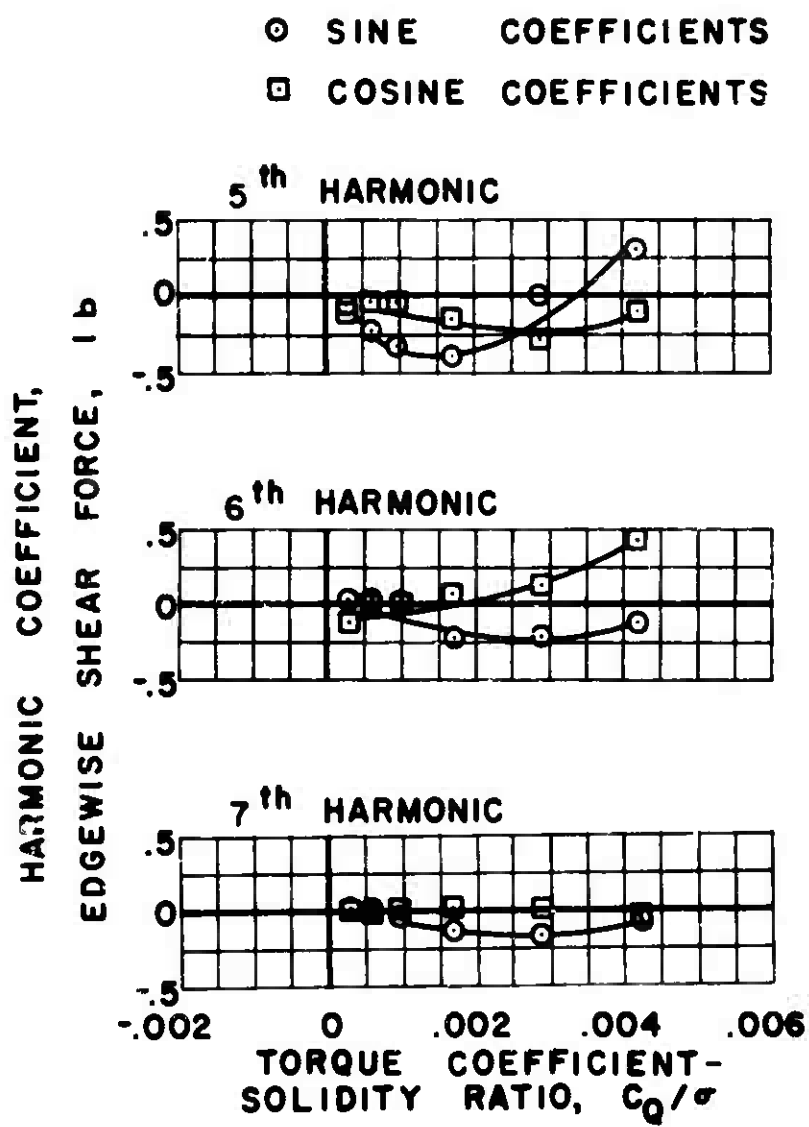
Figure 58(a). Continued.



$\mu = 0.7$ $\alpha_s = -4 \text{ deg.}$

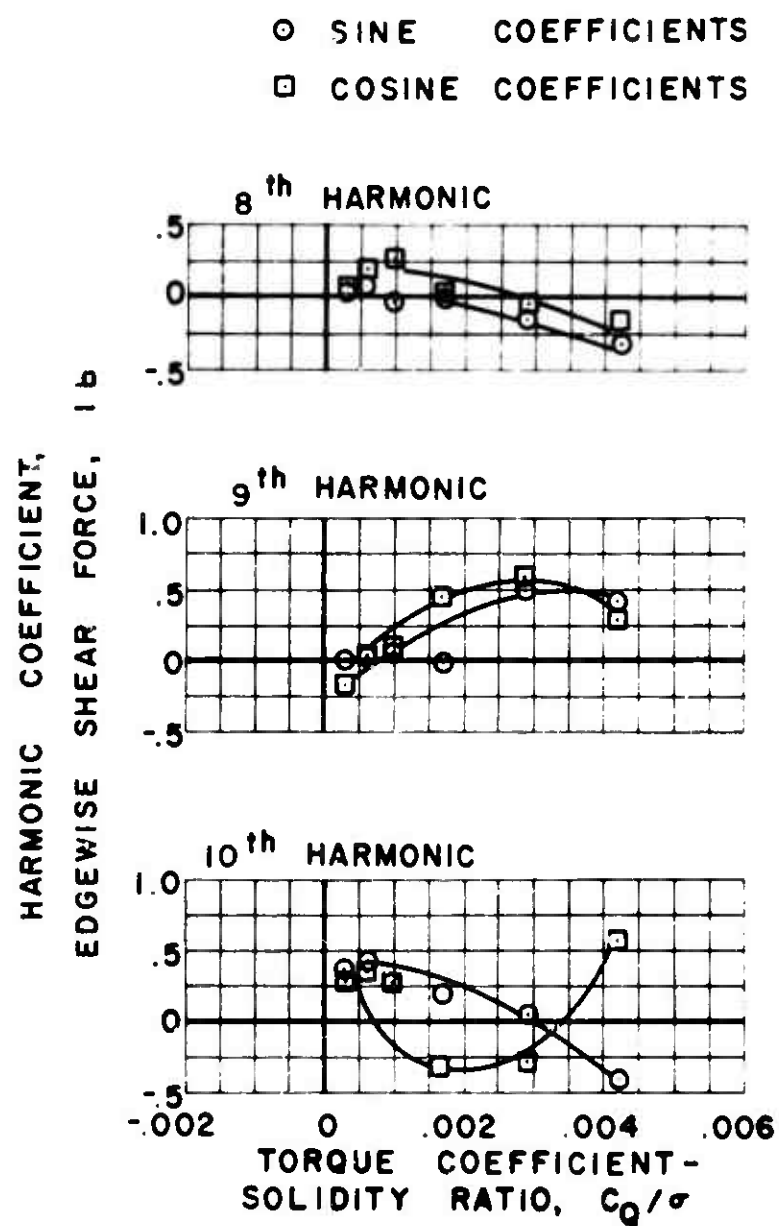
(b) EDGEWISE

Figure 58. Continued.



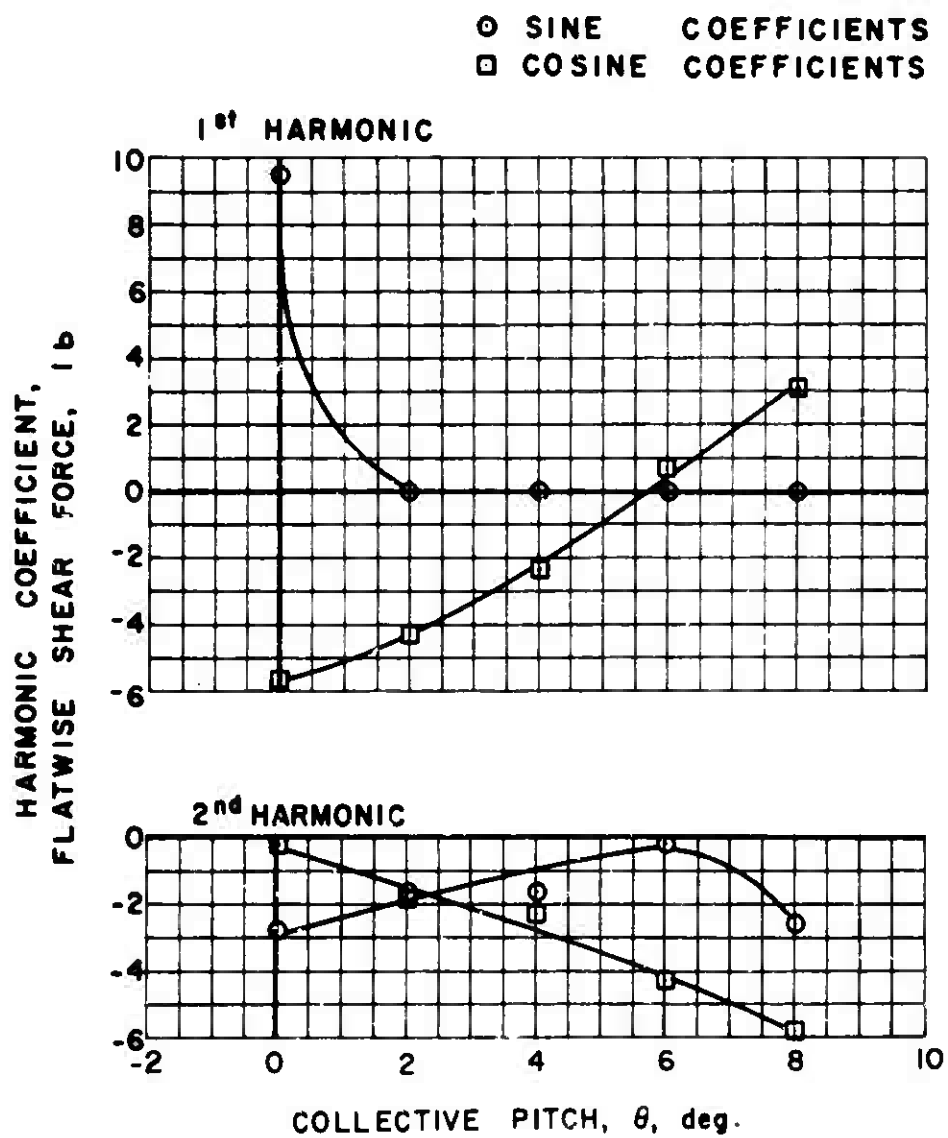
$\mu = 0.7$ $\alpha_s = -4 \text{ deg.}$

Figure 58(b). Continued.



$$\mu = 0.7 \quad \alpha_s = -4 \text{ deg.}$$

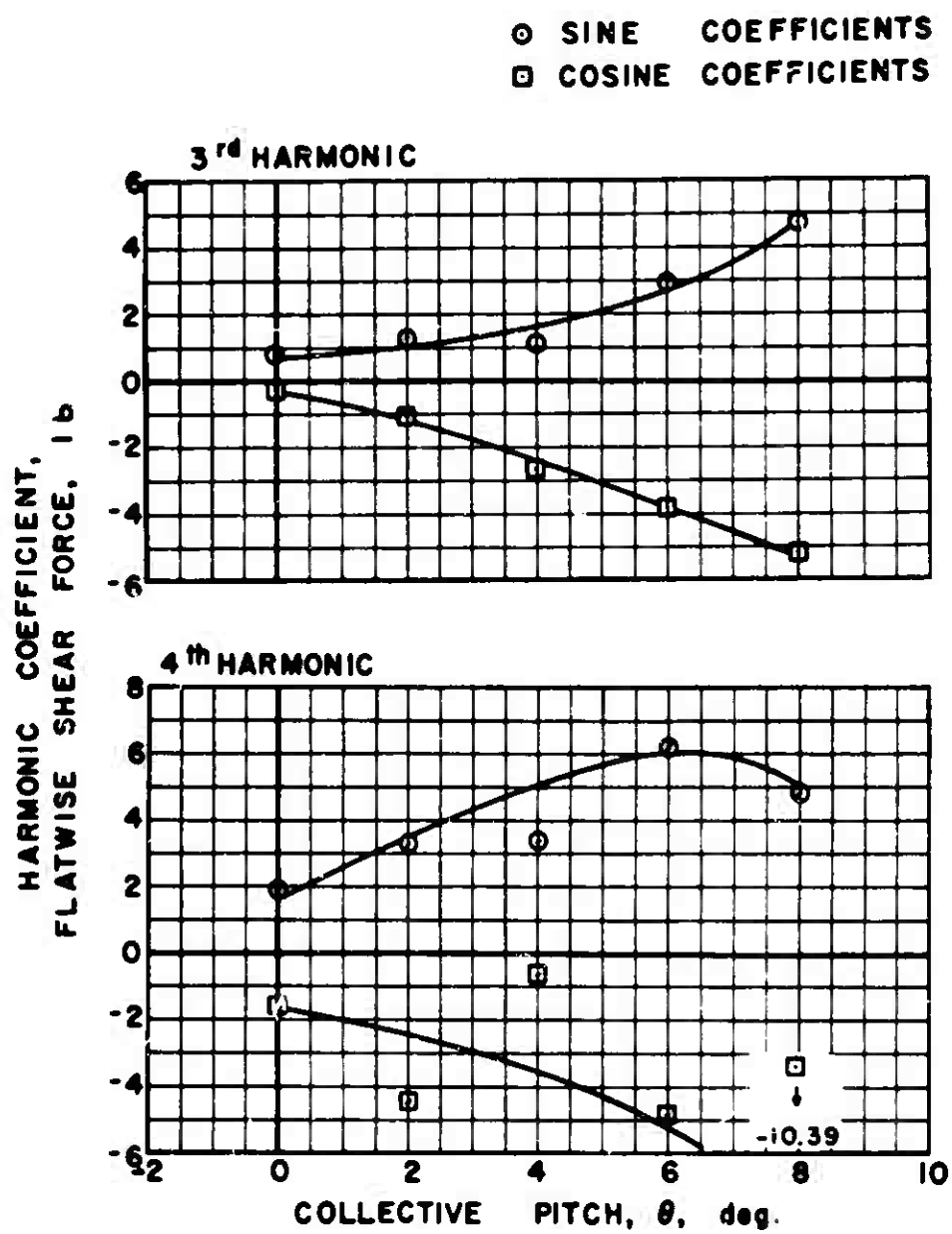
Figure 58(b). Concluded.



$$\mu = 1.0 \quad \alpha_s = 0 \text{ deg.}$$

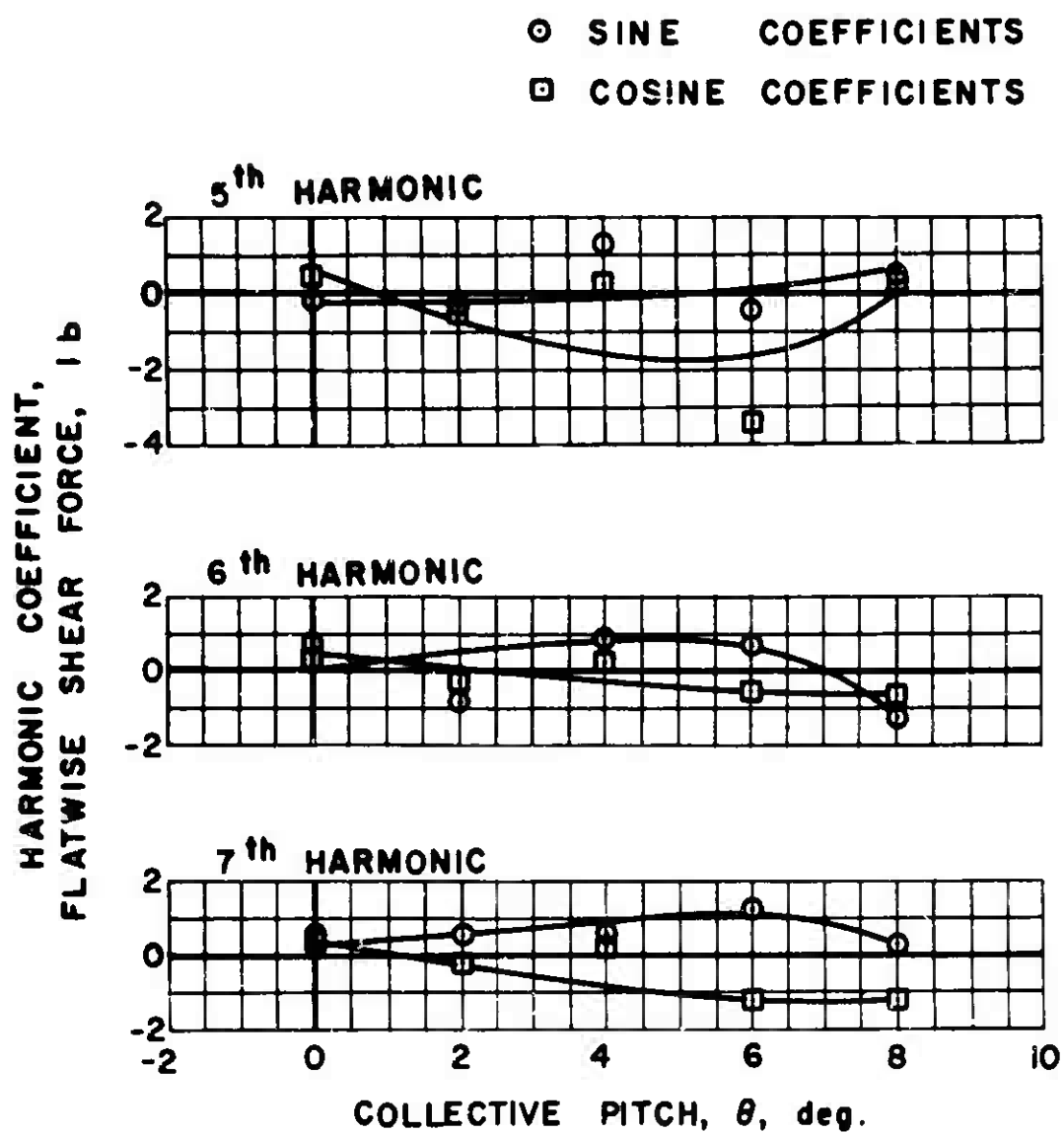
(a) FLATWISE

Figure 59. Experimental Shear Force.



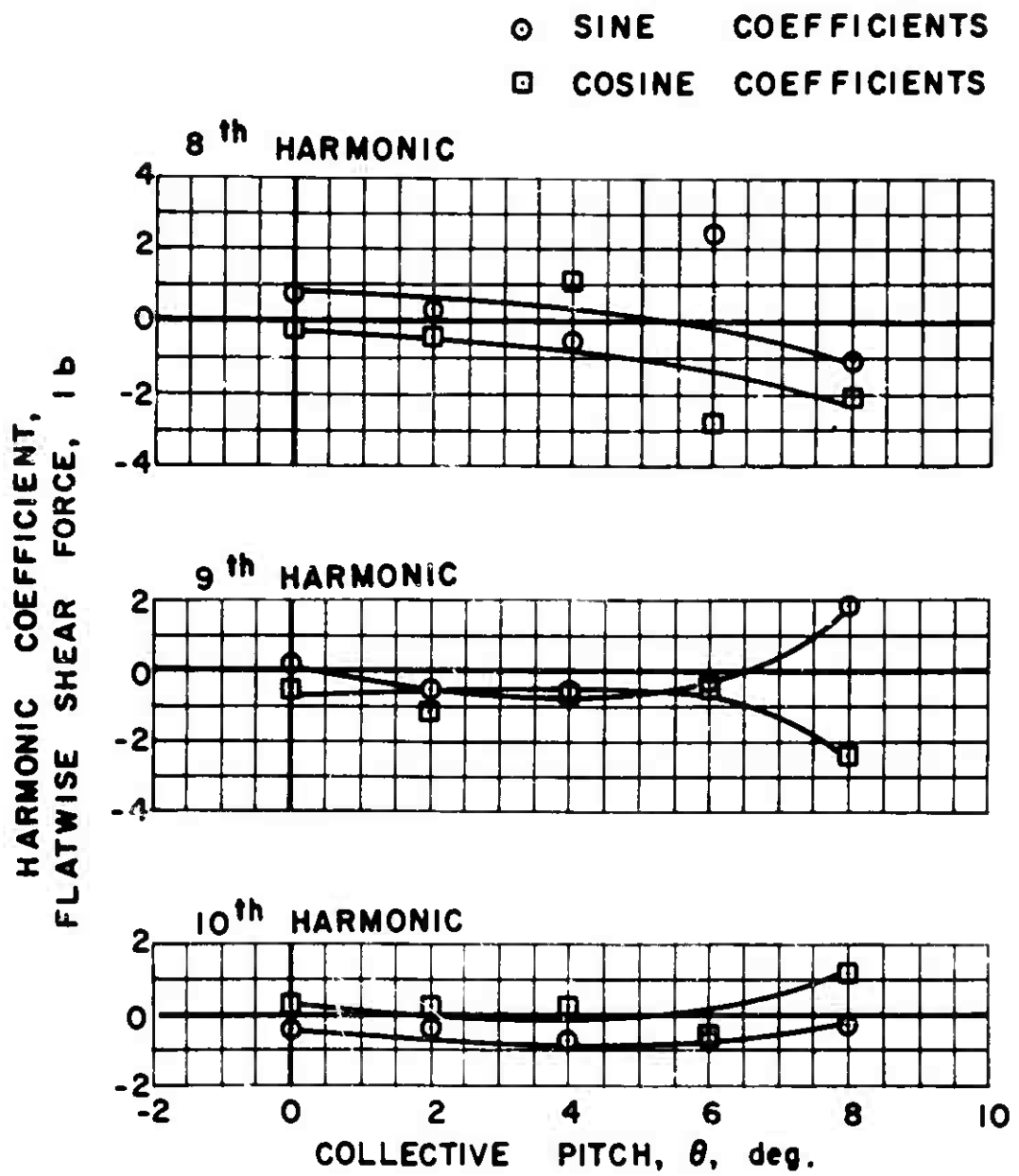
$$\mu = 1.0 \quad \alpha_s = 0 \text{ deg.}$$

Figure 59(a). Continued.



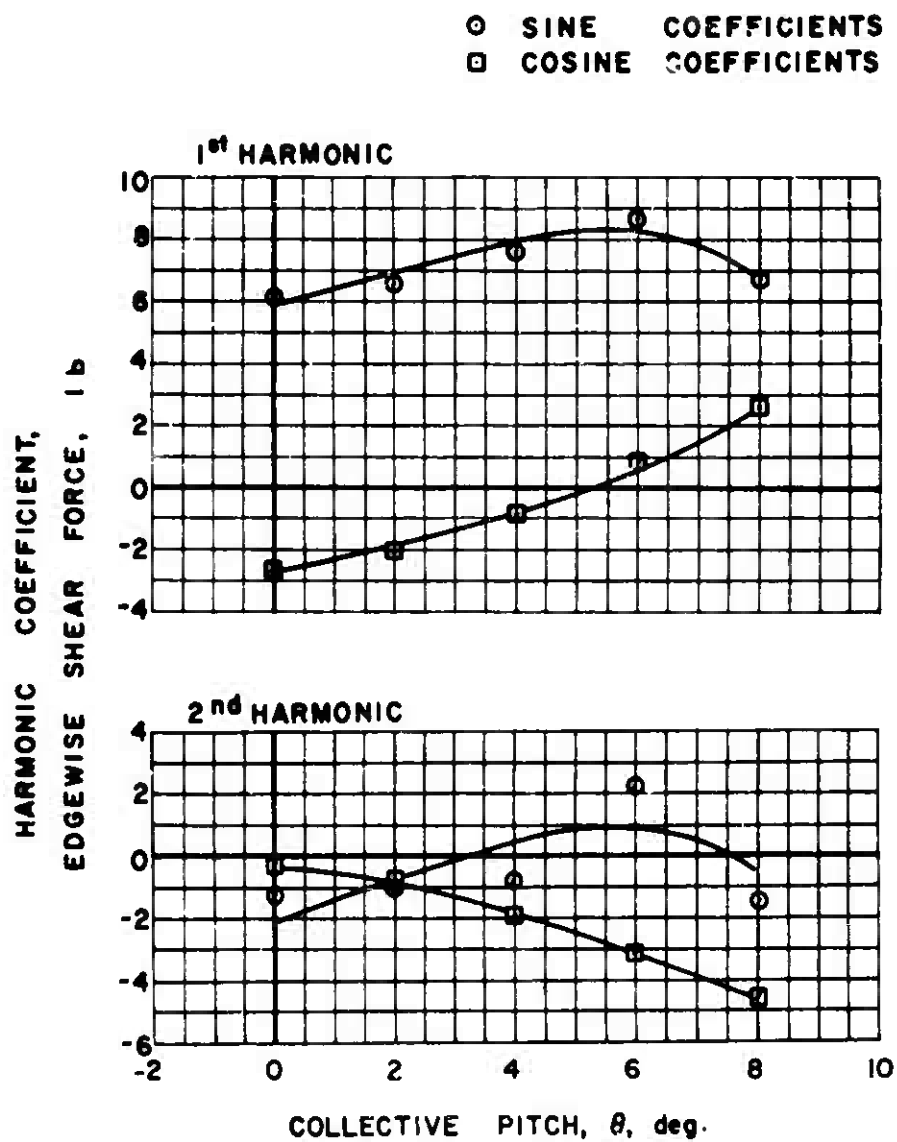
$$\mu = 1.0 \quad \alpha_s = 0 \text{ deg.}$$

Figure 59(a). Continued.



$$\mu = 1.0 \quad \alpha_s = 0 \text{ deg.}$$

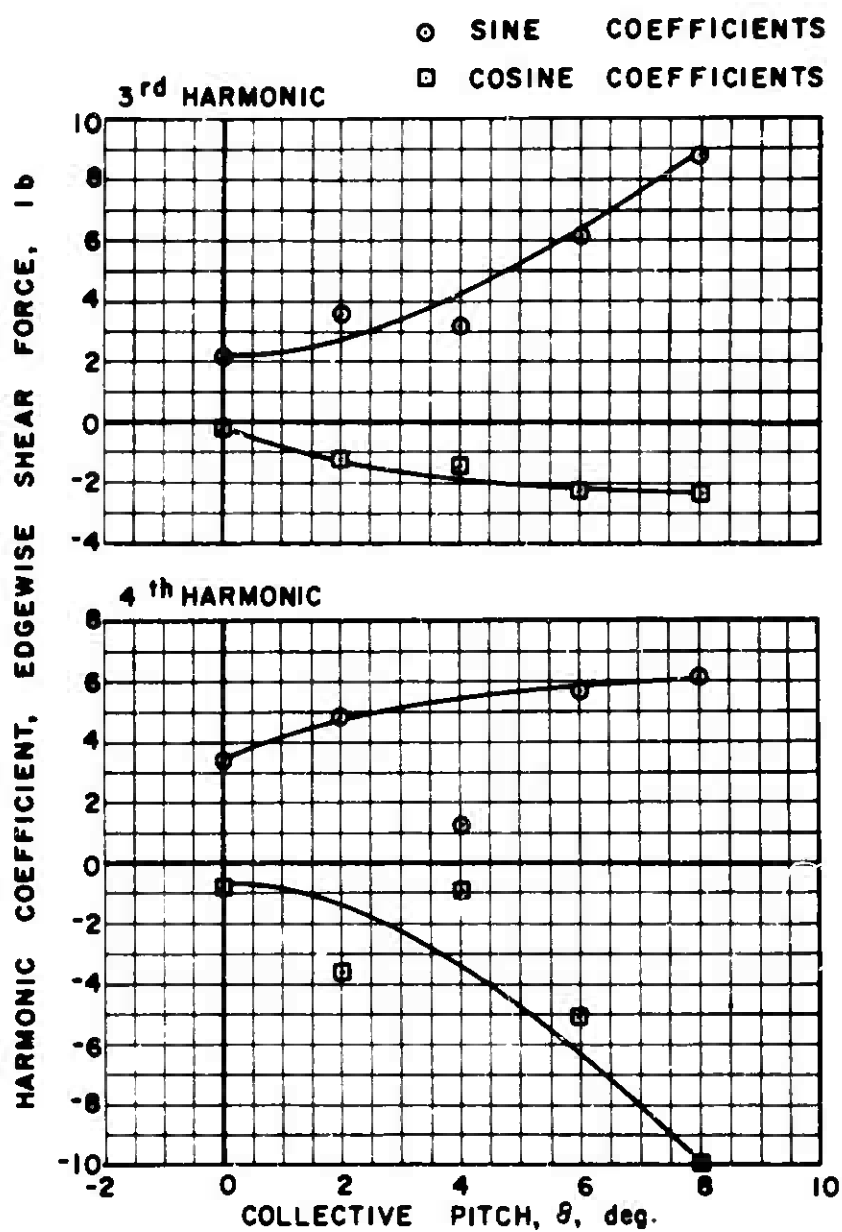
Figure 59(a). Continued.



$\mu = 1.0 \quad \alpha_s = 0 \text{ deg.}$

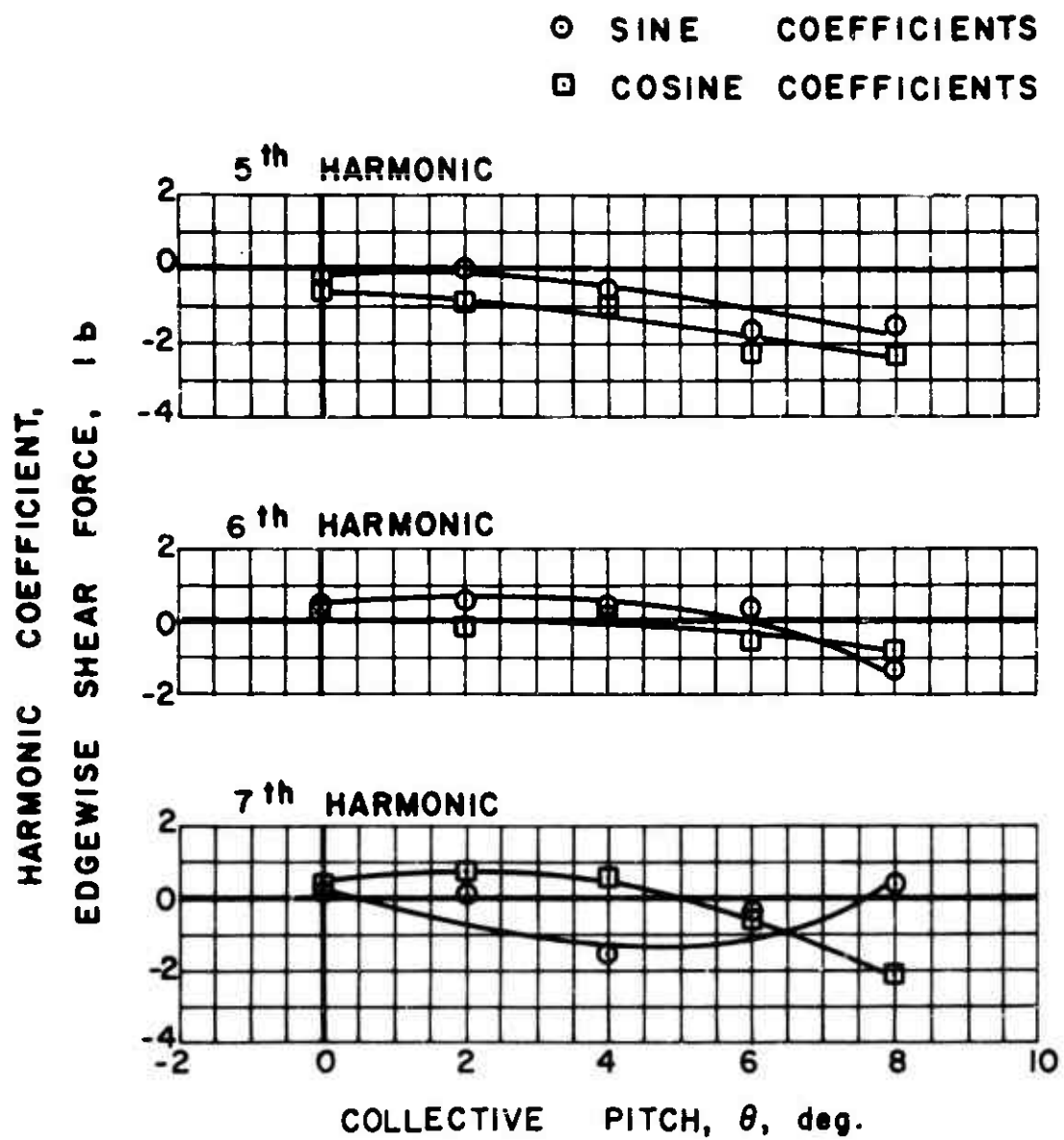
(b) EDGEWISE

Figure 59. Continued.



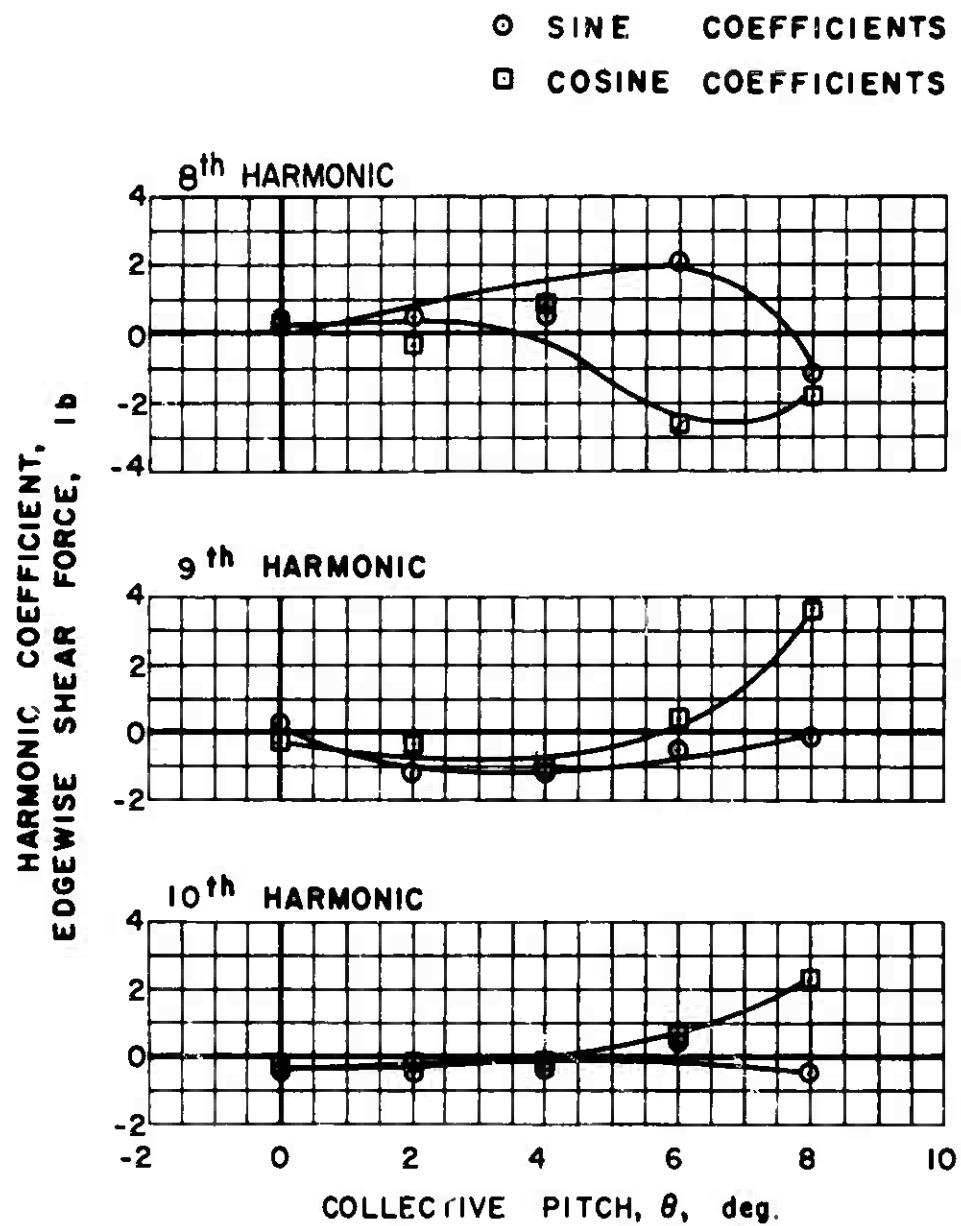
$\mu = 1.0 \quad \alpha_s = 0 \text{ deg.}$

Figure 59(b). Continued.



$$\mu = 1.0 \quad \alpha_s = 0 \text{ deg.}$$

Figure 59(b). Continued.



$$\mu = 1.0 \quad \alpha_s = 0 \text{ deg.}$$

Figure 59(b). Concluded.

APPENDIX II
EXPERIMENTAL RADIAL SHEAR FORCE FIGURES

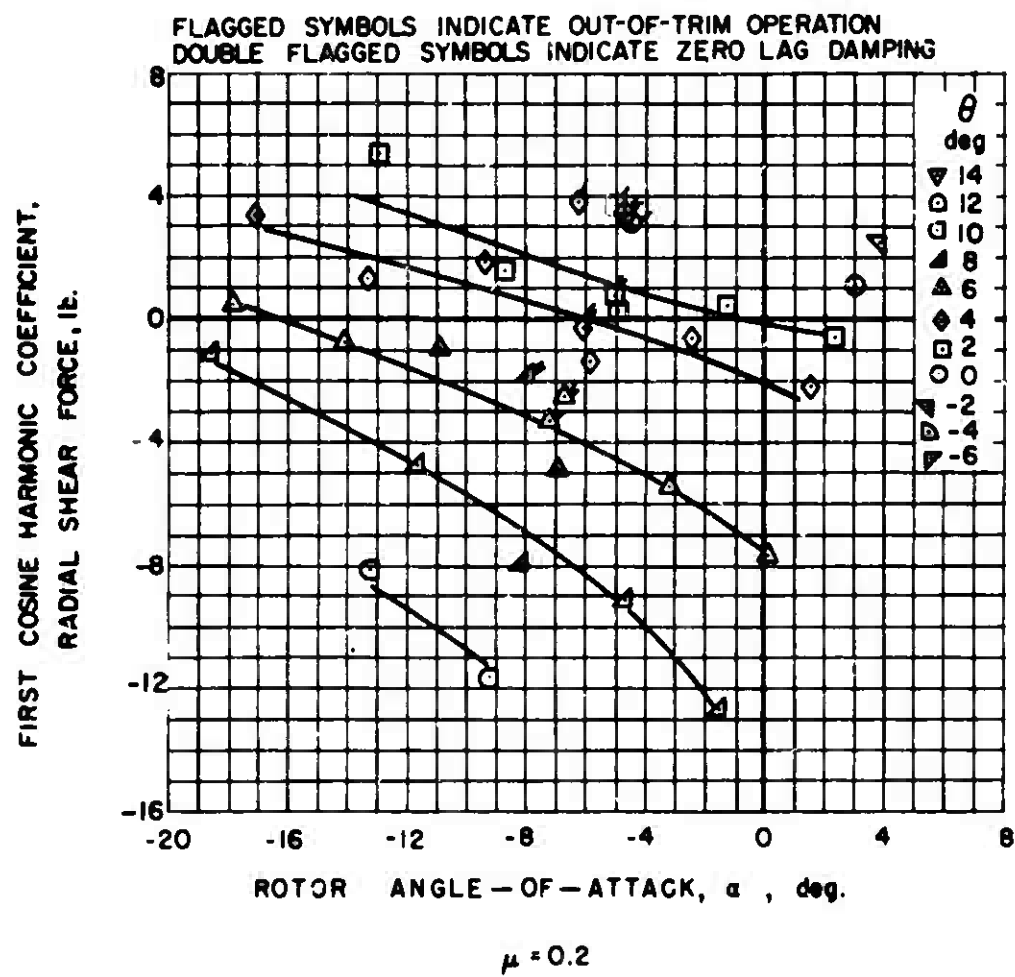


Figure 60. Experimental Radial Shear Force.

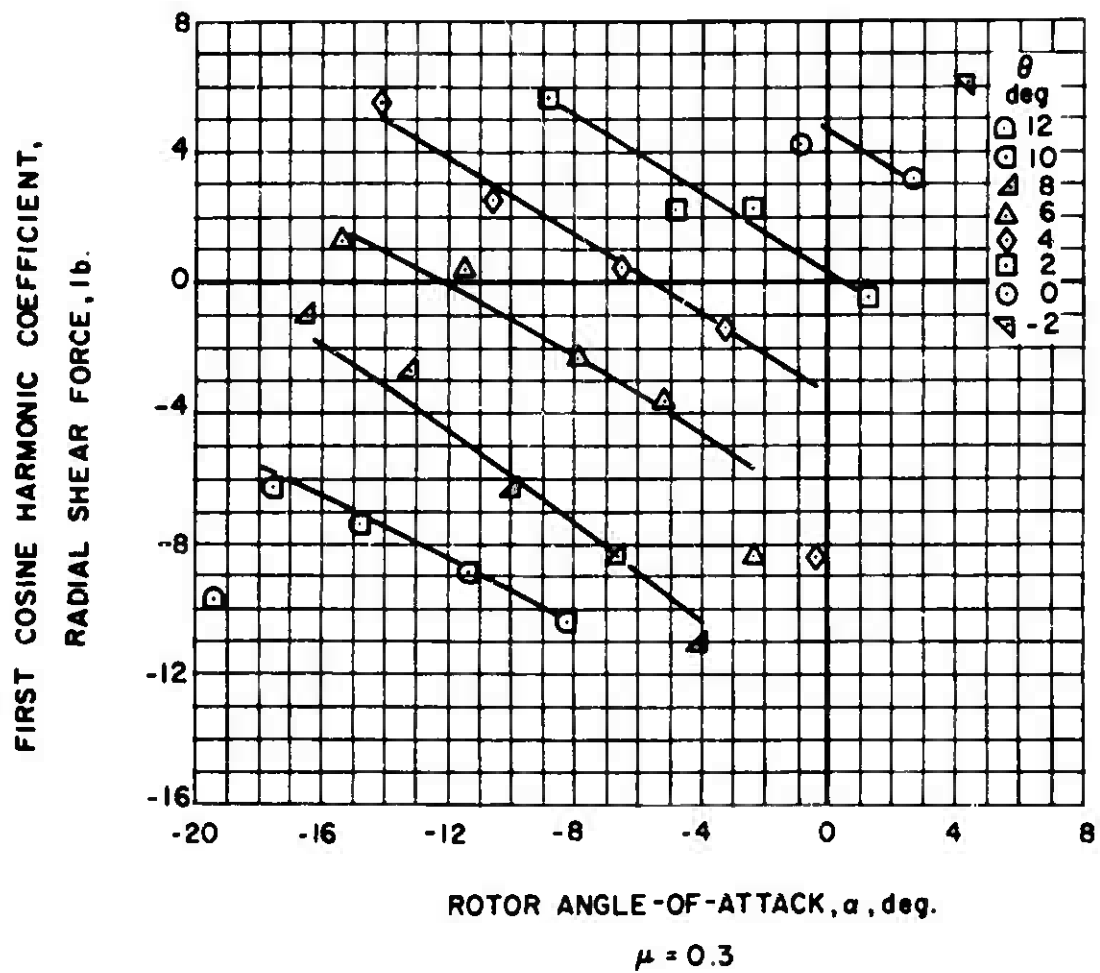


Figure 61. Experimental Radial Shear Force.

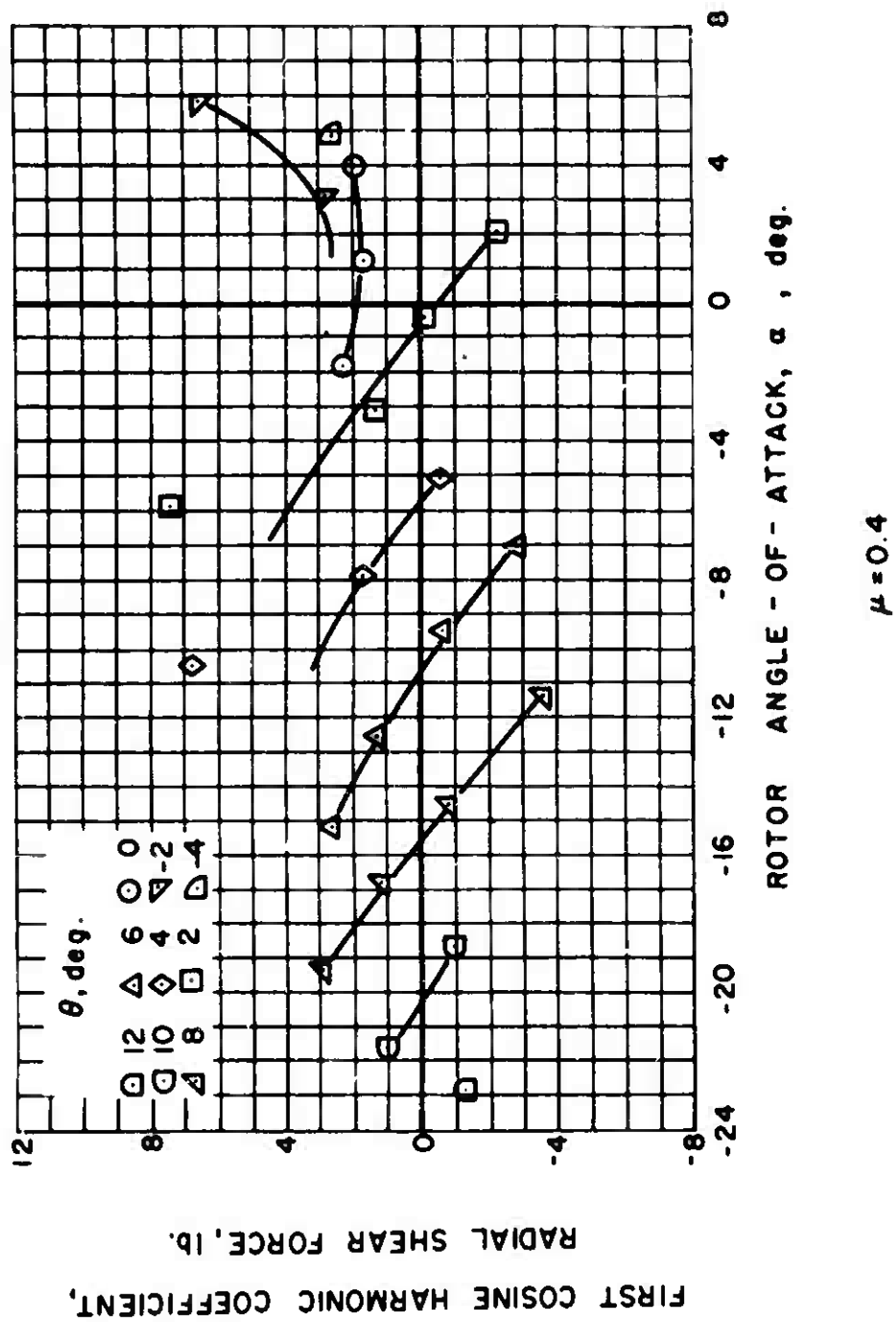


Figure 62. Experimental Radial Shear Force.

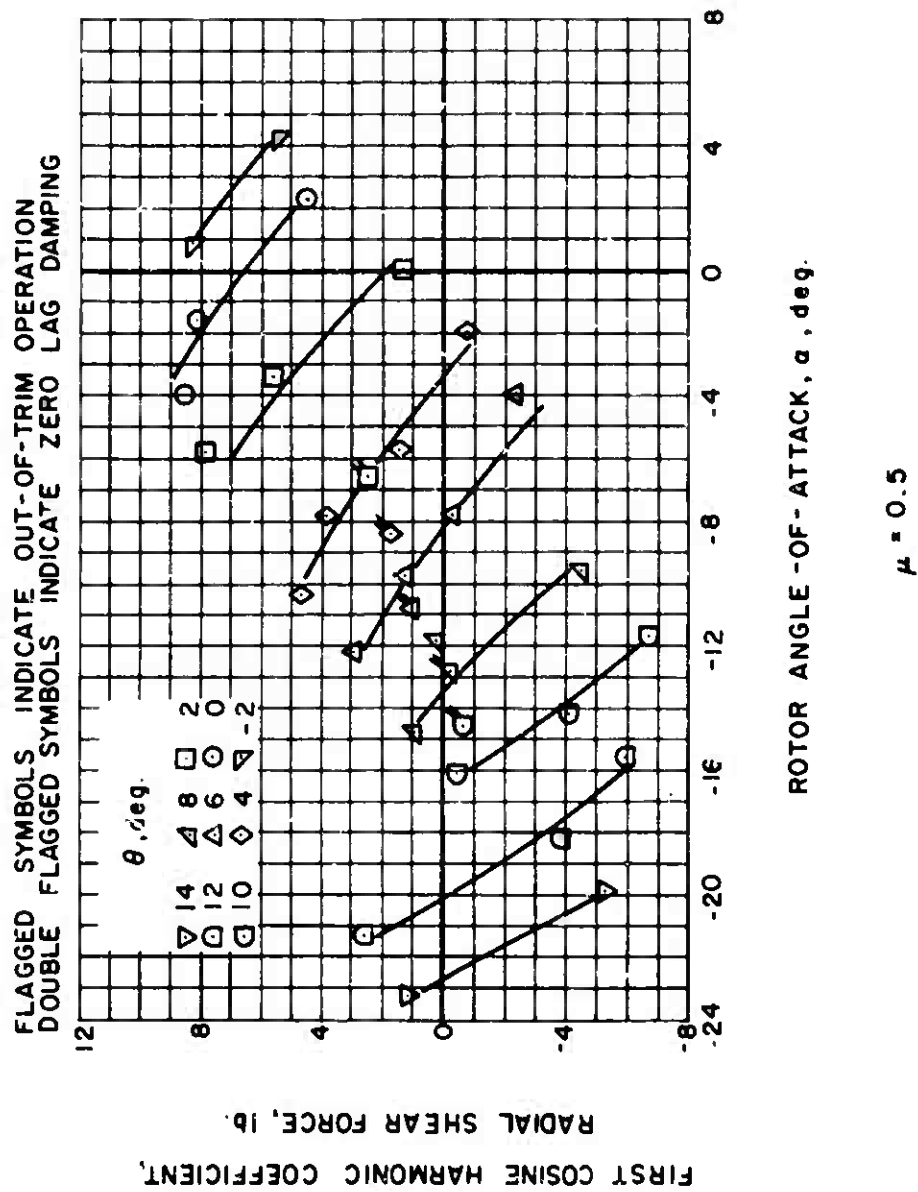


Figure 63. Experimental Radial Shear Force.

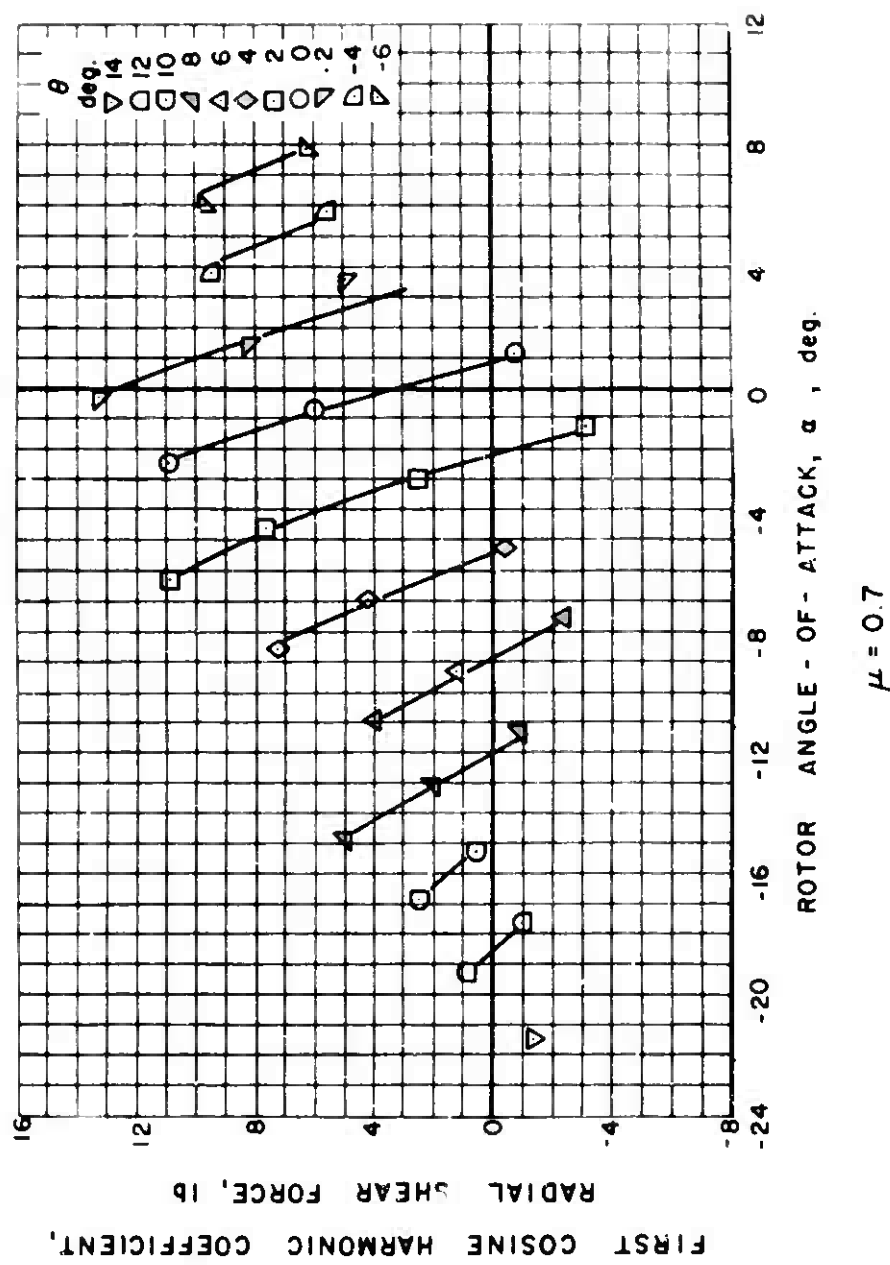
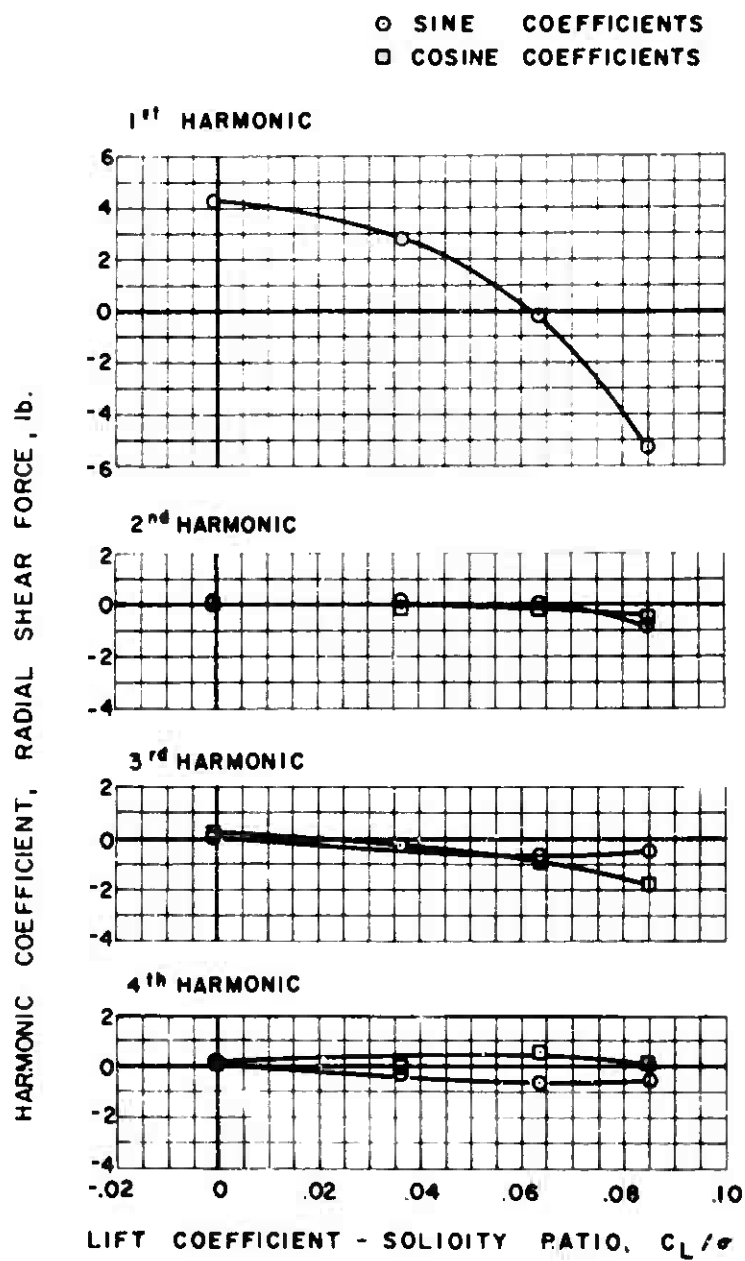
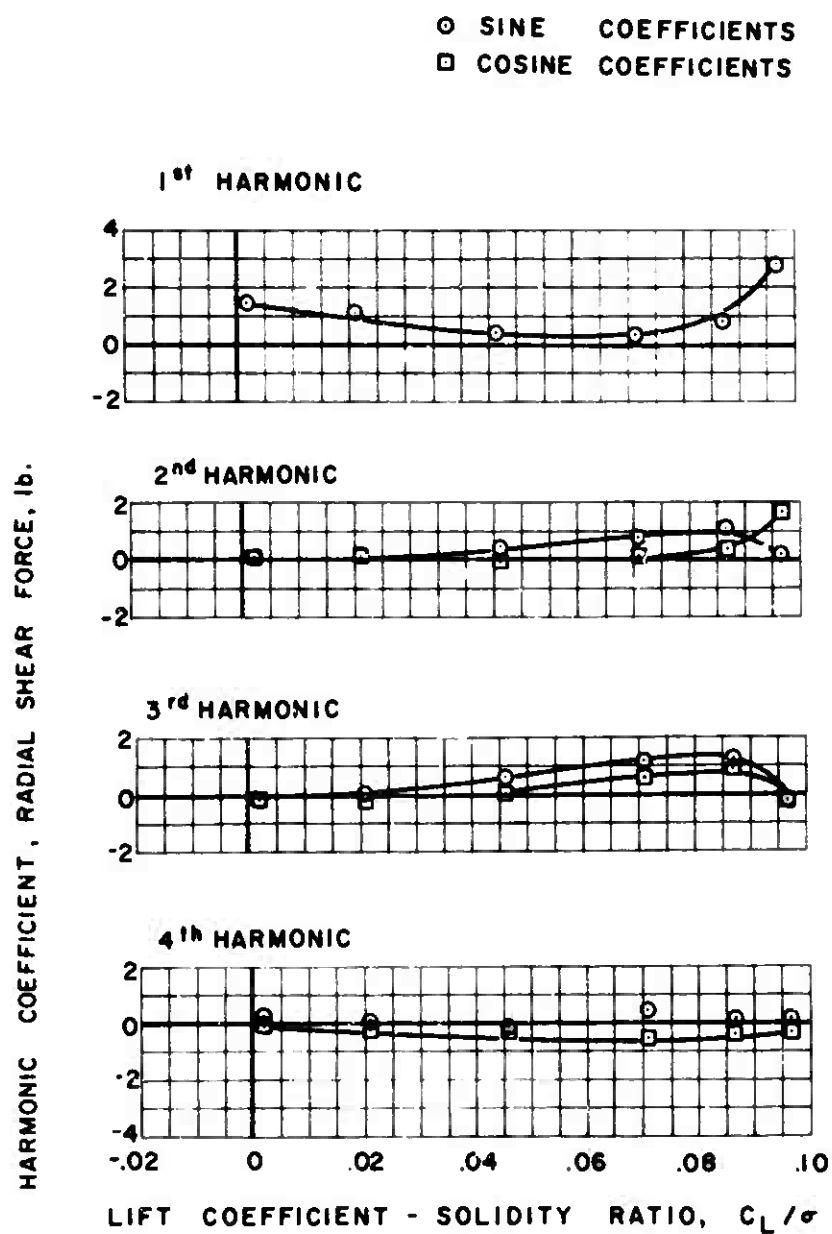


Figure 64. Experimental Radial Shear Force.



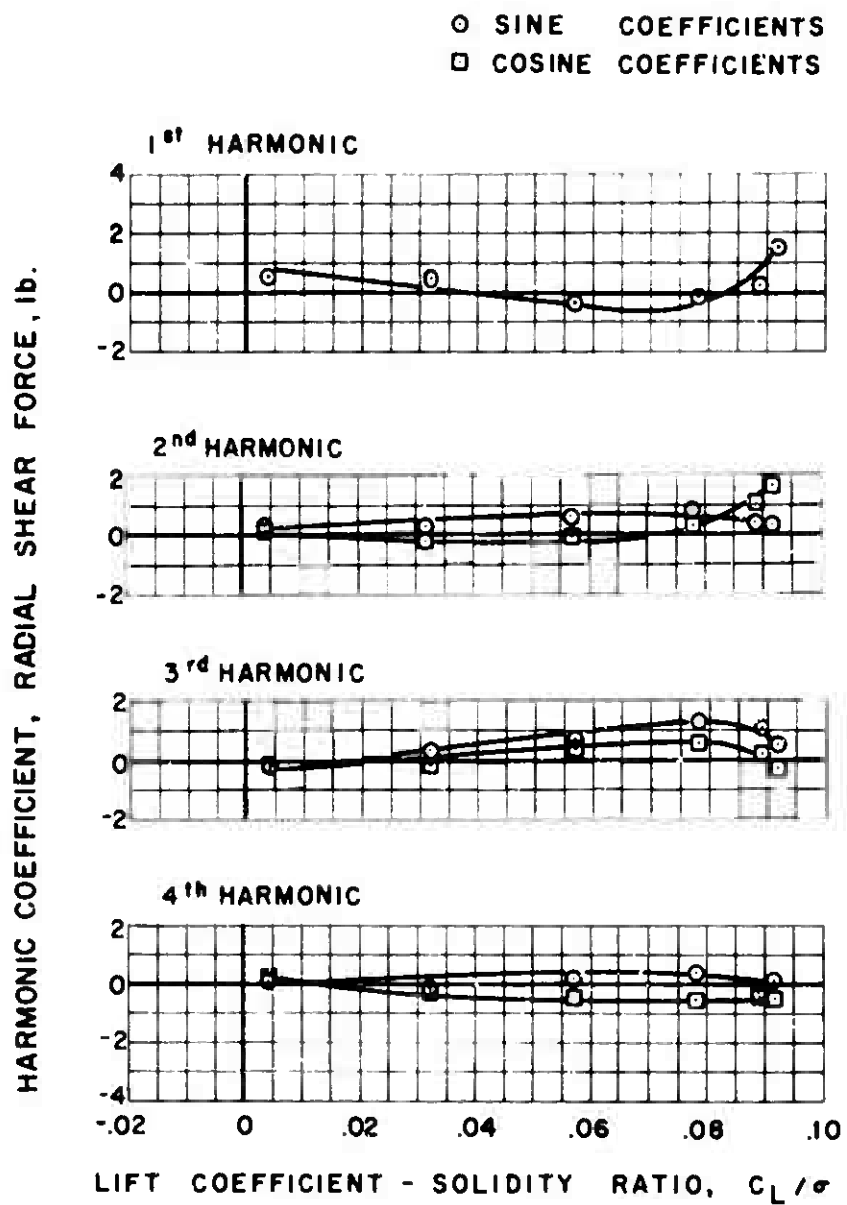
$$\mu = 0.2 \quad \alpha_s = 0 \text{ deg.}$$

Figure 65. Experimental Radial Shear Force.



$$\mu = 0.2 \quad \alpha_s = -4 \text{ deg.}$$

Figure 66. Experimental Radial Shear Force.



$$\mu = 0.2 \quad \alpha_s = -8 \text{ deg.}$$

Figure 67. Experimental Radial Shear Force.

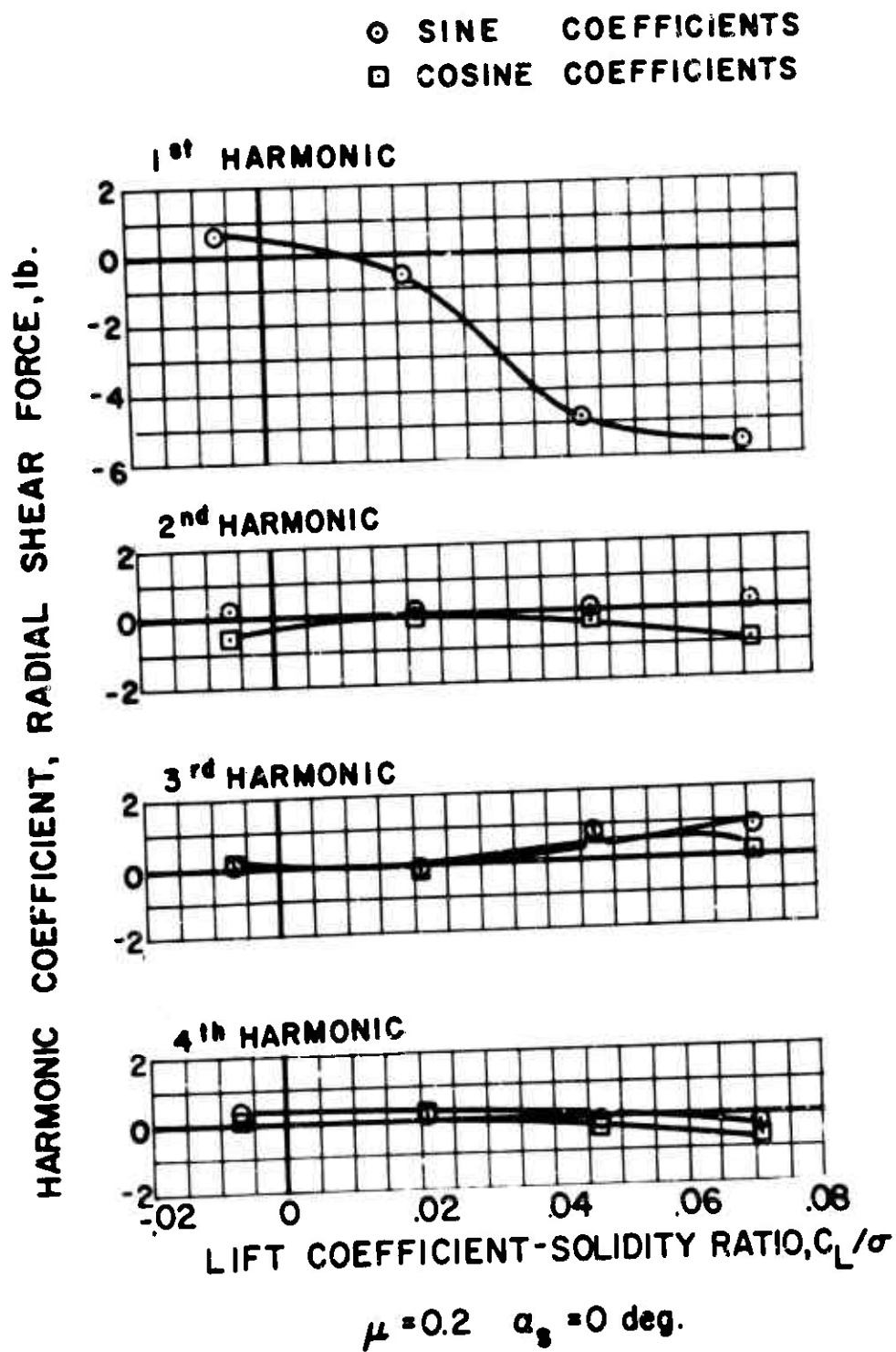
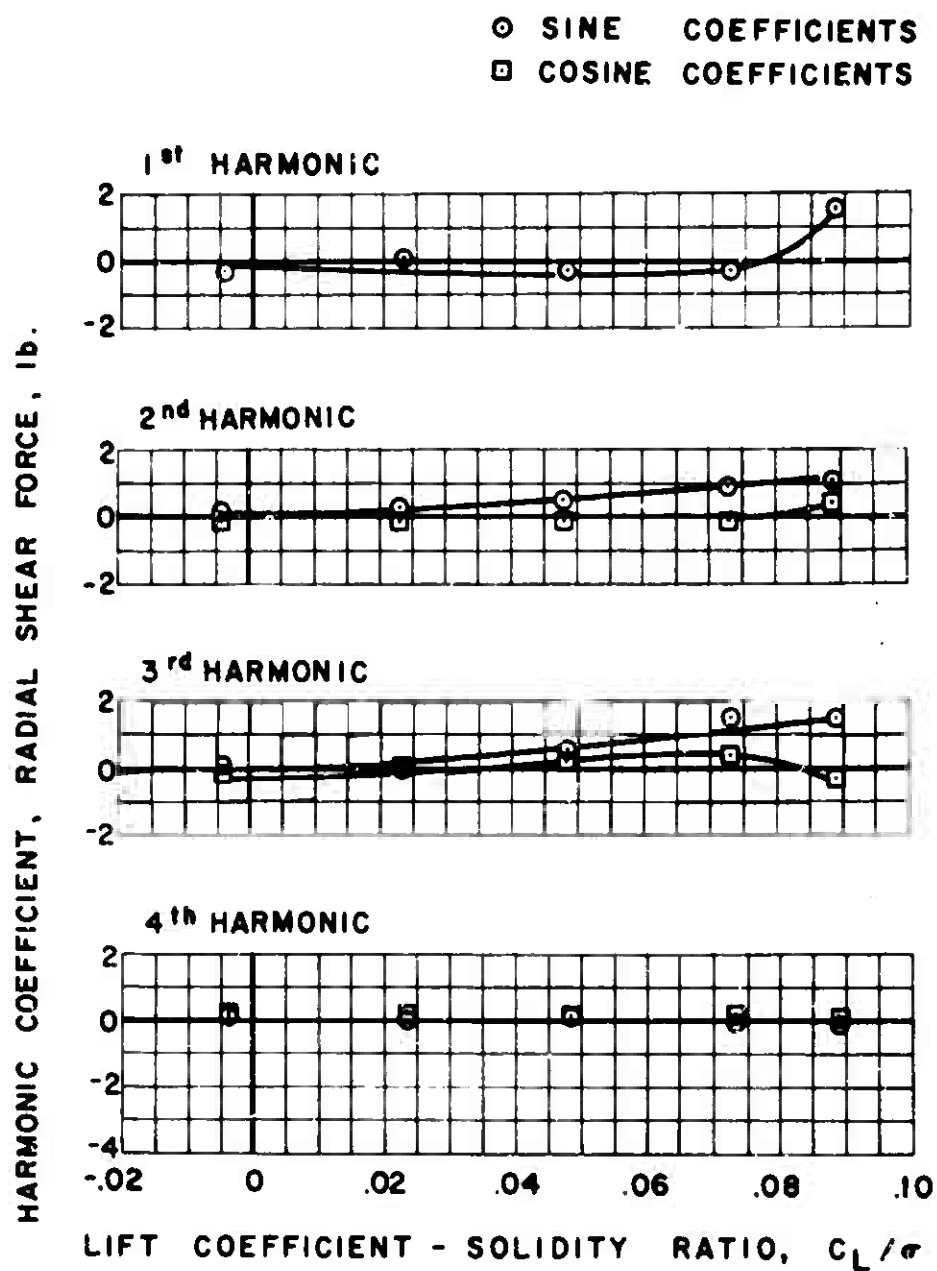
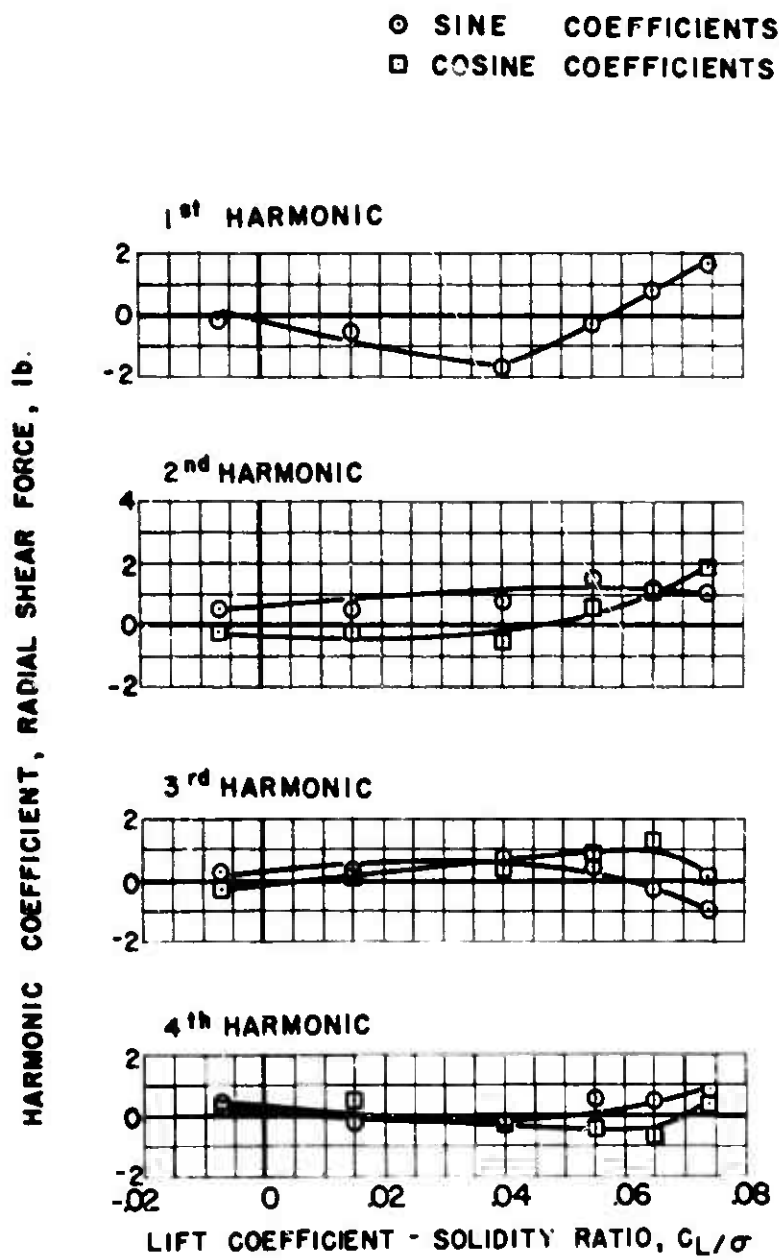


Figure 68. Experimental Radial Shear Force, Out of Trim, -4 Degree Longitudinal Flapping.



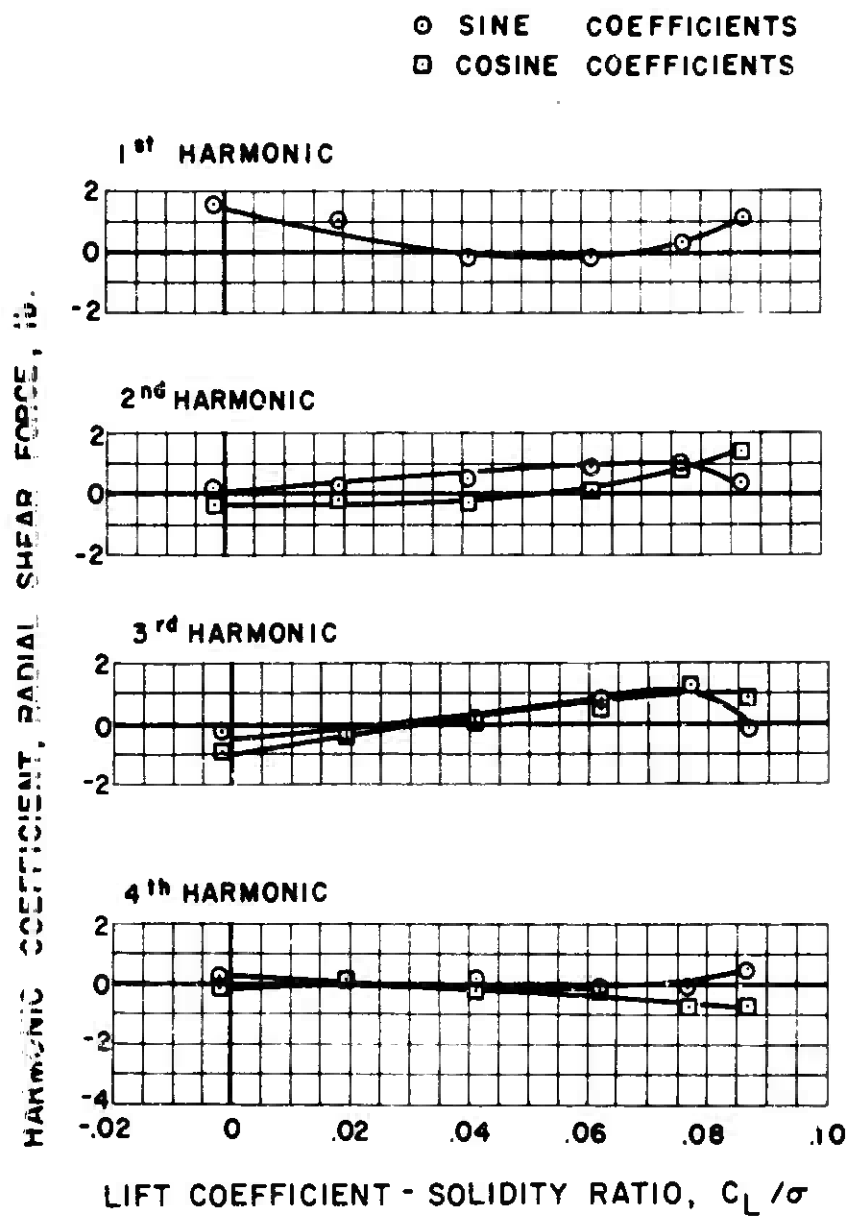
$$\mu = 0.2 \quad \alpha_s = -4 \text{ deg.}$$

Figure 69. Experimental Radial Shear Force, Zero Lag Damping.



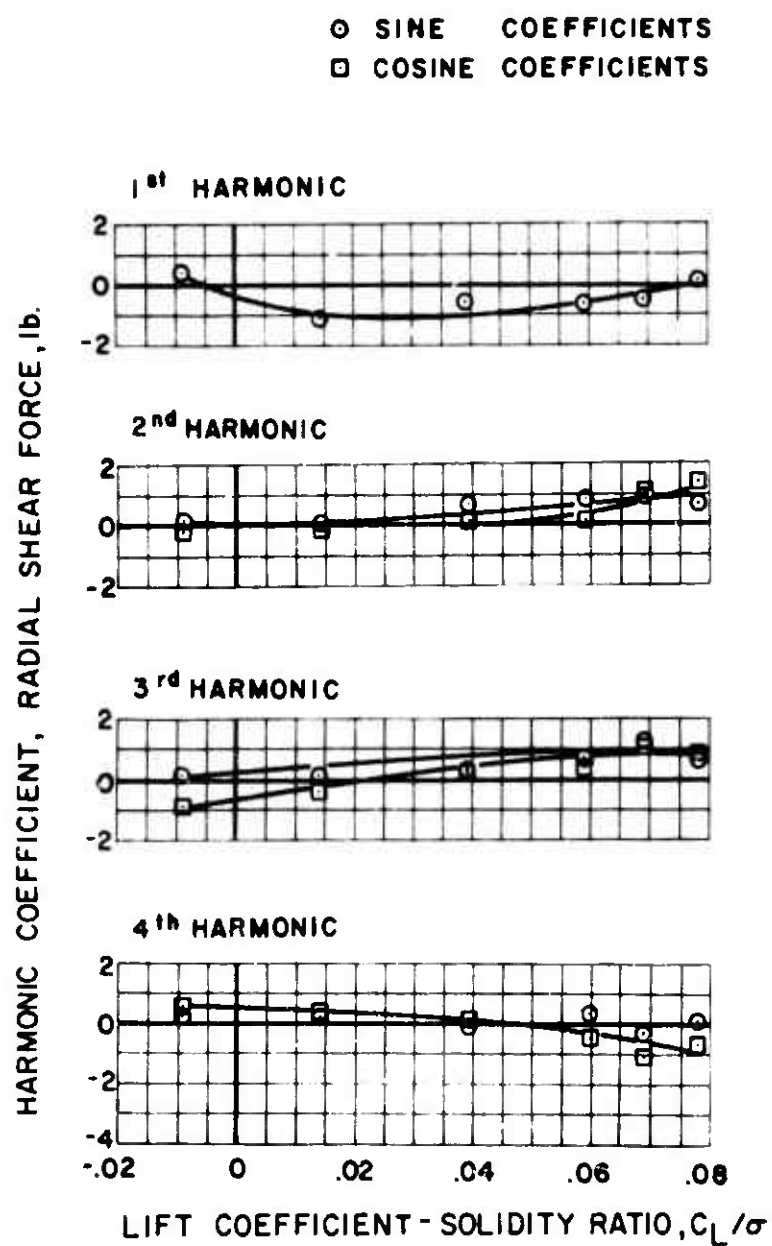
$$\mu = 0.3 \quad \alpha_s = 0 \text{ deg.}$$

Figure 70. Experimental Radial Shear Force.



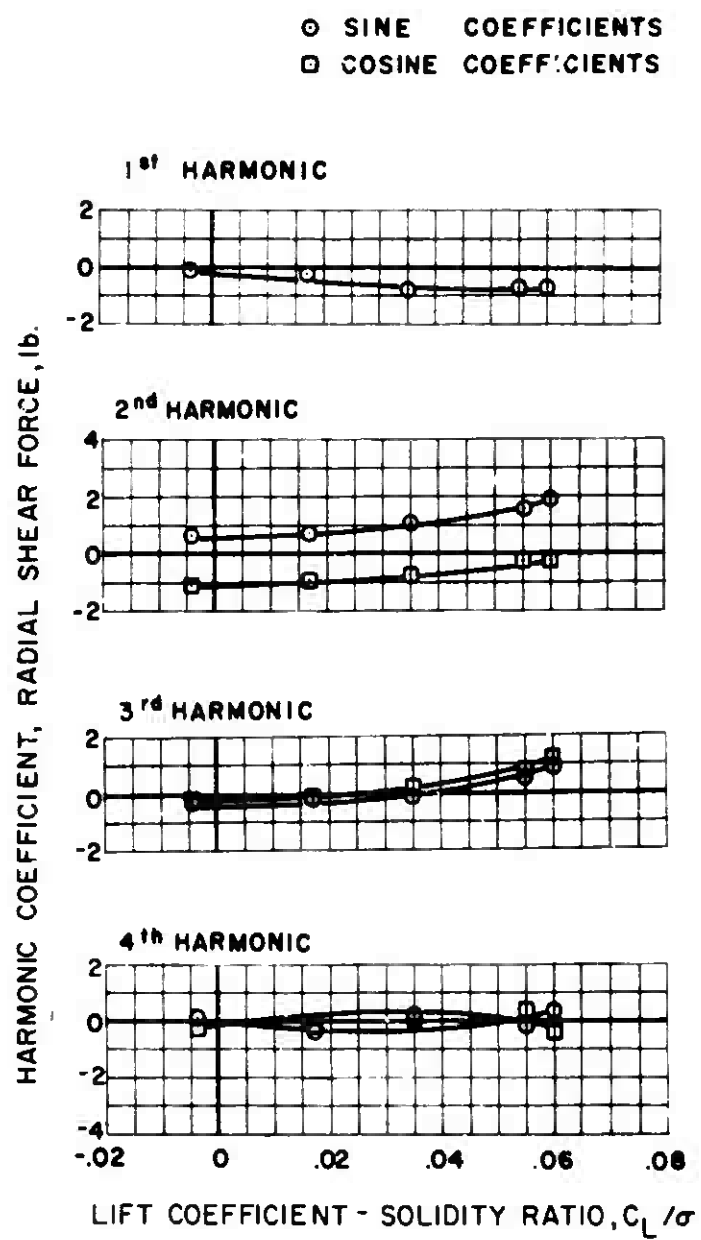
$$\mu = 0.3 \quad \alpha_s = -4 \text{ deg.}$$

Figure 71. Experimental Radial Shear Force.



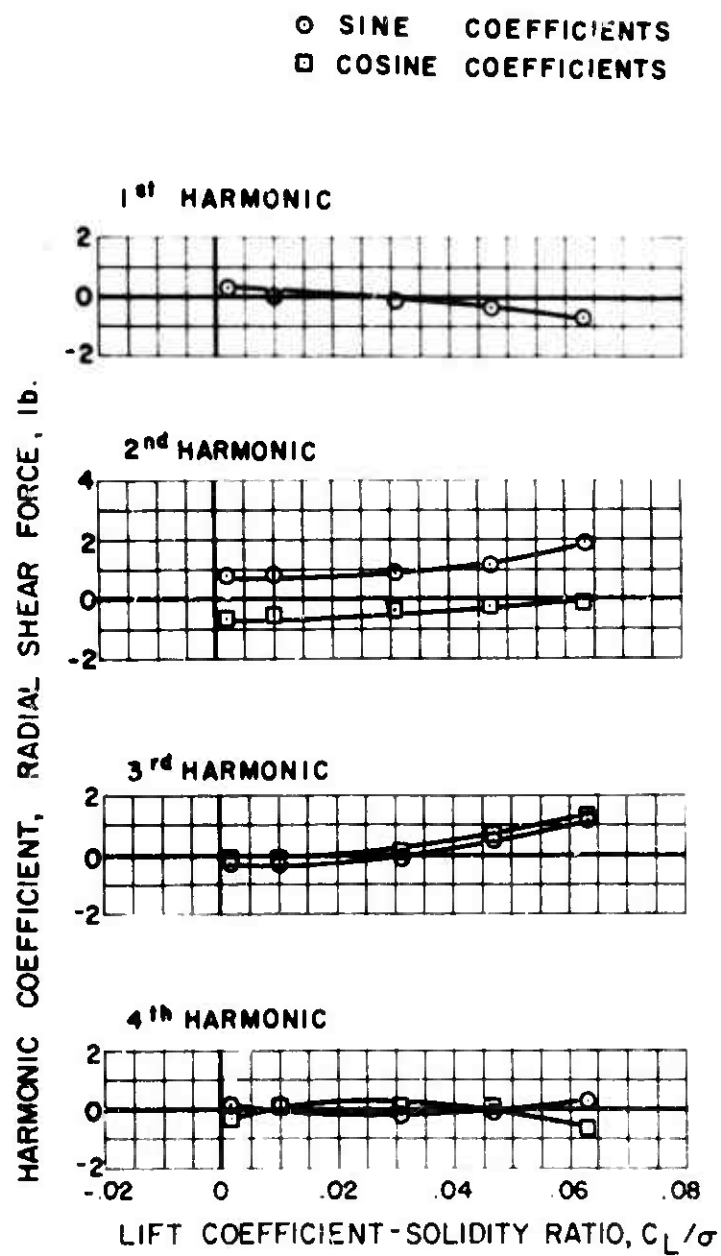
$$\mu = 0.3 \quad \alpha_s = -8 \text{ deg}$$

Figure 72. Experimental Radial Shear Force.



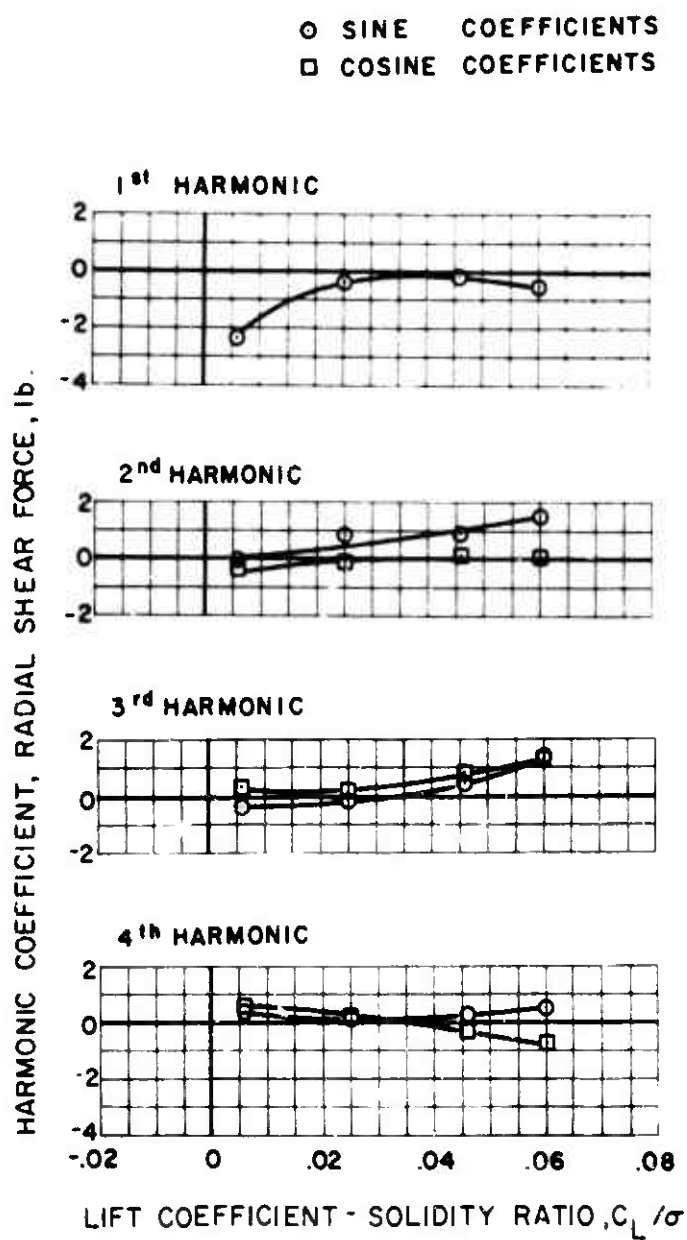
$$\mu = 0.4 \quad \alpha_s = 4 \text{ deg.}$$

Figure 73. Experimental Radial Shear Force.



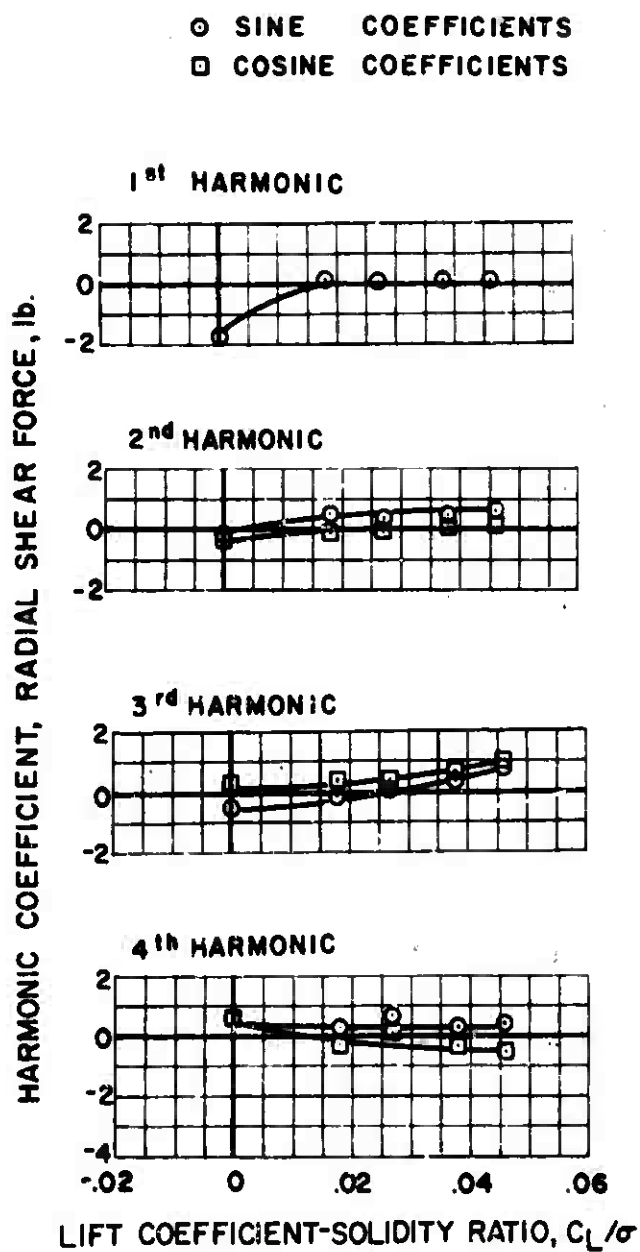
$$\mu = 0.4 \quad \alpha_s = 0 \text{ deg.}$$

Figure 74. Experimental Radial Shear Force.



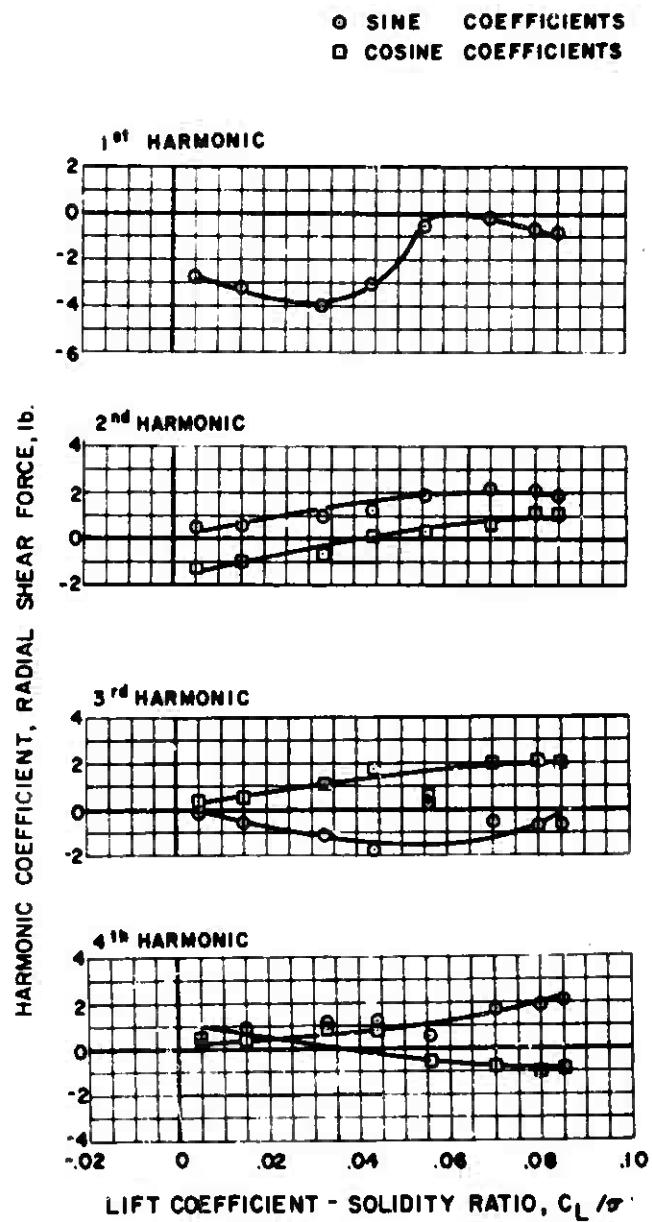
$$\mu = 0.4 \quad \alpha_s = -4 \text{ deg.}$$

Figure 75. Experimental Radial Shear Force.



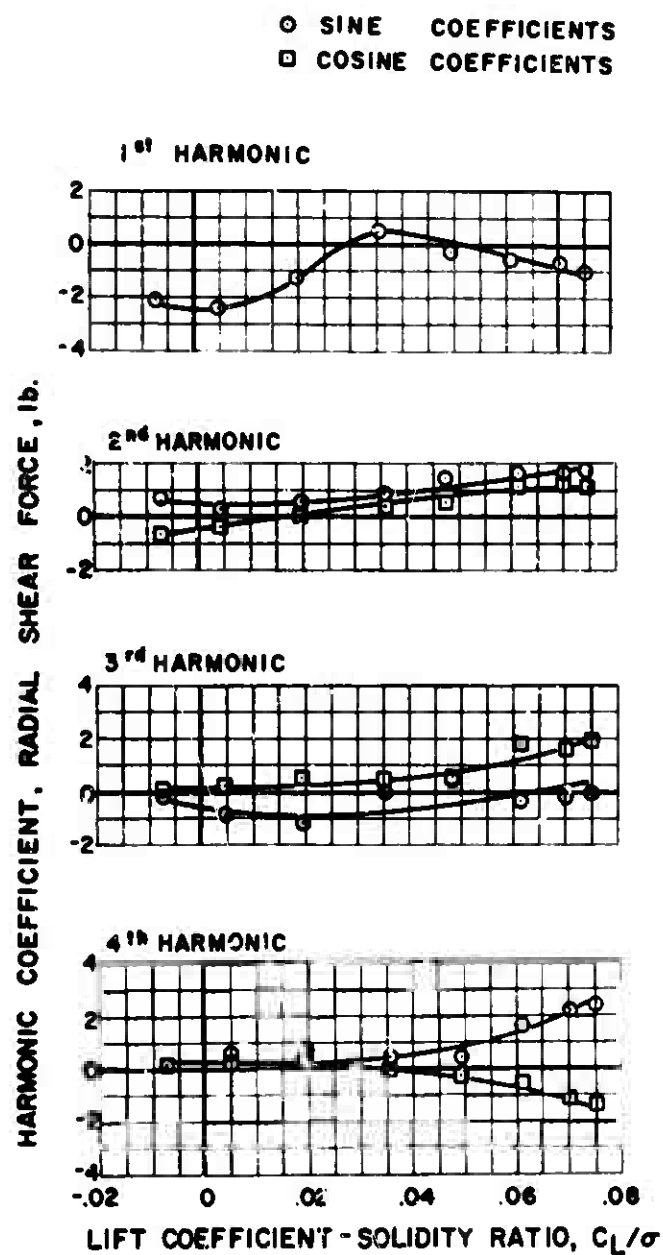
$$\mu = 0.4 \quad \alpha_s = -8 \text{ deg.}$$

Figure 76. Experimental Radial Shear Force.



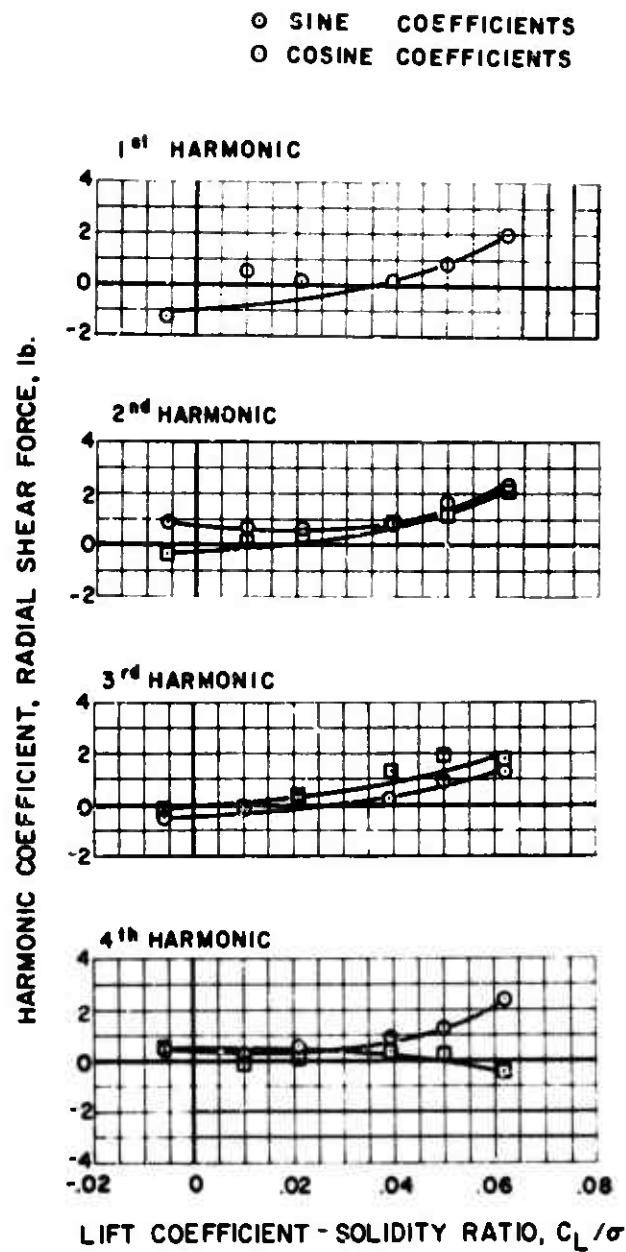
$$\mu = 0.5 \quad \alpha_s = 0 \text{ deg.}$$

Figure 77. Experimental Radial Shear Force.



$\mu = 0.5 \quad \alpha_s = -4 \text{ deg.}$

Figure 78. Experimental Radial Shear Force.



$$\mu = 0.5 \quad \alpha_s = -8 \text{ deg.}$$

Figure 79. Experimental Radial Shear Force.

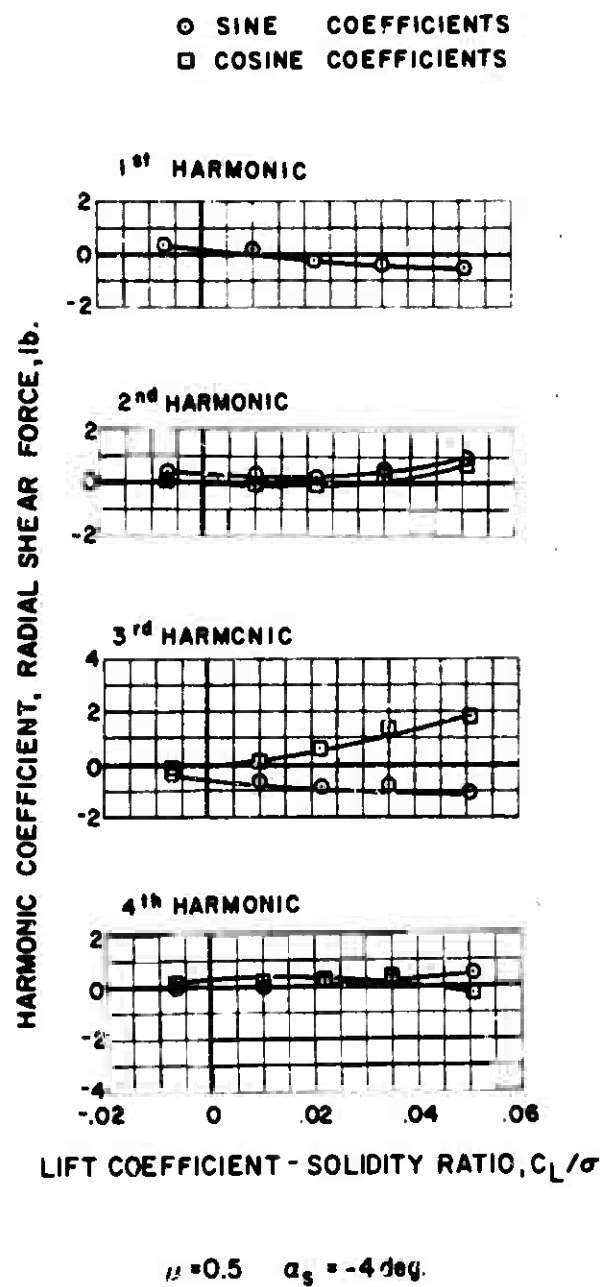
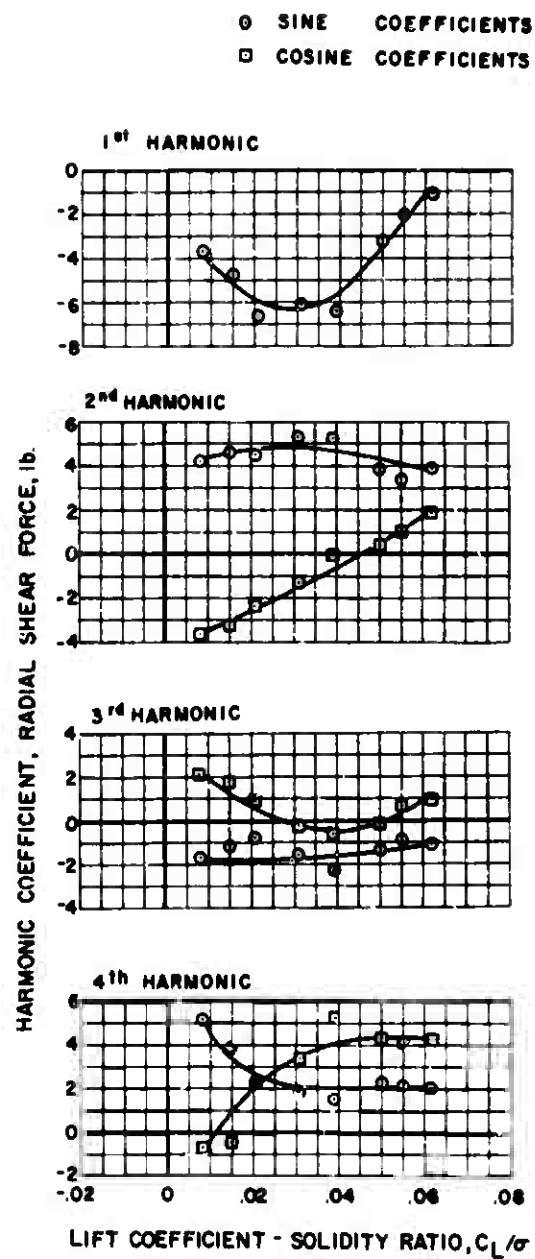


Figure 80. Experimental Radial Shear Force, Zero Lag Damping.



$$\mu = 0.7 \quad \alpha_0 = 4 \text{ deg.}$$

Figure 81. Experimental Radial Shear Force.

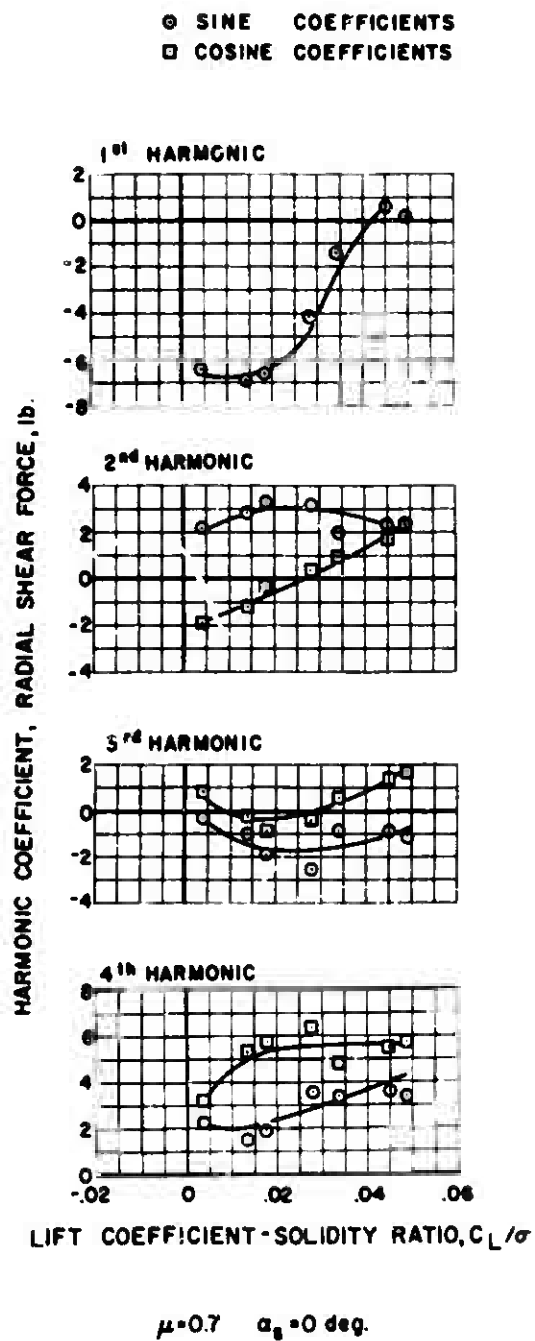
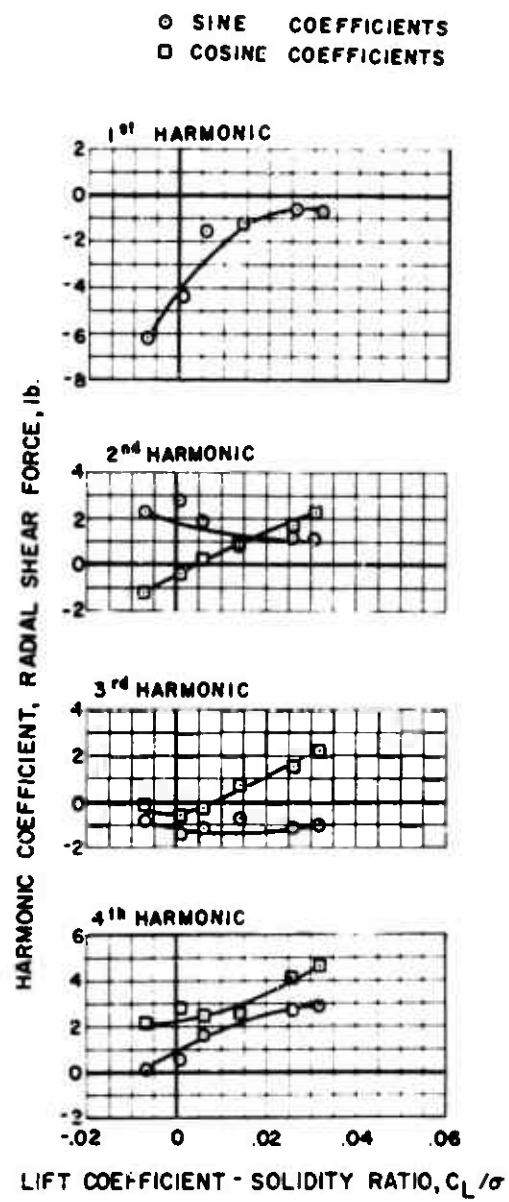
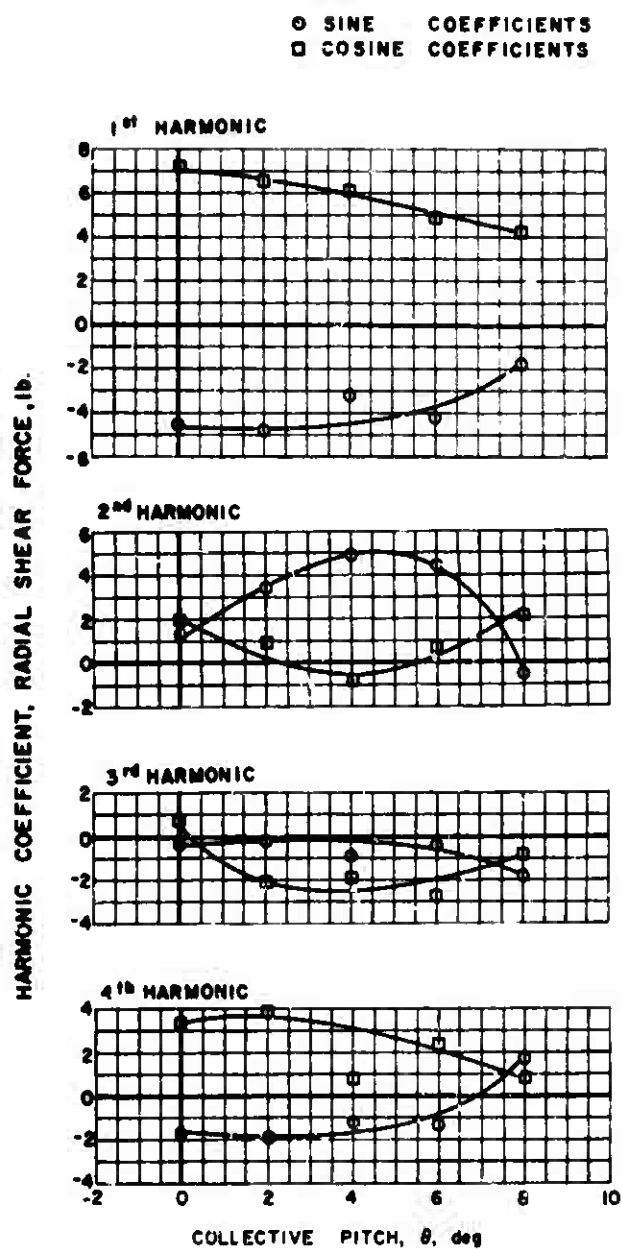


Figure 82. Experimental Radial Shear Force.



$$\mu = 0.7 \quad \alpha_s = -4 \text{ deg.}$$

Figure 83. Experimental Radial Shear Force.

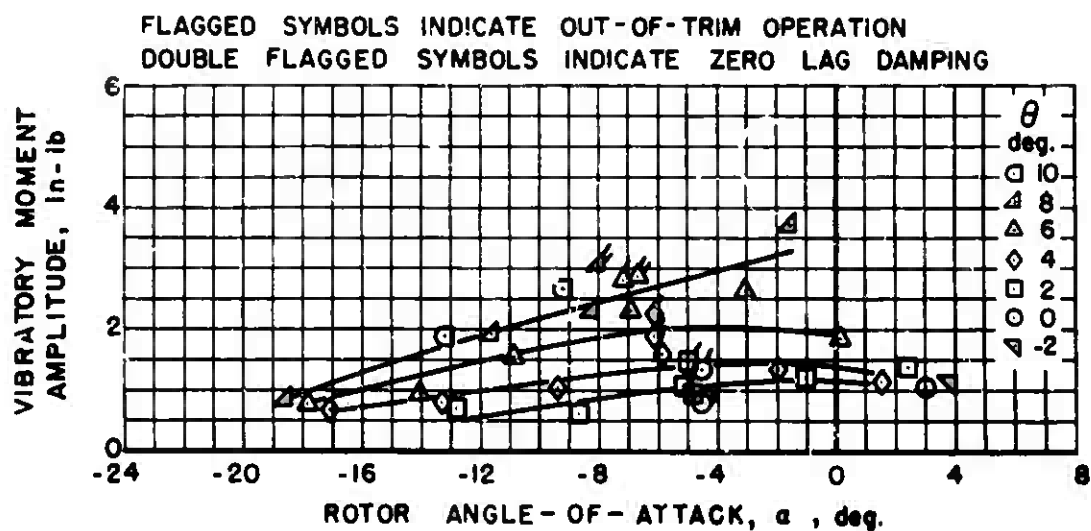


$$\mu = 1.0 \quad \alpha_s = 0 \text{ deg.}$$

Figure 84. Experimental Radial Shear Force.

APPENDIX III

EXPERIMENTAL VIBRATORY MOMENT AMPLITUDE FIGURES

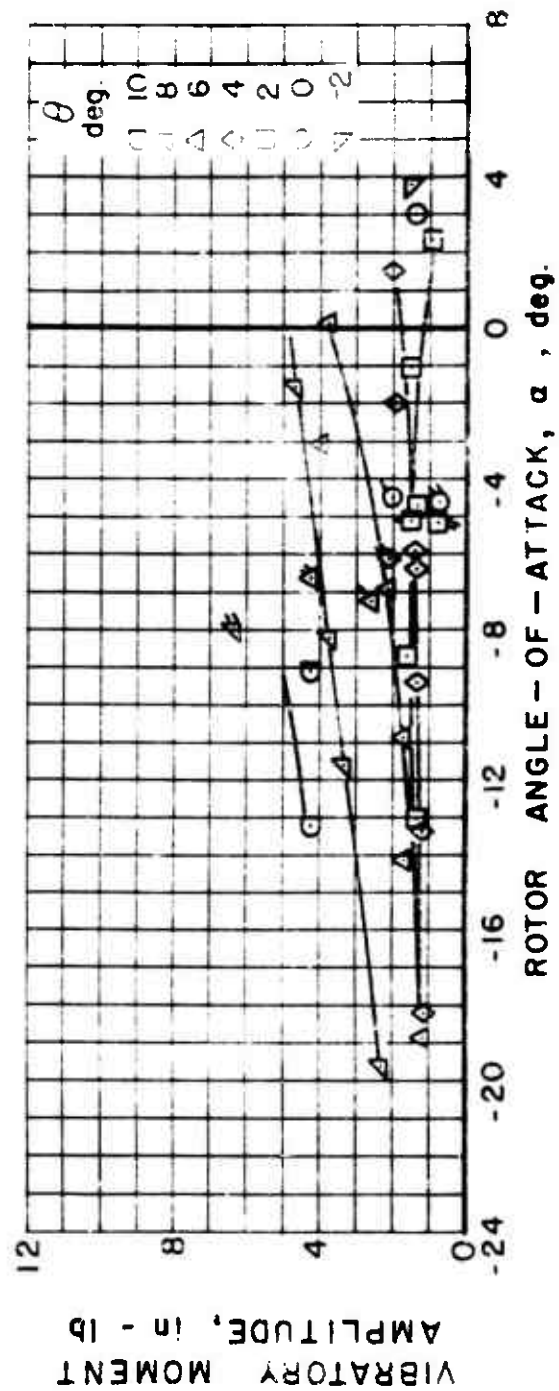


(a) FLATWISE BENDING MOMENT, 21 %R

Figure 85. Experimental Vibratory Moment Amplitude, $\mu = 0.2$.

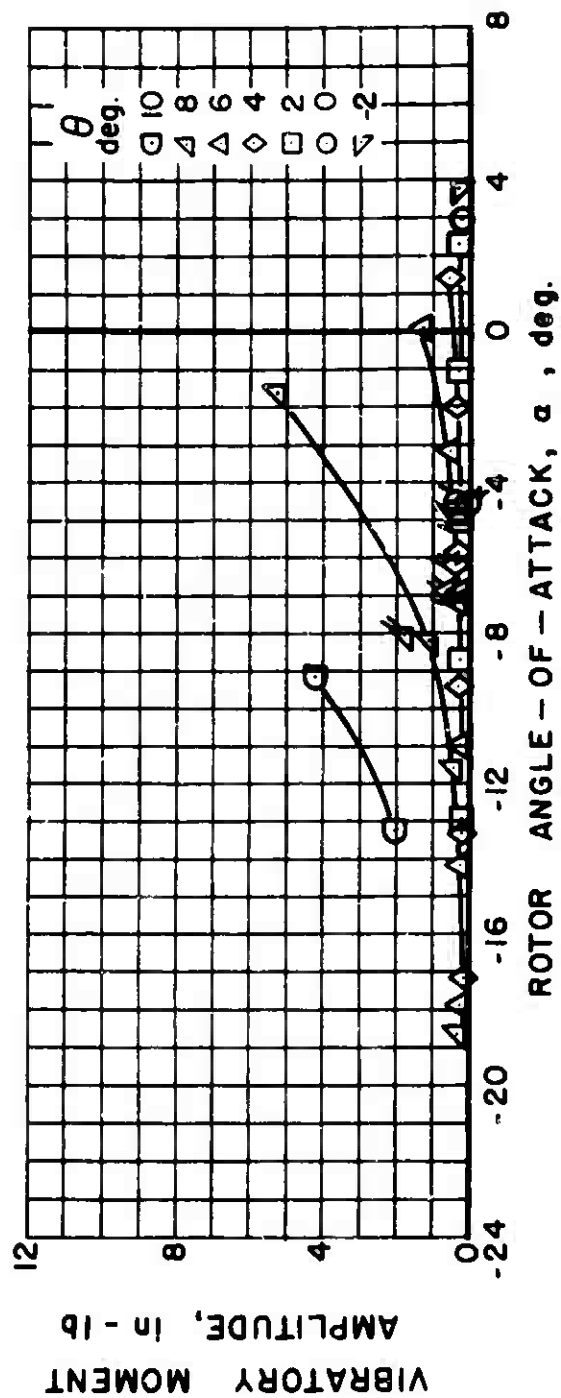
(b) EDGEWISE BENDING MOMENT, 21% R

Figure 85. Continued.



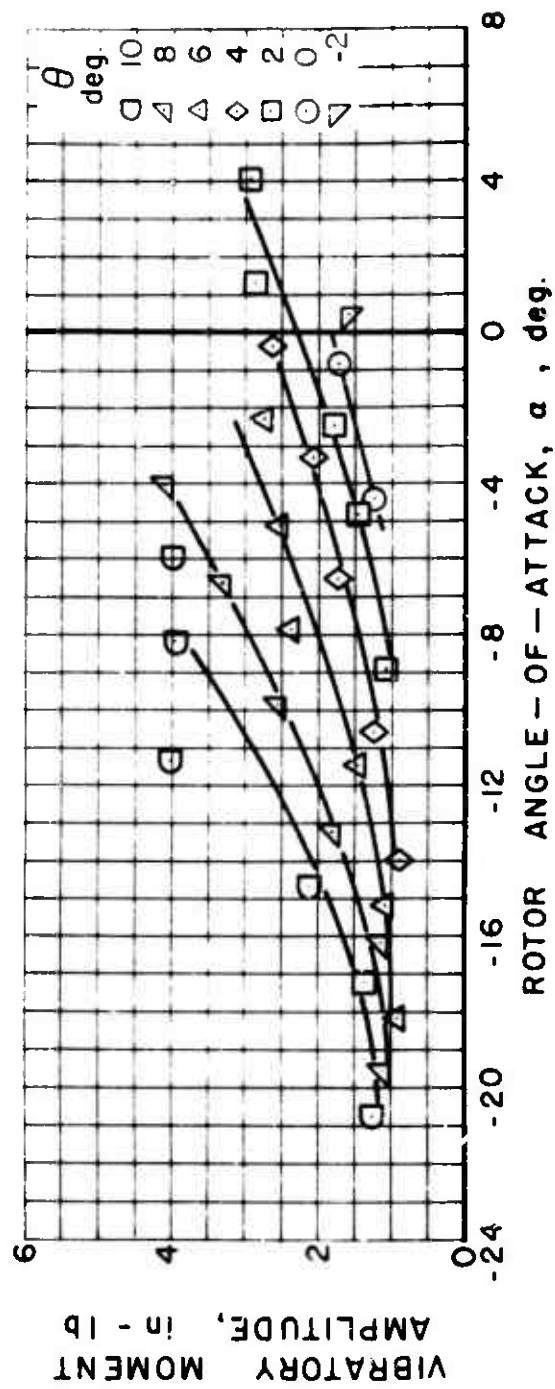
(c) EDGEWISE BENDING MOMENT, 47 % R

Figure 85. Continued.



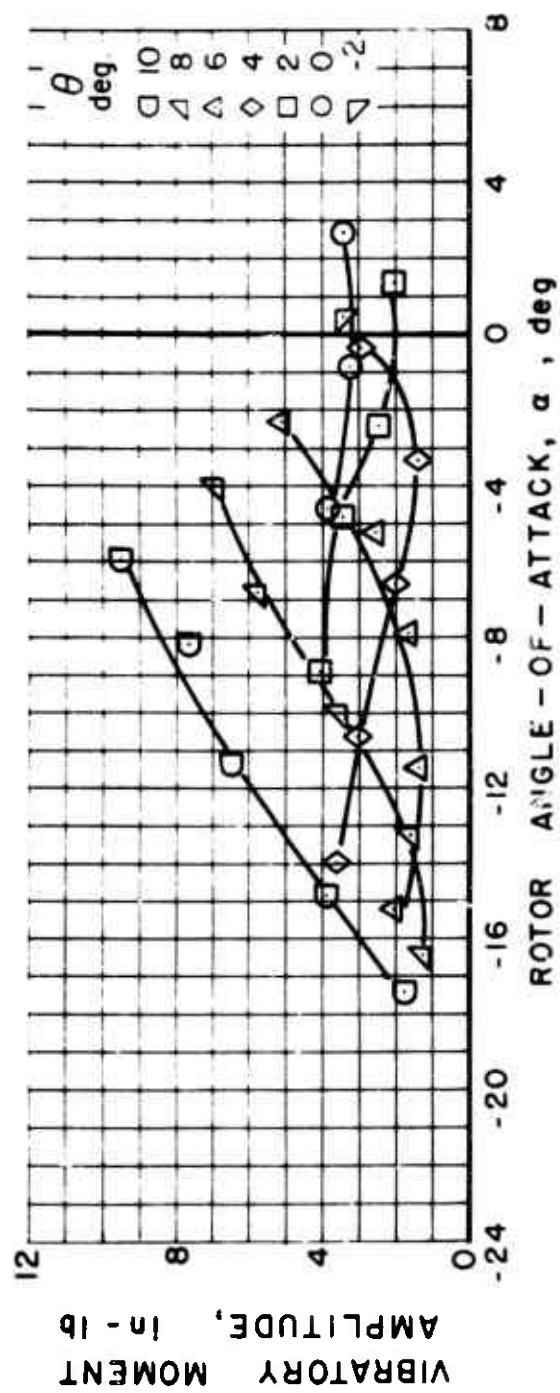
(d) TORSIONAL MOMENT, 17.5 % R

Figure 85. Concluded.



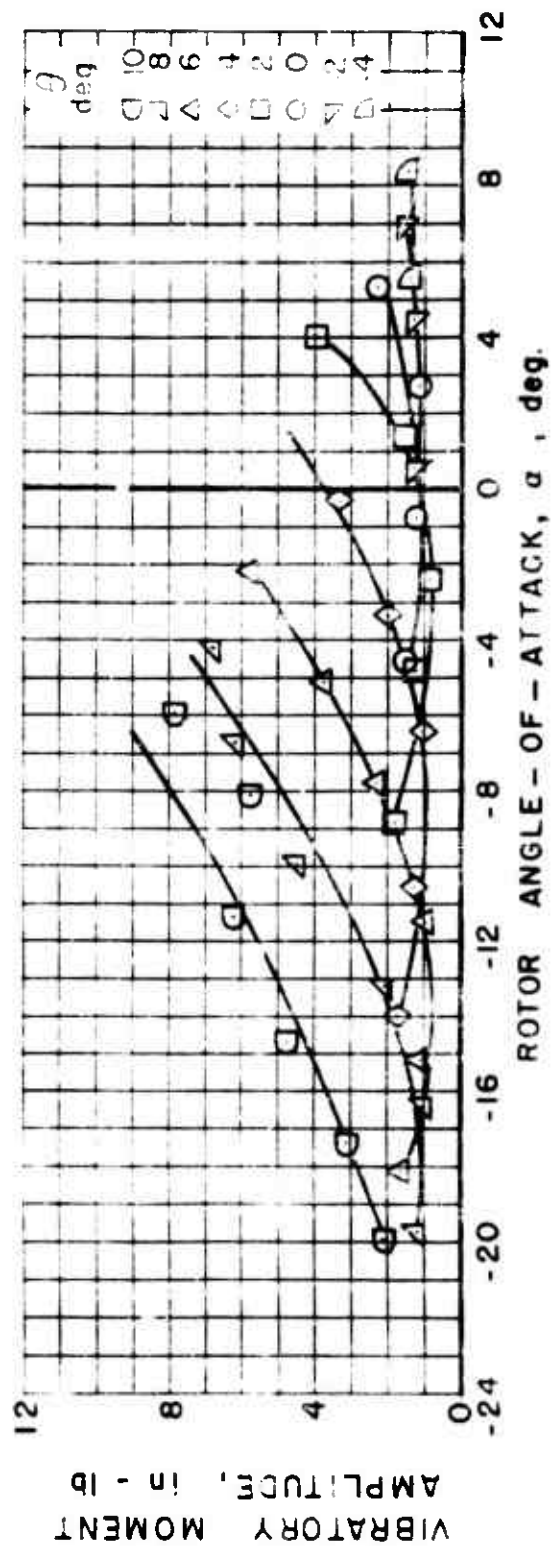
(a) FLATWISE BENDING MOMENT, 21 % R

Figure 86. Experimental Vibratory Moment Amplitude, $\mu = 0.3$.



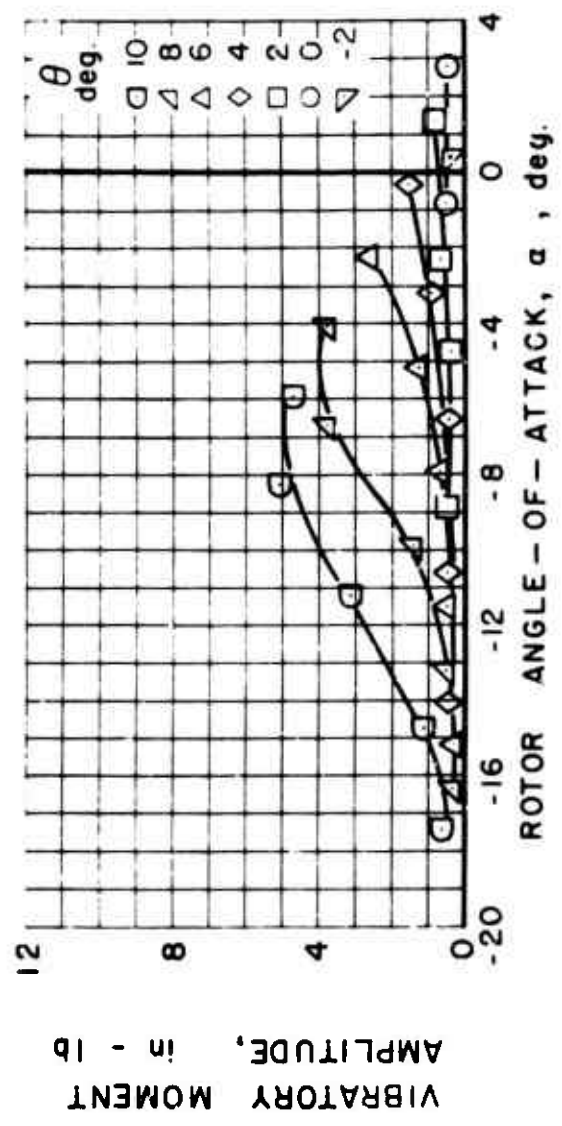
(b) EDGEWISE BENDING MOMENT, 21 % R

Figure 86. Continued.



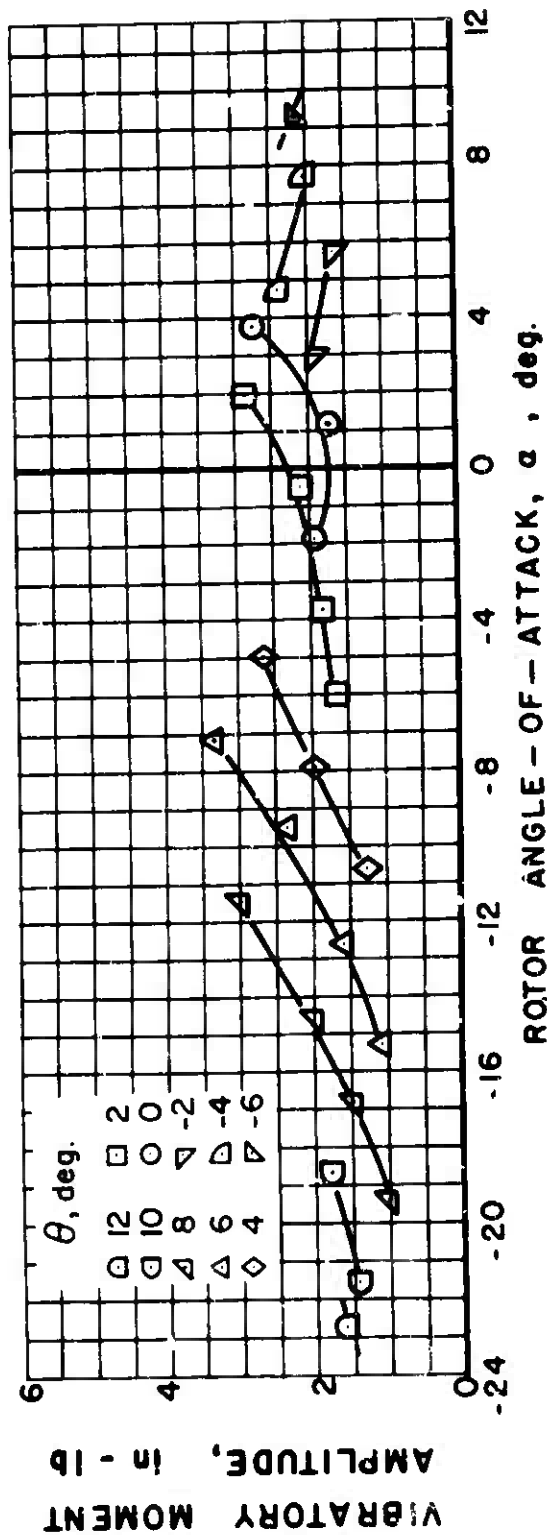
(c) EDGEWISE BENDING MOMENT, 47 % R

Figure 86. Continued.



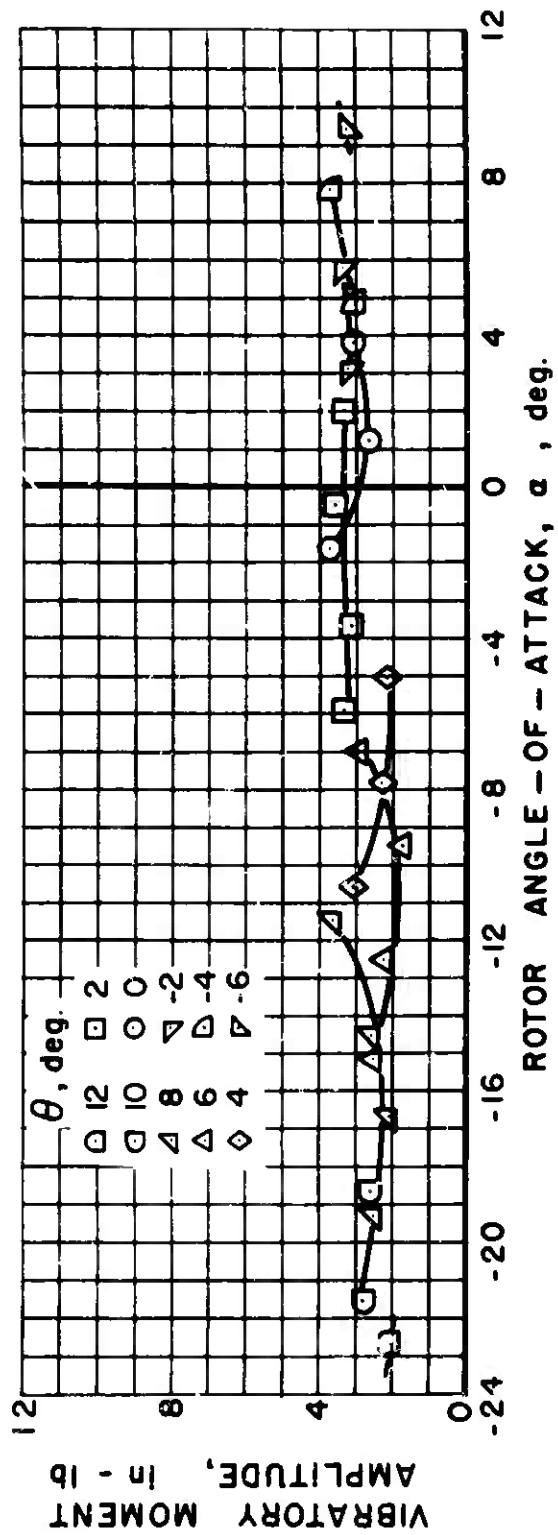
(d) TORSIONAL MOMENT, 17.5 % P

Figure 86. Concluded.



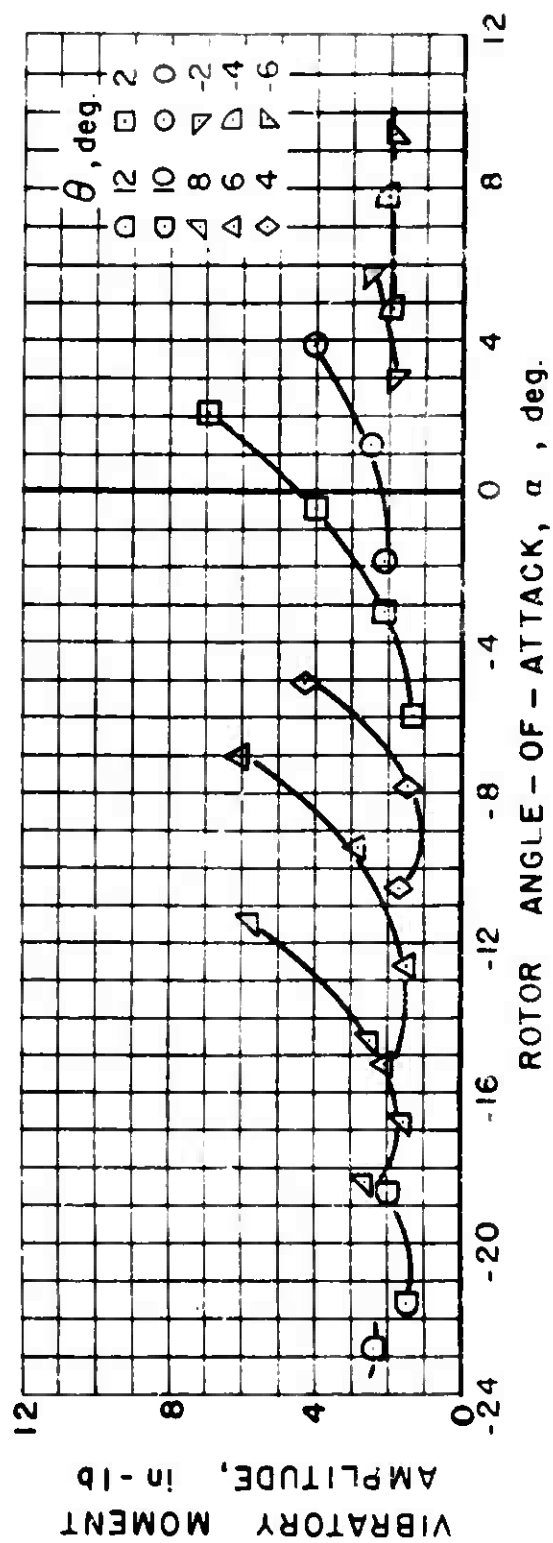
(a) FLATWISE BENDING MOMENT, 21 % R

Figure 87. Experimental Vibratory Moment Amplitude, $\mu = 0.4$.



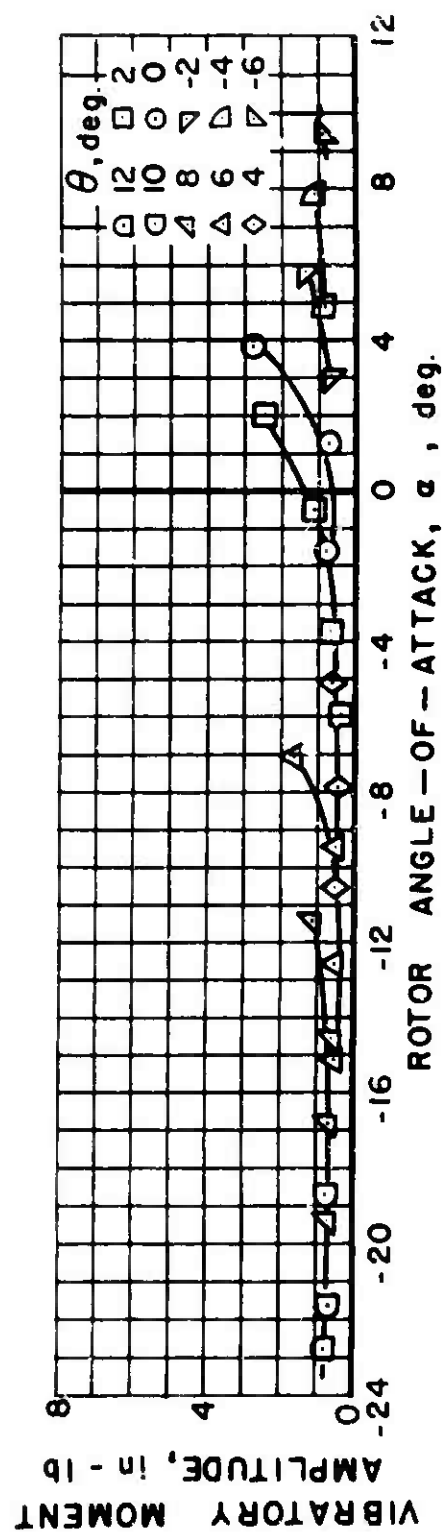
(b) EDGEWISE BENDING MOMENT, 21 %

Figure 87. Continued.



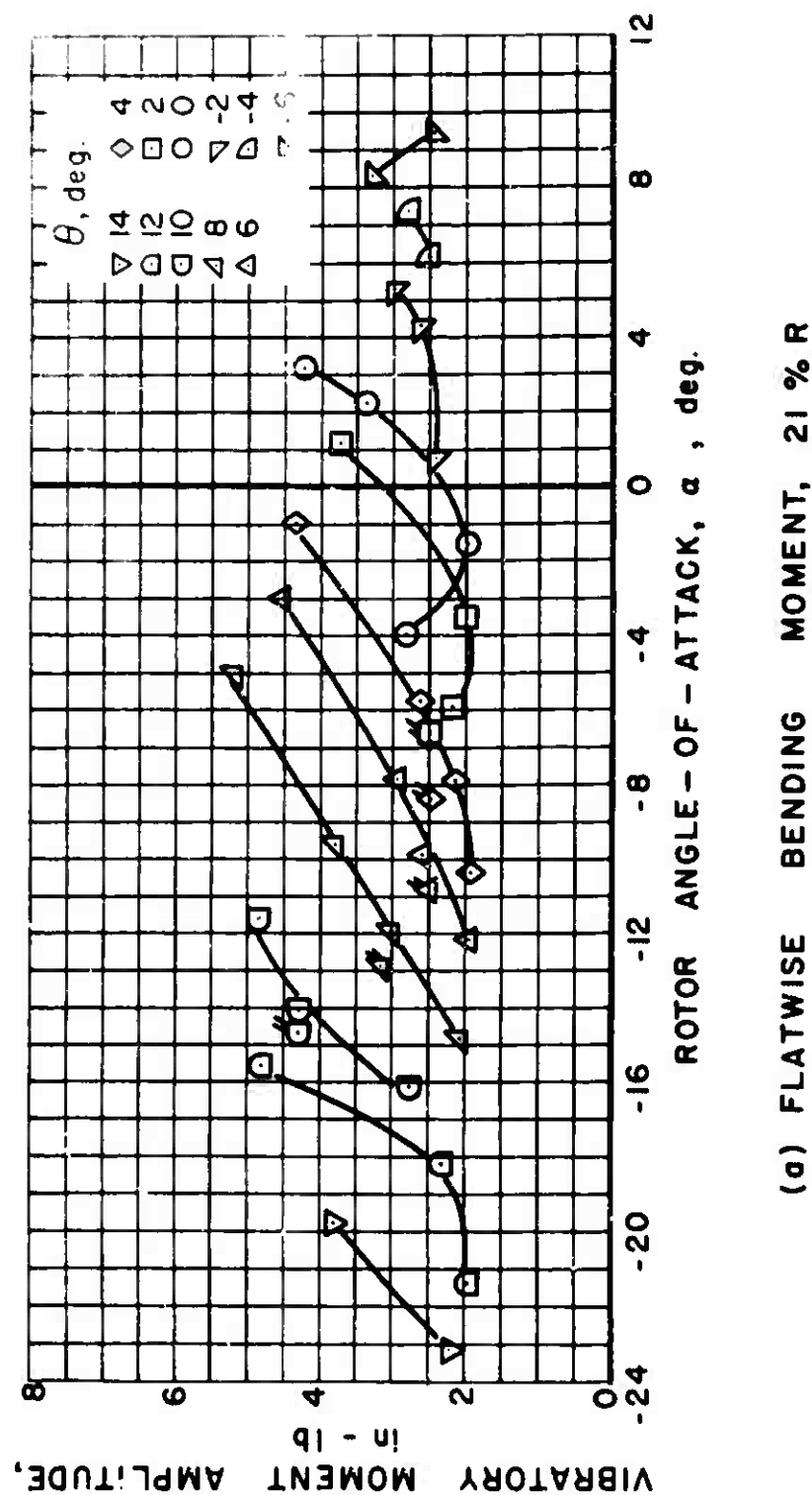
(c) EDGEWISE BENDING MOMENT, 47 % R

Figure 87. Continued.



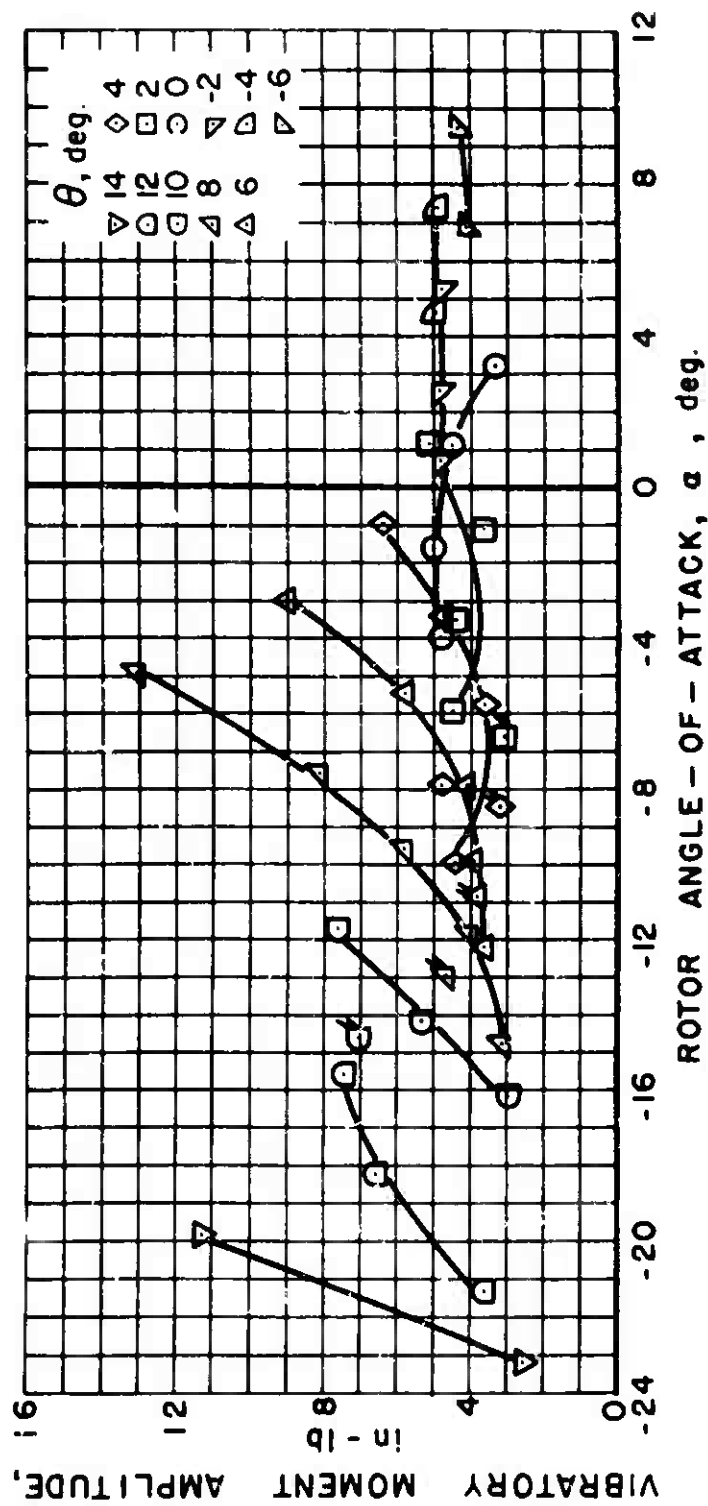
(d) TORSIONAL MOMENT, 17.5 % R

Figure 87. Concluded.



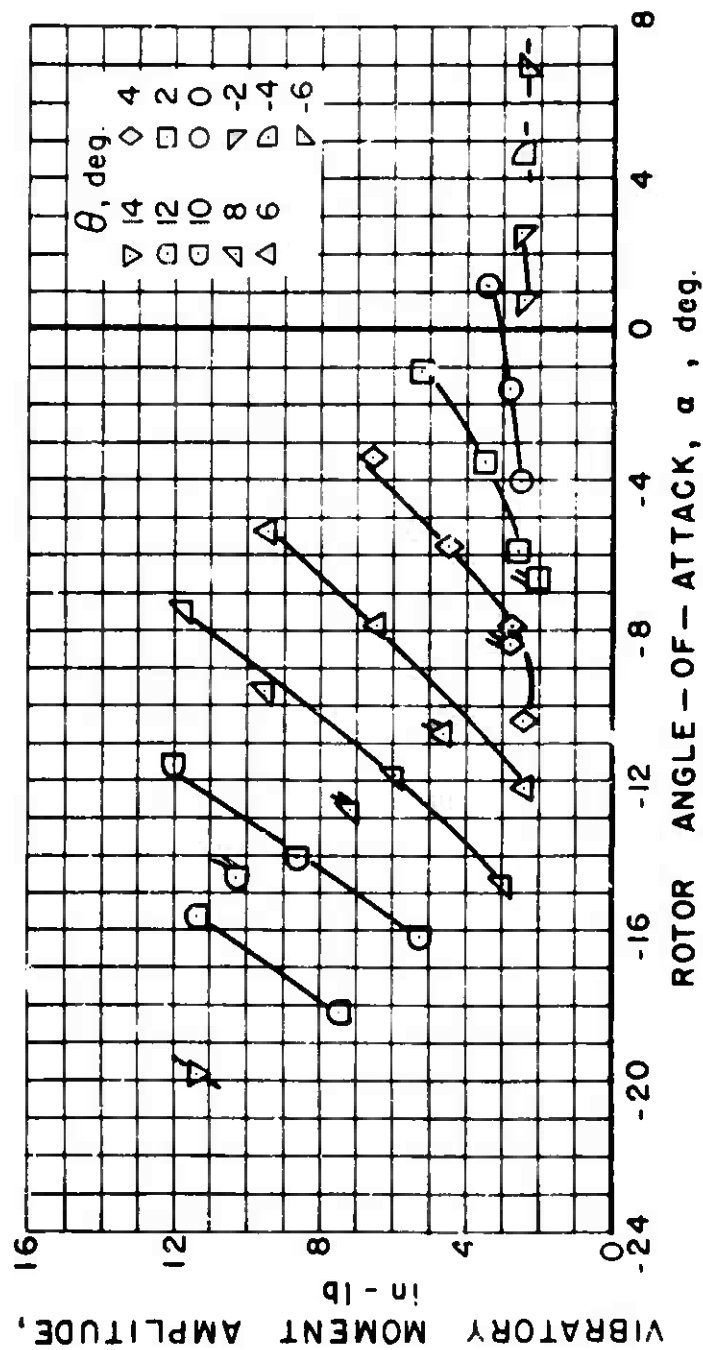
(a) FLATWISE BENDING MOMENT, 21 % R

Figure 88. Experimental Vibratory Moment Amplitude, $\mu = 0.5$.



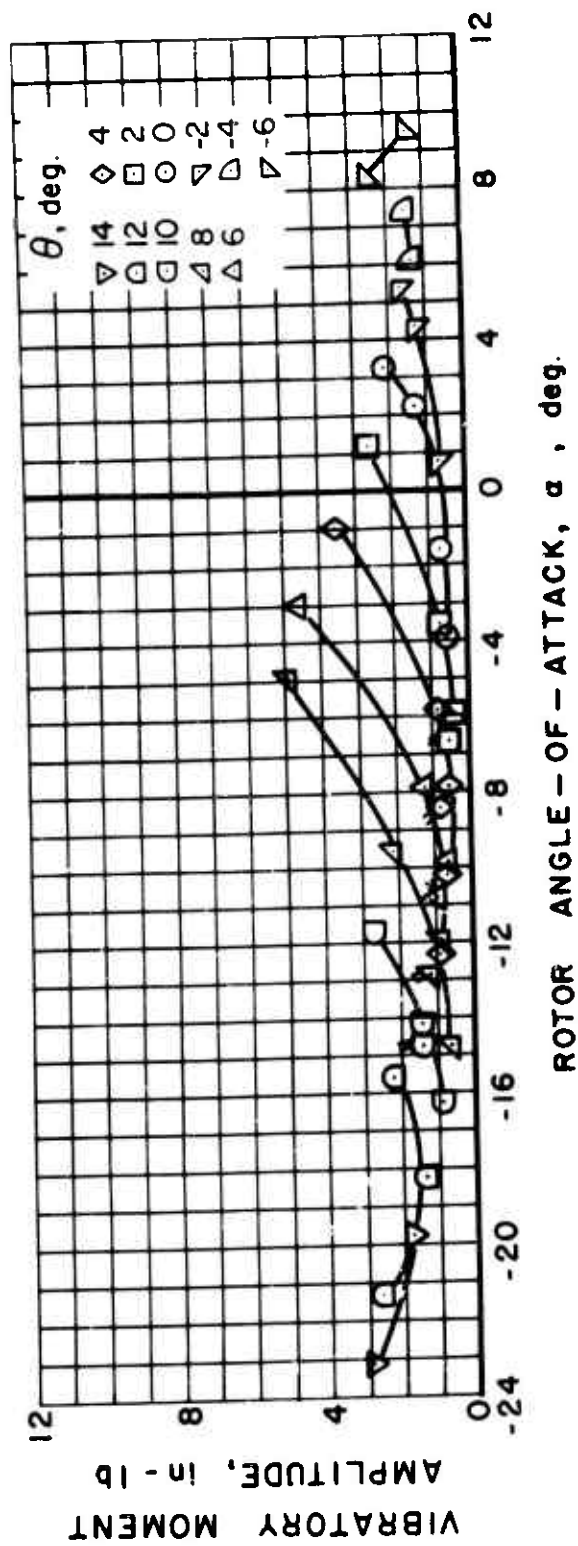
(b) EDGEWISE BENDING MOMENT, 21 % R

Figure 88. Continued.



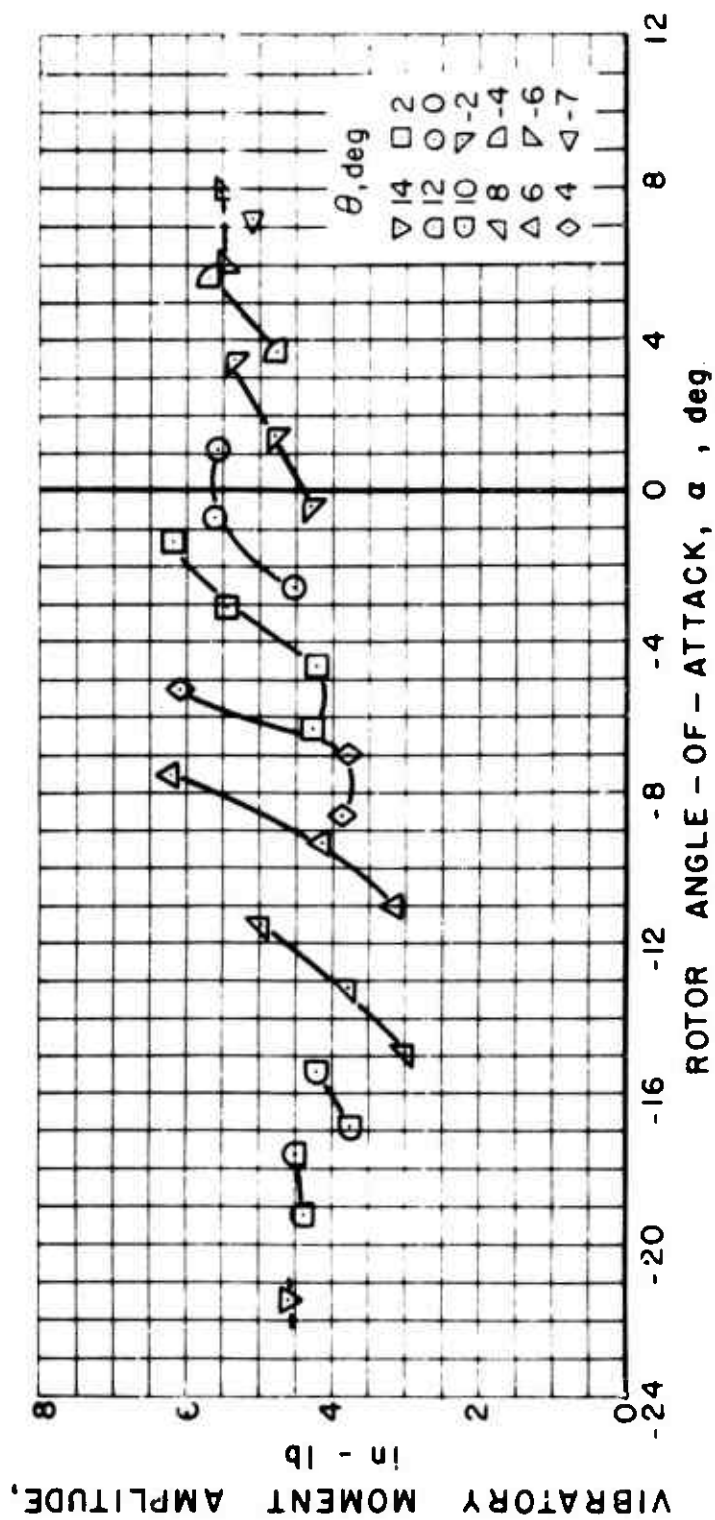
(c) EDGEWISE BENDING MOMENT, 47 % R

Figure 88. Continued.



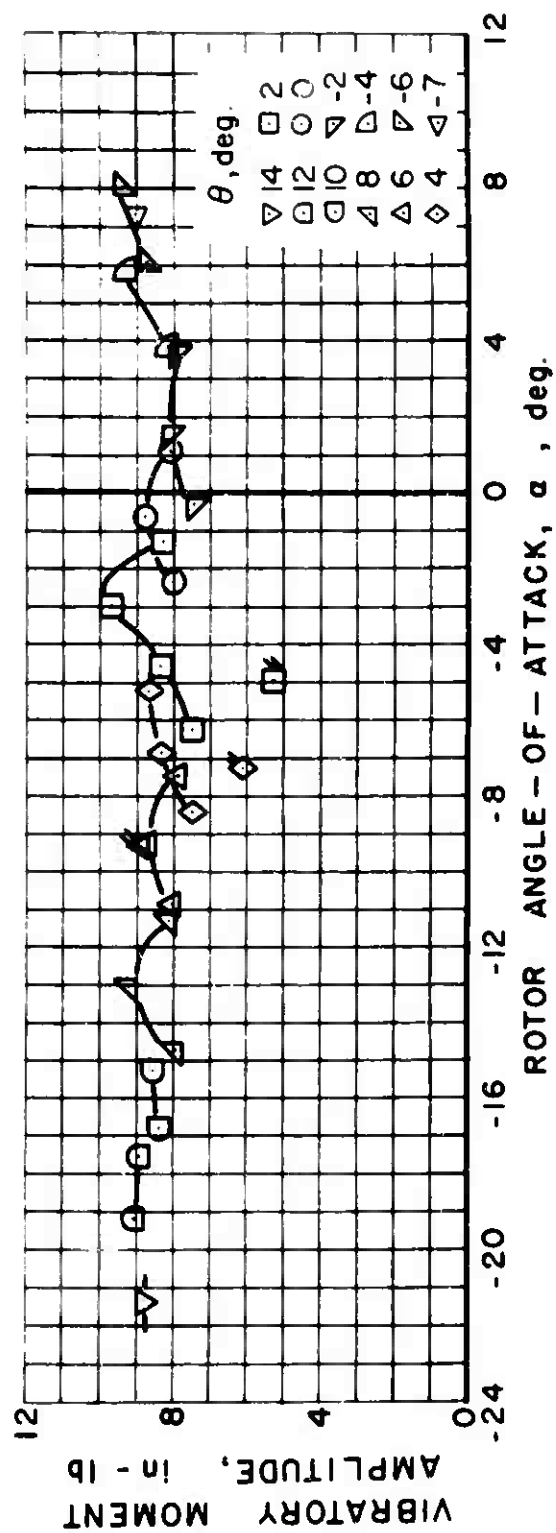
(d) TORSIONAL MOMENT, 17.5 % R

Figure 88. Concluded.



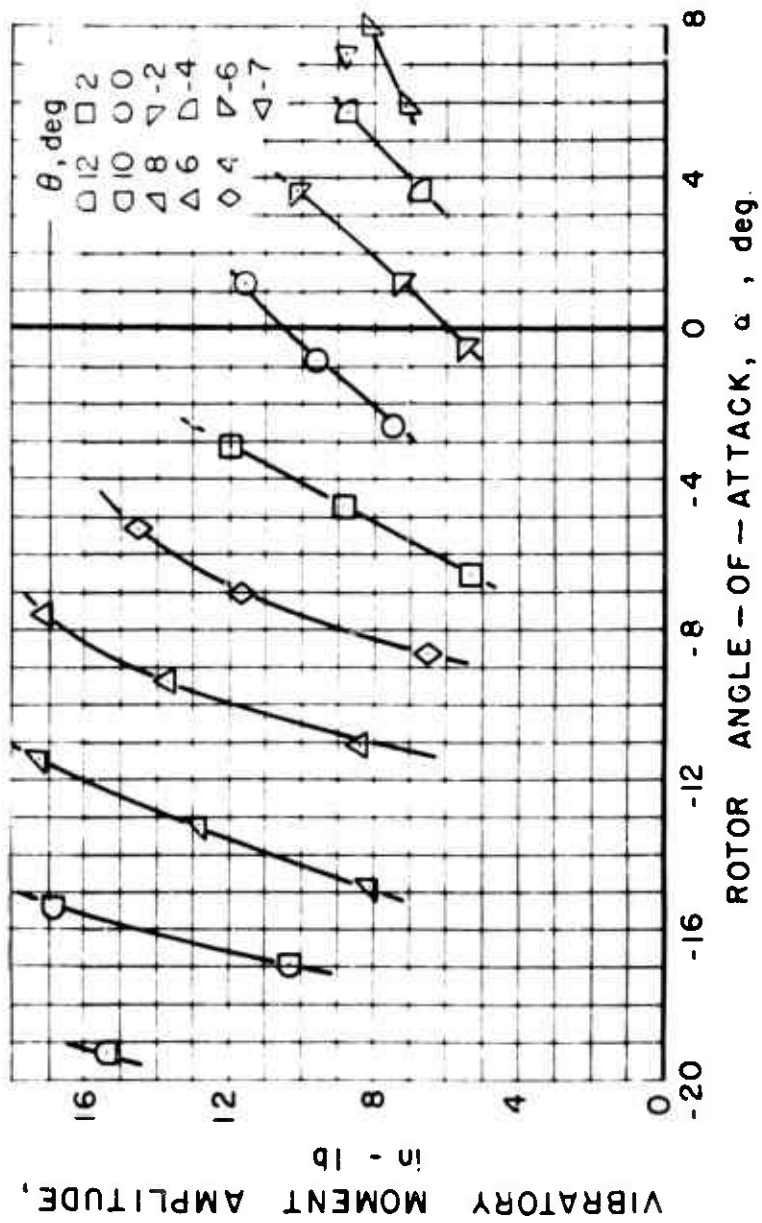
(a) FLATWISE BENDING MOMENT, 21 % R

Figure 89. Experimental Vibratory Moment Amplitude, $\mu = 0.7$.



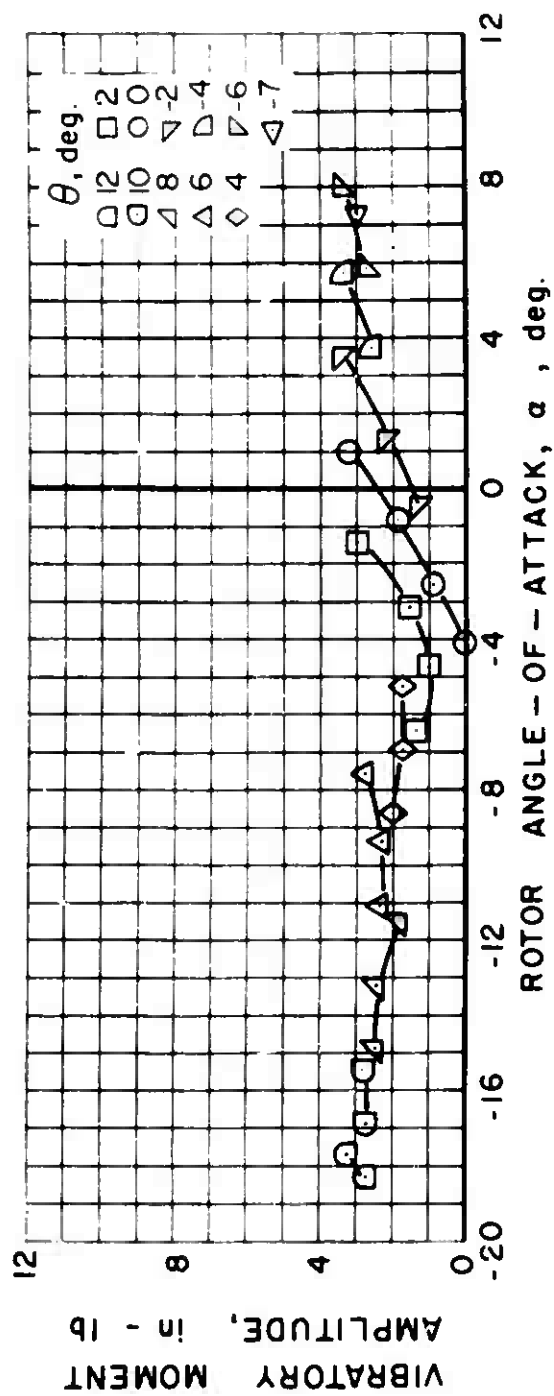
(b) EDGEWISE BENDING MOMENT, 21% R

Figure 89. Continued.



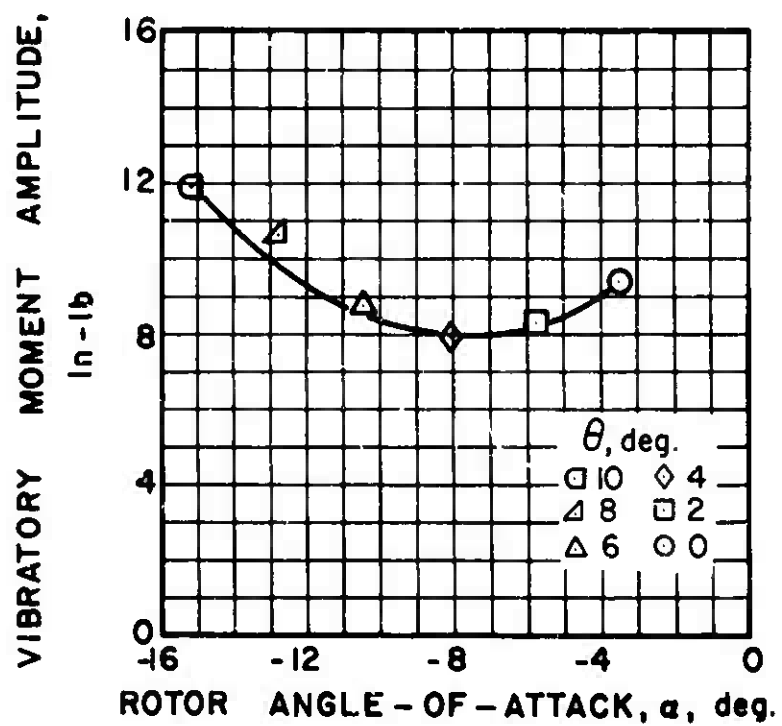
(c) EDGEWISE BENDING MOMENT, 47 % R

Figure 89. Continued.



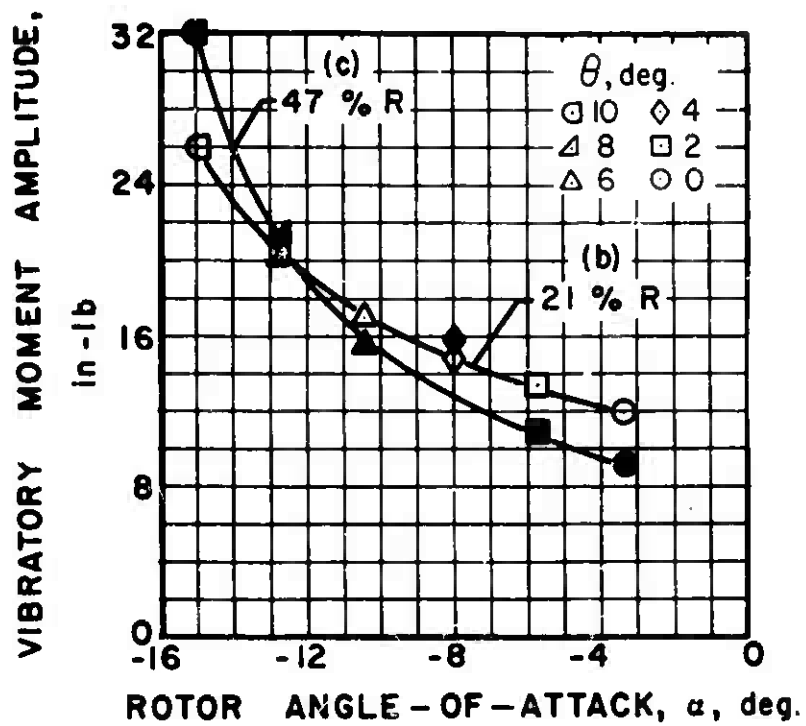
(d) TORSIONAL MOMENT, 17.5 % R

Figure 89. Concluded.



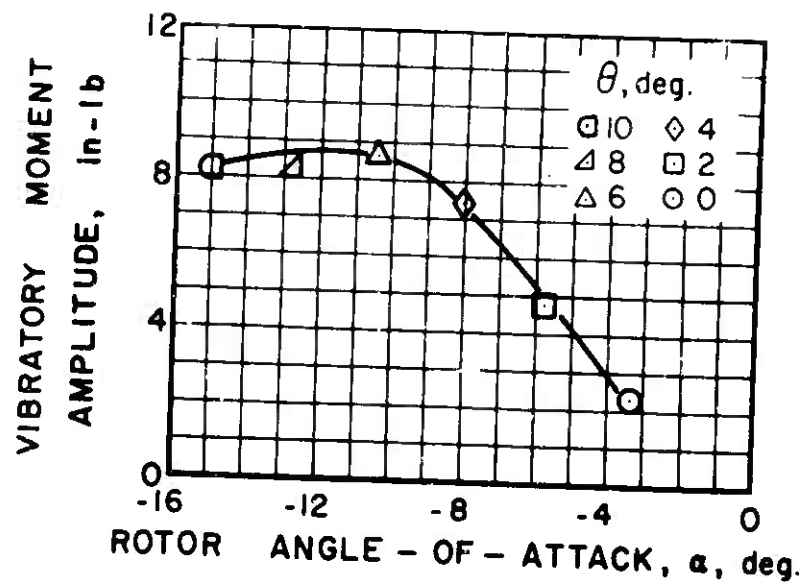
(a) FLATWISE BENDING MOMENT, 21% R

Figure 90. Experimental Vibratory Moment Amplitude, $\mu = 1.0$.



(b) & (c) EDGEWISE BENDING MOMENT

Figure 90. Continued.



(d) TORSIONAL MOMENT, 17.5 % R

Figure 90. Concluded.

APPENDIX IV

EXPERIMENTAL VIBRATORY CONTROL LOAD AMPLITUDE FIGURES

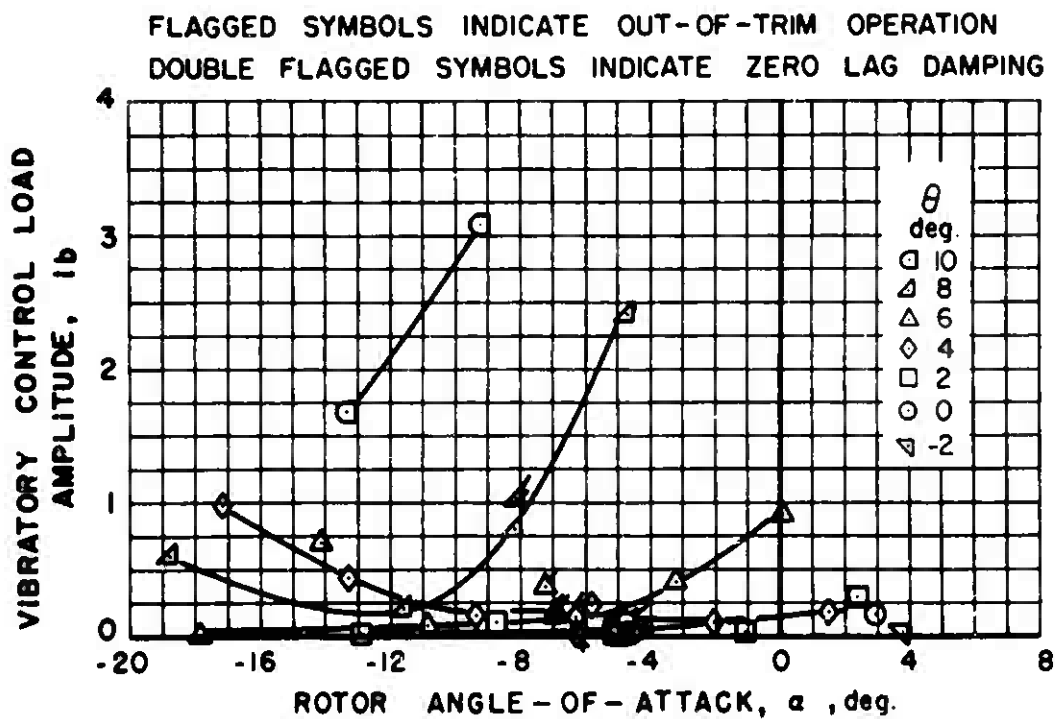


Figure 91. Experimental Vibratory Control Load Amplitude, $\mu = 0.2$.

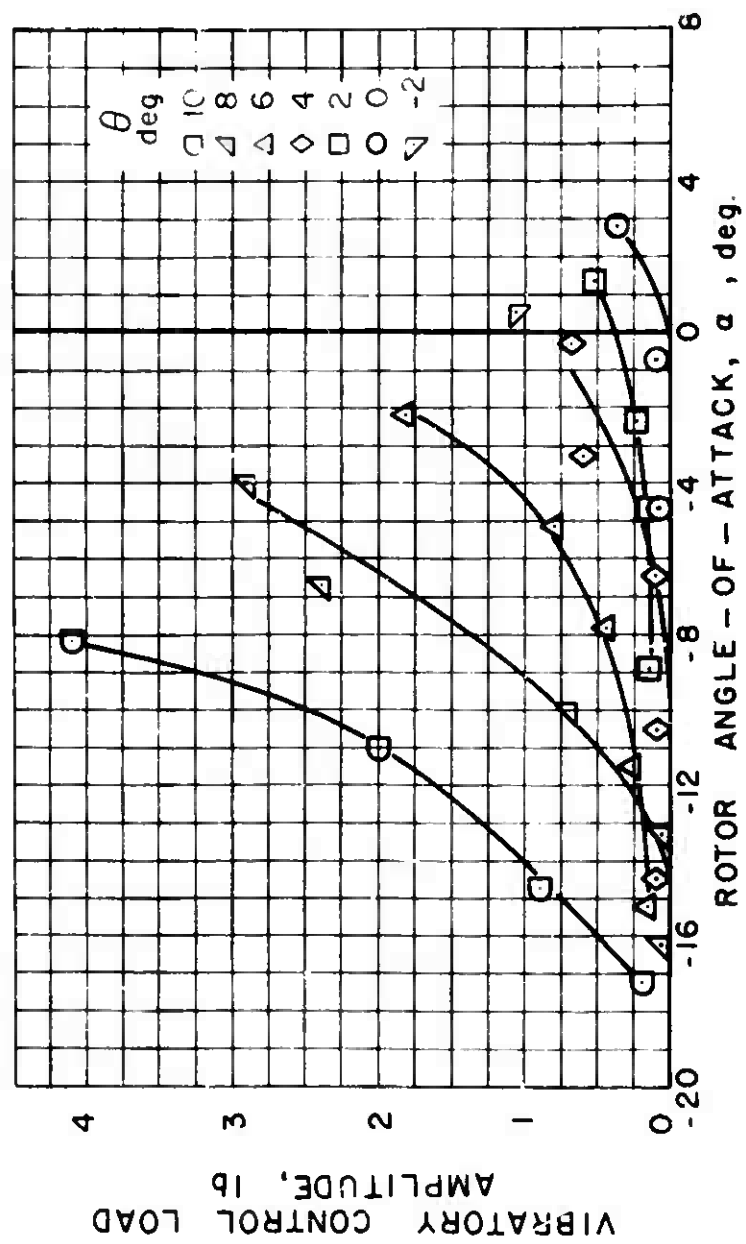


Figure 92. Experimental Vibratory Control Load Amplitude, $\mu = 0.3$.

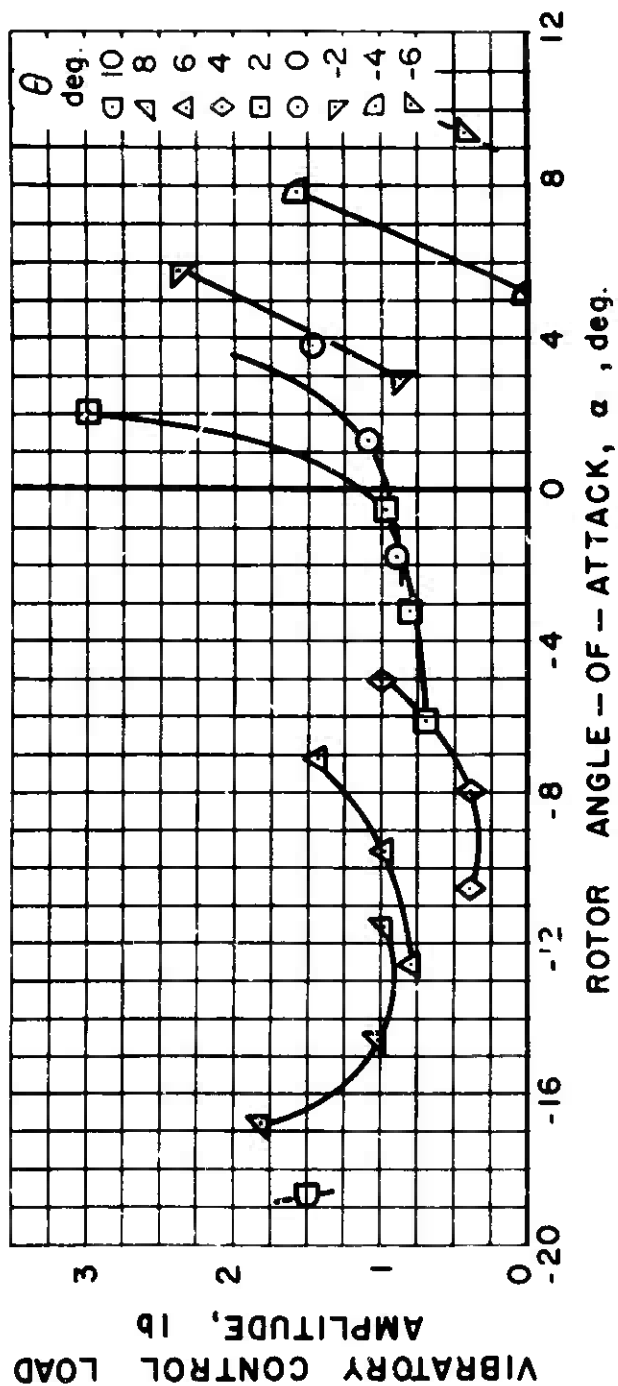


Figure 93. Experimental Vibratory Control Load Amplitude, $\mu = 0.4$.

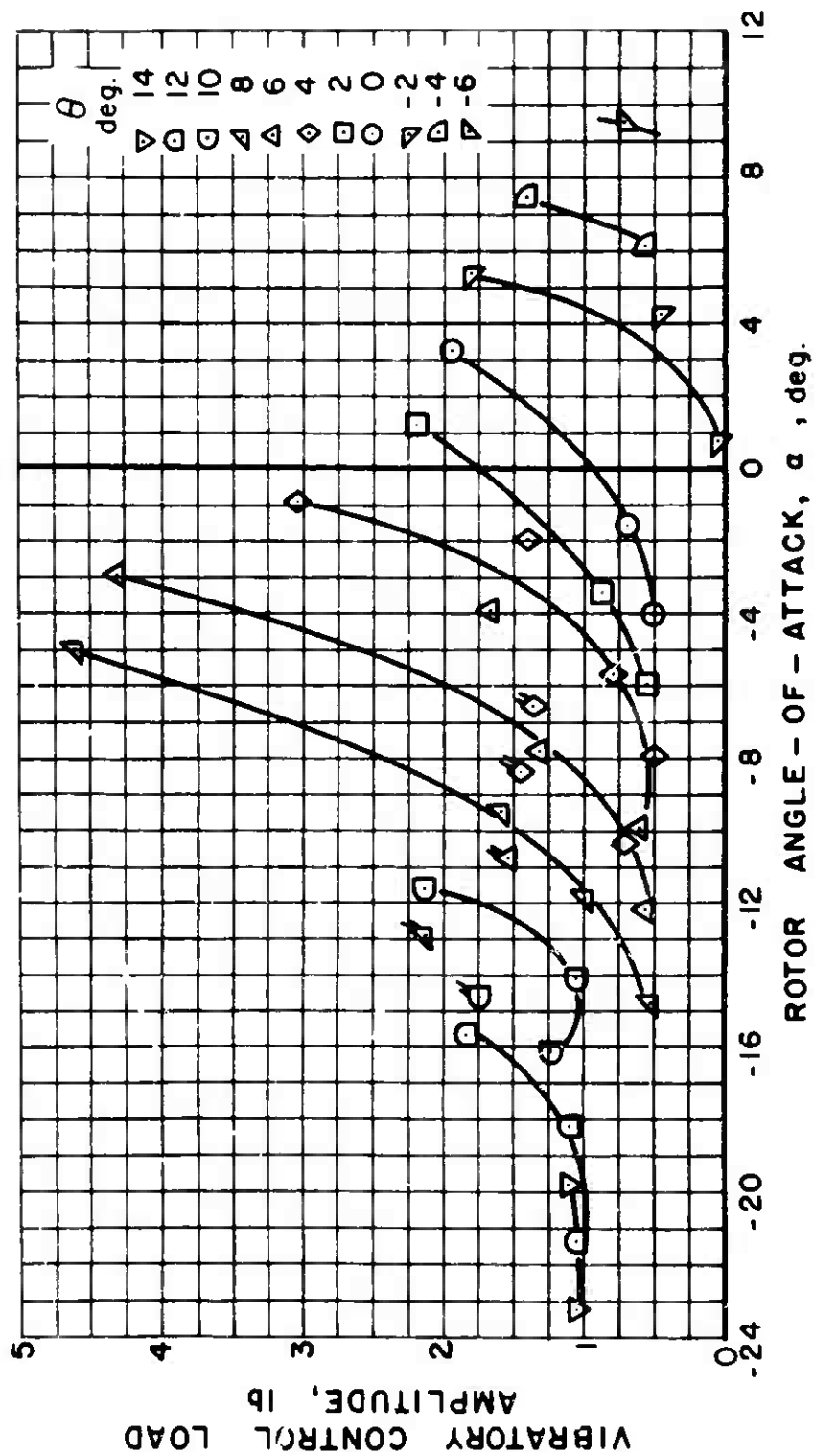


Figure 94. Experimental Vibratory Control Load Amplitude, $\mu = 0.5$.

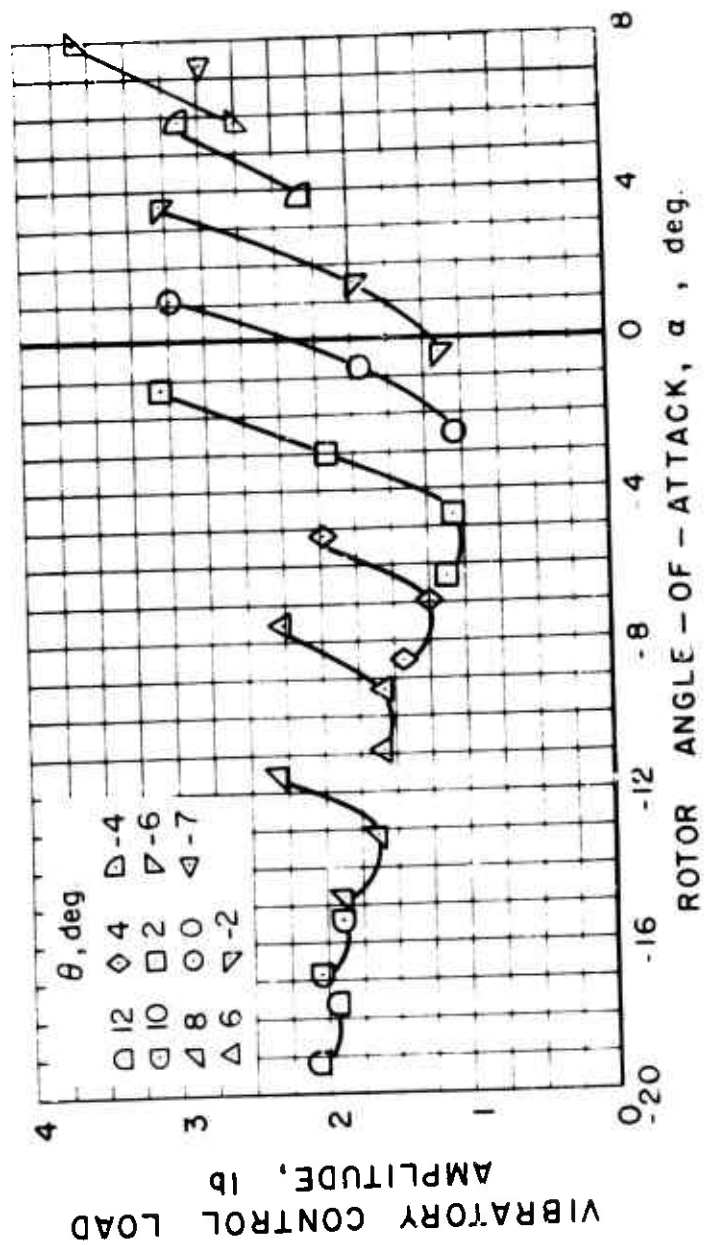


Figure 95. Experimental Vibratory Control Load Amplitude, $\mu = 0.7$.

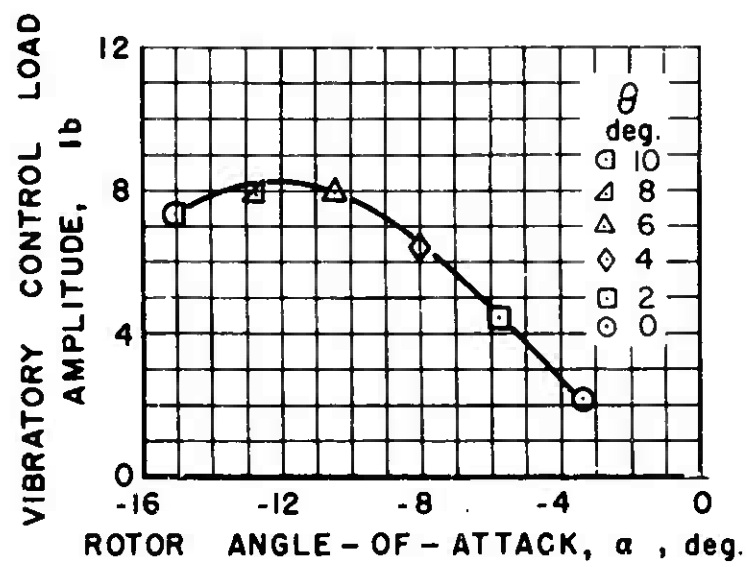


Figure 96. Experimental Vibratory Control Load Amplitude, $\mu = 1.0$.

UNCLASSIFIED

Security Classification

DOCUMENT CONTROL DATA - R & D		
<small>(Security classification of title, body of abstract and indexing annotation must be entered when the overall report is classified)</small>		
1. ORIGINATING ACTIVITY (Corporate author) Sikorsky Aircraft Division of United Aircraft Corp. Stratford, Connecticut		2a. REPORT SECURITY CLASSIFICATION Unclassified
		2b. GROUP
3. REPORT TITLE "Comparison of Theoretical and Experimental Model Rotor Blade Vibratory Shear Forces"		
4. DESCRIPTIVE NOTES (Type of report and inclusive dates)		
5. AUTHOR(S) (First name, middle initial, last name) Lawrence J. Bain		
6. REPORT DATE October 1967	7a. TOTAL NO. OF PAGES 305	7b. NO. OF PAGES 6
8a. CONTRACT OR GRANT NO. DA 44-177-AMC-136(T)	8b. ORIGINATOR'S REPORT NUMBER(S) USAAVLABS Technical Report 66-77	
8c. PROJECT NO. Task 1D 121401A 14203	8d. OTHER REPORT NO(S) (Any other numbers that may be assigned this report) SER-50419	
10. DISTRIBUTION STATEMENT This document has been approved for public release and sale; its distribution is unlimited.		
11. SUPPLEMENTARY NOTES	12. SPONSORING MILITARY ACTIVITY U. S. Army Aviation Material Laboratories Fort Eustis, Virginia	
13. ABSTRACT <p>An investigation was undertaken to obtain quantitative measurements of the vibratory forcing functions from the blades of rotary wing aircraft in the flight speed range encompassing both pure and compound helicopter operation. These measurements were made using dynamically scaled model rotor blades mounted on a specially instrumented rotor head. Testing was accomplished over a range of equivalent forward speeds from 75 to 300 knots and over a range of full-scale rotor lifts from zero to 40,000 lb. In addition to rotor performance, the final data include ten harmonics of the orthogonal blade root shear forces, rotor blade bending moments, and rotor control loads.</p> <p>A portion of the experimental results were correlated with a fully coupled aeroelastic analysis which included the effects of wake induced velocities. It was found that the inclusion of these effects improved the correlation of the flatwise shear forces over that obtained assuming uniform inflow.</p>		

DD FORM 1473

1 NOV 65

(PAGE 1)

S/N 0101-807-6801

UNCLASSIFIED

Security Classification

14 KEY WORDS	LINK A		LINK B		LINK C	
	ROLE	WT	ROLE	WT	ROLE	WT
Helicopter Rotor Blade Vibratory Shear Force Tests Correlations						